

# **Nasal Drying During Pressurised Breathing**

**David Edward White**

**School of Engineering**

**2013**

**A thesis submitted to Auckland University of Technology in fulfilment of the  
degree of Doctor of Philosophy**

## **Dedication**

I dedicate this work to my wife, Kathy, and family, Rosemary and William, who have endured my absence and distracted demeanour during this journey of discovery.

## Abstract

The human nose not only provides the main portal through which air passes to and from our respiratory system, it also plays an important role in maintaining airway health. This function takes the form of heating and humidifying inhaled air to prevent airway drying, as well as trapping and disposing of inhaled particles and pathogens within the mucus lining. The ability of the nose to perform these duties appears compromised during the nasal breathing of pressurised air, with many users reporting symptoms associated with nasal airway drying. There are many situations where nasal breathing of pressurised air occurs. The cause of airway drying is currently not known, but is typically relieved through the use of supplementary humidification.

This investigation examines the role air-pressure has on nasal airway drying by the development of a nasal air-conditioning model to predict inter-nasal airway hydration throughout the breathing cycle during ambient and pressurised breathing. Furthermore, the effect air pressure has on mucosal water supply and airway geometry is investigated in tissue experiments as well as *in-vivo* MRI clinical trials. Together the latter two investigations demonstrate that augmentation in air pressure adversely effects water supply and cause an opposing response in airway geometry between airways.

Implementation of these previously unknown behaviours into the nasal air-conditioning model provides additional new insight into the actual function of the nose and its pathophysiology during pressurised air breathing. For the first time, a different airway hydration status during ambient air breathing is identified between the airways. During inhalation, the patent airway experiences drying that likely disables mucociliary transport, while the patent airway remains fully hydrated. This work sheds new light as to the purpose of the nasal cycle.

Modelling pressurised nasal breathing demonstrates drying occurring within both airways and that supplementary humidification prevents this from occurring by effectively relieving the nose of its air-conditioning function. Modelling also demonstrates how supplementary humidification assists in the removal of entrapped particles and pathogens by providing ideal conditions for mucus transport to occur.

An alternative method to relieve nasal airway drying is proposed. This method maintains normal airway hydration conditions during pressurised air breathing and avoids the problems of perceived stuffiness and congestion commonly encountered with supplementary humidification.

## Table of Contents

List of Figures	xii
List of Tables	xviii
Attestation of Authorship	xix
Publication List	xx
Acknowledgements	xxi
Intellectual Property Rights	xxi
Confidential Material	xxii
Deposit of Thesis in the AUT Library (PGR15)	xxiii
Application for Restricted Access to a Thesis (PGR16)	xxiv
<b>Chapter 1: Introduction</b>	<b>1</b>
<b>1.1 Background</b>	<b>1</b>
<b>1.2 Obstructive Sleep Apnea</b>	<b>1</b>
<b>1.3 Positive Air-Pressure Therapy</b>	<b>3</b>
1.3.1 Pressure Related Symptoms	5
1.3.2 Supplementary Humidification	5
1.3.3 Treatment Adherence	6
<b>1.4 Causes of Nasal Drying</b>	<b>7</b>
<b>1.5 Contributions of this Thesis</b>	<b>7</b>
<b>1.6 Closure</b>	<b>8</b>
<b>Chapter 2: Literature Survey</b>	<b>9</b>
<b>2.1 Introduction</b>	<b>9</b>
<b>2.2 The Human Airways</b>	<b>9</b>
<b>2.3 Nasal Air-Conditioning</b>	<b>10</b>
2.3.1 Anatomical Features	12
2.3.2 Active Control	13
2.3.3 Nasal Cycle	15
2.3.4 Air-Conditioning Morphology	16
2.3.5 Ambient Air-Pressure Measurements	16
2.3.6 Pressure Elicited Change in Nasal Geometry	20
<b>2.4 Airway Surface Liquid</b>	<b>22</b>
2.4.1 Heat and Water Recovery	23

2.4.2	Mucus Entrapment and Clearance	23
2.4.3	ASL Stratification	24
2.4.4	ASL Hydration	26
2.4.5	Mucociliary Transport Dysfunction	26
2.4.6	Hydration/Dehydration Limits	27
<b>2.5</b>	<b>Airway Surface Liquid Water Supply</b>	<b>28</b>
2.5.1	Autonomic Regulation of Airway Surface Liquid Height	29
2.5.2	Purinergic Regulation of Periciliary Liquid Height	29
2.5.2.1	Breathing Stress Stimulation	30
2.5.2.2	Cellular Reabsorption	31
2.5.3	Quantification of PCL Supply and Absorption	31
2.5.3.1	Bronchial, Tracheobronchial and Oral Mucosa	32
2.5.3.2	Nasal Mucosa	33
2.5.3.3	Ambient Pressure	33
<b>2.6</b>	<b>Adult Tidal Breathing</b>	<b>34</b>
<b>2.7</b>	<b>Air Temperature and Humidity Measurements</b>	<b>34</b>
<b>2.8</b>	<b>Review of Air-Conditioning Models</b>	<b>37</b>
2.8.1	Computational Models	38
2.8.2	n-PAP Air-Conditioning Model	49
<b>2.9</b>	<b>Research Hypothesis</b>	<b>51</b>
<b>2.10</b>	<b>Research Plan and Objectives</b>	<b>51</b>
<b>2.11</b>	<b>Closure</b>	<b>54</b>
<b>Chapter 3:</b>	<b>Nasal ASL Hydration Model</b>	<b>55</b>
<b>3.1</b>	<b>Introduction</b>	<b>55</b>
<b>3.2</b>	<b>Model Overview</b>	<b>56</b>
3.2.1	General Description	56
3.2.2	Accounting for Morphology	58
<b>3.3</b>	<b>State-Variable Model Development</b>	<b>60</b>
<b>3.4</b>	<b>Computational Arrangement</b>	<b>61</b>
3.4.1	Variable Computation	61
3.4.2	Data Storage	63
<b>3.5</b>	<b>Model Assumptions</b>	<b>64</b>
<b>3.6</b>	<b>Derivation of State Variables</b>	<b>64</b>

3.6.1	Air/Water Mixture Temperature	64
3.5.2	Airway/Water Species Concentration	67
<b>3.7</b>	<b>Derivation of Input Variables</b>	68
3.7.1	Blood Temperature Distribution	68
3.7.2	Airway Surface Liquid Temperature	69
<b>3.8</b>	<b>Derivation of Intermediate Variables</b>	70
3.8.1	Inter-Nasal Air Mass-Flow Partitioning	70
3.8.2	Convective Heat and Mass Transfer Coefficients	73
<b>3.9</b>	<b>Derivation of Output Variables</b>	74
3.9.1	Airway Surface Liquid Temperature	74
3.9.2	ASL-Air Interface Water Species Concentration	75
3.9.3	Water Flux	77
<b>3.10</b>	<b>Computational Strategy</b>	77
<b>3.11</b>	<b>ASL Water Equivalent Height</b>	79
3.11.1	ASL Height Regulation	80
<b>3.11</b>	<b>Closure</b>	80
<b>Chapter 4:</b>	<b>Morphological Response to n-PAP Breathing – an MRI Investigation</b>	81
<b>4.1</b>	<b>Introduction</b>	81
<b>4.2</b>	<b>Participant Recruitment</b>	81
4.2.1	Ethical Approval	81
4.2.2	Participant Selection and Preparation	82
<b>4.3</b>	<b>MRI Protocol and Data Processing</b>	82
4.3.1	Nasal Cycle Measurement	82
4.3.2	Air Pressure Protocol	82
4.3.2.1	Ambient Air Breathing	83
4.3.2.2	Positive Air-Pressure Breathing	83
4.3.3	MRI protocol	84
4.3.3.1	Region of Interest	84
4.3.3.2	MRI Morphology	85
4.3.3.3	Morphology Image Processing	86
4.3.3.4	MRI Nasal Blood Flow	87
4.3.3.5	Blood Flow Image Processing	88
<b>4.4</b>	<b>Results overview</b>	90

<b>4.5</b>	<b>Nasal Cycle Results</b>	90
4.5.1	Nasal Cycle Discussion	90
<b>4.6</b>	<b>Combined Airway Geometry Results</b>	91
4.6.1	Combined Airway Geometry Discussion	94
<b>4.7</b>	<b>Separate Airway Geometry Results</b>	94
4.7.1	Ambient Pressure Breathing Results	95
4.7.2	Ambient Pressure Breathing Discussion	98
4.7.3	n-PAP Breathing Results	99
4.7.4	n-PAP Discussion	102
4.7.5	Inter-nasal Accumulated Volume Change	103
<b>4.8</b>	<b>Inter-nasal Blood Flow Results</b>	106
4.8.1	Inter-Nasal Blood-Flow Discussion	106
<b>4.9</b>	<b>Closure</b>	108
 <b>Chapter 5: Mucosal ASL Supply Response Air-Pressure – an Experimental Investigation.</b>		109
<b>5.1</b>	<b>Introduction</b>	109
<b>5.2</b>	<b>Tissue Protocol, Equipment, and Data Acquisition</b>	109
5.2.1	Nasal Tissue Model	109
5.2.2	Tissue Protocol	110
5.2.3	Tissue Viability	111
5.2.4	Dissection and Mounting	111
5.2.5	Airway Surface Liquid	112
<b>5.3</b>	<b>Experimental Apparatus</b>	113
5.3.1	Air-Flow Control and Pressure Drop Regulation	114
5.3.2	Water Demand and Measurement	116
5.3.3	Air Humidity and Temperature Measurement	117
<b>5.4</b>	<b>Experimental Protocols and Data Management</b>	118
5.4.1	Calibration	118
5.4.2	Data Acquisition	119
5.4.3	Post-Acquisition Data Processing	120
<b>5.5</b>	<b>Results</b>	120
<b>5.6</b>	<b>Analysis and Discussion</b>	122
5.6.1	Factors Influencing Results	122
5.6.2	Comparison to Previous Results	125

<b>5.7</b>	<b>ASL Water Supply</b>	126
5.7.1	Air-Pressure Suppression	126
5.7.2	Maximal ASL Water Supply	126
<b>5.8</b>	<b>Closure</b>	127
<b>Chapter 6:</b>	<b>Model Results and Observations</b>	128
<b>6.1</b>	<b>Introduction</b>	128
<b>6.2</b>	<b>Introduction to Plots</b>	128
<b>6.3</b>	<b>Ambient Air Breathing</b>	130
6.3.1	Inhalation Air Properties, Flux Levels and ASL Hydration	131
6.3.2	Exhalation Air Properties, Flux Levels and ASL Hydration	132
<b>6.4</b>	<b>Air Mass-Flow Partitioning</b>	133
<b>6.5</b>	<b>Un-Humidified n-PAP Breathing</b>	134
6.5.1	Inhalation Air Properties, Flux Levels and ASL Hydration	135
6.5.2	Exhalation Air Properties, Flux Levels and ASL Hydration	136
<b>6.6</b>	<b>Mucosa Dry Time</b>	137
6.6.1	Un-humidified n-PAP Breathing	137
<b>6.7</b>	<b>n-PAP Breathing with Supplementary Heated Humidification</b>	138
6.7.1	Inhalation Air Properties, Flux Levels and ASL Hydration	140
6.7.2	Exhalation Air Properties, Flux Levels and ASL Hydration	141
<b>6.8</b>	<b>n-PAP Breathing with Non-Heated Supplementary Humidification</b>	142
6.8.1	Inhalation Air Properties, Flux Levels and ASL Hydration	143
6.8.2	Exhalation Air Properties, Flux Levels and ASL Hydration	144
<b>6.9</b>	<b>Closure</b>	145
<b>Chapter 7:</b>	<b>Discussion of Model Results</b>	146
<b>7.1</b>	<b>Introduction</b>	146
<b>7.2</b>	<b>Model Assumption of Laminar Airflow</b>	146
<b>7.3</b>	<b>Nasal Breathing at Ambient Air-Pressure</b>	146
7.3.1	Consequences of ASL dehydration	147
7.3.2	Explanation of the Nasal Cycle	148
<b>7.4</b>	<b>Inhalation of Un-Humidified Pressurised Air</b>	150
7.4.1	Mucosa Dry Time	151
7.4.2	Sleep Quality and the Nasal Cycle	152
<b>7.5</b>	<b>n-PAP Breathing with Supplementary Humidification</b>	153

7.5.1	Heated Supplementary Humidification	153
7.5.2	Non-Heated Supplementary Humidification	153
7.5.3	Supplementary Humidification Debate	154
7.5.3.1	Therapeutic Efficacy and Compliance	154
7.5.3.2	Device Complexity	155
7.5.3.3	Human Factors	155
7.6	Closure	156
<b>Chapter 8:</b>	<b>Alternative to Supplementary Humidification</b>	157
8.1	Introduction	157
8.2	Regulation of Inter-Nasal Air mass-Flow Partitioning	157
8.3	Model Implementation	158
8.4	n-PAP Breathing with Regulated Inter-Nasal Resistances	160
8.4.1	Inhalation Air Properties, Flux Levels and ASL Hydration	161
8.4.2	Exhalation Air Properties, Flux Levels and ASL Hydration	162
8.5	Mucosa Dry Time	162
8.5.1	Absence of Supplementary Humidification	162
8.6	Discussion	163
8.7	Closure	164
<b>Chapter 9:</b>	<b>Conclusions and Future Work</b>	165
9.1	Introduction	165
9.2	Research Hypothesis	165
9.2.1	Inter-Nasal Variation in Geometry	165
9.2.2	Reduction in Mucosal Water Supply	166
9.3	ASL Dehydration During n-PAP Breathing	166
9.4	Nasal Cycle	167
9.5	Alternative to Supplementary Humidification	167
9.6	Recommendations	167
	<b>References</b>	169
	<b>Glossary</b>	183

<b>Appendix A: Air-Conditioning Model Code</b>	187
A1    Main Nose	187
A2    Morphology Acquisition	191
A3    Initiate	195
A4    Morphology Compliance	197
A5    Water Compliance	200
A6    Breath Build	202
A7    Flow Apportionment	203
A8    Breath Phase	204
A9    Start Condition	204
A10   Flux Calculation	216
A11   Phase Corrector	228
A12   Water Regulation	228
 <b>Appendix B: Morphological Response to n-PAP Breathing Experiment</b>	 236
B1    Experimental Protocol and Equipment	236
B1.1  Participant Recruitment	236
B1.2  Participant Preparation	237
B1.3  Measurement of Nasal Cycle	237
B1.4  MRI Scanning	238
B1.5  Air Pressure Protocol	240
B1.6  Nasal Airflow Results	241
B1.7  Region of Interest	242
B1.8  Geometrical Raw Data	243
B1.9  MRI Settings	244
B2:   Ethics Approval	262
B2.1  Application for Ethics Approval	262
B2.2  AUTEC Memorandum of Ethics Approval	285
B2.3  Invitation to Participate	287
B2.4  Participant Information Sheet	288
B2.5  Confidentiality Agreement	293
B2.6  Consent Form	294
B2.7  Demographic Form	296
B2.8  CAMRI MRI Safety and Consent Form	297

B2.9	CAMRI MRI Check List	299
B3	Experimental Data	300
<b>Appendix C: Mucosal ASL Supply Response Air-Pressure Experiment</b>		305
C1	Experimental Protocol and Equipment	305
C1.1	Overview of Experiment	305
C1.2	Dissection and Mounting	306
C1.3	Pre-Test Tissue Viability	307
C1.4	Post-Test Tissue Viability and ASL verification	309
C1.5	Physiological Salt Solution	309
C1.6	Configuration of Test Apparatus	312
C1.7	Pre-Test Sensor Calibration	314
C1.8	Assembly of Desiccant Chamber	314
C1.9	Silica Gel Absorbent	314
C1.10	Assembly of Apparatus in Incubator Space	315
C1.11	Transport Ventilator Air Supply	317
C1.12	Preparation for Augmented Pressure Testing	318
C1.13	Incubator Modification	318
C1.14	Air Pressure Supply	319
C1.15	Incubator Pressure Sensing	320
C1.16	Thermal Stabilisation and Data Acquisition	321
C2:	LabView Program	323
C3:	Orifice Pressure Drop Calculation	325
C4:	Experimental Data and Processing	325
C4.1	Ambient Pressure	326
C4.2	5 cm H <sub>2</sub> O Pressure	330
C4.3	10 cm H <sub>2</sub> O Pressure	334
C4.4	15 cm H <sub>2</sub> O Pressure	338

## List of Figures

Figure 1.1:	Upper airway closure within oropharynx or hypopharynx. ....	3
Figure 1.2:	Patient receiving n-PAP therapy.....	4
Figure 1.3:	Typical supplementary PAP heated humidifier .....	6
Figure 2.1:	Human airway.....	10
Figure 2.2:	Schematic representation of factors of air-conditioning heat and water demand and mucosal water supply which influence ASL hydration status .....	11
Figure 2.3:	Sagittal sectional view through nasal cavity demonstrating functional regions.....	13
Figure 2.4:	Schematic representation of the nasal vasculature.....	14
Figure 2.5:	MRI head coronal scan.....	15
Figure 2.6:	Distribution of combined nasal airway cross-sectional area for African Americans (AA) and European Americans (EA) .....	17
Figure 2.7:	Distribution of combined nasal airway perimeter for African Americans (AA) and European Americans (EA).....	17
Figure 2.8:	Distribution of combined nasal airway perimeter for African Americans (AA) and European Americans (EA).....	18
Figure 2.9:	Canine nasal hydraulic diameter distribution.....	19
Figure 2.10:	Human inter-nasal cross-sectional area distribution.....	20
Figure 2.11:	Nasal compliance representing change in cross-sectional area per unit pressure (cm H <sub>2</sub> O).....	21
Figure 2.12:	Nasal compliance represented as change in volume (cm <sup>3</sup> ) per unit pressure (cm H <sub>2</sub> O).....	21
Figure 2.13:	Mucus layer transport by beating action of motile cilia.....	24
Figure 2.14:	(A) - Mucin release from secretory cells being hydrated within the PCL and moving towards the upper mucus gel layer. (B) – Enlarged view of cilia demonstrating increasing membrane-tethered grafter mucins and mucopolysaccharides.....	25
Figure 2.15:	Two modes of mucociliary transport failure caused by PCL dehydration. (A) Mucus entering interciliary space; (B) Mucus compressing cilia.....	27
Figure 2.16:	(A) Normal ASL hydration enables cilia to extend to full height. (B) Severely dehydrated ASL demonstrating absence of motile cilia. In both images the white bar demonstrates normal PCL height of 7 μm .....	28
Figure 2.17:	Simplified representation of airway submucosal gland demonstrating connection of serous acini cells and mucus tubules to a common duct system.....	29

Figure 2.18: Nasal <i>in-vivo</i> mean end-inspiratory air temperature distribution measured during breathing at rest at room temperature.....	35
Figure 2.19: Air temperature measured <i>in-vivo</i> at head of middle turbinate during breathing at rest. (A) End-inspiratory (B) End-expiratory.....	36
Figure 2.20: Predicted water molar flux during ambient air at rest breathing as a function of non-dimensional distance into conducting airway ( $T=25^{\circ}\text{C}$ , $\text{RH}=35\%$ ).....	39
Figure 2.21: Predicted heat flux as a function of non-dimensional distance into conducting airway model during at rest room breathing.....	40
Figure 2.22: Predicted air temperature distribution as a function of non-dimensional distance into conducting airway model.....	41
Figure 2.23: Air temperature predictions along conducting airway over range of breathing conditions.....	42
Figure 2.24: Air humidity predictions along conducting airway over range of breathing conditions.....	43
Figure 2.25: Predicted normalized ASL height for selected regions along the conducting airway throughout one breath cycle.....	43
Figure 2.26: Simplified nasal geometric model.....	44
Figure 2.27: Results of 2-D nasal model giving temperature distribution along the nasal cavity during peak inhalation of ambient air ( $T=25^{\circ}\text{C}$ , $\text{RH} = 20\%$ ).....	45
Figure 2.28: Predicted lumen air temperature along tracheal/bronchial airways during breathing ambient air ( $T=22^{\circ}\text{C}$ , $\text{RH} = 50\%$ , $V=6 \text{ l/m}$ ).....	46
Figure 2.29: Predicted lumen air relative humidity along tracheal/bronchial airways during breathing ambient air ( $T=22^{\circ}\text{C}$ , $\text{RH} = 50\%$ , $V=6 \text{ l/m}$ ).....	46
Figure 2.30: Predicted lumen air temperature along tracheal/bronchial airways during breathing ambient air ( $T=22^{\circ}\text{C}$ , $\text{RH} = 50\%$ , $V=6 \text{ l/m}$ ).....	47
Figure 2.31: Results of MRI based CFD nasal model. (A) Temperature distribution, (B) Specific Humidity.....	48
Figure 2.32: Results of MRI based CFD nasal model. (A) Average heat flux distribution. (B) Average water flux distribution.....	49
Figure 3.1: Functional representation of the nasal airway.....	58
Figure 3.2: Nasal airway represented as series of co-axial tubes of varying hydraulic diameter.....	59
Figure 3.3: Block diagram of nasal air-conditioning model at time step $t$ .....	60
Figure 3.4: Condensed pictorial representation of model computational strategy.....	62
Figure 3.5: Schematic representation of model storage for one data set.....	63
Figure 3.6 Schematic representation of one small nasal airway section $k$ at a particular time interval $t$ .....	65

Figure 3.7	Adult at-rest single breath air mass-flow.....	70
Figure 3.8:	Symbolic representation of nasal series/parallel resistance network.....	71
Figure 3.9:	Flow diagram of nasal air-conditioning model for segment $k$ at time step $t$ .....	78
Figure 3.10:	Schematic representation of ASL water equivalent height of 10 $\mu\text{m}$ representing the hydration difference between normal and severely dehydrated ASL.....	79
Figure 4.1:	Participant wearing CPAP nasal mask in recumbent position within MRI scanner with head coil fitted.....	84
Figure 4.2:	MRI images showing region of interest spanning the anterior nasal valve to the posterior choanae.....	85
Figure 4.3:	An example of a MRI coronal head image demonstrating the presence of the nasal cycle with patent right airway and congested left airway.....	86
Figure 4.4:	Enlarged MRI coronal nasal image demonstrating the manual segmentation of airway boundaries.....	87
Figure 4.5:	Axial ASL head image demonstrating high cerebral blood flow in brain and congested nasal turbinate by colour intensity.....	88
Figure 4.6:	Arterial spin labelling perfusion image. (A) Ambient breathing. (B) n-PAP 6 cm $\text{H}_2\text{O}$ breathing.....	89
Figure 4.7:	Mid airway ( $X/L=0.5$ ) combined patent and congested airway cross-sectional area at different pressures.....	91
Figure 4.8:	Mid airway ( $X/L=0.5$ ) combined patent and congested airway perimeter at different pressures.....	92
Figure 4.9:	Mid airway ( $X/L=0.5$ ) combined patent and congested airway hydraulic diameter at different pressures.....	92
Figure 4.10:	Total surface area over the region of interest of the combined patent and congested airway hydraulic diameter at different pressures.....	93
Figure 4.11:	Mean cross-sectional area distribution along patent and congested airways at ambient pressure.....	95
Figure 4.12:	Mean perimeter distribution along patent and congested airways at ambient pressure.....	96
Figure 4.13:	Mean hydraulic diameter distribution along patent and congested airways at ambient pressure.....	97
Figure 4.14:	Change in cross-sectional area per unit pressure along patent and congested airways.....	99
Figure 4.15:	Change in perimeter per unit pressure along patent and congested airways.....	100
Figure 4.16:	Change in hydraulic diameter per unit pressure along patent and congested airways.....	101

Figure 4.17: Participant specific accumulated volume change in both patent and congested airways.....	104
Figure 5.1: Intact ASL layer within bovine trachea.....	111
Figure 5.2: Whole trachea immersed in PSS within tissue bath.....	112
Figure 5.3: Schematic representation of apparatus set up within the incubator..	113
Figure 5.4: Schematic of airflow apparatus set-up demonstrating inhalation breath phase and negative pressure distribution along trachea.....	115
Figure 5.5: Schematic of airflow apparatus set-up demonstrating exhalation breath phase and positive pressure distribution along trachea.....	116
Figure 5.6: Schematic of desiccant chamber glass sphere containing silica gel filled bag supported by cantilever strain gauge.....	116
Figure 5.7: Image of glass chamber with cantilever gauge holding desiccant bag.....	117
Figure 5.8: Schematic of air temperature/humidity sensor within slave bellows assembly.....	117
Figure 5.9: Apparatus set up within the incubator.....	118
Figure 5.10: Schematic of desiccant water mass and air temperature/humidity data streams.....	119
Figure 5.11: Desiccant and air absolute humidity during 7 hour test.....	120
Figure 5.12: Mucosal water flux during 7 hour test.....	121
Figure 5.13: Trachea maximal water flux during ambient and augmented pressure.....	121
Figure 5.14: Variation in saturation water vapour concentration over range of pressure augmentation at 37°C.....	124
Figure 6.1: Temporal slices of breath cycle used for inspiration and expiration model results.....	129
Figure 6.2: Inhalation inter-airway temperature ( $T_a$ ), absolute humidity ( $AH$ ), molar water flux ( $N$ ), heat flux ( $Q$ ) and ASL water equivalent height ( $H_{e,ASL}$ ) distribution from rest to maximal change. Mask pressure ambient, $AH=9.2\text{g H}_2\text{O/m}^3$ dry air ( $T=23^\circ\text{C}$ , $RH=45\%$ )...	131
Figure 6.3: Exhalation inter-airway temperature ( $T_a$ ), absolute humidity ( $AH$ ), molar water flux ( $N$ ), heat flux ( $Q$ ) and ASL water equivalent height ( $H_{e,ASL}$ ) distribution from maximal inhalation to maximal exhalation. Mask pressure ambient, $AH=9.2\text{g H}_2\text{O/m}^3$ dry air ( $T=23^\circ\text{C}$ , $RH=45\%$ ).....	132
Figure 6.4: Inter-airway air mass-flow partitioning ratio over range of pressure augmentation.....	133
Figure 6.5: Inhalation inter-airway temperature ( $T_a$ ), absolute humidity ( $AH$ ), molar water flux ( $N$ ), heat flux ( $Q$ ) and ASL water equivalent height ( $H_{e,ASL}$ ) distribution from rest to maximal change. Mask pressure 9 cm $\text{H}_2\text{O}$ , $AH=9.2\text{g H}_2\text{O/m}^3$ dry air ( $T=23^\circ\text{C}$ , $RH=45\%$ ).....	135
Figure 6.6: Inter-nasal hydraulic diameter distribution.....	136

Figure 6.7:	Exhalation inter-airway temperature ( $T_a$ ), absolute humidity ( $AH$ ), molar water flux ( $N$ ), heat flux ( $Q$ ) and ASL water equivalent height ( $H_{e,ASL}$ ) distribution from maximal inhalation to maximal exhalation. Mask pressure 9 cmH <sub>2</sub> O, $AH=9.2\text{g H}_2\text{O/m}^3$ dry air ( $T=23^\circ\text{C}$ , $RH=45\%$ ).....	136
Figure 6.8:	Inter-airway ASL dehydration time distribution for range of pressure augmentation.....	138
Figure 6.9:	Inhalation inter-airway temperature ( $T_a$ ), absolute humidity ( $AH$ ), molar water flux ( $N$ ), heat flux ( $Q$ ) and ASL water equivalent height ( $H_{e,ASL}$ ) distribution from rest to maximal change. Mask pressurise 9 cm H <sub>2</sub> O, $AH=31\text{gH}_2\text{O/m}^3$ dry air. ( $T=30^\circ\text{C}$ , $RH=100\%$ ).....	140
Figure 6.10:	Exhalation inter-airway temperature ( $T_a$ ), absolute humidity ( $AH$ ), molar water flux ( $N$ ), heat flux ( $Q$ ) and ASL water equivalent height ( $H_{e,ASL}$ ) distribution from maximal inhalation to maximal exhalation. Mask pressurise 9 cm H <sub>2</sub> O, $AH=31\text{gH}_2\text{O/m}^3$ dry air. ( $T=30^\circ\text{C}$ , $RH=100\%$ ).....	141
Figure 6.11:	Inhalation inter-airway temperature ( $T_a$ ), absolute humidity ( $AH$ ), molar water flux ( $N$ ), heat flux ( $Q$ ) and ASL water equivalent height ( $H_{e,ASL}$ ) distribution from rest to maximal change. Mask pressurise 9 cm H <sub>2</sub> O, $AH=16.4\text{ gH}_2\text{O/m}^3$ dry air. ( $T=24^\circ\text{C}$ , $RH=75\%$ ).....	143
Figure 6.12:	Exhalation inter-airway temperature ( $T_a$ ), absolute humidity ( $AH$ ), molar water flux ( $N$ ), heat flux ( $Q$ ) and ASL water equivalent height ( $H_{e,ASL}$ ) distribution from maximal inhalation to maximal exhalation. Mask pressurise 9 cm H <sub>2</sub> O, $AH=16.4\text{ gH}_2\text{O/m}^3$ dry air ( $T=24^\circ\text{C}$ , $RH=75\%$ ).....	144
Figure 7.1:	Inter-airway temperature ( $T_a$ ), absolute humidity ( $AH$ ), molar water flux ( $N$ ), heat flux ( $Q$ ) and ASL water equivalent height ( $H_{e,ASL}$ ) distribution from rest to peak inhalation flow. Mask pressure 9 cmH <sub>2</sub> O, $AH=9.2\text{g H}_2\text{O/m}^3$ dry air ( $T=23^\circ\text{C}$ , $RH=45\%$ ). ..	150
Figure 7.2:	Inter-airway ASL dehydration time distribution for range of pressure augmentation.....	151
Figure 8.1:	Change in inter-airway specific air mass-flow resistance over range of pressure augmentation to sustain ASL hydration within left (forced congested) airway.....	158
Figure 8.2:	Inter-airway air mass-flow partitioning ratio over range of pressure augmentation to sustain ASL hydration within left (forced congested) airway.....	159
Figure 8.3:	Inhalation inter-airway temperature ( $T_a$ ), absolute humidity ( $AH$ ), molar water flux ( $N$ ), heat flux ( $Q$ ) and ASL water equivalent height ( $H_{e,ASL}$ ) distribution from rest to maximal change. Mask pressure 9 cmH <sub>2</sub> O, $AH=9.2\text{g H}_2\text{O/m}^3$ dry air ( $T=23^\circ\text{C}$ , $RH=45\%$ ). ..	161
Figure 8.4:	Exhalation inter-airway temperature ( $T_a$ ), absolute humidity ( $AH$ ), molar water flux ( $N$ ), heat flux ( $Q$ ) and ASL water equivalent height ( $H_{e,ASL}$ ) distribution. From maximal inhalation to maximal exhalation. Mask pressure 9 cmH <sub>2</sub> O, $AH=9.2\text{g H}_2\text{O/m}^3$ dry air....	162

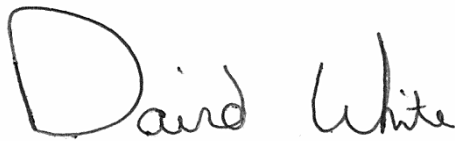
Figure 8.5: Inter-airway ASL dehydration time distribution for range of pressure augmentation.....	163
----------------------------------------------------------------------------------------------------	-----

## List of Tables

Table 2.1: Nasal surface area and volume data obtained from four individuals.	18
Table 2.2: Human cadaver nasal hydraulic diameter data.....	19
Table 2.3: Intra-nasal distribution of air temperature and humidity during quiet breathing at room temperature ( $T=25^{\circ}\text{C}$ , $RH=35\%$ ). (A) Inspiration, (B) expiration.....	36
Table 2.4: Inter-nasal increase in air temperature and humidity during quiet breathing at room temperature ( $T=22^{\circ}\text{C}$ , $RH=35\%$ ). (A) Relative humidity, (B) Temperature.....	37
Table 4.1: Change in inferior turbinate blood volume in response to n-PAP breathing.....	107
Table 6.1: Listing of figures for results during various breathing conditions...	130

### **Attestation of Authorship**

I hereby declare that this submission is my own work and that, to the best of my knowledge and belief, it contains no material previously published or written by another person (except where explicitly defined in the acknowledgements), nor material which to a substantial extent has been submitted for the award of another degree or diploma of a university or other institution of higher learning.

A handwritten signature in black ink that reads "David White". The "D" is large and loops around the "a", and the "White" is written in a cursive style.

.....  
David Edward White

## Publication List

The list of peer reviewed publications made during the course of this investigation is given below:

White, D.E., Al-Jumaily, A.M., Bartley, J and Lu, J., *Correlation of nasal morphology to air-conditioning and clearance function*. Respiratory Physiology & Neurobiology, 2011. **179**, p. 137-141.

White, D.E., Al-Jumaily, A.M., Bartley, J. and Somervell, A., *Nasal air-conditioning during breathing therapy*. Current Respiratory Medicine Reviews, 2011. **7**: p. 213-225.

White, D.E, Al-Jumaily, A.M., Bartley, J. and Lu, J., *Effects of augmented air-pressure on the nasal erectile tissue and blood flow during breathing therapies*. International Mechanical Engineering Conference and Exposition (IMECE) 2011, Denver, Colorado, USA, 13 Nov 2011 -17 Nov 2011.

White, D.E, Al-Jumaily, A.M., Bartley, J. and Hankin, R.K.S., *Nasal morphology and blood flows during augmented air-pressure therapies*. Medical Sciences Congress, 2011, Queenstown, New Zealand, 29 – 31 Aug 2011.

White, D.E, Al-Jumaily, A.M. and Bartley, J., *Nasal air-conditioning during n-PAP therapy*. Medical Sciences Congress, 2011, Queenstown, New Zealand, 9 Dec 2010.

## **Acknowledgements**

It also would not have been possible to complete this work without the support, guidance and sage advice from my supervision team. First and foremost is Dr Jim Bartley who has mentored, inspired and guided me throughout this journey. My sincere gratitude goes to Dr Roy Nates for his technical assistance, assiduous critique and unconditional support. My thanks also go to Associate Professor David I. Wilson for his guidance and support, and to Professor Ahmed Al-Jumaily for motivating me to undertake further study and for his critique of journal papers.

My sincere gratitude goes to Dr Robin Hankin for his statistical assistance, and Associate Professor Brett Cowan, Dr Beau Pontr  and Anna-Maria Lydon, from the Centre of Advance MRI (CAMRI), for guidance with MRI protocol. I wish to acknowledge the support and advice given by my work colleagues Mike Protheroe and Dr Jun Lu, and fellow student Miguel Jo Avila.

Special thanks go to Ivan Batistich of Ivent Research Ltd. for providing ventilator hardware and device advice, and to AUT support staff, Ross Reichardt, Stephen Hartley and Mark Masterton. I would like to thank Professor Steve Henry for providing tissue experimental facilities within Kode Biotech laboratories.

I would like to thank AUT for awarding me a Vice Chancellor's Research Scholarship to assist completion of this work, and the School of Engineering for supporting me throughout this journey.

Approval for a human MRI clinical trial was applied for on behalf of Professor Ahmed Al-Jumaily to the Auckland University of Technology Ethics Committee (AUTEC) and granted under ethics application number 10/121, dated 14<sup>th</sup> July 2010.

## **Intellectual Property Rights**

All original material contained within this thesis pertaining to predicting nasal drying during ambient and pressurised breathing along with the alternative treatment to supplementary humidification belong to David White.

## **Confidential Material**

This thesis contains confidential material that if publically available may jeopardise the future intellectual property rights of the author for patent application or publication.

## Deposit of Thesis in the AUT Library (PGR16)



### FORM PGR15 DEPOSIT OF THESIS/EXEGESIS/DISSERTATION IN THE AUT LIBRARY

**PLEASE NOTE**

- This form must be typed. Handwritten forms will not be accepted.
- The completed and signed form should be bound into the copy of the thesis/exegesis intended for the AUT University Library, i.e. the copy which is printed on acid-free paper.
- If the work is to be treated as confidential or is embargoed for a specified time, form PGR16 must also be completed and bound into the thesis/exegesis.

Student ID No	9012226	Name	David White
Faculty	Design and Creative Technologies	School/Dept	Engineering
Programme	AK3518	Year of submission (for examination)	2013
Research Output	Thesis <input checked="" type="checkbox"/> Exegesis <input type="checkbox"/> Dissertation <input type="checkbox"/>	Points Value	360
Thesis Title	Nasal Drying During Pressurised Breathing		

### DECLARATION

I hereby deposit a print and digital copy of my thesis/exegesis with the Auckland University of Technology Library. I confirm that any changes required by the examiners have been carried out to the satisfaction of my primary supervisor and that the content of the digital copy corresponds exactly to the content of the print copy in its entirety.

This thesis/exegesis is my own work and, to the best of my knowledge and belief, it contains:

- no material previously published or written by another person (except where explicitly defined in the acknowledgements);
- no material which to a substantial extent has been submitted for the award of any other degree or diploma of a university or other institution of higher learning.

### CONDITIONS OF USE

From the date of deposit of this thesis/exegesis or the cessation of any approved access restrictions, the conditions of use are as follows:

1. This thesis/exegesis may be consulted for the purposes of private study or research provided that:
  - (i) appropriate acknowledgement is made of its use;
  - (ii) my permission is obtained before any material contained in it is published.
2. The digital copy may be made available via the Internet by the AUT University Library in downloadable, read-only format with unrestricted access, in the interests of open access to research information.
3. In accordance with Section 56 of the Copyright Act 1994, the AUT University Library may make a copy of this thesis/exegesis for supply to the collection of another prescribed library on request from that library.

### THIRD PARTY COPYRIGHT STATEMENT

I have either used no substantial portions of third party copyright material, including charts, diagrams, graphs, photographs or maps, in my thesis/exegesis or I have obtained permission for such material to be made accessible worldwide via the Internet. If permission has not been obtained, I have asked/will ask the Library to remove the third party copyright material from the digital copy.

Student's Signature

David White

Date

05/11/13

# Application for Restricted Access to a Thesis (PGR16)



## FORM PGR16 APPLICATION FOR RESTRICTED ACCESS TO A THESIS/DISSERTATION/EXEGESIS

**PLEASE NOTE**

- This form must be typed. Handwritten forms will not be accepted.
- Double clicking on the check boxes enables you to change them from not-checked to checked.
- The completed form, signed by the student and the primary supervisor, should be submitted to the appropriate Faculty Postgraduate Office when the thesis/exegesis is lodged for examination. If the application is approved by the Faculty Postgraduate Committee, the form will be signed by the Dean and sent to the University Postgraduate Centre for insertion into the print copies deposited. For more information consult the Postgraduate Handbook.

<b>Student ID No</b>	9012226	<b>Name</b>	David Edward White
<b>Faculty</b>	Design and Creative Technologies	<b>School/Dept</b>	Engineering
<b>Programme</b>	Doctor of Philosophy	<b>Date of submission for examination</b>	5 <sup>th</sup> April 2013
<b>Research Output</b>	<b>Thesis</b> <input checked="" type="checkbox"/> <b>Dissertation</b> <input type="checkbox"/> <b>Exegesis</b> <input type="checkbox"/>	<b>Points Value</b>	360
<b>Thesis Title</b>	Nasal Drying During Pressurised Breathing		

### EMBARGO TIMEFRAME

An embargo is requested on the public availability of the print and digital copies of the above thesis/exegesis from the date of submission for examination (maximum normally 36).

36 months

### EMBARGO CATEGORIES

The thesis/dissertation/exegesis contains confidential or sensitive information which if publicly available may (Tick all that apply)

- ☒ Jeopardise the future intellectual property rights of the author (e.g. a patent application or publication)
- ☐ Breach a prior contractual arrangement with an external organisation
- ☐ Infringe or endanger the right to privacy or cultural respect of an individual or group

### The embargo would apply to

- ☒ The complete thesis/dissertation/exegesis
- ☐ A portion of the work (specify) :

### SIGNATURES

<b>Student</b>		<b>Date</b>	26/03/13
<b>Primary Supervisor</b>	A/P David I Wilson	<b>Date</b>	26 March 2013
<b>Secondary Supervisor</b>		<b>Date</b>	1/4/13
<b>Additional Supervisor</b>		<b>Date</b>	3/4/2013

### RESTRICTED ACCESS APPROVED BY FACULTY DEAN(or delegate)

<b>Signature</b>	<b>Date</b>
------------------	-------------

<b>OFFICE USE</b>	<b>RELEASE</b>
<b>DATE</b>	

## CHAPTER 1

### INTRODUCTION

#### 1.1 Background

In many therapeutic situations gases are delivered under positive pressure to a spontaneously breathing patient. The nose has an important role heating and humidifying inhaled air [1-3], so breathing dry gases through a nasal mask presents an obvious and significant air-conditioning challenge. In this situation, heated or non-heated pass-over type supplementary humidifiers are commonly used to condition inhaled gas to near full water saturation at core body temperature to assist the nose with air-conditioning duties [4-6]. Other forms of breathing therapy, such as nasal positive airway pressure (n-PAP) treatment for obstructive sleep apnea (OSA), utilize pressurised ambient air, but may also require similar supplementary heating and humidification. When breathing air at positive pressures, the nose suffers some form of air-conditioning dysfunction. Symptoms of nasal drying have been attributed to unidirectional air-flow caused by mouth leaks [7-9] but changes in nasal geometry also seems to play a role [10]. Although the benefits of supplementary humidification have been well investigated [4-6, 11-15], the cause(s) of symptoms suggesting nasal airway drying has received little attention. Only one investigation into the effect n-PAP breathing had on nasal air-conditioning could be found in the current literature [16]. Although the functional purposes of the nose are well understood, there is a lack of analytical investigation into how n-PAP breathing influences nasal physiology. Presently the cause(s) of the negative side-effects frequently reported during n-PAP therapy for OSA [13, 14, 17-21] are unknown. Additionally, the current practice of providing supplementary humidification to relieve these symptoms does not seem to improve therapy adherence [13, 15, 21].

#### 1.2 Obstructive Sleep Apnea

Sleep apnea, a disorder characterized by repetitive interruption to spontaneous breathing during sleep, derives its name from the Greek word apnea meaning ‘want of breath’ [22]. This syndrome is defined as complete cessation of breathing airflow lasting at least 10 seconds, whereas a significant reduction (greater than 30%) in airflow is defined as a hypopnea event [23]. There are three types of sleep apnea:

1. Central, where the brain fails to send signals to breathing muscles to initiate breathing (not considered within this study).
2. Obstructive, where collapse of soft tissue structures in the oropharynx or hypopharynx block the air passage (Figure 1.1).
3. Mixed, where a combination of obstructive and central sleep apnea occurs.

The main cause of OSA is thought to be relaxation of the muscles controlling the tone of soft tissue within the oropharynx or hypopharynx during deep sleep [24-26]. Structural abnormalities, such as enlarged tonsils, soft palate abnormalities, large tongue, receding chin and obesity [22, 27, 28], which may cause airway narrowing, can also be contributory.

During sleep the upper airway relaxes (Figure 1.1); closure within this region is thought to occur as a result of the drop in airway internal air-pressure during inhalation [29, 30]. During recumbent sleep, body position can also contribute with gravity also acting to close flaccid soft-tissue airway structures [31]. Forced pauses in breathing, typically, accompanied by snoring, cause a reduction in blood oxygen ( $O_2$ ) and increased carbon dioxide ( $CO_2$ ) levels that trigger an alert in the brain to urgently commence breathing [23]. Continual interruption to the normal deep sleep pattern causes excessive daytime sleepiness and many adverse clinical symptoms including change in personality, depression, irritability, cognitive impairment and reduced libido [32]. OSA sufferers commonly experience excessive daytime sleepiness, snoring, impaired alertness and reduction in cognitive function. OSA can lead to hypertension, ischemic heart disease, myocardial infarction, stroke and premature death [33]. Sufferers are over three times as likely to suffer a motor vehicle accident when compared to the general population [34].

During the year 2000, Sassani *et al.* found that, in the United States, 800,000 vehicle collisions costing US\$15.9 billion and 1,400 lives could be directly attributed to OSA [35]. Sufferers of OSA are also at increased risk of experiencing home or workplace accidents [34]. Although regional variation is likely, in developed countries it is thought that OSA affects between 4% to 6% of the adult population [14, 33], whilst up to 25% display symptoms and risk factors associated with OSA [32, 36, 37]. There is a strong association between OSA and other health conditions such as obesity, cardio-pulmonary arrest, hypertension and arrhythmia as well as congestive heart failure, stroke and type-2 diabetes [23, 32, 38].

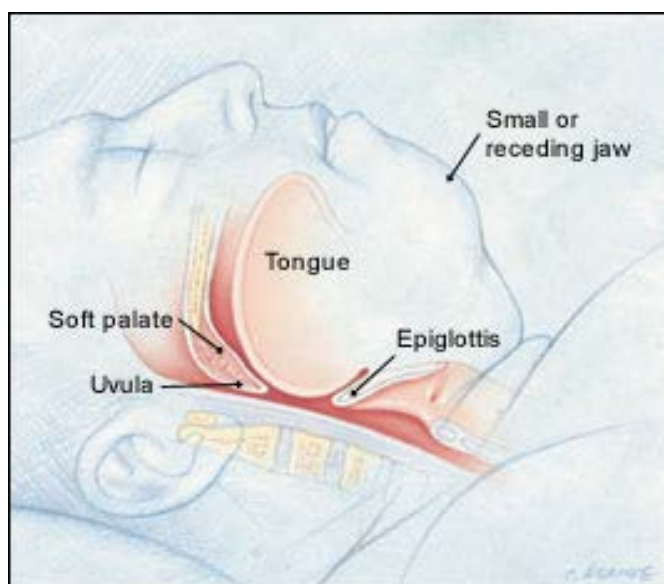


**Figure 1.1: Upper airway closure within oropharynx or hypopharynx. Diagram adapted from [39]**

Recent studies in developing countries have found the adult population is also following a similar trend with increasing levels of OSA being detected [36]. OSA would appear extensive and detrimental OSA within many societies throughout the world.

### **1.3 Positive Air Pressure Therapy**

Treatments for OSA range from tongue and mandibular advancement devices through to invasive surgical intervention; the use of positive airway pressure (PAP) devices is the clinical gold standard because of its low risk, efficacy and relative ease of use [12, 17, 40]. Air pressure, set to a level known as the titration pressure, effectively provides a pneumatic splint, preventing the soft tissue from collapsing thus maintaining airway patency through the oropharynx and hypopharynx (Figure 1.1) during sleep [17, 28, 37]. The degree of pressure required to prevent airway collapse varies between individuals, however clinical guidelines recommend a minimum starting titration pressure of 4 cm H<sub>2</sub>O and a maximum air-pressure of 20 cm H<sub>2</sub>O [41]. Determination of the titration pressure is commonly undertaken within a sleep clinic using a technique called polysomnography - a sleep study methodology where brain function, eye movements, muscle activity and heart rhythm are monitored during the sleep period [22, 23, 37]. Here, titration pressure setting is based on the apnea-hypopnea index

(AHI) [17] or the respiratory disturbance index (RDI) [23] that ranks the number of apnea-hypopnea events per hour against a severity criteria.

There are three common types of PAP therapies used to treat OSA [17, 22]:

1. Continuous positive air-pressure (CPAP) that provides air at a continuous pressure to the spontaneously breathing patient.
2. Bi-level positive air-pressure (Bi-PAP) that switches to a lower air-pressure during exhalation to reduce the effort of breathing due to reduced back-pressure.
3. Auto-titrating positive air-pressure (APAP) that senses the onset or absence of an apnea event and adjusts the air-pressure accordingly.

The choice of PAP therapy is dependent upon many factors including cost and patient comfort. CPAP devices, like the one shown in Figure 1.2, are usually cheaper. The more expensive APAP devices offer (in theory) a lower mean titration pressure since they can account for changes in body position, improving patient comfort and the advantage of compensating for mask leaks [37].

In addition to the range of air-pressure devices, three different types of mask interfaces are commonly used to supply air-pressure to the patient's airways during PAP therapy. These include the nasal mask, the combined nose and mouth mask and the full face mask. Choice of mask interface often depends upon patient preferences and morphological constraints, such as facial geometry or the presence of facial hair.



**Figure 1.2: Patient receiving n-PAP therapy. Picture adapted from [42].**

However, the nasal mask (n-PAP) is the option most preferred for overall comfort and reduced air leaks [43]. This is not surprising given that the nose represents the preferred entry point for air entering the respiratory system [44-47], and serves an important role in maintaining airway health by entrapping inhaled pathogens and pollutants as well as heating and humidifying inhaled air [48, 49]. The mouth on the other hand cannot effectively provide either of these two functions.

Face masks are used when a patient prefers to breathe through both their nose and mouth, but this can lead to airway drying since the nose normally provides about 90% of respiratory system air-conditioning requirements [50, 51]. This type of mask is used in situations when a patient experiences air leakage from the other types of masks, but users frequently report increased claustrophobia when using this form of PAP therapy interface [43].

### **1.3.1 Pressure Related Symptoms**

The nose normally copes with its air-conditioning duties over a wide temperature and humidity range at ambient pressure [45, 52]. However, at elevated pressures, nasal complications have been reported by up to 65% of n-PAP users [10, 13]. The most prevalent side-effects include nasal dryness, crusting, congestion, sneezing, rhinorrhea and/or itching [14, 17-21, 53], however in some extreme cases epistaxis has been reported [10, 18, 19, 21, 53]. These symptoms suggest that the nasal airway experiences mucosal drying [5-7, 10, 15, 17, 54-57]. Whilst these adverse side-effects can be managed through the use of intranasal corticosteroids, antihistamines or anticholinergic sprays, supplementary humidification is more commonly utilized to treat these symptoms and improve patient comfort [10, 12, 17]. Expense and additional side-effects from the long term use of pharmaceutical treatments may be a factor in this choice.

### **1.3.2 Supplementary Humidification**

Supplementary humidification within the PAP breathing system augments the water vapour content of the inhaled air, resulting in the nasal airway experiencing less water loss, whilst conducting its air-conditioning function.



**Figure 1.3: Typical supplementary PAP heated humidifier. Picture from [58].**

Apart from the obvious benefit in alleviating airway dryness and maintaining mucus clearance in patients receiving n-PAP therapies [4, 5, 14, 15, 21, 55], previous studies have also demonstrated the benefits heated humidification has in patients suffering from xerostomia [59] and bronchiectasis [60]. Supplementary heated humidification, which is thought to rehydrate the airway mucosa, benefit patients experiencing oral dryness and poor mucus clearance.

Two types of supplementary humidification are commonly used in n-PAP systems; heated and non-heated. Non-heated, also known as pass-over, humidifiers have air passing over ambient temperature water before entering the mask interface. Heated humidifiers, as shown in Figure 1.3, use the same air circuit, but provide additional water vapour to the air since the heated water raises the equilibrium water vapour pressure causing greater water flux to occur.

### **1.3.3 Treatment Adherence**

The successful treatment of OSA by n-PAP requires adherence to the therapy to enable the therapeutic benefits to be received by the patient. Significantly, some studies into n-PAP therapy adherence have found that by choice, around 75% of patients use this therapy for less than 4 hours per night [17, 61] and around 50% discontinue long-term n-PAP use completely [15]. Despite its popularity in relieving negative symptoms

associated with airway drying, the ability of supplementary humidification to improve adherence to n-PAP treatment is questionable given no improvement occurs when supplementary humidification is introduced [13, 15, 21]. These findings suggest that the cause of patient dissatisfaction with n-PAP therapy might be more complex than simply a case of mucosal drying. They also strongly imply that supplementary humidification is not the panacea for the relief of airway drying symptoms commonly experienced during n-PAP therapy. Any improvement in n-PAP therapy adherence first requires a comprehensive understanding of the causes of airway drying before any advances in symptom relief can occur.

#### **1.4 Causes of Nasal Drying**

Despite extensive studies being undertaken into the symptoms arising from n-PAP treatment and patient compliance, the causes of nasal airway drying have received little attention [16] and are poorly, if at all, understood [10]. The suggestion that mouth leaks cause drying of the nasal mucosa has been proposed [15]. Unidirectional air-flow may be a factor; however symptoms of airway drying still occur when this leak is absent. Nasal drying as a consequence of abnormally large airflows passing through the nose has also been suggested [16], however this seems unlikely given the patient is breathing approximately the same tidal volume during either ambient or n-PAP conditions. A logical and complete explanation as to the causes of nasal mucosal drying has yet to be presented.

#### **1.5 Contributions of this Thesis**

This work will contribute the following to the body of knowledge in this field:

1. A new nasal air-conditioning model to predict change in nasal air mass-flow partitioning between airways and nasal mucosal drying using subject specific morphology.
2. The mechanism and explanation that the symptoms of airway drying are caused by reduced mucosal water supply and change in inter-nasal air mass-flow partitioning.
3. During ambient air breathing, severe airway surface liquid (ASL) dehydration occurs only within the patent nasal airway and the implications of this, in terms

of mucociliary clearance and understanding the purpose of the nasal cycle, are significant.

4. During n-PAP breathing, both nasal airways experience severe ASL dehydration however supplementary humidification prevents this from occurring.
5. Relief from symptoms of nasal drying could be better achieved by regulating inter-nasal air mass-flow partitioning.

## **1.6 Closure**

The causes of apparent nasal drying during n-PAP therapy are currently unknown, although the use of supplementary humidification relieves these symptoms. However, the use of supplementary humidification does not improve the poor patient adherence to n-PAP therapy.

To understand nasal airway drying during n-PAP therapy the influence air pressure has on nasal geometry and mucosal water supply needs to be understood. Modelling of the inter-play between these and other nasal functions during n-PAP tidal breathing is essential to ascertain if this causes change in mucosal hydration levels. The next chapter will discuss nasal physiology and dysfunction associated with n-PAP breathing. Additionally, it will introduce the nasal air-conditioning models currently available and their ability to predict intra-nasal levels of mucosal hydration throughout the breathing cycle.

## CHAPTER 2

### LITERATURE SURVEY

#### 2.1 Introduction

Historically there has been little investigation undertaken into the causes of apparent nasal drying during n-PAP therapy. No investigations using models to simulate nasal pathophysiology during these conditions have previously been undertaken. Earlier models used to study nasal air-conditioning have focused on understanding functional morphology at ambient pressure and have assumed constant parameters of geometry and water supply. These do not represent the conditions found within the nose during n-PAP breathing, as it is already known nasal geometry varies.

Section 2.2 surveys human nasal physiology with regards to understood functions of air-conditioning and filtration. Nasal air-conditioning, anatomical features and pressure elicited change in geometry is then reviewed in more detail in Section 2.3. The ASL, its mucosal supply and pressure induced change are reviewed in Sections 2.4 and 2.5 respectively. Sections 2.6 and 2.7 discuss human tidal breathing and transducer issues when taking *in-vivo* nasal temperature and humidity measurements. Previous mathematical models for air-conditioning within the conducting airways along with their predicted heat and water mass transfer are reviewed in Section 2.8. A research hypothesis, based on the absence of information within the literature, is presented in Section 2.9 and the chapter concludes by detailing the research plan in Section 2.10.

#### 2.2 The Human Airways

According to function, the human airway can be divided into two main regions: the conducting airway (consisting of the nasal cavity, trachea and conducting bronchioles) and the respiratory airway (consisting of respiratory bronchioles and alveoli) where gas exchange occurs [62], as shown in Figure 2.1. In healthy humans, the nose presents the preferred entry point for air entering the conducting airways [44-47] and serves an important role in maintaining airway health by entrapping inhaled pathogens and pollutants as well as heating and humidifying inhaled air [48, 49]. During nasal breathing, the nose also serves to recover around 30% of exhaled heat and water [63] as well as provide a region for olfaction to occur [52].

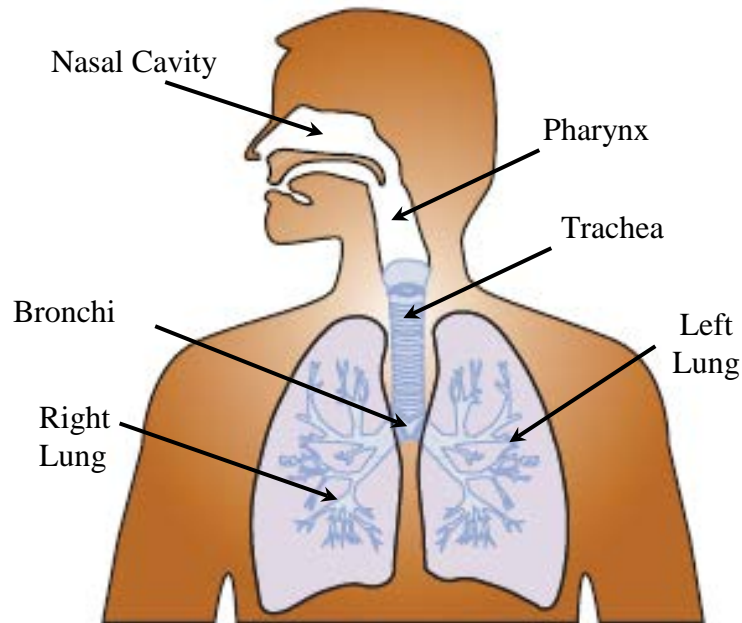


**Figure 2.1: Human airway. Diagram adapted from [62].**

The entire conducting airway is lined with ASL that not only provides the means of entrapment of inhaled pathogens but also is the medium through which heat and water must pass through from the underlying mucosa. This ASL layer provides a thermal and fluid storage buffer between the cyclic demand/ recovery of both heat and water from the inhaled/exhaled air and the mucosal supply. Given symptoms suggesting nasal drying occur during n-PAP breathing it is necessary to quantify both the instantaneous level of air-conditioning heat and water demand/recovery as well as mucosal heat and water supply to determine the change in ASL hydration status. Nasal air-conditioning, mucosal supply and ASL hydration are reviewed in the following sections.

### **2.3 Nasal Air-Conditioning**

The nasal cavity plays an important role in maintaining airway health by conditioning inhaled air to near full saturation at core body temperature to prevent drying of the lower airways [1, 2, 64]. This is achieved by the nose providing supplementary heat and water vapour to the inhaled air. Over a 24 hour rest period, healthy humans normally inhale around 10,000 litres of air which is typically supplemented with around 300 ml of water and 900 kJ of heat energy, when breathing ambient air at 25°C temperature and 50% relative humidity [52, 65]. During quiet breathing, *in vivo*

measurements across the nasal cavity show increased air temperature and humidity levels in an anterior to posterior direction during both inhalation and exhalation [52].

Conditioning of inhaled air is achieved through the combined action of anatomical features, which include complex and narrow internal geometry that regulate heat and water mass convective coefficients [52, 66-68] and vascular/cellular regulatory systems governing tissue heat and water supplies [69]. The conducting airway mucosa is lined with ASL, which provides and recovers both heat and water mass during the inhalation and exhalation breath phases respectively. A schematic representation of this cyclic inter-play occurring between anatomical features regulating the heat and water mass convective coefficients, as well as cellular water and vasculature supplies, is given in Figure 2.2. Because the ASL experiences these cyclic periods of demand and recovery, its hydration status fluctuates throughout the breath cycle.

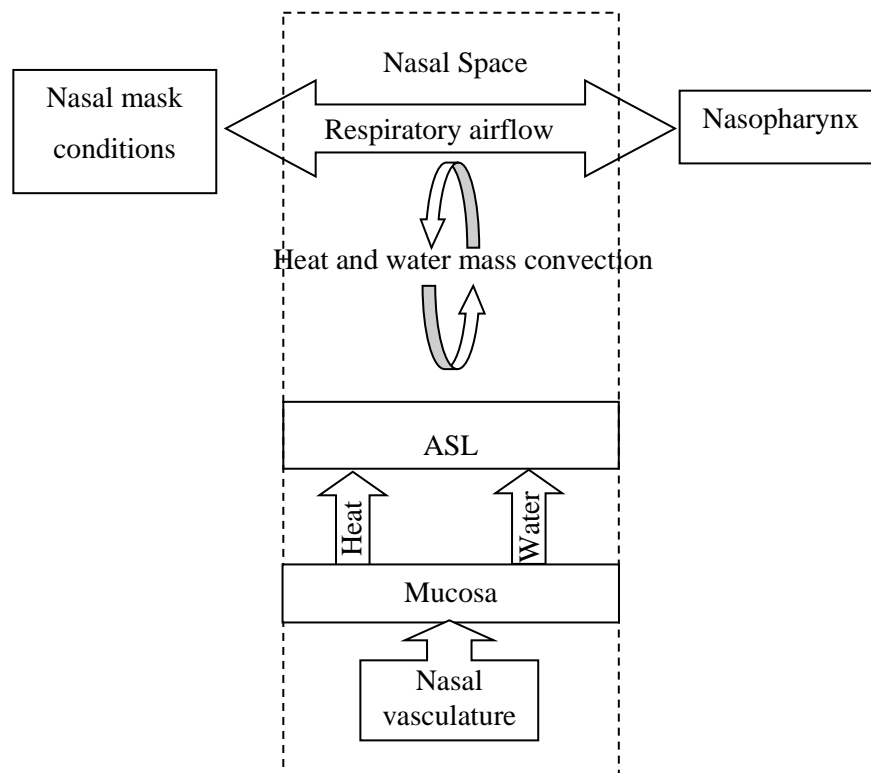


**Figure 2.2: Schematic representation of factors of air-conditioning heat and water demand and mucosal water supply which influence ASL hydration status [69].**

Although the nose provides about 90% of respiratory system air-conditioning requirements [50, 51], further humidification and heating of the inhaled air occurs as it travels through the pharynx and trachea. The ASL lining the conducting airway provides both heat and moisture until the air becomes fully saturated at core body temperature at a position termed as the isothermic saturation boundary (ISB) [70, 71]. The thermal and humidity gradient experienced by the inhaled/exhaled air fluctuates throughout the breathing cycle, causing the location of the ISB to continually move. Changes in ambient air temperature and humidity also cause changes in ISB location. Additionally, recovery of heat and water (discussed in the following section) serves to conserve cellular and vascular supplies [50, 63].

### 2.3.1 Anatomical Features

Previous analysis of nasal air-flow trajectories has identified three functional regions within the two enantiomorphic parts of the airways, enabling nasal morphology to be correlated to respiratory function [72]. Figure 2.3 presents a sagittal sectional view of the nasal cavity and identifies each of these regions:

1. The anterior tract, consisting of the vestibule, isthmus and anterior *cavum nasi*, which act as a curved nozzle-diffuser that stabilizes and redirects airflow across the turbinates.
2. The mid-functional *cavum nasi* tract, consisting of a slit-like space that presents a large mucosal surface area to the airflow.
3. The posterior tract, consisting of the posterior *cavum nasi*, choanae and epipharynx, which act as a curved nozzle to stabilize and redirect the airflow to the lower airways.

Laminar and turbulent airflow regime plays a significant role in heat and water mass transport within the nasal cavity. A reduction in nasal cross-sectional area causes an increase in convective coefficients due to an increase in air velocity. Within the nose, the nasal valve region provides a major dynamic portion of nasal airflow resistance. This region is thought to increase air velocity, which enhances heat and water mass transfer within this region [73, 74].

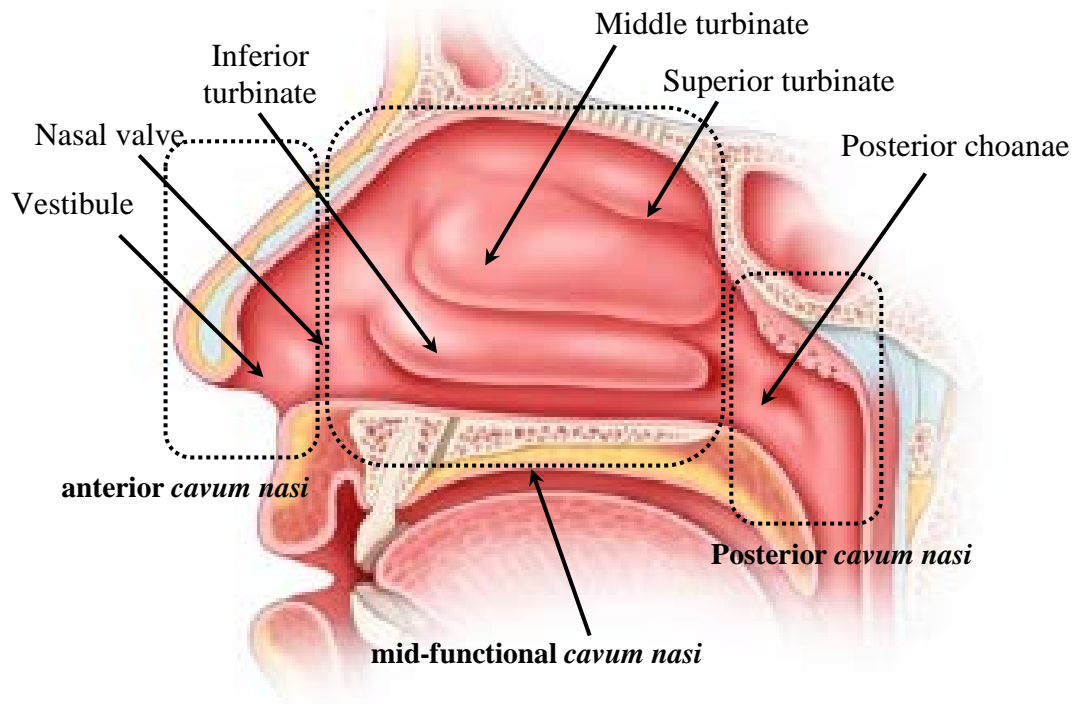


**Figure 2.3: Sagittal sectional view through nasal cavity demonstrating functional regions. Diagram adapted from [72].**

The widening of the air passage posterior to the turbinates causes subsequent slowing of airflow, which enhances deposition of particulate matter to the sticky ASL layer lining the nasal cavity.

### 2.3.2 Active Control

Air-flow within each airway is regulated by blood engorgement of erectile tissue located throughout the nose. Apart from the need to supply oxygen and nutrients to the airway epithelium, it is postulated [75] that arterial blood in-flow within the nasal mucosa supplies the following:

1. Glands providing ASL.
2. Arteriovenous anastomoses (AVAs), thought to control body temperature and tissue water supply.
3. Subepithelial capillaries, which play a role opening intercellular junctions during periods of inflammation.

Drainage of blood from these three sources passes through venous erectile tissues which, when distended, creates a greater obstruction to air passing through the airway.

There are three possible situations that could change erectile tissue swelling, shown by Figure 2.4:

1. Contraction or relaxation of the smooth muscles layering the erectile tissue walls forcing change in blood volume within erectile tissue,
2. Enlargement of the AVAs as part of their temperature and water supply duty causing greater blood inflow to erectile tissue,
3. Contraction of the muscle in the throttle veins causing restriction in blood out-flow from erectile tissue.

In all cases the net result is erectile tissue experiencing periodic blood engorgement and swelling.

Erectile tissue is also located throughout the nasal cavity, including the opposing wall of the septum, and it is at the mid-functional *cavum nasi* region that the inferior, middle and superior turbinates provide the greatest obstruction to airflow. Each turbinate can expand both in width and length. The lower inferior turbinate to extend into and restrict air-flow through the anterior nasal valve region [74].

Within the anteroinferior region of the nasal septum, four arteries anastomose to form a vascular plexus called Kiesselbach's triangle which also contributes to the heating of inhaled air [76]. Around 90% to 95% of all epistaxis episodes occur within this region [76, 77]. The alternating cycle of airflow constriction created by distension of nasal erectile tissue that occurs between each of the airways is discussed in the following section.

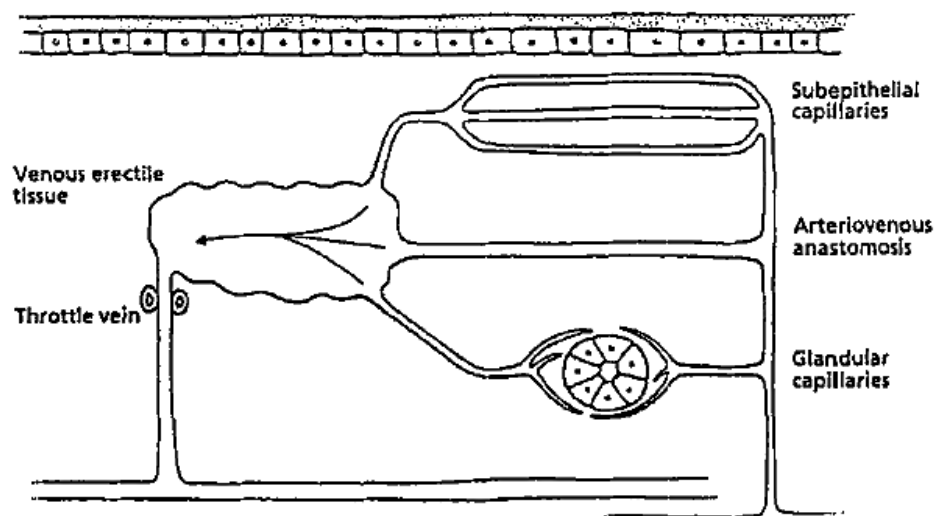


**Figure 2.4: Schematic representation of the nasal vasculature. Diagram from [75].**

### 2.3.3 Nasal Cycle

A proportion of the population, reported as ranging from 20 – 40 % [78-80] to over 80% [79, 81-83], experience periodic congestion/decongestion of the erectile tissue in each side of the nose [83, 84]. Enlarged turbinates obstruct the air-flow through the nasal passage, which is termed 'congested', whilst the un-obstructed airway is termed 'patent'. This 'nasal cycle' results in alternating patent and congested passages within the two enantiomorphic parts of the airway for periods ranging from 1 to 7 hours [85]. The most apparent outcome of this cycle is that it serves to regulate the bias of air mass flow partitioning between that airways [79, 86]. The span of the nasal cycle is made up from combinations of discrete ultradian periods spanning 1-1½ hours [81] and usually go unnoticed since the total nasal airflow resistance remains unchanged [52, 87]. In humans, electroencephalography (EEG) has demonstrated an alternating dominance in cerebral hemispheric activity that correlates directly with the nasal cycle [79, 88, 89].

Figure 2.5 shows a coronal MRI scan demonstrating the alternating patent and congested airway states. Of particular note is the state of inferior and middle turbinate distension within the right (congested) airway. Also seen in this figure is the displaced septum leaning towards the right airway.

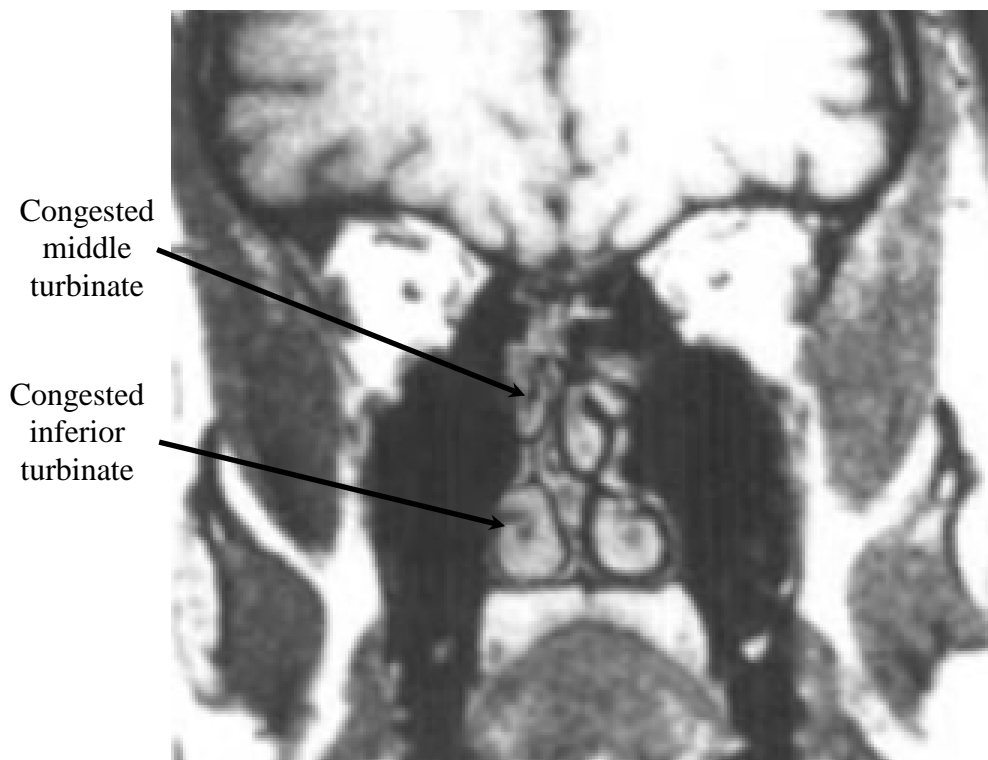


**Figure 2.5: MRI head coronal scan. Image adapted from [90].**

The purpose of the nasal cycle is not fully understood; however, it is thought to control the balance between heat and water fluxes from the ASL [45], as well as enable cells and glands on the congested side to rest and recharge [87]. No definitive work is found in the current literature that analyses or confirms these ideas and there is a need to better understand the purpose of this cycle.

#### **2.3.4 Air-Conditioning Morphology**

Modern imaging techniques such as computer tomography (CT) and MRI have enabled the capture of accurate *in-vivo* nasal geometric information which goes beyond that previously obtained by acoustic rhinometry (AR). Earlier investigations comparing CT and AR cross-sectional data demonstrated a good correlation within the relatively open anterior spaces of the nose [91, 92]. However, AR tends to underestimate cross-sectional area beyond the complex and sometimes obstructed turbinate region [93].

Previous studies correlating the efficacy of nasal air-conditioning to nasal morphology have considered parameters such as surface area to volume ratio in an attempt to assess the influence air velocity and surface area have on heat and water mass convective coefficients [94-96]. This serves well for comparative purposes for the complete nasal airway, but does not provide any detail to describe variation along the lengths of each geometrically complex nasal airway.

#### **2.3.5 Ambient Air-Pressure Measurements**

Within the current literature, investigations into nasal morphology under ambient air-pressure have usually been restricted to either one location or discrete positions along the whole airway. One such investigation into the ecogeographic variation in nasal morphology between forty European Americans (EA) and nine African Americans (AA) assessed the mid nasal region [94]. This area is located immediately posterior to the anterior end of the middle turbinate.

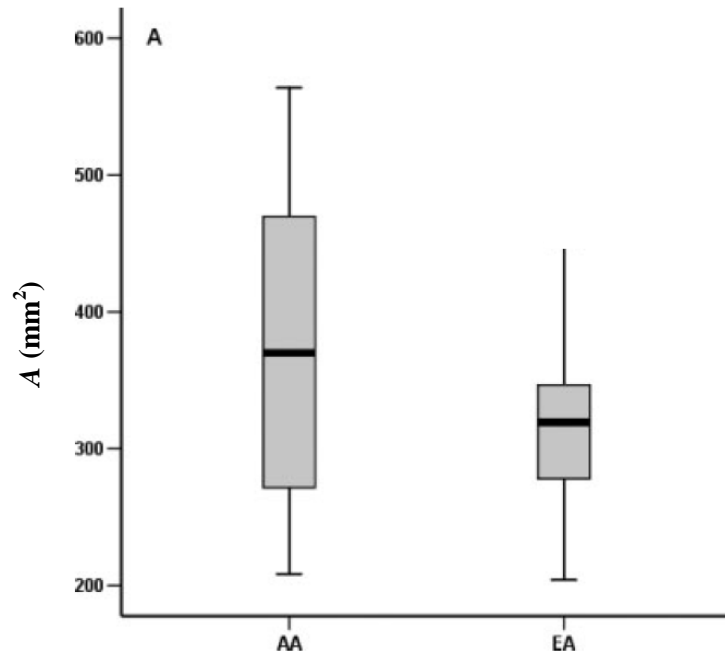


**Figure 2.6: Distribution of combined nasal airway cross-sectional area for African Americans (AA) and European Americans (EA). Graph from [94].**

Yokley *et al.* assessed nasal geometry of cross-sectional area ( $A$ ), perimeter ( $P$ ) and the ratio of  $P/A$ , shown in Figures 2.6, 2.7 and 2.8 respectively. It is noted that  $P/A$  is proportional to the ratio known as the hydraulic diameter ( $D_h$ ), which will be shown to be very relevant in the new work.

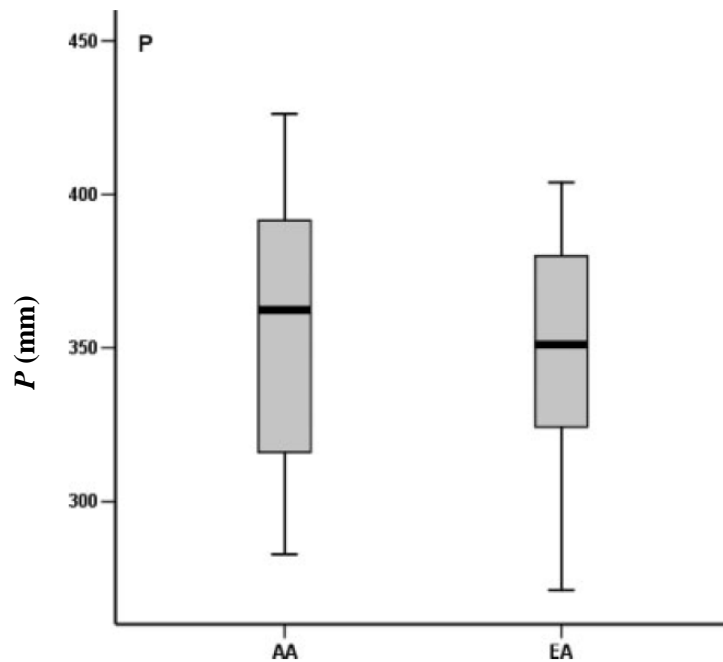


**Figure 2.7: Distribution of combined nasal airway perimeter for African Americans (AA) and European Americans (EA). Graph from [94].**

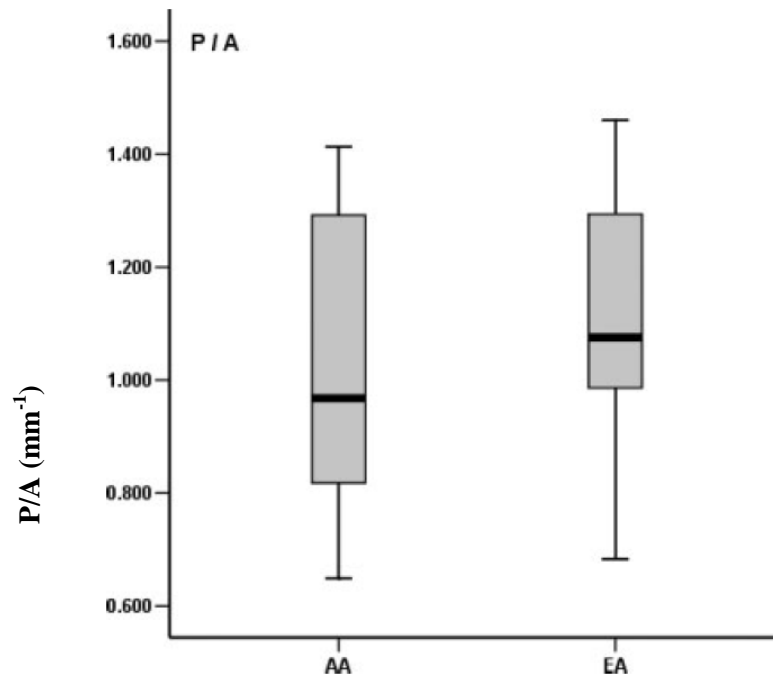


**Figure 2.8: Distribution of combined nasal airway perimeter for African Americans (AA) and European Americans (EA). Graph from [94].**

The justification for analysing the mid airway location was that Yokley *et al.* found a strong correlation coefficient (0.94) between mid-airway geometry and surface area to volume ratio, a more traditional measurement used for quantifying nasal geometry to air-conditioning efficacy. Figure 2.8 presents a ratio of airway  $P/A$ , there is a slight difference demonstrated between the average values of each ethnic group.

Another investigation into the effect nasal anatomy has on air-conditioning efficacy examined the surface area ( $SA$ ) to volume ( $V$ ) ratio of the whole nasal airway in four subjects (Table 2.1) [66].

**Table 2.1: Nasal surface area and volume data obtained from four individuals. Table from [66].**

Subject number	Sex	Height (cm)	Weight (kg)	Surface area (mm <sup>2</sup> )	Volume (mm <sup>3</sup> )	Nasal $SA/V$ (mm <sup>-1</sup> )
A	Male	173	73.0	18,363	17,126	1.07
12	Female	160.7	55.7	15,795	15,305	1.03
14	Male	186.1	74.0	20,714	21,957	0.94
18	Female	170.2	61.2	19,850	23,409	0.85

**Table 2.2: Human cadaver nasal hydraulic diameter data. Table from [97].**

COMP #	REGION	LENGTH	DIAMETER(EQ)
1	MOUTH	9.0	1.25-2.5
2	NASAL VESTIBULE	2.0	1.5
3	NASAL CAVITY	4.0	1.2
4	NASAL TURBINATES	4.0	.425-.880
5	PROXIMAL NASOPH.	1.4	2.0
6	DISTAL NASOPH.	1.9	1.2

Segal *et al.* used a combination of physical and computational fluid dynamics (CFD) modelling techniques to compare the influence nasal morphology has on nasal airflow distribution.

Both of these earlier investigations considered the combined geometry of the whole airway. Only two investigations can be found in the current literature that evaluates geometry at discrete locations along the nasal airway. The first, undertaken by Hanna, considered the geometry along the length of a conducting airway. Little attention was given to the nasal cavity leading to sparse data, Table 2.2, being recorded. Here hydraulic diameter is represented as DIAMETER(EQ), and is defined as the ratio of one quarter of the cross-sectional area divided by the perimeter.

The only *in-vivo* MRI nasal geometric data that can be found in the current literature from comes from an investigation undertaken by Craven *et al.* into canine olfaction [98]. The distribution of hydraulic diameter found by this investigation is presented in Figure 2.9.

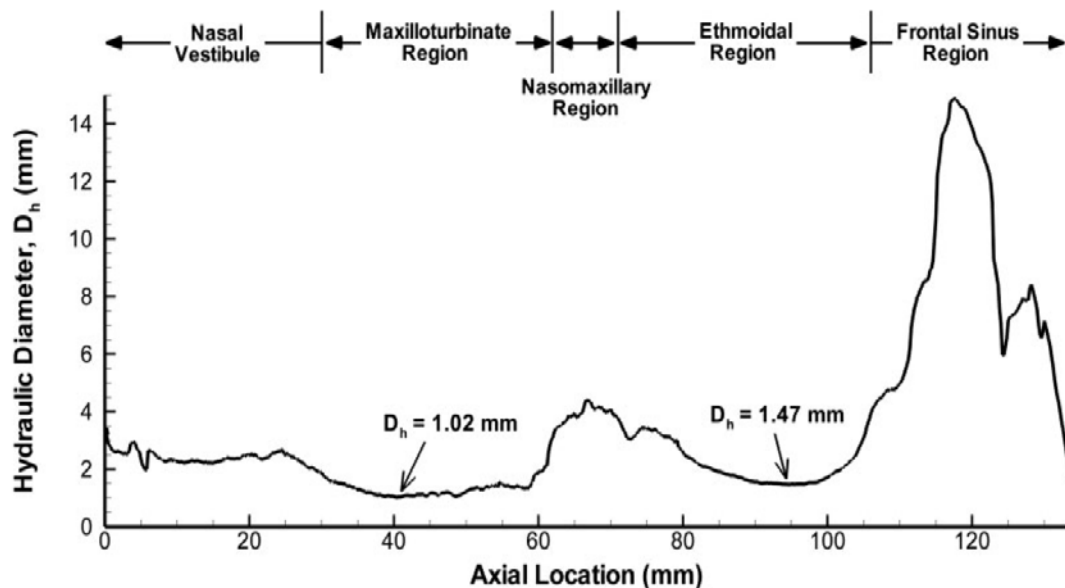


**Figure 2.9: Canine nasal hydraulic diameter distribution. Figure from [98].**

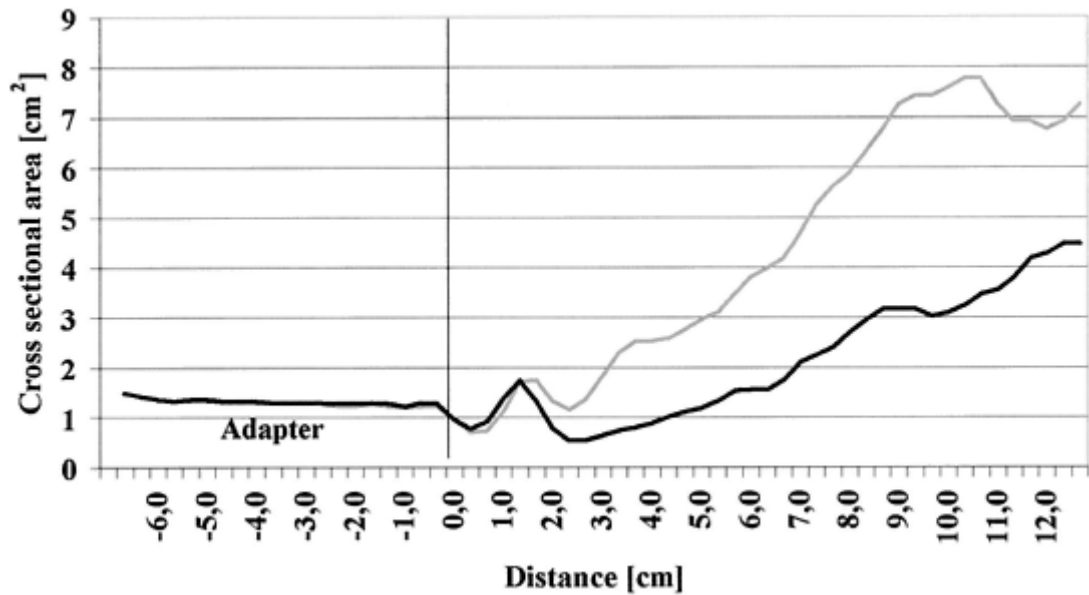


**Figure 2.10: Human inter-nasal cross-sectional area distribution. Graph from [99].**

Out of the investigations into nasal geometry at ambient pressure found in the current literature, only work by Lang *et al.* [99] using AR has considered the difference in cross-sectional area that occurs between the patent and congested airways. As seen in figure 2.10, moving towards the posterior nasal region, the patent airway demonstrates a greater cross-sectional area than that of the congested.

### 2.3.6 Pressure Elicited Change in Nasal Geometry

As discussed in Section 2.3.3, partitioning of the air mass-flow between the two nasal passageways is regulated by variation in nasal cross-sectional area through a periodic cycle of congestion/decongestion of erectile tissue within each side of the nose [84], termed the ‘nasal cycle’. Previous investigations have shown that increases in nasal cross-sectional area can negatively influence its air conditioning ability [95, 100].

The current belief is that pressure elicited change in nasal geometry is caused by a nasal tissue compliance response [101, 102]. Although compliance, a quantification of variation in nasal cross-sectional area in response to pressure change, has previously been investigated, it is not known if this parameter differs between the patent and congested airways. These investigations, using acoustic rhinometry (AR) [101, 102], have demonstrated that this compliance is a function of both tissue elasticity and nasal erectile tissue blood engorgement.

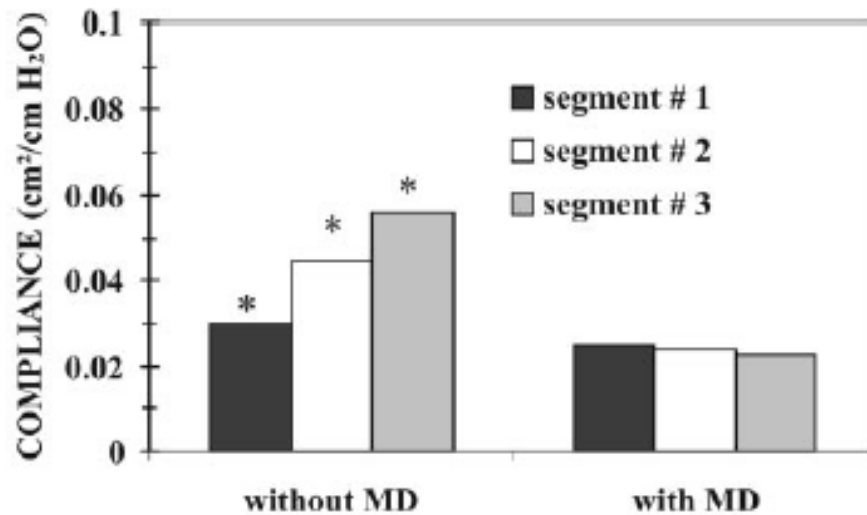


**Figure 2.11: Nasal compliance representing change in cross-sectional area per unit pressure (cm H<sub>2</sub>O). Chart from [102].**

Brugel-Ribere *et al.* [102] considered the effect sub-atmospheric pressures had on airway cross-sectional area because they were interested in airway closure during forced inhalation. Compliance results taken by AR are presented in Figure 2.11 for three locations along the nasal passageway; the anterior tip, middle and posterior regions of the inferior turbinate. The influence activation of nasal erectile tissue had on nasal compliance was also investigated. 0.05% oxymetazoline was sprayed into the nose to decongest erectile tissue venous drainage. This provided mucosal decongestion (MD), shown by Figure 2.11

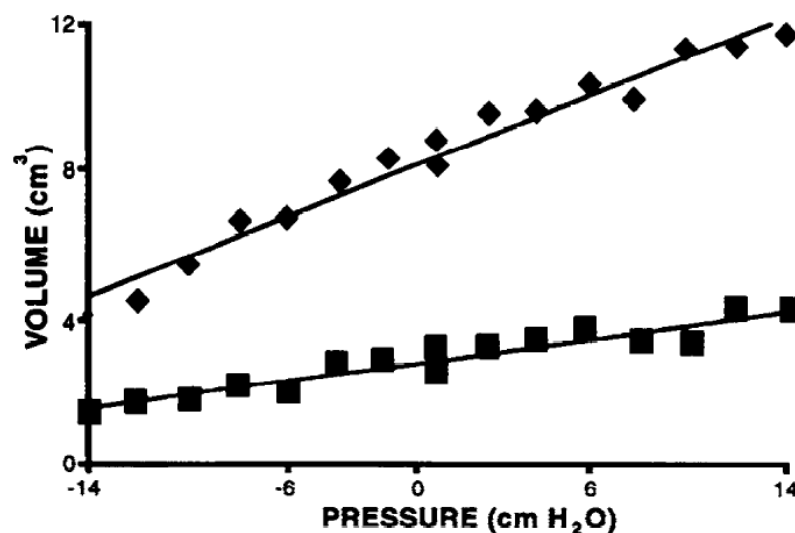


**Figure 2.12: Nasal compliance represented as change in volume (cm<sup>3</sup>) per unit pressure (cm H<sub>2</sub>O). ■ = Nasal valve, ◆ = anterior turbinate regions. Graph from [101].**

Nasal tissue compliance in terms of change in airway volume has also been investigated [101]. Kesavanathan *et al.*, Figure 2.12, considered two locations along the airway, namely the anterior and middle region of the inferior turbinate. Here we see the same trend as found by Brugel-Ribere *et al.* of increasing cross-sectional area (or cross-sectional area per unit volume in the case of Kesavanathan) with increasing air-pressure. Both of these investigations fail to recognize any difference in tissue compliance behavior occurring between the patent and congested airways. Additionally, both relied on the use of AR techniques to undertake these *in-vivo* measurements. From other earlier investigations comparing CT and AR nasal cross-sectional area data, it was found that good correlation can be found within the relatively open anterior spaces of the nose [91, 92], however, AR tends to underestimate nasal cross-sectional area beyond the complex and sometimes obstructed turbinate region [93, 103].

The acquisition of reliable nasal morphological image data comparing ambient and n-PAP breathing does not seem to have been attempted. Quantification of the effect n-PAP breathing has on nasal geometry will be of significant interest given the setting of the current work.

## **2.4 Airway Surface Liquid**

Apart from nasal air-conditioning, the nasal ASL lining the conducting airways also plays an important role in providing protection against pathogens and unwanted contaminants. To achieve this function, this liquid consists of two functional strata – an upper mucus gel blanket overlaying the periciliary liquid (PCL) layer, shown in Figure 2.15. The sticky upper mucus layer provides the important role of entrapment of inhaled pathogens/particles and absorption of gaseous water-soluble air contaminants [20, 104], while the lower PCL layer provides a platform for mucus transportation [105-107]. The lower PCL layer also provides additional protection against infection in the form of a chemical shield provided by active defensins present within this stratum [108]. Although it is commonly known that the ASL consists of two layers, it was only recently that the cause of this stratification and implications for ASL hydration have been further clarified [109]. In addition to providing a source for airway air-conditioning and protection, the ASL layer within the nose also provides a means by which heat and moisture can be recovered from exhaled air through latent heat exchange [52].

Within this section, an overview of heat and moisture recovery from the ASL layer and mucus entrapment and clearance are discussed in Sections 2.4.1 and 2.4.2 respectively. The important relationship of ASL hydration and hydration/height interplay that occurs between the lower PCL and upper mucus layers is discussed in sections 2.4.3 and 2.4.4 respectively. Modes of mucociliary transport dysfunction are discussed in Section 2.4.5 before normal and pathophysiological dehydration limits are defined in terms of osmotic bulk modulus ( $K$ ) in Section 2.4.6.

### **2.4.1 Heat and Water Recovery**

With regards to heat and water mass transfer, inspired air, aided by turbulence, is heated and humidified as it passes through the nasal cavity, causing the ASL to cool when water transfers to the air. However, during exhalation, some of the moisture from the fully saturated warm exhaled air (at near core body temperature) condenses on the ASL, which has previously been cooled during inhalation. Around 30% of exhaled moisture is recovered for use in humidification during the next breathing cycle [52, 63]. The cyclic exchange of latent and sensible heats, as well as the partial water recovery, implies that the ASL acts as a thermal and moisture buffer zone between the nasal air and the underlying mucosa supplying heat and water. This buffering effect possibly reduces the transient fluid requirement from mucosal secretion glands and stabilizes cyclic thermal fluctuations during normal breathing. It may also offer protection from hot air damage due to the fact that ASL has a higher sensible heat capacity than that of air [70].

### **2.4.2 Mucus Entrapment and Clearance**

Within the ASL, the upper mucus blanket overlaying the PCL provides the human airways with the first line of defence against infection, particles and airborne pollutants through entrapment in this sticky layer [20, 110, 111]. The human airways produce around 600-1800 ml of mucus each day, which is transported along the conducting airways, from either the distal airways or nose, to the pharynx where it is either swallowed or expectorated [112, 113]. Swallowed mucus disposes trapped debris and pathogens to the gastrointestinal tract where they are far less likely to survive and cause infection. Additionally, this also supplements the mucus produced within the digestive system [112].

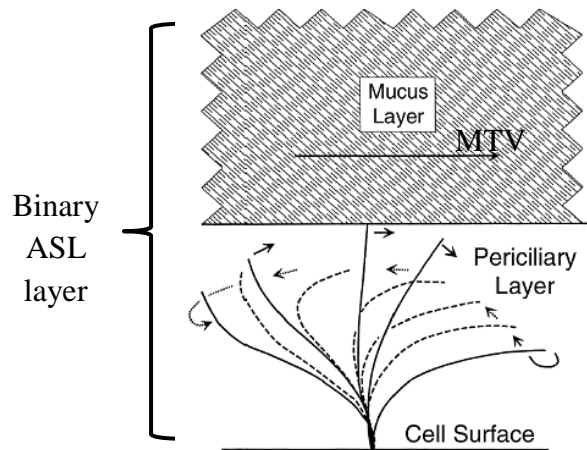


**Figure 2.13: Mucus layer transport by beating action of motile cilia. Figure adapted from [108].**

Within the nose, additional mucus clearance can be achieved through sniffing or blowing of the nose, however this defensive layer is normally transported towards the pharynx by the synchronized beating of cilia protruding from pseudo-stratified columnar epithelial, shown in Figure 2.13.

It is thought that mucociliary transport occurs due to the cilia engaging with the thicker mucus gel layer [114] with a coordinated whip-like motion [115-118]. The cilia beat frequency (CBF) normally ranges from 8 to 15 Hz [108]. The mucociliary transport velocity (MTV) is significantly influenced by the ASL hydration state [107], and during normal hydration the MTV ranges from 3-25 mm/min [119, 120]. It is important that the mucociliary transport system disposes of entrapped pathogens in a timely manner, since bacteria numbers can double in number over a 20 minute period [108]. Continuous transportation of the mucus layer towards the nasopharynx, where it is cleared by swallowing or expectoration, is essential not only for removal of entrapped contaminants [20, 111], but also for nasal air-conditioning [70]. During periods of mucociliary dysfunction, insufficient MTV may lead to a build-up of coalesced mucus hindering both heat and water exchange.

### 2.4.3 ASL Stratification

Until recently, it was thought that the lower PCL layer consisted of a watery, low-viscosity liquid that enabled motile cilia beating to occur which transported and supported the overlaying denser mucus gel blanket [121]. This understanding, termed the ‘two-layer gel-on-liquid’ model, has recently been challenged, since it fails to

explain stratification of the PCL/mucus layers [109]. One concern is that this model does not describe why the gel layer mucin molecules do not descend into the similar sized interciliary spaces and form a single layer. While it has been postulated that the thixotropic action of beating cilia prevents this from occurring, it has been demonstrated that cilia motion is not a factor since particles as small as 40 nm cannot penetrate the PCL layer despite cilia beating having ceased [109].

Recently, research by Button *et al.* [109] has found that membrane-tethered mucins and mucopolysaccharides within the ASL are grafted to the cilia and epithelial surfaces with increasing density from the top of the PCL toward the underlying epithelium as shown by Figure 2.14 (A). These grafted mucins and mucopolysaccharides form the bristles of the ‘brush’ and are believed to propel unwanted particles out from the PCL layer, towards the mucus stratum. This has led to a new ‘gel-on-brush’ model which postulates that ASL stratification occurs as a result of PCL grafted mucin and mucopolysaccharide density gradient being greater than that found in the mucus layer. Here, mucin excretion from goblet and submucosal glands as shown in Figure 2.14 (A) become more hydrated and less dense. This makes them more buoyant than those grafted to the cilia and epithelial surfaces, causing them to float up form into the overlying mucus blanket [109] as shown by the enlarged view in Figure 2.14 (B).

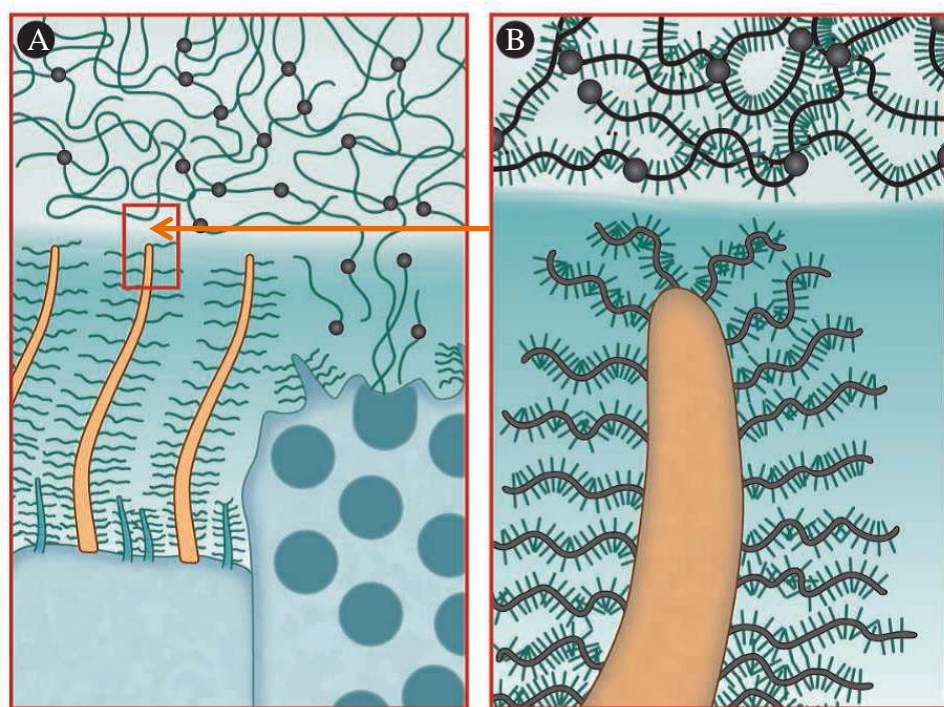


**Figure 2.14: (A) - Mucin release from secretory cells being hydrated within the PCL moving towards the upper mucus gel layer. (B) – Enlarged view of cilia demonstrating increasing membrane-tethered grafter mucins and mucopolysaccharides. Diagram adapted from [113].**

#### 2.4.4 ASL Hydration

It has been long recognised that the PCL height needs to be tightly maintained around 7  $\mu\text{m}$  to ensure efficient mucociliary transport [121, 122]. Within the ASL, the mechanisms by which PCL and mucus height and hydration are achieved are multifaceted, given both of these layers are characterised with differing hydration behaviours. Differentiation in the water drawing power between the PCL and mucus gel layers can be made by considering the parameter of osmotic bulk modulus ( $K$ ) [109]. This parameter is a measure of change in osmotic pressure per unit volume that varies in proportion to mucin density. Significant change in the mucus layer height and water storage occurs during ASL hydration/dehydration, as a consequence of the ungrafted mucins having high water absorbency, characterising this layer with a low  $K$  value. On the other hand, little change in height occurs within the PCL layer during ASL hydration/dehydration as the grafted mucins tend to absorb less water, characterising this layer with a higher  $K$  value. Summarising the ASL hydration/height interplay [109]:

1. During normal ASL hydration/dehydration, water preferentially enters or leaves the mucus layer, causing it to undergo significant changes in height. The PCL layer remains at a relatively constant height of 7  $\mu\text{m}$ , ensuring mucociliary transport is maintained. In essence, the difference in  $K$  values protects the PCL layer from height change over the normal ASL hydration range.
2. Severe ASL dehydration causes water to be drawn from both mucus and PCL layers causing reduction in PCL height and disruption to mucociliary transport.

In what follows, any mention of the 7  $\mu\text{m}$  PCL height actually means an approximate normal physiological value.

#### 2.4.5 Mucociliary Transport Dysfunction

As discussed, a consequence of severe ASL dehydration is a reduction in PCL height causing mucociliary transport dysfunction [70, 122]. Although it has not been investigated, it is speculated that the likely mechanisms by which this could occur may be through mucus filling the interciliary spaces, Figure 2.15 (A), or compression of cilia, Figure 2.15 (B) [109]. Because of its air-conditioning role, nasal breathing when compared to oral breathing has an important role in maintaining ASL hydration within the conducting airways [123, 124].

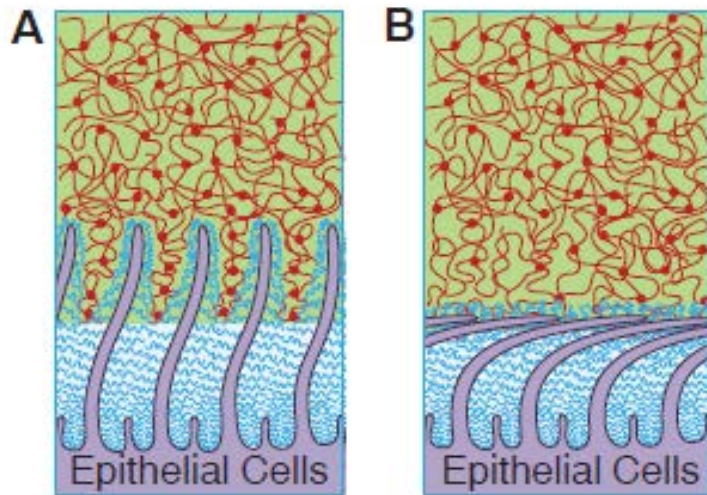


**Figure 2.15: Two modes of mucociliary transport failure caused by PCL dehydration. (A) Mucus entering interciliary space; (B) Mucus compressing cilia. Diagram adapted from [109].**

On the other hand, progressive over humidification through excessive supplementary humidification causes over-hydration of the ASL and a slowing of MTV due to a reduced cilia driving force [70, 125]. If prolonged, over humidification leads to the cessation of ASL transport and the risk of ASL draining into the lungs [70, 71, 125].

Regardless whether dehydration or over-hydration of the ASL occurs, the net result is the same; mucociliary transport will cease. This leads to an increased risk of infection and airway contamination.

#### 2.4.6 Hydration/Dehydration Limits

As discussed in the previous section, severe ASL dehydration exposes the PCL to height loss, which causes failure of mucociliary transport. In this section the difference in mucus osmotic bulk modulus ( $K_{\text{mucus}}$ ) values between the normal and severely dehydrated states is used to determine an ASL water equivalent height range representative of that spanning the range of normal and severely dehydrated ASL hydration status.

Previous investigation has demonstrated that during normal hydration,  $K_{\text{mucus}}$  has been found to be as low as 0.2 kPa [109]. A confocal microscope image of cultured human bronchial epithelium with normally hydrated ASL demonstrates cilia extending to full height, shown by the white bar representing a height of 7  $\mu\text{m}$  in Figure 2.16 (A). On the other hand, severely dehydrated airways demonstrate a  $K_{\text{mucus}}$  as high as 3-8 kPa, leading to PCL height loss of around 4  $\mu\text{m}$  [109].

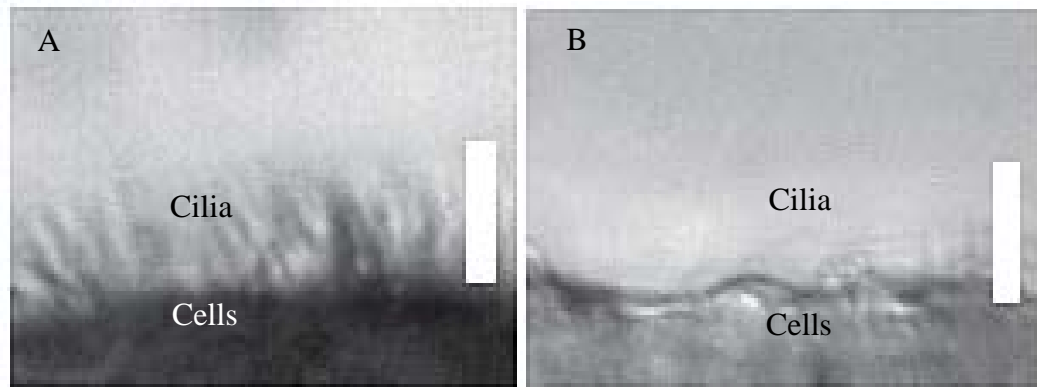


**Figure 2.16: (A) Normal ASL hydration enables cilia to extend to full height. (B) Severely dehydrated ASL demonstrating absence of motile cilia. In both images the white bar demonstrates normal PCL height of 7  $\mu\text{m}$ . Diagram adapted from [109].**

In this situation, a confocal microscope image of cultured human bronchial epithelium demonstrates an absence of motile cilia, whilst the white bar represents the normal cilia height of 7  $\mu\text{m}$  in Figure 2.16 (B). Variation in  $K_{\text{mucus}}$  between the normal and severely dehydrated states corresponds to a mucus layer water volume reduction of around 85% [109]. As previously mentioned, the mucus layer normally acts as a buffer to air-conditioning demands of water supply and recovery during every breath cycle by acting as a fluid reservoir [126].

Mucus height also varies since it is determined by the balance of secretion rate, hydration status and mucociliary transport velocity [110]. Normal *in-vivo* mucus layer height has been reported to range from 0.5  $\mu\text{m}$  [111, 122] up to 10  $\mu\text{m}$  [110]. Exposure to toxic or irritating substances can also greatly increase its height within conducting airways [110].

## 2.5 Airway Surface Liquid Water Supply

Within the nasal mucosa, it is currently thought that regulation of goblet and serous cells within the surface epithelium and submucosal glands provide around 90% of the fluid supply that makes up to the ASL layer lining the airway lumen [127]. Supplementary regulation of PCL height is undertaken by the superficial epithelia lining the conducting airways through stimulation of cellular purinergic pathways. Both the autonomic and purinergic regulation systems are now reviewed in Sections 2.5.1 and 2.5.2 respectively before rates of PCL supply and absorption are reviewed in Section 2.5.3.

### 2.5.1 Autonomic Regulation of Airway Surface Liquid Height

Submucosal glands located below the surface epithelium consist of distal serous acini cells that provide PCL fluid secretion whilst mucus cell tubules, similar to goblet cells found on the superficial epithelium, supply mucus [128]. Both serous acini cells and mucus tubules are connected to a common duct system leading to the airway surface, shown by Figure 2.17.

Within the conducting airways, the secretion rate of these exocrine glands is regulated through three neural pathways of cholinergic, adrenergic and non-cholinergic/non-adrenergic control [129]. It has also been shown that autocrine and/or paracrine mechanisms are also involved in regulating gland secretions [128, 130].

Cholinergic agents, such as methacholine and acetylcholine have been shown to provide a large and rapid increase in ASL height through hydration of the mucus layer by stimulating fluid secretion from the serous cells [131-133].

Goblet cells located on the epithelial lining are also thought to discharge ASL fluid but only in response to local irritation [134]

### 2.5.2 Purinergic Regulation of Periciliary Liquid Height

Supplementary regulation of PCL height and ciliary driving action [135] is undertaken by the mucosa's superficial epithelia lining the conducting airways. Most types of airway epithelial cells, such as Clara and ciliated cells release ions, surfactant, immunoprotective proteins and phospholipids into the PCL layer [62].

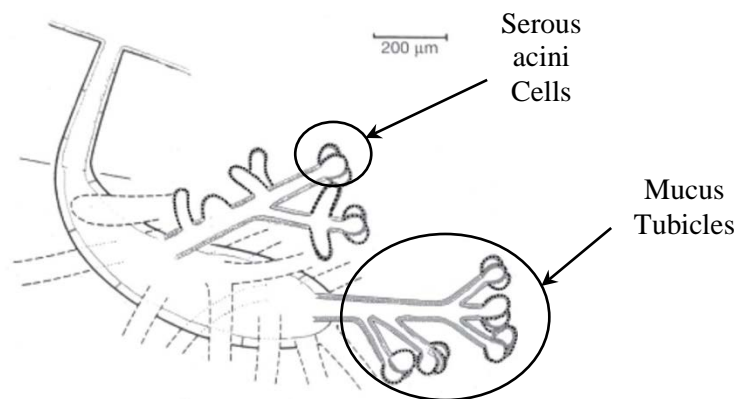


**Figure 2.17: Simplified representation of airway submucosal gland demonstrating connection of serous acini cells and mucus tubules to a common duct system. Diagram adapted from [136].**

The expression and absorption of these substances serves to control trans-epithelial water flow, regulating PCL composition and height [105, 107]. Fluid release occurs during the multiple stress stimuli experienced during tidal breathing [137] and in response to PCL  $\text{Na}^+$  and  $\text{Cl}^-$  balance [105, 107]. This interaction between cellular receptors and mechanical stress causes the opening or blocking of intracellular channels that form the purinergic regulation system.

Breathing stress stimulation of cellular fluid release and the role cellular back-flux has in fine tuning PCL hydration are discussed in Sections 2.5.2.1 and 2.5.2.2 respectively.

### **2.5.2.1 Breathing Stress Stimulation**

Intracellular adenosine triphosphate (ATP) release is triggered by mechanical deformation [138, 139], fluid shear stress [140, 141] and compression or stretch of human airway epithelia [142, 143]. Within the airway mucosa, extracellular release of this signalling molecule occurs during oscillatory pressure fluctuations generated during normal tidal breathing. This stimulus is important in maintaining PCL height and cilia motion to ensure regulation of mucus clearance and the maintenance of a healthy airway by [141, 143]. ATP and other nucleotides from the airway epithelia are released by mechanical forces [107, 144], which are imparted by breathing-induced cyclic shear and pressure stress. These are exerted on the mucosa as oscillatory trans-epithelial breathing pressure fluctuations [107]. Experimental work on tracheal epithelia has shown that ATP release rates are most sensitive over the normal physiological range of oscillatory shear and compressive stress imparted during tidal breathing [107]. Given the airway wall shear stresses experienced during normal breathing are estimated to be as high as 0.3 Pa in the nose [145], compared to around 0.45 Pa in the trachea and lower airway [141], the nasal epithelium probably responds to airway stresses in a similar fashion to that of the trachea. Since goblet cell mucin and PCL volume is increased via epithelial ion transport and also MTV is enhanced by an increase in CBF as a consequence of stress stimuli [135, 146-150], purinergic stress stimulation is also considered part of a natural nasal defence system to wash away noxious contaminants [137, 148].

To emphasise the role stress fluctuations have on stimulating the purinergic regulatory system, recent work on sheep trachea has found that fully humidified unidirectional airflow at 30°C or even 34°C is insufficient to prevent epithelial cell dysfunction or damage due to dehydration from occurring [151]. This is in contrast to the normal

situation where nasal epithelia are frequently exposed to air conditions well below these temperatures and humidity values and no adverse effects are reported. This highlights the importance of cyclic air-stress stimulation in maintaining healthy ASL volume and MTV.

#### **2.5.2.2 Cellular Reabsorption**

Airway epithelia is characterized as having low trans-epithelial resistances [152] and high water permeability [153-155] so as to finely tune the PCL hydration state [156]. This is achieved through continual back-flux occurring during cellular ion and water release [107]. Airway epithelia are considered ‘leaky’ since they are capable of absorbing fluid through cellular tight junctions [157] as well as exchanging intercellular fluid through  $\text{Na}^+$  absorption and  $\text{Cl}^-$  secretion. Given the PCL NaCl concentration is essentially isotonic with the epithelial cells [158], it has been hypothesized [107, 159] that salt secreted by the epithelia is followed by water, to maintain tonicity, resulting in a PCL volume increase. Conversely, if salt is absorbed by the epithelia, water will follow into the cells, resulting in PCL dehydration. Continuous switching of these ion channels between secretion and absorption phenotypes [141, 156] has demonstrated that epithelial water flux fine tunes PCL volume during tidal breathing.

The airway epithelium also actively absorbs fluid to prevent the airway flooding with excess PCL brought up from the lungs. This enables the same PCL height to be maintained throughout the conducting airways [111]. Without reabsorption occurring, excess PCL would occlude the airway lumen given this liquid is transported from the distal airways by the mucociliary system, where it experiences a reduction in aggregate cross-sectional area of around 20,000-fold [160].

#### **2.5.3 Quantification of PCL Supply & Absorption**

As discussed in Section 2.4, it is essential that the PCL layer within the ASL is regulated to maintain a height of 7  $\mu\text{m}$  to ensure a healthy rate of mucociliary transport [107, 115, 161]. Here, air-conditioning water demand or recovery is normally met by changes in mucus hydration. When necessary, rehydration of the mucus layer is achieved from the mucosal surface via the PCL layer.

Within the conducting airway, ASL hydration and mucus supply is predominantly sourced from submucosal glands [127] and goblet cells [111, 162] (as discussed in

Section 2.5.1). Supplementary regulation to maintain the PCL layer within prescribed height limits is also undertaken by the superficial epithelia lining the conducting airways [105, 107, 135]. These cells respond to fluctuations in airway wall pressure and shear stresses generated during tidal breathing and, where necessary, also reabsorb surplus PCL [111]. Although earlier research has demonstrated the beneficial effect cyclic fluctuations in air-flow stresses have on the ability of superficial epithelial cells to regulate PCL height and mucus hydration, the impact PAP has on this regulatory system is currently unknown.

Data corresponding to the *in-vivo* measurement of human nasal ASL flux is absent from the literature. Because of this, a review of ASL flux from within the lower conducting airway and oral mucosa is now undertaken to determine the maximum values of mucosal fluid secretion and absorption within this region, which could be used as indicative extremes for the nasal region.

#### **2.5.3.1 Bronchial, Tracheobronchial and Oral Mucosa**

Early investigations of bronchial and tracheobronchial tissue used a technique of timed exposure to methacholine to stimulate submucosal gland secretion from the airway lumen before rapidly freezing the tissue to lock the ASL layer intact. Change in ASL height was measured by low-temperature scanning electron microscope. Researchers found the maximal ASL volume flux from a human trachea is in the region of  $60 \mu\text{l}/\text{cm}^2\cdot\text{hr}$  and ASL reabsorption occurs at around  $5 \mu\text{l}/\text{cm}^2\cdot\text{hr}$  [134]. Later experimentation using this technique on bovine trachea yielded an increase in ASL height corresponding to a maximal flow rate ranging from  $120 \mu\text{l}/\text{cm}^2\cdot\text{hr}$  [132] to  $150 \mu\text{l}/\text{cm}^2\cdot\text{hr}$  [111]. These investigators also found that the excess ASL was reabsorbed at a rate of around  $5 \mu\text{l}/\text{cm}^2\cdot\text{hr}$  in the following 30 minutes after the stimulus effect of methacholine had ceased. An alternative technique to measure ASL flux exposed porcine bronchi to acetylcholine to stimulate gland liquid secretion [106]. ASL secretion was aspirated by syringe and found to reach a maximal value of  $15.5 \mu\text{l}/\text{cm}^2\cdot\text{hr}$ . Later work using the same technique produced a maximal value of  $14.4 \mu\text{l}/\text{cm}^2\cdot\text{hr}$  [163]. Here the superficial epithelium was removed which isolated the ASL supply to just the submucosal glands and helps explain the reduced magnitude when compared to their earlier measurement. Unfortunately, no rates of excess ASL reabsorption were measured using this technique. More recently, the technique of confocal microscopy has been used to assess reduction in ASL height in cultured human

tracheobronchial epithelial cells. Research into the rate of change in ASL height stimulated by passive forces corresponded to maximal rate of volume reduction, ranging from  $10 \mu\text{l}/\text{cm}^2\cdot\text{hr}$  [164] to  $15 \mu\text{l}/\text{cm}^2\cdot\text{hr}$  [143]. Reduction in ASL height in response to addition of excess liquid has also been measured using this same technique and found to correspond to a maximal initial ASL volume reduction rate of  $2 \mu\text{l}/\text{cm}^2\cdot\text{hr}$  [156].

Other *in-vitro* investigations using radioactive water found water penetration through human oral mucosa tissue ranged from 0.1 to  $40 \mu\text{l}/\text{cm}^2\cdot\text{hr}$  [165]. Here investigators concluded that water flux increased over the interval of testing and also that post-mortem time played a significant role. Disregarding the first 10 minutes of data produced an average water volume flux value of  $4.06 \mu\text{l}/\text{cm}^2\cdot\text{hr}$ . The first investigation into human bronchial water flux using a double capacitance probe technique found ASL induced secretion and baseline absorption values of  $3.6 \mu\text{l}/\text{cm}^2\cdot\text{hr}$  and  $1.2 \mu\text{l}/\text{cm}^2\cdot\text{hr}$  respectively [162].

#### **2.5.3.2 Nasal Mucosa**

The nose is located at the opening of the proximal conducting airway so it is exposed to a significantly greater air-conditioning demand than that encountered when moving toward the ISB, which is located within the distal region [166]. Because of this, it is not possible to directly apply the values of ASL supply and absorption found for the distal conducting airways to that of the proximal airway. Currently there is no data available that quantifies ASL supply and absorption for the nasal mucosa.

#### **2.5.3.3 Ambient Pressure**

Despite the apparent agreement between all of the ASL flux findings previously reviewed in Section 2.5.3.1, comparison of these results to the theoretical ASL flux required to achieve normal *in-vivo* nasal air-conditioning reveals them to be wholly inadequate [52]. Allowing for inhaled air conditions, breathing volume and rate as well as nasal surface area reveals a shortfall of around 1000 times. A strategy to account the additional water supply required within the nose is now undertaken.

One possible method to correlate earlier tracheal ASL flux findings to that required within the nose would be to consider the distribution of submucosal gland duct openings throughout the airway. Here the number of duct openings corresponds to the amount of water flux required to condition inhaled air. For example, porcine airways demonstrate

a near 1000 fold increase in the number of duct openings when moving in the anterior direction between the bronchioles and proximal bronchi [167]. This increase in duct density enables a significant increase in maximal fluid flux from the airway mucosa to occur. The human nose experiences the most severe water flux demands given one of its primary purposes is to heat and humidify inhaled air [1-3]. This is supported by a recent investigation that found a 10 fold increase in gland duct density occurs in the nose when compared to the trachea [168].

The ASL maximal mass efflux and reabsorption rates for the nasal mucosa are currently unknown during either ambient or pressurized tidal breathing conditions. In particular, the influence n-PAP breathing has on the mucosal purinergic system pressure/stress stimulation of ASL secretion/absorption is also unknown. Quantification of the effect n-PAP has on net nasal ASL supply will be of great interest in the context of the present work.

## **2.6 Adult Tidal Breathing**

The human respiratory system responds in an attempt to maintain blood oxygen and carbon-dioxide levels within normal physiological limits [117]. Normal adult at rest tidal breathing varies, however the duration of the inhalation and exhalation phases for a healthy individual typically occurs over a two and three second period respectively [169]. On the other hand, obese adults, a group prone to suffering OSA, typically have an elevated respiratory rate and smaller tidal volumes [170]. It has also been suggested that these individuals also suffer some respiratory muscle function impairment that results in a greater proportion of time during each breath being spend on inhalation [171]. This reported breathing period will be used later for the model input.

## **2.7 Air Temperature and Humidity Measurements**

Previous investigations of *in-vivo* nasal air temperature and humidity during spontaneous breathing have frequently ignored the need to consider the sensor time constant [172-174]. This constant is defined as the time interval taken to achieve a 63.2% response in measurement to a step change in input [175, 176]. This characteristic is particularly important when taking dynamic measurements where the measured variable continuously changes with respect to time and like that found during tidal breathing.

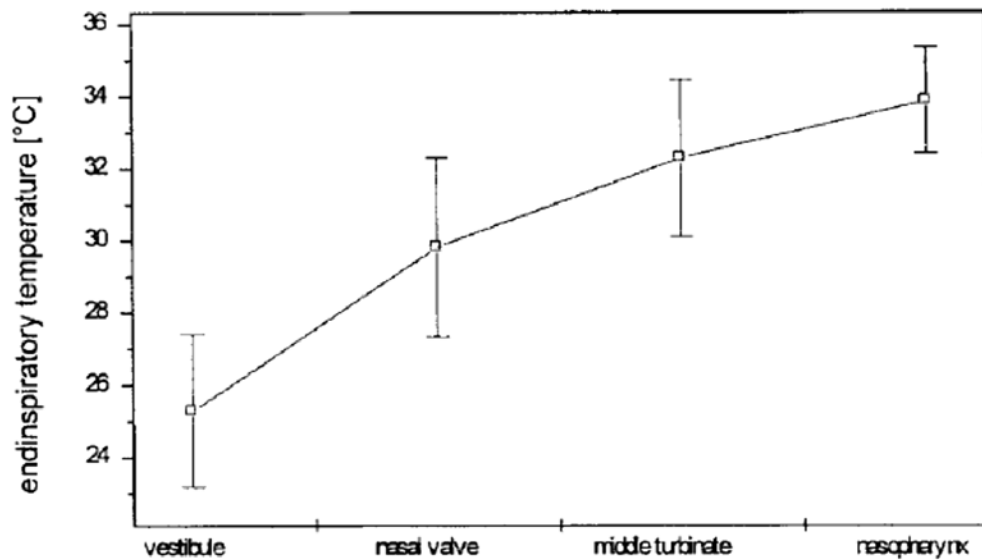


**Figure 2.18: Nasal *in-vivo* mean end-inspiratory air temperature distribution measured during breathing at rest at room temperature ( $T=25^{\circ}\text{C}$ ,  $\text{RH}=35\%$ ). Graph from [49].**

Transducer time response influences both the measurement amplitude and phase relationship and is referred to as dynamic error [175, 176]. As a general rule, the time constant must be much shorter than the period of the measurement [175]. In practice however, if phase is not an issue, a measurement corresponding to 63.2% of the true value is achieved in the time interval corresponding to one time constant while a steady state true measurement is usually achieved within a time interval corresponding to 5 time constants [176].

While some researchers have considered the transducer time constant, they seem to have ignored its relationship to the breath cycle. This had ranged from simply declaring a it had a ‘fast response’ [177] to a 90% response within 2 seconds during sustained high air velocity [178]. Just what was meant by high velocity was not stated and it is unclear if this velocity range falls within the range of airflows normally experienced within the nose. In this case it also seems unrealistic that to think inhalation could last more than four seconds meaning the measurement error due to transducer time constant could be relatively high.

Other research into *in-vivo* nasal temperature distribution has been undertaken (Figures 2.18 and 2.19) using a thermocouple [49, 73] characterized with time constant in still or high-velocity air of 0.4 and 0.1 seconds respectively. The quicker response time of this transducer makes it well suited to taking measurements during the human breath cycle, but the definition of high and low velocity relative to the normal breathing remains unclear.

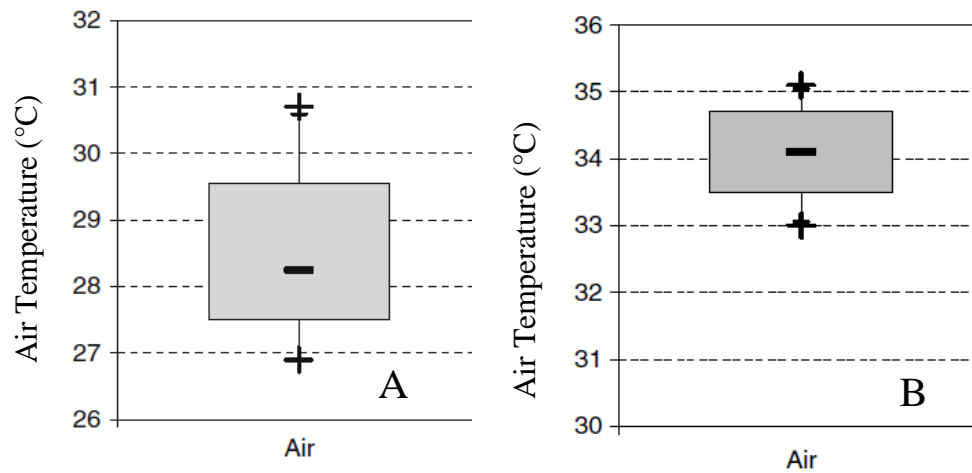


**Figure 2.19: Air temperature measured *in-vivo* at head of middle turbinate during breathing at rest. (A) End-inspiratory (B) end-expiratory. Graphs from [73].**

On the other hand, absolute humidity *in-vivo* measurements during tidal breathing are much more prone to measurement error given the quickest responding thin film transducers have a time constant of around four seconds [179]. Most research that simultaneously measured both *in-vivo* intra-nasal temperature and humidity fails to discriminate between patent and congested airways (Table 2.3) [180]. This effectively means that variation in air mass-flow partitioning between airways, occurring as a consequence of the nasal cycle, is not accounted for. Here, different inter-nasal air velocities simultaneously occurring would have produced variation in transducer response times for each airway.

**Table 2.3: Intra-nasal distribution of air temperature and humidity during quiet breathing at room temperature ( $T=25^{\circ}\text{C}$ ,  $\text{RH}=35\%$ ). (A) Inspiration, (B) expiration. Table from [180].**

Location	Inspiration		
	Temperature ( $^{\circ}\text{C}$ )	Absolute humidity ( $\text{mg H}_2\text{O/l}$ )	
Nasal vestibule	25.3	9.50	A
Nasal valve area	29.8	19.82	
Anterior turbinate area	32.3	23.97	
Nasopharynx	33.9	32.06	
Location	Expiration		
	Temperature ( $^{\circ}\text{C}$ )	Absolute humidity ( $\text{mg H}_2\text{O/l}$ )	
Nasal vestibule	34.2	33.78	B
Nasal valve area	35.1	36.78	
Anterior turbinate area	35.1	37.59	
Nasopharynx	36.2	39.58	

**Table 2.4: Inter-nasal increase in air temperature and humidity during quiet breathing at room temperature (T=22°C, RH=35%). (A) Relative humidity, (B) Temperature. Tables from [181].**

A	Relative humidity (%)	
	Left	Right
Intranasal site		
Nasal valve area	$38.8 \pm 6.1$	$37.2 \pm 6.5$ (n.s.)
Anterior turbinate area	$43.8 \pm 8.1$	$43.8 \pm 9.6$ (n.s.)
B	Temperature (°C)	
	Left	Right
Intranasal site		
Nasal valve area	$3.9 \pm 2.0$	$4.4 \pm 1.6$ (n.s.)
Anterior turbinate area	$5.8 \pm 2.7$	$5.3 \pm 2.3$ (n.s.)

Little nasal *in-vivo* temperature and humidity data is available that accounts for the nasal cycle, however one investigation could be found that focused on the anterior nasal regions (Table 2.4) [181]. Here, the right airway was patent and therefore experienced a greater air mass-flow. Difficulty in gaining clear access along the congested left airway prevented data from being acquired beyond the anterior turbinate area so distribution data is absent from the current literature.

Because humidity transducers are characterized with a relatively long time constant when compared to the breathing cycle, error in all *in-vivo* studies using these sensors is certain. Accurate air temperature and humidity measurements will be of great interest in the setting of the present work.

Within the current literature, only one example of research into the efficacy of nasal air conditioning associated with n-PAP breathing has been found [16]. This investigation was limited to measurements taken prior to or after n-PAP breathing. Results from this work suggest that no reduction in air conditioning occurring across the nose. This finding suggests the negative symptoms experienced during n-PAP therapy occur during the application of air-pressure.

## 2.8 Review of Air-Conditioning Models

During the breathing cycle there is a complex interaction between heat and water demand/recovery and mucosal heat and water supply acting to influence ASL hydration

status. As discussed in Section 2.7, undertaking *in-vivo* nasal mucosal ASL depth, air temperature and humidity measurements along the narrow and convoluted nasal cavity during n-PAP breathing is fraught with challenges that include poor access and the risk of eliciting tissue reactions. Additionally, the best air humidity time constant is still relatively long when compared to the period of the breathing cycle making air measurement errors inevitable. Also, there is presently no means by which accurate *in-vivo* measurements of ASL hydration can be undertaken throughout the nasal cavity. Given all of this, the best way to predict change in ASL hydration along the entire length of both airways during tidal n-PAP breathing is to model the ASL heat and moisture supply and demand occurring between the air and mucosa. Many differing forms of air-conditioning models have been created to better understand this interaction. The techniques used by computational models to predict heat and water mass flux are reviewed in Section 2.8.1.

### **2.8.1 Computational Models**

Computational air-conditioning models commonly require four differential equations of conservation of mass, momentum, convection-diffusion and thermal energy balance [46, 52].

One of the first one-dimensional air-conditioning models of the conducting airway was produced by Hanna *et al.* [97, 166]. Given imaging techniques were not then available; measurement of the complex nasal geometry for use within the model required a series of actions. Here, silicon castings were taken from human cadaver airways to produce a physical airway model. This then enabled local mass transfer coefficient to be empirically determined from naphthalene sublimation techniques. Sherwood ( $Sh$ ) and Schmidt ( $Sc$ ) numbers, representing the ratio of diffusive to convective resistance and momentum to mass diffusivity respectively, were calculated from naphthalene mass loss. Local heat transfer coefficient was calculated by use of the Chilton-Colburn equivalence, where complete analogy was assumed between convective mass and heat coefficients. This then enabled the determination of Nusselt ( $Nu$ ) and Prandtl ( $Pr$ ) numbers, the ratios of conductive to convective resistance and momentum to thermal diffusivity respectively.

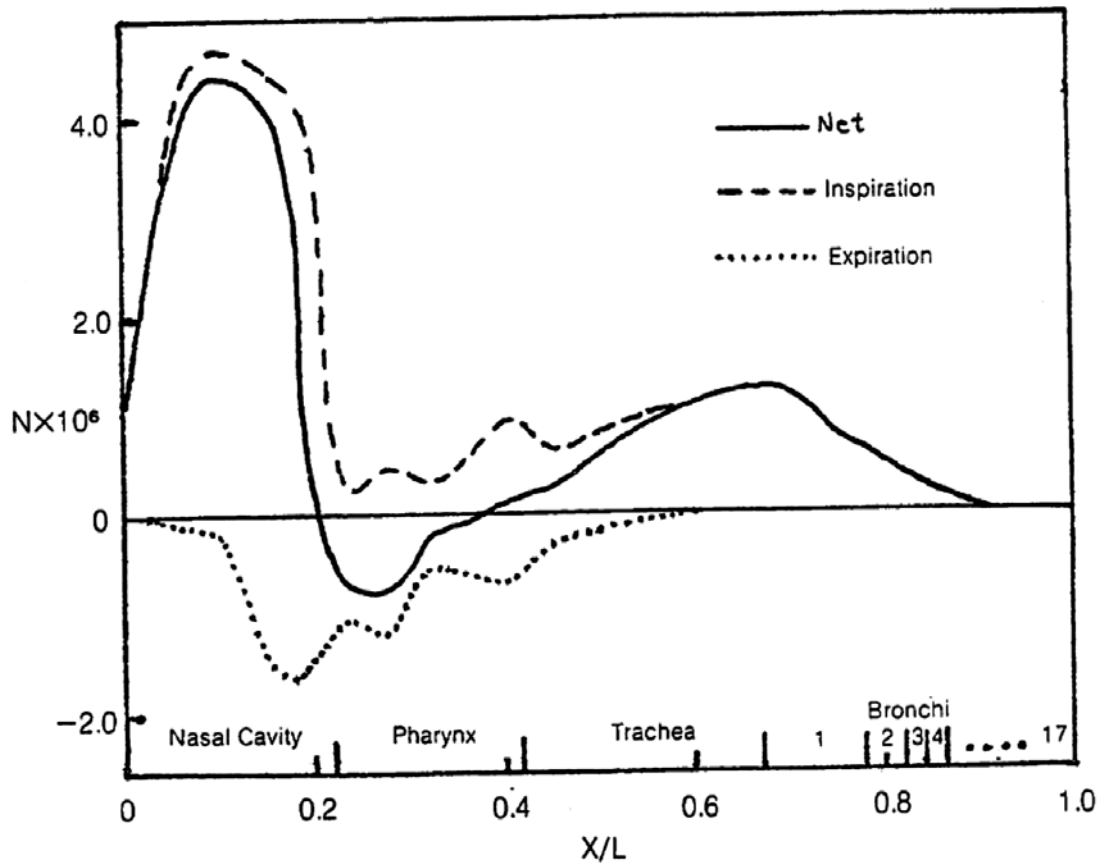


**Figure 2.20: Predicted water molar flux during ambient air at rest breathing as a function of non-dimensional distance into conducting airway ( $T=25^{\circ}\text{C}$ ,  $\text{RH}=35\%$ ). --- Peak inspiration, .... peak expiration, — net. Graph from [97].**

Finally the model morphology within the governing equations was expressed in terms of hydraulic diameter ( $D_h$ ), which enabled local heat and mass transfer coefficients to be calculated throughout the conducting airway.

Results of water molar flux distribution along the conducting airway are presented in Figure 2.20 and given in terms of non-dimensional distance ( $X/L$ ) measured from the nares to the 17<sup>th</sup> bronchi generation.

Of note is the greatest delivery or recovery of water mass along the length of the conducting airway occurring within the nasal cavity. ASL experiences water loss or gain during inhalation or exhalation phases respectively.

Heat flux ( $Q$ ) distribution ( $\text{Watts}/\text{cm}^2\cdot\text{hr}$ ) along the length of the conducting airway for peak inhalation and exhalation is presented in figure 2.21. Like the water molar flux distribution, the majority of transport occurs within the nasal cavity that significantly exceeds that which occurs along the remaining conducting airway. This is not

surprising given Hanna's model utilized the Chilton-Colburn equivalence to determine heat transfer coefficients from experimental mass transfer data.

Results of water molar and heat flux distributions reinforce the view that variation in the air heating demand within the airway, through either reduction or increase in air temperature are predominantly met within the nasal cavity, while little change in heat flux occurs within the distal conducting airways.

The prediction of air temperature ( $T_a$ ) distribution along the length of the conducting airway for the same range of breathing temperatures is presented in figure 2.22. Of note is that the most significant increases in air temperature occur within the nasal cavity. This is in agreement with the substantial rise in air temperature also predicted for this region. These findings of Hanna's model are in agreement with the belief that the nose contributes around 90% of respiratory system air-conditioning requirements [50, 51], as discussed earlier in Section 2.3.

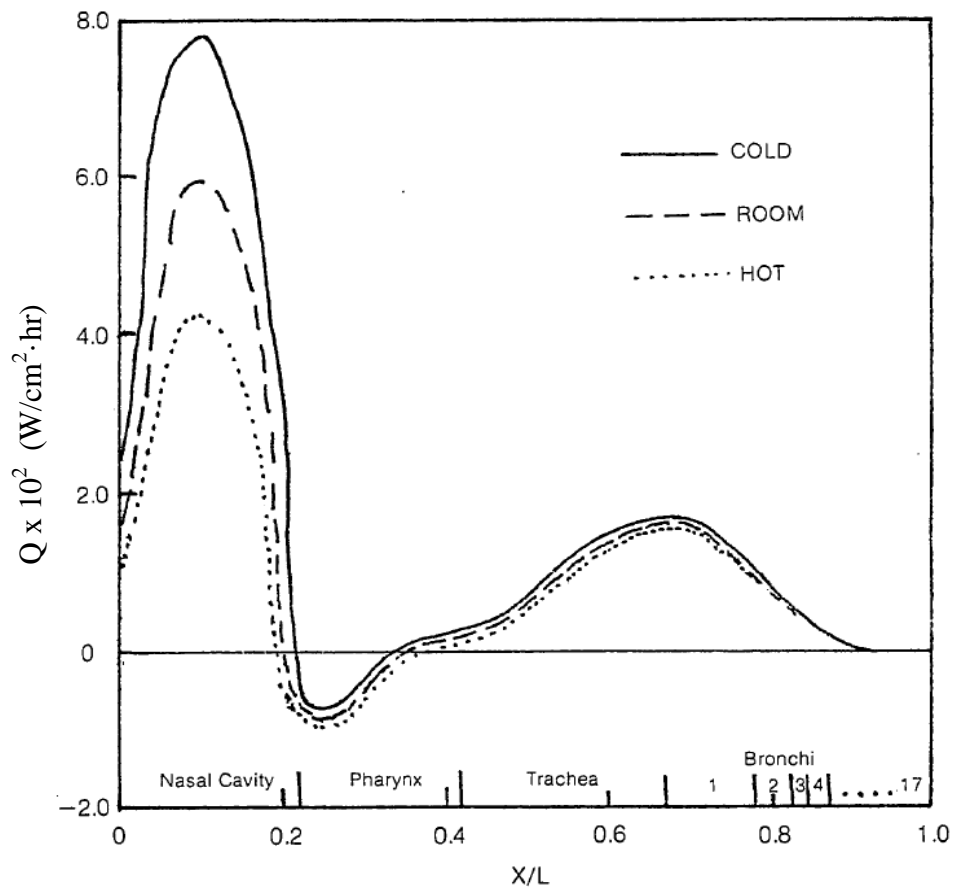


**Figure 2.21: Predicted heat flux as a function of non-dimensional distance into conducting airway model during at rest room breathing. Graph from [97].**

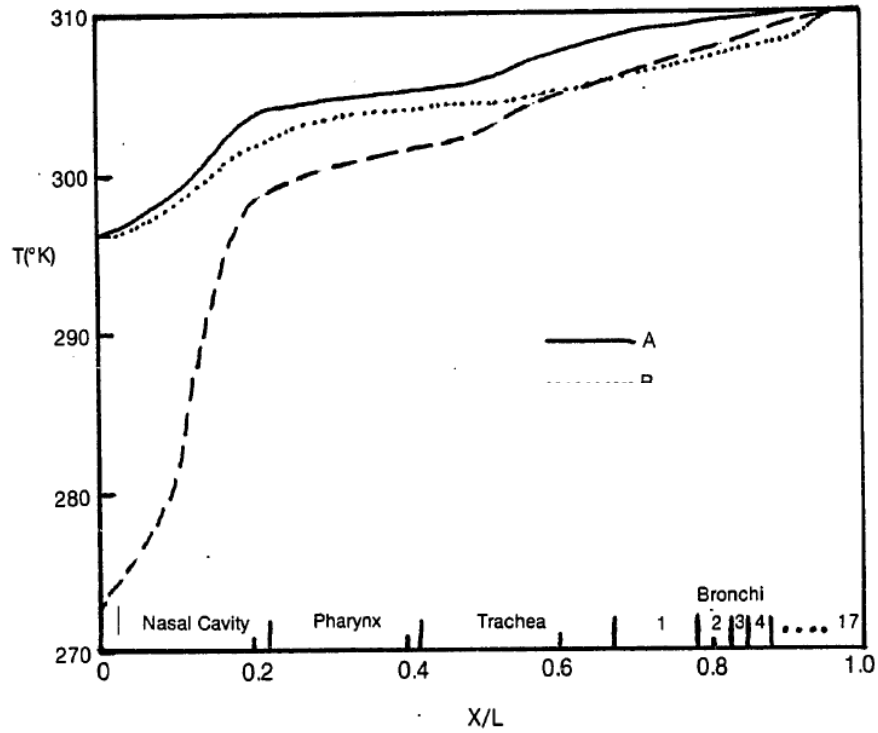


**Figure 2.22: Predicted air temperature distribution as a function of non-dimensional distance into conducting airway model [97]. — Room breathing at rest ( $T=25^{\circ}\text{C}$ ,  $RH=35\%$ ), -- cold air breathing at rest ( $T=0^{\circ}\text{C}$ ,  $RH=0\%$ ), ..... room breathing at maximal flow rate ( $T=25^{\circ}\text{C}$ ,  $RH=35\%$ ,  $V=2000\text{cc/s}$ ). Graph from [97].**

Hanna's model was limited to steady state airflows along the entire length of the conducting airway with only three data sets of nasal geometry recorded during naphthalene testing. This resulted in sparse geometric and local heat and water mass transfer coefficient data being available, which required an iterative solver to fill in the gaps. Although small, changes in air physical and thermodynamic properties along with variation in heat and water mass convective coefficients as a result of temperature change were also not considered. Another limitation was that variation in ASL hydration was not considered. It was assumed that infinite mucosal water supply was available and no allowance was made for the effect of air pressure on airway geometry.

Later computational work by Tsu *et al.* [182-184] built from Hanna's work and included the additional consideration of gas exchange between the airway lumen and mucosa [182].

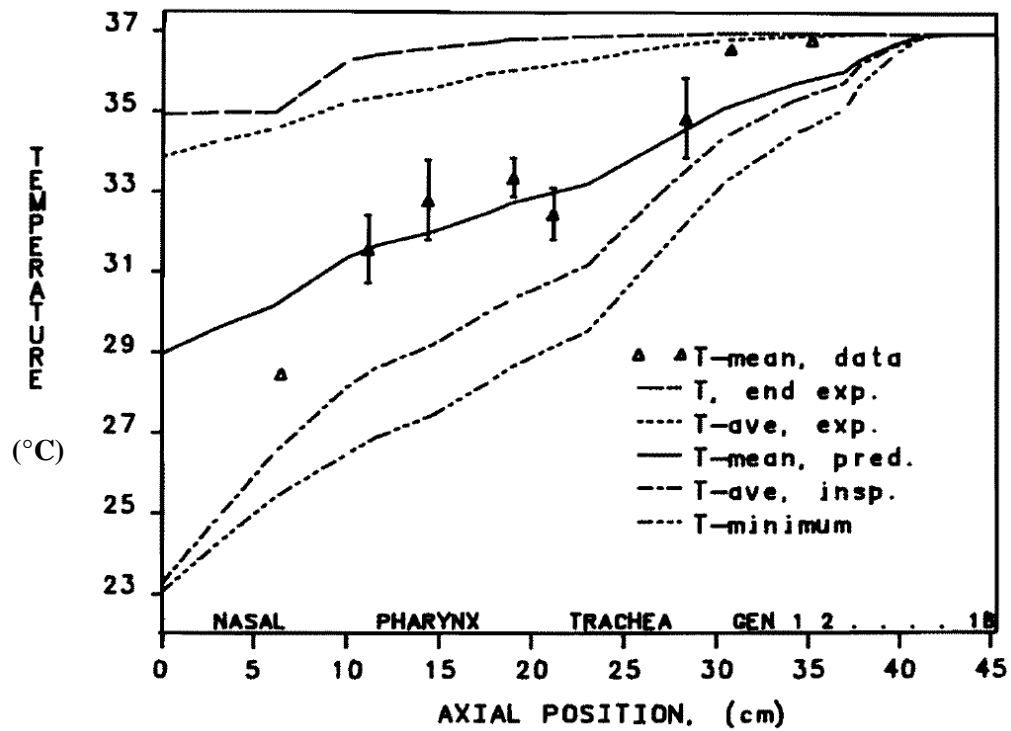


**Figure 2.23: Air temperature predictions along conducting airway over range of breathing conditions. Graph from [182].**

Significantly, this model introduced for the first time the concept of variation in ASL hydration due to evaporation/condensation, however mucosal water flux was not constrained by physiological limits. Although this model ultimately became focused on predicting the relationship between breath and blood alcohol [183, 184], it initially predicted the distribution of air temperature along the conducting airway (Figure 2.23). In this work, air temperature distribution is predicted during nasal breathing over a range of air mass-flow states including end expiratory ( $T_{end\ exp}$ ), average expiratory ( $T_{ave,exp}$ ) and average inspiratory ( $T_{ave, insp}$ ). Mean ( $T_{mean}$ ) and minimum ( $T_{minimum}$ ) temperatures were also predicted. Unfortunately this work concentrated on oral breathing so little detail was given on nasal air temperature distribution.

Tsu *et al.* also predicted the air humidity distribution along the conducting airway (Figure 2.24), but unfortunately did not include the nose. This figure presents predictions for humidity change due to variation in heat transfer correlation (*Change  $h(z)$* ), tissue thickness (*decrease  $\delta R$* ) and capillary bed temperature (*Increase  $T_{head}$* ).

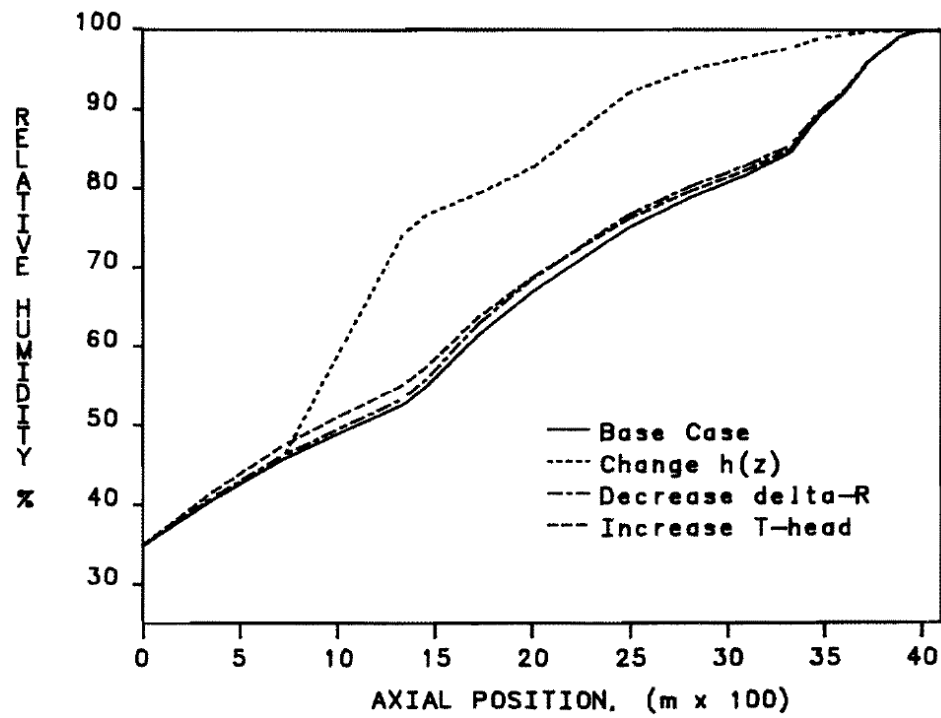


Figure 2.24: Air humidity predictions along conducting airway over range of breathing conditions. Graph from [182].

Finally, using this model, Tsu *et al.* also predicted ASL hydration over one complete breath cycle in terms of relative mucus thickness (Figure 2.25) where 1 represents the minimum allowable level of hydration.

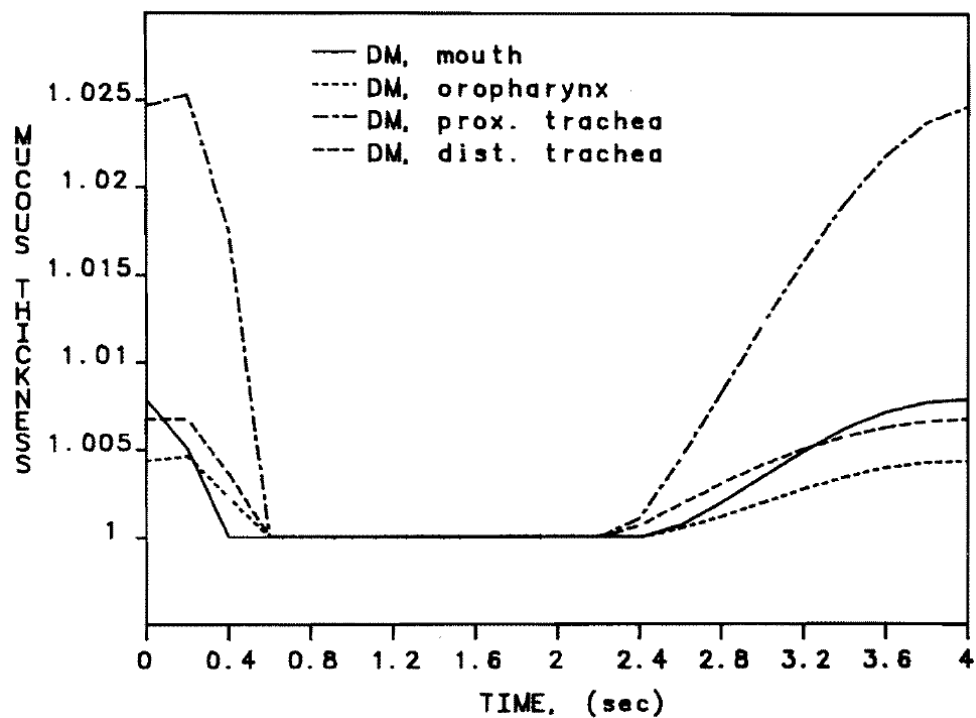


Figure 2.25: Predicted normalized ASL height for selected regions along the conducting airway throughout one breath cycle. Graph from [182].

The different lines shown in Figure 2.25 represent different locations along the conducting airway and time interval is shown along the lower axis. This model predicts that the greatest recovery in ASL height throughout one breath cycle occurs due to condensation within the proximal trachea during oral breathing,. No results for nasal breathing were predicted. Of note is that the ASL does not experience any dehydration beyond its lower limit as a consequence of making the assumption that it has an unlimited mucosal supply.

Although Tsu's model for the first time incorporated the concept of mucosal ASL water supply and accounted for variation in ASL hydration by water loss and recovery it does not account for the effect of air-pressure. It also considered for the first time the effect of the whole breath cycle.

Naftali *et al.* [185] produced an early 2-dimensional nasal air-conditioning model that moved away from using sparse cadaver based geometry to a simplified, but continuous, nose-like shape (Figure 2.26). This new model enabled calculation of air-conditioning parameters around regions where significant change in geometry occurred, since it was not required to calculate regional average flux coefficients.

The predicted distribution of air temperature along the nasal cavity along with a comparison to other work is presented in Figure 2.27.

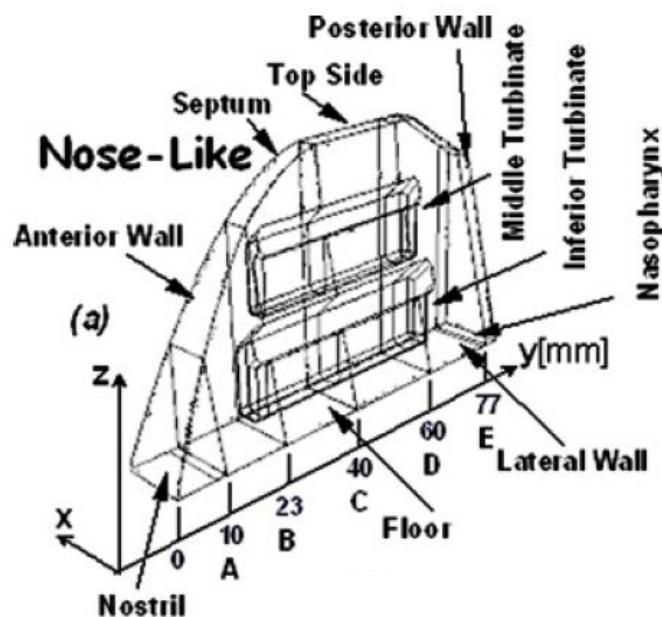
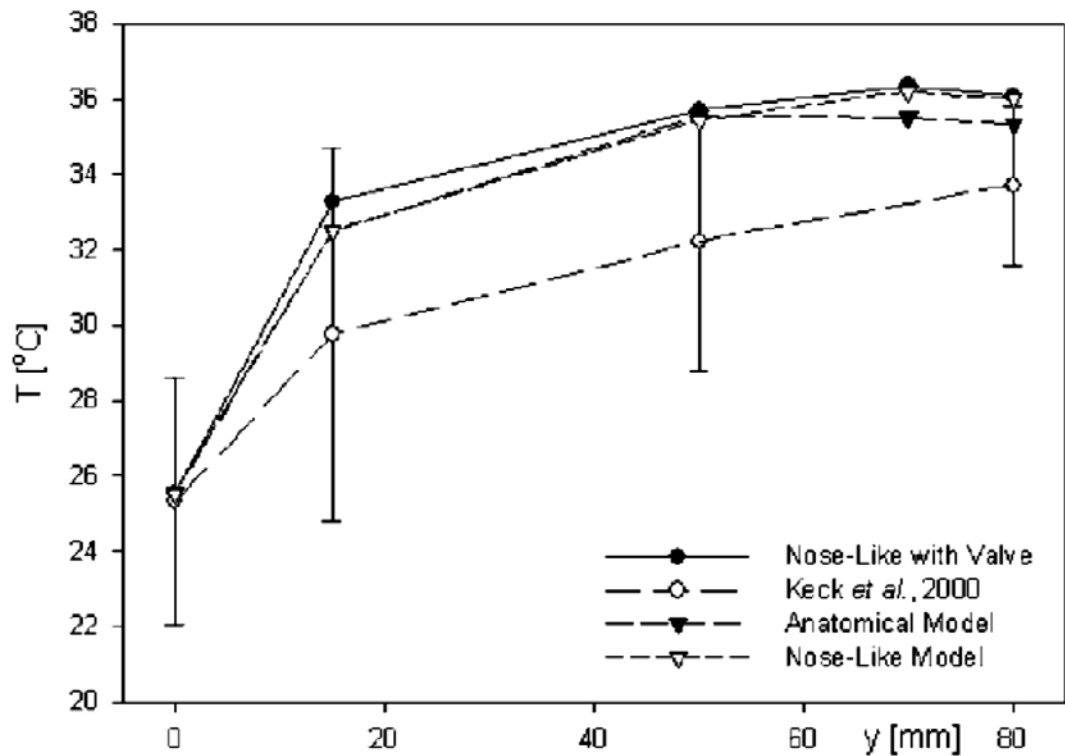


Figure 2.26: Simplified nasal geometric model. Diagram from [185].



**Figure 2.27: Results of 2-D nasal model giving temperature distribution along the nasal cavity during peak inhalation of ambient air ( $T=25^{\circ}\text{C}$ ,  $\text{RH} = 20\%$ ). Graph from [185].**

Despite improving the quality of nasal geometry, when compared to the earlier work, this model remains limited by assuming infinite mucosal water supply, and therefore constant ASL hydration.

More recently, modern imaging techniques, such as CT and MRI, have enabled capture of accurate, subject specific, *in-vivo* sectional conducting airway morphological data [67, 186-189]. These techniques avoid the problem of cadaver tissue shrinkage encountered in *ex-vivo* physical model testing. This improvement, combined with improvements in computational capacity, has enabled more numerically complex models to be undertaken. These have enabled the radial distribution of heat, water vapour and velocity from the trachea to the 16<sup>th</sup> bronchial generation of the conducting airway to be modelled [190-192]. These models have typically assumed the airway morphology consists of a series of circular tubes. Work by Warren *et al.* [193, 194] has resulted in a conducting airway model that incorporates for the first time ASL replenishment by stress induced stimuli of the epithelial purinergic system. This complex model was derived by combining the earlier heat and water model created by Tawhai *et al.* [192] that assumed infinite mucosal water supply with an airway epithelium fluid secretion model developed by Warren *et al.* [193].

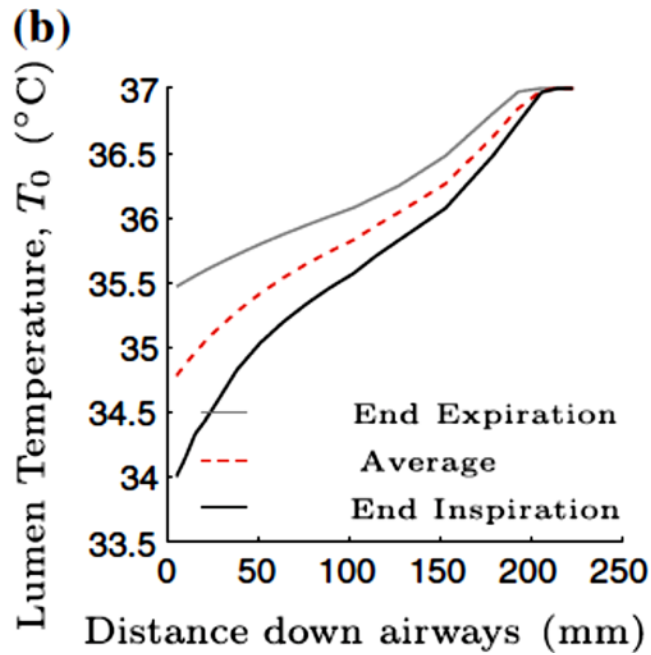


**Figure 2.28: Predicted lumen air temperature along tracheal/bronchial airways during breathing ambient air ( $T=22^{\circ}\text{C}$ ,  $RH = 50\%$ ,  $V=6 \text{ l/m}$ ). Graph from [194].**

Predicted end expiration, end inspiration and average tracheal/bronchial lumen air temperature and relative humidity predictions during tidal breathing of room air are presented in Figures 2.28 and 2.29 respectively. These consider the air conditions at the time periods when expiration and inspiration phases of the breath cycle have just concluded.

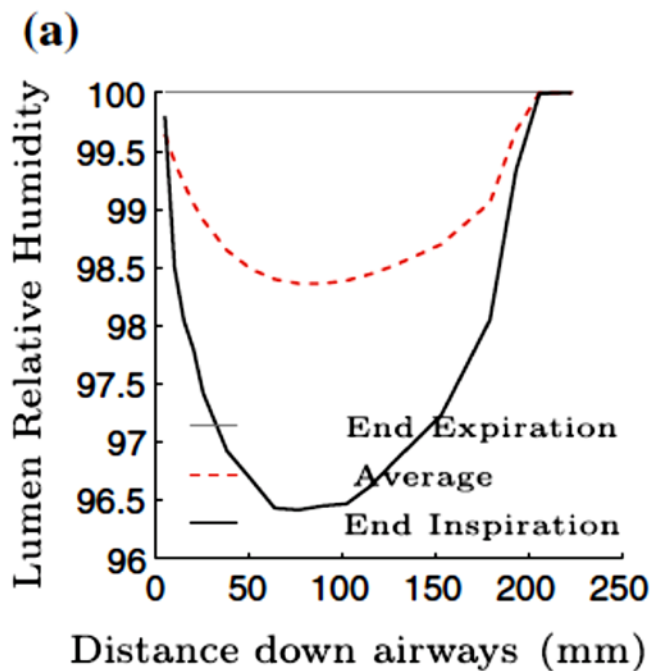


**Figure 2.29: Predicted lumen air relative humidity along tracheal/bronchial airways during breathing ambient air ( $T=22^{\circ}\text{C}$ ,  $RH = 50\%$ ,  $V=6 \text{ l/m}$ ). Graph from [194].**

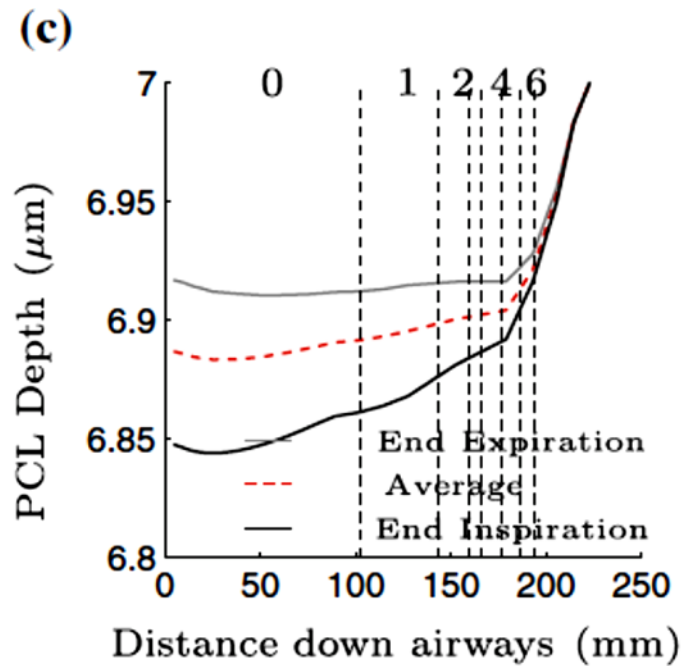


**Figure 2.30: Predicted lumen air temperature along tracheal/bronchial airways during breathing ambient air ( $T=22^{\circ}\text{C}$ ,  $RH = 50\%$ ,  $V=6 \text{ l/m}$ ). Graph from [194].**

Predicted change in ASL depth is presented in Figure 2.30 for a range of the breathing cycle. Included on the figure are the locations of the bronchial generations.

Variation in air properties and heat and water mass convective coefficients due to temperature variation along with the cumulative effects of tidal breathing were accounted for in this model. This model however did not include the nasal airway and airway geometry changes elicited by variation in air pressure.

Garcia *et al.* [189] considered variation in air temperature and water content along one nasal airway (Figure 2.31) using a CFD nasal air-conditioning model. This was undertaken to enable investigation into the change in nasal air-conditioning capacity between a normal nose and the pre and post-operative atrophic nose – a degenerative condition where mucosal tissue shrinks. Although nasal MRI morphological image data was used to construct the airway boundaries there was no attempt to determine variation in ASL height and infinite mucosal water supply was assumed in the model. Additionally, analysis was limited to one airway with unspecified air mass-flow rate. The results of this study show that both air temperature and water content are seen to increase as the air moves down the nasal cavity. The role nasal geometry plays in achieving high nasal heat and water mass transfer is demonstrated by the predicted reduction in heat and water flux during conditions where nasal tissue atrophy has occurred.

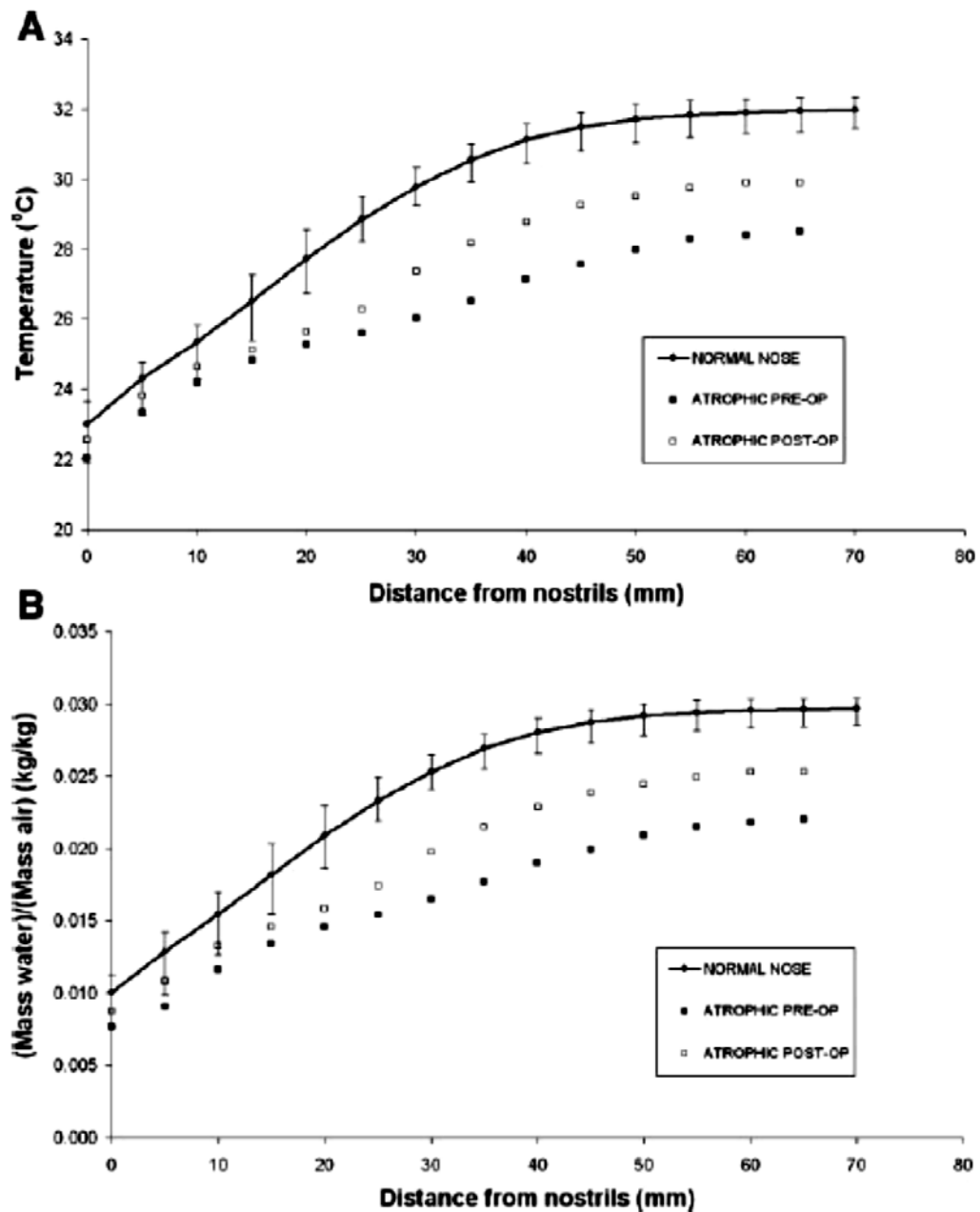


**Figure 2.31: Results of MRI based CFD nasal model. (A) Temperature distribution (B) Specific Humidity. Graphs from [189].**

Circumferential averages of heat and water flux distributions along the nasal airway are shown in Figure 2.32. Again the initial magnitude for both of these fluxes is high in the anterior nasal region, but rapidly drops off as the air moves in the posterior direction.

Despite accurately accounting for the complex nasal geometry, Garcia's CFD model did not account for mucosal ASL supply or pressure elicited change in geometry.

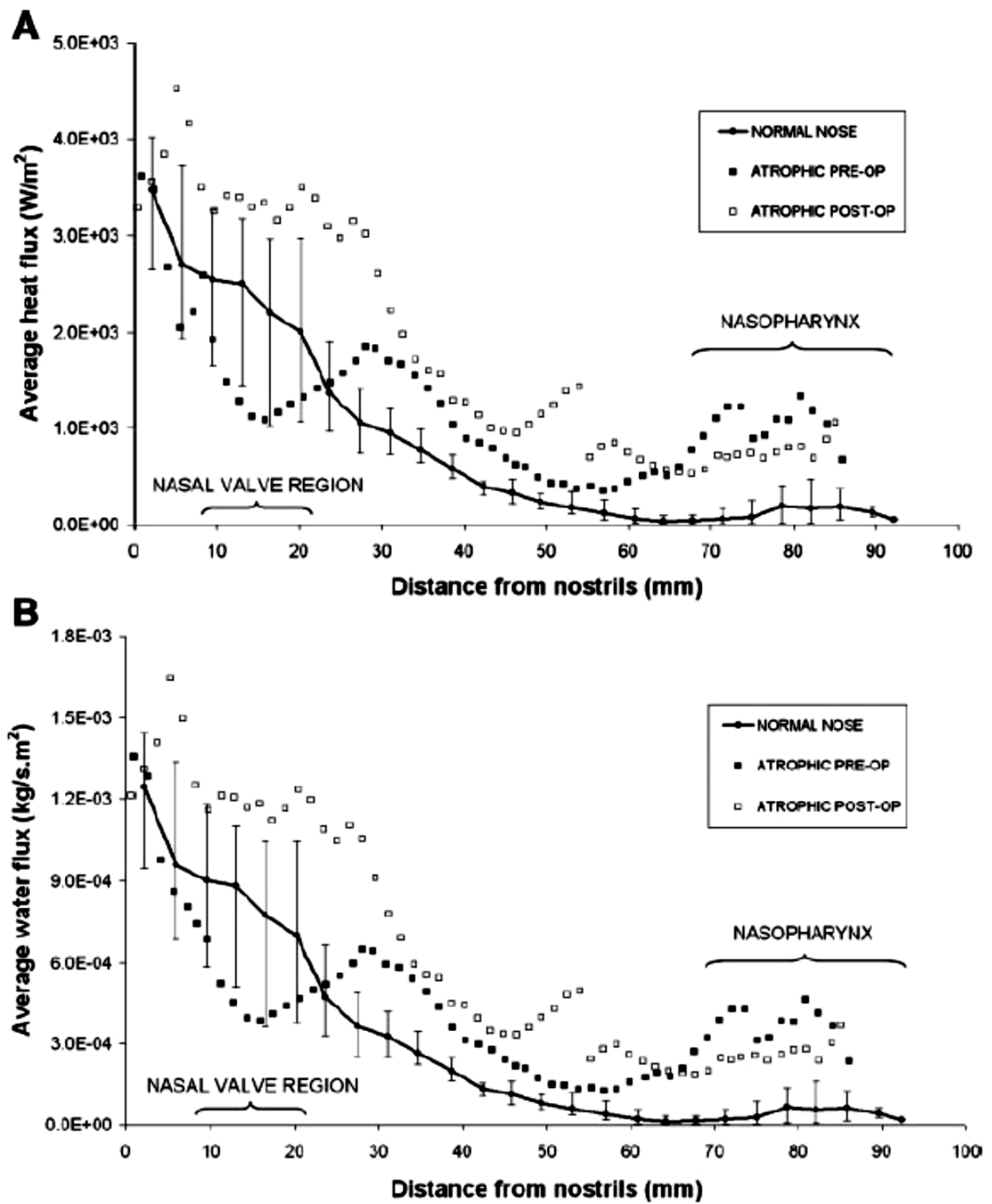


Figure 2.32: Results of MRI based CFD nasal model. (A) Average heat flux distribution. (B) Average water flux distribution. Graphs from [189].

### 2.8.2 n-PAP Air-Conditioning Model

The requirements of an n-PAP air-conditioning model present a unique situation when compared to those previously undertaken.

Interpreting complex inter-nasal morphology within a model requires careful consideration. Although 2- and then 3-dimensional computational studies utilizing simplified nose-like features have enabled the determination of local air temperature

and humidity [46, 185], it has also been shown that quasi-static one-dimensional models such as those developed by Hanna *et al.* [97, 166] and Tsu *et al.* [182] compare well to data measured by *in-vivo* studies [49].

Assumptions of constant temperature and nasal wall water vapor concentrations commonly applied to CFD models ignore the spatial and time dependent distribution occurring at the surface/air interface [195]. Whilst some CFD studies, such as Garcia *et al.* [189], have assumed constant airflow, these ignore the cyclic variation in heat and water mass flux occurring during tidal breathing [45, 76]. Complex unsteady simulations utilizing 3-D CFD models, such as that used by Naftali *et al.* [185], overcomes this issue and results support previous estimates that the nose provides 90% of the heat and water flux required to condition inhaled air over an extreme range of ambient air temperature and humidity [46]. These findings suggest that nasal air-conditioning is virtually independent of environmental conditions which is in support of previous *in vitro* studies [45].

Within the current literature there is an absence of a nasal model that accounts for the influence air mass-flow partitioning has on air-conditioning efficacy. For this work, both the nasal cycle and the effect tissue responses elicited by air pressure have on nasal air mass-flow partitioning still needs to be accounted for. Although nasal wall distention under low pressure has previously been modelled, this was used to predict collapse of the airway during forced inhalation [196]. While numerous models utilizing fixed geometry to predict airway heat and water transfer have been undertaken [97, 166, 182, 185, 189-192, 194], none have considered the influence air pressure has on variation in intra-nasal geometry and resultant change in partitioning of nasal air mass-flow between the two airways.

The assumption of infinite water supply to the mucosal surface simplifies the modeling task and has been applied in many air-conditioning simulations [76, 97, 182, 184, 185, 190-192, 197-200]. Unfortunately, this simple assumption by-passes the issue of airway mucosal drying which is of significant interest to this work. Only Tsu *et al.* [182] and Warren *et al.* [194] have previously considered ASL cellular supply. In these cases only Warren *et al.* included ASL water back-flux within the conducting airway. However, this was however undertaken from the trachea to the 10<sup>th</sup> generation of the bronchi rather than the nasal cavity [194]. Neither did Warren *et al.* consider the influence air pressure had on purinergic stress stimuli of the mucosal ASL supply.

## 2.9 Research Hypothesis

Given n-PAP therapy provides the same ambient air normally breathed but under positive pressure, abnormal airway mucosal drying is likely caused by a physiological response to air pressure rather than a change in air-conditioning demand.

With previous *in-vivo* work having already demonstrated that nasal air-conditioning efficacy is not negatively impacted by n-PAP breathing [16] any further investigation into the symptoms of nasal drying needs to consider the bigger picture. One possibility is that pressure elicited inter-nasal variation in geometry negatively influences the air-conditioning burden carried by each airway. If this were to occur, it may not by itself lead to significant change in overall air-conditioning efficacy; rather, it would negatively influence the air conditioning duty carried within each airway. Here, an increase in airflow through the congested airway will force it to undertake additional heating and humidification during a period of tissue rest and recovery [87]. This change will cause additional demand on mucosal heat and water supply within the congested airway, but may not in the short term lead to a reduction in overall air-conditioning efficiency.

The research hypothesis of this investigation postulates that n-PAP breathing elicits changes in nasal geometry and mucosal ASL water supply that negatively influences inter-nasal heat and water flux. These two alterations combine to cause abnormal ASL hydration distribution along the lengths of both nasal airways. This hypothesis can be divided into two parts:

1. The variation in geometry along the nasal cavity elicited by n-PAP breathing negatively impacts the distribution of heat and water mass flux within the two airways.
2. The increase in static pressure exerted on the airway wall during n-PAP breathing causes a reduction in ASL water supply from airway mucosa.

## 2.10 Research Plan and Objectives

There is a very strong need to identify the causes of negative symptoms associated with mucosal drying and inflammation commonly reported. Not only will this provide researchers with a better understanding of the pathophysiology associated with n-PAP breathing, but could also provide benefits to medical therapy equipment designers and patients. The current practice of using supplementary humidification to relieve

symptoms of drying adds cost as well as complexity and bulk to therapy devices. Patients are also burdened with the need for constant humidifier maintenance and the discomfort associated with breathing heavily heated and humidified air.

To understand how n-PAP breathing causes symptoms of nasal airway drying and inflammation, and develop an improvement to the current practice, it is essential to identify how n-PAP effects the distribution of ASL hydration along both nasal airways. Hence the main aims of the current research are:

- 1. To investigate the influence n-PAP has on the distribution of ASL hydration along each nasal passageway.*
- 2. To investigate and develop alternative solutions to heated humidification that return nasal ASL hydration status to that experienced during ambient air-pressure breathing.*

Three components of ASL hydration dynamics influenced by n-PAP breathing are identified;

1. inter-nasal geometry,
2. mucosal ASL water supply,
3. ASL water demand/recovery during tidal breathing.

There is a need to create an anatomically correct air-conditioning model that can include inter-nasal variation in heat and water mass convection elicited during n-PAP breathing. This would be used to predict how these interactions contribute to nasal ASL dehydration. The model would permit investigation into the differences occurring when breathing at various air-pressure states. This could lead to the development of new methodologies to improve the current practice of relieving negative symptoms through supplementary humidification.

The literature review undertaken in this chapter indicates the absence of any data, or understanding of how n-PAP breathing affects nasal geometry and mucosal ASL water supply. Additionally, there is no research or model that considers the cumulative effect that variation in water flux elicited by the breath cycle has on ASL hydration status along each of the nasal airways.

To address these issues the main research objectives are:

1. Derive a nasal air-conditioning model (Chapter 3)

The aim is to develop a new model that predicts the inter-nasal distribution of ASL hydration along both airways based on the difference between air-conditioning water demand or recovery throughout the breath cycle and mucosal net ASL water supply. This model needs to be validated with earlier *in-vivo* data and also account for variation in nasal geometry and ASL water supply elicited by n-PAP breathing.

2. Quantify change in inter-nasal geometry (Chapter 4)

The current knowledge of the nasal geometric response to n-PAP does not identify any differences occurring between patent and congested airways. Given that inter-nasal air mass-flow partitioning probably has a significant effect on the heat and water mass flux along each airway, it is important that any difference in intra-nasal geometric *in-vivo* response between each airway is quantified. An experimental investigation comparing inter-nasal geometry distribution will attempt to quantify the response of each airway during nasal breathing of pressurized air.

3. Quantify change in ASL water supply (Chapter 5)

Literature describing the two regulatory systems controlling mucosal ASL water supply has been reviewed in this chapter. Cyclic mechanical stresses generated during normal tidal breathing have been shown to play an important role in the regulation of PCL height, but there is no current knowledge on how n-PAP breathing affects this process. An experimental investigation will attempt to quantify ASL water supply suppression elicited by augmented air pressure.

4. Predict inter-nasal ASL hydration status (Chapter 6)

Accurate prediction of the cyclic fluctuations in heat and water mass demand and recovery to and from the airway mucosa is required throughout the breath cycle to enable the degree of ASL hydration along the entire length of both airways to be determined. The objective here is to introduce into the model the experimental results from the nasal geometry and ASL water supply investigations. Comparison of existing *in-vivo* air-conditioning data to model results taken at ambient pressure data will be used to validate the heat and water fluxes occurring within the nose during simulated nasal breathing. Change in

ASL hydration status will be undertaken over a range of air pressures and compared to that of ambient breathing.

5. Propose alternative to supplementary humidification (Chapter 8)

Investigate the feasibility of an alternative solution to supplementary humidification to eliminate the symptoms of nasal mucosal drying. Here the aim is to return the cyclic state of nasal mucosal ASL hydration distribution found during n-PAP breathing to that encountered when breathing ambient pressure air.

## **2.11 Closure**

The literature review of nasal air-conditioning models undertaken has found the need to account for mucosal water supply if ASL hydration status is to be predicted. Additionally, there is also the need to include the effect n-PAP breathing has on nasal airflow partitioning between each airway. Given previous modeling has not included either of these two attributes, development of an appropriate model using accurate subject-specific in-vivo morphological data to simulate conditions over multiple breath cycle is undertaken in Chapter 3.

Appraisal of the current literature corresponding to the change in nasal morphology and ASL supply has identified gaps in the current knowledge. Here, the absence of information corresponding to inter-nasal variation in geometry and suppression in mucosal ASL water supply elicited by n-PAP has initiated the investigations undertaken in Chapter 4 and Chapter 5 respectively.

## CHAPTER 3

### NASAL ASL HYDRATION MODEL

#### 3.1 Introduction

In this chapter, a new state-variable nasal model is used to predict airway surface liquid (ASL) hydration status during ambient and pressurised air breathing. This model predicts change in state variables of air temperature,  $T_a(x,t)$ , and water concentration,  $C_a(x,t)$ , along the nose as a function of both distance (a spatial dimension) and time (a temporal dimension). Although parts of this model are similar to that used by Hanna *et al.* [97, 166], it differs significantly in several aspects including:

1. Geometry based on subject specific *in-vivo* MRI image data.
2. Apportionment of inter-nasal air mass-flow based on nasal air-flow resistance.
3. Mucosal ASL water supply and reabsorption based on physiological data.
4. Water vapour species concentration calculated as a function of both temperature and pressure.
5. Calculation of state variables undertaken over a complete breathing cycle.
6. Determination of ASL hydration status is undertaken along both airways.

Additionally, heat and water mass transfer coefficients are calculated at small incremental distances along the airway, rather than interpolating the sparse empirical data obtained from cadaver studies [97, 166]. The change in model inter-nasal morphology and ASL water supply, both as a function of pressure augmentation, are also included within the model to test both parts of the research hypothesis.

Currently there are no air-conditioning or ASL hydration models that consider the effect n-PAP breathing has on geometry and ASL water supply within the nasal airway, however, various modelling strategies are available. This new model calculates water vapour and heat exchange occurring between the airway surface liquid (ASL) and air using a discretised state-variable modelling approach. It also accounts for inter-nasal air mass-flow partitioning and the affect this has on water and heat flux levels and ASL hydration.

The graphical results of this model are best presented as an animation, given both time and distance are independent variables, but, for the purposes of this work, the results are given in graphical form at discrete time ‘snapshots’ for the length,  $T_a(x)$ ,  $C_a(x) \big|_t$ .

Within this chapter, an overview of the computational model is given first in Section 3.2 before the general state-variable model structure is introduced in Section 3.3. The computational methodology and model assumptions are given in Sections 3.4 and 3.5 respectively. The state, input, intermediate and output variables are derived in Sections 3.6, 3.7, 3.8 and 3.9 respectively. The computational strategy is summarised in Section 3.10 before a means of assessing ASL hydration is discussed in Section 3.11. A listing of the model Matlab™ (MathWorks, Natick, MA, USA) code is given in Appendix A.

## 3.2 Model Overview

### 3.2.1 General Description

The purpose of this new model is to predict the change in nasal ASL hydration occurring along the length of both airways throughout the breath cycle, given the practical limitation of recording accurate *in-vivo* data, previously discussed in Chapter 2. This requires prediction of both heat ( $Q$ ) and water mass ( $m_{ASL}$ ) fluxes from the ASL liquid layer relative to airway distance ( $x$ ) and time ( $t$ ). Depending upon the breath phase, the airway mucosa responds, within defined physiological limits, by supplying or reabsorbing water in an attempt to sustain a constant level of ASL hydration.

Within the nose, thermal and water species concentration gradients exist between the ASL and air, given as the differences ( $T_{ASL}(x,t) - T_a(x,t)$ ) and ( $C_{ASL}(x,t) - C_a(x,t)$ ) respectively. At the commencement of calculations, only the state-variable boundary conditions of air temperature,  $T_a(0,t)$  or  $T_a(L,t)$ , and water species concentration,  $C_a(0,t)$  or  $C_a(L,t)$ , are known. Here, two spatial boundary conditions are given because the temperature and humidity of air entering the nose, comes from either the nasal mask during inhalation ( $x = 0$ ) or the nasopharynx ( $x = L$ ) during exhalation. The remaining variables, required for determination of the thermal and water species gradients and fluxes along the entire airway, are calculated from the deterministic input variables. These consist of the input variables of blood temperature,  $T_b(x)$ , and breath air mass flow,  $m_a(t)$ . Intermediate variables of ASL temperature,  $T_{ASL}(x,t)$ , ASL/Water species concentration,  $C_{ASL}(x,t)$ , and water flux,  $N(x,t)$  are also calculated. These vary along the lengths of both airways so state and input variables are calculated at finely discretised spatial intervals along the lengths of both nasal airways.

The magnitude of heat and water mass flux values depends upon the thermal and water species concentration gradients, and convective film coefficients. These are regulated

by air velocity so variation in concentration gradients and convective coefficients occurs as a consequence of changing air mass-flow throughout the whole breath cycle. Holding the air mass-flow at a constant value, representative of that experienced at a specific time interval of the breath cycle, simplifies this problem. This enables thermal and water species concentration gradients and flux values to be calculated along the lengths of both airways.

Consideration is given to pressure elicited change in nasal geometry to test the first part of the research hypothesis. This states variation in geometry along the nasal cavity elicited by n-PAP breathing negatively impacts the distribution of heat and water mass fluxes within the two airways. Including the affect pressure has on mucosal ASL water supply within the model enables the second part of the research hypothesis to be tested. This states that the increase in static pressure exerted on the airway wall during n-PAP breathing causes a reduction in ASL water supply from airway mucosa.

A lumped parameter approximation of a continuous model, where distance along both airways has been finely discretised, identifies three computational components that can be correlated to the nasal physiology:

1. The mucosa, where heat flows to/from the blood at temperature  $T_b(x)$  by conduction across the mucosa from/to the ASL. This layer of thickness ( $\Delta y_{ASL}$ ) and thermal conductivity ( $\kappa_t$ ) also provides and absorbs water to regulate ASL hydration status within physiological limits.
2. The ASL layer that provides a thermal and hydration buffer to heat and moisture exchange/recovery with the inhaled/exhaled air. The ASL temperature,  $T_{ASL}(x,t)$ , assumed to be equal to that of the mucosa,  $T_m(x,t)$ , regulates the water species concentration,  $C_{ASL}(x,t)$ , at the air-ASL interface. The ASL hydration status, expressed as ASL water equivalent height,  $H_{e,ASL}(x,t)$ , and described in detail in Section 3.11, is a function of the difference between the net difference of mucosal water supply/absorption and water mass flux to/from the air,  $m_{ASL}(x,t)$ .
3. The lumen that conducts the bulk air-flow at temperature  $T_a(x,t)$  and water vapour species concentration,  $C_a(x,t)$ . Here water mass flux,  $m_{ASL}(x,t)$ , and heat flux,  $Q(x,t)$ , pass between the air and ASL in a direction dependent upon thermal and water species concentration gradients.

The model predicts the instantaneous status of inter-nasal ASL hydration by equating the difference between ASL water mass loss or gain and mucosal water resupply or

absorption. This is of great interest to this work as it is likely the key to understanding why symptoms of airway drying occur during n-PAP breathing.

### 3.2.2 Accounting for Morphology

In terms of function, this model considers the interplay in airflow that occurs between both nasal airways, shown schematically in Figure 3.1. This represents an improvement in Hanna's model since it accounts for the physiological changes in inter-nasal geometry elicited during n-PAP breathing. Prediction of intra-nasal resistance for each airway enables the inter-nasal airflow partitioning ratio, a factor which influences the local heat and water mass transfer coefficients, to be calculated. Pressure elicited change in mucosal ASL water supply is also taken into account. Finally, model simulation is also undertaken over a full breath cycle.

To make the model computationally tractable, the spatial dimension is lumped into a series of connected co-axial tubes ( $k$ ) of varying hydraulic diameter as shown in Figure 3.2. Each 'lump', or segment, of thickness 0.78 mm, is taken by MRI techniques normal to the head coronal plane to provide cross-sectional area,  $A(k)$ , and perimeter,  $P(k)$ , data specific to each of the 85 airway segments.

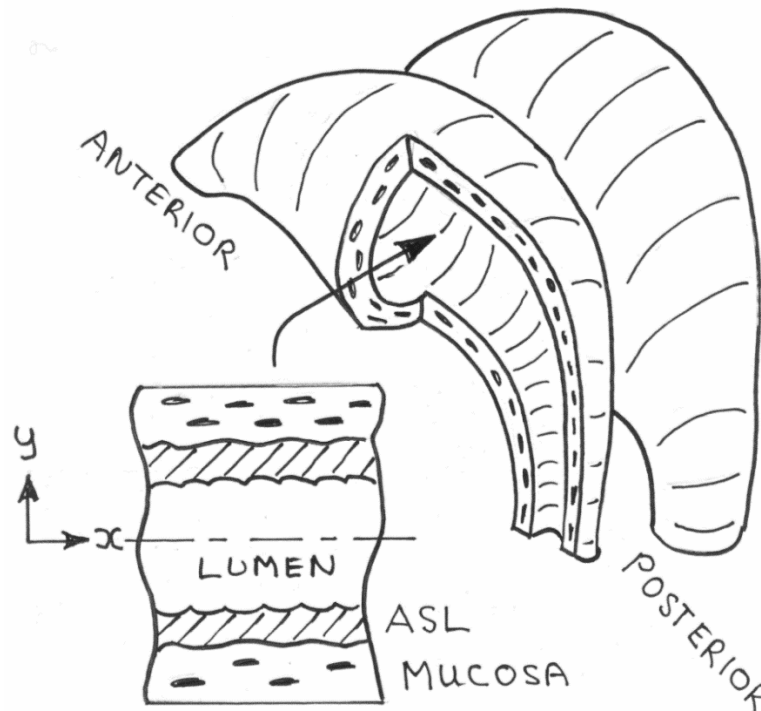


**Figure 3.1: Functional representation of the nasal airway.**

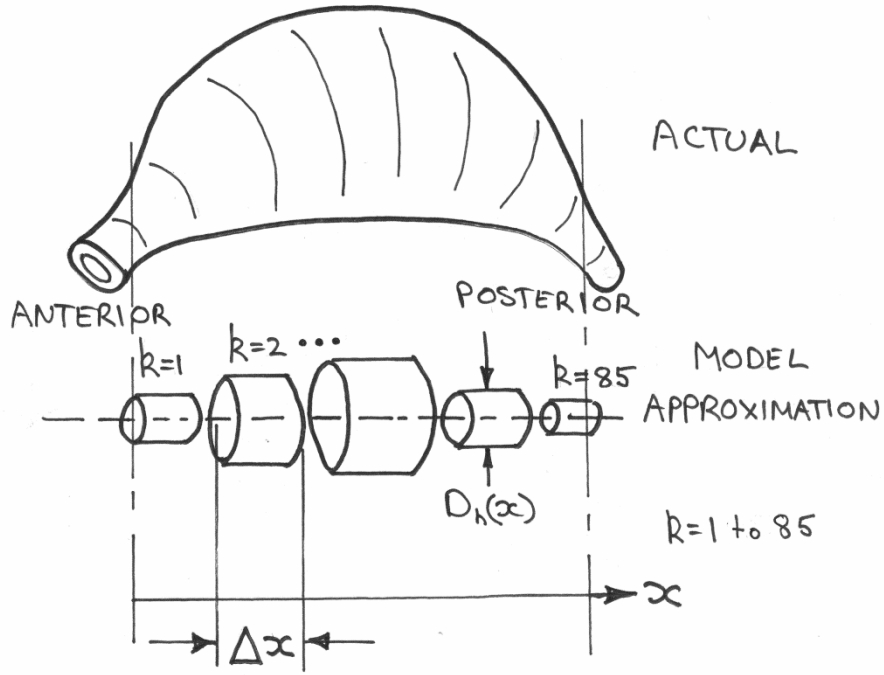


**Figure 3.2: Nasal airway represented as series of co-axial tubes of varying hydraulic diameter.**

The use of the hydraulic diameter enables the analysis of internal fluid flows when the circuits are not circular. In the case of the nasal lumen, the hydraulic diameter is used as a geometric parameter to describe the cross-sectional size. The hydraulic diameter,  $D_h(k)$ , is the characteristic dimension which correlates the airway geometry to heat and mass flux relationships [201-203] and pressure drop [204]. This term, defined as

$$D_h(k) = \frac{4A(k)}{P(k)} \quad (3.1)$$

which represents the ratio of the flow cross-sectional area,  $A(k)$ , to wetted perimeter,  $P(k)$ , perpendicular to the airflow direction.

The constant of 4 used in equation (3.1) enables a round duct to be characterised as having a hydraulic diameter the same as its physical diameter. Using the hydraulic diameter as a cross-sectional dimension also gives the same pressure drop and flow regime as that found in the original multifarious shape. Describing the two complex nasal cavities as a series ( $k$ ) of aligned tubes with a small change in local diameter represents the air-flow paths between the nares and nasopharynx.

### 3.3 State-Variable Model Development

Relationships for the two state variables of air temperature,  $T_a(k, t)$ , and water species concentration,  $C_a(k, t)$ , are derived in the following sections. These two variables contain all the information we need to calculate the system inputs of at each airway location. These are dependent upon the variables derived from blood temperature,  $T_b(k)$ , namely; ASL temperature,  $T_{ASL}(k, t)$ , ASL/air water species concentration,  $C_{ASL}(k, t)$ , and water flux,  $N(k, t)$ . Here,  $T_b(k)$  is considered an input variable.

Dropping the dependence of time ( $t$ ) from the model variables enables the two state-variables to be simultaneously solved using first-order ODEs [205]. The justifications for considering state-variables as only as a function of distance, ( $x$ ), which enables the development of the ODEs, is given later in Sections 3.6.1 and 3.6.2.

Following a standard modelling approach common in systems engineering, initial state-variable initial conditions,  $\mathbf{x}(0)$ , consisting of air temperature,  $T_a(x)$ , and water species concentration,  $C_a(x)$ , are calculated from input variables ( $\mathbf{u}$ ) of blood temperature,  $T_b(x)$  and breath air mass flow rate,  $m_a(t)$ . Intermediate variables of ASL temperature,  $T_{ASL}(x)$ , ASL/air water species concentration,  $C_{ASL}(x)$  and water flux  $N(x)$  are also calculated. Given the model fixed time step, the states of the system are defined as

$$\mathbf{x} \triangleq \left( \begin{bmatrix} T_a \\ C_a \end{bmatrix}, k \right) \quad (3.2)$$

and the external inputs are

$$\mathbf{u} \triangleq \left( \begin{bmatrix} T_b \\ m_a \end{bmatrix}, k \right). \quad (3.3)$$

A block diagram representing the nasal air-conditioning state-variable model at time step  $t$  is presented in Figure 3.4.

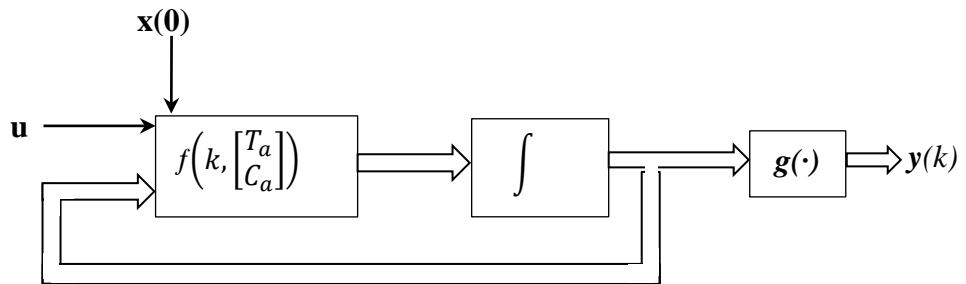


**Figure 3.3: Block diagram of nasal air-conditioning model at time step  $t$ .**

### 3.4 Computational Arrangement

#### 3.4.1 Variable Computation

The sequence by which the model simulates nasal breathing first requires the total airway geometry to be interrogated. This enables airway resistance and hence the ratio of airflow apportionment between airways to be determined. The air mass-flow rate passing down each airway is then apportioned from the total breath content read from an external data file. Section 3.7.2 discusses this breath file in more detail.

Calculations commence with the inhalation phase of the breath cycle at a time increment equal to zero seconds ( $t = 0$ ). During this phase of breathing, the order in which the airway geometry is processing is sequenced from the anterior to the posterior direction.

By way of convention, vector quantities, such as model inputs ( $\mathbf{x}$ ), and matrices, are represented by bold letters while scalar inputs such as airway segment ( $k$ ) are indicated by normal font. Quantities that change with respect to airway location are given in italic font. Starting at the first model segment ( $k = 1$ ), the model reads input variables ( $\mathbf{u}$ ) of blood temperature,  $T_b(x)$ , and breath air mass flow rate,  $m_a(k, t)$ , then simultaneously solves all three of the intermediate variables by applying nasal mask boundary conditions,  $\mathbf{x}(0)$ , of air temperature,  $T_a(k, t)$ , and humidity,  $C_a(k, t)$ . Two of the intermediate variables consist of the ASL temperature,  $T_{ASL}(k, t)$ , calculated from the incoming blood temperature,  $T_b(k)$ , tissue thermal resistance, and water species concentration directly above the ASL,  $C_{ASL}(k, t)$ . This concentration is also dependent upon ASL temperature. These two variables provide the thermal and water species concentration gradient between the air and ASL. This enables the calculation of the third intermediate variable of water flux,  $N(k, t)$ .

Change in the state-variables of air temperature,  $T_a(k, t)$ , and water content,  $C_a(k, t)$ , along the first airway segment ( $k = 1$ ) is determined by solving two ordinary differential equations (ODEs) which requires use of the previously calculated input variables.

Change in ASL hydration along the first segment is determined from the difference between water lost from the ASL to the air and that resupplied by the mucosa.

The model then increments to the next segment along the airway and repeats the calculation of the three model inputs and solving the two ODEs using the results of air temperature and water content determined from the previous segment.

Stepping along the lengths of both airways and solving all three intermediate variables of  $T_{ASL}(k,t)$ ,  $C_{ASL}(k,t)$ , and  $N(k,t)$ , as well as both state-variables of  $T_a(k,t)$  and  $C_a(k,t)$  continues for all 85 airway segments. Once this is done, the time step is incremented by 0.1 seconds and a new apportioned air mass-flow along each airway is calculated from the breath file. The model then repeats this process for all 85 airway sections along both airways before again stepping in time by 0.1 seconds until completion of the inhalation breath phase ( $t = 2$  s). At this point the model changes to process the exhalation phase of breathing. This requires the order in which the nasal geometry is sequenced to be reversed, starting now from the posterior location and moving in an anterior direction. It also requires the boundary conditions of air temperature and humidity to be changed to that found in the nasopharynx. The sequence of stepping the calculations through the model segments then incrementing time continues until the completion of the exhalation phase. A condensed pictorial representation of the model computational strategy is given in Figure 3.4. A complete description detailing the calculation of system inputs is given in Section 3.9 and also shown in Figure 3.9.

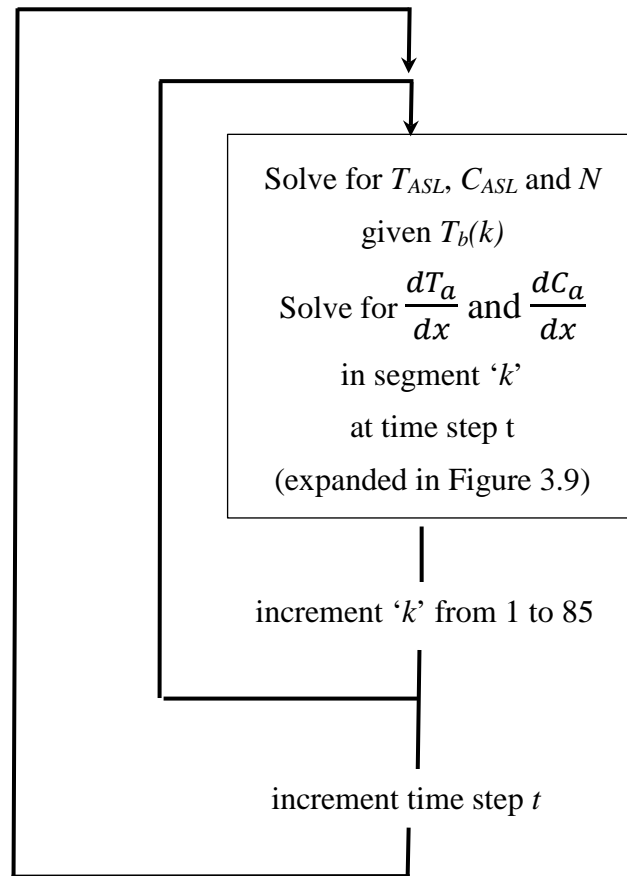


**Figure 3.4: Condensed pictorial representation of model computational strategy.**

This model improves on the previous method of interpolating sparse data from three locations and fixed air mass-flows used by Hanna [97, 166]. It also for the first time accounts for inter-nasal air mass-flow partitioning throughout the whole breath cycle

### 3.4.2 Data Storage

All state, input and intermediate variables, as well other data of interest, are stored in individual 2-dimensional matrices that are indexed in terms of spatial ( $k$ ) and temporal ( $t$ ) dimensions. As mentioned in Section 3.2.1, the state-variable boundary conditions of air temperature,  $T_a(k,t)$ , and water species concentration,  $C_a(k,t)$ , are known. This is because the temperature and humidity of air entering the nose, comes from either the nasal mask during inhalation or the nasopharynx during exhalation. A graphical representation of a data storage matrix demonstrating boundary conditions is given in Figure 3.5.

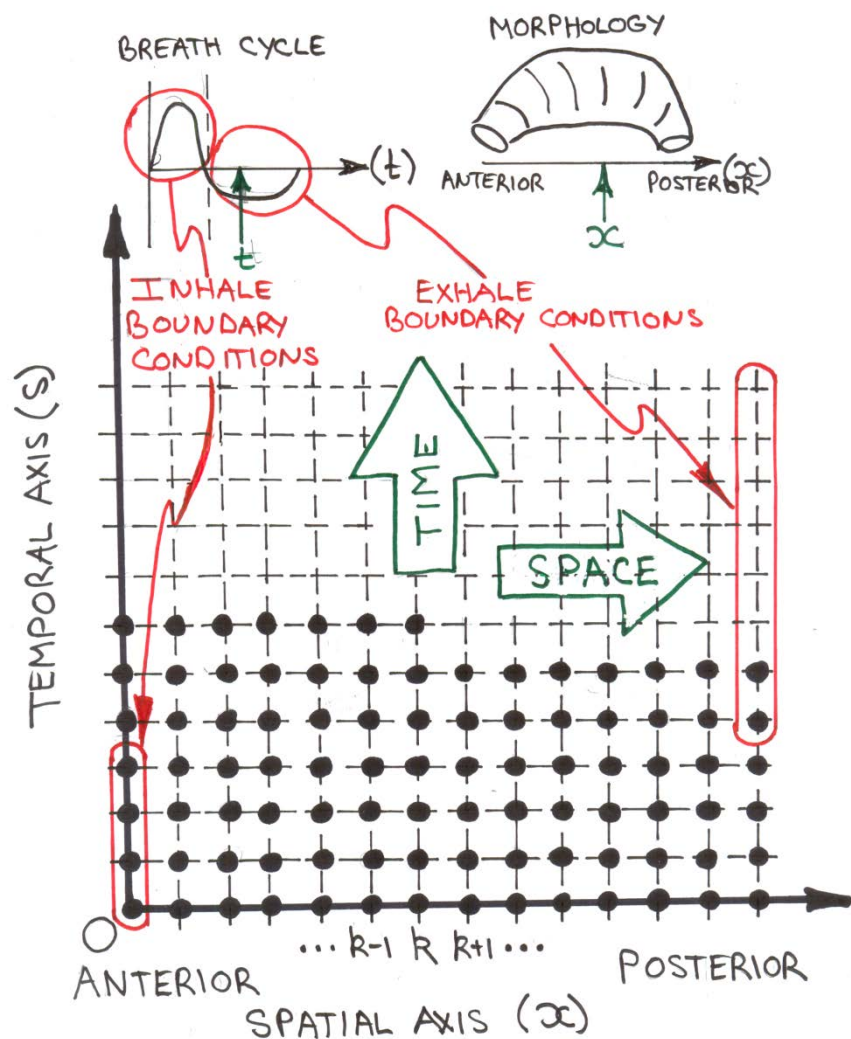


Figure 3.5: Schematic representation of model storage matrix for one data set.

### 3.5 Model Assumptions

To facilitate model development, there are a number of assumptions and simplifications made to reduce computational complexity at a manageable level whilst retaining the key characteristics of the governing processes. These include:

- Axial heat conduction along the airway is assumed to be negligible.
- Air/water vapour mixture is ideally mixed and homogeneous at the end of each position and time interval.
- Air/water vapour mixture flow is one-dimensional in an axial direction.
- Cross-sectional area is discretised across each model segment.
- ASL temperature is the same as that of the mucosa outer surface due to this layer being so thin.

### 3.6 Derivation of State-Variables

In the following sections, equations describing the model state-variables, ( $\mathbf{x}$ ), of air temperature,  $T_a(k, t)$ , and water species concentration,  $C_a(k, t)$ , are determined. The development is at a particular time,  $t$ , so the temporal index is subsequently dropped.

#### 3.6.1 Air/Water Mixture Temperature

Following Hanna's method, applying conservation of energy across a thin airway slice enables the rate of change of air/water mixture temperature,  $T_a(x)$ , to be quantified. Air entering airway segment at time step  $t$  is changed by the heat and water mass flux that occurs between itself and the ASL layer.

The sensible heat per unit area ( $q_s$ ) transferred to the air is in two forms; ASL water mass transfer and thermal convection. With regards to the former, water vapour mass transfer occurs when it leaves the ASL and is heated to the free-stream air temperature,  $T_a$ , given by:

$$q_s(k, t) = m_{ASL}(k, t)C_{p,s}(T_{ASL}(k, t) - T_a(k, t)) \quad (3.4)$$

where ASL water vapour mass flux,  $m_{ASL}(k)$ , of specific heat capacity  $C_{p,s}$  transfers energy as a consequence of the temperature gradient between the ASL and air ( $T_{ASL}(k, t) - T_a(k, t)$ ).

The latter form of sensible heat exchange is also transferred to the air from the ASL by convection, described as

$$q_s(k, t) = h_c(T_{ASL}(k, t) - T_a(k, t)) \quad (3.5)$$

where the temperature difference between the ASL and air, given as  $(T_{ASL}(k, t) - T_a(k, t))$  provides the thermal gradient to drive heat exchange in proportion to the convective heat coefficient,  $h_c(k, t)$ .

Taking an energy balance across each airway segment,  $k$ , shown in Figure 3.6, by equating the difference between in heat energy coming in and going out to heat energy stored during a time period of  $dt$ , results in

$$[\rho_a A(k) C_{p,a} T_{a,(k-1)} - \rho_a A(k) C_{p,a} \left( T_{a,(k-1)} + \frac{dT_a}{dx} dx \right) + h_c(k, t) P(k) dx (T_{ASL}(k, t) - T_a(k, t)) + m_{ASL}(t) P dx C_{p,a} (T_{ASL}(k, t) - T_a(k, t))] dt = \rho_a A(k) dx C_{p,a} dT_a \quad (3.6)$$

for  $k = 2$  through to 85.

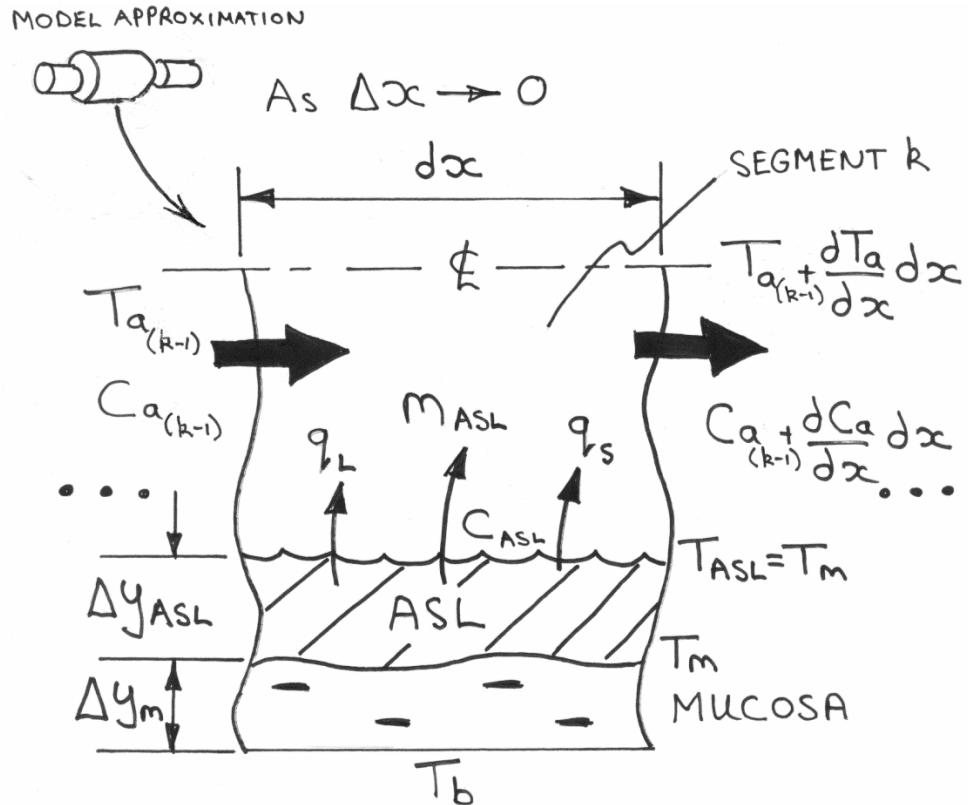


Figure 3.6: Schematic representation of one small nasal airway section  $k$  at a particular time instance,  $t$ .

Cross-sectional area,  $A(k)$  and perimeter,  $P(k)$  data, normal to the head coronal plane, provides geometry detail specific to each airway segment. The first two terms of equation (3.6) account for the change in energy of the air as it passes through the airway segment.

The third term accounts for the sensible heat gained through convective heat transfer occurring between the ASL and air while the fourth term considers the energy exchange occurring as a result of the water vapour leaving the ASL layer.

All of these energy exchanges result in the final term which expresses the net energy exchange as change in air temperature.

By assuming the mean airflow velocity,  $V_k(k,t)$ , within the segment that the ASL water mass flux,  $m_{ASL}(k,t)$ , remains constant over the small time period  $dt$  enables equation (3.6) to be simplified to

$$V_k(k,t) \frac{\partial T_a}{\partial x} + \frac{\partial T_a}{\partial t} = \left( \frac{P(k)}{A(k)} \right) \frac{1}{\rho_a C_{p,a}} \left[ h_c(k,t)(T_{ASL}(k,t) - T_a(k,t)) + m_{ASL}(k,t)C_{ps}(T_{ASL}(k,t) - T_a(k,t)) \right] \quad (3.7)$$

resulting in the air temperature,  $T_a(k,t)$ , being expressed as a function of change in location ( $k$ ) and time ( $t$ ). Substituting the hydraulic diameter definition given by equation (3.1) into the conservation of energy equation (3.7) yields

$$V_k(k,t) \frac{\partial T_a}{\partial x} + \frac{\partial T_a}{\partial t} = \frac{4}{D_h(k)\rho_a C_{p,a}} \left[ h_c(k,t)(T_{ASL}(k,t) - T_a(k,t)) + m_{ASL}(k,t)C_{ps}(T_{ASL}(k,t) - T_a(k,t)) \right] \quad (3.8)$$

where convective heat and ASL water mass fluxes, given as  $h_c(k,t)$  and  $m_{ASL}(k,t)$  respectively, influence air temperature.

Considering the relative mass and specific heat capacity between tissue, water and air and the rate in which the air mass-flow varies during the breathing cycle enables equation (3.8) to be simplified. This is done through estimation of the variation in air temperature,  $T_a$ , as a function of both change in position and time. These values suggest the rate of change of air mass flow rate along each of the nasal passageways during simulated tidal breathing is slow compared to the air temperature response times. From

this equation (3.8) is simplified by assuming a steady state airflow condition enabling the partial differentiation term corresponding to that rate of change of air temperature with respect to time disappear. This equation becomes

$$V_k \frac{dT_a}{dx} = \frac{4}{D_h(k) \rho_a C_{p,a}} \left[ h_c(k) (T_{ASL}(k) - T_a(k)) + m_{ASL}(k) C_{p,s} (T_{ASL}(k) - T_a(k)) \right]. \quad (3.9)$$

Equation (3.9) is the first of two first-order ODEs required for the state-variable nasal air-conditioning model.

### 3.6.2 Air/Water Species Concentration

Using the same approach as used in Hanna's method we are able to express the rate of change of water species concentration within the air,  $C_a(k, t)$ , contained within the control volume, shown earlier in Figure 3.6. This is done by considering conservation of mass between the liquid water and air/water mixture at time step  $t$ .

The rate of change in control volume water species concentration is determined from air velocity,  $V(k, t)$  and airway geometry of cross-sectional area,  $A(k)$  and perimeter,  $P(k)$  which are used to equate the difference between water species concentration entering and leaving the control volume, yielding

$$\left[ V_k A(k) C_{a,(k-1)} - V_k A(k) \left( C_{a,(k-1)} + \frac{\partial C_a}{\partial x} dx \right) \right] dt = P dx \partial C_a \quad (3.10)$$

where simplification produces

$$V_k A(k) \frac{\partial C_a}{\partial x} = P(k) \frac{\partial C_a}{\partial t}. \quad (3.11)$$

We can also express the rate of change in water molar species concentration per unit time, given in equation (3.11), in terms of water species concentration gradient and mass transfer coefficient ( $h_m$ ), given as:

$$\frac{\partial C_a}{\partial t} = h_m(k)(C_{ASL}(k) - C_a(k)) \quad (3.12)$$

Substituting equation (3.12) into equation (3.11) yields

$$V_k \frac{dC_a}{dx} = \left( \frac{P(k)}{A(k)} \right) h_m(k)(C_{ASL}(k) - C_a(k)). \quad (3.13)$$

Simplification, by again substituting hydraulic diameter,  $D_h(k)$ , for airway geometry of perimeter and cross-sectional area, results in the second first-order ODE required for the state-variable nasal air-conditioning model.:

$$V_k \frac{dC_a}{dt} = \frac{4}{D_h(k)} h_m(k)(C_{ASL}(k) - C_a(k)) \quad (3.14)$$

### 3.7 Derivation of Input Variables

In the following sections, model input variables (**u**) of blood temperature,  $Tb(k)$  and breath air mass flow rate,  $m_a(t)$ , are determined. These are subsequently used to calculate intermediate and output variables of ASL temperature,  $T_{ASL}(k)$ , ASL water vapour species concentration at the ASL-air interface,  $C_{asl}(k)$ , and ASL molar water flux,  $N(k)$ .

#### 3.7.1 Blood Temperature Distribution

There are three possible heat sources within the nose: metabolic heat production, conductive heat from surrounding tissue and heat carried by in-flowing blood [166]. Both metabolic and conductive heat sources to the nasal cavity are considered to be small, given the significant sinus cavities and bone structure surrounding this region. This leaves blood in-flow as the primary source of heating within this region. Many variables influence nasal blood temperature distribution since the vascular system responds to external stimuli, such as external temperature change [172, 173], physical exertion [206, 207], body position [208, 209], sleep/awake status [89, 210] or other

forms of autonomic system stimuli [78]. Because of the difficulty in obtaining accurate axial intra-nasal blood temperature distribution, previous researchers have determined that this parameter approximates to be within 0.1°C of the mucosal temperature. This approximation is justified for use in this model given the thin vascular/epithelial wall thickness [166] and its relatively low tissue thermal resistance [211].

Adding to Hanna's model, the intra-nasal blood temperature distribution,  $T_b(k)$  is based on *in-vivo* nasal mucosal temperature data but varies along the length of the airway. The intra-nasal blood temperature distribution used within the model is a linearised representation of the *in-vivo* nasal mucosal temperature found by earlier investigations [49, 50, 73], that found it to increase from 30°C at the anterior nasal valve region to 34°C at the posterior choanae. This is modelled as a function on non-dimensional airway length ( $x/L$ ) that does not change with time. Here, the specific distance along airway ( $x$ ) is expressed as a ratio of the total airway length ( $L$ ) to account for inter-participant variation in nasal geometry and for consistency with earlier investigations [97, 166]. The positive temperature gradient experienced by inhaled air is determined as a function of airway position ( $x/L$ ), given in equation (3.39).

$$T_b(k) = 30 + 4\left(\frac{x}{L}\right) \quad (^\circ\text{C}) \quad (3.15)$$

### 3.7.2 Breath Cycle

Inclusion of a simulated human nasal tidal breathing brings the ability to correlate the rate of change of air mass-flow and consequential heat and water flux levels with rates of ASL water and heat supply or reabsorption.

The variance between the rates of supply and demand enables the rate and hence severity of ASL dehydration (represented in terms of duration and distance along airway) to be computed.

While it is not possible to account for inter-participant variation in tidal breathing volume and frequency as discussed in Section 2.6, for the purposes of this work, the tidal air mass-flow,  $m_a(t)$ , measured from an adult nasal breathing at rest [212], presented in Figure 3.7, will be implemented within the model. As mentioned earlier, this will be done for discrete time intervals ( $t$ ).

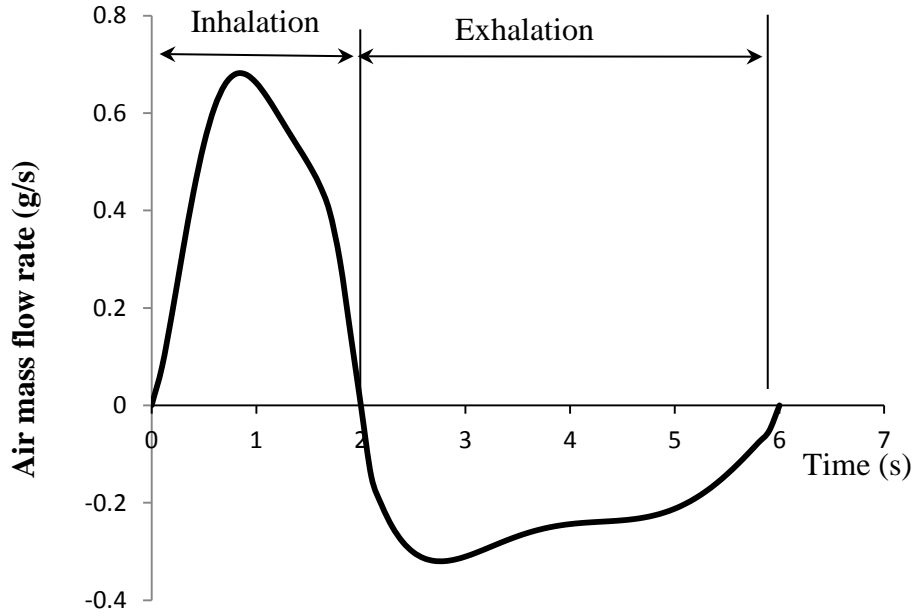


**Figure 3.7: Adult at-rest single breath air-mass-flow, data from [212].**

It is believed that this model treats the nasal airways for the first time as separate passages with each simultaneously sharing a portion of the total breathing mass-flow rate. This is achieved by modelling the nasal airways as a series/parallel resistance network [213], as shown by Figure 3.8.

### 3.8 Derivation of Intermediate Variables

Model parameters regulating heat and water mass flux convection coefficients are dependent upon airway geometry, air fluid properties and airflow regime. All of these intermediate variables are influenced by air mass flow rate which varies as a consequence of tidal breathing and airflow partitioning between the two nasal airways. The methods by which these coefficients are determined are summarised in the following sections.

#### 3.8.1 Inter-Nasal Air Mass-Flow Partitioning

Determination of the resistance to air mass-flow within each airway lump ( $k$ ) requires a number of calculations to be undertaken. This involves three equations governing fluid friction factor,  $f(k)$ , flow regime as predicted by the Reynolds number,  $Re_d(k)$ , and mass continuity are combined with Darcy's equation to predict pressure loss per unit air mass-flow.

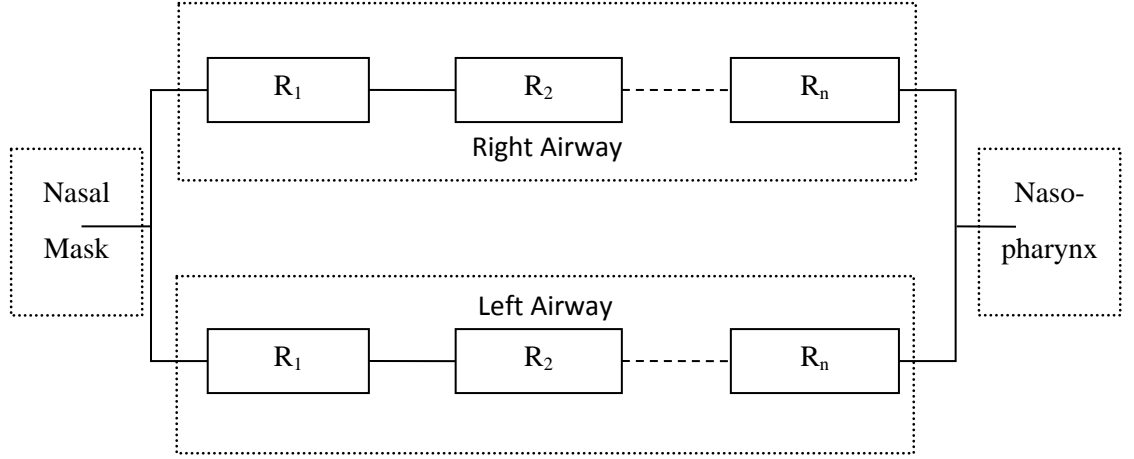


**Figure 3.8: Symbolic representation of nasal series/parallel resistance network.**

Here, the air-flow friction factor,  $f(k)$ , is modelled from an empirical relationship found for two closely spaced plates of infinite length during laminar airflow is given by [121].

$$f(k) = \frac{24}{\text{Re}_d(k)}. \quad (3.16)$$

This is justified by much of the distance between the opposing airway walls not exceeding 3 mm and previous investigations having found that laminar flow occurs throughout most of the nose during peak at-rest air mass-flow [214, 215].

The Reynolds number, based on hydraulic diameter,  $\text{Re}_d(k)$ , given by

$$\text{Re}_d(k) = \frac{\rho V(k) D_h(k)}{\mu}, \quad (3.17)$$

indicates the ratio of inertial to viscous forces [204], where  $\mu$  is the air dynamic viscosity.

The mass continuity equation is given by [204]

$$m_{air}(k) = \rho A(k)V(k) \quad (3.18)$$

which when substituted into equations (3.17) and (3.16) and expressing hydraulic diameter,  $D_h(k)$ , in terms of airway cross-sectional area and perimeter, given as  $A(k)$  and  $P(k)$  respectively, yields

$$f(k) = \frac{6\mu P(k)}{m_{air}(k)} \quad (3.19)$$

Considering Darcy's equation [204];

$$h_f(k) = \frac{f(k)lV^2}{2gD_h(k)} \quad (3.20)$$

where  $l$  represents airway length under consideration, an expression for calculating the airway resistance,  $R(k)$ , within each model lump in terms of pressure head loss,  $h_f(k)$ , per unit air mass-flow,  $m_a$ , can be found. This is done by dividing equation (3.20) by (3.18) to yield;

$$R(k) = \frac{h_f(k)}{m_a} = \frac{3\mu P(k)^2 l}{4\rho^2 A(k)^3 g}. \quad (3.21)$$

The total resistance of each airway is found from summing the resistance of all sections along each airway. Ignoring any difference in potential energy, the total nasal resistance,  $R_{total}$ , can now be found by considering the airways as a parallel resistance network [204, 213]. Each comprising of a number of resisting segments in series, given by

$$\frac{1}{R_{total}} = \frac{1}{\Sigma R_{left}} + \frac{1}{\Sigma R_{right}}. \quad (3.22)$$

The air mass-flow partitioning ratio ( $PR$ ) for each airway can now be determined as a ratio of the total tidal air mass-flow rate by expressing the ratio of total airway resistance to the sum of resistances found in each passageway, given in equations (3.21) and (3.22) for the left and right airways respectively.

$$PR_{left} = \frac{R_{total}}{\Sigma R_{left}} \quad , \quad PR_{right} = \frac{R_{total}}{\Sigma R_{right}} \quad (3.23)$$

### 3.8.2 Convective Heat and Mass Transfer Coefficients

Hanna's model relied on empirically derived heat and mass transfer coefficients. This model uses airway geometry and fluid properties based on pressure and temperature at each lump to determine these coefficients. During heat transfer, the Prantl number ( $Pr$ ) describes the ratio of air dynamic viscosity ( $\nu$ ) to thermal diffusivity ( $\alpha$ )

$$Pr = \frac{\nu}{\alpha} \quad (3.24)$$

and is used in the empirical relationship to predict the dimensionless Nusselt number,  $Nu(k)$ , a ratio of heat transfer coefficients. This is done by assuming laminar flow through two closely spaced plates of infinite length along flow-path distance  $l$  [121], given as

$$Nu(k) = 7.54 + \frac{0.03 \left( \frac{D_h(k)}{l} \right) Re_d(k) Pr}{1 + 0.016 \left[ \left( \frac{D_h(k)}{l} \right) Re_d(k) Pr \right]^{\frac{2}{3}}} \quad (3.25)$$

This assumption is justified by much of the distance between the opposing airway walls not exceeding 3 mm and previous investigations having found that laminar flow occurs throughout most of the nose during peak at-rest air mass-flow [214, 215]. Once found, the Nusselt number can then be applied to yield the convective heat transfer coefficient,  $h_c(k)$ , by considering the thermal conductivity of air ( $k_{t,a}$ ) and airway length under consideration ( $l$ ) [216] as given by

$$h_c(k) = \frac{Nu(k)k_{t,a}}{l}. \quad (3.26)$$

The heat and mass convective transfer governing equations are analogous [211, 216]. This enables prediction of the mass transfer coefficient,  $h_m(k)$ , from that of heat transfer,  $h_c(k)$ , for the same segment. This is done through use of the Lewis number ( $Le$ ) which represents the ratio of thermal to species concentration boundary thickness and is calculated from the ratio of the air/water binary diffusion coefficient ( $D_{ab}$ ) to air thermal diffusivity ( $\alpha$ ), given in equation (3.27) [216].

$$Le = \frac{\alpha}{D_{ab}} \quad (3.27)$$

The Lewis number can be used to calculate the Sherwood number,  $Sh(k)$ , a ratio of convective to diffusive transport used in convective mass transfer. This is achieved by factoring the Nusselt number,  $Nu(k)$ , found by equation (3.25) by the Lewis number calculated in equation (3.27) to yield;

$$Sh(k) = LeNu(k) \quad (3.28)$$

The Sherwood number can then be used to determine the convective mass transfer coefficient,  $h_m(k)$ , by considering the air/water binary diffusion coefficient ( $D_{ab}$ ) and airway length under consideration ( $l$ ).

$$h_m(k) = \frac{Sh(k)D_{ab}}{l} \quad (3.29)$$

### 3.9 Derivation of Output Variables

#### 3.9.1 Airway Surface Liquid Temperature

Water evaporating from the ASL surface leads to latent heat,  $q_l(k)$ , exchange per unit area occurring between this layer and the free-stream air, given as

$$q_l(k) = m_{ASL}(k)h_{fg} \quad (3.30)$$

where the energy per unit mass required for phase change,  $h_{fg}$ , is factored into the water mass flux per unit area,  $m_{ASL}(k)$ .

Applying the same methodology as Hanna and using conservation of energy principles enables the energy flow through the ASL to be determined. This is done by taking an energy balance across an ASL section, previously shown in Figure 3.6. The incoming energy sourced from blood at temperature  $T_b(k)$  through mucosal tissue of thermal conductivity  $k_m$  and thickness  $\Delta y_m$  is compared to latent heat lost ( $h_{fg}$ ) by ASL water mass transfer,  $m_{ASL}(k)$ , and sensible heat lost by convective heat transfer,  $h_c(k)$ . This is driven by the temperature gradient existing between the ASL and air,  $(T_{ASL}(k) - T_a(k))$ , to yield

$$\left[ P(k)dx \frac{k_m}{\Delta y_m} (T_b(k) - T_{ASL}(k)) - m_{ASL}(k)h_{fg} P(k)dx - h_c(k)P(k)dx (T_{ASL}(k) - T_a(k)) \right] dt = \rho_{ASL} \Delta y_{ASL} dx C_{p,ASL} dT_{ASL} \quad (3.31)$$

where ASL temperature,  $T_{ASL}(k)$ , is considered the same as that of the mucosa,  $T_m(k)$ , due to the extremely thin ASL layer present. Further simplification yields

$$\frac{dT_{ASL}}{dt} = \frac{P(k)}{\rho_{ASL} \Delta y_{ASL} C_{p,ASL}} \left[ \frac{k_m}{\Delta y_m} (T_b(k) - T_{ASL}(k)) - m_{ASL}(k)h_{fg} - h_c(k)(T_{ASL}(k) - T_a(k)) \right]. \quad (3.32)$$

Simplification of this equation can now be undertaken using the same justification as that used for calculating the air/water mixture temperature in equation (3.9). This is based on the change in ASL temperature being relatively slow compared to that of the air/water mixture temperature and water flux response times. This enables the rate of change of ASL temperature with respect to time to disappear from equation (3.18), yielding

$$\frac{k_m}{\Delta y_m} (T_b(k) - T_{ASL}(k)) = h_c(k)(T_{ASL}(k) - T_a(k)) + m_{ASL}(k)h_{fg} \quad (3.33)$$

which equates heat energy passing to the ASL from the mucosa to heat leaving this layer into the air, by convective sensible and latent heat loss.

### 3.9.2 ASL-Air Interface Water Species Concentration

The influence change in air pressure,  $P$  and ASL temperature  $T(k)$  has on water species concentration at the ASL-air interface is now undertaken. This is an extension to Hanna's model.

The first stage involves calculating the water saturation vapour pressure,  $P_{st}(k)$ , as a function of temperature,  $T(k)$ , using the Goff-Gratch correlation

$$\log_{10} P_s(k) = -7.9.298 \left( \frac{T_{st}(k)}{T(k)} - 1 \right) + 5.02808 \log_{10} \left( \frac{T_{st}(k)}{T(k)} \right) - 1.3816 \times 10^{-7} \left( 10^{11.344 \left( 1 - \frac{T(k)}{T_{st}(k)} \right)} - 1 \right) + 8.1328 \times 10^{-3} \left( 10^{-3.49149 \left( \frac{T_{st}(k)}{T(k)} - 1 \right)} - 1 \right) + \log_{10} P_{st} \quad (3.34)$$

where  $T_{st}(k)$  represents the saturation temperature,  $P_{st}$  the saturation pressure and  $T(k)$  the reference temperature [217].

The second stage of this process involves the total pressure,  $P_t$ , and saturation pressure,  $P_s(k)$ , calculated by equation (3.34), enabling the humidity ratio,  $\omega(k)$ , to be determined in terms of mass of water per unit mass dry air

$$\omega(k) = \frac{0.622 P_s(k)}{P_t - P_s(k)}. \quad (3.35)$$

Combining the results of (3.35) with air density ( $\rho_a$ ) interpolated from published data [202] and dividing by the molar density of water ( $M$ ) in mol/g yields the water molar concentration at the ASL/air interface

$$C_{ASL}(k) = \frac{\omega(k) \rho_a}{M}. \quad (\text{mols/mm}^3) \quad (3.36)$$

Given the distribution of water vapour molar concentration,  $C_{ASL}(k)$ , at the ASL/air interface is only mildly non-linear with respect to temperature; equation (3.36) is solved over a temperature range of 28 °C to 36 °C. A linear best fit for water vapour molar concentration is used to calculate water vapour molar concentration.

### 3.9.3 Water Flux

The water mass flux between the liquid ASL water lining the airway and the air/water vapour is driven by the water species concentration gradient between the ASL and air ( $C_m(k) - C_a(k)$ ) and convective mass-transfer coefficient,  $h_m(k)$ . With reference to Figure 3.6 and following Hanna's method, ASL water molar flux,  $N(k)$  can be expressed as

$$N(k) = h_m(k)(C_{ASL}(k) - C_a(k)). \quad (3.37)$$

In terms of ASL water mass flux,  $m_{ASL}(k)$ , this can be expressed in units of the same order of magnitude as that used by previous investigators, given by

$$m_{ASL}(k) = \frac{MN(k)}{3600} \quad (\text{g/cm}^2 \cdot \text{hr}) \quad (3.38)$$

where the molar mass of water,  $M$ , is used to convert the flux rate to grams per second.

### 3.10 Computational Strategy

The nasal air-conditioning model consists of a series of five linked governing equations. Two of these are ODEs form the state-variables of air temperature and water species concentration, given by  $T_a(k)$  and  $C_a(k)$  respectively, given by equations (3.9) and (3.14) respectively. System inputs variables are blood temperature,  $T_b(k)$ , given by equation (3.15) and air mass flow,  $m_a(t)$ , described in Section 3.7.2. System outputs of water species concentration at the ASL/air interface,  $C_{ASL}(k)$ , ASL temperature,  $T_{ASL}(k)$ , and molar water flux,  $N(k)$  are described in equations (3.36), (3.33) and (3.37). The inter-relationship between the model state and input variables, and supporting calculations for heat and mass transfer coefficients, breath cycle air mass flow and inter-nasal flow partitioning is graphically presented in Figure 3.9.

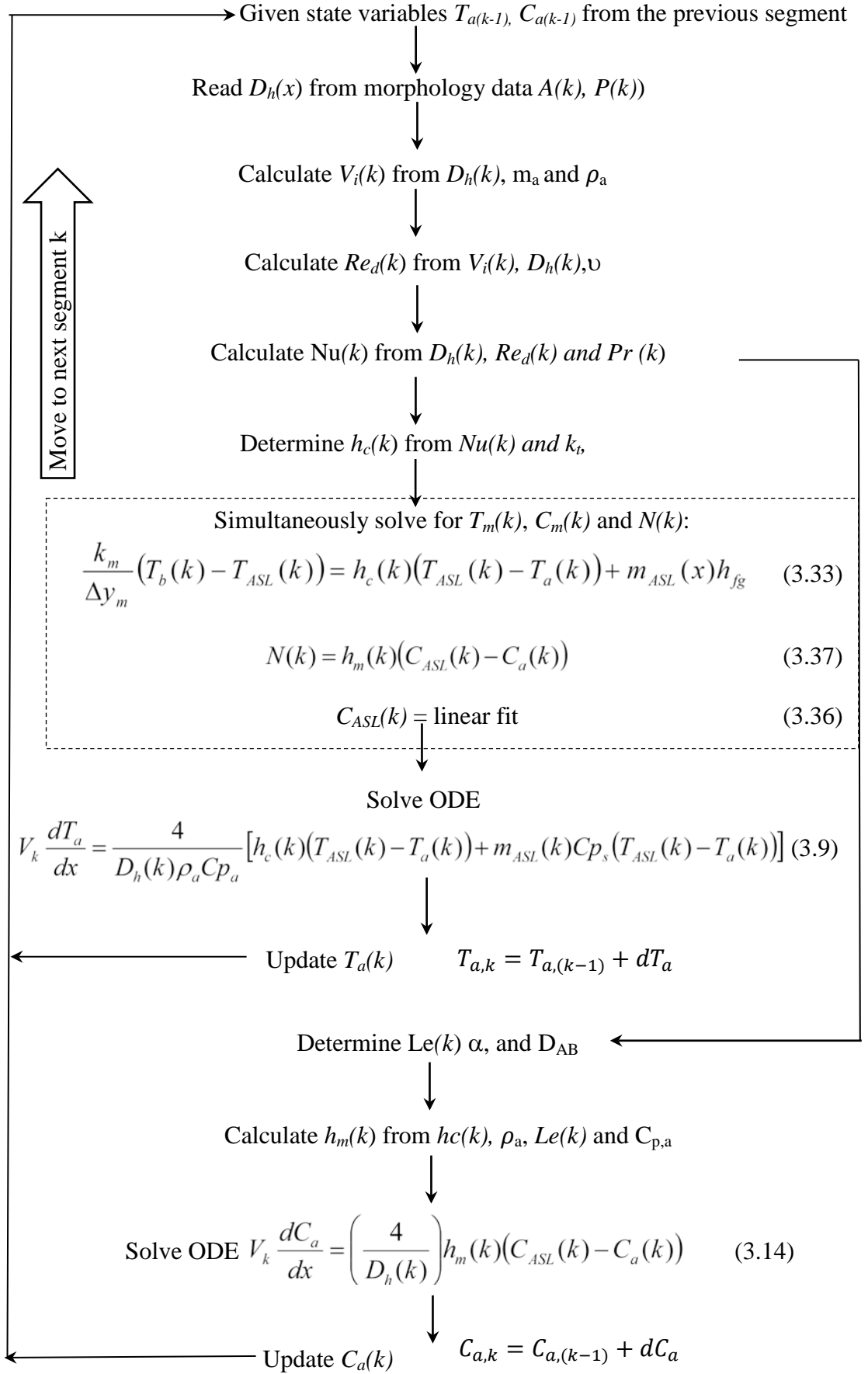


**Figure 3.9: Expanded flow diagram of nasal air-conditioning model for segment  $k$  at time step  $t$ .**

### 3.11 ASL Water Equivalent Height

Adding to Hanna's model, a method by which ASL hydration status can be assessed is now developed. This is done by first considering the normal ASL *in-vivo* hydration/dehydration limits, as discussed in Section 2.4.6. Variation in ASL height, caused by change in hydration status provides a convenient means to correlate water content to ASL height status. Here, an 85% water volume reduction occurs between normal and severe dehydration states and causes the PCL layer to vary by 53% or 4  $\mu\text{m}$  in height [109].

Approximating the osmotic bulk modulus of the PCL ( $K_{PCL}$ ) as being twice that of the mucus ( $K_{mucus}$ ) means the PCL layer experiences half the water loss as that of the mucus layer over the same dehydration range. Over these conditions, the change in mucus layer height (8  $\mu\text{m}$ ) is twice that experienced by the PCL (4  $\mu\text{m}$ ) to yield a total ASL height variation of 12  $\mu\text{m}$ . This height variation can then be equated to an 85% water volume loss during mucus dehydration [109] to yield a variation in ASL water equivalent height ( $H_{e,ASL}$ ) of 10  $\mu\text{m}$  that differentiates between the normal ( $H_{e,ASL} = 10 \mu\text{m}$ ) and severely hydrated ( $H_{e,ASL} = 0 \mu\text{m}$ ) ASL states.

To aid the explanation of this concept,  $H_{e,ASL}$  simply represents the equivalent water volume, in terms of height per unit area, removed from normally hydrated binary layered ASL, to achieve a state of severe mucus and PCL dehydration, characterised by loss of PCL height and cessation of mucociliary transport. This relationship is demonstrated in Figure 3.10.

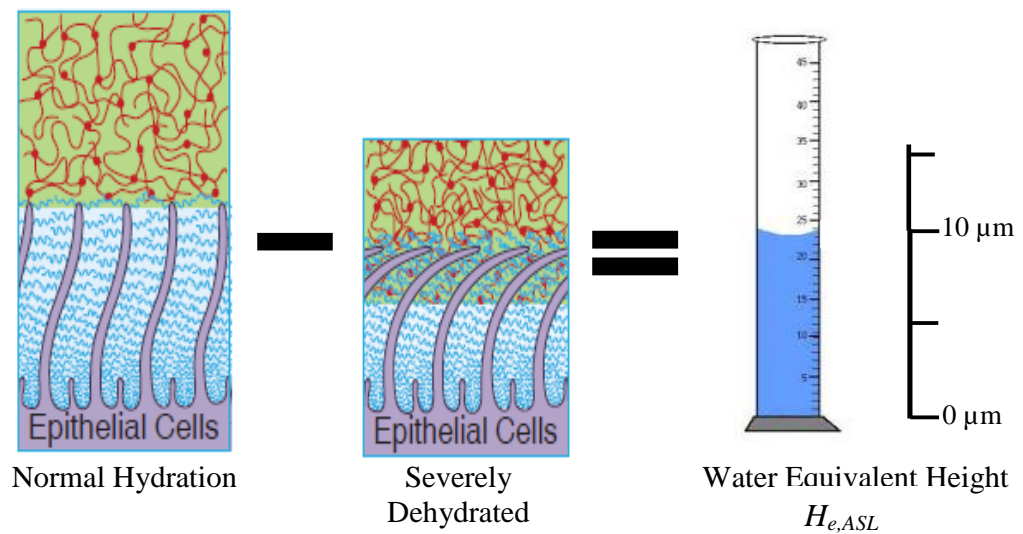


**Figure 3.10: Schematic representation of ASL water equivalent height of 10  $\mu\text{m}$  representing the hydration difference between normal and severely dehydrated ASL. Diagram adapted from [109].**

Within the nasal ASL hydration model, variation in water equivalent height along either airway resulting from the interplay between ASL fluid supply/reabsorption and air-conditioning water demand/recovery flux,  $N(k)$ , serves as an indicator of the instantaneous ASL hydration state.

### **3.11.1 ASL Height Regulation**

The calculation of ASL hydration within the model is based on the physiological supply and demand sources reviewed in Chapter 2. From the definition given in the previous section, mucosal water supply acts in maintain the ASL water equivalent height at 10  $\mu\text{m}$  during periods of water demand or recovery.

During periods of inhalation, where water demand exceeds the cellular maximal supply, the ASL water equivalent height reduces and ASL dehydration occurs. During this situation when the ASL becomes fully dehydrated, water availability for air-conditioning is limited to that of mucosal maximal supply.

During exhalation, moisture condenses causing ASL re-hydration. Under these conditions the ASL water equivalent height may increase beyond 10  $\mu\text{m}$ . When this occurs, the mucosa responds to re-absorb the excess water to try and maintain normal ASL hydration. There is a limit to the amount of water the mucosa can re-absorb and when this is exceeded the ASL becomes over-hydrated. This is demonstrated by the ASL water equivalent height exceeding 10  $\mu\text{m}$ .

## **3.12 Closure**

A one dimensional state variable nasal ASL hydration model has been derived that for the first time accounts for change ASL water hydration over the breath cycle during simulated ambient and n-PAP breathing.

As postulated by the research hypothesis, the two attributes of variation in morphology along the nasal cavity and diminished ASL water supply, both acting in response to n-PAP breathing, are included in the new model. It is now necessary to characterise these air-pressure dependent geometric and water supply behaviours prior to execution of the model within the Matlab environment. This is undertaken in Chapters 4 and Chapter 5 respectively.

## **CHAPTER 4**

### **GEOMETRICAL RESPONSE TO n-PAP BREATHING – AN MRI INVESTIGATION**

#### **4.1 Introduction**

In Chapter 2 it was hypothesized that the change in morphology along each nasal passageway differs between the two nasal passageways during n-PAP breathing, leading to disruption of the normal air-mass-flow partitioning between these two airways. This change could be elicited by change in blood-flow to nasal erectile tissue and may disturb the normal airflow partitioning between these two airways. The purpose of this chapter is to test this hypothesis and determine the inter-nasal morphological response during n-PAP breathing. In the course of this investigation, nasal morphology and blood flow images were acquired from human subjects using MRI scanning techniques during spontaneous breathing of ambient and then pressurised air. This data will also be used as an input into the model.

The experiment was undertaken at the Centre for Advanced MRI (CAMRI), University of Auckland, New Zealand. MRI protocols for the measurement of nasal blood flow using arterial spin labelling techniques had to be developed as this technique had not previously been undertaken under these circumstances. These included the MRI focus on the nose and the requirement for the subject to be undertaking n-PAP breathing during MRI acquisition.

Participant recruitment is discussed in Section 4.2 followed by a description of the nasal cycle measurement equipment and protocol in Section 4.3. Results are overviewed in Sections 4.4 before the nasal cycle, combined and inter-airway geometric results are each discussed in Sections 4.5, 4.6 and 4.7 respectively. Inter-nasal blood-flow results are discussed in Section 4.8. Conclusions are made in Section 4.9.

#### **4.2 Participant Recruitment**

##### **4.2.1 Ethical Approval**

Ethical approval was granted by the Auckland University of Technology Ethics Committee (AUTEC) under application number 10/121 on the 14<sup>th</sup> of July 2010.

Copies of the AUTECH application, supporting documents as well as CAMRI MRI safety and consent forms can be found in Appendix B2.

#### **4.2.2 Participant Selection and Preparation**

Due to the limited MRI time that would be available, it was decided that a maximum of 8 test-runs could be performed. Four male and four female healthy non-smoking adult volunteers, of mixed ethnicity and ages ( $32 \pm 11$  yr) with no prior history of upper airway disease, were chosen for this study, with each participant giving written informed consent. Each participant undertook a visual nasal internal examination by an Ear, Nose and Throat Specialist to ensure the absence of morphological abnormalities such as significantly displaced septum, mucosal inflammation or other nasal pathological conditions. None of the participants had received any form of medication or had consumed food for 2 hours prior to scanning. Additionally, they had not consumed alcohol for 24 hours prior to testing. Appendix B1 contains further information related to participant recruitment, demographic distribution and preparation for imaging.

### **4.3 MRI Protocol and Data Processing**

A summary of the MRI protocol and methodology of data acquisition is presented in the following sections. Further information can be found in Appendix B1.

#### **4.3.1 Nasal Cycle Measurement**

Immediately prior to scanning, all participants undertook a maximal nasal ventilation test using two customized spirometers. These were modified with tailored adaptors that prevented nasal tissue distortion at the nares and measured each nasal passageway separately. This test was performed to determine which was patent, and which was congested. The test was repeated directly upon conclusion of MRI scanning to ascertain if changes in their nasal cycle status had occurred during the image acquisition period. Nasal cycle status was further confirmed during analysis of MRI geometrical data.

#### **4.3.2 Air Pressure Protocol**

One male and one female participant were each allocated an n-PAP setting ranging from 6 to 15 cm H<sub>2</sub>O in 3 cm H<sub>2</sub>O intervals (i.e.: 6, 9, 12 and 15 cm H<sub>2</sub>O).

#### **4.3.2.1 Ambient Air Breathing**

In each case, the first set of images were acquired whilst the participant spontaneously breathed ambient air within the MRI scan room, air-conditioned to be within the range of  $23 \pm 0.5$  °C and 50% RH. Each participant was wearing a nasal mask (Fisher & Paykel Healthcare, Zest Plus) with the air supply hose disconnected at the mask to enable unrestricted breathing of ambient air. Under these conditions two scan sequences were undertaken:

1. Acquisition of morphological image data, taking approximately 7 minutes.
2. Acquisition of blood-flow image data, taking approximately 13 minutes.

#### **4.3.2.2 Positive Air-Pressure Breathing**

Upon completion of initial MRI image acquisition with ambient air-pressure breathing, an air supply hose was connected to the nasal mask and the participant commenced n-PAP breathing with air supplied from a commercially available CPAP air supply unit (Fisher & Paykel Healthcare, HC232 'Sleepstyle'). This unit was located outside the RF screened scan room to avoid interference with the MRI scanner, but was open to the same air-conditioning regulation. This ensured that air at the same temperature and humidity was breathed during ambient and pressurised conditions.

For both patient comfort and to eliminate any transient physiological response, the CPAP air supply unit was pre-set to gradually increase pressure so that it took 20 minutes to achieve the desired nasal mask pressure. During this time period the participant remained relaxed in the supine position within the MRI scanner. Supplementary humidification was not supplied to the pressurised airstream, as this could create a confounding tissue reaction to heated air [12]. Upon completion of this 20 minute settling period, the second phase of image acquisition was undertaken. Here, during spontaneous n-PAP breathing, the same two scan sequences were undertaken over the same time period as previous.

Upon completion of all image acquisition sequences the head coil was removed before the participant sat up, had the nasal mask removed and undertook a second nasal airflow measurement test, as detailed in Section 4.3.1.



**Figure 4.1: Participant wearing CPAP nasal mask in recumbent position within MRI scanner with head coil fitted.**

### **4.3.3 MRI Protocol**

All volunteers were studied in the supine position using head array coil in a 3-tesla scanner (Siemens Magnetom Skyra). The participant's head was firmly positioned through the use of foam wedges before the head coil was locked into position, shown in Figure 4.1. Each participant was initially given 10 minutes to settle into the MRI scanner environment before scanning commenced. This time period also allowed blood flow throughout the body to adjust and stabilize [209]. MRI image acquisition occurred during ambient and n-PAP breathing, as detailed in the previous sections. All MRI sequences acquired image data for the entire head between the ears and above the neck.

#### **4.3.3.1 Region of Interest**

All analysis of nasal physiological parameters was undertaken on coronal scan data spanning the region of interest (ROI) bounded by the anterior portion of the nasal valve to the posterior choana, shown in Figure 4.2. As mentioned, this bifurcated portion of the conducting airway undertakes the majority of air-conditioning through supply and recovery of heat and moisture during nasal breathing.

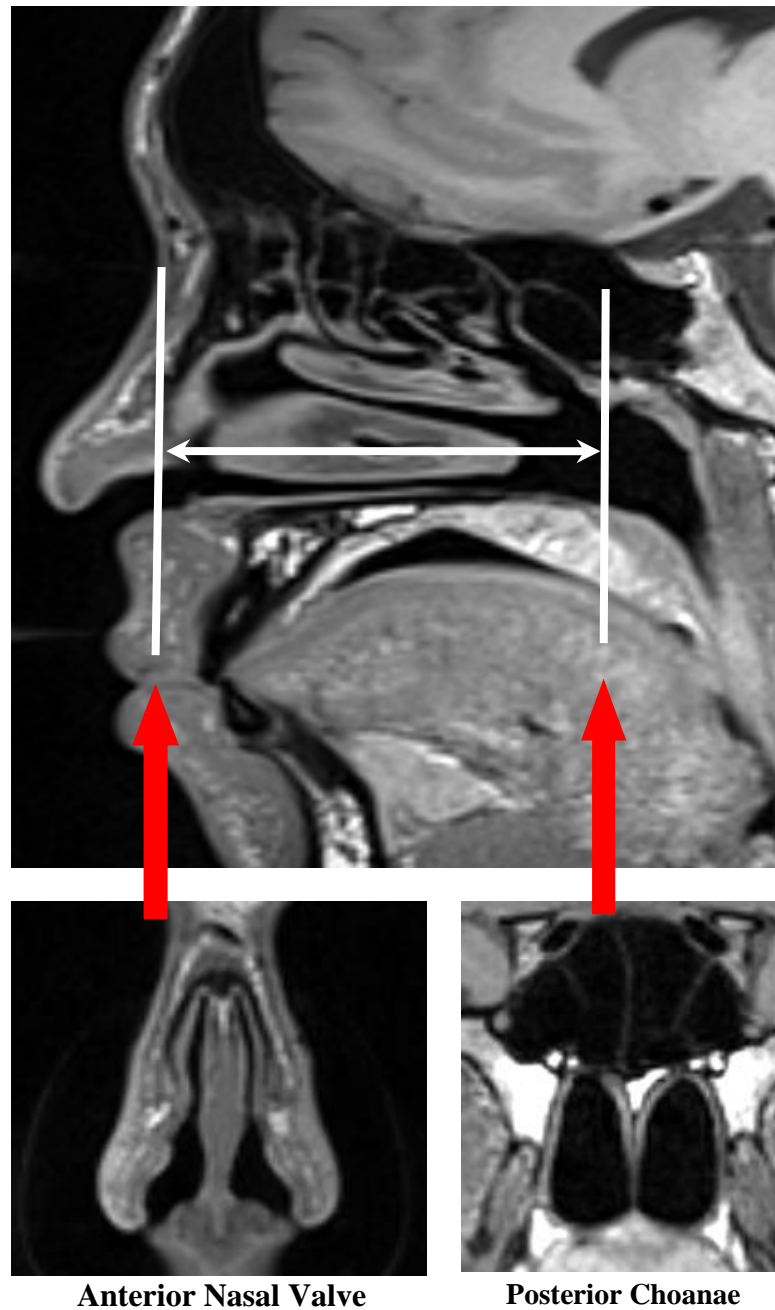


**Figure 4.2: MRI images showing region of interest spanning the anterior nasal valve to the posterior choanae.**

It also contains the active nasal erectile tissue regulating nasal air-flow partitioning between each airway.

#### **4.3.3.2 MRI Morphology**

For morphology image acquisition, the T1-weighted sagittal images were performed using a repetition time (TR) of 700 ms, and an echo time (TE) of 12.0 ms.

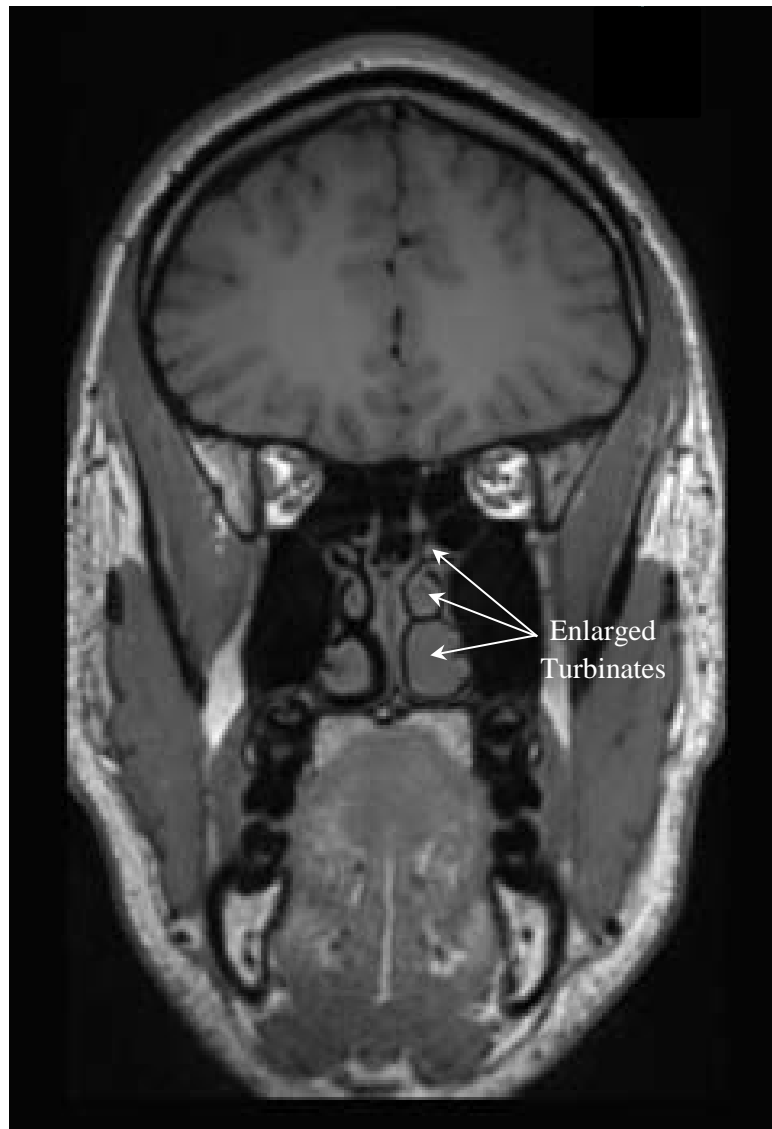


**Figure 4.3: An example of a MRI coronal head image demonstrating the presence of the nasal cycle with patent right airway and congested left airway.**

Slice thickness was 0.78 mm and echo spacing 4.05 ms. Full details of the MRI morphological scan parameters are given in Appendix B1.

#### **4.3.3.3 MRI Morphology Image Processing**

MRI dicom files were collated by the image processing software 3D-Doctor <sup>TM</sup> (Able Software Corp) software and presented as coronal head sections as shown in Figure 4.3. Here, the nasal passageways of this subject demonstrate the presence of the nasal cycle with the left airway being congested to airflow while the right airway is patent. As discussed in Section 2.3.3, the occurrence of the nasal cycle is illustrated by the enlarged turbinates restricting the left airway in this case. On the other hand, within the right airway, the flaccid turbinates are contracted and do not obstruct this airway.

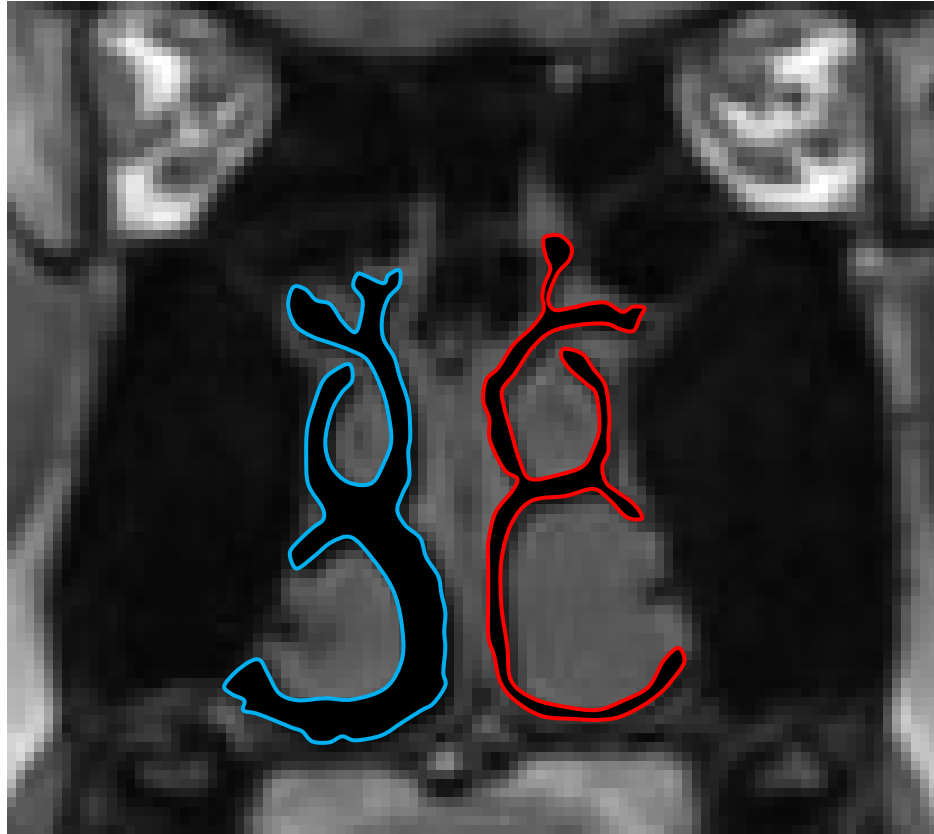


**Figure 4.4: Enlarged MRI coronal nasal image demonstrating the manual segmentation of airway boundaries. — = congested airway, — = patent airway.**

Analysis of nasal morphological attributes within each MRI head coronal scan required the identification of the airway segmentation boundary to be defined. An automatic image boundary segmentation function was provided by the 3D-Doctor <sup>TM</sup> software used during image processing. This was found however to include sinus cavities so airways boundaries were manually traced at 6 x magnification to ensure accurate tracing of the functional airway perimeter.

Morphological data of airway cross-sectional-area ( $A$ ) and perimeter ( $P$ ) were determined using 3D-Doctor <sup>TM</sup> from the airway segmentation boundaries for each coronal slice within the ROI and compiled into a single data file for later analysis. These data files are also used as input to the model during simulation.

#### **4.3.3.4 MRI Nasal Blood-Flow**

Arterial spin labelling techniques were used for blood-flow image acquisition. Here, arterial spin labelling perfusion mode FAIR QII transversal (Axial) images were acquired using a repetition time (TR) of 5 s, and an echo time (TE) of 14.8 ms. Slice

thickness was 4.00 mm, flip angle of 180° and echo spacing 0.5 ms. These settings were selected because they provided adequate detail within a confined and complex region. Duration of scan was approximately 13 minutes. Full details of the MRI arterial spin labelling scan parameters are given in Appendix B1.9.

#### 4.3.3.5 MRI Blood Flow Image Processing

Nasal perfusion was detected using arterial spin-labeling image techniques that offer a non-contact perfusion assessment method that is suited for use while wearing a nasal mask within the MRI environment. Perfusion DICOM format ambient and augmented pressure arterial spin-labeling images were qualitatively analyzed using 3D-Doctor™ by assessing change in visual color representing different amounts of tagged blood volume in-flow into the ROI as shown in Figure 4.5. Intensity of the change in image colour was selected to provide the best contrast in response to tagged blood in-flow for the flow rates present. This setting was maintained constant for all image analysis.

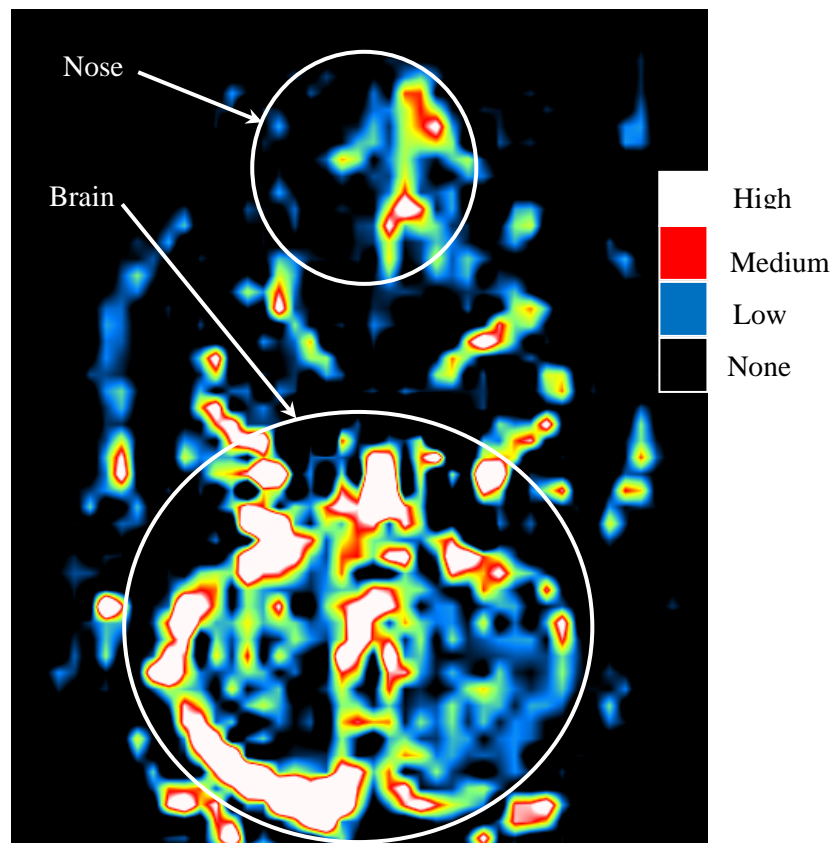


**Figure 4.5: Axial ASL head image demonstrating high cerebral blood flow in brain and congested nasal turbinate by colour intensity.**

Ideally, when using arterial spin-labeling techniques, the transit time for tagged blood to reach the ROI must be short compared to the relaxation spin time ( $T_1$ ), otherwise errors in perfusion measurement become likely [218]. Within the nose, when using these imaging techniques, the low blood flow rate delays the arrival of tagged blood, resulting in lower signal strength which decays over time. This unavoidable fact makes errors in perfusion measurement likely; hence no attempt was made to undertake quantitative measurements of blood flow rates. In this investigation, a qualitative assessment of tagged blood volume was undertaken by visual comparison of the ambient and augmented pressure breathing perfusion images. No meaningful image data could be detected for the congested airway in any participant, suggesting that it was below the sensitivity threshold of this technique [218].

Change in nasal blood-flow was qualitatively assessed through comparison of arterial spin-labeling images. Changes in the patent airway inferior turbinate blood volume in a male participant, as an example, are shown by the difference between ambient and 6 cm  $H_2O$  pressurized images in Figures 4.6A and 4.6B respectively. Comparing the two central upper portions of the mid sections of each image shows an increase in inferior turbinate blood volume (indicated by the elliptical region) occurs under augmented air pressure.

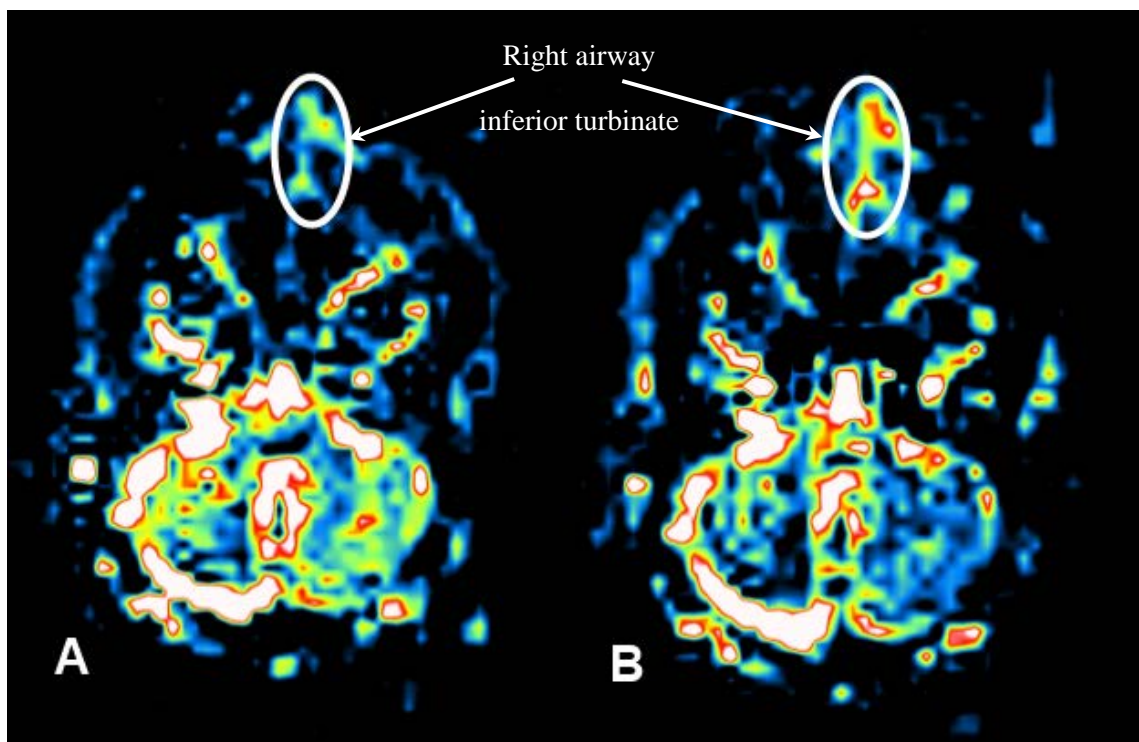


**Figure 4.6: Arterial spin labelling perfusion image. (A) Ambient breathing. (B) 6 cm  $H_2O$  n-PAP breathing.**

## **4.4 Results Overview**

Acquisition of nasal MRI morphology image cross-sectional area and perimeter data has enabled geometrical parameters that influence nasal air-conditioning performance within the ROI during spontaneous n-PAP breathing to be evaluated. As mentioned in Chapter 2, there has been no previously reported research that has sought to develop and use this data, and it should be viewed as one of the unique contributions of this work.

To aid clarity, results are divided into the three sections, each containing their own discussion on the findings. Measurement of nasal cycle is given in Section 4.5, whilst geometric parameters that influence air-conditioning performance are assessed in terms of combined airway geometry and inter-airway geometry in Sections 4.6 and 4.7 respectively. Inter-nasal blood flow results are discussed in Section 4.8.

There is no information from any of the results that supports gender as being a significant factor in the distribution of this data.

## **4.5 Nasal Cycle Results**

All participants demonstrated a clear bias in nasal air mass-flow towards the patent airway and no change in this condition was detected upon completion of the MRI scan period. Given this result, it is assumed that there was no change in the phase of the nasal cycle occurred during this scan period. Specific details of results can be found in Appendix B1.

### **4.5.1 Nasal Cycle Discussion**

The use of spirometry to detect change in the nasal cycle status has previously been shown to yield results comparable to those obtained by rhinomanometry and is recommended for studies of the nasal cycle [219]. Change in air-flow bias between the nasal airways in this experiment would have invalidated both the morphological and blood-flow results since variation in air-flow partitioning requires change in engorgement of nasal erectile tissue through variation in blood flow. Here, not being able to ascertain if this event had just or was about to occur is not an issue since this reciprocal change occurs simultaneously in both airways until changeover is complete [79, 220]. As no change in air-flow bias was detected in these cases, any variation in nasal morphology or blood flow can be attributed to other causes.

#### 4.6 Combined Airway Geometry Results

Within this section, parameters that influence overall nasal air-conditioning performance are considered across both nasal air passageways. This form of analysis has been convenient for other researchers, since it negates the need to account for the status of the nasal cycle or deviated septum [94].

The findings of combined airway cross-sectional area, perimeter and hydraulic diameter results found in this investigation are now compared with results obtained by earlier work by Yokley *et al.* [94] in Figures 4.7, 4.8 and 4.9 respectively. Here, as previously discussed in Section 2.3.4, values were assessed for the mid nasal region, immediately posterior to the anterior end of the middle turbinate.

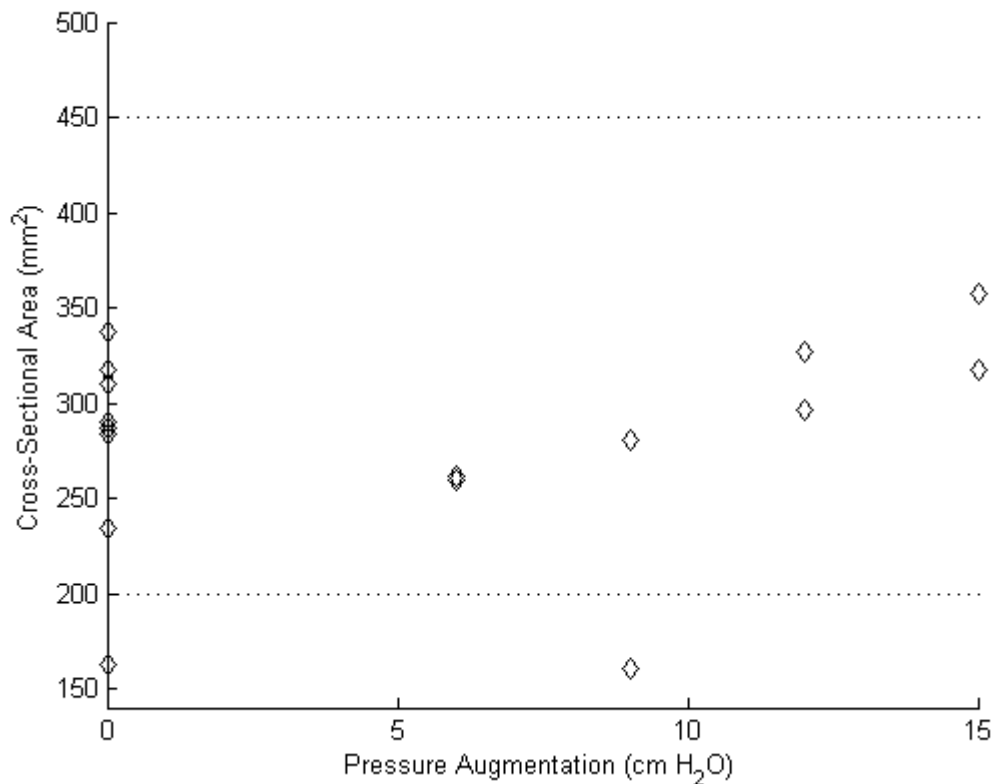


**Figure 4.7: Mid airway (X/L=0.5) combined patent and congested airway cross-sectional area at different pressures. .... = Yokley *et al.* upper and lower limits [94].**

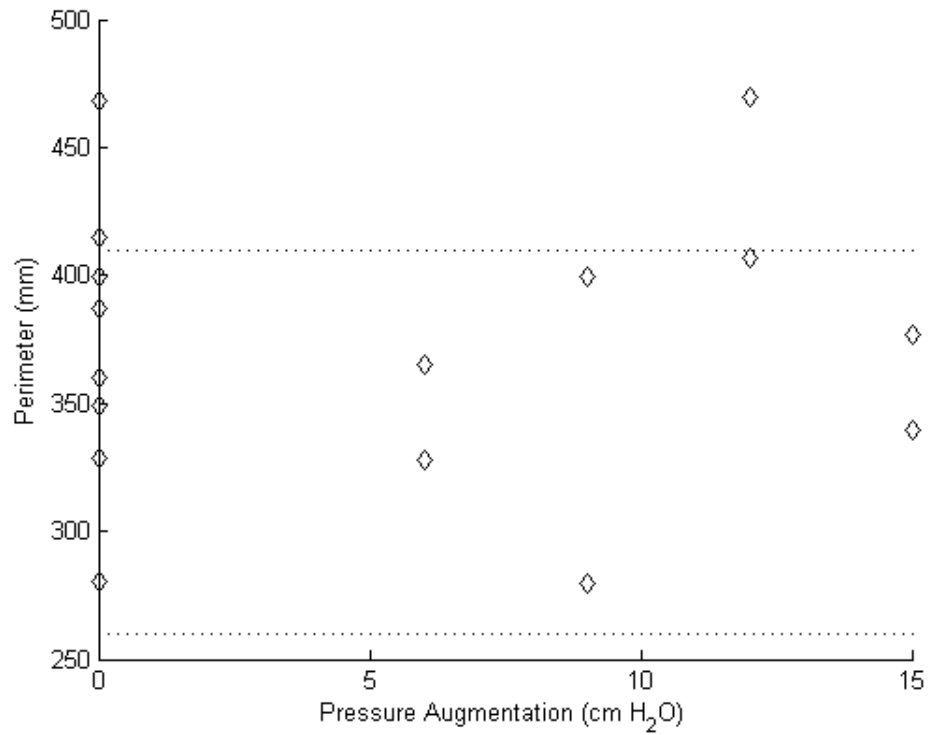


**Figure 4.8: Mid airway (X/L=0.5) combined patent and congested airway perimeter at different pressures. .... = Yokley *et al.* upper and lower limits [94].**

Location along the airway is represented as a dimensionless airway position (X/L), which denotes the fraction of distance from the vestibule to the posterior choanae, spanning the ROI.

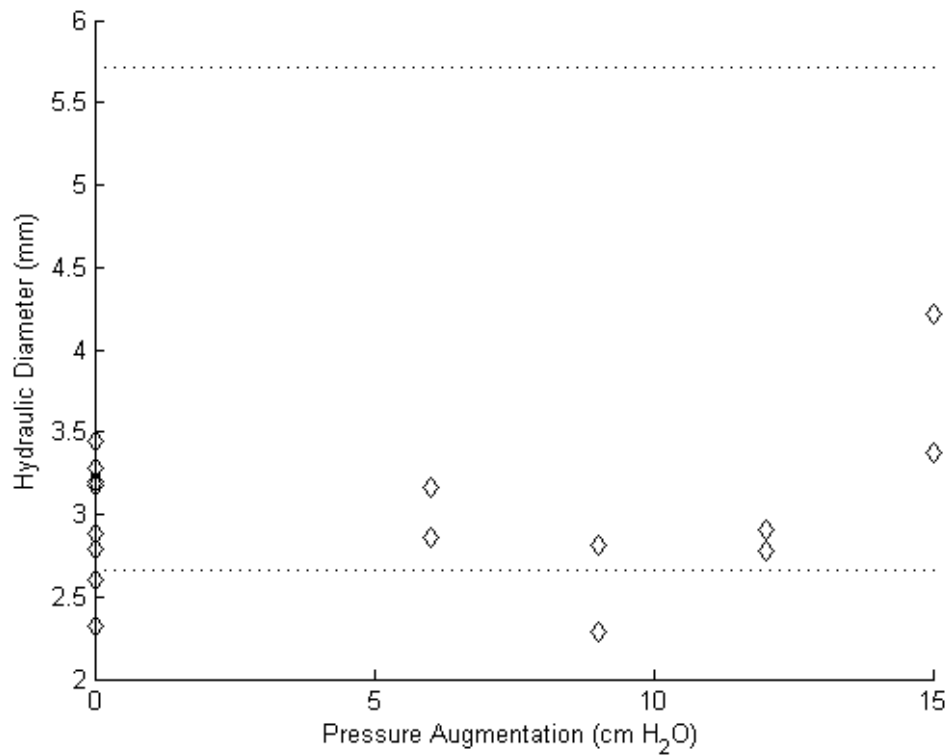


**Figure 4.9: Mid airway (X/L=0.5) combined patent and congested airway hydraulic diameter at different pressures. .... = Yokley *et al.* upper and lower limits [94].**

At this mid-airway location ( $X/L=0.5$ ) all participants demonstrated a combined airway cross-sectional-area within the range found by Yokley *et al.* [94], given by Figure 4.6, apart from one who displayed a lower value at both ambient and 9 cm H<sub>2</sub>O pressure augmentation.

As shown in Figure 4.7, all participants demonstrated a combined airway perimeter within the range previously found by Yokley *et al.* [94] apart from one participant who demonstrated a greater value at both ambient and 12 cm H<sub>2</sub>O pressure augmentation.

All participants experienced a combined airway hydraulic diameter within the range previously found by Yokley *et al.* [94], as shown by Figure 4.8, apart from one who experienced a slightly lower value at both ambient and 9 cm H<sub>2</sub>O pressure. This occurred as a consequence of this individual having a low cross-sectional-area, as previously demonstrated in Figure 4.6.

The justification used by Yokley *et al.* for assessing the mid nasal airway region as a representation of the whole nasal airway air-conditioning capacity [94] seems reasonable given the results of surface area presented in Figure 4.10.

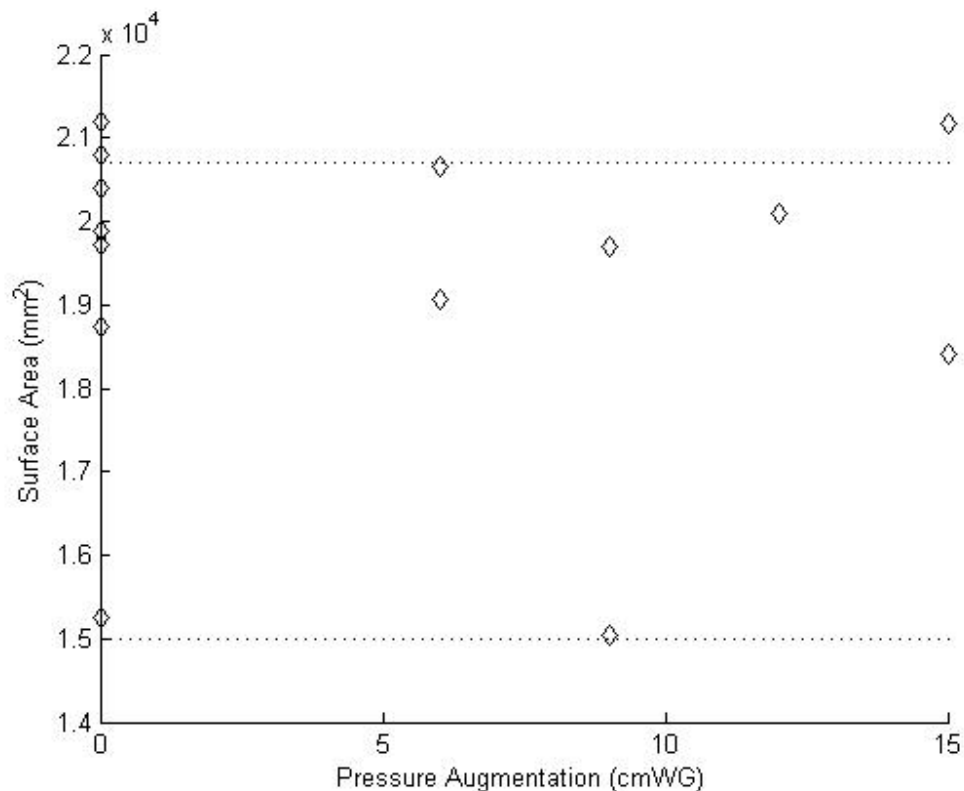


**Figure 4.10: Total surface area over the region of interest of the combined patent and congested airway hydraulic diameter at different pressures. .... = Segal *et al.* upper and lower limits [66].**

The combined airways' surface area, demonstrates good agreement with the upper and lower range of MRI data previously obtained by Segal *et al.* [66]. Of note is one subject in this study that experienced a slightly higher combined airway surface area at both ambient and 15 cm H<sub>2</sub>O pressure than that previously found by Segal *et al.*

#### **4.6.1 Combined Airway Geometry Discussion**

The values of combined nasal airway cross-sectional area, perimeter and hydraulic diameter when breathing ambient pressure air found by this investigation compare well to the earlier work by Yokley *et al.* [94], previously reviewed in Section 2.3.4. The ability of the nasal mucosa geometry to respond to variation in air humidity and temperature through activation of erectile tissue has been previously highlighted by Yokley *et al.* as a variable and could explain the lower grouping of hydraulic diameter results found by this investigation. Adaptation to local environmental conditions of temperature and humidity may have played a part. Additionally, although Segal *et al.* did not identify participants' ethnicity when assessing total nasal surface area, the ethnicity of participants within this study, given in Appendix B, varied from those investigated by Yokley *et al.* It is thought variance in ethnicity may have contributed to the variance found despite this difference only occurring within the decongested airway [94].

The justification of a strong correlation existing between the hydraulic diameter at the mid-airway position and the overall nose surface area to volume ratio by Yokley *et al.* seems justified when comparing the hydraulic diameter results at the mid-airway location and that of total airway surface area, shown by Figures 4.8 and 4.9 respectively. Here the majority of data lies within previously measured limits.

#### **4.7 Separate Airway Geometry Results**

This analysis considers the geometric characteristics along the length of each separate nasal airway. This is a unique analysis as it considers the geometric details of the patent and congested airways separately, while assessing the effect n-PAP breathing has on these parameters. For clarity, the distribution of geometric parameters of cross-sectional area, perimeter and hydraulic diameter at ambient pressure along both the patent and congest airways for all participants are first presented in Section 4.7.1 whilst results corresponding to n-PAP breathing are presented in Section 4.7.3. Comparison is made to previously published data, however this information is sparse given most

research into nasal geometry has considered both passageways together. Comments on these findings are made in Section 4.7.2 and 4.7.4 for ambient and n-PAP breathing respectively. Inter-nasal volume change is also discussed in Section 4.7.5.

#### 4.7.1 Ambient Pressure Breathing Results

The inter-nasal distribution of cross-sectional area along both airways is shown in Figure 4.11. Here, a violin plot showing the distribution at 10% intervals along the length of both the patent and congested airways is presented. Each plot spans the interquartile range with median values ( $n=8$ ) given by bold line. Kernel (probability) density, given by the width of each plot, provides non-parametric probability indicator so standard deviation does not apply. Of note is the separation in the mean cross-sectional area data recorded between the patent and congested airways. Statistical analysis was undertaken using a two-sided paired t-test to a fixed effects linear model to test the null hypothesis that the patent and congested airways have equal mean cross-sectional area value. This found significant variation ( $p < 0.0001$ ) exists between the cross-sectional areas of each airway along all positions considered, thus rejecting the null hypothesis.

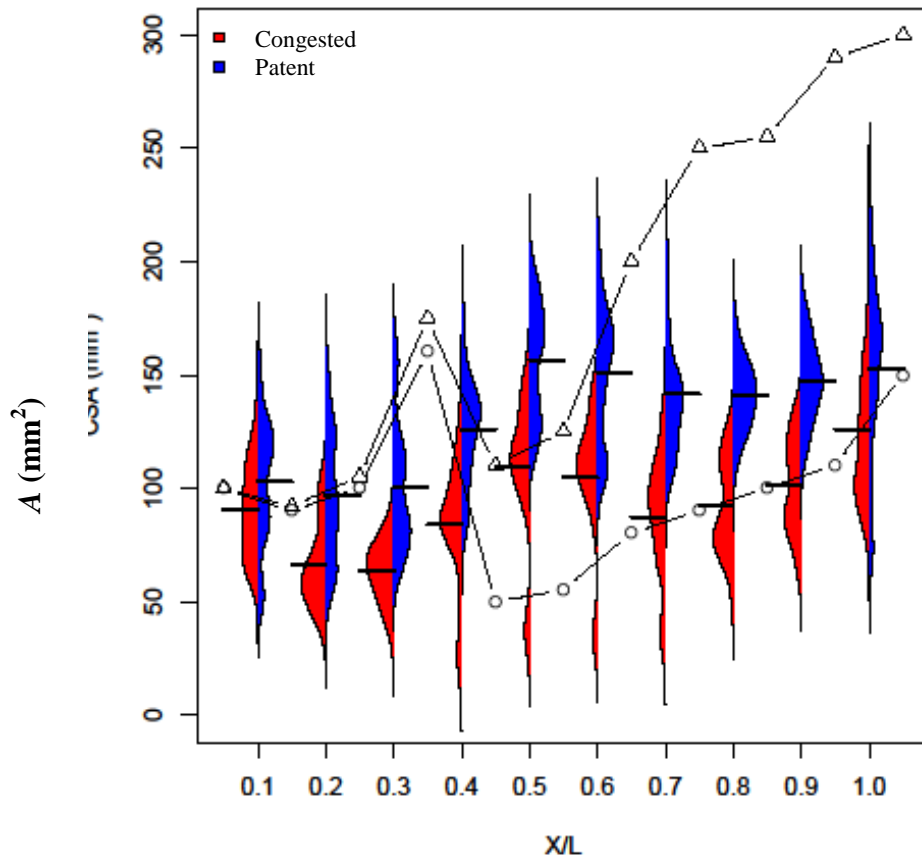


**Figure 4.11: Mean cross-sectional area distribution along patent and congested airways at ambient pressure. ○ = congested airway, Δ = patent airway**  
Lang et al [99].

Also shown are cross-sectional area results from Lang *et al.* that were obtained by the use of rhinomanometry. Mean values of cross-sectional area are presented as thick black lines at set increment along the airway. No statistical comparison is made between the earlier work by Lang *et al.* and this current investigation, given the issues of accuracy associated when using rhinomanometry to measure deep within the nasal cavity, as discussed in Section 2.3.4.

Results of patent and congested airway perimeter distribution along the nasal airway length are presented in Figure 4.12. Using the same statistical analysis to test the null hypothesis that the patent and congested airways have the same perimeter value found insignificant variation ( $p = 0.0615$ ) exists between each airway along all positions considered, thus failing to reject the null hypothesis.

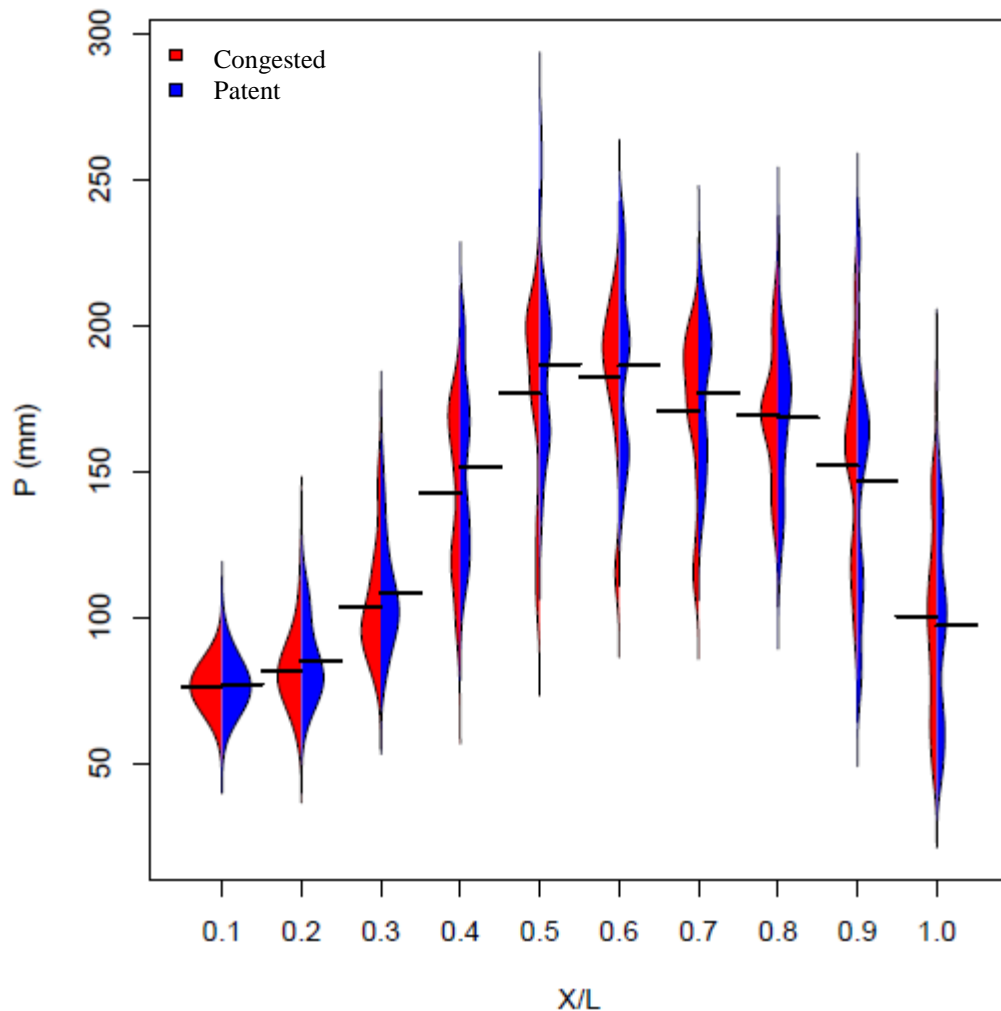


**Figure 4.12: Mean perimeter distribution along patent and congested airways at ambient pressure.**

Unfortunately no comparison to previous results could be made due to the absence of inter-nasal perimeter data within the current literature.

Results of patent and congested airway hydraulic diameter distribution along the nasal airway length are presented in Figure 4.13. Again, using the same statistical analysis, testing the null hypothesis that the patent and congested airways have the same hydraulic diameter value found significant variation ( $p < 0.0001$ ) exists between each airway along all positions considered, thus rejecting the null hypothesis.

Visual comparison can also be made to previous hydraulic diameter data obtained from human cadavers [97] by direct measurement of moulds and live canine MRI measurements [98] as demonstrated in Figure 4.13

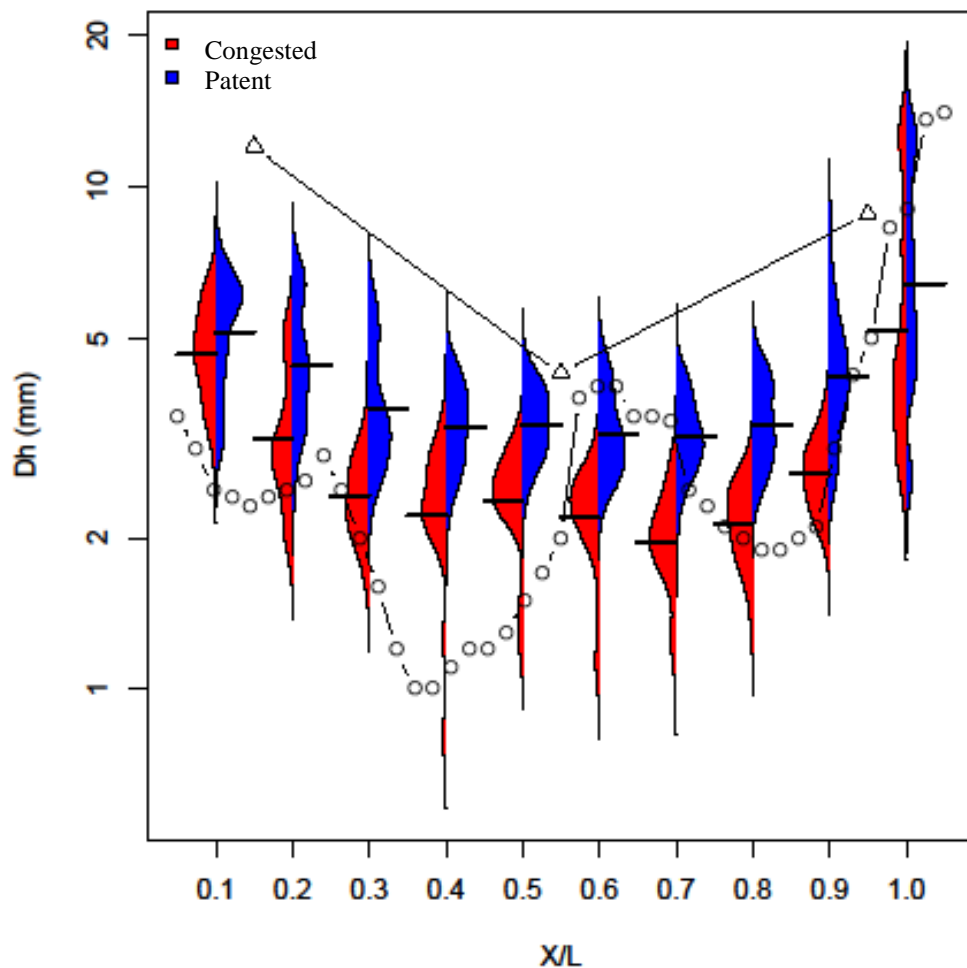


**Figure 4.13: Mean hydraulic diameter distribution along patent and congested airways at ambient pressure.  $\Delta$  = Hanna [97],  $\circ$  = Craven *et al.* [98].**

#### 4.7.2 Ambient Pressure Breathing Discussion

The solid lines in Figures 4.11, 4.12 and 4.13 represent the average value for each parameter recorded at specific airway locations. The trend of change for each parameter can be visually followed along each of the nasal passages.

Comparison of the results for cross-sectional area and perimeter between patent and congested airways, shown in Figures 4.11 and 4.12 respectively, shows the cross-sectional area as the only parameter that varies between airways. Comparison of the distribution of cross-sectional area found by this investigation, Figure 4.9, to that found by Lang *et al.* [99] using acoustic rhinometry (AR) techniques, demonstrates the same variation occurring between patent and congested airways. Of note is the lack of differentiation between patent and congested airways found by Lang *et al.* within the anterior airways region ( $X/L < 0.4$ ). This is contrasted by significant variation between airways found by Lang *et al.* in the posterior airways region ( $X/L > 0.4$ ). Variation between this earlier data and that obtained by this investigation is attributed to AR measurement techniques used by Lang *et al.* Here, the technique of rhinoresistometry measures flow and pressure in order to calculate cross-sectional area and suffers from inherent inaccuracies due to pressure drop and signal attenuation as previously mentioned in Section 2.3.4. This is a major limitation with any AR measurement and results from previous studies using this technique should not be used in situations where accuracy is necessary.

The distribution of hydraulic diameter in both patent and congested airways, Figure 4.13, indicates this parameter follows a similar trend to that of the cross-sectional area. This is not surprising given the lack of difference between patent and congested airway perimeter values. Both of these compare poorly to patent and congested airways measured using the AR techniques [99]. These ranged from 30-60 mm measured at the anterior head of the inferior turbinate (not shown in Figure 4.9). This poor correlation is attributed to the inaccuracies inherent when using AR techniques previously mentioned. For comparison purposes, previous results obtained from human cadaver mouldings by Hanna [97] are shown in this figure. These demonstrate slightly higher values than the data obtained in this research which is probably due to unavoidable tissue shrinkage and the absence of perfusion within cadaveric erectile tissue. Hydraulic diameter values measured using MRI in live canine nasal airways [98] (also shown in Figure 4.12) over the same region demonstrate similar results, both in terms of magnitude and distribution. These close results may be attributed to both human and canine airways

having similar heating and humidifying functional requirements using similar tidal volumes and gives confidence in the veracity of the MRI data obtained. With consideration to all of these factors, there is confidence in the veracity of the inter-nasal geometric data obtained by this work.

### 4.7.3 n-PAP Breathing Results

Having confidence in the veracity of the MRI data found during ambient pressure breathing, the change in geometric parameters of cross-sectional area, perimeter and hydraulic diameter relative to unit pressure augmentation, represented as  $A_p$ ,  $P_p$  and  $D_{h,p}$  respectively, for both the patent and congest airways is now considered in Figures 4.14, 4.15 and 4.16. These results are discussed in Section 4.7.4.

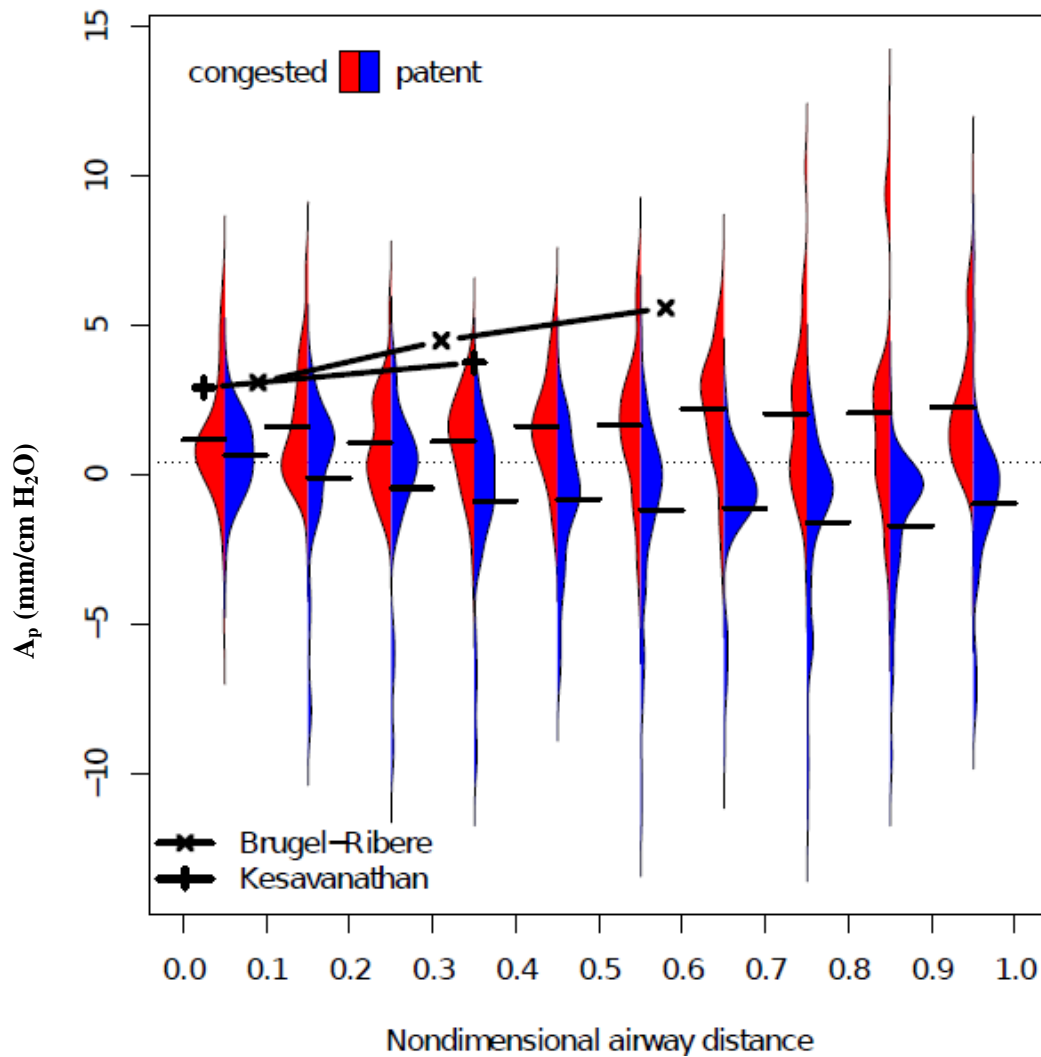


**Figure 4.14:** Change in cross-sectional area per unit pressure along patent and congested airways.  $\times$  = Brugel-Ribere et al [102],  $+$  = Kesavanathan *et al.* [101].

Statistical analysis was undertaken using a two-sided paired t-test to a fixed effects linear model to test the null hypothesis that the patent and congested airways have the same  $A_p$  response. This found significant variation ( $p < 0.0001$ ) exists between the  $A_p$  of each airway apart from the most anterior region where no significant difference was detected ( $p = 0.149$ ), thus failing to reject the null hypothesis. Of particular note are the opposing reactions between the patent and congested airways in response to pressure augmentation. Here the  $A_p$  of the patent airway tends to become smaller, whilst that of the congested airway gets bigger with increasing air-pressure.

For the purposes of comparison, earlier data obtained by AR techniques is also shown on this figure [101, 102]. This work did not distinguish between patent and congested airways. In this study significant variation was found between the median value of the patent and congested airways and the  $A_p$  values obtained from two earlier investigations (2 sided t-test,  $p < 2.1 \times 10^{-16}$ ). Specific airway perimeter distribution shown in Figure 4.15 also demonstrates a slight opposing behaviour between the patent and congested airways occurring.

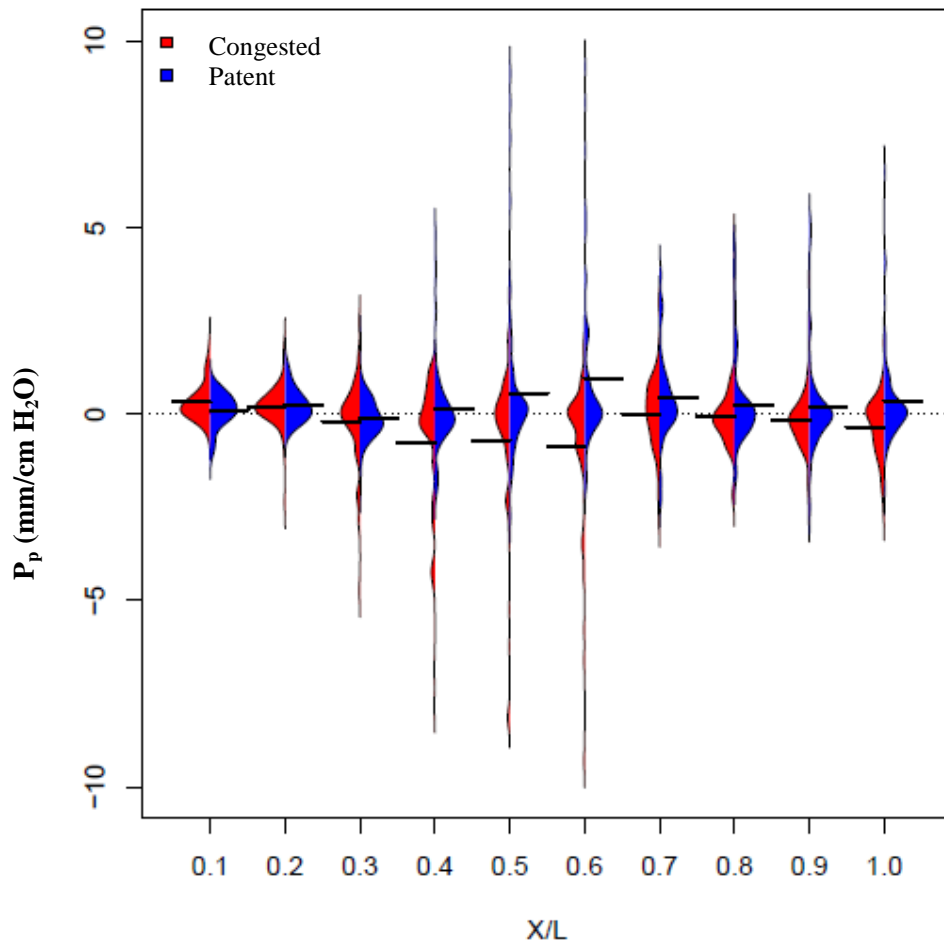


**Figure 4.15: Change in perimeter per unit pressure along patent and congested airways.**

Using the same statistical analysis to test the null hypothesis that the patent and congested airways have the same  $P_p$  value found significant variation ( $p < 0.0001$ ) exists between each airway along all positions considered, thus rejecting the null hypothesis.

As a consequence of the two previous findings, the  $D_{h,p}$  distribution along both airways, shown in Figure 4.16, also demonstrates the same opposing reactions between these two airways in response to pressure augmentation.

An increase in  $D_{h,p}$  can be interpreted as the airway is becoming more circular in cross-section with increasing air-pressure, whilst a decrease indicates the airway becomes more oblate in section. When air-pressure is increased, the patent airway displays a reduction in hydraulic diameter along all but the most anterior portions, while the congested airway experiences an increase along its whole length.

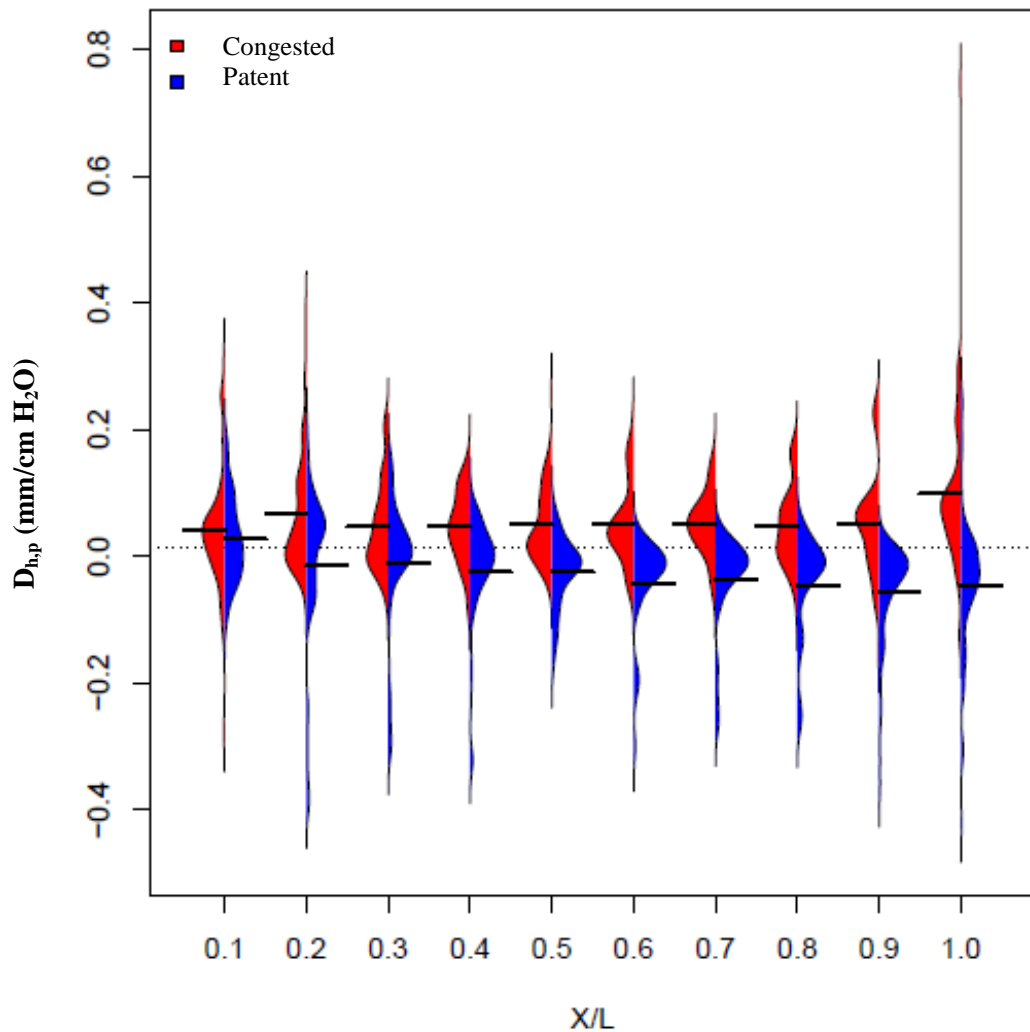


**Figure 4.16: Change in hydraulic diameter per unit pressure along patent and congested airways.**

Again, using the same statistical analysis, testing the null hypothesis that the patent and congested airways have the same  $D_{h,p}$  value found significant variation ( $p < 0.0001$ ) exists between each airway along all but the most anterior position, thus rejecting the null hypothesis.

#### **4.7.4 n-PAP Discussion**

It was previously thought that the cross sectional area within both nasal airways increased by the same amount in response to increasing air-pressure. However, this investigation has found the airways experience a contra-response to augmented pressure. This finding is inconsistent with the current understanding of equal nasal tissue compliance occurring within both airways. Each airway responds differently to air pressure, the congested airway being compliant, whilst the patent airway could better described as ‘defiant’ to air pressure. Because of this differing airway response, the term ‘airway tissue compliance’ previously used by researchers [101, 102] to describe a purely elastic tissue response could be replaced with the more appropriate term. It is suggested that this be named ‘inter-nasal geometric response’.

A simple visual comparison between the  $A_p$  findings of this work, shown by Figure 4.14, and that found in earlier investigations [101, 102] demonstrates the additional information obtained by this investigation. For the purposes of comparison, previous data based on volume change [101] has been recalculated and presented as  $A_p$ . The inter-nasal geometric responses found by this work differ from previous results, not only in terms of magnitude and distribution, but also between patent and congested airways. Here the congested airway is characterized by a rising geometric response when moving posterior, a trend also noted in earlier investigations [101, 102]. Additionally, the magnitude of these findings for this airway is somewhat lower than previously observed values. This variation in magnitude is attributed to the inaccuracies inherent in AR techniques used in the earlier studies. Of note in the findings of this investigation is the different response of the patent airway which shows a contra response to that of the patent airway occurring along its entire length. In both cases this earlier work does not discriminate between patent and congested airways. All earlier reported AR tissue geometric responses to air-pressure have been restricted to the region bound by the nasal valve and middle meatus, as indicated by the shorter distance along the nasal channel. Tissue response behavior posterior to this region has not been

previously investigated due to inaccuracies inherent when using AR techniques previously mentioned.

Findings from this investigation demonstrate that, in the congested airway, both  $A_p$  and  $P_p$  increase during spontaneous n-PAP breathing. This causes the  $D_{h,p}$  of this airway to become greater, meaning the congested airway becomes more round in cross-section along its entire length. On the other hand, the patent airway experiences a reduction in both  $A_p$  and  $P_p$  during spontaneous n-PAP breathing. This causes the  $D_{h,p}$  of this airway to decrease, meaning this airway becomes more oblate in cross-section along.

Unfortunately there is no previous  $P_p$  and  $D_{h,p}$  data in the current literature to compare against the findings of this investigation.

Variation in nasal geometry also occurs during forced inhalation/exhalation due to the compliant nature of airway tissue within the nose [196]. Participants in this investigation were, however, breathing at rest so that pressure gradients generated by slow tidal breathing would have been several orders of magnitude less than that generated during forced inhalation/exhalation [67, 68]. Given this, variation in tissue geometry occurring during image acquisition, as a result of tidal breathing pressure gradients were considered insignificant. Therefore, breath gated image techniques that synchronize image acquisition to breath phase were not considered necessary.

#### **4.7.5 Inter-Nasal Accumulated Volume Change**

Previous investigations have found that laminar airflow occurs throughout the nose during at-rest breathing [221, 222]. This means that the overall airflow resistance across each airway lump per unit mass airflow is inversely proportional to Reynolds number and hence airway cross-sectional area, as described in Section 3.8.1. Significant and sudden change in airway cross-sectional area normally occurs along the length of each nasal passageway, as given in Figure 4.11.

Additional insight into the pressure elicited geometric interplay occurring between the patent and congested nasal airways, and the influence this has on airflow partitioning, can be gained by presenting this data in a new format. This is done to enable visual correlation of pressure elicited change in airway geometry to variation in airflow partitioning between each airway.

The new form of presentation, offered in Figure 4.17, differs from those previously used [101, 102], and that offered in Figure 4.14, in three main aspects:

1. Accumulated change in airway volume is presented since this provides a smooth transition across regions where abrupt change in airway geometry occurs. This is calculated from cross-sectional data taken at equal image slice thicknesses.
2. Results for both patent and congested airways are plotted against two perpendicular axes. This enables the pressure elicited change within each airway to be plotted as a single line.
3. Three regional locations along both airways, given as nasal valve, mid meatus and choanae, are defined by line colour.

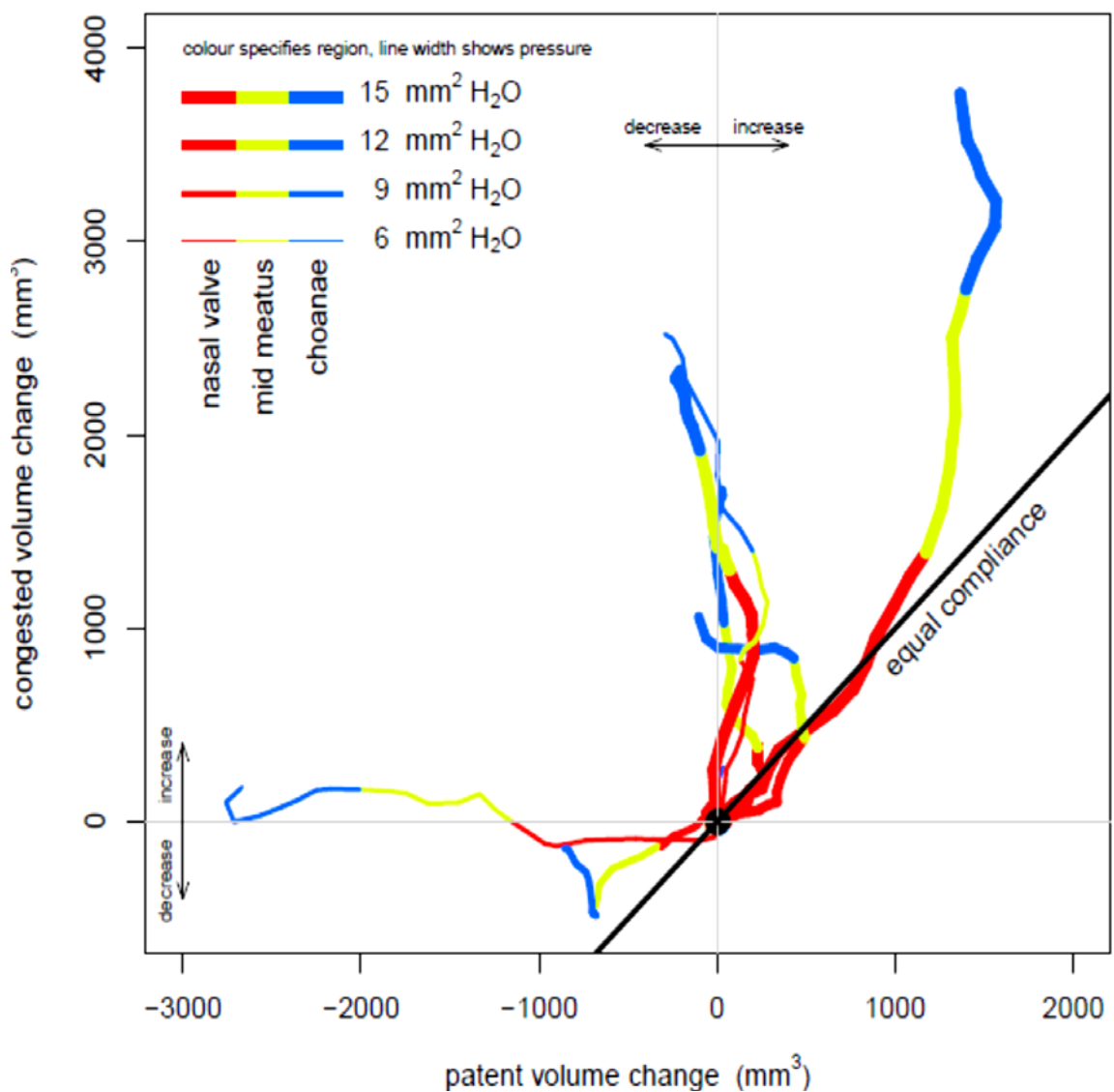


**Figure 4.17: Participant specific accumulated volume change in both patent and congested airways.**

With reference to Figure 4.17, the axes are orientated so that a line representing any individual participant moving in the vertical upward direction away from the origin demonstrates an increase in congested airway accumulated volume. Alternatively, a line moving in the horizontal direction to the right demonstrates an increase in patent airway accumulated volume. Moving either downward or to the left indicates a reduction in both of these parameters whilst simultaneous and equal change in both airways' accumulated volumes is shown in Figure 4.17 by the black line inclined at 45°.

No change in air-flow partitioning between the two airways occurs if the participant's accumulated change volume tracks along this 45° line since change in accumulated volume between airways is equal. This line corresponds to the current understanding of both airways having equal tissue compliance to n-PAP pressure.

It can be clearly seen from Figure 4.17 that only one participant's airways follows anything near equal compliance but this only occurs in their anterior nose. The remaining airway regions of this individual experience a greater increase in congested airway accumulated volume compared to the patent airway. For the remaining seven participants, five experienced an increase in congested airway volume with slight reduction in patent airway volume whilst two demonstrated an almost exclusive reduction in patent airway volume.

The region occupied by the line representing each participant's airways is of particular significance to inter-nasal airflow partitioning. In this case the location for all participants is above the line of equal compliance (dark line inclined at 45°). This indicates that all participants experienced a change in inter-nasal airflow partitioning. This change is characterised by an increase in airflow occurring within the congested airway and a decrease occurring within the patent airway. Any data lines terminating below the line of equal compliance indicates an opposing result but this was not demonstrated during this investigation.

As previously mentioned, it was not possible to ascertain the exact temporal location within the nasal cycle phase of the individuals despite measuring peak airflow from each of the nares. This may have contributed to two participants demonstrating accumulated volume reduction occurring within their patent airways, shown in Figure 4.17.

## **4.8 Inter-Nasal Blood Flow Results**

The qualitative change of this parameter for all participants is given in Table 4.1. Here, four of the participants exhibited increased inferior turbinate blood inflow within the patent airway, in two there was no change and two showed a decrease. No significant differences between male and female data were observed.

### **4.8.1 Inter-nasal Blood-Flow Discussion**

Normally swelling of nasal erectile tissue is not a consequence of increased nasal blood flow [223]; but rather due to the throttling action of drainage veins leading from a network of large anastomosing veins. This action provides the capability for large volume change to occur within this tissue [224].

Nasal airway congestion is normally achieved through the periodic cycle of nasal turbinate engorgement, which is thought to be synchronized to the ultradian cycle [88]. However, this investigation demonstrates that blood flow within the patent nasal airway also changes during n-PAP breathing (Table 4.1). This change may be attributed to the variation in blood flow to different parts of the head. Cerebral blood flow MRI investigations [225-227] using arterial spin-labeling techniques have speculated that the reduced blood flow and volume due to CPAP pressure may be attributed to active arterial vasoconstriction and/or passive compression of capillary and/or venous vessels. This investigation has found both increasing and decreasing blood inflow within the patent airway inferior turbinate (Table 4.1) occurred in all but two of the participants.

The net result of this change is the patent airway displaying an opposing tissue compliance behavior to that of the congested airway that can be attributed to two sources:

1. In the first instance, where turbinate blood inflow increases, this may be attributed to increased arterial blood in-flow to nasal erectile tissue during pressurized breathing. Supporting this belief is the observation that there is still tagged blood entering the patent airway inferior turbinate 20 minutes after commencement of pressurized breathing. This would not have occurred had the arterial in-flow of tagged blood been restricted.

**Table 4.1: Change in inferior turbinate blood volume in response to n-PAP breathing.**

Participant	Gender	Air pressure (cm H <sub>2</sub> O)	Patent airway inferior turbinate blood volume
1	male	6	increased
2	female	6	increased
3	male	9	no change
4	female	9	increased
5	male	12	increased
6	female	12	no change
7	male	15	decreased
8	female	15	decreased

- Alternatively, given half the participants experienced either no change or a reduction in inferior turbinate blood inflow, pressure induced vasoconstriction of blood outflow would reduce the amount of tagged blood being able to enter the ROI.

Both of these possible scenarios are in agreement with earlier cerebral blood flow MRI investigations [225-227].

Regardless of the cause, any tendency for air pressure induced tissue compression within the patent airway appears to be countered by either increased erectile tissue blood volume, achieved either by increased arterial supply or constricted venous drainage. It is believed that the difference in inter-nasal geometric response to air-pressure found by this investigation occurs as a result of change in nasal blood flow occurring within the patent airway. The distribution of tissue airway  $A_p$  along the patent airway, shown in Figure 4.10, suggests change in erectile tissue perfusion occurs not only within the patent airway inferior turbinate but also throughout the whole patent airway cavity.

In this investigation, no arterial spin-labeling blood volume data could be found for the inferior turbinate within the congested airway. This suggests little or no tagged blood inflow to erectile tissue occurs within this airway.

## 4.9 Closure

When considering the complete nasal airway, geometric parameters of cross-sectional area, perimeter and hydraulic diameter were found to be within previously established physiological limits [94] for all participants during the spontaneous breathing of ambient air. Inter-nasal analysis of these same parameters during pressurised breathing has however identified a contra-response occurring between the patent and congested airways. The magnitude and sense of this inter-airway contra response to air-pressure augmentation has been quantified in terms of these geometric parameters or both airways. Since internal air-flow partitioning and heat and mass transfer coefficients are based on local geometry, change in these parameters specific to the state of congestion of each airway must be included within the nasal ASL hydration model.

The use of MRI arterial spin labeling techniques provides a suitable non-invasive method to assess inferior turbinate blood inflow but only within the patent airway. It was found that change in nasal blood flow occurs within the patent airway which explains the opposition to air-pressure force demonstrated by this airway.

The response of mucosal ASL water supply to n-PAP breathing remains currently unknown so this is investigated in the following chapter.

## CHAPTER 5

### MUCOSAL ASL SUPPLY RESPONSE TO AIR PRESSURE – AN EXPERIMENTAL INVESTIGATION.

#### 5.1 Introduction

In Chapter 2 it was hypothesized that nasal breathing of positive air-pressure (n-PAP) negatively influences mucosal ASL water supply through the increase in pressure exerted on the airway wall causing a reduction in airway surface liquid (ASL) water supply. The purpose of this chapter is to test this hypothesis and determine the degree of water supply suppression, if any during n-PAP breathing. This will be achieved by comparing the physiological response in water supply from tissue exposed to normal tidal breathing stresses under both ambient and positive air pressure (PAP) conditions.

Lengths of whole bovine trachea were used as a tissue model given its structural suitability for testing under PAP conditions and its large surface area. Air will pass through this tissue in an oscillating manner simulating tidal breathing. The magnitude of change in maximal rates of tracheal tissue water supply found by this experiment elicited by PAP will later be implemented within the nasal air-conditioning model.

The experiment was undertaken in KODE Biotech laboratories at Auckland University of Technology. The majority of the equipment was custom built, which required novel experimental protocols to be developed.

The tissue protocol is discussed in Section 5.2 followed by a description of the apparatus in Section 5.3. Experimental protocol, results and analysis are given in the following sections. Further details for all of this experiment may be found in Appendix C.

#### 5.2 Tissue Protocol, Equipment, and Data Acquisition

A description of the tissue protocols is given in the following sections.

##### 5.2.1 Nasal Tissue Model

Although ideal, the use of *ex-vivo* nasal mucosa is problematic given the difficulty in isolating this tissue from the surrounding connective tissue and structure. Using an *ex-*

*vivo* whole animal head also presents problems in pneumatically isolating the nasal air channels given the various sinus openings and connections to the ears, eyes and mouth. Additionally, evidence that nasal mucosa can be maintained healthy within a whole head cannot be found in the current literature. As discussed in Chapter 2, previous investigations into mucosal water supply within the conducting airways have been undertaken using bovine bronchial and tracheobronchial tissue [111, 132, 134], human oral mucosa [165] and human tracheal tissue [156, 164, 228]. Despite using a variety of measuring techniques, all of these studies produced similar water supply and reabsorption flux values. Bronchial tissue has the advantage of being easy to isolate and provides a simple pipe-like duct that can be reliably pneumatically sealed. Bovine trachea provides a larger surface area than that offered by human or porcine types and so delivers a greater total water flux. Additionally, it can be immersed in physiological salt solution to maintain cellular health and does not require ethical approval for testing. For these reasons bovine trachea was used for this investigation.

### **5.2.2 Tissue Protocol**

On the day of the test, two litres of physiological salt solution (PSS, composition in mM: 2.4 CaCl<sub>2</sub>, 25.7 NaHCO<sub>3</sub>, 5.6 Glucose Monohydrate, 0.82 MgSO<sub>4</sub>, 1.2 KH<sub>2</sub>PO<sub>4</sub>, 3.39 KCl and 110 NaCl) was made using distilled type 1 (ultrapure) Milli-Q® 18MΩ water. A gas mixture of 95% O<sub>2</sub> and 5 % CO<sub>2</sub> was gassed through the PSS for at least 30 minutes to achieve a pH of 7.4 before being stored in an air-tight glass container.

Fresh trachea tissue was collected from the local abattoir, Auckland Meat Processors. As it did not involve living animals, this experiment was not subject to ethics approval at AUT. Tissue was collected at a pre-determined time from the Abattoir to ensure less than 30 minutes had elapsed after the animal slaughter. Immediately upon collection, any excess connective tissue was removed and chilled PSS was dispersed over the trachea surfaces before it was placed within a plastic bag on ice in a chilled insulated container, to minimize tissue deterioration during the 30 minute journey back to the laboratory.

Preliminary investigations into tissue viability, where whole tracheal tissue was immersed in PSS at 37°C for 24 hours, demonstrated little change in tissue viability occurring over this time period. All testing was performed within this time frame.

### 5.2.3 Tissue Viability

To test tissue viability, an unused portion of the trachea tissue was mounted on a silicon filled petri dish using bent syringe needles before being bathed in PSS. A small drop of Indian ink was then released from a 1 ml Pasteur Pipette into the trachea tissue surface and observed under a Askmnia Citoval SN 43271 microscope at 100X magnification. Confirmation of tissue viability was indicated by the presence of a coherent (synchronised beating) mucociliary transport velocity (MTV) occurring across the mucosa surface. This was visually confirmed by the transport of the small iron particles present within the Indian ink as a result of coordinated motile cilia beating. Post experimentation testing of tissue viability was undertaken on tissue used in the experiment, approximately 7 hours after the experiment commenced. This was undertaken to ensure the tissue had remained viable throughout the duration of the experiment. Alternative means of ascertaining tissue viability not used by this investigation include exposure to pharmaceutical agonists to stimulate cellular secretion and microelectrode analysis of cell secretory current. Further details of tissue viability testing are given in Appendix C1.

### 5.2.4 Dissection and Mounting

Immediately upon arrival, any attached remaining connective tissue was removed and an intact length of tracheal tissue was cut to approximately 300 mm long. The presence of an intact ASL layer was visually confirmed by observation of a wetted internal surface, Figure 5.1. One end of the trachea sample was securely attached to a glass tube of a suitable diameter, so as to be a neat fit within the trachea sample, by three PVC plastic cable ties to ensure a gas-tight seal.

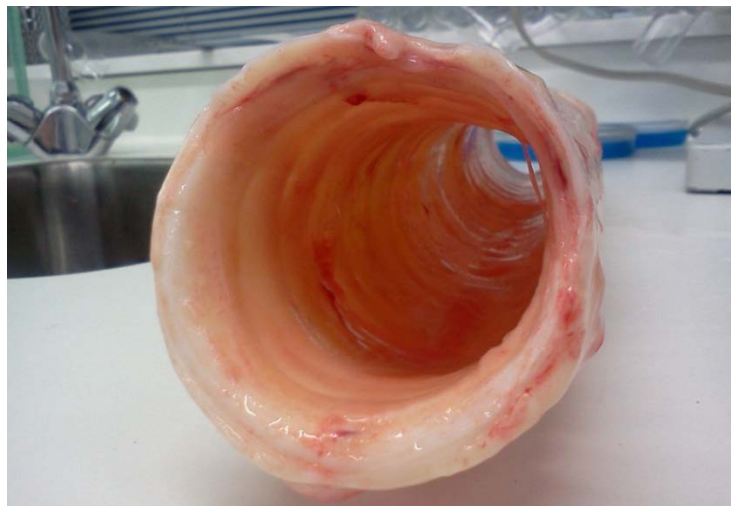


**Figure 5.1: Intact ASL layer within bovine trachea.**



**Figure 5.2: Whole trachea immersed in PSS within tissue bath.**

The trachea sample was then passed through a stainless steel spring, medical grade 6061, to provide a distributed mass to resist buoyancy forces and ensure the trachea remained immersed in the PSS contained within the tissue bath. A second glass tube, also selected to be a neat fit inside the trachea, was inserted into the other end of the trachea and attached in the same manner as the other end. With the two glass pipes firmly sealed to the trachea, the inside of the tissue was rinsed with 100 ml of PSS to remove a red coloured foam contaminant lining the trachea internal surface. Any surplus PSS was allowed to drain from the trachea sample and glass tubing for a period of 3 minutes before the whole trachea and glass tube assembly was immersed in PSS contained within the tissue bath, Figure 5.2.

### **5.2.5 Airway Surface Liquid**

As discussed in Chapter 2, the mucus layer within the ASL normally acts as water volume to buffer the supply and recover of water from inhaled and exhaled air respectively. Because of this, the lower periciliary liquid (PCL) layer remains at a relatively constant height of  $7\mu\text{m}$  [111, 141] so that the mucociliary transportation of the overlaying mucus remains effective.

Overstressing of the trachea water supply in this test will result in ASL dehydration leading to drying of the mucus and PCL layers. During this test, the assumption is made that, provided the mucosal surface remains wetted by the presence of a hydrated

ASL over the full duration of test time (7 hours), any change in ASL water volume within either mucus or PCL layers is insignificant since its total liquid volume is so small. Effectively this means that provided there is a wetted airway surface both prior to, and upon completion of testing, no change in liquid storage within the ASL occurs. This was checked by ensuring the presence of the ASL layer both prior to and immediately after testing.

Maximal rate of mucosal ASL water supply was calculated by from the sum of the rates of change in air water content and water vapour extracted from the air by the desiccant.

### 5.3 Experimental Apparatus

The test apparatus exposes the mucosal surface within the airway luminal space to the same cyclic compressive air pressure and shear air-flow stresses as that experienced *in-vivo*. This is achieved by shuttling a volume of air trapped within two opposing bellow assemblies through activation by a transport ventilator. ASL water demand is created by removing moisture from the air by a desiccant contained within a glass sphere. Air temperature and humidity are monitored throughout the test duration. All of the apparatus is contained within an incubator which also serves as a pressure chamber. A schematic representation of the test apparatus is presented in Figure 5.3.

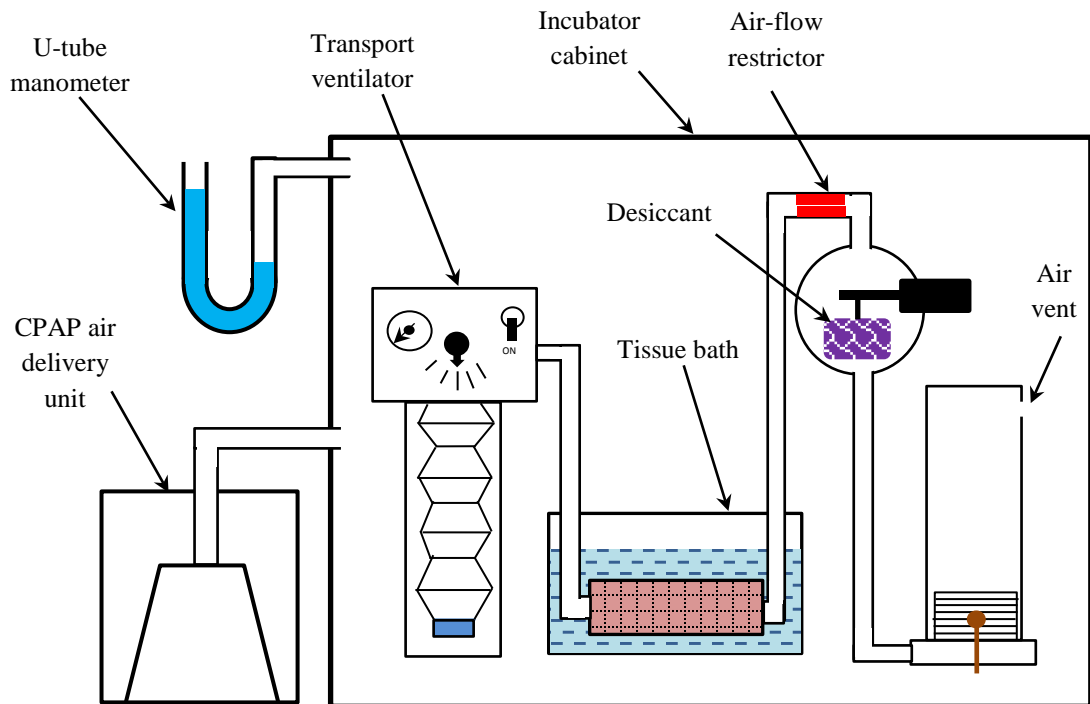


**Figure 5.3: Schematic representation of apparatus set up within the incubator.**

Excluding the tissue mounting system, previously described in Section 5.2.4, the tissue test apparatus, shown in Figure 5.3, consists of three functional sub-systems:

1. Air-flow and pressure drop regulation.
2. ASL water demand and measurement.
3. Air humidity and temperature measurement.

Each of the three apparatus subsystems contained a fixed air volume that was connected using 34 mm diameter thin-wall elastomeric tube to eliminate the transfer of vibration caused by motion of the bellows assemblies to the measuring sensors.

The configuration and operation of each of the apparatus sub-systems are detailed in the following sections before the complete system is discussed. Further detail on each subsystem can be found in the referenced appendices.

### **5.3.1 Air-flow Control and Pressure Drop Regulation**

Simulation of tidal breathing airflow was achieved by moving a fixed volume of air between two elastomeric bellows assemblies, shown schematically by Figure 5.4. To replicate *in-vivo* conditions, where airway epithelial cells experience both cyclic shear and cyclic pressure stresses, requires the airflow to pass in alternative directions through an orifice flow restrictor.

The master driving bellows, actuated by a modified transport ventilator (Ivent Research Ltd.), was inverted and weighted at the free end to ensure that it returned to the extended position when not being driven. In opposition, the slave bellows assembly was mounted in the upright position so that it returned by gravitational forces to the compressed position. Both bellows alternatively expanded and contracted as the trapped air volume was shuttled backward and forwards during actuation by the transport ventilator, simulating a tidal breathing airflow. An orifice, located near the slave bellows assembly provided the same flow resistance as that created by the human nose. Further detail of the pressure drop calculation is given in Appendix C3. The air space surrounding the slave bellows was vented enabling the air pressure within the trapped air volume to be varied and is discussed further in Section 5.4.1. During the inhalation phase of the simulated breath cycle, the trachea ASL and mucosa were exposed to sub ambient air pressure distribution and unidirectional shear stress, as shown by Figure 5.4.

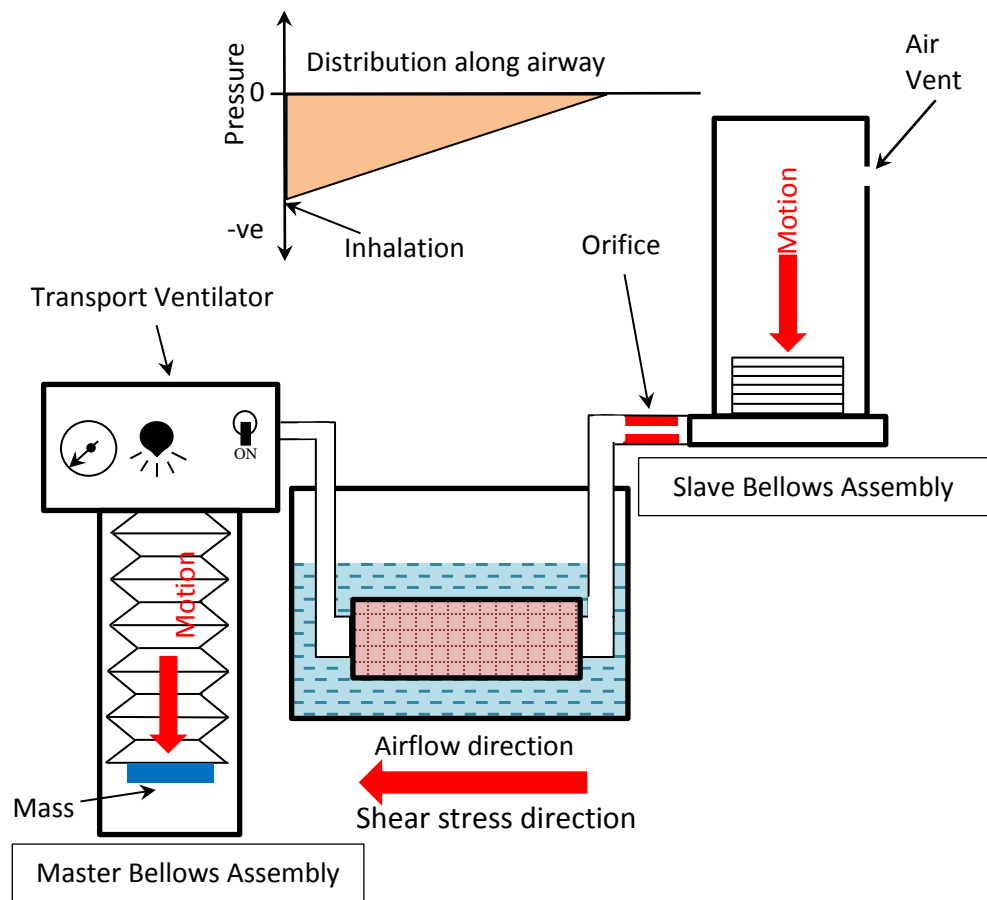


**Figure 5.4: Schematic of airflow apparatus set-up demonstrating inhalation breath phase and negative pressure distribution along trachea.**

For simplicity, ‘sub-ambient’ pressures will be referred to as ‘negative pressures’.

Conversely, during the exhalation phase, trachea epithelial cells experienced a pressure distribution above ambient with shear stress occurring in an opposite direction to that during inhalation, Figure 5.5.

The basis for the size of orifice to achieve the necessary fluctuation in air pressure is given in Appendix C3. This was based on typical pressure differences experienced across the human nose during normal at-rest tidal breathing [200].

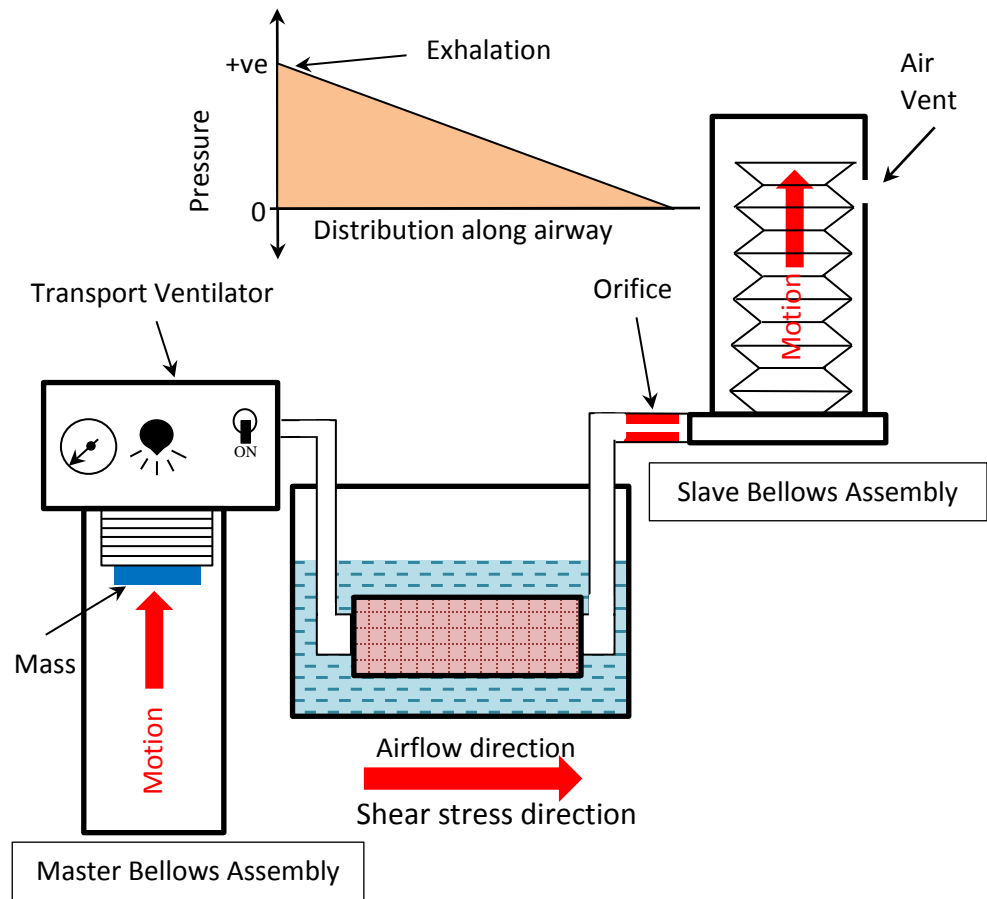


**Figure 5.5: Schematic of airflow apparatus set-up demonstrating exhalation breath phase and positive pressure distribution along trachea.**

### 5.3.2 Water Demand and Measurement.

A glass sphere formed a desiccant chamber within the air circuit. This contained an open weave fabric bag filled with 80 grams of Silica gel desiccant, Figures 5.6 and 5.7.

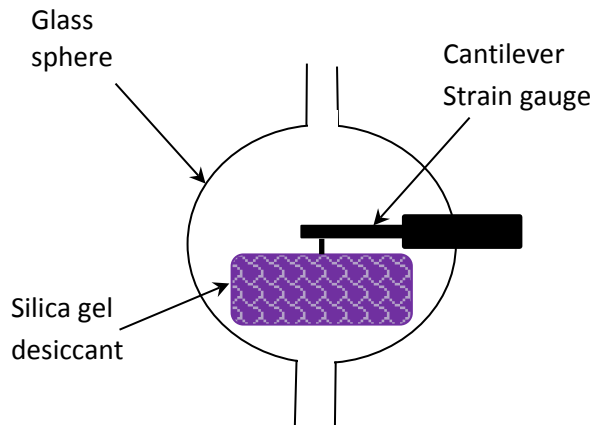


**Figure 5.6: Schematic of desiccant chamber glass sphere containing silica gel filled bag supported by cantilever strain gauge.**



**Figure 5.7: Image of glass chamber with cantilever gauge holding desiccant bag.**

A 100 g full scale cantilever strain gauge (World Precision Instruments FORT 100) supported the desiccant bag within the glass sphere. Water vapour was removed from the air passing through this chamber by the desiccant, resulting in an increase in silica-gel mass, accurately measured by the cantilever strain gauge.

New desiccant was used for each test to ensure consistency of absorption rate in each case.

### **5.3.3 Air Humidity and Temperature Measurement.**

Change in air moisture content was measured by a Sensirion SHT75 air temperature/humidity sensor located within the slave bellows air space, Figure 5.8.

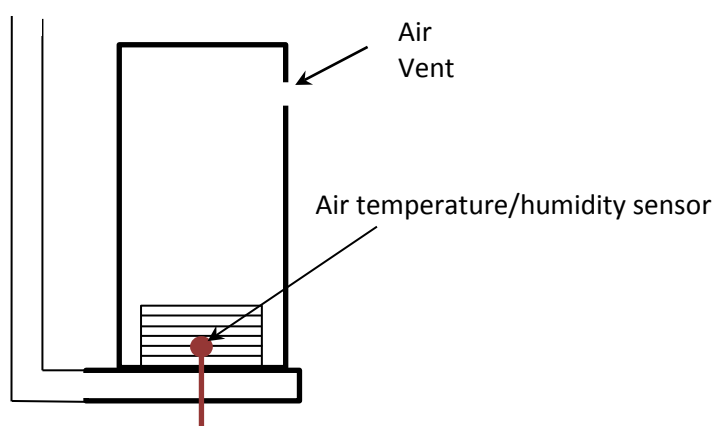


**Figure 5.8: Schematic of air temperature/humidity sensor within slave bellows assembly.**

## 5.4 Experimental Protocols and Data Management

### 5.4.1 Calibration

Prior to each test, the output of the cantilever strain gauge was verified against known calibrated masses. Further information is provided in Appendix C1.

The tissue mounting system containing PSS was placed in a water tank pre-heated by an immersion heater to 37°C and located within an incubator. The test apparatus was then assembled within the incubator space, shown schematically by Figure 5.3 and actual set-up Figure 5.9, trapping 2 litres of ambient air within the closed system. The transport ventilator was then configured to move a tidal volume of 1 litre at a frequency of 6 breaths per minute before the incubator door was closed. The temperature within the incubator space was then gradually raised over a 25 minute period from ambient to 37°C.

When required, pressure augmentation within the incubator space was provided by a CPAP air delivery unit connected by the standard CPAP air hose and pressure measured using a U-tube manometer, shown previously in figure 5.3. This pressure was experienced by the exterior tissue surface since the tissue tank was open at the top, shown previously in Figure 5.2.

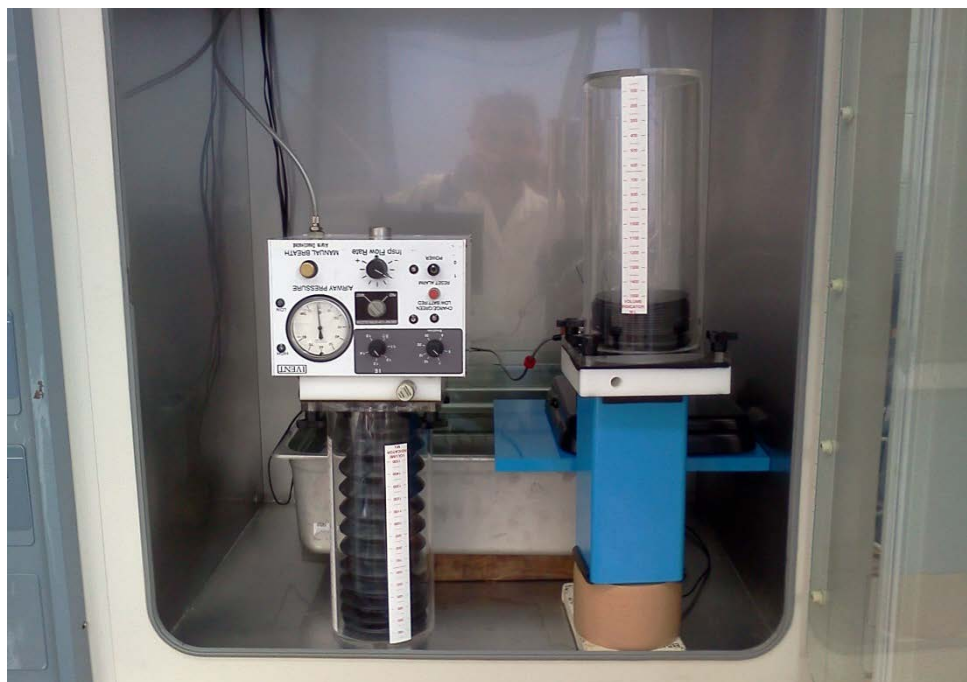


**Figure 5.9: Apparatus set up within the incubator.**

Air pressure was also experienced by the interior tissue surface since the exterior surface of the slave bellows was vented to the incubator space as shown previously in Figure 5.3.

During test, mucosal tissue experienced oscillating stresses associated with normal tidal breathing, whilst simultaneously being exposed to hydrostatic pressure equilibrium across its surfaces equal to the incubator cabinet pressure.

Data acquisition began after the system had been allowed to stabilise at a temperature of 37°C for a 10 minute period.

#### 5.4.2 Data Acquisition

Figure 5.10 illustrates the schematic layout of the data acquisition sub-system. Silica gel mass from the cantilever strain gauge was conditioned and amplified by a World Precision Instruments Transbridge Amplifier (TBM 4M) and continuously transferred to a data acquisition board, National Instruments (DAQMXPC), before being transferred to a PC via USB cable. Also shown in this figure is the data stream from the Sesirion® air humidity/temperature sensor which was pre-conditioned by a Sensirion® Evaluation Kit (model EK-H4) before being transferred to a PC via USB cable.

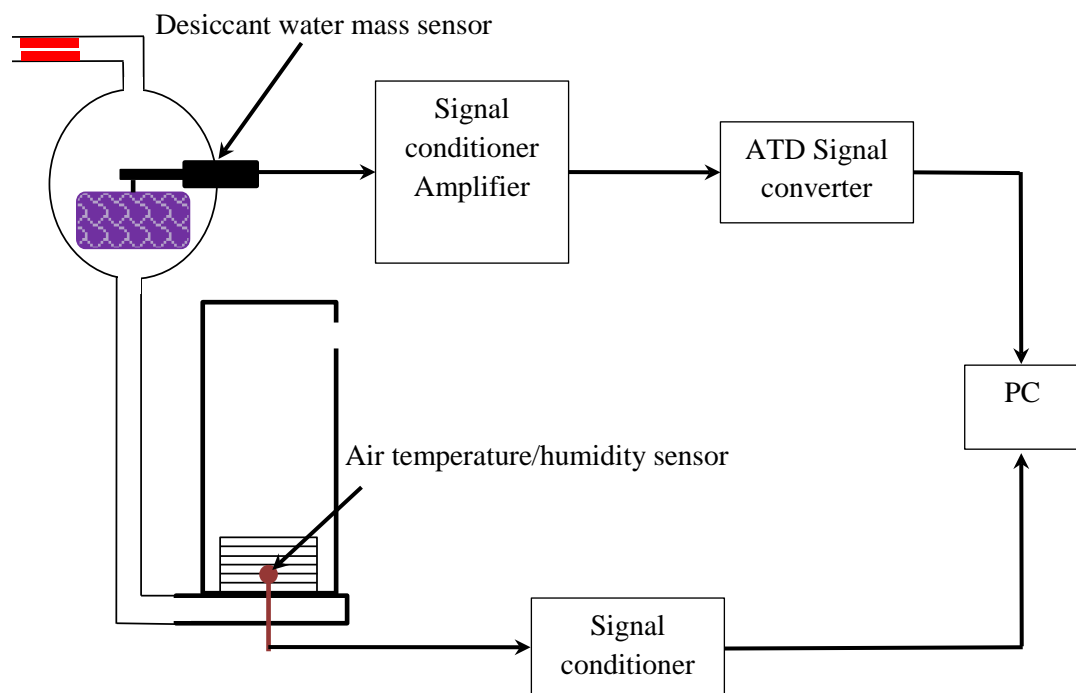


**Figure 5.10: Schematic of desiccant water mass and air temperature/humidity data streams.**

Processing and recording of the desiccant mass and air temperature/humidity data streams was undertaken within a PC using LabVIEW™ 2011 (National Instruments).

### 5.4.3 Post-Acquisition Data Processing

Data corresponding to the mass of water vapour absorbed from the air by the desiccant along with air water vapour content was recorded by the LabView software every 240 seconds for the test duration that spanned a minimum of 7 hours. The sampling time period was selected to reduce the influence of transient vibrations and account for the slow change in air temperature/humidity and desiccant mass occurring within the test apparatus. Upon completion of testing, data was stored in a LabView file using a pressure/date/time naming system. Post processing involved the conversion of these files to text files for input into MatLab™ (MathWorks, Natick, MA, USA) to differentiate the rate of change in each parameter measured as a function of time. Tissue water flux was calculated by adding the rate of change in water mass content in the desiccant to that of the air to yield the rate of water efflux from the tissue surface as demonstrated by equation (5.1).

$$\frac{dm_{eff}}{dt} = \frac{dm_{air}}{dt} + \frac{dm_{dess}}{dt} \quad (5.1)$$

Water flux values for each test undertaken were compiled and plotted using MatLab™.

## 5.5 Results

Data corresponding to one sample giving desiccant mass and the total mass of water vapour contained within the trapped air over a 7 hour period are shown in Figure 5.11.

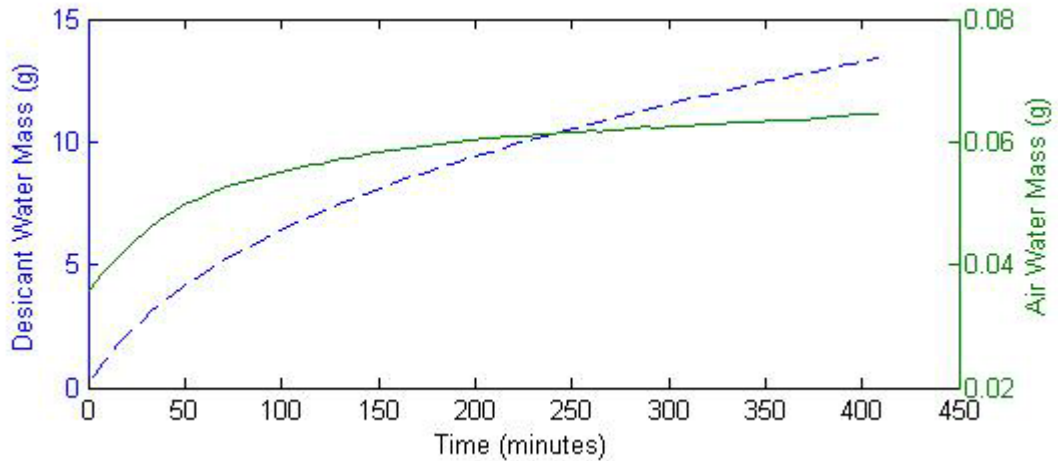


**Figure 5.11: Desiccant and air absolute humidity during 7 hour test. — Air water mass, - - - desiccant water mass.**

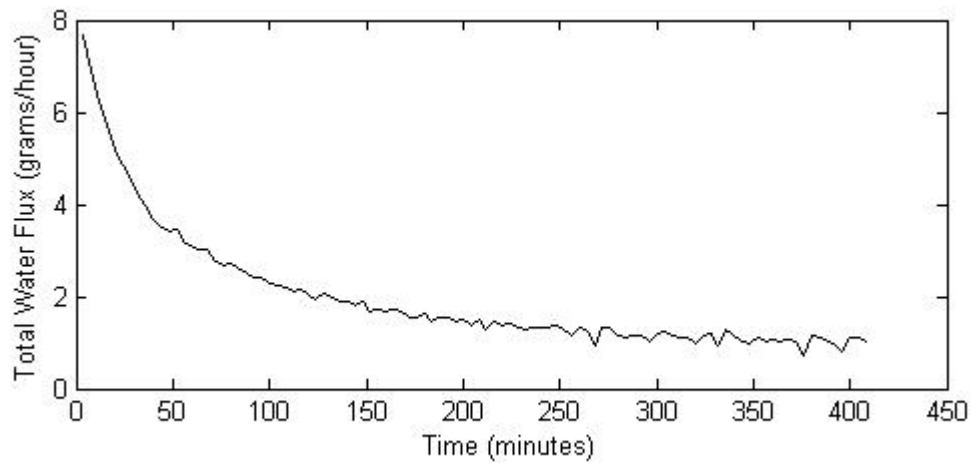


**Figure 5.12: Mucosal water flux during 7 hour test.**

Figure 5.12 presents the same sample where ASL water flux over the 7 hour test period has been determined using the rates of change in desiccant and air water mass as given in equation (5.1). The maximum rate of water flux was compiled for each of the eight samples, each exposed to one pressure level only, and presented at pressure increments of ambient, 5, 10 and 15 cm H<sub>2</sub>O and is given by Figure 5.13. Here, there is a 22% reduction in maximal water flux occurs from 5cm H<sub>2</sub>O PAP.

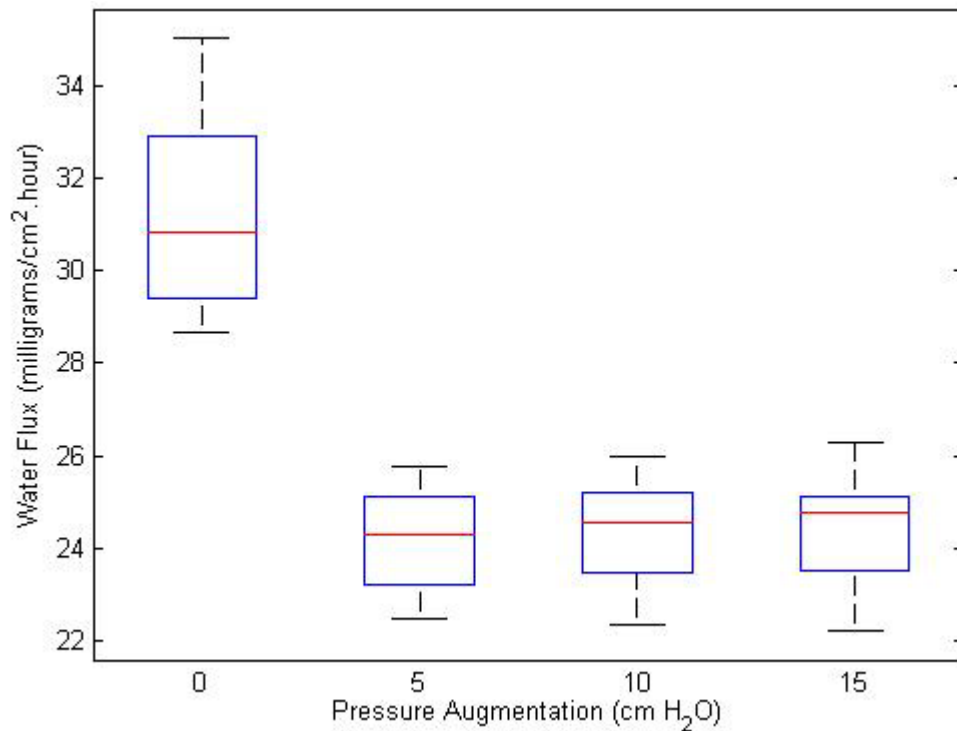


**Figure 5.13: Trachea maximal water flux during ambient and augmented pressure.**

To test the hypothesis that pressure augmentation negatively influences epithelial water flux, variation during simulated PAP breathing was evaluated using a 2-sided linear model. This analysis shows significant difference exists between the ambient and pressurised results ( $p \leq 0.0001$ ) when using a single sided t-test of the null hypothesis that this parameter is the same for all pressures. Additionally, there is no significant variation between all of the PAP results ( $p = 0.716$ ). This accepts the null hypothesis that this parameter is different between ambient and augmented air-pressures.

Correcting for the density of water at 37°C, at ambient pressure, the maximal water flux of 31 mg/cm<sup>2</sup>·hr corresponds to a volume flux rate of 31.2 µl/cm<sup>2</sup>·hr.

## **5.6 Analysis and Discussion**

Within the following sections, a review of factors, which may have influenced these results, is undertaken prior to comparing the ambient water flux results obtained from this experiment to those obtained by other investigators.

### **5.6.1 Factors Influencing Results**

Due to equipment limitations, the incubator air-pressure was found to fluctuate by 2 cm H<sub>2</sub>O for pressures below 5 cm H<sub>2</sub>O. These pressure oscillations were caused by the transport ventilator repeatedly exhausting air within the confines of the incubator enclosure. Here, despite the incubator space having a continuous air leak to atmosphere to stabilize the internal pressure, the ventilator exhaust air contributed sufficient air volume to cause the incubator internal pressure to rise. Increasing the amount of incubator air leak reduced these fluctuations to within 0.5 cm H<sub>2</sub>O; however this caused a drop in incubator temperature due to escaping air heat loss. Although cyclic variation in air pressure has already been proven to stimulate the airway cellular purinergic system [107, 135, 143] fluctuation at these low pressures was still around ten times greater than the normal physiological range [145, 200] and had no relevance in testing the research hypothesis. Because of this, testing was not undertaken at incubator pressures between ambient and 5 cm H<sub>2</sub>O PAP.

The New Zealand Commercial Slaughter Code of Animal Welfare (2010) requires all large mammals to be stunned prior to slaughter [229]. The red coloured foam found within each trachea collected from the abattoir is believed to be a mixture of lung surfactant and blood created by animal convulsions elicited by electrical stunning. This

unavoidable ASL contaminant was rinsed away with PSS, as detailed in Section 5.2.4, prior to testing. Although this rinsing process would have disturbed the ASL rheology and ionic balance necessary for the purinergic regulation system to operate [143, 148, 230], this effect would have been short lived given the high PSS absorption rate within the trachea [153] and rapid restoration of ASL by the airway epithelia [155]. Given the 35 minute interval between rinsing the trachea with PSS and the commencement of measurements taken by this experiment, it is likely the ASL would have returned to the normal rheology and ionic balance necessary for the purinergic system to operate normally.

Another factor that could have potentially influenced the results is the non-linear action of the silica gel desiccant used to remove water vapour from the air. This desiccant is characterised as having a high initial rate of water absorption, which then exponentially diminishes to zero when it has absorbed around 25% of its original mass in water vapour [231]. Further detail on the desiccant performance is contained in Appendix C1. This transient absorption characteristic creates a corresponding variable water demand that diminishes with time. Given the purinergic regulation system attempts to maintain a constant ASL height, its response in terms of ASL flux is then characterized by the applied water demand from the desiccant. This transient response is demonstrated in the air and desiccant water mass data recorded by this experiment. Since we are interested in maximal cellular water flux, the transient nature of the silica gel absorption is not an issue, provided care is taken to ensure each stage of the experiment was undertaken within identical time frames. Compounding this time related variable is the need to operate the experiment for around 35 minutes to achieve thermal stabilization prior to data being recorded. Because of the change in desiccant behaviour, this time delay leads to a slight reduction in the rate in which the silica gel absorbs water vapour. To avoid this issue influencing results, care was taken to ensure that each stage of the experiment was undertaken within identical time frames to ensure replication of tissue loading conditions for all tests undertaken. Care was also taken to ensure the greatest amount of silica gel was used so as to drive the tissue to supply water at its maximal rate whilst not over-stressing the supply so as to cause tissue desiccation and tissue death. During a feasibility study 80 grams of silica gel desiccant achieved these goals for the test apparatus used.

As mentioned in Section 5.2.3, tissue viability was assessed through the presence of active mucociliary transport occurring by observing the motion of Indian ink particles

within the ASL layer. Here it was assumed that the epithelial mucosa, purinergic regulatory system and subepithelial glands were viable if the presence of a coherent mucociliary transport velocity (MTV) could be seen. This assumption is reasonable given the cilial motion that drives the MTV is highly dependent upon ATP and intracellular calcium [147], both of which are regulated by the purinergic system. With this test, non-viable tissue would demonstrate an absence of MTV.

The partial pressure of water vapour directly above the ASL is determined by the temperature of the underlying liquid water which was held constant for this investigation. Change in the molar concentration of water species present in the air diminishes does however occur during conditions of pressure augmentation. This reduction in water vapour content within air over a range of pressures is given in Figure 5.14 which demonstrates a linear relationship between water content in the air and total air pressure over the range considered.

This figure demonstrates there is less than 4 % reduction in water vapour concentration occurring over the ambient to 15 cm H<sub>2</sub>O pressure range. Not only is variation in water vapour concentration very small, it also does not follow the same trend as that of maximal tracheal water flux found by this experiment. Given this, it is unlikely changes in water vapour concentration influenced the results.

The state of mucus hydration could also potentially influence the water vapour pressure above the ASL in situations where a continuous mucus gel layer overlays the watery periciliary liquid (PCL).

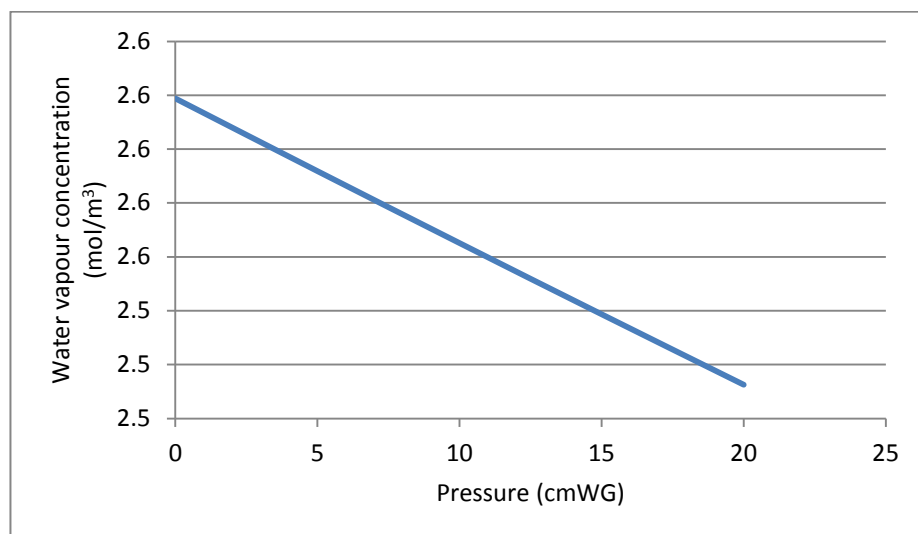


**Figure 5.14: Variation in saturation water vapour concentration over range of pressure augmentation at 37°C.**

Here the hydration state of the mucus determines the equilibrium vapour pressure and this is dependent upon pH and ionic strength [232]. Neutral gels experience a reduction in vapour pressure below 30% hydration but mucus is a polyionic gel, consisting of approximately 98% water 1% salt and 1% glycosylated mucin protein[115], so reduction is likely to occur at much higher hydration levels [166]. The problem of mucus hydration influencing these results was avoided by washing out the trachea prior to testing. This effectively removed any continuous mucus layer within the trachea and ensured the presence of an intact ASL layer both before and after testing.

Not only do temperature and pressure cause change in water vapour pressure and hence influence water flux from the ASL but also changes in chemical concentration of the underlying PCL. Following Raoult's Law, an increase in mole fraction of a chemical component within the ASL layer will cause a corresponding reduction in water mole fraction and water vapour pressure, leading to a subsequent drop in water mass flux. Given the chemical composition and concentration is actively regulated by the epithelial cell purinergic system[233], it is unlikely significant variation in water partial pressure would have occurred during the experiment.

As previously mentioned in 5.2.4, for this test an assumption was made that, provided the ASL volume remains present, any change in ASL water volume is insignificant since its total volume is so small.

### **5.6.2 Comparison to Previous Results**

As discussed in the literature review (Chapter 2) maximal water flux from tracheal tissue under ambient pressure conditions has previously been found to range from 10 – 150  $\mu\text{l}/\text{cm}^2\text{-hr}$  [106, 111, 132, 134, 163, 168]. This compares very well with the findings of this experiment that found a maximal water flux of 31.2  $\mu\text{l}/\text{cm}^2\text{-hr}$  at ambient pressure. This result validates the alternative method used by this experiment to measure tissue water flux and gives confidence to the veracity of findings at augmented air-pressures.

## **5.7 Nasal ASL Water supply**

The following sections discuss variation in nasal ASL water supply.

### **5.7.1 Air-Pressure Suppression**

Although water supply rates at ambient pressure correspond well to those previously reported, this investigation has found that there is a 22% reduction in water supply for all air-pressures above 5 cm H<sub>2</sub>O. It can be speculated that this reduction is most likely due to the cessation of superficial epithelial water supply as a result of excess pressure stress being exerted on the cellular purinergic sensory system. This finding proves the second part of the research hypothesis that stated pressure augmentation will reduce the ASL water supply from the airway mucosa. Within the nasal air-conditioning model, the maximal rate of mucosa water supply to the ASL reduces by 22% for all simulated breathing pressures above 5 cm H<sub>2</sub>O.

Additionally, the findings of this experiment suggest the superficial epithelium can contribute more ASL volume than the 5% previously thought [127] given there was a 22% reduction in water supply.

### **5.7.2 Maximal ASL Water Supply**

As mentioned in Chapter 2, there is an absence of nasal mucosal maximal water supply data from the current literature; however this variable is required for the new nasal ASL hydration model. The point that it is not possible to directly apply the values of ASL supply and absorption found for the distal conducting airways, such as the trachea, to that of the proximal airway, such as the nose has also been made. This is because the distal conducting airway carries a lower air-conditioning load that experienced by the nose. It is however possible to approximate the ratio by which liquid secretion exceeds that absorbed. This can be found by considering the tracheal secretion rates from the ASL flux data reviewed in Chapter 2. By considering the ratio of average secretion to average absorption, discussed in Section 2.5.3.1, secretion is found to exceed absorption by a factor of 3.5. This ratio will be used to determine the absorption rate once the magnitude of the ASL fluid supply has been determined.

A different method of calculating nasal mucosa maximal water flux is now undertaken. This estimation is based on inhaled air conditions, breathing volume and rate which has

already been undertaken for a range of ambient air conditions [52]. By assuming dry inhaled air is fully humidified after passing down one nasal passageway of known typical surface area ( $100 \text{ cm}^2$ ) in one breath cycle, the maximal ASL supply value for the nasal mucosa is calculated at  $7.9 \text{ g/cm}^2\text{-hr}$ . The maximum rate of excess ASL absorption within the nose can now be calculated by dividing this value by the previously determined reabsorption ration (3.5) to yield a maximum PCL reabsorption value of  $2.2 \text{ g/cm}^2\text{-hr}$ .

## **5.8 Closure**

The second part of the research hypothesis that postulated pressure augmentation negatively impacts mucosal ASL water supply has now been demonstrated. Here there is a 22 % reduction in the maximal rate of mucosal water supply occurring at air-pressures above  $5 \text{ cm H}_2\text{O}$ .

Maximal nasal mucosal ASL water supply and reabsorption at ambient pressure has been estimated and can now be applied to the nasal ASL hydration model.

## CHAPTER 6

### MODEL RESULTS AND OBSERVATIONS

#### 6.1 Introduction

In Chapter 2 it was postulated that n-PAP breathing reduces the ASL water supply and also creates abnormal air-flow partitioning between each airway through variation of inter-nasal geometry. The net result of the combination of these two conditions creates abnormal ASL water hydration distributions along both nasal airways.

The findings of change in nasal morphology and mucosal water supply caused by pressure augmentation, determined in chapters 4 and 5 respectively, have now been implemented within the nasal model.

Section 6.2 describes the plot presentations before Section 6.3 presents results from the nasal air-conditioning model during spontaneous breathing at ambient pressure. Where possible, model results are compared to either *in-vivo* results from other studies or earlier model predictions from other research, where *in-vivo* measurements of flux parameters are not available. Inter-nasal air-flow partitioning results presented in Section 6.4 include predictions for breathing at augmented air-pressure. Un-humidified pressurised breathing results are given in Section 6.5, before analysis of mucosa dry time over the breathing cycle for a range of pressure augmentations is presented in Section 6.6. Results of typical supplementary heated humidification and non-heated supplementary humidification are compared in Section 6.7 and Section 6.8 respectively.

Due to the inter-play occurring between results, comments are made throughout each set of findings to explain the complex interactions occurring. A more in-depth discussion and analysis of these results is developed in Chapter 7.

#### 6.2 Introduction to Plots

Model results fluctuate over one breath cycle as a consequence of change in air mass-flow rate and phase of breath cycle as well as variation in the state of ASL hydration. The best way to interpret these results is to view them as an animation, as it gives sense to the rate of change in these parameters during normal tidal breathing. To enable representation of results within this work, data is presented as temporal slices during either the inhalation or exhalation phases of the breath cycle as shown in Figure 6.1.

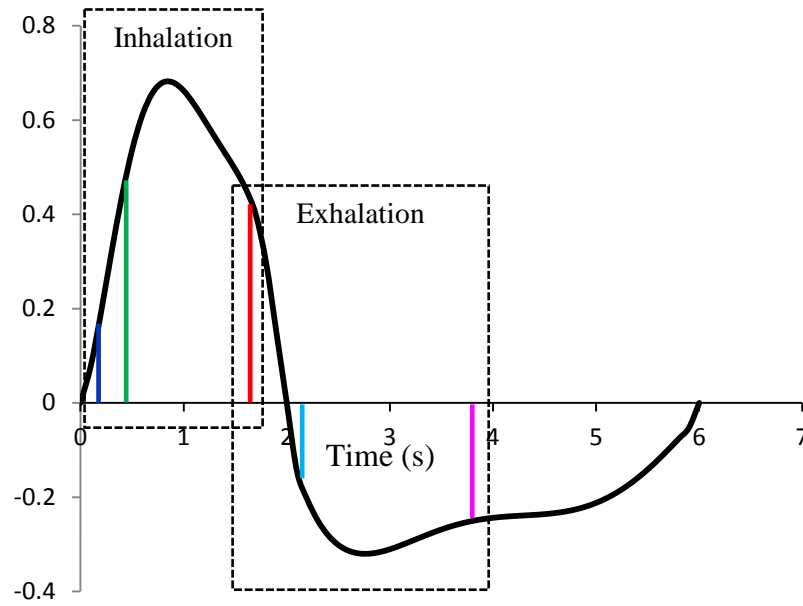


**Figure 6.1: Temporal slices of breath cycle used for inspiration and expiration model results.**

Here, during inhalation, results span the time interval of commencement of inhalation (blue line at  $t = 0.2\text{s}$ ) to where maximal variation in measured parameters occur (red line at  $t = 1.7\text{s}$ ). Data corresponding to an intermediate interval (green line at  $t = 0.4\text{s}$ ) is also shown. Results for expiration span the time interval starting where peak inhalation results (red line,  $t = 1.7\text{s}$ ) occur to where maximal change during exhalation ensues (magenta line,  $t = 3.8\text{s}$ ). Data corresponding to an intermediate interval (cyan line,  $t = 2.1\text{s}$ ) is also given.

To demonstrate the variation in each parameter over either of the two breath phases, arrows are drawn. These start from the data found at the beginning of the breath phase and point to that corresponding to the end. These arrows also lean towards either the distal or proximal direction, as indicated by horizontal X/L axis, to specify airflow trajectory during either phase of the breath cycle. The symbol X is used to represent distance along airway for consistency with earlier publications by Hanna [97, 166].

Graphical results contained within this chapter cover a variety of air conditions during either inhalation or exhalation phases of breathing. These are summarised in Table 6.1.

### 6.3 Ambient Air Breathing

Within this section, subject specific model predictions for inter-nasal distributions of air temperature ( $T_a$ ), absolute humidity ( $AH$ ), water mass flux ( $m_{ASL}$ ), and heat flux ( $Q$ ) are made during simulated nasal breathing at ambient pressure. Additionally it introduces for the first time a prediction of the change in intra-nasal airway surface liquid (ASL) water equivalent height ( $H_{e,asl}$ ) as an indicator of ASL hydration status.

Where possible, results are compared to published *in-vivo* data from other researchers to give confidence as to the veracity of the new model. These results introduce for the first time a prediction of the change in inter-nasal ASL hydration distribution along both nasal airways.

**Table 6.1: Listing of figures for results during various breathing conditions.**

	<b>Inhalation</b>	<b>Exhalation</b>
<b>Ambient air breathing</b>	Figure 6.2	Figure 6.3
<b>Un-humidified n-PAP breathing</b>	Figure 6.5	Figure 6.7
<b>n-PAP breathing with supplementary heated humidification</b>	Figure 6.9	Figure 6.10
<b>n-PAP breathing with non-heated supplementary humidification</b>	Figure 6.11	Figure 6.12

### 6.3.1 Inhalation Air Properties, Flux Levels and ASL Hydration

Model predictions for inter-nasal air temperature ( $T_a$ ), absolute humidity ( $AH$ ), ASL water mass flux ( $m_{ASL}$ ), heat flux ( $Q$ ) and ASL water equivalent height ( $H_{e,ASL}$ ) distributions during the inhalation phase of the breath cycle are shown in Figure 6.2.

The magnitude of peak heat flux within the right (patent) airway, Figure 6.2 (h), is higher than that in the left (congested) airway, Figure 6.2 (g), as a result of the patent airway conducting the majority (67%) of the air mass-flow during ambient pressure breathing, as given by Figure 6.4. Both these results compare well with that predicted by Hanna's model [97]. On the other hand, ASL water mass flux within the anterior region of the right (patent) airway ( $X/L < 0.48$ ), Figure 6.2 (f), is substantially lower than that predicted by Hanna's model [97]. This result is not surprising given Hanna's model featured limitless ASL water supply [97, 166]. Figure 6.2 (j) shows that dehydration of the ASL layer occurs within the anterior region of this airway, which has caused the ASL water mass flux to fall to that of the cellular basal water supply. This was determined in Chapter 5 to be  $7.9 \text{ g/cm}^2\cdot\text{hr}$  and is shown by the horizontal red line in the anterior region ( $X/L < 0.5$ ) in Figure 6.2 (f). Of note in this figure is the slight increment in ASL water mass flux posterior to the mid-region of this airway ( $X/L > 0.5$ ), which is due to the presence of hydrated ASL on the mucosal surface, as given in Figure 6.2 (j). The distribution of ASL water mass flux for the left (congested) airway, Figure 6.2 (e), compares better to that predicted by Hanna's model [97]. This is likely as a consequence of sustained ASL hydration and resultant water availability throughout the inhalation phase of the breath cycle, as shown by Figure 6.2 (i).

Within the right (patent) airway, reduction in ASL water mass flux, shown in Figure 6.2 (f), has lowered the air absolute humidity, Figure 6.2 (d) when compared to that of the left (congested) airway, seen in Figure 6.2 (c). Additionally, reduced latent heat exchange in the right (patent) airway has caused the air temperature distribution, shown in Figure 6.2 (b) to be lower than that found in the left (congested) in Figure 6.2 (a). Even with this inter-airway variation occurring, the distribution of air temperature and ASL water mass flux along both airways compare favourably with previously published *in-vivo* data taken during peak inhalation [50, 73, 180, 181]. This is despite slight variation existing between ambient air conditions of temperature ( $T = 22\text{-}25^\circ\text{C}$ ) and relative humidity ( $RH = 35\text{-}45\%$ ) recorded during these earlier investigations and that used in the model ( $T = 23^\circ\text{C}$  and  $RH = 45\%$ ).

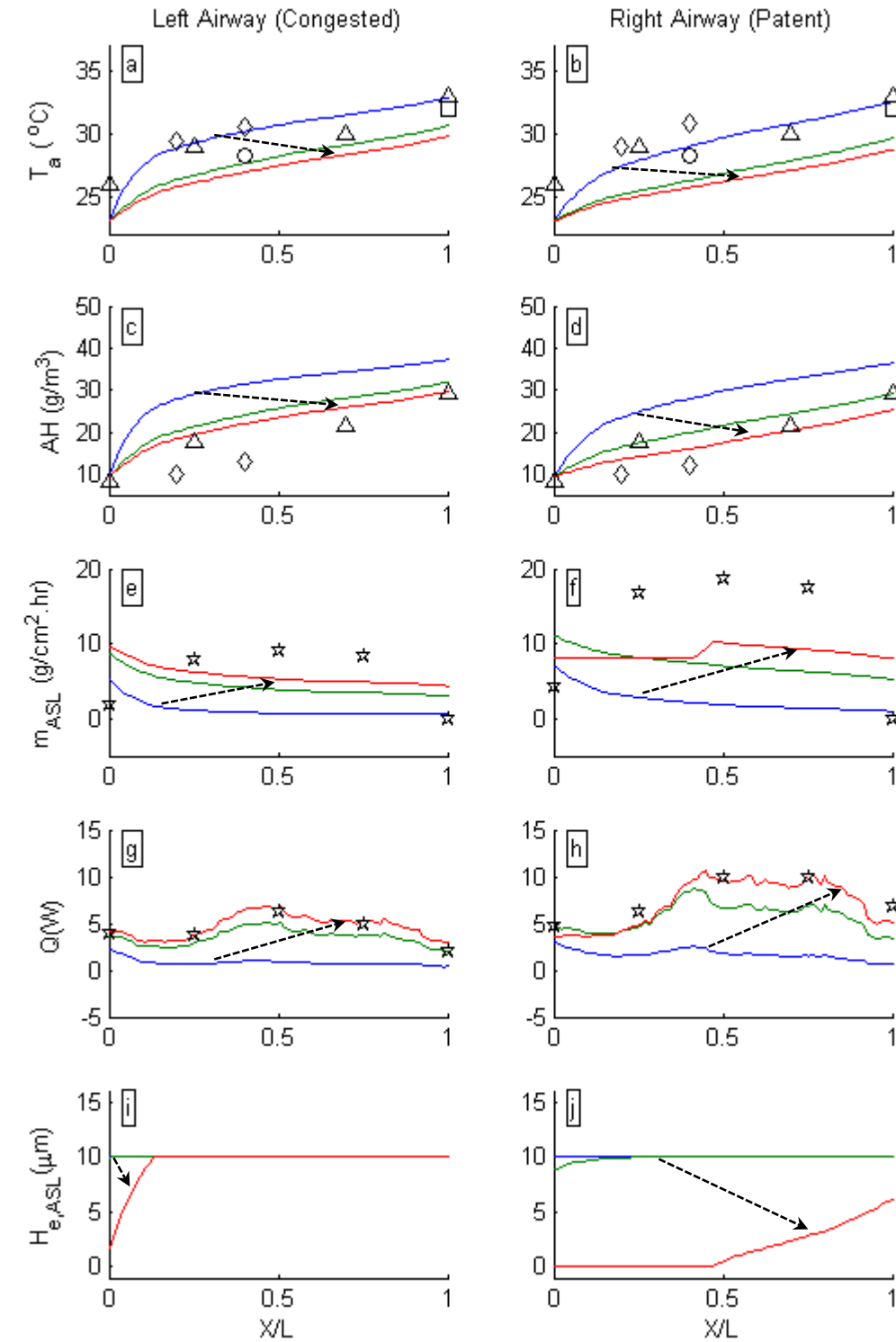


**Figure 6.2: Inhalation inter-airway temperature ( $T_a$ ), absolute humidity ( $AH$ ), molar water flux ( $N$ ), heat flux ( $Q$ ) and ASL water equivalent height ( $H_{e,ASL}$ ) distribution from rest to maximal change. Mask pressure ambient,  $AH=9.2 \text{ g H}_2\text{O/m}^3$  dry air ( $T=23^\circ\text{C}$ ,  $RH=45\%$ ).  $\Delta$  = Keck *et al.* [180],  $\circ$  = Wiesmiller *et al.* [73],  $\diamond$  = Lindemann *et al.* [181],  $\star$  = Hanna [97],  $\square$  = Lindemann *et al.* [50].**

### 6.3.2 Exhalation Air Properties, Flux Levels and ASL Hydration

Model predictions for inter-nasal air temperature, absolute humidity ASL water mass flux, heat flux and ASL water equivalent height distributions during the exhalation phase of the breath cycle are shown in Figure 6.3.

The magnitude of end exhalation ASL water mass and heat flux distributions within the right (patent) airway, shown in Figures 6.3 (f) and 6.3 (h) respectively, is slightly greater than that found in the left (congested) airway in Figures 6.3 (e), and Figure 6.3 (g). This is again a result of the patent airway conducting the majority (67%) of the air mass-flow, as given in Figure 6.4. Results of ASL water mass flux distribution compare well with that predicted by Hanna's model [97], since water supply is not an issue during this phase of breathing as condensation of exhaled water vapour increases ASL hydration. Unfortunately, no published heat flux data can be found to compare to the model results, however, we can see that the heat recovery to the mucosa is around 20-30% of that lost from this surface. This agrees with previous investigations that have found, during the exhalation phase, the nose recovers around 30% of heat and moisture lost during inspiration [63].

Of note is the recovery of ASL hydration status in both the patent airways to normal physiological limits by completion of the exhalation phase. Shown in Figure 6.3 (j), the previously dehydrated anterior region ( $X/L < 0.48$ ) of the right (patent) airway rehydrates due to absorption of water condensed in the ASL surface. Of note is slight over-hydration within the anterior region ( $X/L < 0.3$ ) of this airway due to additional condensation occurring as a result of it carrying a greater portion of exhaled saturated air mass flow (67%) when compared to the left (congested) airway (33%), Figure 6.3 (i). The ASL hydration within the left (congested) airway, shown in Figure 6.3 (i), which had not become dehydrated during inhalation, stabilises at the normal physiological maximal limit.

During peak exhalation, both air temperature and absolute humidity for the left (congested) airway, shown by Figures 6.3 (a) and 6.3 (c) respectively, and right (patent) airway, shown by Figures 6.3 (b) and 6.3 (d) respectively, compare very well to previously published *in-vivo* data [50, 73, 180], despite the slight variation in ambient air conditions previously mentioned in Section 6.2.1.

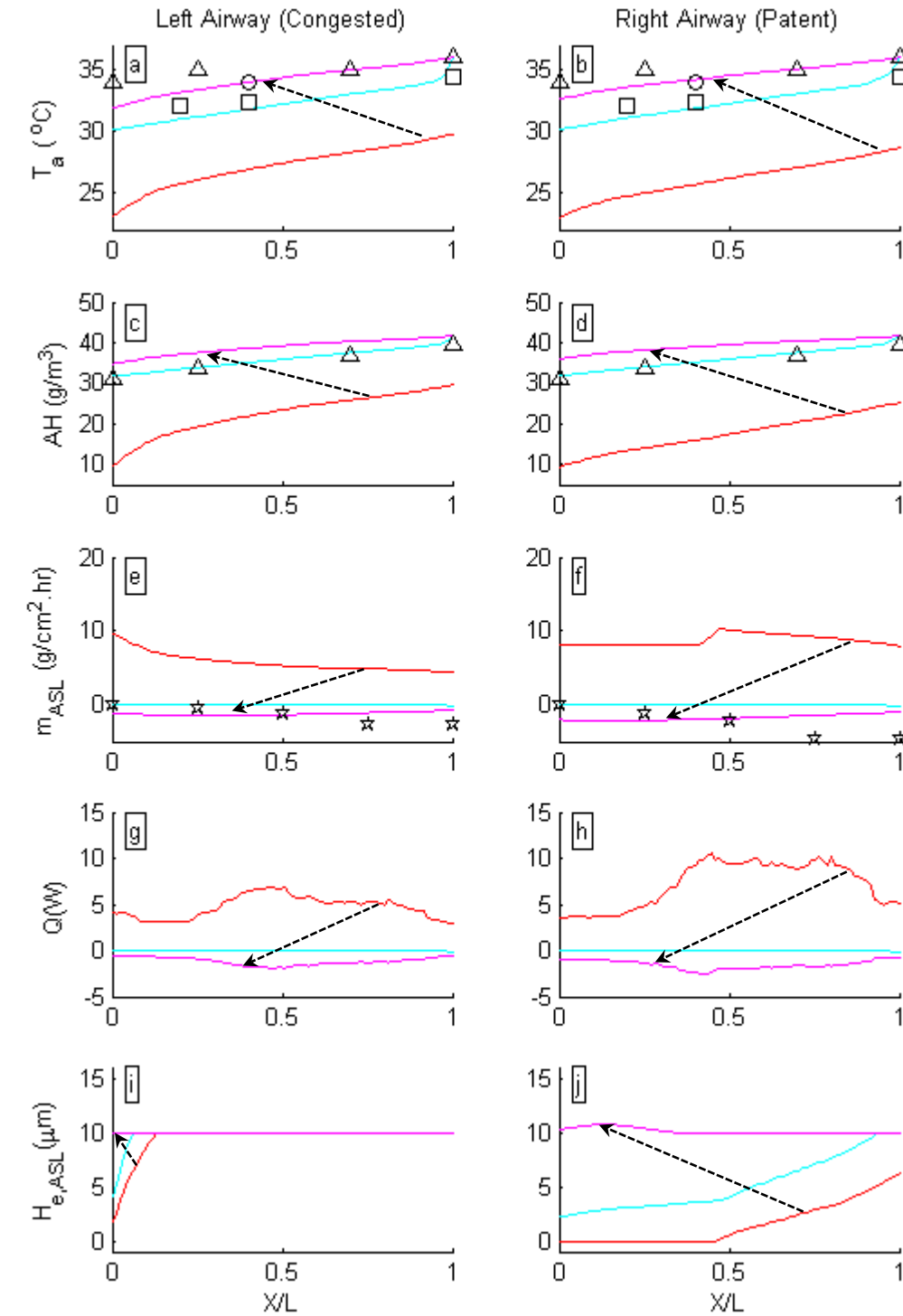


**Figure 6.3: Exhalation inter-airway temperature ( $T_a$ ), absolute humidity ( $AH$ ), molar water flux ( $N$ ), heat flux ( $Q$ ) and ASL water equivalent height ( $H_{e,ASL}$ ) distribution from maximal inhalation to maximal exhalation. Mask pressure ambient,  $AH=9.2\text{g H}_2\text{O/m}^3$  dry air ( $T=23^\circ\text{C}$ ,  $RH=45\%$ ).  $\Delta$  = Keck *et al.* [180],  $\circ$  = Wiesmiller *et al.* [73],  $\star$  = Hanna [97],  $\square$  = Lindemann *et al* [50].**

## 6.4 Air Mass-Flow Partitioning

Model predictions of air mass-flow partitioning between the two nasal passageways over a range of air pressures are shown in Figure 6.4. Here the MRI morphological data from one individual at ambient pressure has been used to predict the percentage of air-mass-flow carried within each airway at ambient pressure and over a range of pressure augmentations, based on the findings discussed in Chapter 4.

At ambient pressure, the patent nasal airway of this individual passes 67% of the air mass-flow while the congested airway passes only 33%. This finding agrees very well with normal range of air-flow partitioning found by Roblin and Eccles who tested 100 people [86]. Given that this is the first nasal air-conditioning investigation that considers air-flow partitioning at augmented pressures, no previous published data on inter-nasal air mass-flow partitioning during n-PAP breathing is available for comparison.

Model predictions of air mass-flow partition ratios for augmented pressures require the application of the nasal geometric response specific to the status of the nasal cycle and pressure augmentation.

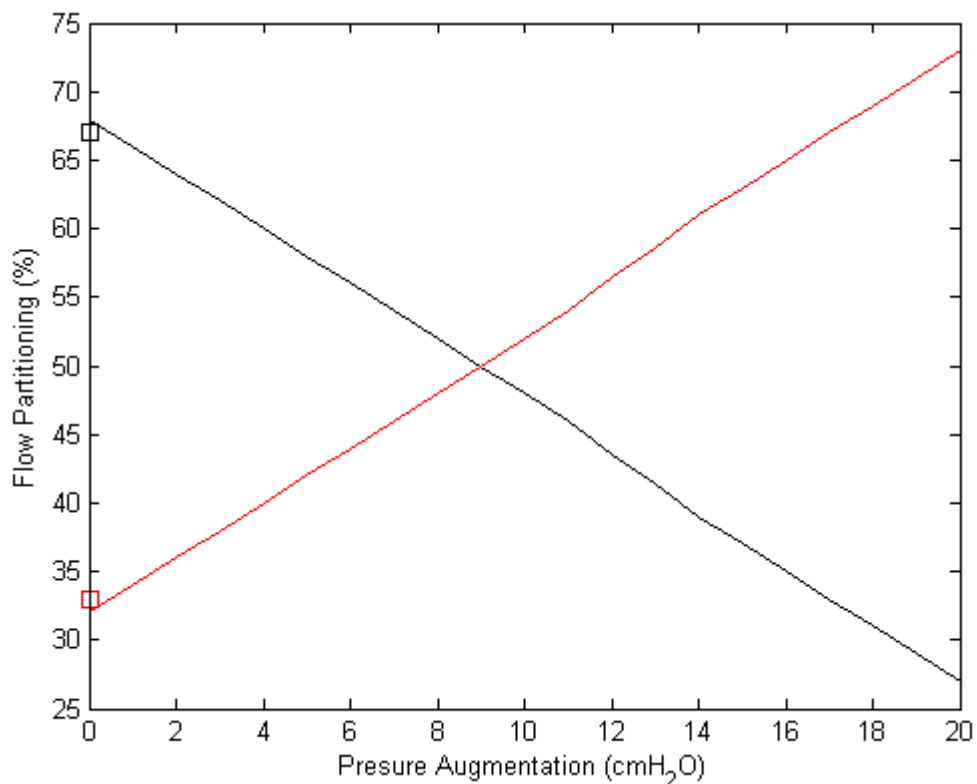


**Figure 6.4: Inter-airway air mass-flow partitioning ratio over range of pressure augmentation. — = right airway, — = left airway. □ = normal patent airway at ambient pressure, ◻ = normal congested airway at ambient pressure. Roblin and Eccles [86].**

The different inter-nasal geometric response between the patent and congested airways during n-PAP breathing, determined in Chapter 4, enables the model to calculate the change in airway resistance. Implementing this data, the model shows that air mass-flow within the right (previously patent) airway decreases with increasing pressure. Conversely, the air mass-flow within the left (previously congested) airway increases, as demonstrated in Figure 6.4. For this particular individual, at a pressure of 9 cm H<sub>2</sub>O, both airways experience an equal air mass-flow rate. In the following sections the model is run at a pressure augmentation of 9 cm H<sub>2</sub>O to simulate this balanced airflow condition, in order to identify the worst possible pathophysiological outcomes for this individual.

## **6.5 Un-Humidified n-PAP Breathing**

Results presented in this section are derived from the model predictions for an individual undertaking simulated 9 cm H<sub>2</sub>O n-PAP breathing, which, as discussed in the previous section, represents for this individual the worst possible scenario for sustaining viable ASL hydration within either of the two airways.

Model predictions for n-PAP breathing are compared to published data at ambient pressure from other sources. This is done as no previously published data acquired during spontaneous n-PAP breathing can be found in the current literature. Despite this variance in pressure status, this comparison will at least provide a means of comparing air-conditioning performance between these two pressure levels.

These results introduce for the first time a prediction of the change in inter-nasal ASL hydration distribution along both nasal airways.

### 6.5.1 Inhalation Air Properties, Flux Levels and ASL Hydration

Model predictions during the inhalation phase of the breath cycle during pressurised breathing are shown in Figure 6.5.

All parameters of air temperature, absolute humidity, ASL water mass flux, heat flux and ASL water equivalent height for the left (previously congested) airway, given in Figures 6.5 (a), 6.5 (c), 6.5 (e), 6.5 (g) and 6.5 (i) respectively, are nearly equal to those found in the right (previously patent) airway, given in Figures 6.5 (b), 6.5 (d), 6.5 (f), 6.5 (h) and 6.5 (j) respectively. This is a consequence of equal air mass-flow occurring within both nasal airways. The only difference in these results occurring between the airways is due to the variation in inter-nasal geometry inherent with this individual. This is demonstrated by the internal hydraulic diameter distribution for both ambient and n-PAP breathing presented in Figure 6.6. The inherent inter-nasal variation in geometry can be seen when comparing the magnitude of the hydraulic diameter distribution between both airways. Of note in Figure 6.6 is the overall reduction in hydraulic diameter experienced by the right (previously patent) airway and increase in that of the left (previously congested) left airway. This pressure elicited change results in the magnitude of the hydraulic diameter along each airway to become nearly identical, causing equal air mass-flows to occur.

Significantly, simultaneous dehydration of the ASL layers along 70-75 % of the anterior airway regions occurs within both the left (previously congested) and right (previously patent) passageways, shown in Figures 6.5 (i) and 6.5 (j) respectively. As a consequence of this, the model has predicted ASL water mass flux to reduce to a level of basal cellular water supply, shown by the horizontal red line in both airways, shown in Figures 6.5 (e) and 6.5 (f). Of note is the slight increment in ASL water mass flux due to the presence of hydrated ASL on the mucosal surface posterior to these locations.

The peak magnitude of heat flux is nearly equal between the left (previously congested) and right (previously patent) airways, shown by Figures 6.5 (g) and 6.5 (h) respectively. These results differ slightly to that predicted by Hanna's model [97] as a result of both airways conducting equal air mass-flow rates.

ASL water mass flux within the anterior region ( $X/L < 0.5$ ) of the left (previously congested) airway, and that of the anterior region ( $X/L < 0.7$ ) of the right (previously patent) airway, shown in Figures 6.5 (e) and 6.5 (f) respectively, are lower than that predicted by Hanna's model [97]. This is a consequence of the ASL being severely dehydrated along these regions and Hanna not accounting for limited ASL water supply.

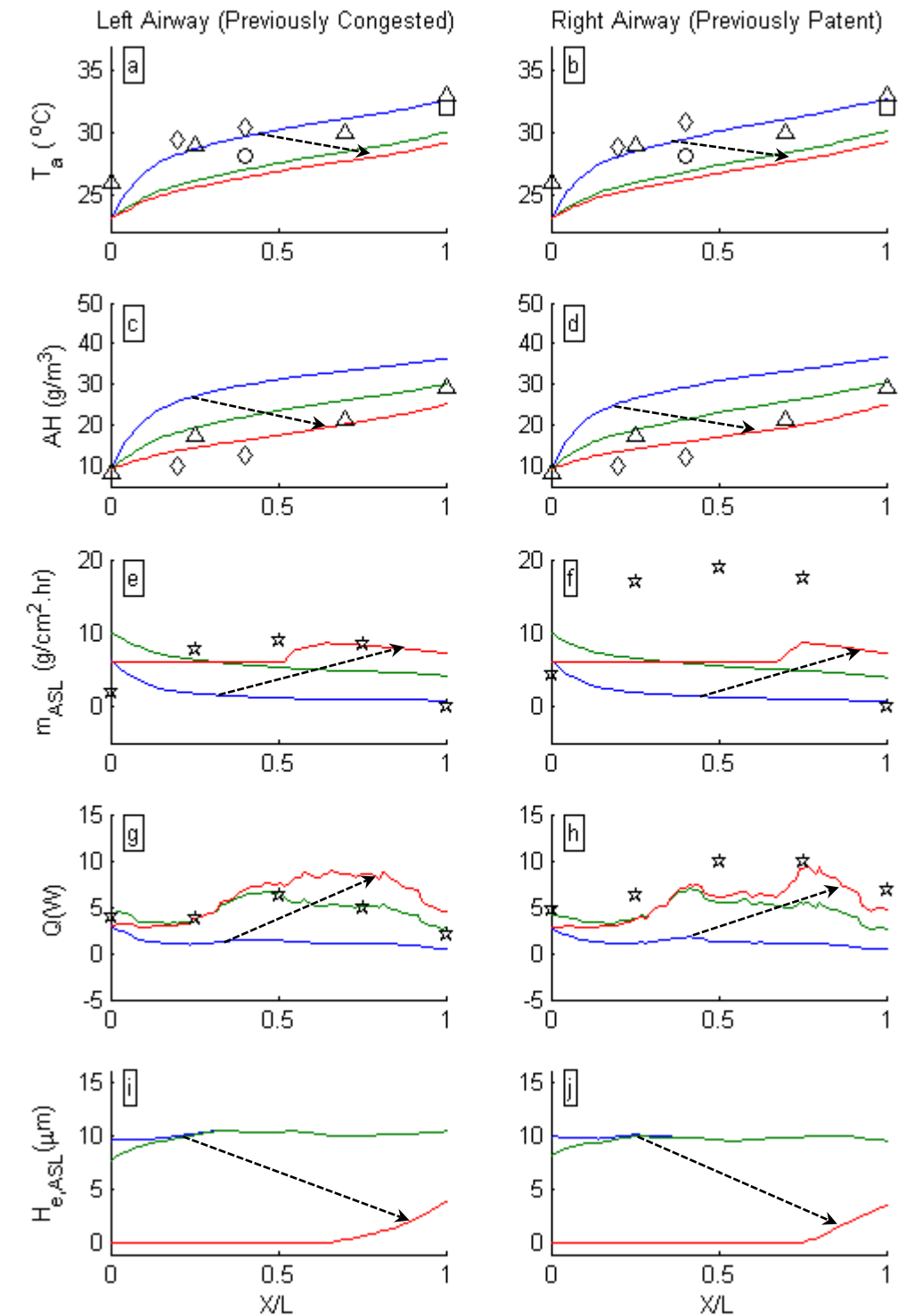


**Figure 6.5: Inhalation inter-airway temperature ( $T_a$ ), absolute humidity ( $AH$ ), molar water flux ( $N$ ), heat flux ( $Q$ ) and ASL water equivalent height ( $H_{e,ASL}$ ) distribution from rest to maximal change. Mask pressure 9 cm  $H_2O$ ,  $AH=9.2g H_2O/m^3$  dry air ( $T=23^\circ C$ ,  $RH=45\%$ ).  $\Delta$  = Keck *et al.* [180],  $\circ$  = Wiesmiller *et al.* [73],  $\diamond$  = Lindemann *et al.* [181],  $\square$  = Lindemann *et al.* [50],  $\star$  = Hanna [97].**

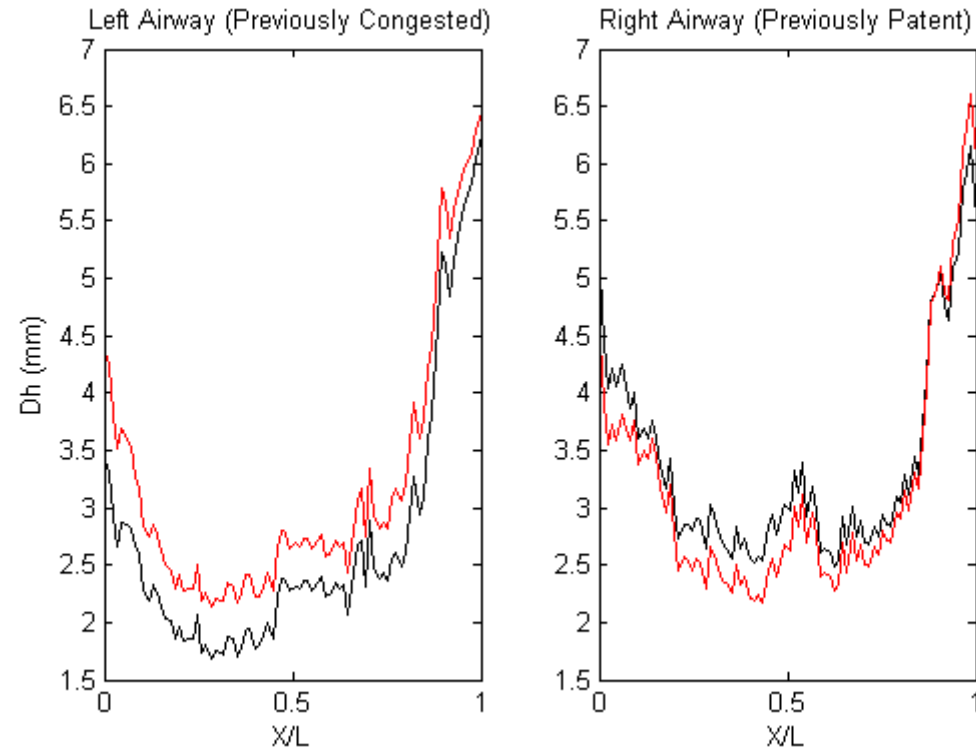


**Figure 6.6: Inter-nasal hydraulic diameter distribution.** — = Ambient pressure, — = 9 cm H<sub>2</sub>O.

### 6.5.2 Exhalation Air Properties, Flux Levels and ASL Hydration

Model predictions during the exhalation phase of the breath cycle during pressurised breathing are shown in Figure 6.7.

As with the inhalation breath phase, all parameters for the left airway are also nearly equal to those found in the right airway. Again, this is a consequence of equal air mass-flows occurring within both airways during n-PAP breathing at 9 cm H<sub>2</sub>O, previously discussed.

As with ambient pressure breathing; the inter-nasal distributions of ASL water mass flux agrees very well with Hanna's model data [97], since water supply is not an issue during this phase of breathing due to condensation of exhaled water vapour increasing ASL hydration. Of note in Figures 6.7 (i) and 6.7 (j) is the recovery of ASL water equivalent height in both airways demonstrating an over-shoot similar to that found in the right (patent at ambient) airway during ambient pressure breathing, shown in Figure 6.3 (j), but of lower magnitude and along their entire lengths.

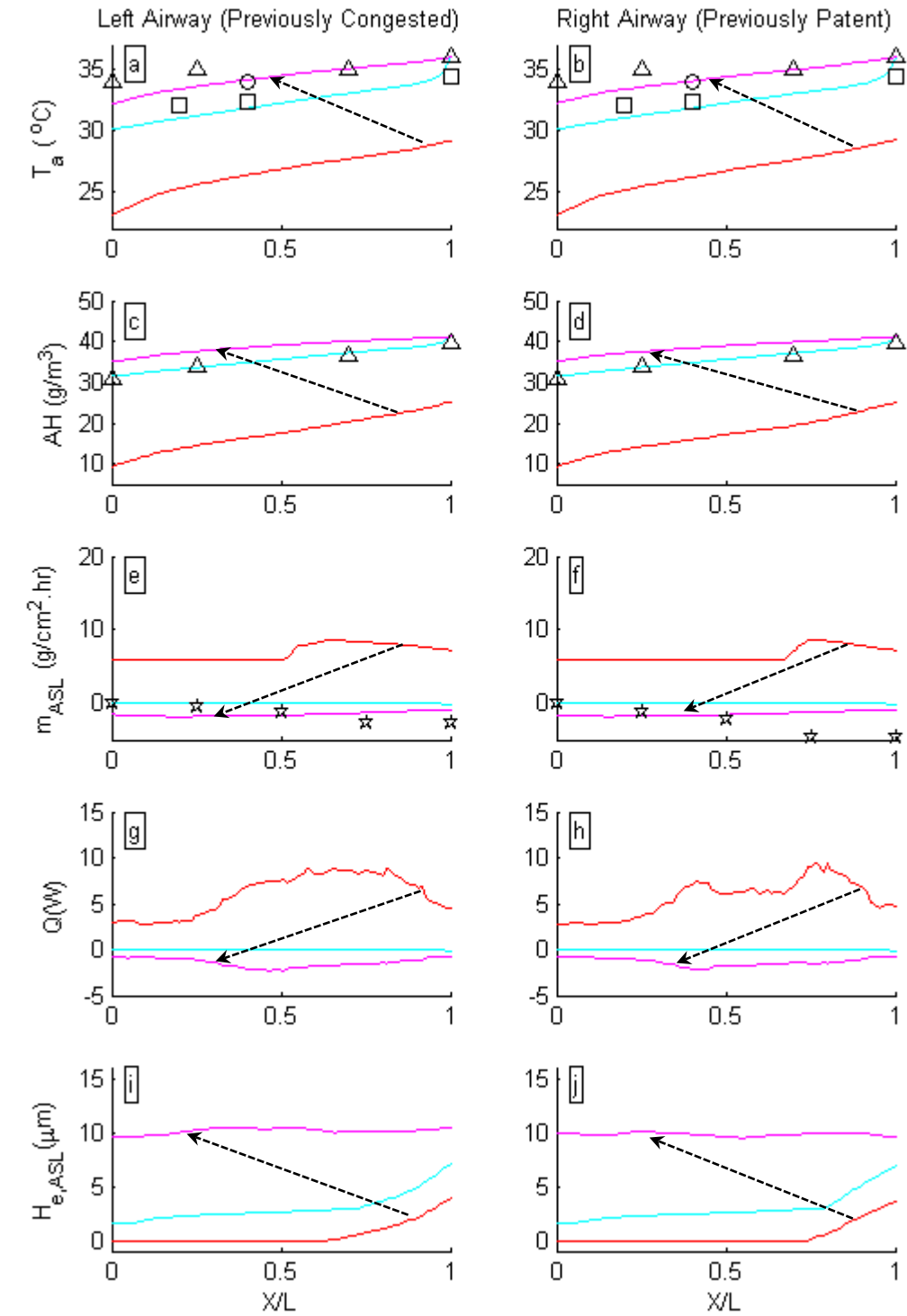


**Figure 6.7: Exhalation inter-airway temperature ( $T_a$ ), absolute humidity ( $AH$ ), molar water flux ( $N$ ), heat flux ( $Q$ ) and ASL water equivalent height ( $H_{e,ASL}$ ) distribution from maximal inhalation to maximal exhalation. Mask pressure 9 cm H<sub>2</sub>O,  $AH=9.2\text{g H}_2\text{O/m}^3$  dry air ( $T=23^\circ\text{C}$ ,  $RH=45\%$ ).  $\Delta$  = Keck *et al.* [180],  $\circ$  = Wiesmiller *et al.* [73],  $\square$  = Lindemann *et al.* [50],  $\star$  = Hanna [97].**

## 6.6 Mucosa Dry Time

The model has demonstrated for the first time that during ambient pressure breathing only the patent airway experiences excessive ASL dehydration. Conversely, during n-PAP breathing (at 9 cm H<sub>2</sub>O) both airways experience periods where excessive ASL dehydration occurs ( $H_{e,asl} = 0 \mu\text{m}$ ). Model predictions of the distance along the airway where excessive ASL dehydration occurs are presented in the following sections. In addition, the time duration that each position exceeds ASL dehydration limits is also presented as a function of pressure augmentation. This is represented as a percentage of the time span for one complete breath cycle which spans 6 seconds. Presenting the ASL hydration results in this format provides an indication as to the severity of the drying event within each airway by considering both the distance affected and the time duration of the event.

### 6.6.1 Un-humidified n-PAP Breathing

Referring to Figure 6.8, the model was configured to constant nasal mask air conditions of temperature ( $T = 23^\circ\text{C}$ ) and humidity ( $RH = 45\%$ ), corresponding to  $AH = 9.2\text{g H}_2\text{O/m}^3$  dry air, and pressures ranging from ambient (black line) to 20 cm H<sub>2</sub>O (magenta line). This enabled the distance and time duration where severe ASL dehydration occurred to be modelled.

An arrow is drawn from the data representing ambient pressure, which points to the data corresponding to the maximal pressure augmentation considered (20 cm H<sub>2</sub>O). Data corresponding to intermediate pressures is also shown. For the breath simulation used, Figure 6.1, a drying time interval of 20% corresponds to a time period of 1.2 seconds.

As already discussed in the earlier sections of this chapter, at ambient pressure it can be seen that the left (congested at ambient pressure) airway experiences no ASL dehydration whilst the right (patent at ambient pressure) airway experiences ASL drying along 48% of its length.

At a n-PAP augmentation of 5 cm H<sub>2</sub>O, the left (congested at ambient pressure) airway experiences ASL dehydration up to 30% along its length. This increases to 85% of its length at 10 cm H<sub>2</sub>O before becoming fully dehydrated for extended time periods along its entire length at pressures above this value.

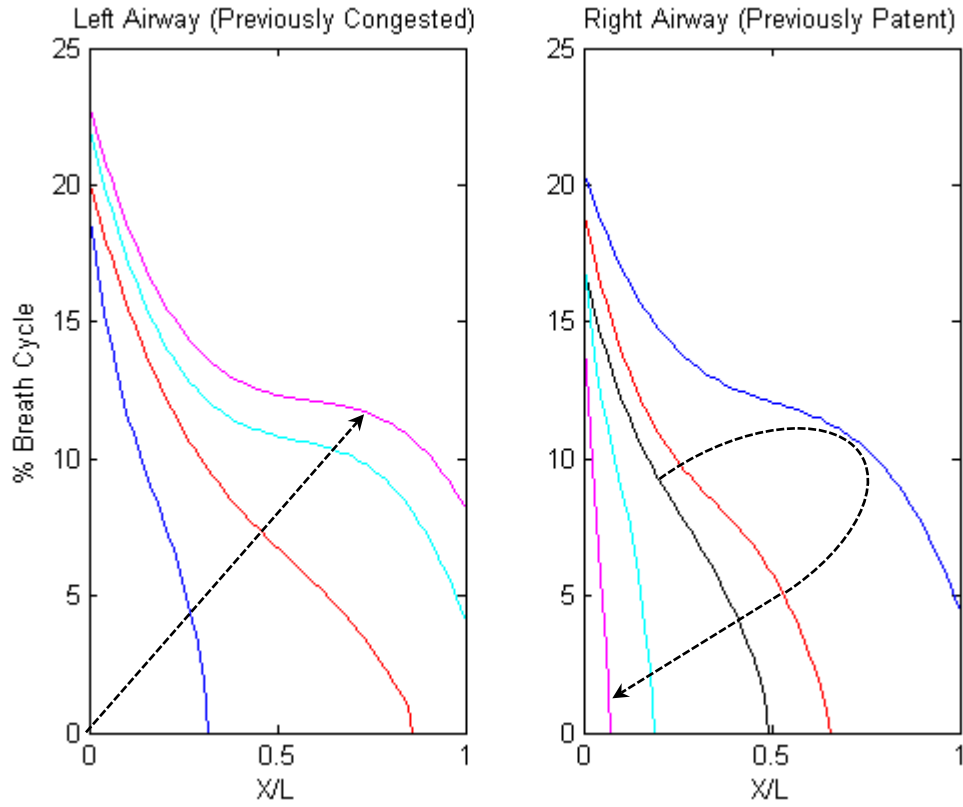


**Figure 6.8: Inter-airway ASL dehydration time distribution for range of pressure augmentation.** — = ambient, — = 5 cm H<sub>2</sub>O, — = 10 cm H<sub>2</sub>O, — = 15 cm H<sub>2</sub>O, — = 20 cm H<sub>2</sub>O.

The right (patent at ambient pressure) airway demonstrates ASL dehydration occurring up to 45% of airway length during ambient pressure breathing. ASL dehydration occurs for a significantly greater time period along the entire length of this airway at a pressure augmentation of 5 cm H<sub>2</sub>O, before progressively reducing at higher pressures.

## 6.7 n-PAP Breathing with Supplementary Heated Humidification

Model predictions for heated and humidified air pressurised to 9 cm H<sub>2</sub>O are presented in this section. Here, nasal mask conditions of absolute humidity and temperature, typical of those delivered by a commercial heated humidifier within a n-PAP breathing therapy device ( $AH = 31 \text{ gH}_2\text{O/m}^3$  dry air and  $Ta = 30^\circ\text{C}$ ) [6], were used. This corresponds to mask air being fully saturated. These results introduce for the first time a prediction of the change in intra-nasal ASL hydration distribution along both airways.

Model predictions for pressurised breathing with typical supplementary humidification are now compared to air temperature and absolute humidity data at ambient pressure

without humidification from other sources. This is due to the absence of published data for the pressurised supplementary humidification condition. Despite this variance in humidification and pressure status, this comparison will at least provide a means of comparing nasal air-conditioning performance between these two conditions.

These results introduce for the first time a prediction of the change in intra-nasal ASL hydration distribution along both airways during simulated heated humidified n-PAP breathing. No analysis of mucosa dry time is required during this simulation since severe ASL dehydration does not occur in either airway.

### 6.7.1 Inhalation Air Properties, Flux Levels and ASL Hydration

As with non-humidified n-PAP breathing, equal air mass-flow occurs within both nasal airways, but enters preheated and humidified. Equal inter-nasal air mass-flows result in all parameters being nearly identical between the left and right airways.

Within both airways, ASL water mass and heat fluxes, given in Figures 6.9 (e) and 6.9 (g) respectively for the left side and Figures 6.9 (f) and 6.9 (h) respectively for the right side, are significantly lower than that predicted by Hanna's model [97]. This is as a result of equal air mass-flow partitioning and more importantly, the inhaled air being pre-heated and humidified so less flux occurs in either airway. Variation in inter-nasal geometry inherent with this individual has little effect on results since these flux levels are so low.

No change in ASL water equivalent height occurs throughout the inhalation cycle in either the left airway, shown in Figure 6.9 (i), or the right airway, shown in Figure 6.9 (j), as a consequence of low water flux demand on ASL hydration.

Because the inhaled air has already been pre-heated and pre-humidified, little increase occurs in air temperature and absolute humidity, given in Figures 6.9 (a) and 6.9 (c) respectively for the left side and Figures 6.9 (b) and 6.9 (d) respectively for the right side, as the air travels along either the airway. Within the anterior regions ( $X/L < 0.2$ ), air temperature distribution between the left and that of the right airways demonstrate a higher value than published *in-vivo* data [49, 50, 73, 181]. There is however better agreement when moving posterior ( $X/L > 0.2$ ). Inhalation of heated and humidified air also causes the absolute humidity distribution between the left and that of the right airways to become significantly higher than published *in-vivo* data [49, 181].

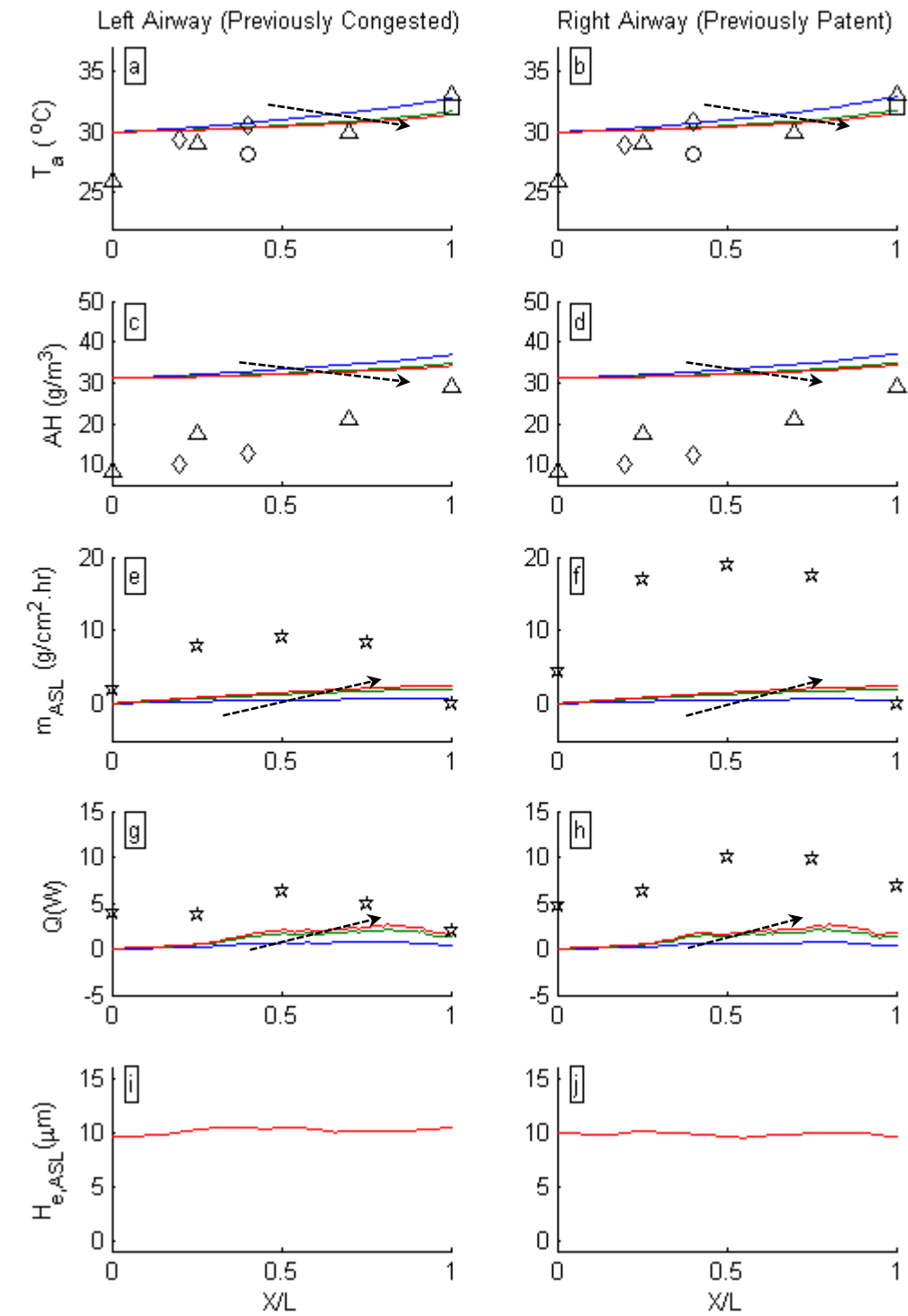


**Figure 6.9: Inhalation inter-airway temperature ( $T_a$ ), absolute humidity ( $AH$ ), molar water flux ( $N$ ), heat flux ( $Q$ ) and ASL water equivalent height ( $H_{e,ASL}$ ) distribution from rest to maximal change. Mask pressurise 9 cm  $H_2O$ ,  $AH=31gH_2O/m^3$  dry air. ( $T=30^\circ C$ ,  $RH=100\%$ ).  $\Delta$  = Keck *et al.* [180],  $\circ$  = Wiesmiller *et al.* [73],  $\diamond$  = Lindemann *et al.* [181],  $\square$  = Lindemann *et al.* [50],  $\star$  = Hanna [97].**

### 6.7.2 Exhalation Air Properties, Flux Levels and ASL Hydration

Model predictions for inter-nasal air temperature, absolute humidity, ASL water mass flux, heat flux and ASL water equivalent height distributions during the exhalation phase of the breath cycle during pressurised breathing are shown in Figure 6.10.

As in the inhalation breath phase, the magnitude and distribution of all parameters are nearly identical between the left and right airways.

As with ambient pressure breathing; the inter-nasal distributions of ASL water mass flux, given in Figures 6.10 (e) and 6.10 (f) for the left and right airways respectively, agree well with Hanna's model data [97], since water supply is not an issue during this phase of breathing as a consequence of exhaled water vapour condensation increasing ASL hydration. Comparison of the ratio of heat and water recovery to that lost is meaningless, since heat flux and ASL water mass flux levels are suppressed during inhalation owing to the air being pre-heated and humidified.

No change in ASL water equivalent height occurs in either the left or right airways, shown in Figures 6.10 (i) or 6.10 (j) respectively. This is not surprising given ASL hydration was not affected in either airway during the inhalation phase.

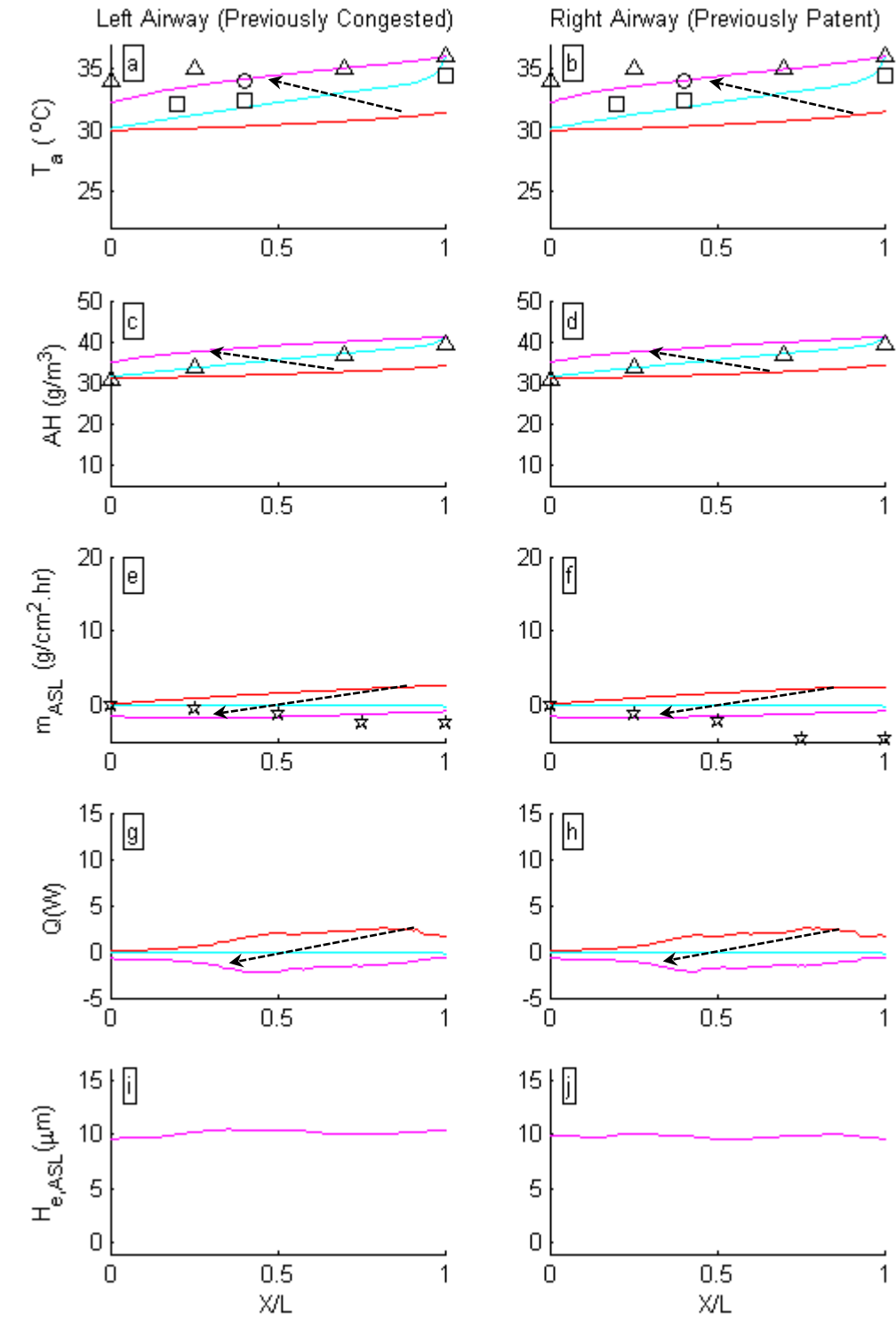


**Figure 6.10: Exhalation inter-airway temperature ( $T_a$ ), absolute humidity ( $AH$ ), molar water flux ( $N$ ), heat flux ( $Q$ ) and ASL water equivalent height ( $H_{e,ASL}$ ) distribution from maximal inhalation to maximal exhalation. Mask pressurise 9 cm  $H_2O$ ,  $AH=31gH_2O/m^3$  dry air. ( $T=30^\circ C$ ,  $RH=100\%$ ).  $\Delta$  = Keck *et al.* [180],  $\circ$  = Wiesmiller *et al.* [73],  $\square$  = Lindemann *et al* [50],  $\star$  = Hanna [97].**

## **6.8 n-PAP Breathing with Non-Heated Supplementary Humidification**

Results presented in this section are derived from the model predictions for an individual nasal breathing air pressurised to 9 cmH<sub>2</sub>O. This air has received supplementary moisture to a level typical of that delivered by a commercial non-heated pass-over type humidifier within a nasal PAP breathing therapy device [6]. This equates to the air within the nasal mask having a relative humidity of 75% and temperature of 24°C.

The purpose of this section is to determine if the use of non-heated humidification can prevent ASL dehydration from occurring within the nasal airways during augmented air-pressure breathing. Model predictions for pressurised breathing with typical non-heated supplementary humidification are compared to published non supplementary humidification data at ambient pressure from other sources, due to the absence of published data for the pressurised supplementary humidification condition.

Similar to the supplementary heated humidification case; the analysis of mucosa dry time during simulated breathing of minimum humidified pressurised air was not undertaken as excessive ASL dehydration did not occur in either airway while breathing under this condition.

### 6.8.1 Inhalation Air Properties, Flux Levels and ASL Hydration

Model predictions during the inhalation phase of the breath cycle during pressurised breathing of minimally humidified air are shown in Figure 6.11.

As in the heated and humidified inhalation results given in Figure 6.9, the magnitude and distribution of all parameters are nearly identical between the left and right airways.

Non-heated humidification leads to increased water mass and heat fluxes occurring along both the left airway, given by Figures 6.11 (e) and 6.11 (g) respectively, and right airway, given by Figures 6.11 (f) and 6.11 (h) respectively. This increase however is only to a level similar to that normally experienced by a congested airway whilst breathing ambient air, as shown by Figures 6.2 (e) and 6.2 (g).

The same change in ASL water equivalent height occurs during peak inhalation in both airways, as shown in Figures 6.11 (j) and 6.11 (i). This is a consequence of equal water flux demand on ASL hydration occurring within both airways. Here, ASL water equivalent height reduces along the anterior regions of both airways ( $X/L < 0.5$ ), however, the ASL remains sufficiently hydrated along both airways during peak inhalation air-flow to maintain mucociliary transport. Compared to the ASL water equivalent height results of inhaling air pressurised to the same pressure, but without supplementary heated humidification, given in Figures 6.5 (i) and 6.5 (j), it can be seen that supplementary non-heated humidification also completely resolves the issue of ASL dehydration occurring.

Since the inhaled air is pre-humidified but not heated, air temperature for both the left and right airways, given in Figures 6.11 (a) and 6.11 (b) respectively, follow the same trend as that found in the left (congested) airway during ambient pressure breathing (Figure 6.2 (a)). Here, this parameter exhibits a slightly lower value than published *in-vivo* data [49, 50, 73, 181] in both airways. Inter-nasal absolute humidity distributions also follow the same trend with both the left and right airways, shown in Figures 6.11 (c) and 6.11 (d) respectively. These both follow the same trend as that found in the congested left (congested) airway during ambient pressure breathing, given in Figure 6.2 (c). As a consequence of non-heated supplementary humidification, the absolute humidity in both airways is slightly higher than published *in-vivo* data [49, 181].

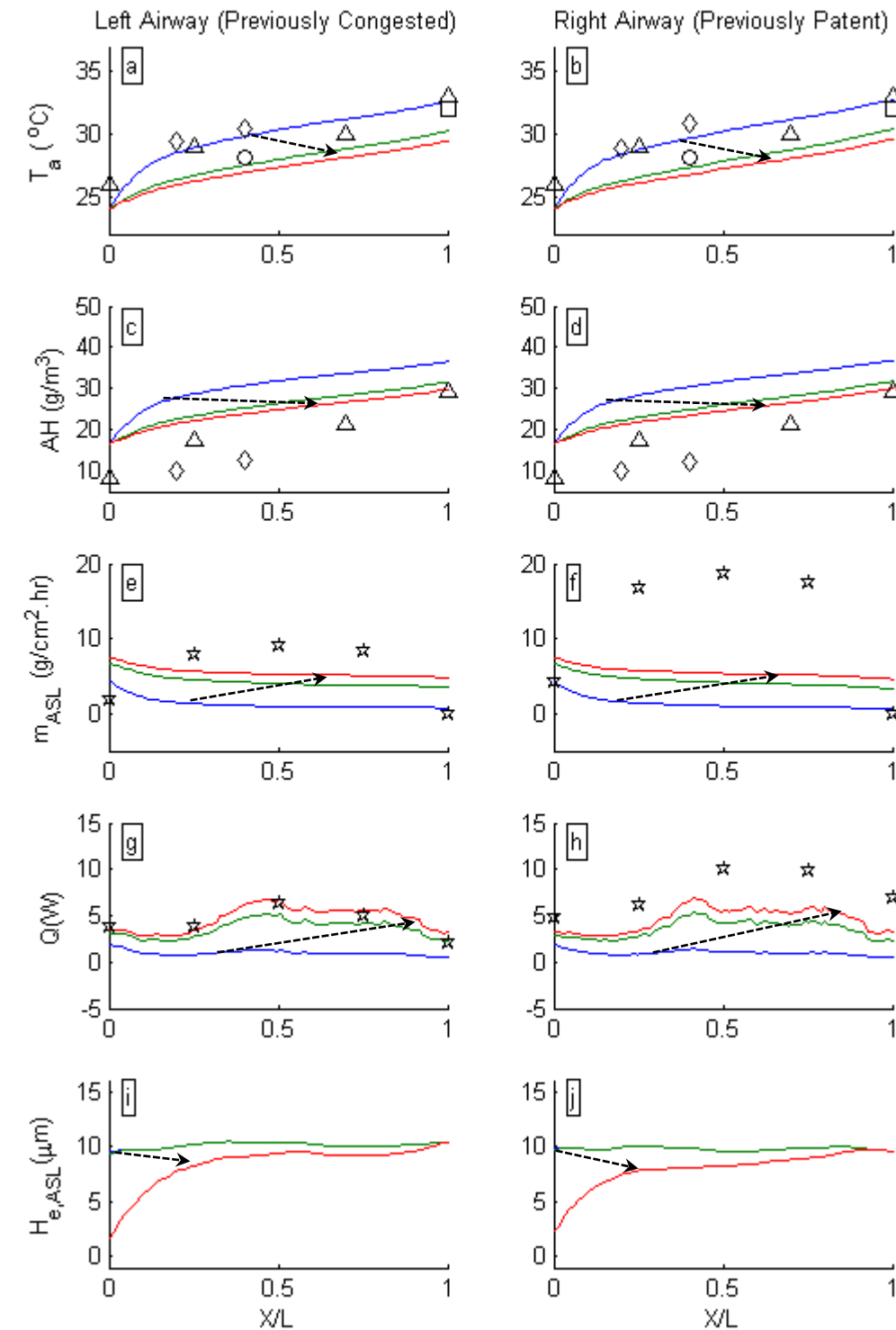


**Figure 6.11: Inhalation inter-airway temperature ( $T_a$ ), absolute humidity ( $AH$ ), molar water flux ( $N$ ), heat flux ( $Q$ ) and ASL water equivalent height ( $H_{e,ASL}$ ) distribution from rest to maximal change. Mask pressurise 9 cm  $H_2O$ ,  $AH=16.4$  g $H_2O$ /m $^3$  dry air. ( $T=24^\circ C$ ,  $RH=75\%$ ).  $\Delta$  = Keck *et al.* [180],  $\circ$  = Wiesmiller *et al.* [73],  $\diamond$  = Lindemann *et al.* [181],  $\square$  = Lindemann *et al.* [50],  $\star$  = Hanna [97].**

### 6.8.2 Exhalation Air Properties, Flux Levels and ASL Hydration

Model predictions during the exhalation phase of the breath cycle during pressurised breathing are shown in Figure 6.12.

As in the inhalation breath phase, all parameters for the left airway are also nearly equal to those found in the right.

Not surprisingly, given the same air conditions occur during exhalation, the inter-nasal distributions of ASL water mass flux agree very well with Hanna's model data [97].

Given that less water demand is made on the ASL, its hydration status recovers quickly with ASL water equivalent height in both airways, shown by Figures 6.12 (i) and 6.12 (j), returning to normal maximal values.

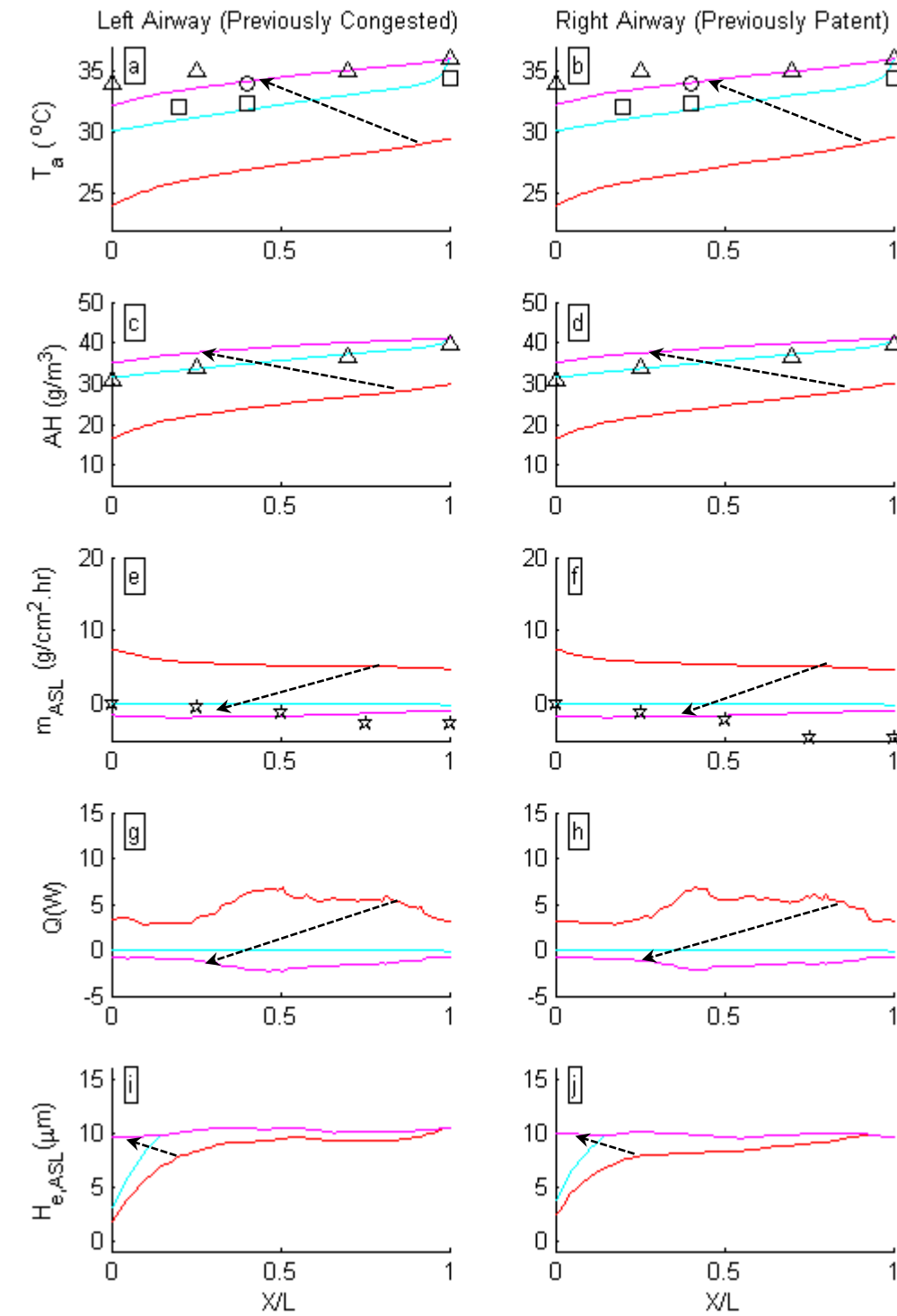


**Figure 6.12:** Exhalation inter-airway temperature ( $T_a$ ), absolute humidity ( $AH$ ), molar water flux ( $N$ ), heat flux ( $Q$ ) and ASL water equivalent height ( $H_{e,ASL}$ ) distribution from maximal inhalation to maximal exhalation. Mask pressurise 9 cm  $H_2O$ ,  $AH=16.4$  g $H_2O$ /m $^3$  dry air ( $T=24^\circ C$ ,  $RH=75\%$ ).  $\Delta$  = Keck *et al.* [180],  $\circ$  = Wiesmiller *et al.* [73],  $\square$  = Lindemann *et al* [50],  $\star$  = Hanna [97].

## **6.9 Closure**

Subject specific results of inter-nasal distribution of air temperature, absolute humidity, ASL water mass flux, heat flux and ASL water equivalent height distributions for both inhalation and exhalation phases of breathing have been found and compared to published data. This has been done for conditions of ambient and n-PAP breathing with no humidification, heated humidification and non-heated humidification. The degree of ASL dehydration, in terms of extent along the airway and time duration, has also been found for ambient and PAP breathing without supplementary humidification. For the first time prediction of change of intra-nasal ASL hydration of both airways is presented.

The complex inter-play between these results has been discussed, however an in-depth analysis is undertaken in Chapter 7.

## CHAPTER 7

### DISCUSSION

#### 7.1 Introduction

This chapter discusses the model results given in Chapter 6 in terms of therapeutic and pathophysiological outcomes. It shows that:

1. The patent airway normally experiences ASL dehydration drying while the congested airway remains normally hydrated.
2. Mucociliary clearance would be compromised in the patent airway during n-PAP breathing.
3. Both airways experience ASL dehydration during n-PAP breathing.
4. Supplementary humidification relieves airway drying in both airways during n-PAP breathing.

The model assumption of laminar flow is revisited in Section 7.2 before ambient air-pressure breathing and un-humidified pressured air breathing are discussed in Sections 7.3 and 7.4 respectively. The benefits and issues surrounding n-PAP breathing with supplementary humidification is then discussed in Section 7.5.

#### 7.2 Model Assumption of Laminar Airflow

For the breath cycle used, the narrow nasal airways suggest that viscous damping forces would dominate over inertial forces, causing laminar airflow to occur. This is demonstrated by the low Reynolds numbers found throughout both airways in this work and is in agreement with other investigations for at-rest breathing [221, 222]. This finding validates the assumption of laminar flow made during model development in Chapter 3.

#### 7.3 Nasal Breathing at Ambient Air-Pressure

The results of model predictions at ambient pressure for air temperature, absolute humidity and heat flux during peak inhalation and exhalation compare well with previous *in-vivo* [50, 73, 180, 181] and model [97] data. As previously mentioned in

Chapter 2, air humidity sensor response time could account for the slight deviation present in Figures 6.2 (a) and 6.2 (b). Additionally, intra-nasal *in-vivo* measurement of both air temperature and absolute humidity is problematic given the difficulty in achieving clear access within the confined nasal spaces, so care needs to be taken when interpreting these *in-vivo* results. Despite this concern, comparison between model and *in-vivo* air temperature and absolute humidity data shows good agreement which suggests the issue of transducer response time is not a problem.

A recovery of around 30% of heat and water mass flux during the exhalation phase, as mentioned in Section 6.2.2, is consistent with an earlier investigation [63]. Of note is the full recovery of ASL hydration status within both airways during the exhalation phase of the breath cycle, shown in Figures 6.3 (i) and 6.3 (j).

Of significance are the model predictions for peak inhalation which give an indication as to how the nose copes with its dual roles of air-conditioning and providing mucociliary clearance. This is indicated by the drop off in ASL water mass flux within the right (patent) airway during peak inhalation, shown in Figure 6.2 (f), caused by severe ASL dehydration occurring along 48% of the anterior nasal region, shown in Figure 6.2 (j). This occurs as a consequence of this airway carrying the greater apportionment (67%) of the air mass-flow. Contrasting this result, the left (congested) airway experiences minor dehydration, shown in Figure 6.2 (i), which does not exceed the ASL hydration limits, as a result of carrying a lesser air mass-flow. While variation in the breath cycle, in terms of amplitude or period, would cause change in the severity and extent of ASL dehydration, it would not change the characteristic difference in ASL hydration behaviour between either of the two airways.

The consequences of ASL dehydration occurring within the patent airway, and not the congested airway, are discussed in the following section.

### **7.3.1 Consequences of ASL dehydration**

Previous investigations into the nasal cycle have found that the mucociliary transport velocity within the congested airway is 2.5 times greater than that found in the patent airway [82]. The findings of this research demonstrate for the first time that during ambient air breathing the patent airway experiences recurring severe ASL dehydration during inhalation. Here, repeated periods of reduction in PCL height, as described in Sections 2.4.4 and 2.4.5, would inhibit mucociliary transport.

The finding of severe ASL dehydration occurring only within the right (patent) airway is new and the implications of this, in terms of delayed mucociliary clearance, are significant.

1. Pathogens entrapped within the sticky mucus layer remain resident within the nasal cavity for a longer time period and can multiply in number [108], as discussed in Section 2.4.2, creating regions of dense population that could penetrate the mucus layer and cause infection.
2. The PCL layer containing active defensins [108], discussed in Section 2.4, becomes reduced in height so presents less of a protective barrier against pathogens entering the mucosal surface.
3. Severe ASL dehydration creates the potential for desiccation of the mucosal surface to occur [70], as discussed in Section 2.4.1, since it is not bathed in aqueous ASL.

These negative outcomes can occur within the patent airway under most conditions of breathing ambient pressure air. The body copes with this by periodically switching the bias of air mass-flow partitioning between the two nasal airways. This limits the exposure time each airway has to endure these adverse ASL drying conditions. This periodic switching is discussed in the following section.

### **7.3.2 Explanation of the Nasal Cycle**

The use of the air-conditioning model has given greater insight into the purpose of the nasal cycle. Understanding that the nose is more than simply a portal by which air passes through the conducting airways is fundamental in comprehending the likely purpose of this recurrent event. In particular, the function of entrapping inhaled pathogens and pollutants requires low air velocities to be effective, whilst the role of air-conditioning requires high air velocities to be operative. Compounding this is the cyclic ASL dehydration occurring in the patent airway with each breath in response to air-conditioning demands. This negatively impacts mucociliary clearance within this airway. Both air conditioning and filtration duties are predominantly carried within the anterior nasal region and must be simultaneously and continuously carried out in order to maintain airway health. The nose copes with this conflict by regulating inter-nasal air mass-flow through change in the nasal cycle.

Switching of the nasal cycle status alternates the primary role carried out by each airway. This is demonstrated in the previously patent airway, stressed from carrying the bulk of the heat and water mass transfer duties and experiencing issues associated with severe ASL dehydration, to become congested. Switching to this state enables its ASL layer to return to an uninterrupted state of hydration that supports continuous and normal mucociliary clearance. On the other hand, the previously congested airway, having had experienced a period of cellular rest and recovery, picks up the bulk of the heat and water mass transfer duties and for a limited time endures issues associated with cyclic severe ASL dehydration. This balancing of heat and water fluxes between airways is consistent with the current understanding of the purpose of the nasal cycle [45] being to control the balance between heat and water fluxes from the ASL [45], as well as enable cells and glands on the congested side to rest and recharge [87]. The new suggestion from this work is that that it also may be a way in which the anterior conducting airway copes with its multiple duties that require the conflicting physiological characteristics of high and low air velocities previously mentioned. It is proposed that the nasal cycle, characterised by recurrent variation in air mass-flow partitioning between each airway, enables each passageway to alternatively take turns in either predominantly undertaking the air-conditioning or clearance roles.

#### 7.4 Inhalation of Un-Humidified Pressurised Air

Results previously presented in Figure 6.5 are now presented in Figure 7.1. For this individual, each airway experiences equal air mass-flow rates during n-PAP breathing un-humidified air at a pressure of 9 cm H<sub>2</sub>O. Under this condition, the distribution and magnitude of air temperature within the left and right airways, shown in Figures 7.1 (a) and 7.1 (b) respectively is lower than that found in previously published *in-vivo* ambient pressure data [49, 50, 73, 181]. On the other hand, distribution of air absolute humidity within the left and right airways, shown in Figures 7.1 (c) and 7.1 (d) respectively, compares well [49, 181]. Despite this apparent agreement, the relatively long humidity transducer response time (4 seconds), as discussed in Section 2.7, likely plays a role in the variation in magnitude found between the *in-vivo* data and model results. In this case, model results of air absolute humidity should be suppressed in both airways given reduced ASL water mass flux has occurred, as indicated by Figures 7.1 (e) and 7.1 (f). Reduction in nasal air-conditioning performance has the net effect of lowering the isothermal saturation boundary (ISB) location and increasing the air-conditioning load within the distal conducting airways [70].

Of significance to this work is severe ASL dehydration occurring along the anterior 60% and 80% lengths of both the left and right nasal airways, as indicated in Figures 7.1 (i) and 7.1 (j). This occurs as a result of the combined change in inter-nasal air mass-flow partitioning and reduced mucosal ASL water supply. ASL dehydration occurs within each airway for slightly different reasons. Within the right airway, reduction in ASL water supply, as discussed in Chapter 5, causes this airway to experience ASL dehydration, despite experiencing a decrease in air mass-flow. On the other hand, the left airway experiences both an increase in air mass-flow and reduction in ASL water supply, both of which contribute to the severity of ASL dehydration.

The cyclic bias of air-conditioning or mucus clearance duties carried out by each airway, discussed in Section 7.2.1, has now been interrupted by severe cyclic ASL dehydration simultaneously occurring along both airways. This situation represents the worst possible scenario for the nose. Any intended change in nasal cycle duty is effectively negated since equal inter-nasal air mass-flows will elicit equal ASL water demands from within both airways. This finding is significant as it identifies and explains for the first time the cause of nasal airway drying during n-PAP breathing that potentially exposes both airways to the pathophysiological outcomes, previously described in section 7.3.1. Under these conditions, change in nasal cycle offers no relief from ASL dehydration.

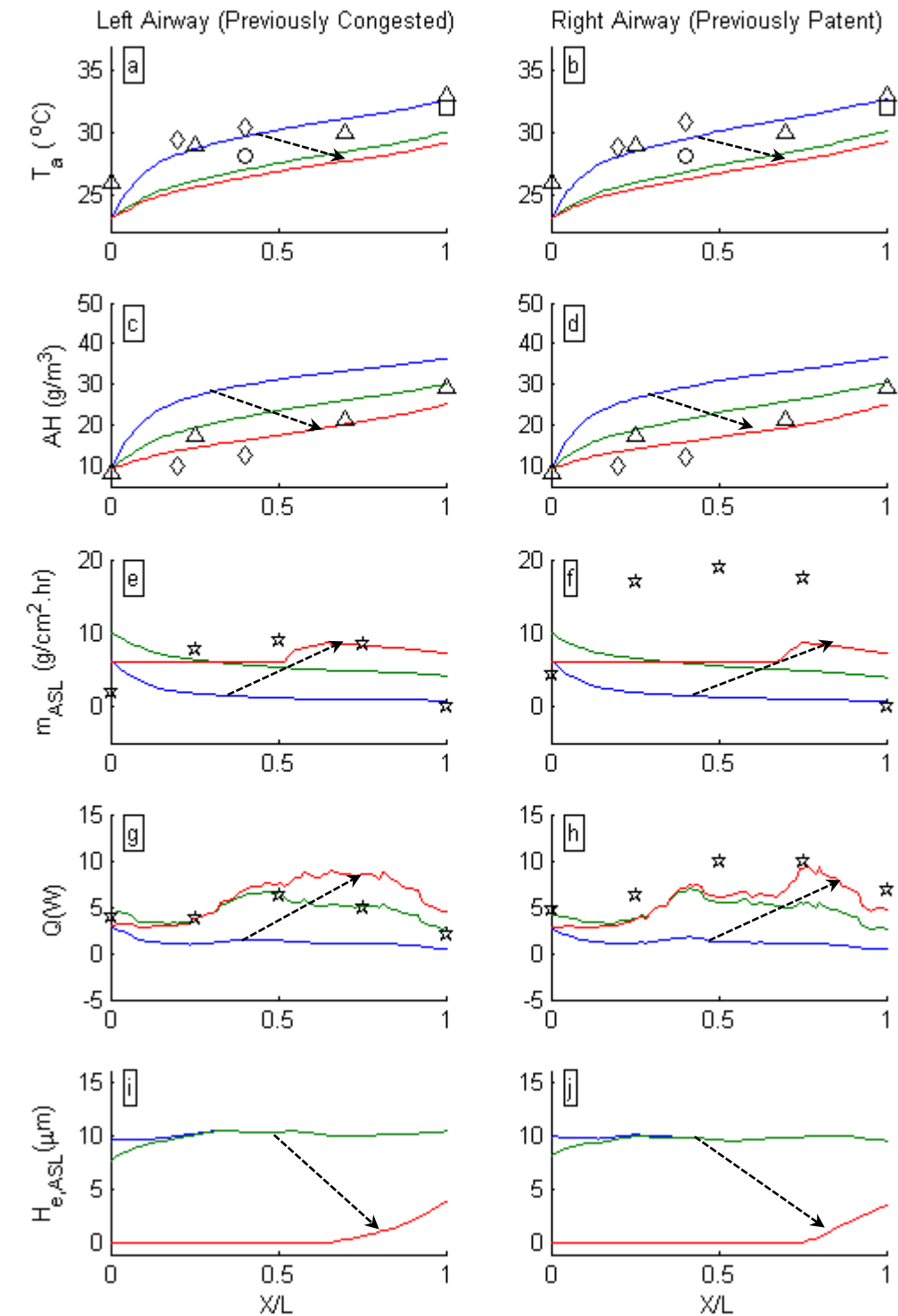


**Figure 7.1: Inhalation inter-airway temperature ( $T_a$ ), absolute humidity ( $AH$ ), molar water flux ( $N$ ), heat flux ( $Q$ ) and ASL water equivalent height ( $H_{e,ASL}$ ) distribution from rest to maximal change. Mask pressure 9 cmH<sub>2</sub>O,  $AH=9.2$ g H<sub>2</sub>O/m<sup>3</sup> dry air ( $T=23^\circ\text{C}$ ,  $RH=45\%$ ).  $\Delta$  = Keck *et al.* [180],  $\circ$  = Wiesmiller *et al.* [73],  $\diamond$  = Lindemann *et al.* [181],  $\star$  = Hanna [97],  $\square$  = Lindemann *et al.* [50].**

During periods of severe ASL dehydration, the availability of ASL water for air-conditioning reduces to that offered by the cellular supply. This drops the rate of ASL water mass flux that can occur to basal levels, as demonstrated in Figures 7.1 (e) and 7.1 (f), which are substantially lower than that predicted by Hanna's model [97]. This result is not surprising given Hanna's model featured limitless ASL water supply [166]. Of note is the increase in ASL water mass flux within both airways, where the ASL is not severely dehydrated.

The severity of ASL dehydration, in terms of airway location and time duration over a range of pressure augmentations, is discussed in the following section.

#### 7.4.1 Mucosa Dry Time

Since n-PAP breathing causes both a reduction in ASL water supply and a proportional change in inter-nasal air mass-flow partitioning, the degree of ASL dehydration varies between each airway under different pressure conditions.

Reference is now made to an inter-airway comparison of exposure time and regional distribution previously presented in Figure 6.8 and reproduced in Figure 7.2.

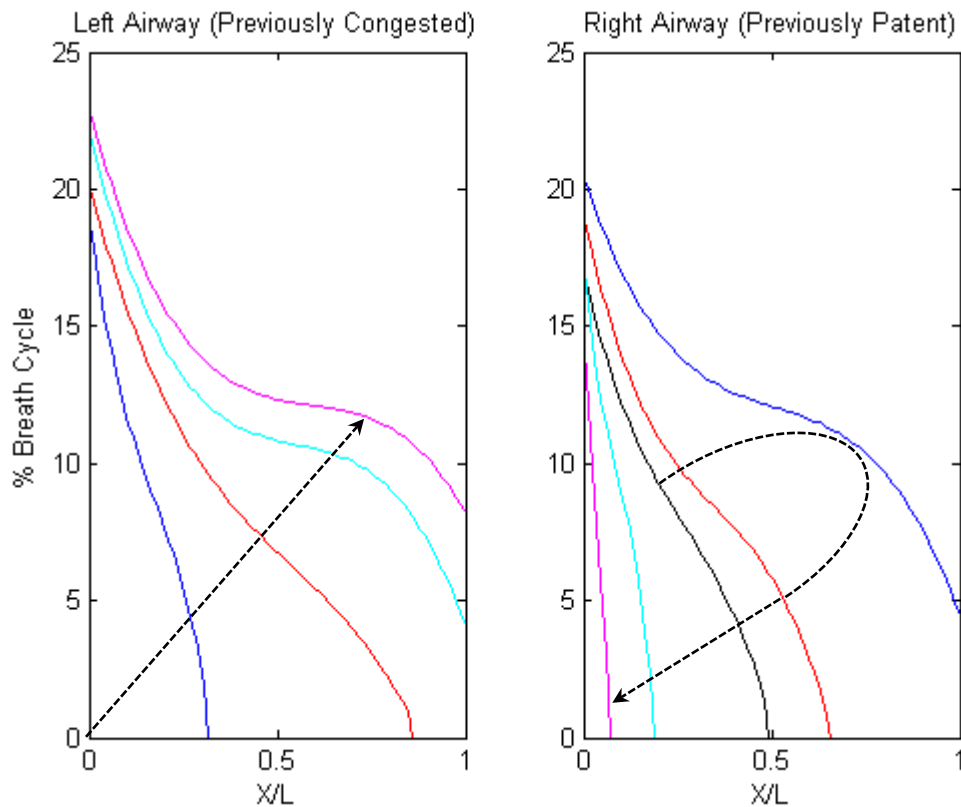


**Figure 7.2: Inter-airway ASL dehydration time distribution for range of pressure augmentation. , — = ambient, — = 5 cmH<sub>2</sub>O, — = 10 cmH<sub>2</sub>O, — = 15 cmH<sub>2</sub>O, — = 20 cmH<sub>2</sub>O**

Based on the individual's nasal geometric data used in the model, at ambient pressure the ASL dehydration within the left (congested) airway remains within normal hydration limits, whilst the right (congested) airway experiences severe ASL dehydration. This affected region extends along 48% of the anterior length of right airway for a time period of 1 second at the most anterior point. Increasing breathing air-pressure above ambient causes increases in both airway length affected and the time duration where severe ASL dehydration has occurred in the left (previously congested) airway. The right (previously patent) airway also initially experiences a similar trend, as a result of increased heat and water mass transfer coefficients, due to a reduction in airway cross-sectional-area. However, further increase in air-pressure causes the air mass-flow resistance within the right (previously patent) airway to increase, which reduces heat and water mass flux levels. These conditions combine to cause a reduction in both the length and duration of severe ASL dehydration in this airway. In summary, increasing breathing pressure increases the degree of severe ASL dehydration occurring within the left (previously congested) airway, but generally reduces that within the right (previously patent) airway. Despite this contra-reaction in ASL dehydration in response to pressure augmentation, neither airway achieves normal ASL hydration levels within the range of air-pressures typically used in n-PAP therapy [56]. Under these conditions, change in the status of the nasal cycle will have little benefit in avoiding the pathological outcomes described in Section 7.3.1.

Episodes of epistaxis occasionally reported during the use of n-PAP therapy can also be attributed to ASL dehydration. Here, the anterior nasal region containing Kiesselbach's triangle is exposed to sustained cycles of severe ASL dehydration, as demonstrated by this investigation. This highly vascular region is commonly thought to contribute to the heating of inhaled air [76] but it is where around 90% to 95% of all epistaxis episodes occur [76, 77]. Here, inflammation of the mucosa has been found to occur during CPAP therapy [12] as a likely consequence of repeated severe ASL dehydration.

#### **7.4.2 Sleep Quality and the Nasal Cycle**

As discussed in Chapter 2, the nasal cycle creates a bias of nasal air mass-flow that alternates from side to side to an ultradian rhythm. Previous studies have demonstrated that forced unilateral nostril breathing can influence this cycle at a central level [234, 235]. This investigation has shown that the inter-nasal airflow bias regulated by the

nasal cycle is interrupted during n-PAP breathing and could lead to the disturbance of normal brain rhythms.

## **7.5 n-PAP Breathing with Supplementary Humidification**

A discussion of both heated and non-heated supplementary humidification results during n-PAP breathing is now undertaken in Section 7.5.1 and 7.5.2 respectively. Issues corresponding to the use of supplementary humidification are then discussed in Section 7.5.3.

### **7.5.1 Heated Supplementary Humidification**

Model simulations indicate that the additional of supplementary heated humidification virtually relieves the nose of its air-conditioning duty. Here low levels of nasal ASL water mass and heat flux occur since the air enters the airways in a pre-heated and humidified state. Benefits of heated supplementary humidification include elevation of both air temperature and absolute humidity above that measured in previous *in-vivo* studies [49, 181] which would cause the ISB to move slightly anterior [70]. This would improve mucociliary transport throughout the conducting airways [59, 70].

Unlike un-humidified n-PAP breathing, the use of supplementary heated humidification ensures the ASL within both airways remains fully hydrated along their entire length and capable of sustaining ideal rates of mucociliary clearance. For this individual and the humidifier setting used, there were no issues of ASL over-hydration predicted during either phase of the breath cycle.

### **7.5.2 Non-Heated Supplementary Humidification**

Results for air temperature, absolute humidity, ASL water mass and heat flux distributions along both airways were nearly equal between airways, but of a lower magnitude than that found with supplementary heated humidification. This result is not surprising given the inhaled air is not pre-heated and carries a lower level of water vapour than that found with heated humidification. For this individual, excessive ASL dehydration did not occur in either airway although both experienced some water loss. This is indicative of the inhaled air containing less water vapour compared to that delivered by supplementary heated humidification.

During exhalation, the distributions of all parameters were nearly identical to those experienced during heated humidification.

### **7.5.3 Supplementary Humidification Debate**

For many n-PAP users, the choice to use supplementary humidification is based on the severity and nature of symptoms experienced [14]. Whilst either heated or non-heated supplementary humidification appears on the surface to be a panacea to the problem of both airways simultaneously experiencing prolonged periods of severe ASL dehydration, there are issues associated with this supplementary therapy. These issues are discussed in the following sections.

#### **7.5.3.1 Therapeutic Efficacy and Compliance**

As mentioned in Chapter 1, heated humidification is commonly utilised to treat symptoms associated with airway drying and improve patient comfort [4, 5, 7], however, its ability to improve treatment adherence and compliance is questionable [13-15, 21]. The sensation of stuffiness associated with breathing heated and humidified air [236] has been linked to elevated nasal lining temperature [179, 237]. Additionally, the quality of sleep may also be negatively affected given the duration of synchronised (non-REM) deep sleep is positively correlated to the blood-flow through heat exchangers regulating body temperature [210, 238]. As discussed in Chapter 2, arteriovenous anastomoses (AVAs) within the nose help regulate body temperature. These AVAs likely experience a reduction in blood flow during periods where heated air is inhaled, leading to a reduction in the time duration of deep sleep. In addition to this, nasal breathing is designed to alternate from side to side in an ultradian cycle. Forced unilateral nostril breathing can influence this cycle at a central level [234, 235] and findings of this work demonstrate an interruption to nasal airflow occurs during n-PAP breathing. Reduction in sleep quality could explain the high level of dissatisfaction and non-compliance commonly demonstrated with n-PAP therapy.

From this investigation, severe ASL dehydration has been shown to occur in both airways during un-humidified n-PAP breathing. Here, the ISB moves further distal within the conducting airways, resulting in the airways proximal to this location being exposed to ASL dehydration [70]. Given that ASL hydration status has been linked to the severity of OSA [124] it seems reasonable to desire that the ASL distal to the nose

remains adequately hydrated at all times. To this end, both heated, and to a lesser extent non-heated, supplementary humidification may help to reduce the severity of an OSA event and potentially enable a lower n-PAP titration pressure to be used.

Use of a heated humidifier also exposes the user to the risk of over humidification of inhaled air [70, 125]. Here, excess water condenses within the conducting airways, over-hydrating and diluting the ASL. This raises the PCL height to a level where mucociliary transport becomes impaired. Thermal damage could also be an issue in this situation due to excessive condensation occurring. The use of non-heated humidification avoids this risk as the ambient temperature limits the amount of water capable of being carried into the airways.

#### **7.5.3.2 Device Complexity**

Providing heated or non-heated humidification therapy adds both cost and complexity to the n-PAP therapeutic device. Heated supplementary humidification commonly features a temperature controller that can be adjusted by the user. Since these systems provide near fully saturated heated air with water vapour above ambient temperature, condensation can occur within the n-PAP system when heat loss occurs. This commonly occurs within the supply hose or nasal mask. Innovative manufacturers can provide a heated air supply hose to overcome this issue; however it adds both to the machine complexity and cost. On the other hand, non-heated supplementary humidifiers do not suffer from condensation, since they do not heat the air above ambient temperature but, as mentioned earlier, these do not deliver the same degree of water vapour.

#### **7.5.3.3 Human factors**

Apart from the matters associated with therapeutic efficacy previously mentioned in Section 7.5.3.1, OSA sufferers have also reported that the size and weight of their n-PAP device is an impediment to their frequent use [28]. Unfortunately, incorporating supplementary humidification to the device increases both of these parameters.

On-going maintenance of the supplementary humidification unit is also an additional burden carried by the user. Here, the water chamber needs to be replenished with distilled water on a daily basis and regularly washed to eliminate any microbial growth.

## **7.6 Closure**

Within this chapter the original model devised findings relating to nasal air-conditioning and resultant ASL dehydration during ambient and n-PAP breathing have been discussed. Additionally, an understanding of the benefits and disadvantages relating to the use of supplementary humidification has also been presented. In the next chapter an alternative to supplementary humidification is proposed.

## CHAPTER 8

### ALTERNATIVE TO SUPPLEMENTARY HUMIDIFICATION

#### 8.1 Introduction

In Chapter 7, the benefits of humidifying air under augmented pressures were discussed. The numerous negative issues associated with this supplementary treatment during n-PAP therapy, for both users and manufacturers, were also highlighted.

In this chapter an alternative technique is proposed that provides relief from symptoms of nasal dysfunction commonly experienced during n-PAP therapy but avoids the undesirable side-effects associated with supplementary humidification.

#### 8.2 Regulation of Inter-Nasal Air Mass-Flow Partitioning

It is proposed that rather than providing supplementary humidification, a much better alternative would be to regulate the resistance of the two parallel nasal airways so that air-flow partitioning between these two passageways mimics that found during normal ambient air breathing. The objective of this is to maintain sufficient ASL hydration within one airway to enable effective mucociliary transport to occur while the other airway undertakes the bulk of air-conditioning duty and subsequently endures ASL dehydration. This mimics the ASL hydration behaviour found during ambient air breathing.

The advantage of such a system would be that the nasal airways would avoid symptoms associated with sustained ASL dehydration without the need for supplementary humidification. This has benefits, both in terms of simplifying and reducing size and mass of equipment however therapeutic benefits may include:

1. The relief of perceived congestion and stuffiness commonly experienced when breathing heated and humidified air [236], as discussed in Section 7.5.3.1.
2. Improved patient satisfaction with n-PAP therapy and improve treatment compliance by returning the nasal air mass-flow partitioning between the two airways back to that normally controlled by the ultradian cycle.

The bias of air mass-flow could also be alternated in the same manner as that experienced during the normal nasal cycle. Here, the airways could switch over duty in

a similar fashion to that experienced during ambient air breathing so that they alternate between states of patency and congestion. This would avoid excessive time periods of mucosal drying. The cycle period could be tuned to the n-PAP conditions which may require shorter period than that of ambient breathing.

### 8.3 Model Implementation

Pressure elicited change of inter-nasal air mass-flow partitioning, causing severe ASL dehydration, can be offset through control of the total air-flow resistance of each airway within the n-PAP system. This would return the ASL hydration status to normal levels, as experienced during ambient air breathing. To achieve this requires separation of each nasal airway circuit and the addition of variable resistance. Model predictions of inter-nasal variation required to achieve this outcome are presented in Figure 8.1. Of note is a slight reduction in overall nasal breathing resistance which will likely go unnoticed by the user.

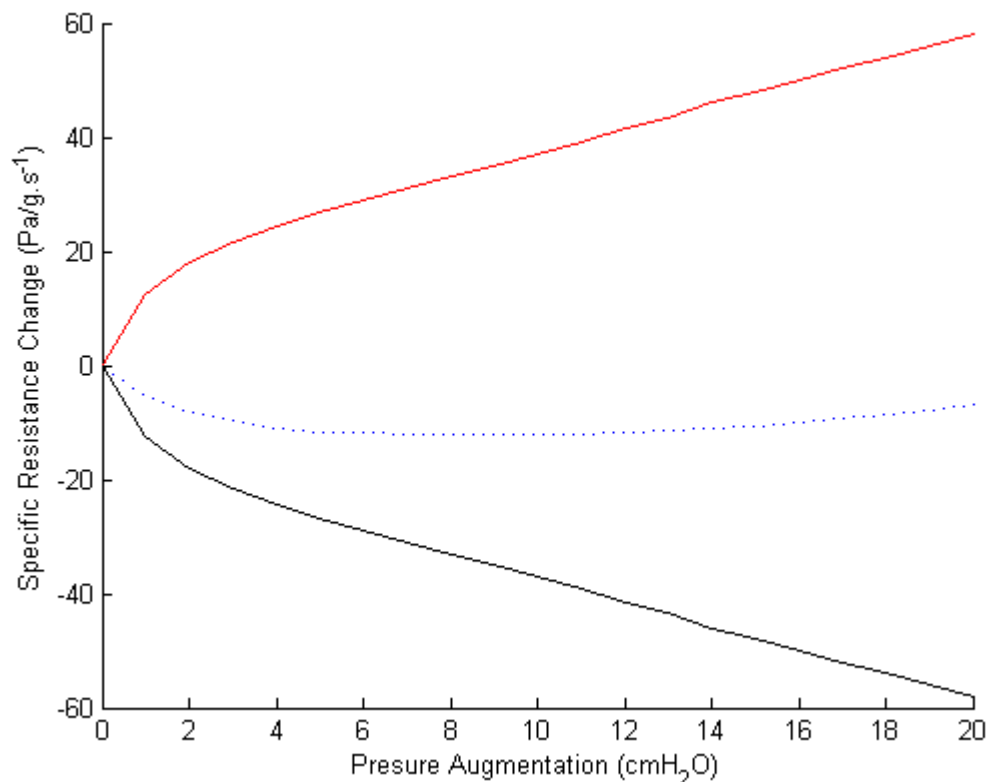


**Figure 8.1: Change in inter-airway specific air mass-flow resistance over range of pressure augmentation to sustain ASL hydration within left (forced congested) airway. — = modified right airway (forced patent), — = modified left airway (forced congested), - - - = overall change in specific nasal airway resistance.**

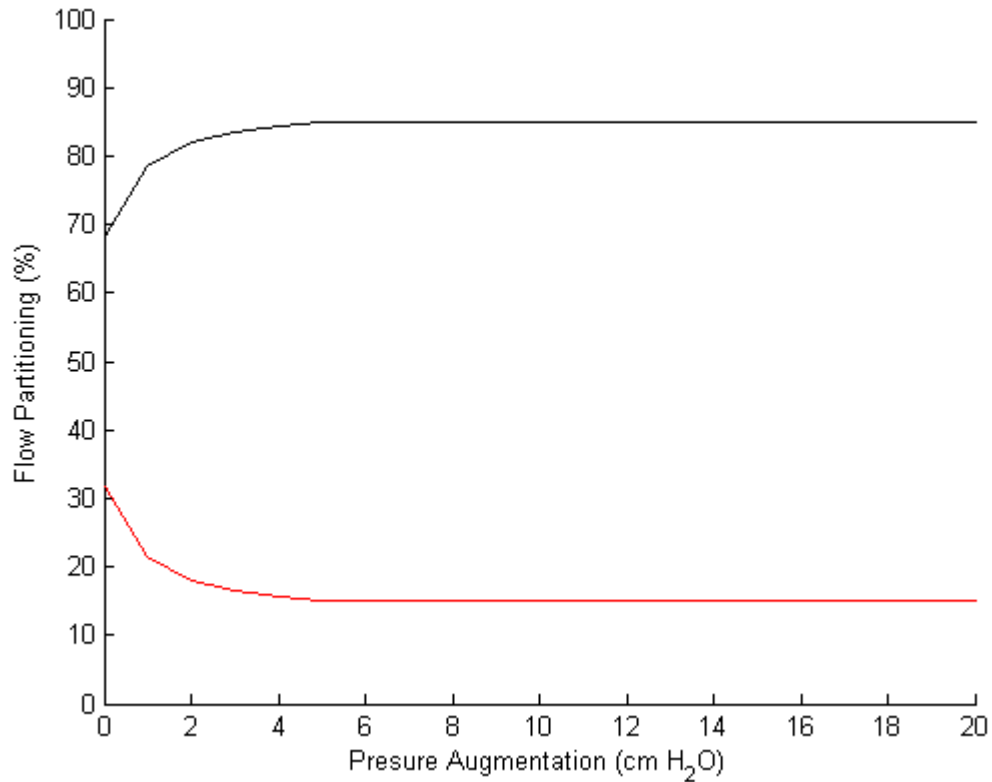


**Figure 8.2: Inter-airway air mass-flow partitioning ratio over range of pressure augmentation to sustain ASL hydration within left (forced congested) airway. — = modified right airway (previously patent), — = modified left airway (previously congested).**

With the change in inter-nasal airway resistance, the inter-nasal air mass-flows and hence ASL hydration status is forced to follow that normally found within the congested and patent airways during ambient air-pressure breathing.

Applying the proposed change in inter-nasal airway resistances given in Figure 8.1 results in the inter-nasal air mass-flow partitioning ratios presented in Figure 8.2.

Reduction in ASL water supply during periods of pressure augmentation is accounted for by biasing the air mass-flow partitioning of each airway as shown in Figure 8.2. This results in more air passing through the right (forced patent) airway and less through the left (forced congested) during breathing at elevated air-pressures. For this individual, the model predicts air-flow through the right (forced patent) airway to increase by around 15%. Conversely, the left (forced congested) airway experiences a 15% drop in air-flow.

#### **8.4 n-PAP Breathing with Regulated Inter-Nasal Resistances**

Results presented in this section are derived from the model predictions for an individual undertaking simulated breathing of ambient air pressurised to 9 cmH<sub>2</sub>O.

As discussed in Chapter 6, this represents the worst possible scenario for sustaining viable ASL hydration within either of the two airways for the specific individual analysed. To relieve airway drying, total inter-nasal resistance is modified in accordance with data given in Figure 8.1 as an alternative to supplying supplementary humidification.

### 8.4.1 Inhalation Air Properties, Flux Levels and ASL Hydration

Model predictions using regulated nasal resistance as a substitute for supplementary humidification are shown in Figure 8.3. These are based on n-PAP breathing at 9 cm H<sub>2</sub>O. This requires the right (forced patent) airway to conduct the majority (85%) of the total air mass-flow. Plots are coloured to represent temporal slices throughout the breath cycle as described in Section 6.2. Arrows are also shown that indicate change from the initial and final results as well as airflow direction.

ASL hydration ( $H_{e,ASL}$ ) demonstrates contrasting states during peak inhalation, as shown in Figures 8.3 (i) and 8.3 (j). This is quite unlike non-humidified n-PAP breathing. As shown, the left (forced congested) airway maintains sufficient ASL hydration to sustain mucociliary transport while the right (forced patent) airway experiences severe dehydration. This demonstrates that regulating inter-nasal resistance during n-PAP breathing could replace supplementary humidification.

As a consequence of differencing ASL hydration states, the left (forced congested) airway experiences higher levels of air temperature ( $T_a$ ) and absolute humidity (AH), shown in Figures 8.3 (a) and (c) respectively when compared to that within the right (forced patent) airway, shown by Figures 8.3 (b) and (d) respectively.

Reduction of the air mass-flow through the left (forced congested) airway has suppressed the ASL heat ( $Q$ ) and water mass flux ( $m_{ASL}$ ) distribution, shown in Figures 8.3 (g) and (e) respectively. On the other hand, increased air mass-flow through the right (forced patent) airway has caused an increase in peak heat flux, shown in Figure 8.3 (h).

Severe ASL dehydration within the right (forced patent) airway has also caused ASL water mass flux to drop to the cellular basal level as indicated by the horizontal line in Figure 8.3 (f).

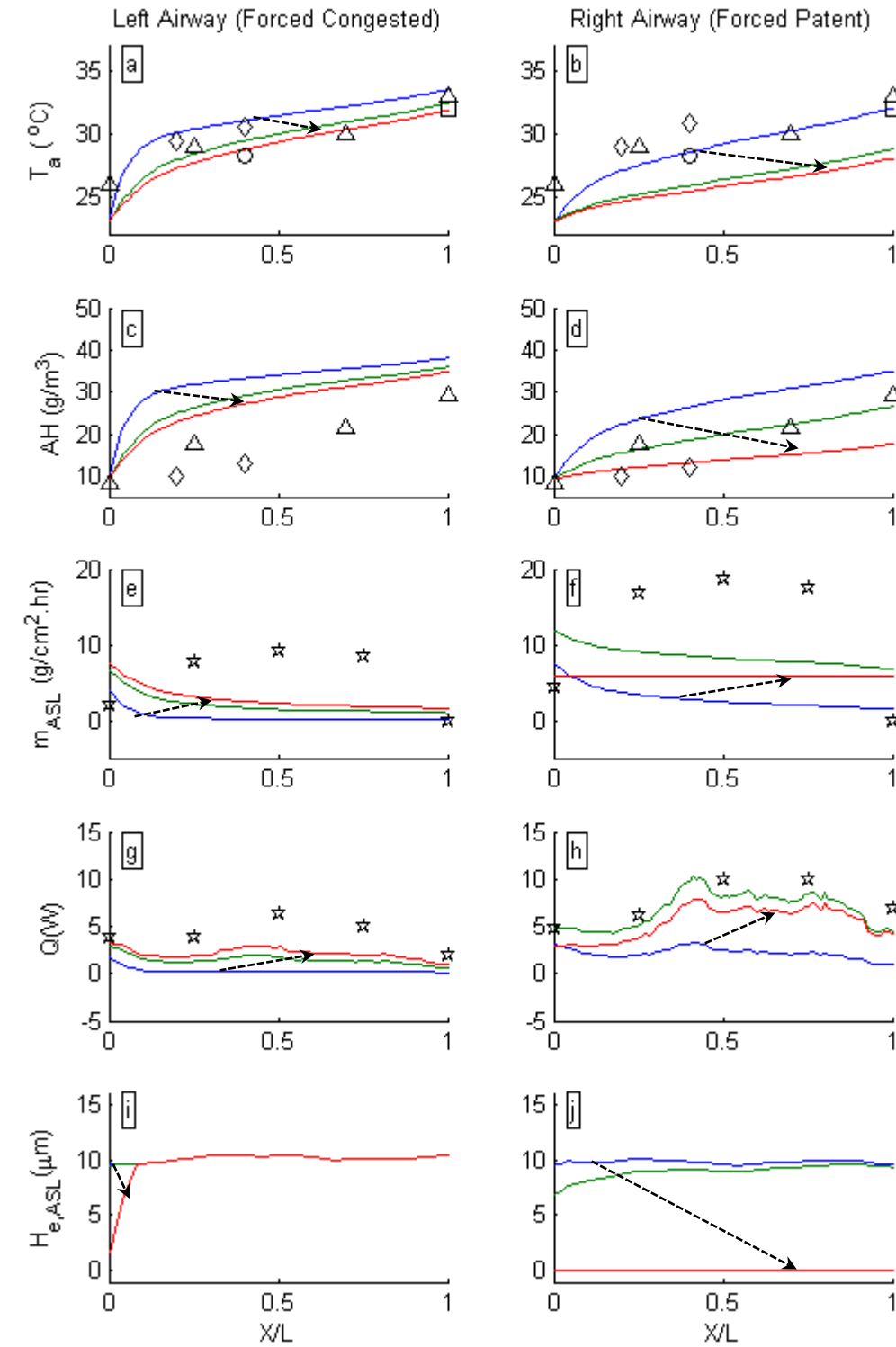


**Figure 8.3:** Inhalation inter-airway temperature ( $T_a$ ), absolute humidity (AH), molar water flux ( $N$ ), heat flux ( $Q$ ) and ASL water equivalent height ( $H_{e,ASL}$ ) distribution from rest to maximal change. Mask pressure 9 cmH<sub>2</sub>O, AH=9.2g H<sub>2</sub>O/m<sup>3</sup> dry air ( $T=23^{\circ}\text{C}$ ,  $RH=45\%$ ).  $\Delta$  = Keck *et al.* [180],  $\circ$  = Wiesmiller *et al.* [73],  $\diamond$  = Lindemann *et al.* [181],  $\square$  = Lindemann *et al.* [50],  $\star$  = Hanna [97].

### 8.4.2 Exhalation Air Properties, Flux Levels and ASL Hydration

During this phase of breathing we again see ASL re-hydrating in both airways, shown in Figures 8.4 (i) for the left (previously congested) airway and Figure 8.4 (j) for the right (forced patent) airway. Of note is the slight over-hydration occurring within the right airway as a consequence of it conducting the bulk (85%) of the exhaled air mass-flow.

### 8.5 Mucosa Dry Time

In Chapter 6, it was demonstrated that only the patent airway experiences excessive ASL dehydration during ambient air-pressure breathing. Conversely, both airways experience periods of excessive ASL dehydration during n-PAP breathing without the use of supplementary humidification. The model will now be used to investigate the effectiveness of the proposed regulated air mass-flow system to limit ASL dehydration under n-PAP conditions.

The following section presents modelled predictions of the severity of dehydration as a function of position and duration. This is given in terms of time duration represented as a percentage of the breath cycle and for a range of pressure augmentation. Presenting the ASL hydration results in this format provides a unique indication as to the severity of the drying event within each airway.

#### 8.5.1 Absence of Supplementary Humidification

With the model configured to nasal mask air conditions of temperature of 23°C and humidity of 45%, and n-PAP pressures ranging from ambient to 20 cmH<sub>2</sub>O enabled the distance and time duration where severe ASL dehydration occurred to be predicted. Results of this simulation are shown in Figure 8.5.

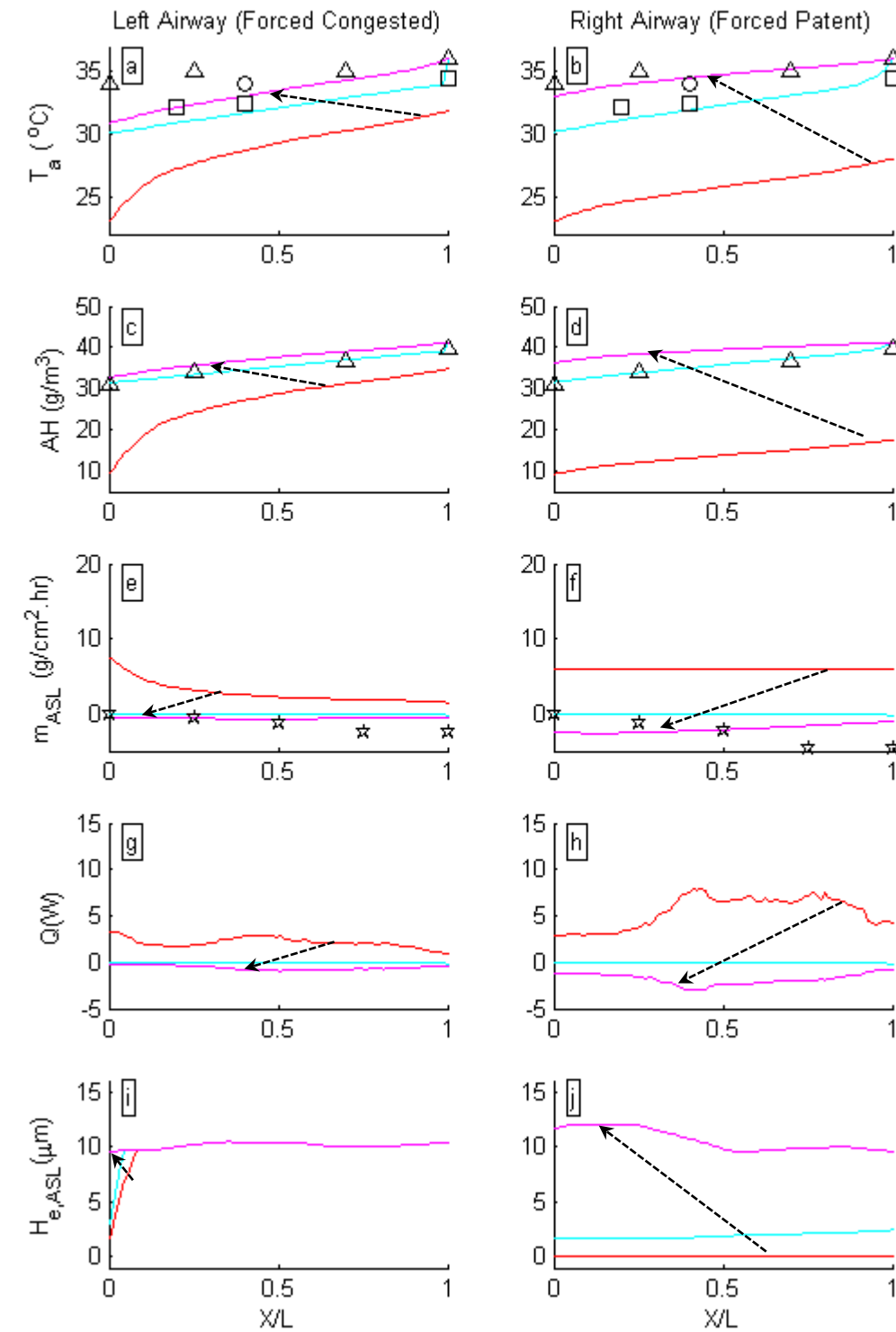


**Figure 8.4: Exhalation inter-airway temperature ( $T_a$ ), absolute humidity ( $AH$ ), molar water flux ( $N$ ), heat flux ( $Q$ ) and ASL water equivalent height ( $H_{e,ASL}$ ) distribution. From maximal inhalation to maximal exhalation. Mask pressure 9 cmH<sub>2</sub>O,  $AH=9.2\text{g H}_2\text{O/m}^3$  dry air ( $T=23^\circ\text{C}$ ,  $RH=45\%$ ).  $\Delta$  = Keck *et al.* [180],  $\circ$  = Wiesmiller *et al.* [73],  $\square$  = Lindemann *et al.* [50],  $\star$  = Hanna [97].**

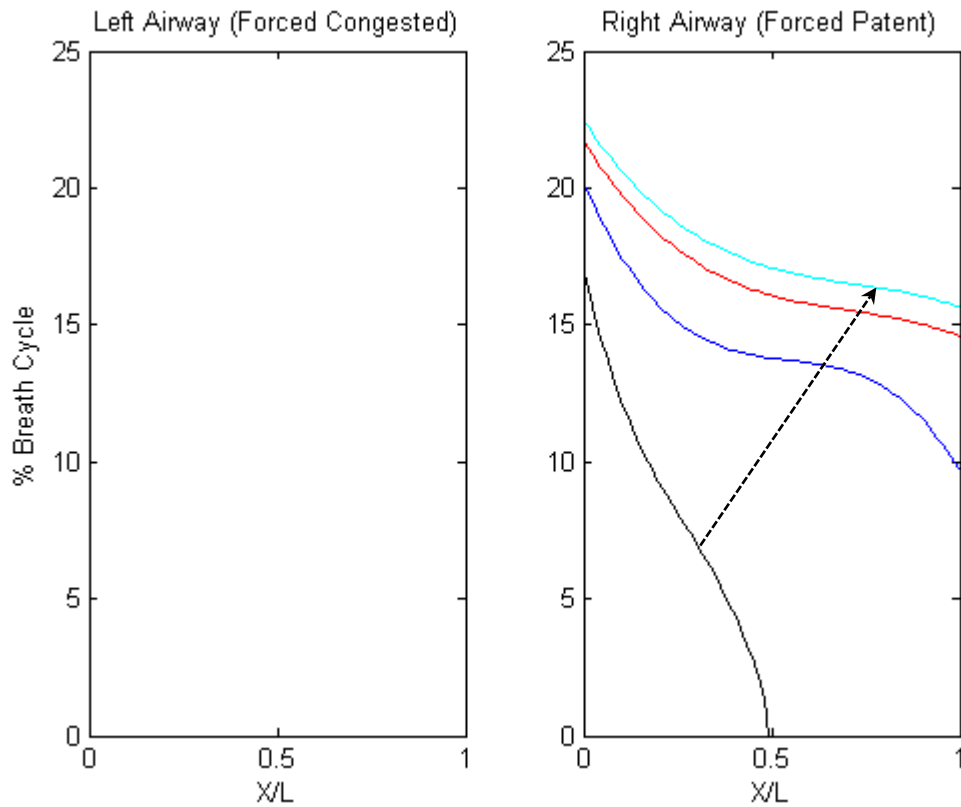


**Figure 8.5: Inter-airway ASL dehydration time distribution for range of pressure augmentation. — = ambient, — = 2 cmH<sub>2</sub>O, — = 4 cmH<sub>2</sub>O, — = 6 to 20 cmH<sub>2</sub>O.**

An arrow is drawn from the data representing ambient pressure which points to the data corresponding to the maximal pressure augmentation considered (20 cmH<sub>2</sub>O). Data corresponding to intermediate pressures are also shown.

As discussed earlier in this chapter, it can be seen from Figure 8.5 that the left (forced congested) airway does not experience severe ASL dehydration at ambient or elevated pressures. The right (forced patent) airway however experiences severe ASL dehydration up to 50% along its length at ambient pressure. At pressures above ambient, the ASL along the whole length of this airway becomes completely dehydrated for increasingly longer time periods.

## 8.6 Discussion

Over the range of pressure tested, regulating inter-nasal air-flow partitioning forces the left (forced congested) airway to experience normal levels of ASL dehydration so mucociliary clearance is not compromised. The right (forced patent) airway, as a

consequence of this regulation, carries the majority of the air-conditioning burden and experiences progressively more severe ASL dehydration, in terms of duration and amount of airway affected.

Whilst this proposed supplementary therapy achieves the goal of mimicking the same alternating ASL hydration conditions as found during ambient pressure breathing, the right (forced patent) airway experiences a more severe ASL drying due to the reduction in ASL water supply, discussed in Chapter 5. Unfortunately this additional drying within the right (forced patent) airway during peak inhalation is unavoidable. The obvious consequence of applying this proposed supplementary therapy is that the conducting airway distal to the nose carries a greater burden of air-conditioning duty. This issue can be ameliorated by increasing the frequency of nasal cycle switching.

Normal variation in nasal morphology, mucosal ASL water supply, breathing patterns and many other factors may also require the bias of inter-nasal air mass-flow partitioning to be tailored to suit an individual's air-conditioning needs. This may also require variation in the frequency in which the nasal cycle is switched. Provided sufficient time is given to enable mucociliary transport to clear entrapped pathogens debris, increasing the frequency seems to be an obvious solution.

## **8.6 Closure**

Within this chapter an alternative therapy has been proposed as a replacement for supplementary humidification used to relieve the symptoms of nasal airway drying. This new proposal offers benefits to the equipment manufacturer, the user and also has the potential to improve treatment efficacy and therapy compliance. This proposal arises from the application of the model developed and data gathered in this research.

## **CHAPTER 9**

### **CONCLUSIONS AND RECOMMENDATIONS.**

#### **9.1 Introduction**

Conclusions are delivered in sections pertaining to coherent outcomes of this work. This is followed by a section making recommendations for future work.

#### **9.2 Research Hypothesis**

The research hypothesis proposed in Chapter 2 suggested that symptoms of apparent nasal drying elicited by n-PAP breathing were caused by the two phenomena discussed in the following sections.

For the first time the multiple causes of severe and abnormal ASL dehydration during n-PAP breathing have been identified. This has been achieved by developing and characterising a nasal air-conditioning model with the findings from studies of inter-nasal air mass-flow partitioning, water supply and nasal geometry. This model has enabled further understanding of the purpose of the nasal cycle and the complex nasal symptoms experienced during n-PAP breathing. It has also allowed an alternative treatment to supplementary humidification to be proposed that potentially could improve patient adherence to n-PAP therapy.

##### **9.2.1 Inter-Nasal Variation in Geometry**

The first part of the research hypothesis proposed that variation in geometry along each cavity elicited by n-PAP breathing negatively impacts the distribution of heat and water mass flux within the two airways. The findings of this investigation, presented in Chapter 4, have quantified and demonstrated that opposing geometric responses occur between the patent and congested airways during n-PAP breathing.

During ambient breathing, the model results demonstrate that the majority of airflow occurs within the patent airway, causing it to experience a greater heat and water mass flux than that in the congested. Implementing the geometric response specific to the nasal cycle status of each airway into the nasal model demonstrates n-PAP breathing alters the normal airflow partitioning. These cause the previously congested airway to

undertake a greater heat and water mass flux duty while the previously patent airway experiences a reduction in these parameters. The model indicates that there is a critical pressure (in this case 9 cm H<sub>2</sub>O) where equal heat and water flux occurs for both nasal airways.

### **9.2.2 Reduction in Mucosal Water Supply**

The second part of the research hypothesis proposed that increased static pressure exerted on the airway wall during n-PAP breathing causes a reduction in ASL water supply from the mucosa. The findings of this investigation, presented in Chapter 5, have demonstrated that the net mucosal ASL water supply reduces by 22% during n-PAP breathing from 5 cm H<sub>2</sub>O.

Modelling nasal air-conditioning, presented in Chapter 6, has demonstrated that at ambient pressure, the mucosal ASL water supply is sufficient to maintain enough ASL hydration to sustain mucociliary clearance within the congested airway. However, during n-PAP breathing, reduction in this supply causes this airway to experience severe ASL dehydration. On the other hand, the patent airway experiences severe ASL dehydration during both ambient and n-PAP breathing.

### **9.3 ASL Dehydration During n-PAP Breathing**

During peak inhalation n-PAP breathing it is predicted that this individual experiences severe ASL dehydration along the anterior 60-80% length of both airways which disables the bias of alternative air-conditioning or mucus clearance duties of each airway. This prediction is significant as it identifies for the first time the cause of nasal airway drying symptoms commonly experienced during n-PAP breathing. Here, unlike ambient air-pressure breathing, both airways experience repeated severe ASL dehydration and a change in the nasal cycle status would not alleviate this condition. This disables mucociliary clearance within both airways and exposes them to the pathophysiological dehydration outcomes described previously. Additionally, the important air-conditioning function carried out by the nose is significantly impaired which could lead to ASL dehydration and lowering of the ISB occurring within the distal conducting airways. This finding is original since previous investigations into nasal air-conditioning and n-PAP breathing have failed to detect airway drying or unfavourable air-conditioning performance.

## **9.4 Nasal Cycle**

The use of a nasal air-conditioning model has given insight into the purpose of the nasal cycle as a means to simultaneously and continuously carry out the conditioning of inhaled air and maintain airway health. This requires the ASL within one airway to remain sufficiently hydrated during peak inhalation to sustain mucociliary clearance. The other airway can however experience severe ASL dehydration as a consequence of it carrying the majority of the air-conditioning burden.

During n-PAP breathing there is a critical pressure, which for this individual is 9 cm H<sub>2</sub>O, where equal levels of heat and water mass flux causes severe ASL dehydration to simultaneously occur in both airways. This disables the mucociliary transport system within both airways and exposes the mucosa to risk of drying or infection.

## **9.5 Alternative to Supplementary Humidification**

The objective of regulating inter-nasal resistance during n-PAP therapy is to maintain normal mucociliary transport within one airway by ensuring the ASL remains sufficiently hydrated. Arising from this work it has been shown that regulating the resistance of the two parallel nasal airways during n-PAP breathing reproduces ASL hydration characteristics experienced during ambient air breathing.

Regulated air mass-flow partitioning would require the bias of air mass-flow to be alternated in the same manner as that experienced during the normal nasal cycle but possibly of a shorter period.

This alternative therapy to supplementary humidification has significant benefits, both in terms of simplifying and reducing size and mass of equipment. Therapeutic benefits may include relief of perceived congestion and stuffiness as well as improved patient satisfaction and treatment adherence.

## **9.6 Recommendations**

The findings of this investigation have identified numerous avenues of future work.

Work to enhance and support the current research could include the following:

1. The nasal model could be advanced to include water diffusion through the mucus layer of the ASL and variation in breathing pattern. This may lead to further alternative breathing therapeutic benefits being identified.
2. Undertake a more extensive MRI clinical study to add data to this original study and monitor other parameters during testing.
3. Develop a method by which ASL water supply from nasal mucosal tissue can be measured during simulated tidal breathing under ambient and pressurized conditions.
4. The nasal model could be further enhanced by considering a 3-dimensional airflow through the nose and the inclusion of ASL water supply being regulated in part through tidal breathing stress stimulation of the mucosa.

The activities that could be undertaken to further the current research findings are:

1. Work is required to ascertain if the conducting airway distal to the nose can cope with the additional air-conditioning duty imposed by regulated air mass-flow partitioning within the nose. This could be in the form of creating a more complex conducting airway model that incorporates the current nasal with an advanced trachea model to predict changes in ISB location, ASL hydration and mucociliary transport velocity.
2. A clinical trial could determine if regulated air mass-flow partitioning and frequency of switch in inter-nasal nasal airflow bias offers benefits in terms of comfort that lead to improved adherence to n-PAP therapy.
3. Investigate, using a clinical sleep trial, the influence of the lack of alternating nasal flow has on the dream cycle and the effect of n-PAP therapy has on brain wave patterns during sleep.
4. Develop a method by which information corresponding to ASL conditions, such as height and ATP content, can be measured during simulated tidal breathing conditions as this may lead to alternative ASL hydration therapies.

## REFERENCES

1. Walker, J.E.C. and Wells, R.E., *Heat and water exchange in the respiratory tract*. Am. J. Med., 1961. **30**(2): p. 259-267.
2. Rouadi, P., Barody, F.M., Abbott, D., Naureckas, E., Solway, J., and Naclerio, R.M., *A technique to measure the ability of the human nose to warm and humidify air*. J. Appl. Physiol., 1999. **87**(1): p. 400-406.
3. Assanasen, P., Barody, F.M., Naureckas, E., Solway, J., and Naclerio, R.M., *Supine position decreases the ability of the nose to warm and humidify air*. J. Appl. Physiol., 2001. **91**(6): p. 2459-2465.
4. Martins de Araujo, M.T., Vieira, S.B., Vasquez, E.C., and Fleury, B., *Heated humidification or face mask to prevent upper airway dryness during continuous positive airway pressure therapy*. Chest, 2000. **117**: p. 142-147.
5. Wiest, G.H., Lehnert, G., Brück, W.M., Meyer, M., Hahn, E.G., and Ficker, J.H., *A heated humidifier reduces upper airway dryness during continuous positive airway pressure therapy*. Respir. Med., 1999. **93**(1): p. 21-26.
6. Wiest, G.H., Fuchs, F.S., Brueckl, W.M., Nusko, G., Harsch, I.A., Hahn, E.G., and Ficker, J.H., *In vivo efficacy of heated and non-heated humidifiers during nasal continuous positive airway pressure (nCPAP)-therapy for obstructive sleep apnoea*. Respir. Med., 2000. **94**(4): p. 364-368.
7. Fischer, Y., Keck, T., Leiacker, R., Rozsasi, A., Rettinger, G., and Gruen, P.M., *Effects of nasal mask leak and heated humidification on nasal mucosa in the therapy with nasal continuous positive airway pressure (nCPAP)*. Sleep Breath, 2008. **12**: p. 353-357.
8. Hayes, M.J., McGregor, F.B., D.N., R., Schroter, R.C., and Pride, N.B., *Continuous nasal positive airway pressure with a mouth leak: effect on nasal mucosal blood flux and nasal geometry*. Thorax, 1995. **50**: p. 1179-1182.
9. Richards, G.N., Cistulli, P.A., Ungar, R.G., Berthon-Jones, M., and Sullivan, C.E., *Mouth leak with nasal continuous positive airway pressure increases nasal airway resistance*. Am. J. Respir. Crit. Care Med., 1996. **154**: p. 182-186.
10. Malik, N.W. and Kenyon, G.S., *Changes in the nasal airway mucosa and in nasal symptoms following continuous positive airway pressure (n-CPAP) for obstructive sleep apnoea*. Australian Journal of Oto-Laryngology, 2004. **7**(1): p. 17-20.
11. Keck, T., Dürr, J., Leiacker, R., Rozsasi, A., Rettinger, G., and Rother, T., *Influence of passive humidification on nasal conditioning*. Am. J. Rhinol., 2006. **20**(5): p. 430.
12. Koutsourelakis, I., Vagiakis, E., Perraki, E., Karatza, M., Magkou, C., Kopaka, M., Roussos, C., and Zakynthinos, S., *Nasal inflammation in sleep apnoea patients using CPAP and effect of heated humidification*. Eur. Respir. J., 2011. **37**(3): p. 587-594.
13. Mador, M.J., Krauz, M., Pervez, A., Pierce, D., and Braun, M., *Effect of heated humidification on compliance and quality of life in patients with sleep apnea using nasal continuous positive airway pressure*. Chest, 2005. **128**(4): p. 2151-2158.
14. Massie, C.A., Hart, R.W., Peralez, K., and Richards, G.N., *Effects of humidification on nasal symptoms and compliance in sleep apnea patients using continuous positive airway pressure*. Chest, 1999. **116**: p. 403-408.

15. Worsnop, C.J., Miseski, S., and Rochford, P.D. *The routine use of humidification with nasal continuous positive airway pressure*. Intern. Med. J., 2009. **99**, DOI: 10.1111/j.1445-5994.2009.01969.x.
16. Sahin-Yilmaz, A., Barody, F.M., DeTineo, M., Cuttance, G., Makinson, D., M. Pinto, J.M., Naureckas, E.T., and Naclerio, R.M., *Effect of changing airway pressure on the ability of the human nose to warm and humidify air*. Ann. Otol. Rhinol. Laryngol., 2008. **117**(7): p. 501-507.
17. Arfoosh, R. and Rowley, J., *Continuous positive airway pressure for obstructive sleep apnea: an update*. Journal of Respiratory Diseases, 2008. **29**(9): p. 365-373.
18. Kalan, A., Kenyon, G.S., Seemungal, T.A.R., and Wedzicha, J.A., *Adverse effects of nasal continuous positive airway pressure therapy in sleep apnoea syndrome*. J. Laryngol. Otol., 1999. **113**(10): p. 888-892.
19. Kreivi, H.R., Virkkula, P., Lehto, J., and Brander, P., *Frequency of upper airway symptoms before and during continuous positive airway pressure treatment in patients with obstructive sleep apnea syndrome*. Respiration, 2010. **80**(6): p. 488-494.
20. Bossi, R., Piatti, G., Roma, E., and Ambrosetti, U., *Effects of long-term nasal continuous positive airway pressure therapy on morphology, function, and mucociliary clearance of nasal epithelium in patients with obstructive sleep apnea syndrome*. Laryngoscope, 2004. **114**(8): p. 1431-1434.
21. Neill, A.M., Wai, H.S., Bannan, S.P.T., Beasley, C.R., Weatherall, M., and Campbell, A.J., *Humidified nasal continuous positive airway pressure in obstructive sleep apnoea*. Eur. Respir. J., 2003. **22**(2): p. 258-262.
22. Madhav, V.N.V., *Diagnosis and management of obstructive sleep apnea*. Journal of International Dental and Medical Research, 2011. **4**(1): p. 35-41.
23. Sunitha, C. and Aravindkumar, S., *Obstructive sleep apnea: Clinical and diagnostic features*. Indian J. Dent. Res., 2009. **20**(4): p. 487-91.
24. Kuna, S.T. and Smickley, J.S., *Superior Pharyngeal Constrictor Activation in Obstructive Sleep Apnea*. Am. J. Respir. Crit. Care Med., 1997. **156**(3): p. 874-880.
25. McGinley, B.M., Schwartz, A.R., Schneider, H., Kirkness, J.P., Smith, P.L., and Patil, S.P., *Upper airway neuromuscular compensation during sleep is defective in obstructive sleep apnea*. J. Appl. Physiol., 2008. **105**(1): p. 197-205.
26. Oliven, R., Tov, N., Odeh, M., Gaitini, L., Steinfeld, U., Schwartz, A.R., and Oliven, A., *Interacting effects of genioglossus stimulation and mandibular advancement in sleep apnea*. J. Appl. Physiol., 2009. **106**(5): p. 1668-1673.
27. Kirkness, J.P., Schwartz, A.R., Schneider, H., Punjabi, N.M., Maly, J.J., Laffan, A.M., McGinley, B.M., Magnuson, T., Schweitzer, M., Smith, P.L., and Patil, S.P., *Contribution of male sex, age, and obesity to mechanical instability of the upper airway during sleep*. J. Appl. Physiol., 2008. **104**(6): p. 1618-1624.
28. Willman, M., Igelström, H., Martin, C., and Åsenlöf, P., *Experiences with CPAP treatment in patients with obstructive sleep apnea syndrome and obesity*. Advances in Physiotherapy, 2012. **14**(4): p. 166-174.
29. Isono, S., Tanaka, A., and Nishino, T., *Dynamic interaction between the tongue and soft palate during obstructive apnea in anesthetized patients with sleep-disordered breathing*. J. Appl. Physiol., 2003. **95**(6): p. 2257-2264.
30. Isono, S., Feroah, T.R., Hajduk, E.A., Brant, R., Whitelaw, W.A., and Remmers, J.E., *Interaction of cross-sectional area, driving pressure, and airflow of passive velopharynx*. J. Appl. Physiol., 1997. **83**(3): p. 851-859.

31. Isono, S., Tanaka, A., Tagaito, Y., Ishikawa, T., and Nishino, T., *Influences of head positions and bite opening on collapsibility of the passive pharynx*. J. Appl. Physiol., 2004. **97**(1): p. 339-346.
32. Hiestand, D.M., Britz, P., Goldman, M., and Phillips, B., *Prevalence of Symptoms and Risk of Sleep Apnea in the US Population: Results From the National Sleep Foundation Sleep in America 2005 Poll*. Chest, 2006. **130**(3): p. 780-6.
33. Giles, T.L., Lasserson, T.J., Smith, B., White, J., Wright, J.J., and Cates, C.J., *Continuous positive airways pressure for obstructive sleep apnoea in adults*. Cochrane Database Syst. Rev. 1996: John Wiley & Sons, Ltd.
34. Rodenstein, D., *Sleep Apnea: Traffic and Occupational Accidents - Individual Risks, Socioeconomic and Legal Implications*. Respiration, 2009. **78**(3): p. 241-8.
35. George, C.F.P., *Sleep Apnea, Alertness, and Motor Vehicle Crashes*. Am. J. Respir. Crit. Care Med., 2007. **176**(10): p. 954-6.
36. Khazaie, H., Najafi, F., Rezaie, L., Tahmasian, M., Sepehry, A.A., and Herth, F.J.F., *Prevalence of Symptoms and Risk of Obstructive Sleep Apnea Syndrome in the General Population*. Archives of Iranian Medicine, 2011. **14**(5): p. 335-8.
37. Hukins, C.A., *Obstructive Sleep Apnea - Management Update*. Neuropsychiatric Disease and Treatment, 2006. **3**(2): p. 309-236.
38. Feng, J., He, Q.-y., Zhang, X.-l., and Chen, B.-y., *Epworth Sleepiness Scale may be an indicator for blood pressure profile and prevalence of coronary artery disease and cerebrovascular disease in patients with obstructive sleep apnea*. Sleep and Breathing, 2012. **16**(1): p. 31-40.
39. Victor, L.D., *Obstructive sleep apnea*. Am. Fam. Physician, 1999. **60**(8): p. 2279-86.
40. Shapiro, G.K. and Shapiro, C.M., *Factors that influence CPAP adherence: an overview*. Sleep and Breathing, 2010. **14**(4): p. 323-35.
41. Kushida, C.A., Chediak, A., Berry, R.B., Brown, L.K., Gozal, D., Iber, C., Parthasarathy, S., Quan, S.F., and Rowley, J.A., *Clinical guidelines for the manual titration of positive airway pressure in patients with obstructive sleep apnea*. Journal of clinical sleep medicine : JCSM : official publication of the American Academy of Sleep Medicine, 2008. **4**(2): p. 157-171.
42. Technology, S.S.D.S. *Snoring Treatments*. 2013; Available from: <http://www.s4sdental.com/information-for-the-public/snoring-sleep-apnoea/about-snoring/snoring-treatments/>.
43. Mortimore, I.L., Whittle, A.T., and Douglas, N.J., *Comparison of nose and face mask CPAP therapy for sleep apnoea*. Thorax, 1998. **53**(4): p. 290-2.
44. Bartley, J., *Breathing Matters: a New Zealand Guide*. 1st. ed 2006, Auckland: Random House. 219.
45. Elad, D., Wolf, M., and Keck, T., *Air-conditioning in the human nasal cavity*. Respir. Physiol. Neurobiol., 2008. **163**(1-3): p. 121-127.
46. Naftali, S., Rosenfeld, M., Wolf, M., and Elad, D., *The air-conditioning capacity of the human nose*. Ann. Biomed. Eng., 2005. **33**(4): p. 545-553.
47. Chhabra, N. and Houser, S.M., *The Diagnosis and Management of Empty Nose Syndrome*. Otolaryngol. Clin. North Am., 2009. **42**(2): p. 311-330.
48. Drettner, B., Falck, B., and Simon, H., *Measurements of the Air Conditioning Capacity of the Nose During Normal and Pathological Conditions and Pharmacological Influence*. Acta Otolaryngol. (Stockh.), 1977. **84**(1-6): p. 266-277.

49. Keck, T., Leiacker, R., Riechelmann, H., and Rettinger, G., *Temperature profile in the nasal cavity*. Laryngoscope, 2000. **110**(4): p. 651-654.
50. Lindemann, J., Leiacker, R., Rettinger, G., and Keck, T., *Nasal mucosal temperature during respiration*. Clin. Otolaryngol., 2002. **27**(3): p. 135-139.
51. Naclerio, R.M., Pinto, J.M., Assanasen, P., and Baroody, F.M., *Observations on the ability of the nose to warm and humidify inspired air*. Rhinology, 2007. **47**: p. 102-111.
52. Wolf, M., Naftali, S., Schroter, R.C., and Elad, D., *Air-conditioning characteristics of the human nose*. J. Laryngol. Otol., 2004. **118**(2): p. 87-92.
53. Johnson, M.K., Carter, R., Nicol, A., Paton, R., and Banham, S.W., *Long-term continuous positive airway pressure (CPAP) outcomes from a sleep service using limited sleep studies and daycase CPAP titration in the management of obstructive sleep apnoea/hypopnoea syndrome*. Chron. Respir. Dis., 2004. **1**(2): p. 83-8.
54. Constantinidis, J., Knobber, D., Steinhart, H., Kuhn, J., and Iro, H., *Fine-structural investigations of the effect of nCPAP-mask application on the nasal mucosa*. Acta Otolaryngol. (Stockh.), 2000. **120**(3): p. 432-437.
55. Rakotonanahary, D., Pelletier-Fleury, N., Gagnadoux, F., and Fleury, B., *Predictive factors for the need for additional humidification during nasal continuous positive airway pressure therapy*. Chest, 2001. **119**(2): p. 460-465.
56. Hollandt, J.H. and Mahlerwein, M., *Nasal breathing and continuous positive airway pressure (CPAP) in patients with obstructive sleep apnea (OSA)*. Sleep and Breathing, 2003. **7**(2): p. 87-93.
57. Devouassoux, G., Lévy, P., Rossini, E., Pin, I., Fior-Gozlan, M., Henry, M., Seigneurin, D., and Pépin, J.-L., *Sleep apnea is associated with bronchial inflammation and continuous positive airway pressure-induced airway hyperresponsiveness*. J. Allergy Clin. Immunol., 2007. **119**(3): p. 597-603.
58. Fisher & Paykel Healthcare Ltd. *Fisher & Paykel Stand-alone HC150 Heated Humidifier*. 2013; Available from: <http://1800cpap.com/fisher-and-paykel-hc150-heated-humidifier.aspx>.
59. Hay, K.D. and Morton, R.P., *Optimal nocturnal humidification for xerostomia*. Head Neck, 2006. **28**(9): p. 792-796.
60. Pasteur, M.C., Bilton, D., and Hill, A.T., *British Thoracic Society guideline for non-CF bronchiectasis*. Thorax, 2010. **65**(Suppl 1): p. i1-i58.
61. Dolan, D.C., Okonkwo, R., Gfullner, F., Hansbrough, J.R., Strobel, R.J., and Rosenthal, L., *Longitudinal comparison study of pressure relief (C-Flex(TM)) vs. CPAP in OSA patients*. Sleep and Breathing, 2009. **13**(1): p. 73-7.
62. Hollenhorst, M.I., Richter, K., and Fronius, M., *Ion Transport by Pulmonary Epithelia*. Journal of Biomedicine and Biotechnology, 2011. **2011**.
63. Cole, P., *Modification of Inspired Air*, in *The Nose: Upper Airway Physiology and the Atmospheric Environment.*, D.F. Proctor and I. Andersen, Editors. 1982, Elsevier Biomedical Press: Amsterdam. p. 351-375.
64. Doorly, D., Taylor, D.J., Franke, P., and Schroter, R.C., *Experimental investigation of nasal airflow*. Proc. Inst. Mech. Eng. [H], 2008. **222**(H4): p. 439-453.
65. Solomita, M. and Samlone, G.C., *Humidification and Noninvasive Ventilation*. Respir. Care, 2007. **52**(1): p. 24-25.
66. Segal, R., Kepler, G., and Kimbell, J., *Effects of differences in nasal anatomy on airflow distribution: A comparison of four individuals at rest*. Ann. Biomed. Eng., 2008. **36**(11): p. 1870.

67. Doorly, D.J., Taylor, D.J., and Schroter, R.C., *Mechanics of airflow in the human nasal airways*. Respiratory Physiology and Cell Neurobiology, 2008. **163**(1-3): p. 100-110.
68. Croce, C., Fodil, R., Durand, M., Sbirlea-Apiou, G., Caillibotte, G., Papon, G.F., Blondeau, J.R., Coste, A., Isabey, D., and Louis, B., *In vitro experiments and numerical simulations of airflow in realistic nasal airway geometry*. Ann. Biomed. Eng., 2006. **34**(6): p. 997-1007.
69. White, D.E., Al-Jumaily, A.M., Bartley, J., and Somervell, A., *Nasal air-conditioning during breathing therapy*. Current Respiratory Medicine Reviews, 2011. **7**: p. 213-225.
70. Williams, R.B., Rankin, N., Smith, T., Galler, D., and Seakins, P., *Relationship Between the Humidity and Temperature of Inspired Gas and the Function of the Airway Mucosa*. Crit. Care Med., 1996. **24**(11): p. 1920-1929.
71. Sottiaux, T.M., *Consequences of Under-and Over-Humidification*. Respir. Care Clin. N. Am., 2006. **12**(2): p. 233-252.
72. Mlynski, G., Grutzenmacher, S., Plontke, S., and Mlynski, B., *Correlation of Nasal Morphology and Respiratory Function*. Rhinology (Utrecht), 2001. **39**(4): p. 197-201.
73. Wiesmiller, K., Keck, T., Leiacker, R., and Lindemann, J., *Simultaneous in vivo measurements of intranasal air and mucosal temperature*. Eur. Arch. Otorhinolaryngol., 2007. **264**(6): p. 615-619.
74. Cole, P., *The four components of the nasal valve*. Am. J. Rhinol., 2003. **17**(2): p. 107-110.
75. Widdicombe, J., *Microvascular anatomy of the nose*. Allergy, 1997. **52**(s40): p. 7-11.
76. Bailie, N., Hanna, B., Watterson, J., and Gallagher, G., *A model of airflow in the nasal cavities: Implications for nasal air conditioning and epistaxis*. Am J Rhinol Allergy, 2009. **23**(3): p. 244-249.
77. Falcon-Chevere, J.L., Giraldez, L., Rivera-Rivera, J.O., and Suero-Salvador, T., *Critical ENT Skills and Procedures in the Emergency Department*. Emerg. Med. Clin. North Am., 2013. **31**(1): p. 29-58.
78. Davis, S.S. and Eccles, R., *Nasal congestion: mechanisms, measurement and medications. Core information for the clinician*. Clin. Otolaryngol., 2004. **29**(6): p. 659-666.
79. Hanif, J., Jawad, S.S.M., and Eccles, R., *The nasal cycle in health and disease*. Clin. Otolaryngol., 2000. **25**(6): p. 461-467.
80. Hasegawa, M., Ohki, M., and Kurita, N., *Effects of posture on the nasal cycle*. Am. J. Rhinol., 1990. **4**(3): p. 101-104.
81. Atanasov, A.I., Dimov, P.D., and Dimitrov, B.D., *Time periods in the nasal cycle during night sleep*. Biol. Rhythm. Res., 2003. **34**(4): p. 355-366.
82. Soane, R.J., Carney, A.S., Jones, N.S., Frier, M., Perkins, A.C., Davis, S.S., and Illum, L., *The effect of the nasal cycle on mucociliary clearance*. Clin Otolaryng Allied Sci, 2001. **26**(1): p. 9-15.
83. Lindemann, J., Leiacker, R., Rettinger, G., and Keck, T., *The relationship between water vapour saturation of inhaled air and nasal patency*. Eur. Respir. J., 2003. **21**(2): p. 313-316.
84. Druce, H.M., *Measurement of nasal mucosal blood flow*. J. Allergy Clin. Immunol., 1988. **81**(3): p. 505-508.
85. Kennedy, D.W., Zinreich, S.J., Kumar, A.J., Rosenbaum, A.E., and Johns, M.E., *Physiologic mucosal changes within the nose and ethmoid sinus: Imaging of the nasal cycle by MRI*. Laryngoscope, 1988. **98**(9): p. 928-933.

86. Roblin, D.G. and Eccles, R., *Normal Range for Nasal Partitioning of Airflow Determined by Nasal Spirometry in 100 Healthy Subjects*. Am. J. Rhinol., 2003. **17**(4): p. 179-83.
87. Eccles, R., *Neurological and pharmacological considerations*, in *The nose: upper airway physiology and the atmospheric environment.*, D.F. Proctor and I. Andersen, Editors. 1982, Elsevier Biomedical Press: Amsterdam. p. 191-214.
88. Shannahoff-Khalsa, D., *The Ultradian Rhythm of Alternating Cerebral Hemispheric Activity*. Int. J. Neurosci., 1993. **70**(3-4): p. 285-298.
89. Shannahoff-khalsa, D.S. and Yates, F.E., *Ultradian Sleep Rhythms of Lateral EEG, Autonomic, and Cardiovascular Activity Are Coupled in Humans*. Int. J. Neurosci., 2000. **101**(1-4): p. 21-43.
90. Cole, P., Haight, J.S.J., Naito, K., and Kucharczyk, W., *Magnetic Resonance Imaging of the Nasal Airways*. Am. J. Rhinol., 1989. **3**(2): p. 63.
91. Çakmak, Ö., Coşkun, M., Çelik, H., Büyüklü, F., and Özlüoğlu, L.N., *Value of acoustic rhinometry for measuring nasal valve area*. Laryngoscope, 2003. **113**(2): p. 295-302.
92. Hilberg, O., Jackson, A.C., Swift, D.L., and Pedersen, O.F., *Acoustic rhinometry: evaluation of nasal cavity geometry by acoustic reflection*. J. Appl. Physiol., 1989. **66**(1): p. 295-303.
93. Cakmak, O., Çelik, H., Cankurtaran, M., and Ozluoglu, L.N., *Effects of Anatomical Variations of the Nasal Cavity on Acoustic Rhinometry Measurements: A Model Study*. Am. J. Rhinol., 2005. **19**(3): p. 262.
94. Yokley, T.R., *Ecogeographic variation in human nasal passages*. Am. J. Phys. Anthropol., 2009. **138**(1): p. 11-22.
95. Lindemann, J., Tsakirpoulou, E., Vital, V., Keck, T., Leiacker, R., Pauls, S., Wacke, F., and Wiesmiller, K.M., *Influence of the turbinate volumes as measured by magnetic resonance imaging on nasal air conditioning*. American Journal of Rhinology and Allergy, 2009. **23**(3): p. 250-254.
96. Noback, M.L., Harvati, K., and Spoor, F., *Climate-related variation of the human nasal cavity*. Am. J. Phys. Anthropol., 2011. **145**(4): p. 599-614.
97. Hanna, L.M., *Modelling of heat and water vapor transport in the human respiratory tract (air-conditioning)*, 1983, University of Pennsylvania: United States -- Pennsylvania.
98. Craven, B.A., Neuberger, T., Paterson, E.G., Webb, A.G., Josephson, E.M., Morrison, E.E., and Settles, G.S., *Reconstruction and Morphometric Analysis of the Nasal Airway of the Dog (Canis familiaris) and Implications Regarding Olfactory Airflow*. Anat Rec (Hoboken), 2007. **290**(11): p. 1325-1340.
99. Lang, C., Grützenmacher, S., Mlynski, B., Plontke, S., and Mlynski, G., *Investigating the Nasal Cycle Using Endoscopy, Rhinoresistometry, and Acoustic Rhinometry*. Laryngoscope, 2003. **113**(2): p. 284-289.
100. Lindemann, J., Sannwald, D., and Wiesmiller, K., *Age-related changes in intranasal air conditioning in the elderly*. The Laryngoscope, 2008. **118**(8): p. 1472-1475.
101. Kesavanathan, J., Swift, D.L., and Bascom, R., *Nasal pressure-volume relationships determined with acoustic rhinometry*. J. Appl. Physiol., 1995. **79**(2): p. 547-553.
102. Brugel-Ribere, L., Fodil, R., Coste, A., Larger, C., Isabey, D., Harf, A., and Louis, B., *Segmental analysis of nasal cavity compliance by acoustic rhinometry*. J. Appl. Physiol., 2002. **93**(1): p. 304-310.
103. Cole, P., *Acoustic rhinometry and rhinomanometry*. Rhinol. Suppl. (Utrecht), 2000. **16**(Supplement): p. 29-34.

104. Winther, B. and Gwaltney, J.R., *Microbiology of Sinusitis*, in *Diseases of the Sinuses - Diagnosis and Management* D.W. Kennedy, W.E. Bolger, and S.J. Zinreich, Editors. 2001, B.C. Decker Inc.: Ontario. p. 77-84.
105. Tarran, R., Trout, L., Donaldson, S.H., and Boucher, R.C., *Soluble Mediators, Not Cilia, Determine Airway Surface Liquid Volume in Normal and Cystic Fibrosis Superficial Airway Epithelia*. J. Gen. Physiol., 2006. **127**(5): p. 591-604.
106. Trout, L., King, M., Feng, W., Inglis, S.K., and Ballard, S.T., *Inhibition of airway liquid secretion and its effect on the physical properties of airway mucus*. Am. J. Physiol. Lung Cell. Mol. Physiol., 1998. **274**(2): p. L258-263.
107. Button, B. and Boucher, R.C., *Role of mechanical stress in regulating airway surface hydration and mucus clearance rates*. Respir. Physiol. Neurobiol., 2008. **163**(1-3): p. 189-201.
108. Knowles, M.R. and Boucher, R.C., *Mucus Clearance as a Primary Innate Defense Mechanism for Mammalian Airways*. J. Clin. Invest, 2002. **109**: p. 571-577.
109. Button, B., Cai, L.-H., Ehre, C., Kesimer, M., Hill, D.B., Sheehan, J.K., Boucher, R.C., and Rubinstein, M., *A Periciliary Brush Promotes the Lung Health by Separating the Mucus Layer from Airway Epithelia*. Science, 2012. **337**(937): p. 937-941.
110. Cone, R.A., *Barrier properties of mucus*. Adv. Drug Delivery. Rev., 2009. **61**(2): p. 75-85.
111. Widdicombe, J.H., *Regulation of the depth and composition of airway surface liquid*. J. Anat., 2002. **201**(4): p. 313-318.
112. Antunes, M.B., Gudis, D.A., and Cohen, N.A., *Epithelium, Cilia, and Mucus: Their Importance in Chronic Rhinosinusitis*. Immunol. Allergy Clin. North Am., 2009. **29**(4): p. 631-643.
113. Dickey, B.F., *Walking on Solid Ground*. Science, 2012. **337**(924): p. 924-925.
114. Silberberg, A., *Rheology of mucus, mucociliary interaction, and ciliary activity*. Cell Motil. Cytoskeleton, 1982. **2**(S1): p. 25-28.
115. Smith, D.J., Gaffney, E.A., and Blake, J.R., *Modelling mucociliary clearance*. Respir. Physiol. Neurobiol., 2008. **163**(1-3): p. 178-188.
116. Brand, R.W. and Isselhard, D.E., *Anatomy of orofacial structures*. 7th ed 2003, St Louis: Mosby. 567.
117. Guyton, A.C. and Hall, J.E., *Textbook of medical physiology*. 10th ed, ed. W. Schmitt 2000, Philadelphia: W.B. Saunders Company. 1064.
118. Stierna, P.L.E., *Physiology, Mucociliary Clearance and Neural Control*, in *Diseases of the Sinuses - Diagnosis and Management*, D.W. Kennedy, W.E. Bolger, and S.J. Zinreich, Editors. 2001, B.C. Decker Inc.: Ontario. p. 35-45.
119. Mygind, N. and Dahl, R., *Anatomy, physiology and function of the nasal cavities in health and disease*. Adv. Drug Delivery. Rev., 1998. **29**(1-2): p. 3-12.
120. Boek, W.M., Graamans, K., Natzijl, H., van Rijk, P.P., and Huizing, E.H., *Nasal mucociliary transport: new evidence for a key role of ciliary beat frequency*. Laryngoscope, 2002. **112**(3): p. 570-573.
121. Refojo, M.F., *Vapor pressure and swelling pressure of hydrogels*. American Chemical Society, Polymer Preprints, Division of Polymer Chemistry, 1975. **16**(2): p. 286-288.
122. Quraishi, M.S., Jones, N.S., and Mason, J., *The rheology of nasal mucus: a review*. Clin. Otolaryngol., 1998. **23**(5): p. 403-413.
123. Kirkness, J.P., Eastwood, P.R., Szollosi, I., Platt, P.R., Wheatley, J.R., Amis, T.C., and Hillman, D.R., *Effect of surface tension of mucosal lining liquid on*

- upper airway mechanics in anesthetized humans*. J. Appl. Physiol., 2003. **95**(1): p. 357-363.
124. Verma, M., Seto-Poon, M., R. Wheatley, J.R., T.C., A., and Kirkness, J.P., *Influence of breathing route on upper airway lining liquid surface tension in humans*. J. Physiol., 2006. **574**(3): p. 859-866.
  125. Williams, R.B., *The Effects of Excessive Humidity*. Respir. Care Clin. N. Am., 1998. **4**(2): p. 215-228.
  126. Randell, S.H., Boucher, R.C., and for the University of North Carolina Virtual Lung, G., *Effective Mucus Clearance Is Essential for Respiratory Health*. Am. J. Respir. Cell Mol. Biol., 2006. **35**(1): p. 20-28.
  127. Lee, R.J. and Foskett, J.K., *Mechanisms of Ca<sup>2+</sup>-stimulated fluid secretion by porcine bronchial submucosal gland serous acinar cells*. Am. J. Physiol. Lung Cell. Mol. Physiol., 2010. **298**(2): p. L210-L231.
  128. Ballard, S.T. and Inglis, S.K., *Liquid secretion properties of airway submucosal glands*. The Journal of Physiology, 2004. **556**(1): p. 1-10.
  129. Rogers, D.F., *Motor control of airway goblet cells and glands*. Respir. Physiol., 2001. **125**(1-2): p. 129-144.
  130. Wine, J.J., *Parasympathetic Control of Airway Submucosal Glands: Central Reflexes and the Airway Intrinsic Nervous System*. Auton. Neurosci. Basic Clin., 2007. **1**(133): p. 35-54.
  131. Choi, J., Joo, N., Krouse, M., Wu, J., Robbins, R., Ianowski, J., Hanrahan, J., and Wine, J., *Synergistic airway gland mucus secretion in response to vasoactive intestinal peptide and carbachol is lost in cystic fibrosis*. J. Clin. Invest., 2007. **117**(10): p. 3118-3127.
  132. Wu, D.X.Y., Lee, C.Y.C., Uyekubo, S.N., Choi, H.K., Bastacky, S.J., and Widdicombe, J.H., *Regulation of the depth of surface liquid in bovine trachea*. Am. J. Physiol. Lung Cell. Mol. Physiol., 1998. **274**(3): p. L388-L395.
  133. Joo, N.S., Wine, J.J., and Cuthbert, A.W., *Lubiprostone stimulates secretion from tracheal submucosal glands of sheep, pigs, and humans*. Am. J. Physiol. Lung Cell. Mol. Physiol., 2009. **296**(5): p. L811-L824.
  134. Widdicombe, J.H., Bastacky, S.J., Wu, D.X., and Lee, C.Y., *Regulation of depth and composition of airway surface liquid*. Eur. Respir. J., 1997. **10**(12): p. 2892-2897.
  135. Davis, C.W. and Lazarowski, E., *Coupling of airway ciliary activity and mucin secretion to mechanical stresses by purinergic signaling*. Respir. Physiol. Neurobiol., 2008. **163**(1-3): p. 208-213.
  136. Wu, J.V., Krouse, M.E., and Wine, J.J., *Acinar origin of CFTR-dependent airway submucosal gland fluid secretion*. Am. J. Physiol. Lung Cell. Mol. Physiol., 2007. **292**(1): p. L304-L311.
  137. Théâtre, E., Bours, V., and Oury, C., *A P2X Ion Channel-Triggered NF-[kappa]B Pathway Enhances TNF-[alpha]-Induced IL-8 Expression in Airway Epithelial Cells*. Am. J. Respir. Cell Mol. Biol., 2009. **41**(6): p. 705-713.
  138. Knight, G.E., Bodin, P., De Groat, W.C., and Burnstock, G., *ATP is released from guinea pig ureter epithelium on distension*. Am. J. Physiol. Renal Physiol., 2002. **282**(2): p. F281-288.
  139. Homolya, L., Steinberg, T.H., and Boucher, R.C., *Cell to cell communication in response to mechanical stress via bilateral release of ATP and UTP in polarized epithelia*. J. Cell Biol., 2000. **150**(6): p. 1349-1359.
  140. Lazarowski, E.R., Tarran, R., Grubb, B.R., van Heusden, C.A., Okada, S.F., and Boucher, R.C., *Nucleotide release provides a mechanism for airway surface liquid homeostasis*. J. Biol. Chem., 2004. **279**(35): p. 36855-36864.

141. Tarran, R., Button, B., Picher, M., Paradiso, A.M., Ribeiro, C.M., Lazarowski, E.R., Zhang, L., Collins, P.L., Pickles, R.J., Fredberg, J.J., and Boucher, R.C., *Normal and Cystic Fibrosis Airway Surface Liquid Homeostasis*. J. Biol. Chem., 2005. **280**(42): p. 35751-35759.
142. Basser, P.J., McMahon, T.A., and Griffith, P., *The mechanism of mucus clearance in cough*. J. Biomech. Eng., 1989. **111**(4): p. 288-297.
143. Button, B., Picher, M., and Boucher, R.C., *Differential effects of cyclic and constant stress on ATP release and mucociliary transport by human airway epithelia*. J. Physiol., 2007. **580**(2): p. 577-592.
144. Ahmed, B., *Comparison of nasal prong pressure and thermistor measurements for detecting respiratory events during sleep*. Respiration, 2004. **71**(4): p. 385-390.
145. Elad, D., Naftali, S., Rosenfeld, M., and Wolf, M., *Physical stresses at the air-wall interface of the human nasal cavity during breathing*. J. Appl. Physiol., 2006. **100**(3): p. 1003-1010.
146. Lieb, T., Frei, C.W., Frohock, J.I., Bookman, R.J., and Salathe, M., *Prolonged increase in ciliary beat frequency after short-term purinergic stimulation in human airway epithelial cells*. J. Physiol., 2002. **538**(2): p. 633-646.
147. Zhang, L. and Sanderson, M.J., *Oscillations in ciliary beat frequency and intracellular calcium concentration in rabbit tracheal epithelial cells induced by ATP*. J. Physiol., 2003. **546**(3): p. 733-749.
148. Bucheimer, R.E. and Linden, J., *Purinergic regulation of epithelial transport*. J. Physiol., 2004. **555**(2): p. 311-321.
149. Sanderson, M.J. and Dirksen, E.R., *Mechanosensitivity of cultured ciliated cells from the mammalian respiratory tract: implications for the regulation of mucociliary transport*. Proc. Natl. Acad. Sci. U. S. A., 1986. **83**: p. 7302-7306.
150. Leuba, D., De Ribaupierre, Y., and Kucera, P., *Ion transport, ciliary activity, and mechanosensitivity of sinus mucosa: an in vitro study*. American Journal of Physiology - Lung and Cellular Molecular Physiology, 1996. **271**(3): p. L349-358.
151. Kilgour, E., Rankin, N., Ryan, S., and Pack, R., *Mucociliary function deteriorates in the clinical range of inspired air temperature and humidity*. Intensive Care Med., 2004. **30**: p. 1491-1494.
152. Franklin, H.E. and Patricio, S., *Na-K-Cl cotransport in chloride-transporting epithelia*. Ann. N. Y. Acad. Sci., 1985. **456**: p. 187-197.
153. Crews, A., Taylor, A.E., and Ballard, S.T., *Liquid transport properties of porcine tracheal epithelium*. J. Appl. Physiol., 2001. **91**(2): p. 797-802.
154. Farinas, J., Kneen, M., Moore, M., and Verkman, A.S., *Plasma membrane water permeability of cultured cells and epithelia measured by light microscopy with spatial filtering*. J. Gen. Physiol., 1997. **110**: p. 283-296.
155. Matsui, H., Davis, C.W., Tarran, R., and Boucher, R.C., *Osmotic water permeabilities of cultured, well-differentiated normal and cystic fibrosis epithelia*. J. Clin. Invest., 2000. **105**(10): p. 1419-1427.
156. Tarran, R., Grubb, B.R., Gatzky, J.T., and Davis, C.W., *The Relative Roles of Passive Surface Forces and Active Ion Transport in the Modulation of Airway Surface Liquid Volume and Composition*. J. Gen. Physiol., 2001. **118**(2): p. 223-236.
157. Nilsson, H.E., Dragomir, A., Lazorova, L., Johannesson, M., and Roomans, G.M., *CFTR and tight junctions in cultured bronchial epithelial cells*. Exp. Mol. Pathol., 2010. **88**(1): p. 118-127.

158. Knowles, R.M., Robinson, J.M., Wood, R.E., Pue, C.A., Mentz, W.M., and Wager, G.C., *Ion composition of airway surface liquid of patients with cystic fibrosis as compared with normal and disease-control subjects*. J. Clin. Invest., 1997. **100**(10): p. 2588-2595.
159. Boucher, R.C., *Molecular insights into the physiology of the 'thin film' of airway surface liquid*. J. Physiol., 1999. **516**(3): p. 631-638.
160. Kilburn, K.H., *A hypothesis for pulmonary clearance and its implications*. Am. Rev. Respir. Dis., 1968. **98**(3): p. 449-&.
161. Houtmeyers, E., Gosselink, R., Gayan-Ramirez, G., and Decramer, M., *Regulation of mucociliary clearance in health and disease*. Eur. Respir. J., 1999. **13**(5): p. 1177-1188.
162. Jiang, C., Finkbeiner, W.E., Widdicombe, J.H., McCray, P.B., and Miller, S.S., *Altered fluid transport across airway epithelium in cystic fibrosis*. Science, 1993. **262**(5132): p. 424-427.
163. Ballard, S.T., Trout, L., Bebök, Z., Sorscher, E.J., and Crews, A., *CFTR involvement in chloride, bicarbonate, and liquid secretion by airway submucosal glands*. Am. J. Physiol. Lung Cell. Mol. Physiol., 1999. **277**(4): p. L694-L699.
164. Tarran, R., Button, B., and Boucher, R.C., *Regulation of Normal and Cystic Fibrosis Airway Surface Liquid Volume by Phasic Shear Stress*. Annu. Rev. Physiol., 2006. **68**: p. 543-561.
165. Adams, D., *Penetration of water through human and rabbit oral mucosa in vitro*. Arch. Oral Biol., 1974. **19**(10): p. 865-IN11.
166. Hanna, L.M. and Scherer, P.W., *Regional control of local airway heat and water vapor losses*. J. Appl. Physiol., 1986. **61**(2): p. 624-632.
167. Ballard, S.T., Fountain, J.D., Inglis, S.K., Corboz, M.R., and Taylor, A.E., *Chloride secretion across distal airway epithelium: relationship to submucosal gland distribution*. Am. J. Physiol. Lung Cell. Mol. Physiol., 1995. **268**(3): p. L526-L531.
168. Cho, H.-J., Joo, N.S., and Wine, J.J., *Defective Fluid Secretion from Submucosal Glands of Nasal Turbinates from CFTR<sup>-/-</sup> and CFTR[delta]F508/[delta]F508 Pigs*. PLoS ONE, 2011. **6**(8).
169. Cerny, F.J. and Ucer, C., *Arm work interferes with normal ventilation*. Appl. Ergon., 2004. **35**(5): p. 411-415.
170. McMurray, R. and Ondrak, K., *Effects of being overweight on ventilatory dynamics of youth at rest and during exercise*. Eur. J. Appl. Physiol., 2011. **111**(2): p. 285-292.
171. Chlif, M., Keochkerian, D., Choquet, D., Vaidie, A., and Ahmaidi, S., *Effects of obesity on breathing pattern, ventilatory neural drive and mechanics*. Respir. Physiol. Neurobiol., 2009. **168**(3): p. 198-202.
172. Abbott, D.J., Baroody, F.M., Naureckas, E., and Naclerio, R.M., *Elevation of Nasal Mucosal Temperature Increases the Ability of the Nose to Warm and Humidify Air*. Am. J. Rhinol., 2001. **15**(1): p. 41.
173. Assanasen, P., Baroody, F.M., Naureckas, E., and Naclerio, R.M., *Warming of feet elevates nasal mucosal surface temperature and reduces the early response to nasal challenge with allergen*. J. Allergy Clin. Immunol., 1999. **104**(2): p. 285-293.
174. Assanasen, P., Baroody, F.M., Naureckas, E., Solway, J., and Naclerio, R.M., *The Nasal Passage of Subjects with Asthma Has a Decreased Ability to Warm and Humidify Inspired Air*. Am. J. Respir. Crit. Care Med., 2001. **164**(9): p. 1640-1646.

175. Doebelin, E.O., *Measurement Systems - Application and Design*. 4th ed, ed. J. Corrigan and M. Luhrs 1990, New York: McGraw-Hill. 960.
176. Bryan, G.T., *Control Systems* 1984, Toronto: Hodder and Stoughton. 320.
177. Cain, J.B., Livingstone, S.D., Nolan, R.W., and Keefe, A.A., *Respiratory heat loss during work at various ambient temperatures*. *Respir. Physiol.*, 1990. **79**(2): p. 145-150.
178. Rozsasi, A., Leiacker, R., and Keck, T., *Nasal conditioning in perennial allergic rhinitis after nasal allergen challenge*. *Clin. Exp. Allergy*, 2004. **34**(7): p. 1099-1104.
179. Zhao, K., Blacker, K., Luo, Y., Bryant, B., and Jiang, J., *Perceiving Nasal Patency through Mucosal Cooling Rather than Air Temperature or Nasal Resistance*. *PLoS ONE*, 2011. **6**(10): p. e24618.
180. Keck, T., Leiacker, R., Heinrich, A., Kuhnemann, S., and Rettinger, G., *Humidity and temperature profile in the nasal cavity*. *Rhinology*, 2000. **38**(4): p. 167-171.
181. Lindemann, J., Leiacker, R., Stehmer, V., Rettinger, G., and Keck, T., *Intranasal temperature and humidity profile in patients with nasal septal perforation before and after surgical closure*. *Clinical Otolaryngology & Allied Sciences*, 2001. **26**(5): p. 433-437.
182. Tsu, M.E., Babb, A.L., Ralph, D.D., and Hlastala, M.P., *Dynamics of Heat, Water and Soluble Gas Exchange in the Human Airways: I. A Model Study*. *Ann. Biomed. Eng.*, 1988. **16**(6): p. 547-571.
183. Tsu, M.E., Babb, A.L., and Hlastala, M.P. *Breathing pattern affects the airway exchange of heat, water, and soluble gases*. in *Engineering in Medicine and Biology Society, 1989. Images of the Twenty-First Century., Proceedings of the Annual International Conference of the IEEE Engineering in*. 1989.
184. Tsu, M.E., Babb, A.L., Sugiyama, E.M., and Hlastala, M.P., *Dynamics of soluble gas exchange in the airways: II. Effects of breathing conditions*. *Respir. Physiol.*, 1991. **83**(3): p. 261-276.
185. Naftali, S., Schroter, R.C., Shiner, R.J., and Elad, D., *Transport phenomena in the human nasal cavity: a computational model*. *Ann. Biomed. Eng.*, 1998. **26**: p. 831-839.
186. Lindemann, J., Keck, T., Wiesmiller, K., Sander, B., Brambs, H.J., Rettinger, G., and Pless, D., *A Numerical Simulation of Intranasal Air Temperature During Inspiration*. *Laryngoscope*, 2004. **114**(6): p. 1037-1041.
187. Pless, D., Keck, T., Wiesmiller, K., Rettinger, G., Aschoff, A.J., Fleiter, T.R., and Lindemann, J., *Numerical simulation of air temperature and airflow patterns in the human nose during expiration*. *Clin. Otolaryngol.*, 2004. **29**(6): p. 642-647.
188. Lindemann, J., Keck, T., Wiesmiller, K., Sander, B., Brambs, H.J., Rettinger, G., and Pless, D., *Nasal air temperature and airflow during respiration in numerical simulation based on multislice computed tomography scan*. *Am. J. Rhinol.*, 2006. **20**(2): p. 219-223.
189. Garcia, G.J.M., Bailie, N., Martins, D.A., and Kimbell, J.S., *Atrophic rhinitis: a CFD study of air conditioning in the nasal cavity*. *J. Appl. Physiol.*, 2007. **103**(3): p. 1082-10925.
190. Daviskas, E., Gonda, I., and Anderson, S.D., *Mathematical modeling of heat and water transport in human respiratory tract*. *J. Appl. Physiol.*, 1990. **69**(1): p. 362-372.
191. Daviskas, E., Gonda, I., and Anderson, S.D., *Local airway heat and water vapour losses*. *Respir. Physiol.*, 1991. **84**(1): p. 115-132.

192. Tawhai, M.H. and Hunter, P.J., *Modeling Water Vapor and Heat Transfer in the normal and the Intubated Airways*. Ann. Biomed. Eng., 2003. **32**(4): p. 609-622.
193. Warren, N.J., Tawhai, M.H., and Crampin, E.J., *A mathematical model of calcium-induced fluid secretion in airway epithelium*. J. Theor. Biol., 2009. **259**(4): p. 837-849.
194. Warren, N., Crampin, E., and Tawhai, M., *The Role of Airway Epithelium in Replenishment of Evaporated Airway Surface Liquid From the Human Conducting Airways*. Ann. Biomed. Eng., 2010. **38**(12): p. 3535-3549.
195. Bogdanffy, M.S. and Sarangapani, R., *Physiologically-based kinetic modeling of vapours toxic to the respiratory tract*. Toxicol. Lett., 2003. **138**(1-2): p. 103-117.
196. Fodil, R., Brugel-Ribere, L., Croce, C., Sbirlea-Apiou, G., Larger, C., Papon, J.-F., Delclaux, C., Coste, A., and Louis, B., *Inspiratory flow in the nose: A model coupling flow and vasoerectile tissue distensibility*. J. Appl. Physiol., 2005. **98**: p. 288-295.
197. Keyhani, K., *Numerical modeling of airflow and mass transfer in the human nasal cavity*, 1995, University of Pennsylvania: United States -- Pennsylvania. p. 238.
198. Poon, C.S., *Respiratory Models and Control*, in *The Biomedical Engineering Handbook, Second Edition. 2 Volume Set* 1999, CRC Press.
199. Welch, W.R. and Tracy, C.R., *Respiratory water loss: A predictive model*. J. Theor. Biol., 1977. **65**(2): p. 253-265.
200. Wen, J., Inthavong, K., Tu, J., and Wang, S., *Numerical simulations for detailed airflow dynamics in a human nasal cavity*. Respir. Physiol. Neurobiol., 2008. **161**(2): p. 125-135.
201. Holman, J.P., *Heat Transfer*. SI Metric ed. Mechanical Engineering Series, ed. P.N. Rao 1989, Singapore: McGraw-Hill. 676.
202. Incropera, F.P. and DeWitt, D.P., *Fundamentals of Heat and Mass Transfer*. 3rd ed 1990, New York: John Wiley & Sons. 919.
203. Mills, A.F., *Heat Transfer*. International ed 1992, Boston: Irwin. 888.
204. White, F.M., *Fluid Mechanics*. 3rd ed 1979, New York: McGraw-Hill. 736.
205. Golten, J. and Verwer, A., *Modelling of Dynamic Systems*, in *Control System Design and Sumulation* 1991, McGraw-Hill: London. p. 41-45.
206. Marconi, T.F., Richard, L.V., and Kelerson, M.C.P., *Evaluation of nasal volume by acoustic rhinometry before and after physical exercise*. Am. J. Rhinol., 2006. **20**(3): p. 269.
207. Dallimore, N.S. and Eccles, R., *Changes in Human Nasal Resistance Associated With Exercise, Hyperventilation and Rebreathing*. Acta Otolaryngol. (Stockh.), 1977. **84**(1-6): p. 416-421.
208. Hellgren, J., Yee, B.J., Dungan, G., and Grunstein, R.R., *Altered Positional Regulation of Nasal Patency in Patients with Obstructive Sleep Apnea Syndrome*. Eur. Arch. Otorhinolaryngol., 2009. **266**: p. 83-87.
209. Ko, J.-H., Kuo, T.B.J., and Lee, G.-S., *Effect of postural change on nasal airway and autonomic nervous system established by rhinomanometry and heart rate variability analysis*. Am. J. Rhinol., 2008. **22**(2): p. 159.
210. Azzaroni, A. and Parmeggiani, P.L., *Synchronized sleep duration is related to tonic vasoconstriction of thermoregulatory exchangers*. J. Sleep Res., 1995. **4**(1): p. 41-47.
211. Datta, A.K., *Biological and Bioenvironmental Heat and Mass Transfer*. 1st ed 2002, New York: CRC Press. 383.

212. White, D.E., *Breathing therapy air delivery unit: simulation, design and development*, in *School of Engineering*2003, Auckland University of Technology: Auckland. p. 144.
213. Douglas, J.F., Gasiorek, J.M., and Swaffield, J.A., *Fluid Mechanics*. 3rd ed 1995, Singapore: Longman 819.
214. Guan-xia, X., Jie-Min, Z., Hong-Yan, J., Jian-Feng, L., Liang-Wan, R., and Gen, X., *Computational fluid dynamics simulation of airflow in the normal nasal cavity and paranasal sinuses*. Am. J. Rhinol., 2008. **22**(5): p. 477.
215. Hörschler, I., Schröder, W., and Meinke, M., *On the assumption of steadiness of nasal cavity flow*. J. Biomech., 2010. **43**(6): p. 1081-1085.
216. Incoropera, F.P. and DeWitt, D.P., *Fundamentals of Heat and Mass Transfer*. 3rd ed 1990, New York: John Wiley & Sons. 918.
217. Prusaczyk, W.K., *Precise water vapor pressure value calculations*. Comput. Biol. Med., 1989. **19**(2): p. 129-130.
218. Wong, E.C., Cronin, M., Wu, W.-C., Inglis, B., Frank, L.R., and Liu, T.T., *Velocity-selective arterial spin labeling*. Magn. Reson. Med., 2006. **55**(6): p. 1334-1341.
219. Hanif, J., Ron, E., and Suhair, S.M.J., *Use of a Portable Spirometer for Studies on the Nasal Cycle*. Am. J. Rhinol., 2001. **15**(5): p. 303-6.
220. Eccles, R., *The Central Rhythm of the Nasal Cycle*. Acta Otolaryngol. (Stockh.), 1978. **86**(5-6): p. 464-468.
221. Subramaniam, R.P., Richardson, R.B., Morgan, K.T., Kimbell, J.S., and Guilmette, R.A., *Computational Fluid Dynamics Simulations of Inspiratory Airflow in the Human Nose and Nasopharynx*. Inhal. Toxicol., 1998. **10**(2): p. 91-120.
222. Hahn, I., Scherer, P.W., and Mozell, M.M., *Velocity profiles measured for airflow through a large-scale model of the human nasal cavity*. J. Appl. Physiol., 1993. **75**(5): p. 2273-2287.
223. Kurita, N., Hasegawa, M., Ohki, M., and Watanabe, I., *Nasal resistance and nasal blood flow in postural changes*. Acta Otolaryngol. (Stockh.), 1988. **106**(5): p. 448 - 452.
224. Cauna, N., *Blood and nerve supply of the nasal lining*, in *The nose: upper airway physiology and the atmospheric environment*, D.F. Proctor and I. Andersen, Editors. 1982, Elsevier Biomedical Press: Amsterdam. p. 45-66.
225. Kolbitsch, C., Lorenz, I., H, Hörmann, C., Schocke, M., Kremser, C., Zschiegner, F., Felber, S., and Benzer, A., *The impact of increased mean airway pressure on contrast-enhanced MRI measurement of regional cerebral blood flow (rCBF), regional cerebral blood volume (rCBV), regional mean transit time (rMTT), and regional cerebrovascular resistance (rCVR) in human volunteers*. Hum. Brain Mapp., 2000. **11**(3): p. 214-222.
226. Keller, E., Nadler, A., Alkadhi, H., Kollias, S.S., Yonekawa, Y., and Niederer, P., *Noninvasive measurement of regional cerebral blood flow and regional cerebral blood volume by near-infrared spectroscopy and indocyanine green dye dilution*. Neuroimage, 2003. **20**(2): p. 828-839.
227. Lorenz, I.H., Kolbitsch, C., Hörmann, C., Schocke, M., Kremser, C., Zschiegner, F., Felber, S., and Benzer, A., *Increasing mean airway pressure reduces functional MRI (fMRI) signal in the primary visual cortex*. Magn. Reson. Imaging, 2001. **19**(1): p. 7-11.
228. Jiang, C., Finkbeiner, W.E., Widdicombe, J.H., and Miller, S.S., *Fluid transport across cultures of human tracheal glands is altered in cystic fibrosis*. J. Physiol., 1997. **501**(3): p. 637-647.

229. Committee, N.A.W.A., *Commercial Slaughter*, in *Animal Welfare (Commercial Slaughter) Code of Welfare 2010*, M.o.A.a. Forestry, Editor 2010, Ministry of Agriculture and Forestry: Wellington.
230. Schwiebert, E.M., *Extracellular autocrine nucleotide signalling in a microenvironment: integrative physiology in a minute volume of airway surface liquid*. The Journal of Physiology, 2007. **580**(2): p. 359-360.
231. Sorbent-Systems. *Desiccant Chart Comparisons*. 2012; Available from: [http://www.sorbentsystems.com/desiccants\\_charts.html](http://www.sorbentsystems.com/desiccants_charts.html).
232. Verdugo, P., *Hydration kinetics of exocytosed mucins in cultured secretory cells of the rabbit trachea: a new model*. Ciba Found. Symp., 1984. **109**: p. 212-225.
233. Matsui, H., Randell, S.H., Peretti, S.W., Davis, C.W., and Boucher, R.C., *Coordinated Clearance of Periciliary Liquid and Mucus from Airway Surfaces*. J. Clin. Invest, 1998. **102**(6): p. 1125-1131.
234. Jella, S.A. and Shannahoff-khalsa, D.S., *The effects of unilateral forced nostril breathing on cognitive performance*. Int. J. Neurosci., 1993. **73**(1-2): p. 61-68.
235. Shannahoff-khalsa, D.S., Boyle, M.R., and Buebel, M.E., *The Effects of Unilateral Forced Nostril Breathing on Cognition*. Int. J. Neurosci., 1991. **57**(3-4): p. 239-249.
236. Reinikainen, L.M. and Jaakkola, J.J.K., *Significance of humidity and temperature on skin and upper airway symptoms*. Indoor Air, 2003. **13**(4): p. 344-352.
237. Willatt, D.J. and Jones, A.S., *The role of the temperature of the nasal lining in the sensation of nasal patency*. Clinical Otolaryngology & Allied Sciences, 1996. **21**(6): p. 519-523.
238. Ishiura, D., Karashima, A., Katayama, N., and Nakao, M., *Integrated model incorporating circadian phase dynamics and the thermoregulatory mechanism of sleep*. Sleep & Biological Rhythms, 2007. **5**(4): p. 259-270.

## GLOSSARY

### Abbreviations

AH	Air absolute humidity
APAP	Auto-titrating positive air pressure
AR	Acoustic Rhinometry
ASL	Airway surface liquid
ATP	Adenosine triphosphate
AVA	Arteriovenous anastomoses
Bi-PAP	Bi-level positive air pressure
CBF	Cilia beat frequency
CFD	Computational Fluid Dynamics
CO <sub>2</sub>	Carbon dioxide
CT	Computer tomography
EEG	Electroencephalography
ISB	Isothermal saturation boundary
MD	Mucosal decongestion
MRI	Magnetic resonance imaging
MTV	Mucociliary transport velocity
n-PAP	Nasal positive air pressure
OSA	Obstructive sleep apnea
O <sub>2</sub>	Oxygen
PAP	Positive air pressure
PCL	Periciliary liquid
PR	Partition ratio

## Nomenclature

$A$	Cross sectional area	$\text{cm}^2$
$C$	Water species concentration	$\text{mol}/\text{cm}^3$
$C_p$	Specific heat capacity at constant pressure	$\text{J}/\text{g} \cdot ^\circ\text{C}$
$D$	Diameter	$\text{m}$
$D_{ab}$	Binary diffusion coefficient	$\text{m}^2/\text{s}$
$f$	Friction factor	
$g$	Gravity	$\text{m}/\text{s}^2$
$He$	Water equivalent height	$\mu\text{m}$
$h_c$	Convective heat transfer coefficient	$\text{W}/\text{cm}^2 \cdot ^\circ\text{C}$
$h_f$	Friction head loss	$\text{m}$
$h_{fg}$	Enthalpy fluid-gas mixture	$\text{J}/\text{g}$
$h_m$	Convective mass transfer coefficient	$\text{m}/\text{s}$
$K$	Osmotic bulk modulus	$\text{Pa}$
$k_t$	Thermal conductivity coefficient	$(\text{w}/\text{m} \cdot ^\circ\text{C})$
$L, \ell$	Length	$\text{cm}$
$Le$	Lewis Number	
$M$	Molar mass	$\text{mol}/\text{g}$
$m$	Mass flux	$\text{g}/\text{cm}^2 \cdot \text{hr}$
$N$	Molar mass flux	$(\text{mol}/\text{cm}^2 \cdot \text{s})$
$Nu$	Nusselt number	
$P$	Wetted perimeter	$\text{cm}$
$P$	Pressure	$\text{Pa}$
$Pr$	Prandtl number	
$Q$	Heat flux	$\text{W}/\text{cm}^2$
$q$	Specific heat flux	$\text{W}/\text{cm}^2 \cdot \text{g}$
$R$	Resistance	$\text{Pa} \cdot \text{s}/\text{g}$

$Re$	Reynolds number	
$Sc$	Schmidt number	
$Sh$	Sherwood number	
$T$	Temperature	°C
$t$	Time	s
$V$	Velocity	cm/s
$X$	Distance along airway	cm
$\Delta y_t$	Mucosal thickness	μm
$\alpha$	Air thermal diffusivity	m <sup>2</sup> /s
$\rho$	Density	g/cm <sup>3</sup>
$\kappa$	Thermal conductivity	W/m·K
$\mu$	Dynamic viscosity	N.s/m <sup>2</sup>
$\nu$	Kinematic viscosity	m <sup>2</sup> /s
$\omega$	Humidity Ratio	g H <sub>2</sub> O/g dry air

### Subscripts

$ASL$	Airway surface liquid
$a$	Air
$b$	Blood
$c$	Convection
$d$	Diameter
$e$	Equivalent
$h$	hydraulic
$i$	Initial
$l$	Latent heat
$m$	Mucosa, mass transfer

$p$	Per unit pressure
$p_{CL}$	Periciliary Liquid
$s$	Sensible heat
$s$	Water vapour saturation
$st$	Steam saturation
$t$	Total, thermal

## APPENDIX A: AIR-CONDITIONING MODEL CODE

The general configuration detailing the implementation of the computational nasal model within the MatLab is now given. Here an overview of the structure main programme is given before each of the supporting eleven function files are presented. Files corresponding to the implementation of the model with MatLab are referenced in the appropriate sections. Where necessary, fluid or tissue properties that vary with pressure and temperature are interpolated from look-up tables created from published data.

### A1 Main Nose

From a functional perspective, *Main Nose* can be considered to consist of two separate portions, shown schematically in Figure B1. Here, the first set up portion serves to read an individual's MRI nasal morphology data, configure pressure related variables related to geometry and ASL water supply and air mass-flow apportionment between airways.

The second cyclic portion of the programme repetitively calculates the magnitude of parameters along the length of each nasal airway for each time interval corresponding to a change in air mass-flow rate to simulate patient breathing.

Selection of individual MRI morphological data and initial conditions of air pressure, temperature and relative humidity along with ASL water equivalent height are entered. Model simulation for number of breath cycles and size of time step for Euler solving technique are also entered. Individual nasal geometry is then acquired directly from 3D-Doctor data files to exclude bias from manual analysis. The remaining initial conditions are then calculated before the geometry is modified in accordance with the inter-nasal geometry pressure response. Mucosal water supply is also determined as function of mask pressure before nasal airflow partitioning is calculated. Subsequently a While loop is entered that steps through the calculation of model variables along the length of the airway. Order of calculation is determined as a function of breath phase. The While loop terminates upon completion when the calculations of variables spanning the simulation time interval are complete. This is defined by the desired number of breaths.

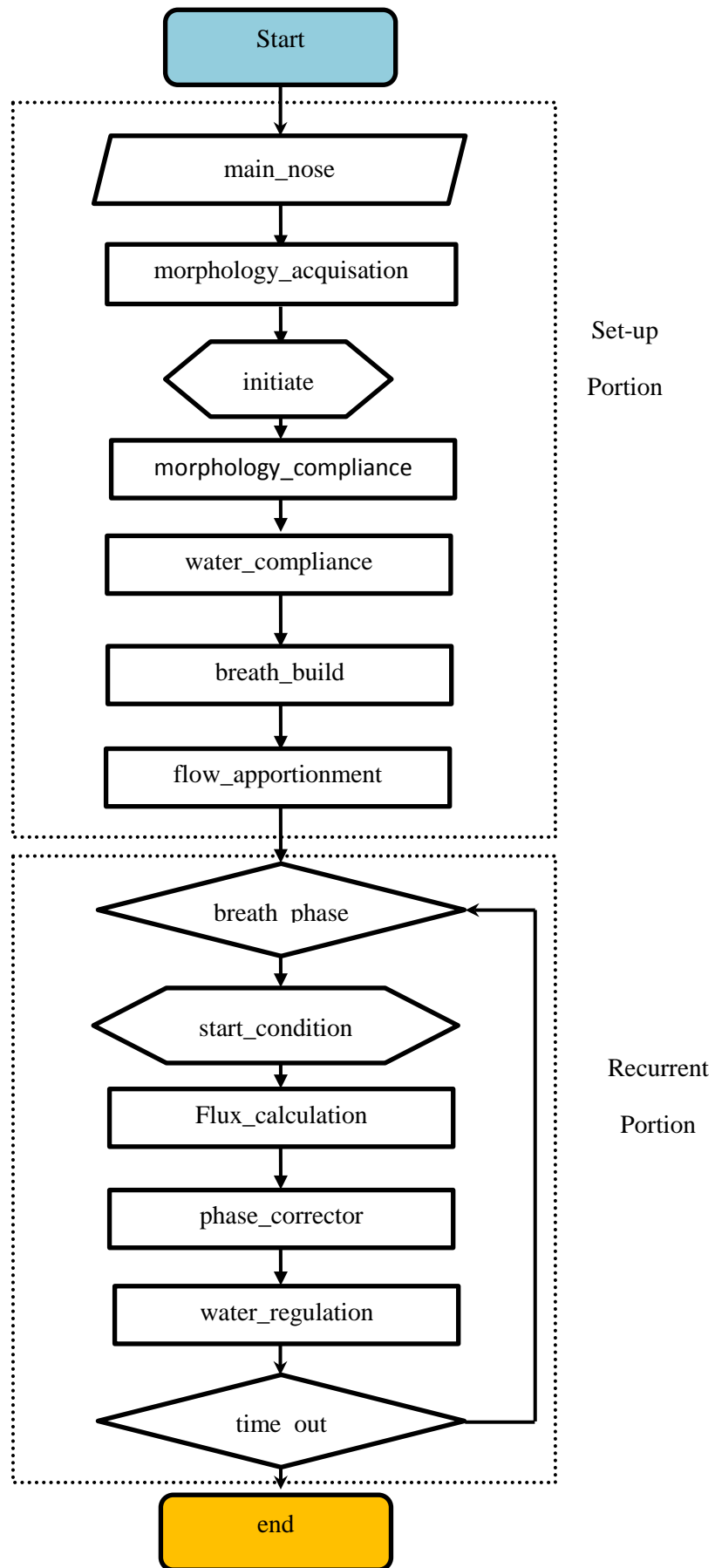


**Figure A1: Schematic functional representation of the main nose programme.**

```

%% Created by D White 9th January 2012

%MAIN NOSE PROGRAM
%This programme is the central logic processor that connects with
functions to undertake specific tasks.
clear

% IMAGE DATA
participant_num=118; % pre-select of one participant.
slice_thickness=0.78; % pre-select based on MRI slices.

%PATIENT BREATHING
bpm=9; % temporary pre-select in breaths per minute.
tv=1; % temporary pre-select in litres.

%MASK CONDITIONS
mask_pressure=9; % mask pressure augmentation (cmWG).
mask_temp=23; % temporary pre-select based on mask temp (degree C).
mask_rh=45; % temporary pre-select based on mask RH.

%NP CONDITIONS
np_temp=36; % temporary pre-select based on 36 degree C lung temp.
np_rh=95; % temporary pre-select based on 95% lung RH.

%ASL DEPTH
asl_height_nominal=0.010; % Equivalent normal physiological asl height
in mm (micrometres).

%BREATH CYCLE
number_breath=2; % total time period being assessed - each breath
takes 6 seconds.

%SIMULATION
time_step=0.1; % time increment for calculation time step in seconds.

%% Call up morphology_acquisition function to acquire and compile left
& right airway morphology matrices
[morphology_right,morphology_left,patent_airway]=morphology_acquisatio
n(participant_num);

%% Call up initiate to undertake initial calculation of input
parameters
[water_molar_mass,asl_height_left,asl_height_right,density_water,asl_w
ater_mass_mean_left,asl_water_mass_mean_right,time,asl_water_mass_left
,asl_water_mass_right,asl_water_mass_max_left,asl_water_mass_max_right
,asl_water_mass_min_left,asl_water_mass_min_right,time_out,mask_ah,np_
ah,store_count,Ca_left,Ca_right,Cm_left,Cm_right,Ta_left,Ta_right,Tm_l
eft,Tm_right,N_left,N_right,Q_left,Q_right,air_ah_left,air_ah_right]=i
nitiate(asl_height_nominal,morphology_left,morphology_right,number_bre
ath,slice_thickness,mask_temp,mask_rh,mask_pressure,np_temp,np_rh,time
_step);

%% Call up morphology_compliance to calculate delta CSA & perimeter
parameters
[morphology_right,morphology_left,delta_csa,delta_perimeter]=morpholog
y_compliance(morphology_right,morphology_left,mask_pressure,patent_air
way);

%% Call up water_compliance to calculate maximum cellular water supply
and ASL mass distribution.

```

```

[asl_water_mass_backflux_left,asl_water_mass_backflux_right,cellular_w
ater_mass_efflux_max_left,cellular_water_mass_efflux_max_right]=water_
compliance(morphology_left,morphology_right,slice_thickness,mask_press
ure,time_step);
%% Call up breath_build function to create tidal breathing over
duration of simulation
[breath]=breath_build(time_out);

%% Call up flow_apportionment to calculate airflow partitioning between
patent and congested airway
[partition_ratio_left,partition_ratio_right]=flow_apportionment(slice_
thickness,morphology_left,morphology_right);

% assign air mass flow matrices that will be filled with each cycle
air_mass_flow_rate_right=zeros(1,time_out/time_step+1);
air_mass_flow_rate_left=zeros(1,time_out/time_step+1);

% pre-allocating matrix size for speed
asl_water_mass_flux_left=zeros(length(morphology_left(:,1)),1);
asl_water_mass_flux_right=zeros(length(morphology_right(:,1)),1);
cellular_water_mass_efflux_left=zeros(length(morphology_left(:,1)),1);
cellular_water_mass_efflux_right=zeros(length(morphology_right(:,1)),1
);

%% cycle through parameter calculations for each time step for
duration of breathing time interval
while time<=time_out;

%% Call up breath_phase to determine if order of morphology
processing, i.e. nare to np or vise versa.
[phase]=breath_phase(breath,time);

%% Call up start_condition to determine initial Ca, Ta, Cm, Tm & N
parameters
[mucosa_thickness,Kt,position_count,asl_water_mass_flux_left,asl_water
_mass_flux_right,asl_water_mass_left,asl_water_mass_right,asl_water_ma
ss_max_left,
asl_water_mass_max_right,reynolds_number_left,reynolds_number_right,hm
_left,hm_right,hc_left,hc_right,nusselt_number_left,nusselt_number_rig
ht,hydraulic_diameter_left,hydraulic_diameter_right,Ca_right,Ca_left,T
a_right,Ta_left,Cm_left,Cm_right,Tm_left,Tm_right,N_left,N_right,morph
ology_left,morphology_right,Q_left,Q_right,air_velocity_right,air_velo
city_left,air_ah_right,air_ah_left,air_mass_flow_rate_right,air_mass_f
low_rate_left]=start_condition(breath,partition_ratio_right,partition_
ratio_left,phase,mask_temp,mask_ah,np_temp,np_ah,morphology_left,morph
ology_right,Ca_left,Ca_right,Cm_left,Cm_right,Ta_left,Ta_right,Tm_left
,Tm_right,N_left,N_right,Q_left,Q_right,air_ah_left,air_ah_right,store
_count,time,slice_thickness,asl_water_mass_left,asl_water_mass_right,a
sl_water_mass_max_left,asl_water_mass_max_right,asl_water_mass_flux_le
ft,asl_water_mass_flux_right,time_step,asl_water_mass_backflux_left,as
l_water_mass_backflux_right,cellular_water_mass_efflux_left,cellular_w
ater_mass_efflux_right,mask_pressure);

%% Call up flux_calculation to determine remaining Ca, Ta, Cm, Tm & N
parameters
[Ca_right,Ca_left,Ta_right,Ta_left,Cm_left,Cm_right,Tm_left,Tm_right,N
_left,N_right,Q_left,Q_right,air_velocity_right,air_velocity_left,air_
ah_right,air_ah_left,reynolds_number_left,reynolds_number_right]=flux_
calculation(hm_left,hm_right,hc_left,hc_right,nusselt_number_left,nuss
elt_number_right,reynolds_number_left,reynolds_number_right,hydraulic_
diameter_left,hydraulic_diameter_right,morphology_left,morphology_righ
t,store_count,slice_thickness,Ca_right,Ca_left,Ta_right,Ta_left,Cm_lef

```

```

t,Cm_right,Tm_left,Tm_right,N_left,N_right,Q_left,Q_right,air_velocity_
_right,air_velocity_left,air_mass_flow_rate_right,air_mass_flow_rate_l
eft,air_ah_right,air_ah_left,phase,asl_water_mass_left,asl_water_mass_
right,time_step,asl_water_mass_backflux_left,asl_water_mass_backflux_r
ight,cellular_water_mass_efflux_left,cellular_water_mass_efflux_right,
Kt,mucosa_thickness,water_molar_mass,mask_pressure);

%% call up phase_corrector to correct order of both morphology
matricies
[asl_water_mass_flux_left,asl_water_mass_flux_right,morphology_left,mo
rphology_right,phase,Ca_left,Ca_right,Cm_left,Cm_right,Ta_left,Ta_righ
t,Tm_left,Tm_right,N_left,N_right,Q_left,Q_right,air_ah_left,air_ah_r
ight,asl_water_mass_left,asl_water_mass_right,asl_water_mass_max_left,a
sl_water_mass_max_right,asl_water_mass_min_left,asl_water_mass_min_rig
ht,cellular_water_mass_efflux_max_left,cellular_water_mass_efflux_max_
right]=phase_corrector(morphology_left,morphology_right,phase,Ca_left,
Ca_right,Cm_left,Cm_right,Ta_left,Ta_right,Tm_left,Tm_right,N_left,N_r
ight,Q_left,Q_right,air_ah_left,air_ah_right,asl_water_mass_left,asl_w
ater_mass_right,asl_water_mass_max_left,asl_water_mass_max_right,asl_w
ater_mass_min_left,asl_water_mass_min_right,cellular_water_mass_efflux
_max_left,cellular_water_mass_efflux_max_right,asl_water_mass_flux_lef
t,asl_water_mass_flux_right);

%% Call up water_regulation to calculate water flux and storage levels
[asl_height_left,asl_height_right,cellular_water_mass_efflux_left,cell
ular_water_mass_efflux_right,asl_water_mass_flux_left,asl_water_mass_f
lux_right,asl_water_mass_left,asl_water_mass_right]=water_regulation(c
ellular_water_mass_efflux_left,cellular_water_mass_efflux_right,slice_
thickness,morphology_left,morphology_right,N_left,N_right,asl_water_ma
ss_left,asl_water_mass_right,cellular_water_mass_efflux_max_left,cellu
lar_water_mass_efflux_max_right,store_count,time_step,asl_water_mass_f
lux_left,asl_water_mass_flux_right,asl_water_mass_mean_left,asl_water_
mass_mean_right,density_water,asl_height_left,asl_height_right,asl_wat
er_mass_backflux_left,asl_water_mass_backflux_right);

%% call up counter to repeat calculations for next increment in breath
or end program
[time,store_count]=counter(time,store_count,time_step);
end

```

## A2 Morphology Acquisition

*Morphology\_Acquisition* extracts the individual's nasal morphological nasal data of cross sectional area, perimeter and location directly from 3-D Doctor data files and compiles them over the region of interest.

```

%% M File created by D White 9th January 2012
function
[morphology_right,morphology_left,patent_airway]=morphology_acquisatio
n(participant_num)
%patient_data acquires and compiles MRI CSA and perimeter data into
two matricies - patent and congested.
%Input arguments:
%patient_num=patient MRI trial number.
%Output Arguments:

```

```

%morphology_right=right airway morphology matrix spanning X/L=0 to
X/L=1.
%morphology_left=left airway morphology matrix spanning X/L=0 to
X/L=1.

%% Temporary resource of input information - REMOVE LATER

%participant_num=104; % temporary pre-select of one participant

%% Allocating file parameters to be read.
%Create array of data to be read as well as first and last image
planes of interest.
if participant_num==104;
    filename=('104 Ambient Nasal CSA Data.txt');
    roi_start=189;
    roi_finish=274;
    patent_airway=0; % 0=right airway, 1=left airway.
elseif participant_num==118;
    filename=('118 Ambient Nasal CSA Data.txt');
    roi_start=153;
    roi_finish=238;
    patent_airway=0; % 0=right airway, 1=left airway.
elseif participant_num==101;
    filename=('101 Ambient Nasal CSA Data.txt');
    roi_start=147;
    roi_finish=225;
    patent_airway=1; % 0=right airway, 1=left airway.
elseif participant_num==106;
    filename=('106 Ambient Nasal CSA Data.txt');
    roi_start=147;
    roi_finish=228;
    patent_airway=0; % 0=right airway, 1=left airway.
elseif participant_num==107;
    filename=('107 Ambient Nasal CSA Data.txt');
    roi_start=164;
    roi_finish=246;
    patent_airway=1; % 0=right airway, 1=left airway.
elseif participant_num==109;
    filename=('109 Ambient Nasal CSA Data.txt');
    roi_start=157;
    roi_finish=229;
    patent_airway=0; % 0=right airway, 1=left airway.
elseif participant_num==108;
    filename=('108 Ambient Nasal CSA Data.txt');
    roi_start=149;
    roi_finish=236;
    patent_airway=1; % 0=right airway, 1=left airway.
elseif participant_num==115;
    filename=('115 Ambient Nasal CSA Data.txt');
    roi_start=145;
    roi_finish=221;
    patent_airway=1; % 0=right airway, 1=left airway.
end

%% Open text file and sort out rows labelled 'patent'

fid = fopen(filename,'r');
y = 0;
z=1;% counter for indexing loading of data_array

```

```

patent_data=zeros(1,500);
while feof(fid) == 0

    tline = fgetl(fid);
    matches = strfind(tline, 'Patent');

    num = length(matches);
    if num > 0
        y = y + num;

        x{y}=sscan(tline); % convert tline string data into numbers
        %% inset image plane area and perimeter data into matrix.
        x{1,1}{1,3}=0; %get rid of string variable
        patent_data(z,1)=x{1,y}{1,3}; %Obtaining slice number value of 3rd
        column in row 1 from top level cell
        patent_data(z,2)=x{1,y}{1,8}; %Obtaining Area value of 8th column in
        row 1 from top level cell
        patent_data(z,3)=x{1,y}{1,12}; %Obtaining perimeter value from 12th
        column in row 1 from top level cell
        z=z+1;

    end
end

fclose(fid);

%% Select slices within range of desired slices.

[c]=find(patent_data(:,1)>=roi_start & patent_data(:,1)<=roi_finish);%
finding column numbers that fall within desired region of interest.

%% reversing slice order
A=[]; % clearing matrix B for each iterative step

%% filling matrix

A(:,1)=patent_data(c(:,1),1); % Transferring desired slice position data
into area_array
A(:,2)=patent_data(c(:,2),2); % Transferring desired area data into
area_array
A(:,3)=patent_data(c(:,3),3); % Transferring desired perimeter data into
area_array

%% Reverse ordering matrix given largest number represents anterior
slice
patent=sortrows(A,-1);

%% changing column 1 of patent matrix to read X/L
patent(:,1)=(A(end,1)-A(1:end,1)+A(1,1)-A(end,1))/(A(1,1)-A(end,1));

    %% Open text file and sort out rows labelled 'congested'
    %fid = fopen(Z,'r');

    %data_array=slice_data(filename); % call m-file process_data which
    pulls out numbers & strings from txt file

    fid = fopen(filename,'r');
    y = 0;
    z=1;% counter for indexing loading of data_array

```

```

congested_data=zeros(1,500);
while feof(fid) == 0
    tline = fgetl(fid);
    matches = strfind(tline, 'Congested');

    num = length(matches);
    if num > 0
        y = y + num;

        x{y}=sscan(tline); % convert tline string data into numbers
        %% inset image plane area and perimeter data into matrix.
        x{1,1}{1,3}=0; %get rid of string variable
        congested_data(z,1)=x{1,y}{1,3}; %Obtaining slice number value of 3rd
        column in row 1 from top level cell
        congested_data(z,2)=x{1,y}{1,8}; %Obtaining Area value of 8th column
        in row 1 from top level cell
        congested_data(z,3)=x{1,y}{1,12}; %Obtaining perimeter value from 12th
        column in row 1 from top level cell
        z=z+1;

    end
end

fclose(fid);

%%
B=[]; % clearing matrix B for each iterative step

%% filling matrix

B(:,1)=congested_data(c(:),1); % Transferring desired slice position
data into area_array
B(:,2)=congested_data(c(:),2); % Transferring desired area data into
area_array
B(:,3)=congested_data(c(:),3); % Transferring desired perimeter data
into area_array

%% Reverse ordering matrix given largest number represents anterior
slice
congested=sortrows(B,-1);

%% changing column 1 of congested matrix to read X/L
congested(:,1)=(B(end,1)-B(1:end,1)+B(1,1)-B(end,1))/(B(1,1)-
B(end,1));

%% Compile participant results into left and right matrices

if patent_airway==0;
    morphology_right(:,:)=patent(:,:);
    morphology_left(:,:)=congested(:,:);
elseif patent_airway==1;
    morphology_right(:,:)=congested(:,:);
    morphology_left(:,:)=patent(:,:);
end

```

### A3 Initiate

*Initiate* assigns data matrices and calculates the initial input parameters of nasal mask and nasopharynx air temperature and humidity and number of breath cycles. Initial ASL water equivalent mass for the first model lump is also calculated.

```
% M File created by D White 9th January 2012
function[water_molar_mass,asl_height_left,asl_height_right,density_water,asl_water_mass_mean_left,asl_water_mass_mean_right,time,asl_water_mass_left,asl_water_mass_right,asl_water_mass_max_left,asl_water_mass_max_right,asl_water_mass_min_left,asl_water_mass_min_right,time_out,mask_ah,np_ah,store_count,Ca_left,Ca_right,Cm_left,Cm_right,Ta_left,Ta_right,Tm_left,Tm_right,N_left,N_right,Q_left,Q_right,air_ah_left,air_ah_right]=initiate(asl_height_nominal,morphology_left,morphology_right,number_breath,slice_thickness,mask_temp,mask_rh,mask_pressure,np_temp,np_rh,time_step)
%period,num_cycles,mask_temp,mask_rh,mask_ah,np_temp,np_rh,np_ah,%time_step,time,store_count,
%time_out,,;
%tm_initial,n_initial)
%initiate calculates initial model parameters based on data input.
%input arguments:
%asl_depth_max=selected maximum desirable asl depth in micrometres.
%asl_depth_min=selected minimum desirable asl depth in micrometres.
%period=time period of nasal cycle in minutes.
%num_cycles=number of nasal cycle changes to be included in model run time.
%mask_temp=temperature of air delivered to nasal mask in degrees celcius.
%mask_rh=relative humidity of air delivered to nasal mask.
%np_temp=temperature of air in nasophrynx during exhalation degrees celcius.
%np_rh=relative humidity of air in nasophrynx during exhalation.
%Output arguments:
%% fixed property details

density_water=0.001; %(g/mm^3)
water_molar_mass=18; % molar mass of water g/mol

%% variable property details
% air density
density_air_data_matrix=[7 1.265e-6;17 1.220e-6;27 1.177e-6;37 1.141e-6;47 1.106e-6];
%density_air=1.177e-6; %(g/mm^3) air density function of temp, Cengel, Table A.7, p824.

%% Assigning time_step
time=0; %setting time counter to zero.

%% Assigning store_count
store_count=1; %setting matrix storage index to one.

%% Calculating simulation run-time
time_out=number_breath*6;
```

```

%% pre-allocating matrix size for speed
asl_water_mass_left=zeros(length(morphology_left(:,1)),time_out/time_step+1);
asl_water_mass_right=zeros(length(morphology_right(:,1)),time_out/time_step+1);

asl_water_mass_max_left=zeros(length(morphology_left(:,1)),1);
asl_water_mass_max_right=zeros(length(morphology_right(:,1)),1);

asl_water_mass_min_left=zeros(length(morphology_left(:,1)),1);
asl_water_mass_min_right=zeros(length(morphology_right(:,1)),1);

asl_water_mass_mean_left=zeros(length(morphology_left(:,1)),1);
asl_water_mass_mean_right=zeros(length(morphology_right(:,1)),1);

asl_height_left=zeros(length(morphology_left(:,1)),1);
asl_height_right=zeros(length(morphology_right(:,1)),1);

%% Calculating asl_mass for time=0 based on initial asl_depth_mean

for position_count=1:1:length(morphology_right(:,1));

    %Calculating initial asl_mass_mean based on asl_height_nominal
    asl_water_mass_mean_left(position_count,1)=morphology_left(position_count,3)*asl_height_nominal*slice_thickness*density_water;
    asl_water_mass_mean_right(position_count,1)=morphology_right(position_count,3)*asl_height_nominal*slice_thickness*density_water;
    %asl water mass per lump = perimeter x mean depth x slice thickness (mm) x density (g)

    %Calculating asl_mass for time=0 based on initial asl_depth_mean
    asl_water_mass_left(position_count,1)=asl_water_mass_mean_left(position_count,1);
    asl_water_mass_right(position_count,1)=asl_water_mass_mean_right(position_count,1);
    %asl water mass per lump = perimeter x mean depth x slice thickness (mm) x density (g)

end

%% calculate total pressure for later use in determining humidity ratio
total_pressure=(mask_pressure/100)*9.81*1000+101325; %(Pa)

%% Calculate absolute humidity
%MASK
mask_saturation_vapour_pressure=(10^(-7.90298*(373.16/(mask_temp+273))-1)+5.02808*log10(373.16/(mask_temp+273))-1.3816*1e-7*(10^(11.344*(1-(mask_temp+273)/373.16))-1)+8.1328*1e-3*(10^(-3.49149*(373.16/(mask_temp+273))-1))+log10(1013.246)))*100;
% Goff-Gratch Equation is used to calculate water partial pressure.

%mask water vapour pressure proportioned to mask relative humidity
mask_water_vapour_pressure=mask_rh/100*mask_saturation_vapour_pressure;

% calculate humidity ratio
mask_humidity_ratio=(0.622*mask_water_vapour_pressure)/(total_pressure-mask_water_vapour_pressure);

```

```

mask_density_air=interp1(density_air_data_matrix(:,1),density_air_data_matrix(:,2),mask_temp,'linear');

% calculation of mask air water species concentration in mol/mm^3
Ca_mask=mask_humidity_ratio*mask_density_air/18;

mask_ah=Ca_mask*water_molar_mass*10^9; %(g/m^3)

%NASOPHARYNX
np_saturation_vapour_pressure=(10^(-7.90298*(373.16/(np_temp+273))-1)+5.02808*log10(373.16/(np_temp+273))-1.3816*1e-7*(10^(11.344*(1-(np_temp+273)/373.16))-1)+8.1328*1e-3*(10^(-3.49149*(373.16/(np_temp+273)-1))-1)+log10(1013.246)))*100;
% Goff-Gratch Equation is used to calculate water partial pressure.

%nasopharynx water vapour pressure proportioned to nasopharynx relative humidity
np_water_vapour_pressure=np_rh/100*np_saturation_vapour_pressure;

% calculate humidity ratio
np_humidity_ratio=(0.622*np_water_vapour_pressure)/(total_pressure-np_water_vapour_pressure);

np_density_air=interp1(density_air_data_matrix(:,1),density_air_data_matrix(:,2),np_temp,'linear');

% calculation of nasopharynx air water species concentration in mol/mm^3
Ca_np=np_humidity_ratio*np_density_air/18;

np_ah=Ca_np*water_molar_mass*10^9; %(g/m^3)

%% pre-allocating matrices for use later
Ca_left=zeros(length(morphology_left(:,1)),1);
Ca_right=zeros(length(morphology_right(:,1)),1);
Cm_left=zeros(length(morphology_left(:,1)),1);
Cm_right=zeros(length(morphology_right(:,1)),1);
Ta_left=zeros(length(morphology_left(:,1)),1);
Ta_right=zeros(length(morphology_right(:,1)),1);
Tm_left=zeros(length(morphology_left(:,1)),1);
Tm_right=zeros(length(morphology_right(:,1)),1);
N_left=zeros(length(morphology_left(:,1)),1);
N_right=zeros(length(morphology_right(:,1)),1);
Q_left=zeros(length(morphology_left(:,1)),1);
Q_right=zeros(length(morphology_right(:,1)),1);
air_ah_left=zeros(length(morphology_left(:,1)),1);
air_ah_right=zeros(length(morphology_right(:,1)),1);

```

## A4 Morphology Compliance

*Morphology Compliance* modifies airway geometry of cross sectional area and perimeter along the entire length of both airways in accordance with the response to air-pressure.

%% M File created by D White 10th January 2012

```
function
[morphology_right,morphology_left,delta_csa,delta_perimeter]=morpholog
y_compliance(morphology_right,morphology_left,mask_pressure,patent_air
way)
%modifies airway morphology to account for active compliance response
and calculates
%offset in airway parameters
%Input arguments:
%morphology_right.
%morphology_left.
%mask_pressure.
%Output Arguments:
%morphology_right - right airway morphology modified for active
compliance response.
%morphology_left - left airway morphology modified for active
compliance response.
%delta_csa - difference in modified csa between both airways.
%delta_perimeter - difference in modified perimeter between both
airways.

%% assigning area and perimeter compliance data matrices

% congested [X/L, area compliance, perimeter compliance]
compliance_matrix_congested=[0.05 1.1987 0.3170;0.15 1.6261
0.2113;0.25 1.0848 -0.1943;0.35 1.1309 -0.7740;0.45 1.6317 -0.6979;
0.55 1.6679 -0.8512;0.65 2.2235 0.0067;0.75 2.0535 -0.0644;0.85
2.0796 -0.1659;0.95 2.2631 -0.3623];

% patent [X/L, area compliance, perimeter compliance]
compliance_matrix_patent=[0.05 0.6985 0.1179;0.15 -0.0832 0.2412;0.25
-0.4353 -0.1067;0.35 -0.8611 0.1445;
0.45 -0.8077 0.5497;0.55 -1.1682 0.9711;0.65 -1.1064 0.4560;0.75 -
1.5780 0.2508;0.85 -0.6047 -0.0020;0.95 -0.9467 0.3527];

%% compile compliance matrices in accordance with data sets along
airway

% compile area and perimeter compliance tables for patent and
congested airways
compliance_congested=interp1(compliance_matrix_congested(:,1),complan
ce_matrix_congested(:,2),morphology_left(:,1),'linear','extrap');
% formulate compliance congested matrix taylored to the same length
and X/L positions as current patient

compliance_patent=interp1(compliance_matrix_patent(:,1),compliance_mat
rix_patent(:,2),morphology_right(:,1),'linear','extrap');
% formulate compliance congested matrix taylored to the same length
and X/L positions as current patient

%% calculating new CSA morphology for both airways due to tissue
compliance
if patent_airway==0; % if right airway is patent then left is
congested, modify congested and patent airway CSA in accordance with
respective area compliance.

morphology_left(:,2)=morphology_left(:,2)+(compliance_congested(:,2)*m
ask_pressure);
```

```

    % modify left (congested) morphology CSA based on taylored
congested compliance matrix and pressure augmentation
    % modified left morphology distribution = original distribution +
increase due to CSA compliance.

morphology_right(:,2)=morphology_right(:,2)+(compliance_patent(:,2)*ma
sk_pressure);
    % modified right (patent) morphology distribution = original
distribution + increase due to CSA compliance.
    % modified right morphology distribution = original distribution +
increase due to CSA compliance.

elseif patent_airway==1; % if left airway is patent then right is
congested, modify congested and patent airway CSA in accordance with
respective area compliance.

morphology_left(:,2)=morphology_left(:,2)+(compliance_patent(:,2)*mask
_pressure);
    % modify patent morphology CSA based on taylored congested
compliance matrix and pressure augmentation
    % modified left morphology distribution = original distribution +
increase due to CSA compliance.

morphology_right(:,2)=morphology_right(:,2)+(compliance_congested(:,2)
*mask_pressure);
    % modify congested morphology CSA based on taylored congested
compliance matrix and pressure augmentation
    % modified left morphology distribution = original distribution +
increase due to CSA compliance.

end

%% calculating new perimeter morphology for both airways due to tissue
compliance
if patent_airway==0; % if right airway is patent then left is
congested, modify congested and patent airway parimeter in accordance
with respective perimeter compliance.

morphology_left(:,3)=morphology_left(:,3)+(compliance_congested(:,3)*m
ask_pressure);
    % modify left (congested) morphology parimeter based on taylored
congested compliance matrix and pressure augmentation
    % modified left morphology distribution = original distribution +
increase due to perimeter compliance.

morphology_right(:,3)=morphology_right(:,3)+(compliance_patent(:,3)*ma
sk_pressure);
    % modified right (patent) morphology distribution = original
distribution + increase due to perimeter compliance.
    % modified right morphology distribution = original distribution +
increase due to perimeter compliance.

elseif patent_airway==1; % if left airway is patent then right is
congested, modify congested and patent airway CSA in accordance with
respective area compliance.

```

```

morphology_left(:,3)=morphology_left(:,3)+(compliance_patent(:,3)*mask_
_pressure);
    % modify patent morphology CSA based on taylored congested
compliance matrix and pressure augmentation
    % modified left morphology distribution = original distribution +
increase due to perimeter compliance.

morphology_right(:,3)=morphology_right(:,3)+(compliance_congested(:,3)
*mask_pressure);
    % modify congested morphology perimeter based on taylored
congested compliance matrix and pressure augmentation
    % modified right morphology distribution = original distribution +
increase due to parimeter compliance.

end

%% calculating delta_csa values

if patent_airway==0; % if right airway is patent, subtract congested
(left) csa from patent (right) csa.
    delta_csa(:,:)=morphology_right(:,2)-morphology_left(:,2);

elseif patent_airway==1; % if left airway is patent, subtract
congested (right) csa from patent (left) csa.
    delta_csa(:,:)=morphology_left(:,2)-morphology_right(:,2);

end

%% calculating delta_perimeter values

if patent_airway==0; % if right airway is patent, subtract congested
(left) perimeter from patent (right) perimeter.
    delta_perimeter(:,:)=morphology_right(:,3)-morphology_left(:,3);

elseif patent_airway==1; % if left airway is patent, subtract
congested (right) perimeter from patent (left) perimeter.
    delta_perimeter(:,:)=morphology_left(:,3)-morphology_right(:,3);

end
end

```

## A5 Water Compliance

*Water Compliance* calculates the amount of net mucosal water supply in accordance with level of air-pressure. Initial ASL water equivalent mass along the entire airway region of interest is also calculated.

```

%% M File created by D White 11th January 2012
function
[asl_water_mass_backflux_left,asl_water_mass_backflux_right,cellular_w
ater_mass_efflux_max_left,cellular_water_mass_efflux_max_right]=water_

```

```

compliance(morphology_left,morphology_right,slice_thickness,mask_pressure,time_step)
%water_compliance acquires
%representing
%Input arguments:
%morphology_left.
%morphology_right.
%asl_depth_mean.
%slice_thickness.
%mask_pressure.
%period.
%Output Arguments:
%asl_water_mass_left.
%asl_water_mass_right.
%cellular_water_mass_supply_left.
%cellular_water_mass_supply_right.
%cellular_water_mass_storage_left.
%cellular_water_mass_storage_right.

%% assigning water supply data matrix

cell_specific_water_efflux_matrix=[0 2.25e-5;5 1.65e-5; 10 1.65e-5; 15
1.65e-5]; % [0 8.8e-6;5 6.6e-6; 10 6.6e-6; 15 6.6e-6]; % Nett water
supply from tissue test trial
% pressure augmentation, water efflux g/(mm^2.s)

asl_specific_water_back_flux=6.23e-6; % continuous asl water backflux
based on Button Boucher (2008)

% setting specific cellular water supply based on pressure
augmentation
cell_specific_water_efflux_max=interp1(cell_specific_water_efflux_matrix(:,1),cell_specific_water_efflux_matrix(:,2),mask_pressure,'linear','extrap')+asl_specific_water_back_flux;

%% pre-allocating matrix size for speed
cellular_water_mass_efflux_max_left=zeros(length(morphology_left(:,1)),1);
cellular_water_mass_efflux_max_right=zeros(length(morphology_right(:,1)),1);
asl_water_mass_backflux_left=zeros(length(morphology_left(:,1)),1);
asl_water_mass_backflux_right=zeros(length(morphology_right(:,1)),1);

%% Increment to repeat parameter calculation for each airway position
X/L from 2nd position to X/L=1
for position_count=1:1:length(morphology_right(:,1));

%% calculate maximum cellular water supply accounting for water supply
compliance
%LEFT
cellular_water_mass_efflux_max_left(position_count,1)=morphology_left(
position_count,3)*slice_thickness*cell_specific_water_efflux_max*time_step;
% cellular water mass supply maximum = surface area x specific maximum
cellular water supply x time step (g)

%RIGHT
cellular_water_mass_efflux_max_right(position_count,1)=morphology_right(
position_count,3)*slice_thickness*cell_specific_water_efflux_max*time_step;
% cellular water mass supply maximum = surface area x specific maximum
cellular water supply x time step (g)

```

```

%% calculate continuous asl back-flux
%LEFT
asl_water_mass_backflux_left(position_count,1)=morphology_left(position_count,3)*slice_thickness*asl_specific_water_back_flux*time_step;
% cellular water mass supply maximum = surface area x specific asl
water back-flux x time step (g)

%RIGHT
asl_water_mass_backflux_right(position_count,1)=morphology_right(position_count,3)*slice_thickness*asl_specific_water_back_flux*time_step;
% cellular water mass supply maximum = surface area x specific asl
water back-flux x time step (g)

end

```

## A6 Breath Build

*Breath Build* reads by interpolation a single breath text file, data shown in Figure 3.3, and compiles a matrix of breathing air mass-flow spanning the total modelling time period of interest.

```

%% M File created by D White 10th January 2012
function [breath]=breath_build(time_out)
%breath_build acquires single at rest breath text file and produces
breath matrix
%representing continuous tidal breathing over time duration of
simulation.
%Input arguments:
%time_step=simulation time increments.
%time_out=total simulation run time.
%Output Arguments:
%breath=tidal breath matrix spanning total simulation time.

%% Open text file and sort out rows labelled 'patent'
breath=importdata('breath.txt');

%% Build breath matrix covering duration of simulation
index=1; % time matrix index counter
while index<(time_out/0.1)-59;
    breath((index+61),1)=(6+index*0.1); %incrementing time by one
time step withion breath matrix
    breath((index+61),2)=breath(index+1,2);
    %copy repeated air mass flow rate data to subsequent cells
    index=index+1; % increment counter
end
end

```

## A7 Flow Apportionment

Flow Apportionment calculates the air mass-flow partition ratio between each of the two nasal airways. It does this by considering the total resistance of each airway and that of the combined airways, as detailed in Section 3.8. Importantly, this is done after the two airways have had their geometry modified in response to air-pressure augmentation.

```
% M File created by D White 11th January 2012
function
[partition_ratio_left,partition_ratio_right]=flow_apportionment(slice_
thickness,morphology_left,morphology_right)
%flow_apportionment calculates airflow mass partitioning between
patent & congested airways
%Input arguments:
%morphology_left.
%morphology_right.
%slice_thickness.
%breath.
%time.
%Output Arguments:
%partition_ratio_left.
%partition_ratio_right.

%% specify constants used in calculation
dynamic_viscosity_air=1.85e-8; % air dynamic viscosity (g/mm^2.s)
T=300K at atmospheric pressure Cengel p874
density_air=1.177e-6; % air density (g/mm^3) T=300K at atmospheric
pressure Cengel p874
gravity=9.81e3; % gravitational constant (mm/s^2);

%% calculating airway series resistance
% LEFT
resistance_left(:,:)=(3*dynamic_viscosity_air*slice_thickness*morpholo
gy_left(:,3).^2)./(4*gravity*density_air^2.*morphology_left(:,2).^3);
% left airway series resistance/unit mass airflow = (dynamic viscosity
x
% length x unit air mass flow)/(2 x density^2 x csa left^3 x gravity

%RIGHT
resistance_right(:,:)=(3*dynamic_viscosity_air*slice_thickness*morphol
ogy_right(:,3).^2)./(4*gravity*density_air^2.*morphology_right(:,2).^3
);
% right airway series resistance/unit mass airflow = (dynamic
viscosity x
% length x unit air mass flow)/(2 x density^2 x csa right^3 x gravity

%% calculating total resistance
inverse_resistance_total=1/sum(resistance_left)+1/sum(resistance_right
);
resistance_total=1/inverse_resistance_total;
% applying parallel resistance analysis

%% calculating partition ratio between airways
% LEFT
partition_ratio_left=resistance_total/sum(resistance_left);
```

```
% calculation ratio of total air mass flowing through left airway

% RIGHT
partition_ratio_right=resistance_total/sum(resistance_right);
% calculation ratio of total air mass flowing through left airway
```

## A8 Breath Phase

*Breath Phase* reads the compiled breath matrix spanning the time period of interest to determine whether the air-mass-flow rate is for inhalation or exhalation. Here, both the direction in which the model processes the nasal morphology and also the initial air conditions are determined.

```
%% M File created by D White 11th January 2012
function [phase]=breath_phase(breath,time)
%breath_phase identifies whether airflow is inhale or exhale to enable
%morphology to be processed in the correct order i.e. nare to np or vice
%versa.
%input arguments:
%breath=breathing matrix over simulation run time.
%time=model simulation time.
%Output Arguments:
%phase=marker for inhale or exhale breathing phase.

%% reading breath matrix to correlate air mass flow rate to simulation
time
air_mass_flow_rate=interp1(breath(:,1),breath(:,2),time,'nearest');

%% determining breath phase
if air_mass_flow_rate<=0;
    phase='inhale';
elseif air_mass_flow_rate==0
    phase='inhale';
else
    phase='exhale';
end
```

## A9 Start Condition

*Start Condition* uses data from the previous function file to order the data matrices so that the sequence of calculation goes anterior to posterior using nasal mask air conditions of air temperature and water species concentration. Alternatively, during the exhalation phase, the data matrices are configured so that the sequence of calculation commences posterior and moves anterior using nasopharynx air conditions of air temperature and water species concentration. These two air conditions are then used to

solve the linear ODE equations (3.10) and (3.11) for air temperature and mid-stream lumen water species concentration. Using these new values, the non-linear algebraic equations (3.12) and (3.13) along with linear algebraic equation (3.17) can be solved to calculate mucosal temperature, air/ASL interface water species concentration and water flux which provides all of the data required for the first airway location.

```

%% M File created by D White 16th January 2012
function
[mucosa_thickness,Kt,position_count,asl_water_mass_flux_left,asl_water_
_mass_flux_right,asl_water_mass_left,asl_water_mass_right,asl_water_ma
ss_max_left,
asl_water_mass_max_right,reynolds_number_left,reynolds_number_right,hm
_left,hm_right,hc_left,hc_right,nusselt_number_left,nusselt_number_rig
ht,hydraulic_diameter_left,hydraulic_diameter_right,Ca_right,Ca_left,T
a_right,Ta_left,Cm_left,Cm_right,Tm_left,Tm_right,N_left,N_right,morph
ology_left,morphology_right,Q_left,Q_right,air_velocity_right,air_velo
city_left,air_ah_right,air_ah_left,air_mass_flow_rate_right,air_mass_f
low_rate_left]=start_condition(breath,partition_ratio_right,partition_
ratio_left,phase,mask_temp,mask_ah,np_temp,np_ah,morphology_left,morph
ology_right,Ca_left,Ca_right,Cm_left,Cm_right,Ta_left,Ta_right,Tm_left
,Tm_right,N_left,N_right,Q_left,Q_right,air_ah_left,air_ah_right,store
_count,time,slice_thickness,asl_water_mass_left,asl_water_mass_right,a
sl_water_mass_max_left,asl_water_mass_max_right,asl_water_mass_flux_le
ft,asl_water_mass_flux_right,time_step,asl_water_mass_backflux_left,as
l_water_mass_backflux_right,cellular_water_mass_efflux_left,cellular_w
ater_mass_efflux_right,mask_pressure)
%start_condition assigns initial values of Ca, Ta, Cm, Tm & N based
on
%phase of breathing cycle
%input arguments:
%breath
%partition_ratio_right
%partition_ratio_left
%phase
%mask_temp.
%mask_ah
%np_temp.
%np_ah
%morphology_left.
%morphology_right.
%store_count.
%time.
%Output Arguments:
%Ca_right
%Ca_left
%Ta_right
%Ta_left
%Cm_left
%Cm_right
%Tm_left
%Tm_right
%N_left
%N_right
%morphology_left.
%morphology_right.

%% Fixed property values

```

```

Kt = 0.0048; % mucosal wall conductivity coefficient (W/mm.K)
(modelled as human skin) %from Datta Table C4, p335.
mucosa_thickness=0.05; % estimated mucosal thickness (mm) (Hanna)
water_molar_mass=18; % molar mass of water g/mol

%% determine start air conditions and order of morphology calculation
based on breathing phase

% initiating X/L position counter for each property matrix
position_count=1;

if strcmp(phase,'inhale'); %air initially enters from mask and flows
to nasopharynx
% no need to resequence morphology matrices

    Ta_right(position_count,store_count)=mask_temp; % using mask
air temp conditions at start of every time cycle
    Ta_left(position_count,store_count)=mask_temp; % % using mask
air temp conditions at start of every time cycle
    Ca_right(position_count,store_count)=(mask_ah*10^-
9/water_molar_mass); % assigning Ca initial value by converting ah
(g/m^3) to mol/mm^3
    Ca_left(position_count,store_count)=(mask_ah*10^-
9/water_molar_mass); % assigning Ca initial value by converting ah
(g/m^3) to mol/mm^3
    Tb=30+(4/length(morphology_left(:,1)))*(position_count-1); %
blood temperature as a function of airway position (C) linear from 30
to 34 degrees based on airflow moving anterior to posterior

else %air initially enters from nasopharynx and flows to nares

    morphology_right=flipud(morphology_right); %flip morphology_right
matrix upsidedown to reverse order
    morphology_left=flipud(morphology_left); %flip morphology_left
matrix upsidedown to reverse order
    Ca_left=flipud(Ca_left);
    Ca_right=flipud(Ca_right);
    Cm_left=flipud(Cm_left);
    Cm_right=flipud(Cm_right);
    Ta_right=flipud(Ta_right);
    Ta_left=flipud(Ta_left);
    Tm_left=flipud(Tm_left);
    Tm_right=flipud(Tm_right);
    N_left=flipud(N_left);
    N_right=flipud(N_right);
    Q_left=flipud(Q_left);
    Q_right=flipud(Q_right);
    air_ah_left=flipud(air_ah_left);
    air_ah_right=flipud(air_ah_right);
    asl_water_mass_left=flipud(asl_water_mass_left);
    asl_water_mass_right=flipud(asl_water_mass_right);
    asl_water_mass_max_left=flipud(asl_water_mass_max_left);
    asl_water_mass_max_right=flipud(asl_water_mass_max_right);
    asl_water_mass_flux_left=flipud(asl_water_mass_flux_left);
    asl_water_mass_flux_right=flipud(asl_water_mass_flux_right);

    Ta_right(position_count,store_count)=np_temp; % using np air temp
conditions at start of every time cycle
    Ta_left(position_count,store_count)=np_temp; % using np air temp
conditions at start of every time cycle

```

```

Ca_right(position_count,store_count)=(np_ah*10^-
9/water_molar_mass); % assigning Ca initial value by converting ah
(g/m^3) to mol/mm^3
Ca_left(position_count,store_count)=(np_ah*10^-
9/water_molar_mass); % assigning Ca initial value by converting ah
(g/m^3) to mol/mm^3
Tb=34-(4/length(morphology_left(:,1)))*(position_count-1); % blood
temperature as a function of airway position (C) linear from 34 to 30
degrees based on airflow moving posterior to anterior

end

%% Variable property values as function of air and water temperature
specific_heat_capacity_dry_air_data_matrix=[7 1.008;17 1.007;27
1.005;37 1.005;47 1.006];
%(J/g.K) air specific heat capacity, Cengel, Table A.7, p824.

specific_heat_capacity_water_vapour_data_matrix=[2 1.859e-3;27 1.864e-
3;52 1.871e-3];
%(J/g.K) specific_heat_capacity_water_vapour, Rogers & Mayhew, p17.

if store_count==1
    % use air temperature from adjacent upstream lump to get started

specific_heat_capacity_dry_air_left=interp1(specific_heat_capacity_dry
_air_data_matrix(:,1),specific_heat_capacity_dry_air_data_matrix(:,2),
Ta_left(position_count,store_count),'linear');

specific_heat_capacity_dry_air_right=interp1(specific_heat_capacity_dr
y_air_data_matrix(:,1),specific_heat_capacity_dry_air_data_matrix(:,2)
,Ta_right(position_count,store_count),'linear');

specific_heat_capacity_water_vapour_left=interp1(specific_heat_capacit
y_water_vapour_data_matrix(:,1),specific_heat_capacity_water_vapour_da
ta_matrix(:,2),Tb,'linear');% note blood temp used as no mucosa temp
yet

specific_heat_capacity_water_vapour_right=interp1(specific_heat_capaci
ty_water_vapour_data_matrix(:,1),specific_heat_capacity_water_vapour_d
ata_matrix(:,2),Tb,'linear');% note blood temp used as no mucosa temp
yet

    % airway water saturation pressure based on mucosa temperature
(pa)
    saturation_vapour_pressure_left=(10^(-7.90298*(373.16/(Tb+273))-
1)+5.02808*log10(373.16/(Tb+273))-1.3816*1e-7*(10^(11.344*(1-
(Tb+273)/373.16))-1)+8.1328*1e-3*(10^(-3.49149*(373.16/(Tb+273)-1))-
1)+log10(1013.246)))*100;% note blood temp used as no mucosa temp yet
    saturation_vapour_pressure_right=(10^(-7.90298*(373.16/(Tb+273))-
1)+5.02808*log10(373.16/(Tb+273))-1.3816*1e-7*(10^(11.344*(1-
(Tb+273)/373.16))-1)+8.1328*1e-3*(10^(-3.49149*(373.16/(Tb+273)-1))-
1)+log10(1013.246)))*100;% note blood temp used as no mucosa temp yet

else

specific_heat_capacity_dry_air_left=interp1(specific_heat_capacity_dry
_air_data_matrix(:,1),specific_heat_capacity_dry_air_data_matrix(:,2),
Ta_left(position_count,store_count-1),'linear');

specific_heat_capacity_dry_air_right=interp1(specific_heat_capacity_dr

```

```

y_air_data_matrix(:,1),specific_heat_capacity_dry_air_data_matrix(:,2)
,Ta_right(position_count,store_count-1),'linear');

specific_heat_capacity_water_vapour_left=interp1(specific_heat_capacity_water_vapour_data_matrix(:,1),specific_heat_capacity_water_vapour_data_matrix(:,2),Tm_left(position_count,store_count-1),'linear');

specific_heat_capacity_water_vapour_right=interp1(specific_heat_capacity_water_vapour_data_matrix(:,1),specific_heat_capacity_water_vapour_data_matrix(:,2),Tm_right(position_count,store_count-1),'linear');

    % airway water saturation pressure based on mucosa temperature
    (pa)
    saturation_vapour_pressure_left=(10^(-
7.90298*(373.16/(Tm_left(position_count,store_count-1)+273))-
1)+5.02808*log10(373.16/(Tm_left(position_count,store_count-1)+273))-
1.3816*1e-7*(10^(11.344*(1-(Tm_left(position_count,store_count-
1)+273)/373.16))-1)+8.1328*1e-3*(10^(-
3.49149*(373.16/(Tm_left(position_count,store_count-1)+273)-1))-
1)+log10(1013.246)))*100;
    saturation_vapour_pressure_right=(10^(-
7.90298*(373.16/(Tm_right(position_count,store_count-1)+273))-
1)+5.02808*log10(373.16/(Tm_right(position_count,store_count-1)+273))-
1.3816*1e-7*(10^(11.344*(1-(Tm_right(position_count,store_count-
1)+273)/373.16))-1)+8.1328*1e-3*(10^(-
3.49149*(373.16/(Tm_right(position_count,store_count-1)+273)-1))-
1)+log10(1013.246)))*100;

end

%calculate total pressure
total_pressure=(mask_pressure/100)*9.81*1000+101325;

% calculate humidity ratio
humidity_ratio_left=(0.622*saturation_vapour_pressure_left)/(total_pressure-saturation_vapour_pressure_left);
humidity_ratio_right=(0.622*saturation_vapour_pressure_right)/(total_pressure-saturation_vapour_pressure_left);

% calculate specific heat capacity of moist air
specific_heat_capacity_air_left=specific_heat_capacity_dry_air_left+humidity_ratio_left*specific_heat_capacity_water_vapour_left;
specific_heat_capacity_air_right=specific_heat_capacity_dry_air_right+humidity_ratio_right*specific_heat_capacity_water_vapour_right;

density_air_data_matrix=[7 1.265e-6;17 1.220e-6;27 1.177e-6;37 1.141e-6;47 1.106e-6];
%density_air=1.177e-6; %(g/mm^3) air density function of temp, Cengel, Table A.7, p824.
if store_count==1
    % use air temperature from adjacent upstream lump to get started

density_air_left=interp1(density_air_data_matrix(:,1),density_air_data_matrix(:,2),Ta_left(position_count,store_count),'linear');

density_air_right=interp1(density_air_data_matrix(:,1),density_air_data_matrix(:,2),Ta_right(position_count,store_count),'linear');
else

```

```

density_air_left=interp1(density_air_data_matrix(:,1),density_air_data_matrix(:,2),Ta_left(position_count,store_count-1),'linear');

density_air_right=interp1(density_air_data_matrix(:,1),density_air_data_matrix(:,2),Ta_right(position_count,store_count-1),'linear');
end

air_thermal_conductivity_coefficient_data_matrix=[7 2.55e-5;17 2.61e-5;27 2.67e-5;37 2.74e-5;47 2.81e-5];
%conductivity coefficient of air (W/mm.K) function of temp and pressure from Cengel, Table A-7, p824
if store_count==1
    % use air temperature from adjacent upstream lump to get started

air_thermal_conductivity_coefficient_left=interp1(air_thermal_conductivity_coefficient_data_matrix(:,1),air_thermal_conductivity_coefficient_data_matrix(:,2),Ta_left(position_count,store_count),'linear');

air_thermal_conductivity_coefficient_right=interp1(air_thermal_conductivity_coefficient_data_matrix(:,1),air_thermal_conductivity_coefficient_data_matrix(:,2),Ta_right(position_count,store_count),'linear');
else

air_thermal_conductivity_coefficient_left=interp1(air_thermal_conductivity_coefficient_data_matrix(:,1),air_thermal_conductivity_coefficient_data_matrix(:,2),Ta_left(position_count,store_count-1),'linear');

air_thermal_conductivity_coefficient_right=interp1(air_thermal_conductivity_coefficient_data_matrix(:,1),air_thermal_conductivity_coefficient_data_matrix(:,2),Ta_right(position_count,store_count-1),'linear');
end

air_kinematic_viscosity_data_matrix=[7 13.91;17 14.77;27 15.66;37 16.54;47 14.77];
%kinematic viscosity of air(mm^2/s) function of temp and pressure from Cengel, Table A-7, p824
if store_count==1
    % use air temperature from adjacent upstream lump to get started

air_kinematic_viscosity_left=interp1(air_kinematic_viscosity_data_matrix(:,1),air_kinematic_viscosity_data_matrix(:,2),Ta_left(position_count,store_count),'linear');

air_kinematic_viscosity_right=interp1(air_kinematic_viscosity_data_matrix(:,1),air_kinematic_viscosity_data_matrix(:,2),Ta_right(position_count,store_count),'linear');
else

air_kinematic_viscosity_left=interp1(air_kinematic_viscosity_data_matrix(:,1),air_kinematic_viscosity_data_matrix(:,2),Ta_left(position_count,store_count-1),'linear');

air_kinematic_viscosity_right=interp1(air_kinematic_viscosity_data_matrix(:,1),air_kinematic_viscosity_data_matrix(:,2),Ta_right(position_count,store_count-1),'linear');
end

air_thermal_diffusivity_data_matrix=[-23 15.9;27 22.5;77 29.9];
% air thermal diffusivity (mm^2/s^2) function of temp from Incropera & DeWitt, Table A.4, pA15

```

```

if store_count==1

air_thermal_diffusivity_left=interp1(air_thermal_diffusivity_data_matrix(:,1),air_thermal_diffusivity_data_matrix(:,2),Ta_left(position_count,store_count),'linear');

air_thermal_diffusivity_right=interp1(air_thermal_diffusivity_data_matrix(:,1),air_thermal_diffusivity_data_matrix(:,2),Ta_right(position_count,store_count),'linear');
else

air_thermal_diffusivity_left=interp1(air_thermal_diffusivity_data_matrix(:,1),air_thermal_diffusivity_data_matrix(:,2),Ta_left(position_count,store_count-1),'linear');

air_thermal_diffusivity_right=interp1(air_thermal_diffusivity_data_matrix(:,1),air_thermal_diffusivity_data_matrix(:,2),Ta_right(position_count,store_count-1),'linear');
end

hfg_data_matrix=[10 2479;15 2466;20 2454;25 2442;30 2430;35 2418;39 2409];
%enthalpy of fusion (J/g) function of temp and pressure from Cengel, Table A-12a, p835

if store_count==1

hfg_left=interp1(hfg_data_matrix(:,1),hfg_data_matrix(:,2),Ta_left(position_count,store_count),'linear');

hfg_right=interp1(hfg_data_matrix(:,1),hfg_data_matrix(:,2),Ta_right(position_count,store_count),'linear');
else

hfg_left=interp1(hfg_data_matrix(:,1),hfg_data_matrix(:,2),Ta_left(position_count,store_count-1),'linear');

hfg_right=interp1(hfg_data_matrix(:,1),hfg_data_matrix(:,2),Ta_right(position_count,store_count-1),'linear');
end

%% Varying property values as function of water temperature
water_air_binary_diffusion_coefficient_data_matrix=[7 22.7;12 23.3;17 24.0;22 24.8;27 25.6;32 26.1;37 27.0;42 27.8];
%water/air binary diffusion coefficient (mm^2/s) as a function of temperature, Fig1, p E23-11.
if store_count==1

water_air_binary_diffusion_coefficient_left=interp1(water_air_binary_diffusion_coefficient_data_matrix(:,1),water_air_binary_diffusion_coefficient_data_matrix(:,2),Tb,'linear');
    %use blood temperature for first iteration

water_air_binary_diffusion_coefficient_right=interp1(water_air_binary_diffusion_coefficient_data_matrix(:,1),water_air_binary_diffusion_coefficient_data_matrix(:,2),Tb,'linear');
else

water_air_binary_diffusion_coefficient_left=interp1(water_air_binary_diffusion_coefficient_data_matrix(:,1),water_air_binary_diffusion_coefficient_data_matrix(:,2),Tm_left(position_count,store_count-1),'linear');

```

```

water_air_binary_diffusion_coefficient_right=interp1(water_air_binary_
diffusion_coefficient_data_matrix(:,1),water_air_binary_diffusion_coef
ficient_data_matrix(:,2),Tm_right(position_count,store_count-
1),'linear');
end

%% calculating initial hydraulic diameters
hydraulic_diameter_left(position_count,1)=4*morphology_left(1,2)/morph
ology_left(1,3); % mm
hydraulic_diameter_right(position_count,1)=4*morphology_right(1,2)/mor
phology_right(1,3); %mm

%% calculating air velocities in intial lump
air_mass_flow_rate=interp1(breath(:,1),breath(:,2),time,'linear');
% reading breath matrix to correlate air mass flow rate to simulation
time

% correct for negative value of air mass flow
if air_mass_flow_rate<0;
    air_mass_flow_rate=air_mass_flow_rate*-1; % changing negative
air mass flow numbers to positive during inhale cycle
end

%% calculating and storing air mass flow for each passageway with
respect to time
air_mass_flow_rate_right(1,store_count)=air_mass_flow_rate*partition_r
atio_right;
air_mass_flow_rate_left(1,store_count)=air_mass_flow_rate*partition_ra
tio_left;

%% calculating air velocities for each nasal passageway and storing in
matricies
air_velocity_left(position_count,store_count)=(air_mass_flow_rate_left
(1,store_count))/(density_air_left*(pi/4)*hydraulic_diameter_left(posi
tion_count,1)^2);%morphology_left(position_count,2));
air_velocity_right(position_count,store_count)=(air_mass_flow_rate_rig
ht(1,store_count))/(density_air_right*pi/4*hydraulic_diameter_right(po
sition_count,1)^2);%morphology_right(position_count,2));

%% calculating reynolds numbers
reynolds_number_left(position_count,1)=air_velocity_left(position_coun
t,store_count)*hydraulic_diameter_left(position_count,1)/air_kinematic
_viscosity_left;
reynolds_number_right(position_count,1)=air_velocity_right(position_co
unt,store_count)*hydraulic_diameter_right(position_count,1)/air_kinema
tic_viscosity_right;

%% calculating prandtl numbers
prandtl_number_left=air_kinematic_viscosity_left/air_thermal_diffusivi
ty_left; % calculating prandtl number left airway
prandtl_number_right=air_kinematic_viscosity_right/air_thermal_diffusi
vity_right; % calculating prandtl number right airway

%% calculating nusselt numbers - two parallel plates laminar flow
nusselt_number_left=7.54+((0.03*(hydraulic_diameter_left(position_coun
t,1)/slice_thickness)*reynolds_number_left(position_count,1)*prandtl_n
umber_left)/(1+0.016*((hydraulic_diameter_left(position_count,1)/slice
_thickness)*reynolds_number_left(position_count,1)*prandtl_number_left
)^(2/3)));
nusselt_number_right=7.54+((0.03*(hydraulic_diameter_right(position_co
unt,1)/slice_thickness)*reynolds_number_right(position_count,1)*prandtl

```

```

l_number_right)/(1+0.016*((hydraulic_diameter_right(position_count,1)/
slice_thickness)*reynolds_number_right(position_count,1)*prandtl_numbe
r_right)^(2/3)));

%% computing convective heat transfer coefficients (hc)
hc_left(position_count,1)=nusselt_number_left(position_count,1)*air_th
ermal_conductivity_coefficient_left/slice_thickness; % first
calculation of left side heat convection coefficient (w/cm^2.K)
hc_right(position_count,1)=nusselt_number_right(position_count,1)*air_
thermal_conductivity_coefficient_right/slice_thickness; % first
calculation of right side heat convection coefficient (w/cm^2.K)

%% Calculating mass transfer coefficient
lewis_number_left=air_thermal_diffusivity_left/water_air_binary_diffus
ion_coefficient_left; %Lewis number
lewis_number_right=air_thermal_diffusivity_right/water_air_binary_diff
usion_coefficient_right; %Lewis number

hm_left(position_count,1)=hc_left(position_count,1)/(density_air_left*
specific_heat_capacity_air_left*(lewis_number_left)^(2/3));
%convective mass transfer coefficient as a function of heat transfer
coefficient.
hm_right(position_count,1)=hc_right(position_count,1)/(density_air_rig
ht*specific_heat_capacity_air_right*(lewis_number_right)^(2/3));
%convective mass transfer coefficient as a function of heat transfer
coefficient.

%% calculating gradient and y-intercept for linear approximation of Cm
based on Tm for left airway
% pre-allocating matrix for speed.
Cm=zeros(1,8);
density_air=zeros(1,8);

for temp=28:1:36; % span mucosal temperature from 28-36 degrees C

saturation_vapour_pressure=(10^(-7.90298*(373.16/(temp+273))-
1)+5.02808*log10(373.16/(temp+273))-1.3816*1e-7*(10^(11.344*(1-
(temp+273)/373.16))-1)+8.1328*1e-3*(10^(-3.49149*(373.16/(temp+273))-
1))-1)+log10(1013.246))*100;
% Goff-Gratch Equation is used to calculate water partial pressure.

% calculate humidity ratio
mucosa_humidity_ratio=(0.622*saturation_vapour_pressure)/(total_pressu
re-saturation_vapour_pressure);

density_air(1,temp-
27)=interp1(density_air_data_matrix(:,1),density_air_data_matrix(:,2),
temp,'linear');

% Cm temperate data
Cm(1,temp-27)=temp;

% calculation of mask air water species concentration in mol/mm^3
Cm(2,temp-27)=mucosa_humidity_ratio*density_air(1,temp-27)/18;

end
% determine gradient and slope
P = polyfit(Cm(1,:),Cm(2,:),1);

% assign values
Cm_gradient=P(1,1);

```



```

(hm_left(position_count,1)*Ca_left(position_count,store_count));
Cm_intercept];
    x=(A\b).';
    N_left(position_count,store_count) = x(1,3); % assigning
initial value for N_left

    % test for insufficient ASL water mass to meet total demand
    if
N_left(position_count,store_count)>(asl_water_mass_left(position_count
,store_count-
1)+cellular_water_mass_efflux_left(position_count,store_count-1)-
asl_water_mass_backflux_left(position_count,1))/(morphology_left(positi
on_count,3)*slice_thickness*water_molar_mass*time_step);
        N_left(position_count,store_count) =
(asl_water_mass_left(position_count,store_count-
1)+cellular_water_mass_efflux_left(position_count,store_count-1)-
asl_water_mass_backflux_left(position_count,1))/(morphology_left(positi
on_count,3)*slice_thickness*water_molar_mass*time_step);%+cellular_wa
ter_mass_efflux_left(position_count,store_count-1)-
asl_water_mass_backflux_left(position_count,1);

Tm_left(position_count,store_count)=((Kt/mucosa_thickness)*Tb+hc_left(
position_count,1)*Ta_left(position_count,store_count)-
water_molar_mass*N_left(position_count,store_count)*hfg_left)/(Kt/muco
sa_thickness+hc_left(position_count,1));
    Cm_left(position_count,store_count)=
Ca_left(position_count,store_count)+N_left(position_count,store_count)
/hm_left(position_count,1);

    else % where sufficient asl water mass is present on mucosa
        Cm_left(position_count,store_count)= x(1,1); % assigning
initial value for Cm_left
        Tm_left(position_count,store_count)= x(1,2); % assigning
initial value for Tm_left
        %N_left(position_count,store_count) = x(1,3); % assigning
initial value for N_left
    end

end

%% Compute initial conditions for Cm Tm & N right

switch store_count; % for first time iteration need to use initial
start value of asl water mass mean
    case {1}

        % initial calculation for change in mucosa parameters
        A=[0 (Kt/mucosa_thickness+hc_right(position_count,1))
(water_molar_mass*hfg_right);hm_right(position_count,1) 0 -1;1 -
1*Cm_gradient 0];

        b=[((Kt/mucosa_thickness)*Tb+(hc_right(position_count,1)*Ta_right(posi
tion_count,store_count)));
(hm_right(position_count,1)*Ca_right(position_count,store_count));
Cm_intercept];
        y=(A\b).';
        N_right(position_count,store_count) = y(1,3); % assigning
initial value for N_right

        % test for insufficient ASL water mass to meet total demand
        if
N_right(position_count,store_count)>asl_water_mass_right(position_coun

```

```

t,store_count)/(morphology_right(position_count,3)*slice_thickness*water_molar_mass*time_step);
    N_right(position_count,store_count) =
asl_water_mass_right(position_count,store_count)/(morphology_right(position_count,3)*slice_thickness*water_molar_mass*time_step);

Tm_right(position_count,store_count)=((Kt/mucosa_thickness)*Tb+hc_right(position_count,1)*Ta_right(position_count,store_count)-
water_molar_mass*N_right(position_count,store_count)*hfg_right)/(Kt/mucosa_thickness+hc_right(position_count,1));
    Cm_right(position_count,store_count)=
Ca_right(position_count,store_count)+N_right(position_count,store_count)/hm_right(position_count,1);

    else % where sufficient asl water mass is present on mucosa
        Cm_right(position_count,store_count)= y(1,1); % assigning initial value for Cm_right
        Tm_right(position_count,store_count)= y(1,2); % assigning initial value for Tm_right
        %N_right(position_count,store_count) = y(1,3); % assigning initial value for N_right
    end

    otherwise % for subsequent time iteration use previous asl water mass

        % initial calculation for change in mucosa parameters
        A=[0 (Kt/mucosa_thickness+hc_right(position_count,1))
(water_molar_mass*hfg_right);hm_right(position_count,1) 0 -1;1 -1*Cm_gradient 0];

b=[((Kt/mucosa_thickness)*Tb+(hc_right(position_count,1)*Ta_right(position_count,store_count)));
(hm_right(position_count,1)*Ca_right(position_count,store_count));
Cm_intercept];
        y=(A\b).';
        N_right(position_count,store_count) = y(1,3); % assigning initial value for N_right

        % test for insufficient ASL water mass to meet total demand
        if
N_right(position_count,store_count)>(asl_water_mass_right(position_count,store_count-1)+cellular_water_mass_efflux_right(position_count,store_count-1)-
asl_water_mass_backflux_right(position_count,1))/(morphology_right(position_count,3)*slice_thickness*water_molar_mass*time_step);
            N_right(position_count,store_count) =
(asl_water_mass_right(position_count,store_count-1)+cellular_water_mass_efflux_right(position_count,store_count-1)-
asl_water_mass_backflux_right(position_count,1))/(morphology_right(position_count,3)*slice_thickness*water_molar_mass*time_step);

Tm_right(position_count,store_count)=((Kt/mucosa_thickness)*Tb+hc_right(position_count,1)*Ta_right(position_count,store_count)-
water_molar_mass*N_right(position_count,store_count)*hfg_right)/(Kt/mucosa_thickness+hc_right(position_count,1));
            Cm_right(position_count,store_count)=
Ca_right(position_count,store_count)+N_right(position_count,store_count)/hm_right(position_count,1);

        else % where sufficient asl water mass is present on mucosa

```

```

        Cm_right(position_count,store_count)= y(1,1); % assigning
initial value for Cm_right
        Tm_right(position_count,store_count)= y(1,2); % assigning
initial value for Tm_right
        %N_right(position_count,store_count) = y(1,3); % assigning
initial value for N_right
        end

end

%% calculate heat flux (Q) and form storage matrix
Q_left(position_count,store_count)=(hc_left(position_count,1)*(Tm_left
(position_count,store_count)-
Ta_left(position_count,store_count))+N_left(position_count,store_count
)*water_molar_mass*hfg_left)*morphology_left(position_count,3)*slice_t
hickness;
Q_right(position_count,store_count)=(hc_right(position_count,1)*(Tm_righ
t(position_count,store_count)-
Ta_right(position_count,store_count))+N_right(position_count,store_cou
nt)*water_molar_mass*hfg_right)*morphology_right(position_count,3)*sli
ce_thickness;

%% calculate air absolute humidity based on water molar flux (N)
if strcmp(phase,'inhale'); %air initially enters from mask and flows
to nasopharynx
    air_ah_right(position_count,store_count)=mask_ah;
    air_ah_left(position_count,store_count)=mask_ah;

else %air initially enters from nasopharynx and flows to mask
    air_ah_right(position_count,store_count)=np_ah;
    air_ah_left(position_count,store_count)=np_ah;
end

```

## A10 Flux Calculation

Flux Calculation predicts air temperature and water species concentration for the next model lump along the airway using the Euler method for solving the linear ODE equations (3.8) and (3.9). Using these new values, the non-linear algebraic equations (3.10) and (3.11) along with linear algebraic equation (3.15) can be solved for mucosal temperature and ASL/air interface water species concentration along with ASL water flux. This stepping process is undertaken along the whole length of both airways for each air-mass-flow rate within the breath file.

```

%% M File created by D White 17th January 2012
function
[Ca_right,Ca_left,Ta_right,Ta_left,Cm_left,Cm_right,Tm_left,Tm_right,N
_left,N_right,Q_left,Q_right,air_velocity_right,air_velocity_left,air_

```

```

ah_right,air_ah_left,reynolds_number_left,reynolds_number_right]=flux_
calculation(hm_left,hm_right,hc_left,hc_right,nusselt_number_left,nuss
elt_number_right,reynolds_number_left,reynolds_number_right,hydraulic_
diameter_left,hydraulic_diameter_right,morphology_left,morphology_righ
t,store_count,slice_thickness,Ca_right,Ca_left,Ta_right,Ta_left,Cm_lef
t,Cm_right,Tm_left,Tm_right,N_left,N_right,Q_left,Q_right,air_velocity_
right,air_velocity_left,air_mass_flow_rate_right,air_mass_flow_rate_l
eft,air_ah_right,air_ah_left,phase,asl_water_mass_left,asl_water_mass_
right,time_step,asl_water_mass_backflux_left,asl_water_mass_backflux_r
ight,cellular_water_mass_efflux_left,cellular_water_mass_efflux_right,
Kt,mucosa_thickness,water_molar_mass,mask_pressure)
%start_condition assigns initial values of Ca, Ta, Cm, Tm & N based
on
%phase of breathing cycle
%input arguments:
%breath
%partition_ratio_right
%partition_ratio_left
%phase
%mask_temp.
%mask_ah
%np_temp.
%np_ah
%morphology_left.
%morphology_right.
%store_count.
%time.
%slice_thickness.
%Output Arguments:
%Ca_right
%Ca_left
%Ta_right
%Ta_left
%Cm_left
%Cm_right
%Tm_left
%Tm_right
%N_left
%N_right
%morphology_left.
%morphology_right.

%% Fixed property values
%mucosa_thickness=0.05; % estimated mucosal thickness (mm) (Hanna)
%water_molar_mass=18; % molar mass of water g/mol

%Kt = 0.0048; % mucosal wall conductivity coefficient (W/mm.K) (Hanna)
%from Datta Table C4, p335.
%water_air_binary_diffusion_coefficient=25.38; % water/air_binary
diffusion coefficient at atmospheric pressure (mm^2/s) from Datta,
Table D3, p348.
%air_thermal_diffusivity=22.1; % air thermal diffusivity (mm^2/s^2)
function of temp and pressure from Cengel, Table A-19, p874
%air_kinematic_viscosity=15.7; %kinematic viscosity of air(mm^2/s)
function of temp and pressure from Cengel, Table A-19, p874
%hfg=2257; %enthalpy of fusion (J/g) function of temp and pressure
from Cengel, Table A-3, p846
%air_thermal_conductivity_coefficient=2.61e-5; %conductivity
coefficient of air (W/mm.K) function of temp and pressure from Cengel,
Table A-19, p874
%density_air=1.177e-6; % (g/mm^3) air density function of temp and
pressure from Cengel, Table A-19, p875

```

```

%specific_heat_capacity_water=4.180; % (J/g.K) water specific heat
capacity function of temp and pressure from Cengel, Table A-3, p847
%specific_heat_capacity_air=1.005; % (J/g.K) air specific heat
capacity function of temp and pressure from Cengel, Table A-19, p874

%% Increment to repeat parameter calculation for each airway position
X/L from 2nd position to X/L=1
for position_count=2:1:length(morphology_right(:,1));

% calculating blood temperature specific to airway location and breath
phase
if strcmp(phase,'inhale'); %air initially enters from mask and flows
to nasopharynx
    Tb=30+(4/length(morphology_left(:,1)))*(position_count-1); % blood
temperature as a function of airway position (C) linear from 30 to 34
degrees based on airflow moving anterior to posterior.

else %air initially enters from nasopharynx and flows to nares
    Tb=34-(4/length(morphology_left(:,1)))*(position_count-1); % blood
temperature as a function of airway position (C) linear from 34 to 30
degrees based on airflow moving posterior to anterior.
end

%% Variable property values as function of air temperature
specific_heat_capacity_dry_air_data_matrix=[7 1.008;17 1.007;27
1.005;37 1.005;47 1.006];
%(j/gK) air specific heat capacity at 300K, Cengel, Table A.7, p824.

specific_heat_capacity_water_vapour_data_matrix=[2 1.859e-3;27 1.864e-
3;52 1.871e-3];
% (J/g.K) specific_heat_capacity_water_vapour, Rogers & Mayhew, pl7.

if store_count==1
    % use air temperature from adjacent upstream lump to get started

specific_heat_capacity_dry_air_left=interp1(specific_heat_capacity_dry
_air_data_matrix(:,1),specific_heat_capacity_dry_air_data_matrix(:,2),
Ta_left(position_count-1,store_count),'linear');

specific_heat_capacity_dry_air_right=interp1(specific_heat_capacity_dr
y_air_data_matrix(:,1),specific_heat_capacity_dry_air_data_matrix(:,2)
,Ta_right(position_count-1,store_count),'linear');

specific_heat_capacity_water_vapour_left=interp1(specific_heat_capacit
y_water_vapour_data_matrix(:,1),specific_heat_capacity_water_vapour_da
ta_matrix(:,2),Tm_left(position_count-1,store_count),'linear');% note
use adjacent mucosa temp for 1st iteration

specific_heat_capacity_water_vapour_right=interp1(specific_heat_capaci
ty_water_vapour_data_matrix(:,1),specific_heat_capacity_water_vapour_d
ata_matrix(:,2),Tm_right(position_count-1,store_count),'linear');%
note use adjacent mucosa temp for 1st iteration

    % airway water saturation pressure based on mucosa temperature
(pa)
    saturation_vapour_pressure_left=(10^(-
7.90298*(373.16/(Tm_left(position_count-1,store_count)+273))-
1)+5.02808*log10(373.16/(Tm_left(position_count-1,store_count)+273))-
1.3816*1e-7*(10^(11.344*(1-(Tm_left(position_count-
1,store_count)+273)/373.16))-1)+8.1328*1e-3*(10^(-
3.49149*(373.16/(Tm_left(position_count-1,store_count)+273)-1)))-

```

```

1)+log10(1013.246))) *100;% note use adjacent mucosa temp for 1st
iteration
    saturation_vapour_pressure_right=(10^(-
7.90298*(373.16/(Tm_right(position_count-1,store_count)+273)-
1)+5.02808*log10(373.16/(Tm_right(position_count-1,store_count)+273))-
1.3816*1e-7*(10^(11.344*(1-(Tm_right(position_count-
1,store_count)+273)/373.16))-1)+8.1328*1e-3*(10^(-
3.49149*(373.16/(Tm_right(position_count-1,store_count)+273)-1))-
1)+log10(1013.246))) *100;% note use adjacent mucosa temp for 1st
iteration

    else

specific_heat_capacity_dry_air_left=interp1(specific_heat_capacity_dry
_air_data_matrix(:,1),specific_heat_capacity_dry_air_data_matrix(:,2),
Ta_left(position_count,store_count-1),'linear');

specific_heat_capacity_dry_air_right=interp1(specific_heat_capacity_dr
y_air_data_matrix(:,1),specific_heat_capacity_dry_air_data_matrix(:,2)
,Ta_right(position_count,store_count-1),'linear');

specific_heat_capacity_water_vapour_left=interp1(specific_heat_capacit
y_water_vapour_data_matrix(:,1),specific_heat_capacity_water_vapour_da
ta_matrix(:,2),Tm_left(position_count,store_count-1),'linear');

specific_heat_capacity_water_vapour_right=interp1(specific_heat_capaci
ty_water_vapour_data_matrix(:,1),specific_heat_capacity_water_vapour_d
ata_matrix(:,2),Tm_right(position_count,store_count-1),'linear');

    % airway water saturation pressure based on mucosa temperature
(pa)
    saturation_vapour_pressure_left=(10^(-
7.90298*(373.16/(Tm_left(position_count,store_count-1)+273)-
1)+5.02808*log10(373.16/(Tm_left(position_count,store_count-1)+273))-
1.3816*1e-7*(10^(11.344*(1-(Tm_left(position_count,store_count-
1)+273)/373.16))-1)+8.1328*1e-3*(10^(-
3.49149*(373.16/(Tm_left(position_count,store_count-1)+273)-1))-
1)+log10(1013.246))) *100;
    saturation_vapour_pressure_right=(10^(-
7.90298*(373.16/(Tm_right(position_count,store_count-1)+273)-
1)+5.02808*log10(373.16/(Tm_right(position_count,store_count-1)+273))-
1.3816*1e-7*(10^(11.344*(1-(Tm_right(position_count,store_count-
1)+273)/373.16))-1)+8.1328*1e-3*(10^(-
3.49149*(373.16/(Tm_right(position_count,store_count-1)+273)-1))-
1)+log10(1013.246))) *100;

end

%calculate total pressure
total_pressure=(mask_pressure/100)*9.81*1000+101325;

% calculate humidity ratio
humidity_ratio_left=(0.622*saturation_vapour_pressure_left)/(total_pre
ssure-saturation_vapour_pressure_left);
humidity_ratio_right=(0.622*saturation_vapour_pressure_right)/(total_p
ressure-saturation_vapour_pressure_left);

% calculate specific heat capacity of moist air
specific_heat_capacity_air_left=specific_heat_capacity_dry_air_left+hu
midity_ratio_left*specific_heat_capacity_water_vapour_left;

```

```

specific_heat_capacity_air_right=specific_heat_capacity_dry_air_right+
humidity_ratio_right*specific_heat_capacity_water_vapour_right;

density_air_data_matrix=[7 1.265e-6;17 1.220e-6;27 1.177e-6;37 1.141e-
6;47 1.106e-6];
%density_air=1.177e-6; %(g/mm^3) air density function of temp, Cengel,
Table A.7, p824.
if store_count==1
    % use air temperature from adjacent upstream lump to get started

density_air_left=interp1(density_air_data_matrix(:,1),density_air_data
_matrix(:,2),Ta_left(position_count-1,store_count),'linear');

density_air_right=interp1(density_air_data_matrix(:,1),density_air_dat
a_matrix(:,2),Ta_right(position_count-1,store_count),'linear');
else

density_air_left=interp1(density_air_data_matrix(:,1),density_air_data
_matrix(:,2),Ta_left(position_count,store_count-1),'linear');

density_air_right=interp1(density_air_data_matrix(:,1),density_air_dat
a_matrix(:,2),Ta_right(position_count,store_count-1),'linear');
end

air_thermal_conductivity_coefficient_data_matrix=[7 2.55e-5;17 2.61e-
5;27 2.67e-5;37 2.74e-5;47 2.81e-5];
%conductivity coefficient of air (W/mm.K) function of temp and
pressure from Cengel, Table A-7, p824
if store_count==1
    % use air temperature from adjacent upstream lump to get started

air_thermal_conductivity_coefficient_left=interp1(air_thermal_conducti
vity_coefficient_data_matrix(:,1),air_thermal_conductivity_coefficient
_data_matrix(:,2),Ta_left(position_count-1,store_count),'linear');

air_thermal_conductivity_coefficient_right=interp1(air_thermal_conduct
ivity_coefficient_data_matrix(:,1),air_thermal_conductivity_coefficien
t_data_matrix(:,2),Ta_right(position_count-1,store_count),'linear');
else

air_thermal_conductivity_coefficient_left=interp1(air_thermal_conducti
vity_coefficient_data_matrix(:,1),air_thermal_conductivity_coefficient
_data_matrix(:,2),Ta_left(position_count,store_count-1),'linear');

air_thermal_conductivity_coefficient_right=interp1(air_thermal_conduct
ivity_coefficient_data_matrix(:,1),air_thermal_conductivity_coefficien
t_data_matrix(:,2),Ta_right(position_count,store_count-1),'linear');
end

air_kinematic_viscosity_data_matrix=[7 13.91;17 14.77;27 15.66;37
16.54;47 14.77];
%kinematic viscosity of air(mm^2/s) function of temp and pressure from
Cengel, Table A-7, p824
if store_count==1
    % use air temperature from adjacent upstream lump to get started

air_kinematic_viscosity_left=interp1(air_kinematic_viscosity_data_matr
ix(:,1),air_kinematic_viscosity_data_matrix(:,2),Ta_left(position_coun
t-1,store_count),'linear');

```

```

air_kinematic_viscosity_right=interp1(air_kinematic_viscosity_data_matrix(:,1),air_kinematic_viscosity_data_matrix(:,2),Ta_right(position_count-1,store_count),'linear');
    else

air_kinematic_viscosity_left=interp1(air_kinematic_viscosity_data_matrix(:,1),air_kinematic_viscosity_data_matrix(:,2),Ta_left(position_count,store_count-1),'linear');

air_kinematic_viscosity_right=interp1(air_kinematic_viscosity_data_matrix(:,1),air_kinematic_viscosity_data_matrix(:,2),Ta_right(position_count,store_count-1),'linear');
end

air_thermal_diffusivity_data_matrix=[-23 15.9;27 22.5;77 29.9];
% air thermal diffusivity (mm^2/s^2) function of temp from Incropera & DeWitt, Table A.4, pA15
if store_count==1

air_thermal_diffusivity_left=interp1(air_thermal_diffusivity_data_matrix(:,1),air_thermal_diffusivity_data_matrix(:,2),Ta_left(position_count-1,store_count),'linear');

air_thermal_diffusivity_right=interp1(air_thermal_diffusivity_data_matrix(:,1),air_thermal_diffusivity_data_matrix(:,2),Ta_right(position_count-1,store_count),'linear');
else

air_thermal_diffusivity_left=interp1(air_thermal_diffusivity_data_matrix(:,1),air_thermal_diffusivity_data_matrix(:,2),Ta_left(position_count,store_count-1),'linear');

air_thermal_diffusivity_right=interp1(air_thermal_diffusivity_data_matrix(:,1),air_thermal_diffusivity_data_matrix(:,2),Ta_right(position_count,store_count-1),'linear');
end

hfg_data_matrix=[10 2479;15 2466;20 2454;25 2442;30 2430;35 2418;39 2409];
%enthalpy of fusion (J/g) function of temp and pressure from Cengel, Table A-12a, p835
if store_count==1

hfg_left=interp1(hfg_data_matrix(:,1),hfg_data_matrix(:,2),Ta_left(position_count-1,store_count),'linear');

hfg_right=interp1(hfg_data_matrix(:,1),hfg_data_matrix(:,2),Ta_right(position_count-1,store_count),'linear');
else

hfg_left=interp1(hfg_data_matrix(:,1),hfg_data_matrix(:,2),Ta_left(position_count,store_count-1),'linear');

hfg_right=interp1(hfg_data_matrix(:,1),hfg_data_matrix(:,2),Ta_right(position_count,store_count-1),'linear');
end

%% Varying property values as function of mucosa temperature
specific_heat_capacity_water_data_matrix=[7 4.203;12 4.192;17 4.186;22 4.181;27 4.178;37 4.174;47 4.174];
%specific heat capacity of water (J/gK) function of temperature from Cengel, Table A.8, p830

```

```

if store_count==1

specific_heat_capacity_water_left=interp1(specific_heat_capacity_water_data_matrix(:,1),specific_heat_capacity_water_data_matrix(:,2),Tm_left(position_count-1,store_count),'linear');

specific_heat_capacity_water_right=interp1(specific_heat_capacity_water_data_matrix(:,1),specific_heat_capacity_water_data_matrix(:,2),Tm_right(position_count-1,store_count),'linear');
else

specific_heat_capacity_water_left=interp1(specific_heat_capacity_water_data_matrix(:,1),specific_heat_capacity_water_data_matrix(:,2),Tm_left(position_count,store_count-1),'linear');

specific_heat_capacity_water_right=interp1(specific_heat_capacity_water_data_matrix(:,1),specific_heat_capacity_water_data_matrix(:,2),Tm_right(position_count,store_count-1),'linear');
end

water_air_binary_diffusion_coefficient_data_matrix=[7 22.7;12 23.3;17 24.0;22 24.8;27 25.6;32 26.1;37 27.0;42 27.8];
%water/air binary diffusion coefficient (mm^2/s) as a function of temperature, Fig1, p E23-11.
if store_count==1

water_air_binary_diffusion_coefficient_left=interp1(water_air_binary_diffusion_coefficient_data_matrix(:,1),water_air_binary_diffusion_coefficient_data_matrix(:,2),Tm_left(position_count-1,store_count),'linear');

water_air_binary_diffusion_coefficient_right=interp1(water_air_binary_diffusion_coefficient_data_matrix(:,1),water_air_binary_diffusion_coefficient_data_matrix(:,2),Tm_right(position_count-1,store_count),'linear');
else

water_air_binary_diffusion_coefficient_left=interp1(water_air_binary_diffusion_coefficient_data_matrix(:,1),water_air_binary_diffusion_coefficient_data_matrix(:,2),Tm_left(position_count,store_count-1),'linear');

water_air_binary_diffusion_coefficient_right=interp1(water_air_binary_diffusion_coefficient_data_matrix(:,1),water_air_binary_diffusion_coefficient_data_matrix(:,2),Tm_right(position_count,store_count-1),'linear');
end

%% calculating next hydraulic diameters
hydraulic_diameter_left(position_count,1)=4*morphology_left(position_count,2)/morphology_left(position_count,3);
hydraulic_diameter_right(position_count,1)=4*morphology_right(position_count,2)/morphology_right(position_count,3);

%% calculating air velocities in lump

%%calculating air velocities for each nasal passageway and storing in matrices
air_velocity_left(position_count,store_count)=air_mass_flow_rate_left(:,store_count)/(density_air_left*(pi/4)*(hydraulic_diameter_left(position_count,1)^2));%morphology_left(position_count,2));

```

```

air_velocity_right(position_count,store_count)=air_mass_flow_rate_right(:,store_count)/(density_air_right*pi/4*hydraulic_diameter_right(position_count,1)^2);%morphology_right(position_count,2)); %

%% calculating reynolds numbers
reynolds_number_left(position_count,1)=air_velocity_left(position_count,store_count)*hydraulic_diameter_left(position_count,1)/air_kinematic_viscosity_left;
reynolds_number_right(position_count,1)=air_velocity_right(position_count,store_count)*hydraulic_diameter_right(position_count,1)/air_kinematic_viscosity_right;

%% calculating prandtl numbers
prandtl_number_left=air_kinematic_viscosity_left/air_thermal_diffusivity_left; % calculating prandtl number left
prandtl_number_right=air_kinematic_viscosity_right/air_thermal_diffusivity_right; % calculating prandtl number left

%% calculating nusselt numbers - earlier version
nusselt_number_left(position_count,1)=7.54+((0.03*(hydraulic_diameter_left(position_count,1)/slice_thickness)*reynolds_number_left(position_count,1)*prandtl_number_left)/(1+0.016*((hydraulic_diameter_left(position_count,1)/slice_thickness)*reynolds_number_left(position_count,1)*prandtl_number_left)^(2/3)));
nusselt_number_right(position_count,1)=7.54+((0.03*(hydraulic_diameter_right(position_count,1)/slice_thickness)*reynolds_number_right(position_count,1)*prandtl_number_right)/(1+0.016*((hydraulic_diameter_right(position_count,1)/slice_thickness)*reynolds_number_right(position_count,1)*prandtl_number_right)^(2/3)));

%% computing convective heat transfer coefficients (hc)
hc_left(position_count,1)=nusselt_number_left(position_count,1)*air_thermal_conductivity_coefficient_left/slice_thickness; % first calculation of left side heat convection coefficient (w/cm^2.K)
hc_right(position_count,1)=nusselt_number_right(position_count,1)*air_thermal_conductivity_coefficient_right/slice_thickness; % first calculation of right side heat convection coefficient (w/cm^2.K)

%% Calculating mass transfer coefficient
%% Calculating mass transfer coefficient
lewis_number_left=air_thermal_diffusivity_left/water_air_binary_diffusion_coefficient_left; %Lewis number
lewis_number_right=air_thermal_diffusivity_right/water_air_binary_diffusion_coefficient_right; %Lewis number

hm_left(position_count,1)=hc_left(position_count,1)/(density_air_left*specific_heat_capacity_air_left*(lewis_number_left)^(2/3));
%convective mass transfer coefficient as a function of heat transfer coefficient.
hm_right(position_count,1)=hc_right(position_count,1)/(density_air_right*specific_heat_capacity_air_right*(lewis_number_right)^(2/3));
%convective mass transfer coefficient as a function of heat transfer coefficient.

%% compute next Ta and Ca values for next position using Ca Cm Ta Tm & N values from previous position
Ca_left(position_count,store_count)=Ca_left(position_count-1,store_count)+hm_left(position_count-1,1)/hydraulic_diameter_left(position_count-1,1)*(Cm_left(position_count-1,store_count)-Ca_left(position_count-1,store_count))*slice_thickness/air_velocity_left(position_count-1,store_count);

```

```

Ca_right(position_count,store_count)=Ca_right(position_count-
1,store_count)+hm_right(position_count-
1,1)/hydraulic_diameter_right(position_count-
1,1)*(Cm_right(position_count-1,store_count)-Ca_right(position_count-
1,store_count))*slice_thickness/air_velocity_right(position_count-
1,store_count);

Ta_left(position_count,store_count)=Ta_left(position_count-
1,store_count)+slice_thickness/(air_velocity_left(position_count-
1,store_count)*hydraulic_diameter_left(position_count-
1,1)*density_air_left*specific_heat_capacity_air_left)*(hc_left(positi
on_count-1,1)*(Tm_left(position_count-1,store_count)-
Ta_left(position_count-
1,store_count))+specific_heat_capacity_water_left*water_molar_mass*N_l
eft(position_count-1,store_count)*(Tm_left(position_count-
1,store_count)-Ta_left(position_count-1,store_count)));
Ta_right(position_count,store_count)=Ta_right(position_count-
1,store_count)+slice_thickness/(air_velocity_right(position_count-
1,store_count)*hydraulic_diameter_right(position_count-
1,1)*density_air_right*specific_heat_capacity_air_right)*(hc_right(pos
ition_count-1,1)*(Tm_right(position_count-1,store_count)-
Ta_right(position_count-
1,store_count))+specific_heat_capacity_water_right*water_molar_mass*N_
right(position_count-1,store_count)*(Tm_right(position_count-
1,store_count)-Ta_right(position_count-1,store_count)));

%% calculating gradient and y-intercept for linear approximation of Cm
based on Tm for left airway
% pre-allocating matrix for speed.
Cm=zeros(1,8);
density_air=zeros(1,8);

for temp=28:1:36; % span mucosal temperature from 28-36 degrees C

saturation_vapour_pressure=(10^(-7.90298*(373.16/(temp+273))-
1)+5.02808*log10(373.16/(temp+273))-1.3816*1e-7*(10^(11.344*(1-
(temp+273)/373.16))-1)+8.1328*1e-3*(10^(-3.49149*(373.16/(temp+273))-
1))-1)+log10(1013.246))*100;
% Goff-Gratch Equation is used to calculate water partial pressure.

% calculate humidity ratio
mucosa_humidity_ratio=(0.622*saturation_vapour_pressure)/(total_pressu
re-saturation_vapour_pressure);

density_air(1,temp-
27)=interp1(density_air_data_matrix(:,1),density_air_data_matrix(:,2),
temp,'linear');

% Cm temperate data
Cm(1,temp-27)=temp;

% calculation of mask air water species concentration in mol/mm^3
Cm(2,temp-27)=mucosa_humidity_ratio*density_air(1,temp-27)/18;

end
% determine gradient and slope
P = polyfit(Cm(1,:),Cm(2,:),1);

% assign values
Cm_gradient=P(1,1);
Cm_intercept=P(1,2);

```

```

%% Compute left Cm Tm & N values for next position using Ta & Ca
values for this position
% initial calculation for change in mucosa parameters
    A=[0 (Kt/mucosa_thickness+hc_left(position_count,1))
(water_molar_mass*hfg_left);hm_left(position_count,1) 0 -1;1 -
1*Cm_gradient 0];

b=[((Kt/mucosa_thickness)*Tb+(hc_left(position_count,1)*Ta_left(positi
on_count,store_count)));
(hm_left(position_count,1)*Ca_left(position_count,store_count));
Cm_intercept];
    x=(A\b).';
    N_left(position_count,store_count) = x(1,3); % assigning
initial value for N_left

switch store_count; % for first iteration need to use initial start
value of asl water mass mean

    case 1 % test for insufficient ASL water mass to meet total
demand
        if
N_left(position_count,store_count)>asl_water_mass_left(position_count,
store_count)/(morphology_left(position_count,3)*slice_thickness*water_
molar_mass*time_step);
            N_left(position_count,store_count)
=asl_water_mass_left(position_count,store_count)/(morphology_left(posi
tion_count,3)*slice_thickness*water_molar_mass*time_step);%+cellular_w
ater_mass_efflux_left(position_count,1)-
asl_water_mass_backflux_left(position_count,1);

Tm_left(position_count,store_count)=((Kt/mucosa_thickness)*Tb+hc_left(
position_count,1)*Ta_left(position_count,store_count)-
water_molar_mass*N_left(position_count,store_count)*hfg_left)/(Kt/muco
sa_thickness+hc_left(position_count,1));
            Cm_left(position_count,store_count)=
Ca_left(position_count,store_count)+N_left(position_count,store_count)
/hm_left(position_count,1);

            else % where sufficient asl water mass is present on mucosa
                Cm_left(position_count,store_count)= x(1,1); % assigning
initial value for Cm_left
                Tm_left(position_count,store_count)= x(1,2); % assigning
initial value for Tm_left
                %N_left(position_count,store_count) = x(1,3); % assigning
initial value for N_left
            end

        otherwise % for subsequent iteration use previous asl water mass

            % initial calculation for change in mucosa parameters
            %
            A=[0 (Kt/mucosa_thickness+hc_left(position_count,1))
(water_molar_mass*hfg_left);hm_left(position_count,1) 0 -1;1 -0.1148e-
9 0];
            %
b=[((Kt/mucosa_thickness)*Tb+(hc_left(position_count,1)*Ta_left(positi
on_count,store_count)));
(hm_left(position_count,1)*Ca_left(position_count,store_count)); -
1.7306e-9];
            %
            x=(A\b).';
            %
            N_left(position_count,store_count) = x(1,3); % assigning
initial value for N_left

```

```

        % test for insufficient ASL water mass to meet total demand
        if
N_left(position_count,store_count)>(asl_water_mass_left(position_count
,store_count-
1)+cellular_water_mass_efflux_left(position_count,store_count-1)-
asl_water_mass_backflux_left(position_count,1))/(morphology_left(positi
on_count,3)*slice_thickness*water_molar_mass*time_step);
            N_left(position_count,store_count) =
(asl_water_mass_left(position_count,store_count-
1)+cellular_water_mass_efflux_left(position_count,store_count-1)-
asl_water_mass_backflux_left(position_count,1))/(morphology_left(positi
on_count,3)*slice_thickness*water_molar_mass*time_step);%+cellular_wa
ter_mass_efflux_left(position_count,1)-
asl_water_mass_backflux_left(position_count,1);

Tm_left(position_count,store_count)=( (Kt/mucosa_thickness)*Tb+hc_left(
position_count,1)*Ta_left(position_count,store_count)-
water_molar_mass*N_left(position_count,store_count)*hfg_left)/(Kt/muco
sa_thickness+hc_left(position_count,1));
            Cm_left(position_count,store_count)=
Ca_left(position_count,store_count)+N_left(position_count,store_count)
/hm_left(position_count,1);

        else % where sufficient asl water mass is present on mucosa
            Cm_left(position_count,store_count)= x(1,1); % assigning
initial value for Cm_left
            Tm_left(position_count,store_count)= x(1,2); % assigning
initial value for Tm_left
            %N_left(position_count,store_count) = x(1,3); % assigning
initial value for N_left
        end

end

%% Compute right Cm Tm & N values for next position using Ta & Ca
values for next position

% initial calculation for change in mucosa parameters
A=[0 (Kt/mucosa_thickness+hc_right(position_count,1))
(water_molar_mass*hfg_right);hm_right(position_count,1) 0 -1;1 -
1*Cm_gradient 0];

b=[((Kt/mucosa_thickness)*Tb+(hc_right(position_count,1)*Ta_right(posi
tion_count,store_count)));
(hm_right(position_count,1)*Ca_right(position_count,store_count));
Cm_intercept];
y=(A\b).';
            N_right(position_count,store_count) = y(1,3); % assigning
initial value for N_right

switch store_count; % for first iteration need to use initial start
value of asl water mass mean
    case 1 % test for insufficient ASL water mass to meet total
demand
        if
N_right(position_count,store_count)>asl_water_mass_right(position_coun
t,store_count)/(morphology_right(position_count,3)*slice_thickness*wat
er_molar_mass*time_step);
            N_right(position_count,store_count) =
asl_water_mass_right(position_count,store_count)/(morphology_right(pos
ition_count,3)*slice_thickness*water_molar_mass*time_step);

```

```

Tm_right(position_count,store_count)=( (Kt/mucosa_thickness)*Tb+hc_right
t(position_count,1)*Ta_right(position_count,store_count)-
water_molar_mass*N_right(position_count,store_count)*hfg_right)/(Kt/mu
cosa_thickness+hc_right(position_count,1));
    Cm_right(position_count,store_count)=
Ca_right(position_count,store_count)+N_right(position_count,store_coun
t)/hm_right(position_count,1);

        else % where sufficient asl water mass is present on mucosa
            Cm_right(position_count,store_count)= y(1,1); % assigning
initial value for Cm_right
            Tm_right(position_count,store_count)= y(1,2); % assigning
initial value for Tm_right
            %N_right(position_count,store_count) = y(1,3); % assigning
initial value for N_right
        end

        otherwise % for subsequent iteration use previous asl water mass

            % test for insufficient ASL water mass to meet total demand
            if
N_right(position_count,store_count)>(asl_water_mass_right(position_cou
nt,store_count-
1)+cellular_water_mass_efflux_right(position_count,store_count-1)-
asl_water_mass_backflux_right(position_count,1))/(morphology_right(pos
ition_count,3)*slice_thickness*water_molar_mass*time_step);
                N_right(position_count,store_count) =
(asl_water_mass_right(position_count,store_count-
1)+cellular_water_mass_efflux_right(position_count,store_count-1)-
asl_water_mass_backflux_right(position_count,1))/(morphology_right(pos
ition_count,3)*slice_thickness*water_molar_mass*time_step);

Tm_right(position_count,store_count)=( (Kt/mucosa_thickness)*Tb+hc_right
t(position_count,1)*Ta_right(position_count,store_count)-
water_molar_mass*N_right(position_count,store_count)*hfg_right)/(Kt/mu
cosa_thickness+hc_right(position_count,1));
            Cm_right(position_count,store_count)=
Ca_right(position_count,store_count)+N_right(position_count,store_coun
t)/hm_right(position_count,1);

            else % where sufficient asl water mass is present on mucosa
                Cm_right(position_count,store_count)= y(1,1); % assigning
initial value for Cm_right
                Tm_right(position_count,store_count)= y(1,2); % assigning
initial value for Tm_right
                %N_right(position_count,store_count) = y(1,3); % assigning
initial value for N_right
            end

        end

%% calculate heat flux (Q) based on summing convective and latent heat
fluxes.
Q_left(position_count,store_count)=(hc_left(position_count,1)*(Tm_left
(position_count,store_count)-
Ta_left(position_count,store_count))+N_left(position_count,store_count
)*water_molar_mass*hfg_left)*morphology_left(position_count,3)*slice_t
hickness;
Q_right(position_count,store_count)=(hc_right(position_count,1)*(Tm_righ
t(position_count,store_count)-
Ta_right(position_count,store_count))+N_right(position_count,store_cou

```

```

nt)*water_molar_mass*hfg_right)*morphology_right(position_count,3)*slice_thickness;

%% calculate air absolute humidity and form storage matrix

% calculating new air ah based on water molar flux (N)
air_ah_right(position_count,store_count)=
Ca_right(position_count,store_count)*water_molar_mass/1e-
9;%air_ah_right(position_count-
1,store_count)+(N_right(position_count,store_count)*water_molar_mass*m
orphology_right(position_count,3)*slice_thickness*time_step)/(morphology
gy_right(position_count,2)*slice_thickness*1e-6);
air_ah_left(position_count,store_count)=Ca_left(position_count,store_c
ount)*water_molar_mass/1e-9;%air_ah_left(position_count-
1,store_count)+(N_left(position_count,store_count)*water_molar_mass*mo
rphology_left(position_count,3)*slice_thickness*time_step)/(morphology
_left(position_count,2)*slice_thickness*1e-6);

end

```

## A11 Phase Corrector

*Phase Corrector* returns the data matrices to their original order sequence if they have been reconfigured to account for the exhalation breath phase.

```

%% M File created by D White 31st January 2012
function
[asl_water_mass_flux_left,asl_water_mass_flux_right,morphology_left,mo
rphology_right,phase,Ca_left,Ca_right,Cm_left,Cm_right,Ta_left,Ta_righ
t,Tm_left,Tm_right,N_left,N_right,Q_left,Q_right,air_ah_left,air_ah_rig
ht,asl_water_mass_left,asl_water_mass_right,asl_water_mass_max_left,a
sl_water_mass_max_right,asl_water_mass_min_left,asl_water_mass_min_rig
ht,cellular_water_mass_efflux_max_left,cellular_water_mass_efflux_max_
right]=phase_corrector(morphology_left,morphology_right,phase,Ca_left,
Ca_right,Cm_left,Cm_right,Ta_left,Ta_right,Tm_left,Tm_right,N_left,N_r
ight,Q_left,Q_right,air_ah_left,air_ah_right,asl_water_mass_left,asl_w
ater_mass_right,asl_water_mass_max_left,asl_water_mass_max_right,asl_w
ater_mass_min_left,asl_water_mass_min_right,cellular_water_mass_efflux
_max_left,cellular_water_mass_efflux_max_right,asl_water_mass_flux_lef
t,asl_water_mass_flux_right)
%phase_corrector detects exhalation cycle and corrects order of left
and right morphology matrices
%%Input arguments:
%morphology_left.
%morphology_right.
%Output Arguments:
%morphology_left
%morphology_right.

if strcmp(phase,'exhale'); %sensing for exhale cycle having being
calculated

```

```

        morphology_right=flipud(morphology_right); %flip morphology_right
matrix from upsidedown to correct order
        morphology_left=flipud(morphology_left); %flip morphology_left
matrix from upsidedown to correct order
        Ca_left=flipud(Ca_left);
        Ca_right=flipud(Ca_right);
        Cm_left=flipud(Cm_left);
        Cm_right=flipud(Cm_right);
        Ta_right=flipud(Ta_right);
        Ta_left=flipud(Ta_left);
        Tm_left=flipud(Tm_left);
        Tm_right=flipud(Tm_right);
        N_left=flipud(N_left);
        N_right=flipud(N_right);
        Q_left=flipud(Q_left);
        Q_right=flipud(Q_right);
        air_ah_left=flipud(air_ah_left);
        air_ah_right=flipud(air_ah_right);
        asl_water_mass_left=flipud(asl_water_mass_left);
        asl_water_mass_right=flipud(asl_water_mass_right);
        asl_water_mass_max_left=flipud(asl_water_mass_max_left);
        asl_water_mass_max_right=flipud(asl_water_mass_max_right);
        asl_water_mass_min_left=flipud(asl_water_mass_min_left);
        asl_water_mass_min_right=flipud(asl_water_mass_min_right);
        asl_water_mass_flux_left=flipud(asl_water_mass_flux_left);
        asl_water_mass_flux_right=flipud(asl_water_mass_flux_right);

end

```

## A12 Water Regulation

*Water Regulation* calculates the new water equivalent mass in each model lump. This is based on the water equivalent top-up that is calculated from the difference between the water lost to or recovered from the air, water lost by tissue water reabsorption and the tissue water supply. Both reabsorption and supply are limited to a maximal amount, as discussed in Chapter 2. Calculation of water equivalent mass is undertaken along the whole length of both airways for each air-mass-flow rate within the breath file..

```

%% M File created by D White 26th January 2012
function
[asl_height_left,asl_height_right,cellular_water_mass_efflux_left,cell
ular_water_mass_efflux_right,asl_water_mass_flux_left,asl_water_mass_f
lux_right,asl_water_mass_left,asl_water_mass_right]=water_regulation(c
ellular_water_mass_efflux_left,cellular_water_mass_efflux_right,slice_
thickness,morphology_left,morphology_right,N_left,N_right,asl_water_ma
ss_left,asl_water_mass_right,cellular_water_mass_efflux_max_left,cellu
lar_water_mass_efflux_max_right,store_count,time_step,asl_water_mass_f
lux_left,asl_water_mass_flux_right,asl_water_mass_mean_left,asl_water_
mass_mean_right,density_water,asl_height_left,asl_height_right,asl_wat
er_mass_backflux_left,asl_water_mass_backflux_right)

%start_condition assigns initial values of Ca, Ta, Cm, Tm & N based
on phase of breathing cycle

```

```



```

```

asl_water_mass_flux_left(position_count,store_count)-
asl_water_mass_backflux_left(position_count,1);
% subsequent iterations
end

    %% for left airway - equating one of three conditions and actions
    based on asl mass status

    if
interim_asl_water_mass_left(position_count,1)<asl_water_mass_mean_left(
position_count,1)
    % asl water mass below minimum value
    asl_water_left='low'; %requires water
    elseif
interim_asl_water_mass_left(position_count,1)>asl_water_mass_max_left(
position_count,1)
    %asl water mass above maximum value
    asl_water_left='over'; %over full
    else
    asl_water_left='within'; %within limits;
    % asl water mass within limits
    end

switch asl_water_left % taking action based on asl water mass levels

    %***** asl requires water top
up*****

    case {'low'} %requires water;

    % calculating cellular water mass efflux based on asl water mass
    status

desired_cellular_water_mass_efflux_left(position_count,1)=asl_water_ma
ss_mean_left(position_count,1)-
interim_asl_water_mass_left(position_count,1);

% testing for efflux supply level
    if
desired_cellular_water_mass_efflux_left(position_count,1)<=cellular_wa
ter_mass_efflux_max_left(position_count,1)
    % efflux demand is less than cellular supply

cellular_water_mass_efflux_left(position_count,store_count)=desired_ce
llular_water_mass_efflux_left(position_count,1);
    else % where efflux level exceeds cellular supply

cellular_water_mass_efflux_left(position_count,store_count)=cellular_w
ater_mass_efflux_max_left(position_count,1);
    end

    % applying mass continuity across asl
    if store_count==1 % first iteration

asl_water_mass_left(position_count,store_count)=asl_water_mass_left(po
sition_count,store_count)+cellular_water_mass_efflux_left(position_cou
nt,store_count)-asl_water_mass_flux_left(position_count,store_count)-
asl_water_mass_backflux_left(position_count,1);

```

```

        else % subsequent itterations

asl_water_mass_left(position_count,store_count)=asl_water_mass_left(po
sition_count,store_count-
1)+cellular_water_mass_efflux_left(position_count,store_count)-
asl_water_mass_flux_left(position_count,store_count)-
asl_water_mass_backflux_left(position_count,1);
        end
        % ensuring no negative asl water mass
        if
asl_water_mass_left(position_count,store_count)<0;%asl_water_mass_min_
left(position_count,1)
                asl_water_mass_left(position_count,store_count)=0;
        end

%***** asl over full
%*****
        %case {'over'} %over full;

        % calculating cellular water mass return efflux based on asl
water mass status

%desired_cellular_water_mass_efflux_left(position_count,1)=asl_water_m
ass_max_left(position_count,1)-
interim_asl_water_mass_left(position_count,1);
        % negative desired efflux value

%cellular_water_mass_efflux_left(position_count,store_count)=0;%desire
d_cellular_water_mass_efflux_left(position_count,1);
        % copying over negative efflux

        %if store_count==1 % first itteration

%asl_water_mass_left(position_count,store_count)=asl_water_mass_max_le
ft(position_count,1)+cellular_water_mass_efflux_left(position_count,st
ore_count)-asl_water_mass_flux_left(position_count,1);
        %else % subsequent itterations

%asl_water_mass_left(position_count,store_count)=asl_water_mass_max_le
ft(position_count,1)+cellular_water_mass_efflux_left(position_count,st
ore_count)-asl_water_mass_flux_left(position_count,1);
        %end
        % ensuring no negative asl water mass
        %if
asl_water_mass_left(position_count,store_count)<0;%asl_water_mass_min_
left(position_count,1)
                %asl_water_mass_left(position_count,store_count)=0;
        %end

% ***** asl between limits
%*****
        case {'within'} %within limits;
                cellular_water_mass_efflux_left(position_count,store_count)=0;
                if store_count==1 % first itteration

asl_water_mass_left(position_count,store_count)=asl_water_mass_left(po
sition_count,store_count)-
asl_water_mass_flux_left(position_count,store_count)-
asl_water_mass_backflux_left(position_count,1)+cellular_water_mass_eff
lux_left(position_count,store_count);
                else % subsequent itterations

```

```

asl_water_mass_left(position_count,store_count)=asl_water_mass_left(po
sition_count,store_count-1)-
asl_water_mass_flux_left(position_count,store_count)-
asl_water_mass_backflux_left(position_count,1)+cellular_water_mass_eff
lux_left(position_count,store_count);
    end

    % ensuring no negative asl water mass
    if asl_water_mass_left(position_count,store_count)<0
%asl_water_mass_min_left(position_count,1)
        asl_water_mass_left(position_count,store_count)=0;
    end
end % finish switch based on asl height

%% Calculating asl height based on asl mass
asl_height_left(position_count,store_count)=asl_water_mass_left(positi
on_count,store_count)/(density_water*morphology_left(position_count,3)
*slice_thickness);

%% RIGHT AIRWAY

% recalculating asl water mass based on water mass flux and asl water
mass
% back-flux
if store_count==1 % first itteration

interim_asl_water_mass_right(position_count,1)=asl_water_mass_right(po
sition_count,store_count)-
asl_water_mass_flux_right(position_count,store_count)-
asl_water_mass_backflux_right(position_count,1);
else
interim_asl_water_mass_right(position_count,1)=asl_water_mass_right(po
sition_count,store_count-1)-
asl_water_mass_flux_right(position_count,store_count)-
asl_water_mass_backflux_right(position_count,1);
% subsequent itterations
end

    %% for right airway - equating one of three conditions and actions
based on asl mass status

    if
interim_asl_water_mass_right(position_count,1)<asl_water_mass_mean_rig
ht(position_count,1)
        % asl water mass below minium value
        asl_water_right='low'; %requires water
    elseif
interim_asl_water_mass_right(position_count,1)>asl_water_mass_max_righ
t(position_count,1)
        % asl water mass above maximum value
        asl_water_right='over'; %over full
    else
        asl_water_right='within'; %within limits;
    % asl water mass within limits
    end

switch asl_water_right % taking action based on asl water mass levels

```

```

%***** asl requires water top
up*****

    case {'low'} %requires water;

    % calculating cellular water mass efflux based on asl water mass
    status

    desired_cellular_water_mass_efflux_right(position_count,1)=asl_water_m
    ass_mean_right(position_count,1)-
    interim_asl_water_mass_right(position_count,1);

    % testing for efflux supply level
    if
    desired_cellular_water_mass_efflux_right(position_count,1)<=cellular_w
    ater_mass_efflux_max_right(position_count,1)
        % efflux demand is less then cellular supply

    cellular_water_mass_efflux_right(position_count,store_count)=desired_c
    ellular_water_mass_efflux_right(position_count,1);
        else % where efflux level exceeds cellular supply

    cellular_water_mass_efflux_right(position_count,store_count)=cellular_
    water_mass_efflux_max_right(position_count,1);
        end

        % applying mass continuity across asl
        if store_count==1 % first itteration

    asl_water_mass_right(position_count,store_count)=asl_water_mass_right(
    position_count,store_count)+cellular_water_mass_efflux_right(position_
    count,store_count)-
    asl_water_mass_flux_right(position_count,store_count)-
    asl_water_mass_backflux_right(position_count,1);
        else % subsequent itterations

    asl_water_mass_right(position_count,store_count)=asl_water_mass_right(
    position_count,store_count-
    1)+cellular_water_mass_efflux_right(position_count,store_count)-
    asl_water_mass_flux_right(position_count,store_count)-
    asl_water_mass_backflux_right(position_count,1);
        end
        % ensuring no negative asl water mass
        if
    asl_water_mass_right(position_count,store_count)<0;%asl_water_mass_min
    _right(position_count,1)
            asl_water_mass_right(position_count,store_count)=0;
        end
%***** asl over full
*****
    %case {'over'} %over full;

    % calculating cellular water mass return efflux based on asl
    water mass status

    %desired_cellular_water_mass_efflux_right(position_count,1)=asl_water_
    mass_max_right(position_count,1)-
    interim_asl_water_mass_right(position_count,1);
        % negative desired efflux value
        %cellular_water_mass_efflux_right(position_count,store_count)=
    0;%desired_cellular_water_mass_efflux_right(position_count,1);
        % copying over negative efflux

```

```

        %if store_count==1 % first itteration

%asl_water_mass_right(position_count,store_count)=asl_water_mass_max_r
ight(position_count,1)+cellular_water_mass_efflux_right(position_count
,store_count)-asl_water_mass_flux_right(position_count,1);
        %else % subsequent itterations

%asl_water_mass_right(position_count,store_count)=asl_water_mass_max_r
ight(position_count,1)+cellular_water_mass_efflux_right(position_count
,store_count)-asl_water_mass_flux_right(position_count,1);
        %end
        % ensuring no negative asl water mass
        %if
asl_water_mass_right(position_count,store_count)<0;%asl_water_mass_min
_right(position_count,1)
                %asl_water_mass_right(position_count,store_count)=0;
        %end
% ***** asl between limits
% *****
        case {'within'} %within limits;

cellular_water_mass_efflux_right(position_count,store_count)=0;
        if store_count==1 % first itteration

asl_water_mass_right(position_count,store_count)=asl_water_mass_right(
position_count,store_count)-
asl_water_mass_flux_right(position_count,store_count)-
asl_water_mass_backflux_right(position_count,1)+cellular_water_mass_ef
flux_right(position_count,store_count);
                else % subsequent itterations

asl_water_mass_right(position_count,store_count)=asl_water_mass_right(
position_count,store_count-1)-
asl_water_mass_flux_right(position_count,store_count)-
asl_water_mass_backflux_right(position_count,1)+cellular_water_mass_ef
flux_right(position_count,store_count);
                end

        % ensuring no negative asl water mass
        if
asl_water_mass_right(position_count,store_count)<0;%asl_water_mass_min
_right(position_count,1)
                asl_water_mass_right(position_count,store_count)=0;
        end

end % finish switch based on asl height

%% Calculating asl height based on asl mass
asl_height_right(position_count,store_count)=asl_water_mass_right(posi
tion_count,store_count)/(density_water*morphology_right(position_count
,3)*slice_thickness);

end

end

```

## APPENDIX B MORPHOLOGICAL RESPONSE TO N-PAP BREATHING

### B1 Experimental Protocol and Equipment

Supplementary information pertaining to the MRI investigation into air-pressure elicited change in nasal geometry during n-PAP breathing is contained within this appendix.

#### B1.1 Participant Recruitment

Posters were located around the University campus inviting participants to contact the Research Manager. Participant Information Sheet was sent to non-smoking respondents who, if wishing to proceed, had a meeting with the Research Manager to discuss the project in detail and ask questions. During this meeting the Demographic, Consent and Centre for Advance MRI (CAMRI) Safety and Consent and Confidentiality Agreement forms were completed and signed. Copies of these forms can be found in Appendix B2. Participants then undertook a visual nasal internal examination by ENT specialist, Dr Jim Bartley, to screen out those with morphological abnormalities, such as displaying a significantly displaced septum, mucosa inflammation or other nasal pathological conditions. The range of age, gender, ethnic diversity and number of participants, shown in Table B1.1, was limited by the respondents volunteering to participate and also research funding available. Given these constraints, eight participants were selected for MRI scanning from the eligible participants on the basis of achieving as broad a distribution of age, ethnicity and gender possible.

**TableB1.1: Distribution of Participant Details**

Age	Gender	Ethnicity
22	Male	Asian
21	Male	Indian
53	Female	European
30	Male	European
29	Male	Middle Eastern
35	Female	Asian
33	Female	South American
26	Female	European

After receiving ethical approval; eight healthy participants, ages ranging from 18 to 56 years of mixed gender and ethnicity, undertook head MRI scans during the nasal breathing of ambient then augmented air pressure delivered by a commercially available continuous positive pressure (CPAP) device.

### **B1.2 Participant Preparation**

All participants were not receiving any form of medicine, had not consumed food or drink 2 hours or alcohol 24 hours prior to undertaking the scan.

Standard preparation and safety procedures for MRI scanning were followed. Essentially these involved the participant removing footwear, all jewelry, watches and any other metallic items along with all external clothing before dressing in a gown.

### **B1.3 Measurement of nasal cycle**

The status of the nasal cycle was determined by comparing the simultaneous maximal voluntary ventilation (MVV) of each nare. Measurement was performed by two 'EasyOne' electronic spirometers, each modified by removal of the spirtette mouthpiece section to enable the fitting of a plastic conic adaptor shaped to seal around one nare, shown in Figure B1.1.

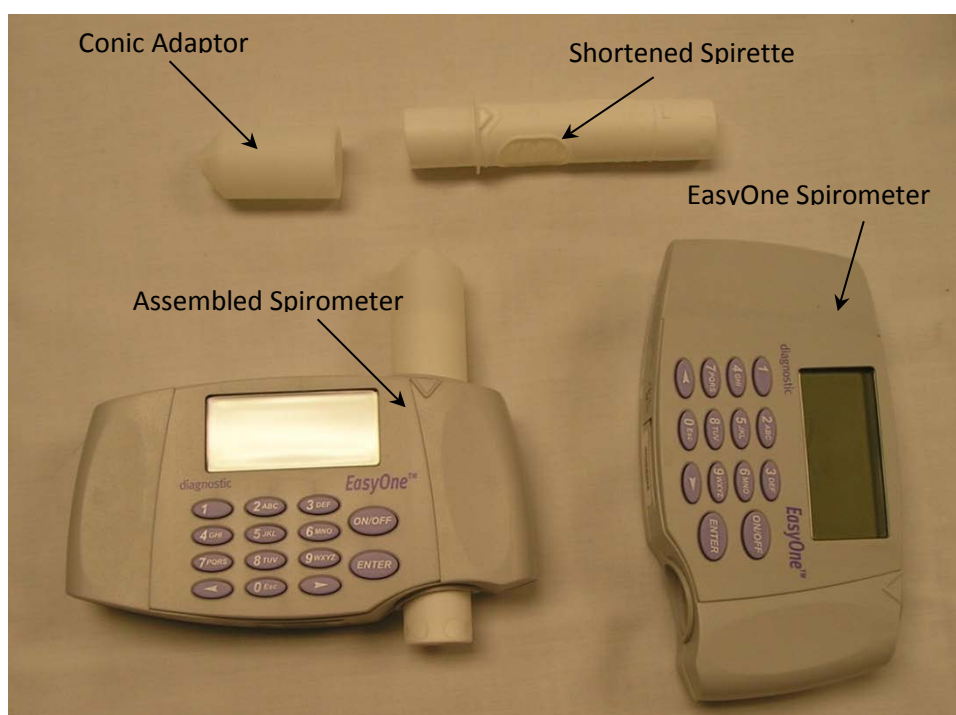


**Figure B1.1: 'EasyOne' Spirometer with modified spirtette.**



**Figure B1.2: ‘EasyOne’ Electronic Spirometers adapted for independent nare airflow measurement.**

With both of the two spirometers configured to record MVV, each conic spirette adaptor was firmly engaged into the nare, shown by Figure B1.2, to form an air-tight seal. The participant then undertook at least three breath cycles through the nose whilst MVV for each nare was then recorded.

Nasal Airflow measurement was repeated upon completion of the MRI scanning sequences to ascertain if there had been any change in nasal cycle during the scanning period.

#### **B1.4 MRI Scanning**

Upon completion of the pre-scan nasal airflow test, the participant entered the MRI scanning room where the CPAP nasal mask was fitted before assuming the recumbent position on the MRI table. All volunteers were studied using head array coil in a 3-Tesla scanner (Siemens Magnetom Skyra). The participant’s head was firmly positioned through the use of foam wedges before the head coil was locked into position, shown by Figure B1.3.



**Figure B1.3: Participant wearing CPAP nasal mask in recumbent position within Siemens 'Skyra' 3-Tesla MRI scanner with head coil fitted.**

Each participant was initially given 10 minutes to settle into the MRI scanner environment before scanning commenced. MRI image acquisition occurred in two phases, the first being whilst the participant spontaneously breathed ambient air within the MRI scan room, air-conditioned to be with the range of  $23 \pm 0.5$  °C and 50% RH. Here each participant was wearing a nasal mask (Fisher & Paykel Healthcare, Zest Plus) but the air supply hose was not connected so they breathed ambient air. Under these conditions two scan sequences were undertaken, the first to acquire morphological image data and the second ASL image data.

Upon completion of the first image acquisition phase the air supply hose was connected to the nasal mask and the participant commenced breathing augmented pressure air supplied from a commercially available CPAP air supply unit (Fisher & Paykel Healthcare, HC232 'Sleepstyle'). This unit was located outside the RF screened scan room to avoid interference with the MRI scanner but was open to the same air-conditioning regulation as the MRI scan room. The air supply hose passed through a wall gland fitting, shown by Figure B1.4, which is normally used for delivery of anesthetic or other types of breathing gas.



**Figure B1.4: Fisher & Paykel HC 232 ‘Sleep Style’ CPAP air supply unit located external to MRI scanning suite.**

For both patient comfort and to eliminate any transient physiological response, the CPAP air supply unit was pre-set to gradually increase pressure so that it took 20 minutes to achieve the desired nasal mask pressure. During this time period the participant remained relaxed in the recumbent position within the MRI scanner and supplementary humidification was not supplied to the pressurised airstream. Upon completion of this settling period, the second phase of image acquisition was undertaken. Here the two scan sequences of acquisition of morphological image data and ASL image data were repeated using the same imaging parameters. All MRI sequences acquired image data for the entire head between the ears and neck.

Upon completion of all image acquisition sequences the head coil was removed before the participant sat up, had the nasal mask removed and undertook a second nasal airflow measurement test.

### **B1.5 Air Pressure Protocol**

Most applications of breathing therapy, either through delivery of anesthetic, ventilation or by CPAP, typically range from 6 cm H<sub>2</sub>O up to a maximum of 20 cm H<sub>2</sub>O.

**Table B1.2: Distribution of Participant Breathing Pressure.**

<b>Pressure (cm H<sub>2</sub>O )</b>	<b>Male Participant Number</b>	<b>Female Participant Number</b>
15	108	115
12	107	109
9	101	106
6	104	118

Prescribed pressure depends upon many patient related variables so it is desirable to test a range of pressures representative of those commonly experienced during therapy, typically from 6 to 15 cm H<sub>2</sub>O. Being limited to eight participants, and given the desire to have two participants at each pressure increment, it was decided to randomly allocate one male and one female to pressure settings ranging from 6 to 15 cm H<sub>2</sub>O in steps of 3 cm H<sub>2</sub>O.

#### **B1.6 Nasal Airflow Results**

All participants demonstrated a clear bias in nasal airflow, with no change in this condition occurring throughout the duration of the MRI scanning trial. Results are shown in Table B1.3.

Given this result, it is assumed that there was no change in the phase of the nasal cycle and hence no variation in nasal blood flow regulating nasal volumes. These results do not, however, suggest that there was no change in capillary blood flows due to other factors that may influence heating and fluid supply to the nasal mucosa.

**Table B1.3: Distribution of Participant Nasal Airflow Details**

<b>Participant</b>	<b>Pre-Test MVV (litres/min)</b>		<b>Post-Test MVV (litres/min)</b>		<b>Patent Nasal Passage</b>	<b>Change in Nasal Cycle</b>
	<b>Right Nare</b>	<b>Left Nare</b>	<b>Right Nare</b>	<b>Left Nare</b>		
101	not detected	<b>10.3</b>	not detected	<b>12.6</b>	Left	No
104	<b>9.8</b>	8.9	<b>8.6</b>	6.8	Right	No
106	<b>11.4</b>	10.5	<b>11.1</b>	Not detected	Right	No
107	4.6	<b>8.0</b>	6.3	<b>6.7</b>	Left	No
108	8.1	<b>8.5</b>	11.6	<b>13.5</b>	Left	No
109	<b>6.9</b>	5.7	<b>7.8</b>	7.1	Right	No
115	not detected	<b>13.5</b>	not detected	<b>6.5</b>	Left	No
118	<b>9.5</b>	7.4	<b>8.2</b>	7.7	Right	No

**B1.7 Region of Interest**

All analysis of nasal physiological parameters was undertaken for the region bounded by the anterior portion of the nasal valve to the posterior choanae, shown in Figure B1.5. Not only does this region undertake the majority of nasal air-conditioning through supply and recovery of heat and moisture recovery during nasal breathing but also the bifurcated portion of the upper airway which contains the majority of active nasal erectile tissue.

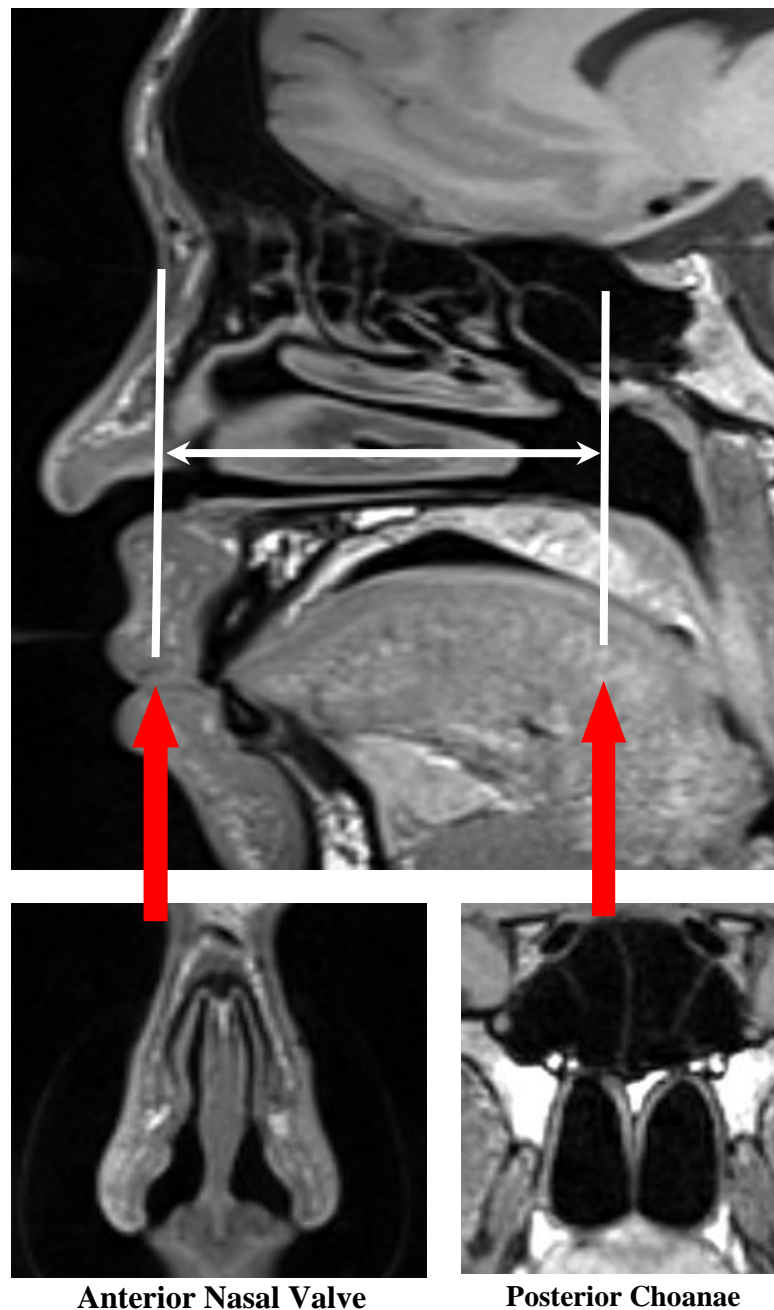


**Figure B1.5: MRI images showing region of interest spanning the anterior nasal valve to the posterior choanae.**

Characterization of individual airway response to augmented air pressure is possible when evaluating each separate airway.

### **B1.8 Geometrical Raw Data**

All MRI positional, cross sectional and perimeter data for both patent and congested airways is presented in in Table B1.4 for both ambient and n-PAP breathing. All data was read directly from files created by 3D-Doctor image analysis software using Matlab code. This was necessary to eliminate the possibility of bias during manual analysis.

## B1.9: MRI Settings

SIEMENS MAGNETOM Skyra syngo MR D11

-----  
\\USER\Research\AUT\ASL\localizer  
TA:0:13 PAT:Off Voxel size:0.5×0.5×7.0 mm Rel. SNR:1.00 :fl  
-----

### Properties

Prio Recon	On
Before measurement	
After measurement	
Load to viewer	On
Inline movie	Off
Auto store images	On
Load to stamp segments	On
Load images to graphic segments	On
Auto open inline display	Off
Wait for user to start	Off
Start measurements	single

### Routine

Nr. of slice groups	1
Slices	3
Dist. factor	20 %
Position	Isocenter
Orientation	Sagittal
Phase enc. dir.	A >> P
AutoAlign	---
Phase oversampling	0 %
FoV read	250 mm
FoV phase	100.0 %
Slice thickness	7.0 mm
TR	8.6 ms
TE	4.00 ms
Averages	2
Concatenations	3
Filter	Prescan Normalize, Elliptical filter
Coil elements	HE1-4

### Contrast

TD	0 ms
MTC	Off
Magn. preparation	None
Flip angle	20 deg
Fat suppr.	None
Water suppr.	None
SWI	Off
Averaging mode	Short term
Measurements	1

Reconstruction		Magnitude
Multiple series		Each measurement
<b>Resolution</b>		
Base resolution		256
Phase resolution		90 %
Phase partial Fourier		Off
Interpolation		On
PAT mode		None
Image Filter		Off
Distortion Corr.		Off
TD		0 ms
Unfiltered images		Off
Prescan Normalize		On
Normalize		Off
B1 filter		Off
Raw filter		Off
Elliptical filter		On
Mode		Inplane
<b>Geometry</b>		
Nr. of slice groups	3	
Slices	1	
Dist. factor	20 %	
Position	Isocenter	
Phase enc. dir.	A >> P	
Phase oversampling	0 %	
Multi-slice mode	Sequential	
Series	Interleaved	
Saturation mode	Standard	
Nr. of sat. regions	0	
Position mode	Offcenter-Shift	
Fat suppr.	None	
Water suppr.	None	
Special sat.	None	
Special sat.	None	
Set-n-Go Protocol	Off	
Table position	P	
Inline Composing	Off	
<b>System</b>		
Body	Off	
HE1	On	
HE3	On	
NE1	Off	
HE2	On	
HE4	On	
NE2	Off	
SP5	Off	
SP6	Off	
SP7	Off	
SP8	Off	

SP1	Off
SP2	Off
SP3	Off
SP4	Off
Position mode	Offcenter-Shift
Positioning mode	REF
Table position	H
Table position	0 mm
MSMA	S - C - T
Sagittal	R >> L
Coronal	A >> P
Transversal	F >> H
Save uncombined	Off
Coil Combine Mode	Adaptive Combine
AutoAlign	---
Auto Coil Select	Off
Shim mode	Tune up
Adjust with body coil	Off
Confirm freq. adjustment	Off
Assume Dominant Fat	Off
Assume Silicone	Off
Adjustment Tolerance	Auto
? Ref. amplitude 1H	0.000 V
Position	Isocenter
Rotation	0.00 deg
R >> L	350 mm
A >> P	263 mm
F >> H	350 mm
Frequency 1H	123.258794 MHz
Correction factor	1
SRFExcit 1H	46.457 V
Gain	High
Table position	0 mm
Img. Scale. Cor.	1.000
Physio	
1st Signal/Mode	None
Segments	1
Tagging	None
Magn. preparation	None
Dark blood	Off
Resp. control	Off
Inline	
Inline Composing	Off
Distortion correction	Off
Sequence	
Introduction	On
Dimension	2D
Phase stabilisation	Off
Averaging mode	Short term
Multi-slice mode	Sequential
Asymmetric echo	Allowed
Contrasts	1

Bandwidth	320 Hz/Px
Flow comp.	No
Allowed delay	0 s
RF pulse type	Normal
Gradient mode	Normal
Excitation	Slice-sel.
RF spoiling	On
TX/RX delta frequency	0 Hz
TX Nucleus	None
TX delta frequency	0 Hz
Coil elements	HE1-4
Acquisition duration	0 ms
Mode	Off
<b>BOLD</b>	
Subtract	Off
Liver registration	Off
Save images	On
Autoscaling	Off
Scaling factor	1
Offset	0
Subtrahend	1
Subtraction indices	
StdDev	Off
Std-Dev-Sag	Off
Std-Dev-Cor	Off
Std-Dev-Tra	Off
Std-Dev-Time	Off
MIP-Sag	Off
MIP-Cor	Off
MIP-Tra	Off
MIP-Time	Off
Radial MIP	Off
Save original images	On
Distortion Corr.	Off
MapIt	None
Contrasts	1
Save original images	On
Wash - In	Off
Wash - Out	Off
TTP	Off
PEI	Off
MIP - time	Off
Number of radial views	1
Axis of radial views	L-R
MPR Sag	Off
MPR Cor	Off
MPR Tra	Off

SIEMENS MAGNETOM Skyra syngo MR D11

---

\\USER\Research\AUT\ASL\t1\_space\_sag\_iso\_0.78

-----  
Properties

Prio Recon	Off
Before measurement	
After measurement	
Load to viewer	On
Inline movie	Off
Auto store images	On
Load to stamp segments	On
Load images to graphic segments	Off
Auto open inline display	Off
Wait for user to start	Off
Start measurements	single

## Routine

Nr. of slab groups	1
Slabs	1
Position	L1.9 A4.6 F11.9 mm
Orientation	S > C-3.0
Phase enc. dir.	A >> P
AutoAlign	---
Phase oversampling	0 %
Slice oversampling	9.1 %
FoV read	250 mm
FoV phase	100.0 %
Slice thickness	0.78 mm
TR	700 ms
TE	12.0 ms
Concatenations	1
Filter	Raw filter, Prescan Normalize
Coil elements	HE1-4

## Contrast

MTC	Off
Magn. preparation	None
Fat suppr.	None
Water suppr.	None
Restore magn.	On
Measurements	1
Reconstruction	Magnitude
Multiple series	Each measurement

## Resolution

Base resolution	320
Phase resolution	100 %
Phase partial Fourier	Off
Interpolation	Off
PAT mode	GRAPPA
Accel. factor PE	2
Ref. lines PE	24
Reference scan mode	Integrated
Image Filter	Off
Distortion Corr.	Off
Accel. factor 3D	1

Unfiltered images	Off
Prescan Normalize	On
Normalize	Off
B1 filter	Off
Raw filter	On
Intensity	Weak
Slope	0
Elliptical filter	Off
Slice resolution	91 %
Slice partial Fourier	Off
Geometry	
Nr. of slab groups	1
Slabs	1
Position	L1.9 A4.6 F11.9 mm
Phase enc. dir.	A >> P
Phase oversampling	0 %
Slice oversampling	9.1 %
Slices per slab	176
Series	Interleaved
Nr. of sat. regions	0
Position mode	Offcenter-Shift
Fat suppr.	None
Water suppr.	None
Special sat.	None
Special sat.	None
Set-n-Go Protocol	Off
Table position	P
Inline Composing	Off
Restore magn.	On
System	
Body	Off
HE1	On
HE3	On
NE1	Off
HE2	On
HE4	On
NE2	Off
SP5	Off
SP6	Off
SP7	Off
SP8	Off
SP1	Off
SP2	Off
SP3	Off
SP4	Off
Position mode	Offcenter-Shift
Positioning mode	FIX
Table position	H
Table position	0 mm
MSMA	S - C - T
Sagittal	R >> L
Coronal	A >> P

Transversal	F >> H
Save uncombined	Off
Coil Combine Mode	Adaptive Combine
AutoAlign	---
Auto Coil Select	Off
Shim mode	Tune up
Adjust with body coil	Off
Confirm freq. adjustment	Off
Assume Dominant Fat	Off
Assume Silicone	Off
Adjustment Tolerance	Auto
? Ref. amplitude 1H	0.000 V
Position	Isocenter
Rotation	0.00 deg
R >> L	350 mm
A >> P	263 mm
F >> H	350 mm
Frequency 1H	123.258794 MHz
Correction factor	1
SRFExcit 1H	244.167 V
! Gain	High
Table position	0 mm
Img. Scale. Cor.	1.000
Physio	
1st Signal/Mode	None
Trigger delay	0 ms
Magn. preparation	None
Dark blood	Off
Resp. control	Off
Inline	
Inline Composing	Off
Distortion correction	Off
Sequence	
Introduction	On
Dimension	3D
Elliptical scanning	On
Reordering	Linear
Bandwidth	625 Hz/Px
Flow comp.	No
Allowed delay	30 s
Echo spacing	4.05 ms
Adiabatic-mode	Off
Turbo factor	38
Echo train duration	166
RF pulse type	Normal
Gradient mode	Fast
Excitation	Non-sel.
Flip angle mode	T1 var
TX/RX delta frequency	0 Hz
TX Nucleus	None
TX delta frequency	0 Hz
Coil elements	HE1-4

Acquisition duration	0 ms
Organ under exam.	None
<b>BOLD</b>	
Subtract	Off
Save images	On
Autoscaling	Off
Scaling factor	1
Offset	0
Subtrahend	1
Subtraction indices	
StdDev	Off
Std-Dev-Sag	Off
Std-Dev-Cor	Off
Std-Dev-Tra	Off
Std-Dev-Time	Off
MIP-Sag	Off
MIP-Cor	Off
MIP-Tra	Off
MIP-Time	Off
Radial MIP	Off
Save original images	On
Distortion Corr.	Off
Save original images	On
Number of radial views	1
Axis of radial views	L-R
MPR Sag	Off
MPR Cor	Off
MPR Tra	Off

# SIEMENS MAGNETOM Skyra syngo MR D11

\\USER\Research\AUT\ASL\ASL\_3D\_tra\_iso TI 2000\_ambient  
TA:3:05 Voxel size:4.0×4.0×4.0 mm Rel. SNR:1.00 :tgse

## Properties

Prio Recon	Off
Before measurement	
After measurement	
Load to viewer	On
Inline movie	Off
Auto store images	On
Load to stamp segments	Off
Load images to graphic segments	Off
Auto open inline display	Off
Wait for user to start	Off
Start measurements	single

## Routine

Nr. of slab groups	1
Slabs	1
Dist. factor	50 %
Position	L0.0 A9.4 F24.0 mm

Orientation	Transversal
Phase enc. dir.	A >> P
AutoAlign	---
Phase oversampling	0 %
Slice oversampling	20.0 %
FoV read	256 mm
FoV phase	100.0 %
Slice thickness	4.00 mm
TR	5000 ms
TE	14.8 ms
Averages	1
Concatenations	1
Filter	Prescan Normalize
Coil elements	HE3,4
Contrast	
Flip angle	180 deg
Fat suppr.	Fat sat.
Averaging mode	Long term
Measurements	2
Delay in TR	0 ms
Reconstruction	Magnitude
Multiple series	Off
Perfusion mode	FAIR QII
Bolus Duration	700 ms
Inversion Time	syngo.MR.ProtBasic.Interop.ValueArray
Inversion Array Size	1
Averaging mode	CONSTANT
Suppression Mode	GRAY-WHITE
Resolution	
Base resolution	64
Phase resolution	98 %
Phase partial Fourier	Off
Interpolation	Off
Distortion Corr.	Off
Hamming	Off
Prescan Normalize	On
Raw filter	Off
Elliptical filter	Off
Slice partial Fourier	Off
Geometry	
Nr. of slab groups	1
Slabs	1
Dist. factor	50 %
Position	L0.0 A9.4 F25.0 mm
Phase enc. dir.	A >> P
Phase oversampling	0 %
Slice oversampling	20.0 %
Slices per slab	32
Multi-slice mode	Interleaved
Series	Ascending
Nr. of sat. regions	0
Position mode	Offcenter-Shift

Fat suppr.	Fat sat.
Special sat.	None
Special sat.	None
Set-n-Go Protocol	Off
Table position	P
Inline Composing	Off
System	
Body	Off
L4	Off
HE1	Off
HE3	On
NE1	Off
HE2	Off
HE4	On
NE2	Off
SP5	Off
SP6	Off
SP7	Off
SP8	Off
SP1	Off
SP2	Off
SP3	Off
SP4	Off
Position mode	Offcenter-Shift
Positioning mode	REF
Table position	F
Table position	0 mm
MSMA	S - C - T
Sagittal	R >> L
Coronal	A >> P
Transversal	F >> H
Coil Combine Mode	Sum of Squares
AutoAlign	---
Auto Coil Select	Off
Shim mode	Standard
Adjust with body coil	Off
Confirm freq. adjustment	Off
Assume Dominant Fat	Off
Assume Silicone	Off
Adjustment Tolerance	Auto
? Ref. amplitude 1H	0.000 V
Position	L0.0 A9.4 F25.0 mm
Rotation	0.00 deg
R >> L	256 mm
A >> P	256 mm
F >> H	128 mm
Frequency 1H	123.258794 MHz
Correction factor	1
ExtRefocRF 1H	498.100 V
Gain	Low
Table position	1 mm
Img. Scale. Cor.	1.000

Physio		
1st Signal/Mode		None
Segments	9	
Inline		
Inline Composing		Off
Distortion correction		Off
Sequence		
Introduction		Off
Dimension		3D
Averaging mode		Long term
Multi-slice mode		Interleaved
Reordering		Centric
Bandwidth		2604 Hz/Px
Free echo spacing		Off
Echo spacing		0.5 ms
Turbo factor		18
EPI factor	21	
RF pulse type		Normal
Gradient mode		Fast
TX/RX delta frequency		0 Hz
TX Nucleus		None
TX delta frequency		0 Hz
Coil elements		HE3,4
Acquisition duration		0 ms
BOLD		
Delay in TR		0 ms
Distortion Corr.		Off

#### SIEMENS MAGNETOM Skyra syngo MR D11

\\USER\Research\AUT\ASL\ASL\_3D\_tra\_iso\_15cmWG  
TA:3:05 Voxel size:4.0×4.0×4.0 mm Rel. SNR:1.00 :tgse

Properties		
Prio Recon		Off
Before measurement		
After measurement		
Load to viewer		On
Inline movie		Off
Auto store images		On
Load to stamp segments		Off
Load images to graphic segments		Off
Auto open inline display		Off
Wait for user to start		Off
Start measurements		single
Routine		
Nr. of slab groups		1
Slabs	1	
Dist. factor		50 %
Position		L0.0 A11.2 H4.8 mm
Orientation		T > S0.4

Phase enc. dir.	A >> P
AutoAlign	---
Phase oversampling	0 %
Slice oversampling	20.0 %
FoV read	256 mm
FoV phase	100.0 %
Slice thickness	4.00 mm
TR	5000 ms
TE	14.8 ms
Averages	1
Concatenations	1
Filter	Prescan Normalize
Coil elements	HE3,4
Contrast	
Flip angle	180 deg
Fat suppr.	Fat sat.
Averaging mode	Long term
Measurements	2
Delay in TR	0 ms
Reconstruction	Magnitude
Multiple series	Off
Perfusion mode	FAIR QII
Bolus Duration	700 ms
Inversion Time	syngo.MR.ProtBasic.Interop.ValueArray
Inversion Array Size	1
Averaging mode	CONSTANT
Suppression Mode	GRAY-WHITE
Resolution	
Base resolution	64
Phase resolution	98 %
Phase partial Fourier	Off
Interpolation	Off
Distortion Corr.	Off
Hamming	Off
Prescan Normalize	On
Raw filter	Off
Elliptical filter	Off
Slice partial Fourier	Off
Geometry	
Nr. of slab groups	1
Slabs	1
Dist. factor	50 %
Position	L0.0 A11.2 H4.8 mm
Phase enc. dir.	A >> P
Phase oversampling	0 %
Slice oversampling	20.0 %
Slices per slab	32
Multi-slice mode	Interleaved
Series	Ascending
Nr. of sat. regions	0
Position mode	Offcenter-Shift
Fat suppr.	Fat sat.

Special sat.	None
Special sat.	None
Set-n-Go Protocol	Off
Table position	P
Inline Composing	Off
System	
Body	Off
HE1	Off
HE3	On
NE1	Off
HE2	Off
HE4	On
NE2	Off
SP5	Off
SP6	Off
SP7	Off
SP8	Off
SP1	Off
SP2	Off
SP3	Off
SP4	Off
Position mode	Offcenter-Shift
Positioning mode	REF
Table position	H
Table position	0 mm
MSMA	S - C - T
Sagittal	R >> L
Coronal	A >> P
Transversal	F >> H
Coil Combine Mode	Sum of Squares
AutoAlign	---
Auto Coil Select	Off
Shim mode	Standard
Adjust with body coil	Off
Confirm freq. adjustment	Off
Assume Dominant Fat	Off
Assume Silicone	Off
Adjustment Tolerance	Auto
? Ref. amplitude 1H	0.000 V
Position	L0.0 A11.2 H4.8 mm
Rotation	-2.30 deg
R >> L	256 mm
A >> P	256 mm
F >> H	128 mm
Frequency 1H	123.258794 MHz
Correction factor	1
ExtRefocRF 1H	498.100 V
Gain	Low
Table position	0 mm
Img. Scale. Cor.	1.000
Physio	
1st Signal/Mode	None

Segments	9
Inline	
Inline Composing	Off
Distortion correction	Off
Sequence	
Introduction	Off
Dimension	3D
Averaging mode	Long term
Multi-slice mode	Interleaved
Reordering	Centric
Bandwidth	2604 Hz/Px
Free echo spacing	Off
Echo spacing	0.5 ms
Turbo factor	18
EPI factor	21
RF pulse type	Normal
Gradient mode	Fast
TX/RX delta frequency	0 Hz
TX Nucleus	None
TX delta frequency	0 Hz
Coil elements	HE3,4
Acquisition duration	0 ms
BOLD	
Delay in TR	0 ms
Distortion Corr.	Off

#### SIEMENS MAGNETOM Skyra syngo MR D11

\\USER\Research\AUT\ASL\t1\_space\_sag\_iso\_0.78\_15cmWG  
 TA:7:25 PAT:2 Voxel size:0.8×0.8×0.8 mm Rel. SNR:1.00 :spcR

Properties	
Prio Recon	Off
Before measurement	
After measurement	
Load to viewer	On
Inline movie	Off
Auto store images	On
Load to stamp segments	On
Load images to graphic segments	Off
Auto open inline display	Off
Wait for user to start	Off
Start measurements	single
Routine	
Nr. of slab groups	1
Slabs	1
Position	L1.9 A4.6 F11.9 mm
Orientation	S > C-3.0
Phase enc. dir.	A >> P
AutoAlign	---
Phase oversampling	0 %

Slice oversampling	9.1 %
FoV read	250 mm
FoV phase	100.0 %
Slice thickness	0.78 mm
TR	700 ms
TE	12.0 ms
Concatenations	1
Filter	Raw filter, Prescan Normalize
Coil elements	HE1-4
Contrast	
MTC	Off
Magn. preparation	None
Fat suppr.	None
Water suppr.	None
Restore magn.	On
Measurements	1
Reconstruction	Magnitude
Multiple series	Each measurement
Resolution	
Base resolution	320
Phase resolution	100 %
Phase partial Fourier	Off
Interpolation	Off
PAT mode	GRAPPA
Accel. factor PE	2
Ref. lines PE	24
Reference scan mode	Integrated
Image Filter	Off
Distortion Corr.	Off
Accel. factor 3D	1
Unfiltered images	Off
Prescan Normalize	On
Normalize	Off
B1 filter	Off
Raw filter	On
Intensity	Weak
Slope	0
Elliptical filter	Off
Slice resolution	91 %
Slice partial Fourier	Off
Geometry	
Nr. of slab groups	1
Slabs	1
Position	L1.9 A4.6 F11.9 mm
Phase enc. dir.	A >> P
Phase oversampling	0 %
Slice oversampling	9.1 %
Slices per slab	176
Series	Interleaved
Nr. of sat. regions	0
Position mode	Offcenter-Shift
Fat suppr.	None

Water suppr.	None
Special sat.	None
Special sat.	None
Set-n-Go Protocol	Off
Table position	P
Inline Composing	Off
Restore magn.	On
System	
Body	Off
HE1	On
HE3	On
NE1	Off
HE2	On
HE4	On
NE2	Off
SP5	Off
SP6	Off
SP7	Off
SP8	Off
SP1	Off
SP2	Off
SP3	Off
SP4	Off
Position mode	Offcenter-Shift
Positioning mode	FIX
Table position	H
Table position	0 mm
MSMA	S - C - T
Sagittal	R >> L
Coronal	A >> P
Transversal	F >> H
Save uncombined	Off
Coil Combine Mode	Adaptive Combine
AutoAlign	---
Auto Coil Select	Off
Shim mode	Tune up
Adjust with body coil	Off
Confirm freq. adjustment	Off
Assume Dominant Fat	Off
Assume Silicone	Off
Adjustment Tolerance	Auto
? Ref. amplitude 1H	0.000 V
Position	Isocenter
Rotation	0.00 deg
R >> L	350 mm
A >> P	263 mm
F >> H	350 mm
Frequency 1H	123.258794 MHz
Correction factor	1
SRFExcit 1H	244.167 V
! Gain	High
Table position	0 mm

Img. Scale. Cor.	1.000
Physio	
1st Signal/Mode	None
Trigger delay	0 ms
Magn. preparation	None
Dark blood	Off
Resp. control	Off
Inline	
Inline Composing	Off
Distortion correction	Off
Sequence	
Introduction	On
Dimension	3D
Elliptical scanning	On
Reordering	Linear
Bandwidth	625 Hz/Px
Flow comp.	No
Allowed delay	30 s
Echo spacing	4.05 ms
Adiabatic-mode	Off
Turbo factor	38
Echo train duration	166
RF pulse type	Normal
Gradient mode	Fast
Excitation	Non-sel.
Flip angle mode	T1 var
TX/RX delta frequency	0 Hz
TX Nucleus	None
TX delta frequency	0 Hz
Coil elements	HE1-4
Acquisition duration	0 ms
Organ under exam.	None
BOLD	
Subtract	Off
Save images	On
Autoscaling	Off
Scaling factor	1
Offset	0
Subtrahend	1
Subtraction indices	
StdDev	Off
Std-Dev-Sag	Off
Std-Dev-Cor	Off
Std-Dev-Tra	Off
Std-Dev-Time	Off
MIP-Sag	Off
MIP-Cor	Off
MIP-Tra	Off
MIP-Time	Off
Radial MIP	Off
Save original images	On
Distortion Corr.	Off

Save original images	On
Number of radial views	1
Axis of radial views	L-R
MPR Sag	Off
MPR Cor	Off
MPR Tra	Off

## B2: Ethics Approval

Ethical approval was sought from the Auckland University of Technology Ethics Committee (AUTEC) under application number 10/121 and granted on the 14<sup>th</sup> of July 2010. Copies of all of the forms relating to the ethics application can be found in the following appendices.

### B2.1 Application for Ethics Approval

**Auckland University of Technology Ethics Committee  
(AUTEC)**

**EA1**

**APPLICATION FOR ETHICS APPROVAL FOR RESEARCH PROJECTS**



---

*Please read the notes at the end of the form before submitting this application.*

### General Information

#### Project Title

*If you will be using a different title in documents to that being used as your working title, please provide both, clearly indicating which title will be used for what purpose.*

Feasibility study into the use of magnetic resonance imaging (MRI) to detect change in internal nasal geometry and blood flow during nasal breathing therapy.

#### Applicant Name and Qualifications

*When the researcher is a student (including staff who are AUT students), the applicant is the principal supervisor. When the researcher is an AUT staff member undertaking research as part of employment or a staff member undertaking research as part of an external qualification, the applicant is the researcher. Staff should refer to Section 11.4 of Applying for Ethics Approval: Guidelines and Procedures to check requirements for ethics approval where they are studying at another institution.*

Professor Ahmed Al-Jumaily

Doctor of Philosophy (Mechanical Engineering), PhD, 1977

Master of Science (Mechanical Engineering), MSME, 1973

Bachelor of Science (Mechanical Engineering), BSc, 1971

#### Applicant's School/Department/Academic Group/Centre

Institute of Biomedical Technologies

#### Applicant's Faculty

Design and Creative Technologies

#### Student Details

*Please complete this section only if the research is being undertaken by a student as part of an AUT qualification.*

#### Student Name(s):

David White

**Student ID Number(s):**

9012226

**Completed Qualification(s):**

Master of Engineering, 2003.

Bachelor of Engineering (Mechanical), 1996.

New Zealand Certificate in Engineering (Mechanical) 1986.

Trade Certification (Automotive Engineering), 1982.

**E-mail address:**

david.white@aut.ac.nz

**School/Department/Academic Group/Centre**

School of Engineering / Institute of Biomedical Technologies (IBTec)

**Faculty**

Design and Creative Technologies

**Name of the qualification for which this research is being undertaken:**

Doctor of Philosophy (PhD) in Engineering

**Research Output**

*Please state whether your research will result in a thesis or dissertation or a research paper or is part of coursework requirements.*

The research will result in the publication of a thesis which will be lodged in the AUT Library and a (potential) number of research papers that will be published in international journals and refereed conference proceedings.

**Details of Other Researchers or Investigators**

*Please complete this section only if other researchers, investigators or organisations are involved in this project. Please also specify the role any other researcher(s), investigator(s) or organisation(s) will have in the research.*

**Individual Researcher(s) or Investigator(s)**

*Please provide the name of each researcher or investigator and the institution in which they research.*

David White, PhD candidate, Institute of Biomedical Technologies (IBTEC), AUT

Dr Andrew Sommervell, Fisher & Paykel Healthcare Ltd. (Second Supervisor)

Dr Jim Bartley, Auckland District Health Board (ADHB). (Third Supervisor)

**Research or Investigator Organisations**

*Please provide the name of each organisation and the city in which the organisation is located.*

Centre for Advanced MRI (CAMRI), University of Auckland.

**Are you applying concurrently to another ethics committee?**

*If your answer is yes, please provide full details, including the meeting date, and attach copies of the full application and approval letter if it has been approved.*

No

## Declaration

The information supplied is, to the best of my knowledge and belief, accurate. I have read the current Guidelines, published by the Auckland University of Technology Ethics Committee, and clearly understand my obligations and the rights of the participant, particularly with regard to informed consent.

\_\_\_\_\_  
Signature of Applicant

\_\_\_\_\_  
Date

*(In the case of student applications the signature must be that of the Supervisor)*

\_\_\_\_\_  
Signature of Student

\_\_\_\_\_  
Date

*(If the research is a student project, both the signature of the Supervisor, as the applicant, and the student are required)*

## Authorising Signature

\_\_\_\_\_  
Signature of Head

\_\_\_\_\_  
Name of  
Faculty/Programme/School/Centre

\_\_\_\_\_  
Date

## General Project Information

### Project Duration

#### Approximate Start Date of Primary Data Collection

02 August 2010

#### Approximate Finish Date of Complete Project

31 December 2011

### Are funds being obtained specifically for this project?

*If your answer is yes, then you must complete section G of this Application Form.*

No.

### Types of persons participating as participants

*Please indicate clearly every one of the following categories that applies to those participating in your research.*

#### Researcher's students

Yes

#### Adults (20 years and above)

Yes

#### Legal minors (16 to 20 years old)

No

#### Legal minors (under 16 years old)

No

#### Members of vulnerable groups

*e.g. persons with impairments, limited understanding, etc. If your answer is yes, please provide a full description.*

No

**Hospital patients**

No

**Prisoners**

No

**Does this research involve use of human remains, tissue or body fluids which does not require submission to a Regional Ethics Committee?**

*e.g. finger pricks, urine samples, etc. (please refer to section 13 of the AUTC Guidelines). If your answer is yes, please provide full details of all arrangements, including details of agreements for treatment, etc.*

No

**Does this research involve potentially hazardous substances?**

*e.g. radioactive materials (please refer to section 15 of the AUTC Guidelines). If your answer is yes, please provide full details.*

No

**Research Instruments**

**Does the research include the use of a written or electronic questionnaire or survey?**

*If your answer is yes, please attach to this application form a copy of the finalised questionnaire or survey in the format that it will be presented to participants.*

No

**Does the research involve the use of focus groups or interviews?**

*If the answer is yes, please indicate how the data will be recorded (e.g. audiotape, videotape, note-taking). When interviews or focus groups are being recorded, you will need to make sure there is provision for explicit consent on the Consent Form and attach to this Application Form examples of indicative questions or the full interview or focus group schedule.*

No

**Does the research involve the use of observation?**

*If the answer is 'Yes', please attach to this application a copy of the observation protocol that will be used.*

No

**Does the research involve the use of other research instruments such as performance tests?**

*If the answer is yes, please attach to this application a copy of the protocols for the instruments and the instruments that will be used to record results.*

Yes – Magnetic Resonance Imaging (MRI).

**Who will be transcribing or recording the data?**

*If someone other than the researcher will be transcribing the interview or focus group records or taking the notes, you need to provide a confidentiality agreement with this Application Form.*

The Centre for Advanced MRI (CAMRI) will be collecting data for this project. The Researcher and CAMRI radiologist will be acquiring the MRI image data.

All research assistants will be required to sign confidentiality agreements to protect the participant's privacy.

## **How does the design and practice of this research implement each of the three principles of the Treaty of Waitangi (Partnership, Participation and Protection) in the relationships between the researcher and other participants?**

*Please refer to Section 2.5 of AUTECH's Applying for Ethics Approval: Guidelines and Procedures (accessible in the Ethics Knowledge Base online via <http://www.aut.ac.nz/about/ethics>) and to the relevant Frequently Asked Questions section in the Ethics Knowledge Base.*

Each of the three principles of the Treaty of Waitangi in terms of partnership, participation and protection is incorporated in the design and implementation of this research through the following points:

### **Partnership**

- Dialogue between the researchers and participants will occur covering the justification for this research, the purpose and rationale behind the procedures to be undertaken as well as answering questions relating to this work. After consent has been offered by the participant to proceed; throughout the feasibility study confirmation will be sought from the participant that the procedure is being conducted in a courteous and considerate manner.
- By ensuring a continual dialogue occurs between participants and researchers throughout the duration of this feasibility study where each explains the justification and rationale for actions undertaken will ensure both parties act honourably and in good faith to each other. This will also involve seeking permission from the other party prior to undertaking any procedure.
- Applied breathing therapy is utilised in many situations, ranging from the application of oxygen or other gases in hospital to nasal continuous positive airway pressure (n-CPAP) therapy for treatment of obstructive sleep apnoea (OSA), so this research are not designed to specifically benefit the participants and/or their social or cultural group. Outcomes of this research are intended to assist anyone undergoing nasal applied breathing therapy.

### **Participation**

- The role of the participants is to undertake two comparative MRI scans - one whilst breathing ambient air and the other whilst breathing pressurised air. Each participant will also have their nasal airflow measured both prior to and post MRI scan.
- Participants will be asked to assess their nasal symptoms both prior to and post MRI scan but will not influence the nature of the research, its aims, or its methodology.
- Each participant will share information regarding the status of their nasal symptoms. Image data acquired by MRI will require the participant to be involved in conducting the research by consenting to undertake comparative head MRI scans.
- None of the participants will have a formal role as stakeholder and being screened for having no respiratory ailment will most likely not benefit in the near future.

- Research outputs will not contain any reference to individual participants or enable them to be identified in any way as only summary findings will be published. Because of this, participants will have no role in the research outputs but they will be invited to view the summary results on the Research Institute (IBTec) website.

### **Protection**

- Protection of the participant from deceit, harm and coercion has been designed into the feasibility study in three ways. Firstly, the information supplied by the Participant Information Sheet will ensure they are aware of the rationale, purpose and methodology. Secondly, the participant understands that their participation is entirely voluntary and they can choose to withdraw at any time and for any reason prior to completion of the feasibility study. Thirdly, throughout the feasibility study there will be a dialogue between the researchers and participant to communicate not only procedures and seek permission for these to proceed but also to enable the participant to express concerns and remain informed. Included in this dialogue will be the communication of any discomfort experienced by the participant and any mitigating action undertaken by the researchers.
- Privacy of the participants and researchers will be protected through a process of ensuring that the participants remain anonymous to each other and the only contact they have will be directly with the researchers. Data collected by the researchers, specific to each participant, will be stored using a reference number that can only be referred back to the participant through the demographic data form that is held securely in a separate location to the data.
- Management of the power imbalance inherent in the relationship between participants and researchers will be managed through a process of continual dialogue where procedures are explained and justified by the researchers and the seeking of consent from the participant prior to proceeding.
- Respect for participant cultural or other diversity of the participant will be ensured through a process of continual dialogue where procedures are explained and justified by the researchers and the seeking of consent from the participant prior to proceeding.

### **Does this research target Maori participants?**

No

#### **If 'Yes', what consultation has been undertaken when designing the research?**

*Please identify the group(s) with whom consultation has occurred and provide evidence of their support and any impact this consultation had on the design of the research. Researchers are advised to read the Health Research Council's Guidelines for researchers on health research involving Maori, available via the Ethics Knowledge Base.*

N/A

### **Does this research target participants of particular cultures or social groups?**

*Please refer to Section 2.5 of AUTECH's Applying for Ethics Approval: Guidelines and Procedures (accessible in the Ethics Knowledge Base online via <http://www.aut.ac.nz/about/ethics>) and to the relevant Frequently Asked Questions section in the Ethics Knowledge Base.*

No

If 'Yes' please identify which cultures or social groups are being targeted and how their cultures or social groups are being considered in the research design.

N/A

If your answer to B.9 was 'Yes', what consultation has occurred with these cultures or social groups in the design of the research?

*Please identify the group(s) with whom consultation has occurred and provide evidence of their support and any impact this consultation had on the design of the research.*

N/A

**Is there a need for translation or interpreting?**

*If your answer is 'Yes', please provide copies of any translations with this application and any Confidentiality Agreement required for translators or interpreters.*

No

## Project Details

*Please describe the project details in language which is, as far as possible, free from jargon and comprehensible to lay people.*

**Aim of project:**

*Please explain the broad scope and purpose of the project and state concisely how the type of information being sought will achieve the project's aims. Please give the specific hypothesis(es), if any, to be tested.*

The aim of this feasibility study is threefold:

1. To ascertain if changes in internal nasal geometry occurs by comparing MRI data of the nasal cavity before and during applied nasal breathing therapy.
2. To gather 3-D nasal geometry data prior to and during applied breathing therapy to enable volume and area analysis to be undertaken at a later date.
3. To quantify if changes in nasal blood flow occurs by comparing MRI data of the nasal arteries before and during applied nasal breathing therapy. Specifically the main arteries supplying blood to the nasal cavity are of interest. These include the anterior and posterior ethmoid arteries, the sphenopalatine artery and the superior labial artery.

The acquisition of internal nasal geometry has been achieved before using MRI, however, this technique has not previously been used to detect changes in geometry during applied breathing therapy.

The MRI measurement technique of Arterial Spin Labelling (ASL) has not previously been used to measure nasal blood flow and therefore the aim of this feasibility study is to test if this technique can detect any changes under vary air pressure conditions.

**Why are you proposing this research?**

*(ie what are its potential benefits to participants, researcher, wider community, etc?)*

Over 6% of the adult population in the western world suffer obstructive sleep apnoea (OSA) which is most commonly treated through application of nasal continuous positive airway pressure (n-CPAP) breathing therapy. Like other nasal applied breathing therapies, about 40% of n-CPAP users report a range of nasal problems that include sneezing, itching, crusting or dry nose. Conversely the opposite symptoms of nasal congestion and/or runny nose

are also commonly reported. In most cases these symptoms were not present prior to therapy being applied and are indicative of failure of the nose to adequately heat and humidify inhaled air. Within the human body nasal air-conditioning is directly controlled by autonomic and purinergic regulation systems, however the mechanism(s) by which nasal applied breathing therapy affects these regulation systems is currently unknown.

In order to better understand the body's nasal air-conditioning response to nasal applied breathing therapy, a predictive model of nasal air-conditioning response to this therapy is being developed. Within this model it is essential to simplify the vast array of variables by incorporating those that are important and excluding those that are insignificant to ensure the model fits real life situations. In this case nasal geometry and vasculature flow are of interest to the researcher.

Variation in nasal geometry is predicted to have a significant influence in heat and mass transfer within the nose and, although there is no evidence at present, it appears likely that air pressure could compress the soft erectile tissue contained within the nasal cavity. Collecting data on nasal geometry will enable computational predictive calculations to be undertaken for application within the predictive air-conditioning model.

Changes in nasal blood flow will influence both heat and gland fluid supply, however there is no evidence supporting the hypothesis that air pressure influences nasal blood flow. Although it is considered unlikely that this will occur, this needs to be demonstrated for the pressure ranges typically encountered during n-CPAP therapy before being excluded from the predictive air-conditioning model.

The simultaneous recorded data from this feasibility study will be used for designing and testing the predictive air-conditioning model. The predictive nasal air-conditioning model will enable development of new and improved nasal breathing therapy devices that will benefit the wider community through better health management.

### **Background:**

*Please provide sufficient information, including relevant references, to place the project in perspective and to allow the project's significance to be assessed. Where appropriate, provide one or two references to the applicant's (or supervisor's) own published work in the relevant field.*

The human nose is important for our respiratory wellbeing as it provides not only the first line of particulate defence by filtration but also conditions inhaled air to become near fully water saturated at core body temperature to protect the lower airways from drying when exposed to the extremes of temperature and humidity that exist in our world [1, 2].

A range of different gases are delivered at slightly elevated pressures to a nasal mask to treat a range of patient respiratory ailments ranging from lung infection or injury through to obstructive sleep apnoea (OSA) where the upper airway collapses during deep sleep, leading to repetitive hypoxia and arousal. OSA is associated with daytime sleepiness, hypertension, and many other pathological conditions [3] as well as increased risk of work and vehicle accidents. In the western world this is a relatively common condition affecting around 2% of adult females and 4% of adult males with those obese or with abnormal airways being most prone to suffering from this ailment [4].

There are however some side effects to nasal applied breathing therapy with over 40% of n-CPAP users reporting symptoms that include crusty or dry nose, congestion, sneezing, rhinorrhea or nasal itching is seemingly created by changes in the ability of the nose to condition inhaled ambient air under slightly elevated pressures [4-13]. These symptoms can be classified into two groups:

1. Crusting or dry nose, – all symptoms of upper airway mucosal drying. This may be treated by pre-therapy use of oily nose drops [8] or more commonly through post-therapy saline spray.
2. Nasal congestion, nasal itch and/or rhinorrhea – due to nasal inflammation. This may be treated with a topical nasal steroid spray, saline nasal spray or a topical anticholinergic drug, such as ipratropium.

Heated humidification is commonly utilized as a non-pharmaceutical alternative to treat these symptoms and improve patient comfort, however, reports that this may not improve treatment compliance are conflicting [14, 15]. The suggestion has been made that these symptoms could have existed prior to therapy being initiated, however, they commonly disappear upon cessation of breathing treatment [10]. Currently there is no clear explanation as to why apparent nasal mucosal dysfunction occurs, particularly during the absence of oral mouth leak, when breathing ambient air at slightly elevated pressures.

Both the autonomic and purinergic systems regulating nasal heating and water supply play a regulatory role in nasal air-conditioning, however, the influence elevated air pressure has on these two systems is poorly understood. Matching the nasal mask temperature and humidity conditions to that required by the patient rather than fully heating and humidifying the breathing gas to core body conditions found in the lungs offers both equipment energy savings and reduction in negative treatment side-effects such as over heating or over humidification.

The project aims at determining if changes in nasal geometry or blood flow occur during the application of nasal applied breathing therapy, such as nasal continuous positive airway pressure (n-CPAP), and to provide data that can then be implemented in a nasal air-conditioning predictive model. This predictive model will be used to further our understanding of nasal air-conditioning and enable optimised air delivery conditions to be identified on which new therapy devices can be developed.

#### **Procedure:**

**Explain the philosophical and/or methodological approach taken to obtaining information and/or testing the hypothesis(es).**

The MRI data of internal nasal geometry and blood flow specific to the nasal arteries will be recorded for differing conditions of breathing. Comparison will be made between nasal geometry and blood flow data gathered during breathing air under ambient conditions and then pressurised by a commercially available n-CPAP device. This MRI data will be used to identify if any variation in nasal geometry or blood flow occurs that would lead to change in nasal heat and water mass flow within the nose. It may also be used within computational packages to predict the magnitude of these values. The occurrence, if any, of changes in nasal geometry or nasal blood flow needs to be established to validate any assumptions made in developing a predictive nasal air-conditioning model.

Pressurised patient air will be supplied by a commercially available n-CPAP system at a level considered to be at the maximal end of what is normally prescribed by obstructive sleep apnoea (OSA) sleep physicians. Airflow through both nostrils will be simultaneously measured both prior to and immediately after the MRI test to determine if the participant's nasal cycle has switched during scanning. Data and images gathered will be used to determine if n-CPAP air pressure causes variation in nasal geometry and nasal artery blood flow. Results will be incorporated in a predictive mathematical model of nasal air-conditioning.

**State in practical terms what research procedures or methods will be used.**

The MRI device will be used to record 2D and 3D nasal geometry as well as nasal blood flow using arterial spin labelling (ASL) technique during patient breathing of both ambient air and air under elevated pressure utilising a commercially available n-CPAP breathing therapy device. A head coil will be utilised within the MRI device to serve a number of different imaging functions. ASL involves modifying the conventional MRI hydrogen molecule spin in the nasal blood stream to be orthogonal to the magnetic field for a short period of time, during which its path is tracked and blood flow velocity then calculated.

**State how information will be gathered and processed.**

Step 1: Participant's age, gender, ethnicity and state of upper respiratory health will be recorded on Demographic Data form.

Step2: Participant airflow through each nostril will be simultaneously measured and peak airflow recorded to determine phase of participant's nasal cycle.

Step 3: A nasal mask without an air supply hose will be fit to the participant who will then assume the recumbent position within the MRI machine. The MRI head coil will then be positioned over their head.

Step 4: After a suitable settling time to enable the participant to settle in, the MRI device will record the nasal space geometry as well as the nasal arterial blood flow data.

Step 5: The air hose from the n-CPAP air delivery unit will then be connected to the participant's nasal mask and ambient air pressurised to 14 cm H<sub>2</sub>O supplied to the participant.

Step 6: After a suitable settling time the MRI device will record comparative data of nasal space geometry and nasal arterial blood flows. All MRI image data will be stored by computer.

Step 7: Upon completion of MRI data acquisition, the participant airflow through each nostril will again be simultaneously measured and peak airflow recorded.

Step 6: Data will be analysed using suitable computer software.

**State how your data will be analysed.**

Internal nasal geometry during ambient air breathing will be compared to images recorded during nasal breathing during exposure to elevated air pressure.

3 D data for each of the participants will be analysed within computational packages to estimate any volume change utilising standard MRI computational analysis package.

Nasal blood flow will be measured using arterial spin labelling (ASL) techniques and analysis software.

Nasal airflow through each nostril, both prior to and post MRI, will be compared to determine if change in the nasal cycle has occurred during testing as this will have an influence on nasal blood flow and geometry.

**Provide the statistical or methodological justification for this.**

Previous measurements of nasal airflow using cadaver (dead people), plastination (plastic impregnation of tissue), ultrasound or MRI imaging techniques all correlate well to *in-vivo* measurements, however, none of these investigations have considered the effect air pressure has on *in-vivo* nasal geometry and blood flow through soft tissue deformation. MRI data can provide this information.

Comparison of *in-vivo* nasal geometry and arterial flows between ambient and pressurised breathing will validate or disprove the hypothesis that these parameters are independent of applied breathing therapy air pressure. This feasibility study aims to test if MRI and arterial spin labelling (ASL) techniques can detect any change under these conditions.

## References

*Please include the references for your responses to this section in the standard format used in your discipline.*

1. Wolf, M., S. Naftali, R.C. Schroter, and D. Elad, *Air-conditioning characteristics of the human nose*. J. Laryngol. Otol., 2004. **118**(2): p. 87-92.
2. Sahin-Yilmaz, A., F.M. Baroody, M. DeTineo, G. Cuttance, D. Makinson, J.M. M. Pinto, E.T. Naureckas, and R.M. Naclerio, *Effect of changing airway pressure on the ability of the human nose to warm and humidify air*. Ann. Otol. Rhinol. Laryngol., 2008. **117**(7): p. 501-507.
3. Barnes, M., R.D. McEvoy, S. Banks, N. Tarquinio, C.G. Murray, N. Vowles, and R.J. Pierce, *Efficacy of Positive Airway Pressure and Oral Appliance in Mild to Moderate Obstructive Sleep Apnea*. Am. J. Respir. Crit. Care Med., 2004. **170**(6): p. 656.
4. Wiest, G.H., F.S. Fuchs, W.M. Brueckl, G. Nusko, I.A. Harsch, E.G. Hahn, and J.H. Ficker, *In vivo efficacy of heated and non-heated humidifiers during nasal continuous positive airway pressure (nCPAP)-therapy for obstructive sleep apnoea*. Respir. Med., 2000. **94**(4): p. 364-368.
5. Constantinidis, J., D. Knobber, H. Steinhart, J. Kuhn, and H. Iro, *Fine-structural investigations of the effect of nCPAP-mask application on the nasal mucosa*. Acta Otolaryngol. (Stockh.), 2000. **120**(3): p. 432-437.
6. Malik, N.W. and G.S. Kenyon, *Changes in the nasal airway mucosa and in nasal symptoms following continuous positive airway pressure (n-CPAP) for obstructive sleep apnoea*. Australian Journal of Oto-Laryngology, 2004. **7**(1): p. 17-20.
7. Worsnop, C.J., S. Miseski, and P.D. Rochford *The routine use of humidification with nasal continuous positive airway pressure*. Intern. Med. J., 2009. **9999**, DOI: 10.1111/j.1445-5994.2009.01969.x.
8. Wiest, G.H., G. Lehnert, W.M. Brück, M. Meyer, E.G. Hahn, and J.H. Ficker, *A heated humidifier reduces upper airway dryness during continuous positive airway pressure therapy*. Respir. Med., 1999. **93**(1): p. 21-26.

9. Rakotonanahary, D., N. Pelletier-Fleury, F. Gagnadoux, and B. Fleury, *Predictive factors for the need for additional humidification during nasal continuous positive airway pressure therapy*. Chest, 2001. **119**(2): p. 460-465.
10. Hollandt, J.H. and M. Mahlerwein, *Nasal breathing and continuous positive airway pressure (CPAP) in patients with obstructive sleep apnea (OSA)*. Sleep and Breathing, 2003. **7**(2): p. 87-93.
11. Fischer, Y., T. Keck, R. Leiacker, A. Rozsasi, G. Rettinger, and P.M. Gruen, *Effects of nasal mask leak and heated humidification on nasal mucosa in the therapy with nasal continuous positive airway pressure (nCPAP)*. Sleep Breath, 2008. **12**: p. 353-357.
12. Devouassoux, G., P. Lévy, E. Rossini, I. Pin, M. Fior-Gozlan, M. Henry, D. Seigneurin, and J.-L. Pépin, *Sleep apnea is associated with bronchial inflammation and continuous positive airway pressure-induced airway hyperresponsiveness*. J. Allergy Clin. Immunol., 2007. **119**(3): p. 597-603.
13. Arfoosh, R. and J. Rowley, *Continuous positive airway pressure for obstructive sleep apnea: an update*. Journal of Respiratory Diseases, 2008. **29**(9): p. 365-373.
14. Mador, M.J., M. Krauza, A. Pervez, D. Pierce, and M. Braun, *Effect of heated humidification on compliance and quality of life in patients with sleep apnea using nasal continuous positive airway pressure*. Chest, 2005. **128**(4): p. 2151-2158.
15. Massie, C.A., R.W. Hart, K. Peralez, and G.N. Richards, *Effects of humidification on nasal symptoms and compliance in sleep apnea patients using continuous positive airway pressure*. Chest, 1999. **116**: p. 403-408.

## Participants

### Who are the participants?

Adults between the ages of 20 ~ 60 years with healthy upper respiratory tract and able to wear a nasal mask that seals on the face can participate in this research. This includes those who have experienced trauma to the face.

### What criteria are to be used in recruiting the participants?

Non smokers with no history of OSA or sinus complaints will be recruited as participants; anyone who meets the age and respiratory health criteria will be recruited.

### What criteria are to be used for selecting participants from those recruited?

It is desired that participants cover a range of age, gender and ethnicity representative of the population so they will be selected in order to fulfil this goal.

### Are there any potential participants who will be excluded?

*If your answer is yes, please detail the criteria for exclusion.*

Yes, those who have had an upper respiratory infection within the last two weeks prior to participating in study.

A visual nasal examination will be undertaken by an ENT specialist, Dr Jim Bartley, to ascertain the presence of healthy nasal mucosa, absence of nasal polyps or turbinate abnormalities, such as infection or other conditions that may influence nasal airflow regulation.

People with metallic implants, pacemakers or are pregnant will be excluded. Those currently undergoing n-CPAP therapy will also be excluded.

**Are there any potential conflicts of interest or possible coercive influences in the professional, social, or cultural relationships between the researcher and the participants (e.g. dependent relationships such as teacher/student; parent/child; employer/employee; pastor/congregation etc.)?**

No

**If your answer was 'Yes', please identify the nature of the relationships concerned and provide full information about the processes being incorporated into the research design to mitigate any adverse affects that may arise from them.**

N/A

**How many participants will be selected?**

8 participants will be selected.

**What is the reason for selecting this number?**

This is a feasibility study since arterial spin labelling (ASL) techniques have never been used before to attempt to detect any change in nasal blood flow that may occur during applied breathing therapy.

Natural variation in nasal morphology means every participant will be unique so there is no justification in seeking an average determination of nasal geometry and blood flows. Data will only be collected at ambient and elevated air pressure to validate or disprove the hypothesis that nasal morphology and vasculature flows are independent of applied air pressure.

Access to the MRI suite is being charged out at a discounted student research rate of \$550/hr and, since this is a feasibility study, the number of participants selected is based on available funding.

**Provide a statistical justification where applicable, if you have not already provided one in C.4 5. above.**

Being a feasibility study, statistical justification is not applicable.

**Is there a control group?**

*If your answer is yes, please describe and state how many are in the control group.*

No. Each individual will be their own control.

**Describe in detail the recruitment methods to be used.**

*If you will be recruiting by advertisement or email, please attach a copy to this Application Form*

Posters will be used to advertise the feasibility study for non-smoking people.

People enquiring in response to the posters will be sent a Participant Information Sheet which provides further detail information and also invites them to participate in the study.

Those who respond to the Participant Information Sheet by contacting the Project Manager, signalling they wish to participate in this study, will then be interviewed by the Project Manager which provides an arena for informed dialogue to occur.

A screening process will then be undertaken to exclude those who are unsuited to undertake this feasibility study and to provide the desired population sample variety. The final sample of participants selected will be notified and a mutually agreeable time will be arranged for the study to be undertaken.

Prior to undertaking the MRI scan the participant will be requested to sign the Consent Form.

### **How will information about the project be given to participants?**

*(e.g. in writing, verbally). A copy of information to be given to prospective participants is to be attached to this Application Form. If written information is to be provided to participants, you are advised to use the Information Sheet exemplar.*

General information will initially be given from the poster; however, more detailed and specific information will be given to prospective participants by the Participant Information Sheet. Those who respond and wish to participate in the study will be interviewed by the Project Manager which provides an arena for detailed informed dialogue to occur and further information to be given.

### **Will the participants have difficulty giving informed consent on their own behalf?**

*Consider physical or mental condition, age, language, legal status, or other barriers. If the answer is yes, please provide full details.*

No

### **If participants are not competent to give fully informed consent, who will consent on their behalf?**

The MRI image data will only be recorded for those people who give informed consent on their own.

### **Will these participants be asked to provide assent to participation?**

*If the answer is yes, please attach a copy of the assent form which will be used. Please note that assent is not the same as consent (please refer to the Glossary in Appendix A of the ATEC Guidelines and Procedures.*

N/A

### **Will consent of participants be gained in writing?**

*If the answer is yes, please attach a copy of the Consent Form which will be used. If the answer is No, please provide the reasons for this.*

Yes. Participants will discuss the objectives and data acquisition process with the Project Manager prior to reading and completing the consent form. Time to ensure the consent is both informed and voluntary will vary depending upon the discussion and questions raised but should take around 10 to 20 minutes.

### **Will the participants remain anonymous to the researcher?**

*Please note that anonymity and confidentiality are different. If the answer is yes, please state how, otherwise, if the answer is no, please describe how participant privacy issues and confidentiality of information will be preserved.*

No

### **In the final report will there be any possibility that individuals or groups could be identified?**

*If the answer is yes, please explain how and why this will happen.*

No. Only aggregate data will be reported, in such a form that no individuals or groups can be identified from it.

**Will feedback or findings be disseminated to participants (individuals or groups)?**

*If the answer is yes, please explain how this will occur and ensure that this information is included in the Information Sheet.*

A summary of the trends noted in the measurements will be made available to participants through the Institute's website.

**Will the findings of this study be of particular interest to specific cultures or social groups?**

*If your answer is 'Yes', please identify how the findings will be made available to them.*

No

## Other Project Details

**Where will the project be conducted?**

*Please provide the name/s of the Institution/s, town/s, city or cities, region or country that best answers this question.*

Data will be collected in the Centre for Advance MRI (CAMRI) Auckland, New Zealand. Data will be stored and archived at both the secure office of the Researcher at the AUT City Campus.

**Who is in charge of data collection?**

The Project Manager (David White) will be in charge of data collection.

**Who will interact with the participants?**

The Project Manager (David White) will interact with the participants.

**What ethical risks are involved for participants in the proposed research?**

*Please consider the possibility of moral, physical, psychological or emotional risks to participants, including issues of confidentiality and privacy. Researchers are urged to consider this issue from the perspective of the participants, and not only from the perspective of someone familiar with the subject matter and research practices involved.*

The MRI scan may detect nasal disorders unrelated to this project but potentially significant to the health of the participant. Depending upon their desire to be notified, as indicated on the participant Consent Form, if this were to occur the participant may be contacted in a private and confidential manner and advised to seek advice from their medical practitioner.

**Are the participants likely to experience any discomfort, embarrassment (physical, psychological, social) or incapacity as a result of the research's procedures?**

The nasal continuous positive airway pressure (n-CPAP) form of breathing therapy has been prescribed for over 30 years and symptoms relate to minor pressure augmentation. These commonly include increased breathing effort during exhalation, puffy eyes, sensation of pressure in the ears or feeling bloat. If experienced, these symptoms are temporary and normally disappear upon cessation of treatment.

MRI techniques have been used in the clinical environment for the past 20 years. No physical discomforts or incapacity have been noted in people who used these techniques. Common MRI side effects are

related to the noise generated during testing which include headaches, dizziness, sweating, nausea, fatigue. If experienced, these symptoms are temporary, mostly caused by the noise during scan and diminish upon cessation of treatment.

**If there are risks, please identify their probability and describe how they will be mitigated.**

*Please describe how these will be minimised or mitigated (e.g. participants do not need to answer a question that they find embarrassing or they may terminate an interview or there may be a qualified counsellor present in the interview or the findings will be reported in a way that ensures that participants cannot be individually identified, etc.) Possible risks and their mitigation should be fully described in the Information Sheets for participants.*

Symptoms related to nasal continuous positive airway pressure (n-CPAP) breathing therapy commonly disappear upon cessation of treatment. If these become a problem then the machine will be turned off.

MRI side effects are temporary and mostly caused by the noise during scan. These symptoms commonly disappear upon cessation of treatment and if these become a problem then the machine will be turned off.

Participants will be advised to seek professional medical advice in the occurrence of detection of nasal disorders, unrelated to this project but potentially significant to their health.

**If the participants are likely to experience any discomfort, embarrassment, or incapacity, what provision for counselling has been made, either with AUT Counselling (who also provide an online service) or with other counselling professionals (this is to be at no charge to the participants)?**

*Please refer to section 2.3 of AUTECH's Applying for Ethics Approval: Guidelines and Procedures in the Ethics Knowledge Base. If the answer is No, please explain the arrangements which have been made to have qualified personnel available to deal with unexpected adverse physical or psychological consequences?*

N/A

**What risks are involved for the researcher(s) in the proposed project (such as physical, social, psychological, or safety risks)?**

*If this project will involve interviewing participants in private homes, undertaking research overseas, or going into similarly vulnerable situations, then a Researcher Safety protocol should be designed and appended to this application.*

None.

**Will there be any other physical hazards introduced to AUT staff and/or students through the duration of this project?**

*If the answer is yes, please provide details of management controls which will be in place to either eliminate or minimise harm from these hazards (e.g. a hazardous substance management plan).*

No

**Is deception of participants involved at any stage of the research?**

*If the answer is yes, please provide full details of and rationale for the deception. Please refer to Section 2.4 of AUTECH's Applying for Ethics Approval: Guidelines and Procedures when considering this question.*

No

**How much time will participants have to give to the project?**

The preparing and scanning time for MRI is about 40 minutes. Given that it takes between 5-10 minutes to recruit participants and gain informed consent from them and another 10 minutes to conduct pre and post MRI

nasal airflow examination. The participant will have to give about 1 hr to the project.

**Will any information on the participants be obtained from third parties?**

*If the answer is yes, please provide full details. This includes use of third parties, such as employers, in recruitment.*

No

**Will any identifiable information on the participants be given to third parties?**

*If the answer is Yes, please provide full details.*

No

**Provide details of any payment, gift or koha and, where applicable, level of payment to be made to participants.**

*Please refer to Section 2.1 of the AUTECH's Applying for Ethics Approval: Guidelines and Procedures and Appendix A of that document for AUTECH's policy on Payment and Koha, especially in relation to recruitment.*

Payment as compensation for travel and parking expenses in the form of fuel vouchers to the value of \$50/participant.

## **Data and Consent Forms**

**Who will have access to the data?**

Only David White, Research Manager and Researcher, will have access to the data.

**Are there plans for future use of the data beyond those already described?**

*The applicant's attention is drawn to the requirements of the Privacy Act 1993 (see Appendix I). If there are future plans for the use of the data, then this needs to be explained in the Information Sheets for participants.*

No.

**Where will the data be stored once the analysis is complete?**

*Please provide the exact storage location. AUTECH normally requires that the data be stored securely on AUT premises in a location separate from the consent forms. If you are proposing an alternative arrangement, please explain why.*

The recorded data will be stored within an external hard drive locked in the office of the Research Manager (David White).

**For how long will the data be stored after completion of analysis?**

*AUTECH normally requires that the data be stored securely for six years. If you are proposing an alternative arrangement, please explain why.*

10 years.

**Will the data be destroyed?**

*If the answer is yes, please describe how the destruction will be effected. If the answer is no, please provide the reason for this.*

Yes. The original data will be stored for a period of 10 years from the completion of the project. After this period, the original data will be securely deleted from the secure hard drive.

**Who will have access to the Consent Forms?**

Only the Project Manager and Researcher will have access to the consent forms.

### **Where will the completed Consent Forms be stored?**

*Please provide the exact storage location. AUTECH normally requires that the Consent Forms be stored securely on AUT premises in a location separate from the data. If you are proposing an alternative arrangement, please explain why.*

The consent forms will be stored securely and separate to the data in the offices of the Institute of Biomedical Technologies (IBTECH) at the AUT City Campus.

### **For how long will the completed Consent Forms be stored?**

*AUTECH normally requires that the Consent Forms be stored securely for six years. If you are proposing an alternative arrangement, please explain why.*

10 years; we will be destroying the consent forms with the recorded dataset.

### **Will the Consent Forms be destroyed?**

*If the answer is yes, please describe how the destruction will be effected. If the answer is no, please provide the reason for this.*

Yes; consent forms will be shredded.

## **Material Resources**

**Has an application for financial support for this project been (or will be) made to a source external to AUT or is a source external to AUT providing (or will provide) financial support for this project?**

No

*If the answer to G.1 was 'yes', please provide the name of the source, the amount of financial support involved, and clearly explain how the funder/s are involved in the design and management of the research.*

N/A

**Has the application been (or will it be) submitted to an AUT Faculty Research Grants Committee or other AUT funding entity?**

*If the answer is yes, please provide details.*

Yes

*If the answer to G.2 was 'yes', please provide the name of the source, the amount of financial support involved, and clearly explain how the funder/s are involved in the design and management of the research.*

The Institute of Biomedical Technologies (IBTECH) is providing funding of \$5,000 as part of its ongoing research initiative in respiratory devices and therapies. The Institute Director is the applicant of this ethics approval.

**Is funding already available, or is it awaiting decision?**

*Please provide full details.*

Funding is available as on date of application.

The Institute of Biomedical Technologies (IBTECH) has funding available to support this project.

The MRI device and operator are charged out at a student research rate of \$550/hr by The Centre for Advance MRI (CAMRI).

Compensation for travel and parking expenses amounts to \$50/ participant in the form of fuel vouchers.

**Please provide full details about the financial interest, if any, in the outcome of the project of the researchers, investigators or research organisations mentioned in Part A of this application.**

None - Internal research for Researcher PhD study.

## Other Information

**Have you ever made any other related applications?**

*If the answer is yes, please provide the AUTECH application / approval number(s)*

No

## Checklist

*Please ensure all applicable sections of this form have been completed and all appropriate documentation is attached as incomplete applications will not be considered by AUTECH.*

Section A	General Information Completed	<input checked="" type="checkbox"/>
	Signatures/Declaration Completed	<input checked="" type="checkbox"/>
Section B	Project General Information Completed	<input checked="" type="checkbox"/>
Section C	Project Details Completed	<input checked="" type="checkbox"/>
Section D	Participant Details Completed	<input checked="" type="checkbox"/>
Section E	Other Project Details Completed	<input checked="" type="checkbox"/>
Section F	Data & Consent Forms Details Completed	<input checked="" type="checkbox"/>
Section G	Material Resources Completed	<input checked="" type="checkbox"/>
Section H	Other Information Completed	<input checked="" type="checkbox"/>

**Spelling and Grammar Check** (please note that a high standard of spelling and grammar is required in documents that are issued with AUTECH approval)

☒

### Attached Documents (where applicable)

Participant Information Sheet(s)	<input checked="" type="checkbox"/>
Consent Form(s)	<input checked="" type="checkbox"/>
Questionnaire(s)	N/A
Indicative Questions for Interviews or Focus Groups	N/A
Observation Protocols	N/A
Recording Protocols for Tests	N/A
Advertisement(s)	<input checked="" type="checkbox"/>
Hazardous Substance Management Plan	N/A
Any Confidentiality Agreement(s)	<input checked="" type="checkbox"/>
Other Documentation	N/A

*Before submitting this application, please note the following:*

❖ *If you think that your research may be of low ethical risk, use the EA8RA self assessment form to make sure that this is the correct form for your application;*

- ❖ *Incomplete or incorrectly formatted applications will not be considered by AUTEK;*
- ❖ *Please check online for the most recent version of this form before submitting your application;*
- ❖ *Please do not alter the formatting of this form or delete any sections. If a particular question is not applicable to your research, please state that as your response to that question;*

*This form needs to be submitted, along with all associated documents as follows:*

- ❖ *In printed form;*
- ❖ *With the required signatures in sections A.8 and A.9;*
- ❖ *Single sided;*
- ❖ *Using clips rather than staples;*
- ❖ *By 4 pm on the agenda closing date at:*

*The AUTEK Secretariat  
Room WO201, WO Building  
56 Wakefield Street, City Campus.*

- ❖ *The Internal Mail Code is D-89. If sending applications by Internal Mail, please ensure that they are posted at least two days earlier to allow for any delay that may occur.*

## Auckland University of Technology Ethics Committee (AUTEK)

**EA8RA**

### SELF ASSESSMENT OF RESEARCH PROJECTS FOR ETHICS APPROVAL



*Please read the notes at the end of the form before submitting this application.*

## General Information

### Project Title

Feasibility study into the use of magnetic resonance imaging (MRI) to detect change in internal nasal geometry and blood flow during nasal breathing therapy.

### Applicant Name and Qualifications

*When the researcher is a student (including staff who are AUT students), the applicant is the principal supervisor. When the researcher is an AUT staff member undertaking research as part of employment or a staff member undertaking research as part of an external qualification, the applicant is the researcher.*

Professor Ahmed Al-Jumaily

Doctor of Philosophy (Mechanical Engineering), PhD, 1977

Master of Science (Mechanical Engineering), MSME, 1973

Bachelor of Science (Mechanical Engineering), BSc, 1971

### Student Name(s)

*Please complete this section only if the researcher is a student*

David White

## Assessment of Ethical Risk

*The following sections will help assess the risk of your research project causing physical or psychological harm to participants and whether the nature of any harm is minimal and no more than is normally encountered in daily life.*

**Note: Student researchers are required to review the completed form with their supervisor.**

## **Risk of Harm**

**Does your project involve situations in which the researcher may be at risk of harm?**

No

**Does your project involve use of a questionnaire or interview or other research process, whether or not it is anonymous, which might reasonably be expected to cause discomfort, embarrassment, anxiety or psychological or spiritual harm to any or some participants?**

No

**Does your project involve processes that are potentially disadvantageous to a person or group, such as the collection of information, images etc. which may expose that person/group to discrimination or criticism?**

No

**Does your project involve collection of information of illegal behaviour(s) gained during the research which could place the participants at current or future risk of criminal or civil liability or be damaging to their financial standing, employability, professional or personal relationships?**

No

**Does your project involve any form of physically invasive procedure on volunteer participants, such as the collection of blood, body fluid or tissue samples, exercise regimes, physical restraint or physical examination?**

No

**Does your project involve the administration of any form of drug, medicine (other than in the course of standard medical procedure), or placebo?**

No

**Does your project involve physical pain, beyond mild discomfort?**

No

**Does your project involve the intentional recruitment of participants who are staff or students of AUT. (Note: section 6.1 of AUTECH's *Applying for Ethics: Guidelines and Procedures* provides an exception for audit or evaluation purposes only)?**

No

**Does your project involve any AUT teaching which involves the participation of AUT students for the demonstration of procedures or phenomena which have a potential for harm?**

No

**Does your project involve participants who are in any sort of dependent relationship to the researchers?**

No

## **Informed and Voluntary Consent**

**Does your project involve the use of oral consent of participants rather than written consent?**

No

**Does your project involve participants who are unable to give informed consent?**

No

Does your project involve your (or your supervisor's) own students as participants (Note: section 6.1 of AUTECH's *Applying for Ethics: Guidelines and Procedures* provides an exception for audit or evaluation purposes only)?

No

Does your project involve the participation of children aged 8 years or younger?

No

Does your project involve the participation of children aged sixteen years or younger where parental consent is not being sought?

No

Does your project involve participants who are in a dependent situation, such as people with a disability, or residents of a hospital, nursing home or prison or patients highly dependent on medical care?

No

Does your project involve participants who are vulnerable (e.g. the elderly, prisoners, persons who have suffered abuse, persons who are not competent in English, new immigrants)?

No

Does your project involve the use of previously collected information or biological samples for which there was no explicit consent for this research?

No

### Privacy or Confidentiality

Does your project involve any research about organisational practices where information of a personal or sensitive nature may be collected and where participants may be identified?

No

### Deception

Does your project involve deception of the participants, including concealment and covert observations except in a public place?

No

### Conflict of Interest

Does your project involve a conflict of interest situation for the researcher (where the researcher has more than one role or interest e.g. teacher/researcher, treatment provider/researcher, employer/researcher? (*Financial interests in research outcomes, sponsorship, etc. should be declared here*))

Yes. The researcher & student, David White is also a lecturer at AUT.

### Payment to Participants

Does your project involve payments or other financial inducements (other than koha, reasonable reimbursement of travel expenses or time, or entry into a modest prize draw) to participants?

No

### Procedural Issues

Does your project involve a requirement by an outside organisation (e.g. a funding organisation or a journal in which you wish to publish) for AUTECH approval?

No

## Other Issues

Does your project involve any ethical issues which may mean that the research is not low risk, other than those mentioned above?

No

*If your answer was yes, please briefly describe the issues involved.*

## Applying for Ethics Approval

### If your answer to **ALL** the above questions is 'No'

*Please complete the EA8 application form for low ethical risk approvals and send it together with this completed self-assessment to your AUTECH Faculty Representative. If you work outside a faculty, please send them to the Ethics Coordinator who will forward them to the AUTECH Faculty Representative in the most appropriate faculty for the subject matter of the research.*

### If your answer to **at least one** of the above questions is 'Yes'

*If you have answered 'Yes' to one or more of the above questions, you will normally need to submit a full EA1 application form to AUTECH, through the Ethics Coordinator. However, if you consider that the reasons why you responded 'yes' do not take the research out of the low ethical risk category, you may wish to consult your AUTECH faculty representative or the Ethics Coordinator before submitting a full application.*

*Before submitting this application, please note the following:*

- ❖ *Incomplete or incorrectly formatted applications will not be considered by AUTECH;*
- ❖ *Please check online for the most recent version of this form before submitting your application;*
- ❖ *Please do not alter the formatting of this form or delete any sections. A response is required for each question in part B.*

*This form needs to be submitted, along with a completed EA8 application form and all associated documents as follows:*

- ❖ *In electronic form;*
- ❖ *By 4 pm on the submission date to:*

*The AUTECH Faculty Representative for your Faculty (contact details for the AUTECH Faculty Representatives is available online in the Ethics Knowledge Base, accessible via <http://www.aut.ac.nz/about/ethics>).*

## B2.2 AUTC Memorandum of Ethics Approval



# MEMORANDUM

## Auckland University of Technology Ethics Committee (AUTC)

---

To: Ahmed Al-Jumaily  
From: **Charles Grinter** Ethics Coordinator  
Date: 14 July 2010  
Subject: Ethics Application Number 10/121 **Feasibility study into the use of magnetic resonance imaging (MRI) to detect change in internal nasal geometry and blood flow during nasal breathing therapy.**

---

Tena koe Ahmed

Thank you for providing written evidence as requested. I am pleased to advise that it satisfies the points raised by the Auckland University of Technology Ethics Committee (AUTC) at their meeting on 14 June 2010 and that I approved your ethics application. This delegated approval is made in accordance with section 5.3.2.3 of AUTC's *Applying for Ethics Approval: Guidelines and Procedures* and is subject to endorsement at AUTC's meeting on 9 August 2010.

Your ethics application is approved for a period of three years until 14 July 2013.

I advise that as part of the ethics approval process, you are required to submit the following to AUTC:

- A brief annual progress report using form EA2, which is available online through <http://www.aut.ac.nz/research/research-ethics>. When necessary this form may also be used to request an extension of the approval at least one month prior to its expiry on 14 July 2013;
- A brief report on the status of the project using form EA3, which is available online through <http://www.aut.ac.nz/research/research-ethics>. This report is to be submitted either when the approval expires on 14 July 2013 or on completion of the project, whichever comes sooner;

It is a condition of approval that AUTC is notified of any adverse events or if the research does not commence. AUTC approval needs to be sought for any alteration to the research, including any alteration of or addition to any documents that are provided to participants. You are reminded that, as applicant, you are responsible for ensuring that research undertaken under this approval occurs within the parameters outlined in the approved application.

Please note that AUTC grants ethical approval only. If you require management approval from an institution or organisation for your research, then you will need to make the arrangements necessary to obtain this.

When communicating with us about this application, we ask that you use the application number and study title to enable us to provide you with prompt service. Should you have any further enquiries regarding this matter, you are welcome to contact Charles Grinter, Ethics Coordinator, by email at [ethics@aut.ac.nz](mailto:ethics@aut.ac.nz) or by telephone on 921 9999 at extension 8860.

On behalf of the AUTEK and myself, I wish you success with your research and look forward to reading about it in your reports.

On behalf of Madeline Banda Executive Secretary  
**Auckland University of Technology Ethics Committee**

Cc: David White davidwhite@aut.ac.nz

# **Invitation to Participate in Breathing Therapy Feasibility Study**



**Image of nasal mask on face  
(Mayo Foundation for Medical Education and Research)**

The Institute of Biomedical Technologies (IBTec) within AUT University is conducting research aimed to improve patient comfort during into the use nasal applied breathing therapy.

To assist in this research, non- smoking adults between the ages of 20 to 60 years with good respiratory health are invited to participate in the collection of data using magnetic resonance imaging (MRI) techniques.

If you have are able to wear a nasal mask, have no recent history of upper airway or sinus infection, do not suffer any respiratory condition or allergy (mild asthma excluded), are interested in having a nasal examination and then participating in this feasibility study or require further information, please contact the Research Manager:

David White

Ph (09) 921-9999 ext. 8352

[david.white@aut.ac.nz](mailto:david.white@aut.ac.nz)

**Approved by the Auckland University of Technology Ethics Committee on 14<sup>th</sup> July 2010,  
AUTEC Reference number 10/121.**

# Participant Information Sheet



## **Date Information Sheet Produced:**

27 May 2010

## **Project Title**

Feasibility study into the use of magnetic resonance imaging (MRI) to detect changes in internal nasal geometry and blood flow during nasal breathing therapy.

## **An Invitation**

My name is David White, a researcher who is undertaking this task as part of my study towards a Doctor of Philosophy degree (PhD).

As part of my research work I am developing a mathematical model capable of predicting the optimum nasal mask conditions for patients undertaking nasal applied breathing therapy. This therapy ranges from situations where breathing gases are delivered during hospital care or during continuous positive air pressure (n-CPAP) therapy used to treat obstructive sleep apnoea (OSA), a condition of temporary choking during sleep which effects over 6% of the adult population of the western world. To achieve an accurate model we require data on the geometry and blood flow behaviour of the human nose during the application of nasal breathing therapy, in this case n-CPAP and we invite non-smoking adults between the ages of 20 ~ 60 years with healthy upper respiratory tract and no history of sinus complains or suffering OSA to participate in this research.

Your participation is entirely voluntary and you may withdraw at any time prior to the completion of data collection.

## **What is the purpose of this research?**

The primary purpose of this research is to improve patient comfort during nasal applied breathing therapy by matching the delivered air conditions to that best suited to the patient's response to elevated air pressure. In order to achieve this a mathematical model predicting the optimum nasal mask air conditions to best suit the patient's needs is being developed. To enable development of this model, we first need to establish what changes in nasal geometry and blood flow occurs when the nose is exposed to elevated air pressure typical of that used during nasal applied breathing therapy. We want to undertake comparative measurement of nasal geometry and blood flow during breathing of ambient air and then pressurised air from an n-CPAP device.

## **How was I chosen for this invitation?**

You have responded to posters advertising this study which invited non- smoking adults between the ages of 20 ~ 60 years and with good respiratory health to participate in this research.



**Image of nasal mask on face (Mayo Foundation for Medical Education and Research)**

Also, you can wear a nasal mask that seals on your face, have no recent history of upper airway or sinus infection or allergy and do not suffer any respiratory condition (mild asthma excluded)

### **What will happen in this research?**

The aim of this project is to identify and quantify changes in nasal geometry and blood flow created by the application of n-CPAP breathing therapy.



Prior to undertaking the MRI scan your nose will be examined by an ear, nose & throat (ENT) specialist to ensure the absence of any problems, such as swelling due to infection, which may influence the study. Prior to commencing the MRI scan, a nasal mask will be placed over your nose. During the scan process you will breathe ambient air and then air under a slight pressure which will be delivered to the mask whilst you lay relaxed in the MRI machine.

**Image of MRI machine and head coil (Philips Healthcare)**

Images of nasal geometry and nasal blood flow will be recorded using a magnetic resonance imaging (MRI) device. To enable measurement of nasal blood flows a technique called Arterial Spin Labelling (ASL) will be used. This involves modifying the conventional MRI hydrogen molecule spin in the nasal blood stream to be at right-angles to the magnetic field for a short period of time, during which its path is tracked and blood flow velocity then calculated.

The data will be used to establish if changes in nasal geometry and blood flow are significant and require incorporation into the predictive nasal air-conditioning model.

### **What are the discomforts and risks?**

The n-CPAP form of nasal applied breathing therapy has been prescribed for over 20 years. There have been reports of physical discomfort, limited to that associated with minor pressure augmentation, such as increased breathing effort during exhalation, puffy eyes, pressure equalisation in the ears or sensation of bloat but these disappear upon cessation of treatment. If this becomes a problem then the machine will be switched off.

The MRI techniques for image acquisition have been used in the clinical environment for a large part of the past 20 years. No physical discomforts or incapacity have been noted in people who used these techniques. Common [MRI side effects](#) are headaches, dizziness, sweating, nausea, fatigue. These symptoms of MRI side effect are temporary, mostly caused by the noise during the scan. If this becomes a problem then the machine will be switched off.

Participants may feel concerned should MRI reveal nasal abnormalities and should this occur they will be referred to their General Practitioner if this is indicated in the Consent Form.

**How will my privacy be protected?**

Although your name will be recorded on the Consent Form this will only be accessed by the Project Manager for administrative purposes. Only anonymous data will be available for publications and presentation of the research.

Only myself as researcher will have access to the anonymous data.

The data will be securely stored within a separate hard drive locked within the researcher's office. Consent form and Patient Questionnaires will be securely stored at the Institute of Biomedical Technologies, where access to it will be controlled.

Please note that the recorded data will be archived and securely stored for 10 years then destroyed.

**What are the costs of participating in this research?**

Your participation will require approximately 60 minutes of your time and not more than 80 minutes.

**How is this research being funded?**

The Institute of Biomedical Technologies (IBTec), part of AUT University, is internally funding this research.

**What are the benefits of this study?**

IBTec intends to publish the results of this study in journal papers or conference proceedings and will benefit from ongoing research output in respiratory breathing therapies and devices. The results of this study may lead to improved breathing therapies being utilised to improve patient comfort and treatment compliance.

**What compensation is available for injury or negligence?**

In the unlikely event of a physical injury as a result of your participation in this study, rehabilitation and compensation for injury by accident may be available from the Accident Compensation Corporation, providing the incident details satisfy the requirements of the law and the Corporation's regulations.

**What opportunity do I have to consider this invitation?**

You are welcome to consider this invitation for as long as it takes you to make up your mind whether you would like to participate or not. We are happy to answer any questions that you may have.

Furthermore, since your participation is entirely voluntary, you may choose to withdraw at any time and for any reason prior to the completion of data collection.

**How do I agree to participate in this research?**

Contact the Project Manager who will then arrange for an appointment at a mutually agreeable time. The purpose of this meeting is to discuss your health state, confirm that you're a non-smoker, have had no recent history of upper airway infection or allergy, having no metallic implants or pacemaker fitted, are not pregnant and not be under any current form of medication. Due to the magnetic forces generated by MRI,

safety protocols require the removal of all metallic items and in particular care needs to be given if there is the possibility that metal fragments may be embedded in your eyes.

An ear nose and throat (ENT) specialist will undertake an internal examination of your nose in order to diagnose suitability for the study.

A selection process will then be undertaken screening all respondents to provide a sample of participants who cover a range of age, gender and ethnicity representative of the population. All respondents will be notified of the results of this screening process.

Participants selected will arrange with the Project Manager a mutually agreeable time to undertake the MRI scan and are requested to avoid food or drink intake and physical exercise for at least 2 hours prior to testing and no alcohol must be ingested in the 24 hours prior to testing.

You will be requested to sign a consent form prior to undertaking the scan.

All participants will receive fuel vouchers as compensation for travel and parking expenses.

You may also keep this participation information sheet if you wish to.

**Will I receive feedback on the results of this research?**

Yes. Summary and findings of this research will be given on the Institute of Biomedical Technologies website, [www.ibtec.org.nz](http://www.ibtec.org.nz). You are welcome to check the website at a later date to view these results of this research.

Participants will only be contacted directly in confidence should they wish to be and if MRI reveals nasal abnormalities. Should this occur, participants will be referred to their General Practitioner.

**Whom do I contact for further information about this research?**

***Researcher Contact Details:***

Name: David White   email: david.white@aut.ac.nz      Phone: 921-9999 extn. 8352

***Project Manager Contact Details:***

Name: David White   email: david.white@aut.ac.nz      Phone: 921-9999 extn. 8352

***Project Supervisor Contact Details:***

Name: Ahmed Al-Jumaily   email: ahmed.aljumaily@aut.ac.nz      Phone: 921-9777

**What do I do if I have concerns about this research?**

Any concerns regarding the nature of this project should be notified in the first instance to the Project Supervisor or the Project Manager. Their contact details are listed above.

Concerns regarding the conduct of the research should be notified to the Executive Secretary, AUTECH, Madeline Banda, *madeline.banda@aut.ac.nz* , 921 9999 extn. 8044.

**Approved by the Auckland University of Technology Ethics Committee on 14<sup>th</sup> July 2010, AUTECH Reference number 10/121.**

# Confidentiality Agreement



*Project title:* Feasibility study into the use of magnetic resonance imaging (MRI) to detect change in internal nasal geometry and blood flow during nasal breathing therapy.

*Project Supervisor:* Professor Ahmed Al-Jumaily

*Researcher:* **David White**

---

- ☐ I understand that all the material I will be asked to record is confidential.
- ☐ I understand that the contents of the Consent Forms, tapes, or interview notes can only be discussed with the researchers.
- ☐ I will not keep any copies of the information nor allow third parties access to them.

Intermediary's ..... signature:

Intermediary's ..... name:

Intermediary's Contact Details (if appropriate):

.....  
.....  
.....  
.....

Date:

Project Supervisor's Contact Details (if appropriate):

.....  
.....  
.....

**Approved by the Auckland University of Technology Ethics Committee on 14<sup>th</sup> July 2010, AUTEK Reference number 10/121.**

*Note: The Intermediary should retain a copy of this form.*

# Consent Form



**Project title:** Feasibility study into the use of magnetic resonance imaging (MRI) to detect changes in internal nasal geometry and blood flow during nasal breathing therapy.

**Project Manager:** David White      **Project Supervisor:** Ahmed Al-Jumaily

**Researcher:** David White      **Participant Number:**

---

- I have read and understood the information provided about this research project in the Information Sheet dated 13 April 2010.
- I have had the opportunity to ask questions and have them answered.
- I understand that I may withdraw any information that I have provided for this project at any time prior to data collection without being disadvantaged in any way.
- I agree to discuss my health condition and answer all questions asked correctly to the best of my knowledge.
- I am a non-smoker, have had no recent history of upper airway or sinus infection or allergy and do not suffer any respiratory condition (mild asthma excluded). Also that I have no metallic implants, do not have a pacemaker, am not pregnant and am not under any current form of medication.
- I agree to take part in this research and have my nose examined by an ear, nose and throat (ENT) specialist to ensure the absence of infection, swelling or other conditions that may influence nasal airflow.
- I agree to undertake a nasal air-flow test.
- I agree to have my nasal geometry and nasal blood flow images recorded by MRI whilst wearing a nasal mask. I am aware that this information will be maintained for a period of 10 years.
- I am aware that the MRI image and data collected from this project may be used in journal and conference publications of this research. A summary of this activity and global findings may be given on the Institute of Biomedical Technologies website, [www.ibtec.org.nz](http://www.ibtec.org.nz), in an anonymous form to overview the research work being undertaken within the Institute.

In the event that a condition which is assessed to be a clinical abnormality is detected through performing a scan on you, you will be informed of this and will be advised to consult your general practitioner or other health professional of your choice. Because the images are not routinely reviewed by a radiologist we are unable to perform diagnostic scans for medical purposes of areas where you have known abnormalities. You should be aware that once you have been informed that a clinical abnormality has been detected through performing a scan on you this could affect your ability to obtain insurance whether or not you take the matter further.

Participant's signature: ..... Date: .....

Participant's name: .....

Participant's Contact Details:

.....

.....

***Approved by the Auckland University of Technology Ethics Committee on 14<sup>th</sup>  
July 2010 AUTEC Reference number 10/121***

*Note: A copy of the completed consent form will be mailed to the address provided.*

# Demographic Form



**Project title:** Feasibility study into the use of magnetic resonance imaging (MRI) to detect changes in internal nasal geometry and blood flow during nasal breathing therapy.

**Project Manager:** David White      **Project Supervisor:** Ahmed Al-Jumaily

**Researchers:** David White

**Participant Number:**

---

- Age:.....
- Gender:.....
- Ethnicity:.....
- Confirmation of non-smoker status ☐ (please tick)
- State of Respiratory Health:

***Approved by the Auckland University of Technology Ethics Committee on 14<sup>th</sup> July 2010 AUTEK Reference number 10/121***

## B2.8 CAMRI MRI Safety and Consent Form



### MRI SAFETY AND CONSENT FORM

Name \_\_\_\_\_

Date of Birth \_\_\_\_/\_\_\_\_/\_\_\_\_ NHI \_\_\_\_\_

Weight \_\_\_\_\_ kg Height \_\_\_\_\_ cm

Magnetic Resonance Imaging involves the use of an extremely powerful magnet.  
For your **safety** please answer the following questions

Have you had a previous MRI scan? ☐yes ☐no

Do you have **or** have you **ever** had a cardiac pacemaker? ☐yes ☐no

Do you have a brain aneurysm clip? ☐yes ☐no

Have you **ever** had an injury to the **eye** with a metallic object or fragment? ☐yes ☐no

Have you had any previous surgery? ☐yes ☐no

**Please list** \_\_\_\_\_

Do you have any allergies to medications? ☐yes ☐no

**Please list** \_\_\_\_\_

Do you have any of the following:

Anaemia, blood disorders, kidney disease or seizures? ☐yes ☐no

### FEMALE PATIENTS

Is there any chance that you could be pregnant? ☐yes ☐no

Are you currently breastfeeding? ☐yes ☐no

**PLEASE ANSWER THE QUESTIONS ON THE BACK OF THIS SHEET**

### DO YOU HAVE ANY OF THE FOLLOWING?

Implanted cardiac defibrillator ☐yes ☐no

- Implanted electronic or magnetic device ☐yes  
☐no
- Metallic stent, filter or coil ☐yes  
☐no
- Cochlear implant or other ear implant ☐yes  
☐no
- Heart valve prosthesis ☐yes  
☐no
- Any type of prosthesis (eye, limb etc) ☐yes  
☐no
- Joint replacement ☐yes  
☐no
- Screws, plates or wires in bones or joints ☐yes  
☐no
- Shunt (spinal, intraventricular, or heart) ☐yes ☐no
- Vascular or drug access port or catheter ☐yes ☐no
- Radiation seeds or implants ☐yes ☐no
- Medication patches (Nicotine or hormone) ☐yes ☐no
- Tattoo or permanent makeup ☐yes ☐no
- Dentures or partial plate ☐yes ☐no
- Hearing aid ☐yes ☐no
- Shrapnel, bullets or other metal ☐yes ☐no

### BEFORE ENTERING THE MR SCAN ROOM

You must remove all metallic objects, including jewellery, watches, keys, coins, credit cards, pens, cell phones, hearing aids, clothing with metallic zips and fasteners, metallic threads, or glitter finishes. You may be asked to change into a gown.

Owing to the loud noises emitted by the MR system, you will be given headphones or ear plugs to protect your hearing.

**If you answer YES or are uncertain regarding any of the above, please contact us on (09) 303 5966 prior to your appointment.**

### USE OF YOUR IMAGES

As a University it may be useful to use your images (without your name or other identifying details) for all or some of the following purposes -

- education and training by Centre for Advanced MRI staff
- scientific publications, reports and presentations
- University teaching
- publicity material for the Centre for Advanced MRI
- the Centre for Advanced MRI website and websites of organisations we collaborate with (e.g. Siemens the manufacturer of the machine)
- publicity materials for non-profit organisations
- television documentaries or other public interest media
- databases that may be published on the internet

I give consent for my images to be used for the above purposes provided that all details that could allow me to be identified have been removed

☐yes ☐no

I confirm that the above information is correct to the best of my knowledge.

Signature \_\_\_\_\_ Date \_\_\_\_/\_\_\_\_/\_\_\_\_

Screening form checked by \_\_\_\_\_

## B2.9 CAMRI MRI Check List



### MRI Trial checklist

Before commencing any trial or research study, researchers must provide the Centre for Advanced MRI with the following documentation.

#### **(A) Ethics**

- ☐ (a) Ethics application  
This should include a copy of the ethics application to ensure that MRI has been appropriately included. Also included should be the Patient Information Sheet and Consent Form.
- ☐ (b) Ethics Approval letter  
Ethical approvals, where required, should have been obtained. Dates must be valid.
- ☐ (c) Incidental findings policy  
This will be provided to the researcher who must be aware of and follow this policy.

#### **(B) Project**

- ☐ (a) Copy of the grant or application
- ☐ (b) Quote questionnaire  
This is a simple one page summary – a template can be downloaded from [www.mri.auckland.ac.nz](http://www.mri.auckland.ac.nz)
- ☐ (c) Papers (optional)  
Copies of up to three relevant papers containing similar MRI protocols to those proposed for the study. Preferable with scan protocols from a Siemens scanner.

#### **(C) Procedures**

- ☐ (a) Patient registration  
Description of how patients will be registered on the scanner (this will be electronically attached to every image). Sample can be downloaded from [www.mri.auckland.ac.nz](http://www.mri.auckland.ac.nz)
- ☐ (b) Scan protocol  
This will describe the images to be acquired and the relevant MRI parameters. This will usually be compiled in association and with the help of CAMRI staff.

**(D) Signed Quote**

☐

The formal quote from CAMRI must have been accepted and signed by the principal investigator

Signed \_\_\_\_\_

Date \_\_\_\_\_

**B3 Experimental Data**

The image data of airway cross sectional area and perimeter was automatically read from 3-D Doctor files into Matlab to avoid transcription error. Due to the volume of data, this is presented in a graphical form. Included with each set of results are data for the patent and congested airways.

Participant 104    Pressure Ambient/5 cm H<sub>2</sub>O    Congested left    Patent Right

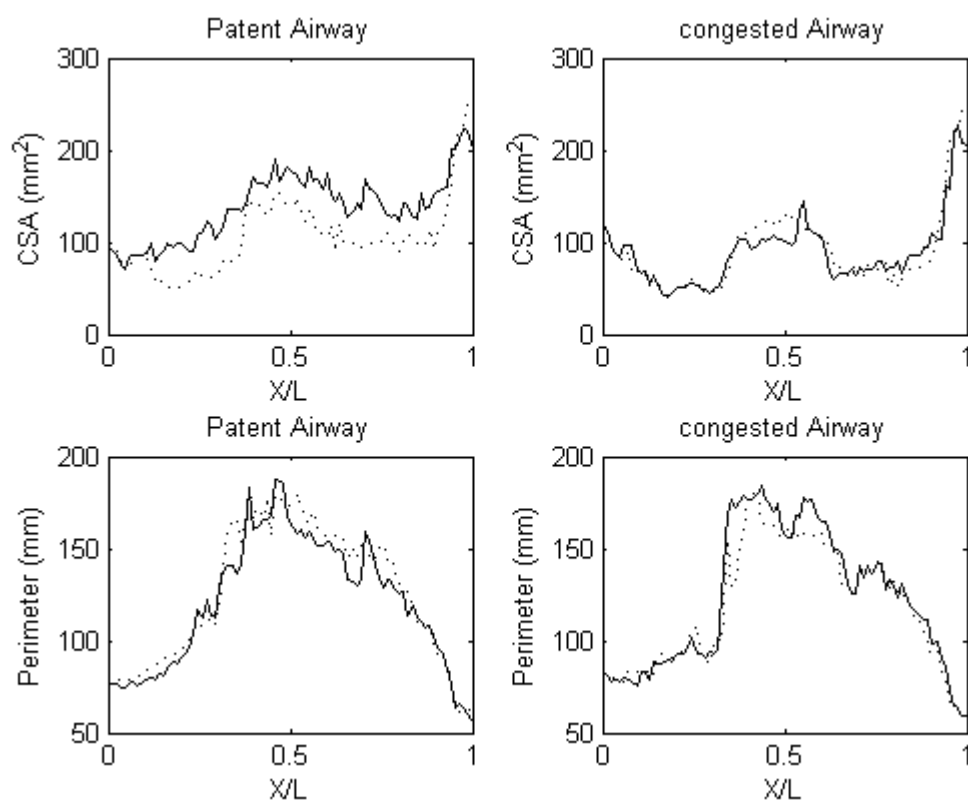


**Figure B3.1: Airway geometric data. — Ambient, - - - - pressurized.**

Participant 118    Pressure Ambient/5 cm H<sub>2</sub>O    Congested left    Patent Right

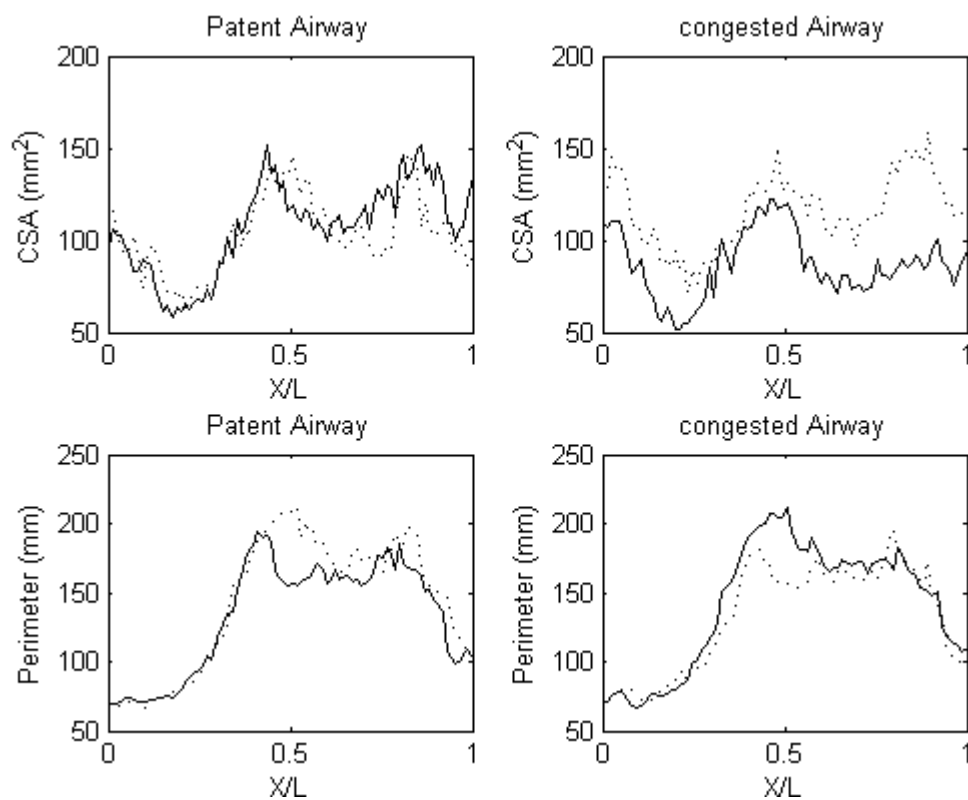


**Figure B3.2: Airway geometric data. — Ambient, - - - - pressurized.**

Participant 101    Pressure Ambient/10 cm H<sub>2</sub>O    Congested left    Patent Right

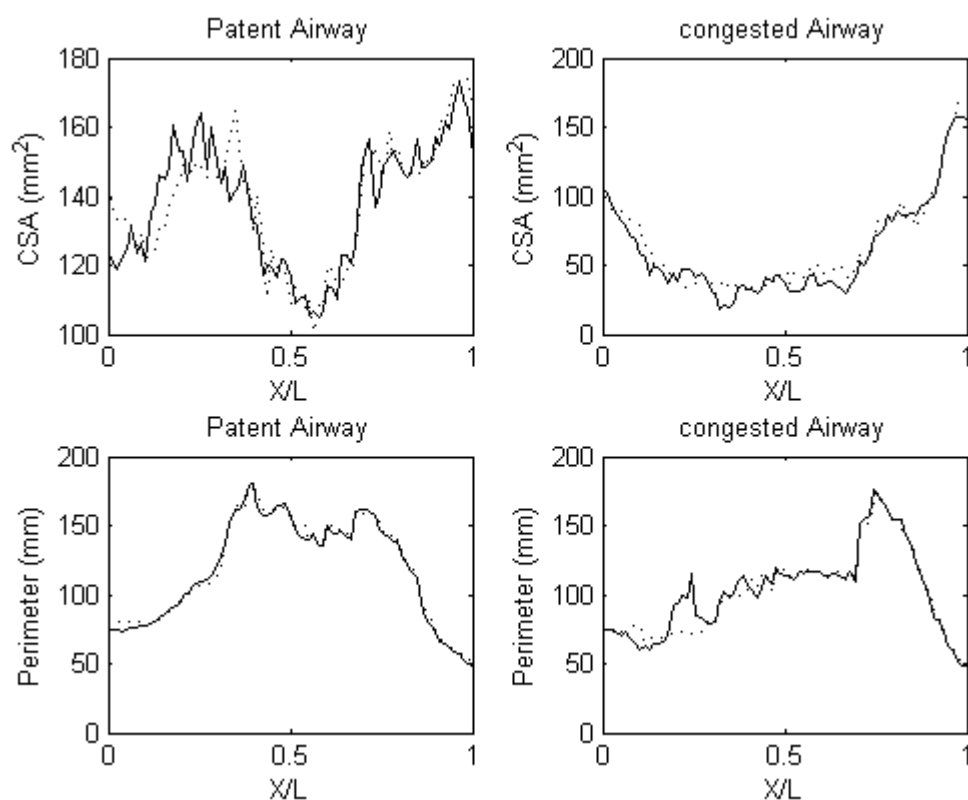


**Figure B3.3: Airway geometric data. — Ambient, - - - pressurized.**

Participant 106    Pressure Ambient/10 cm H<sub>2</sub>O    Congested left    Patent Right

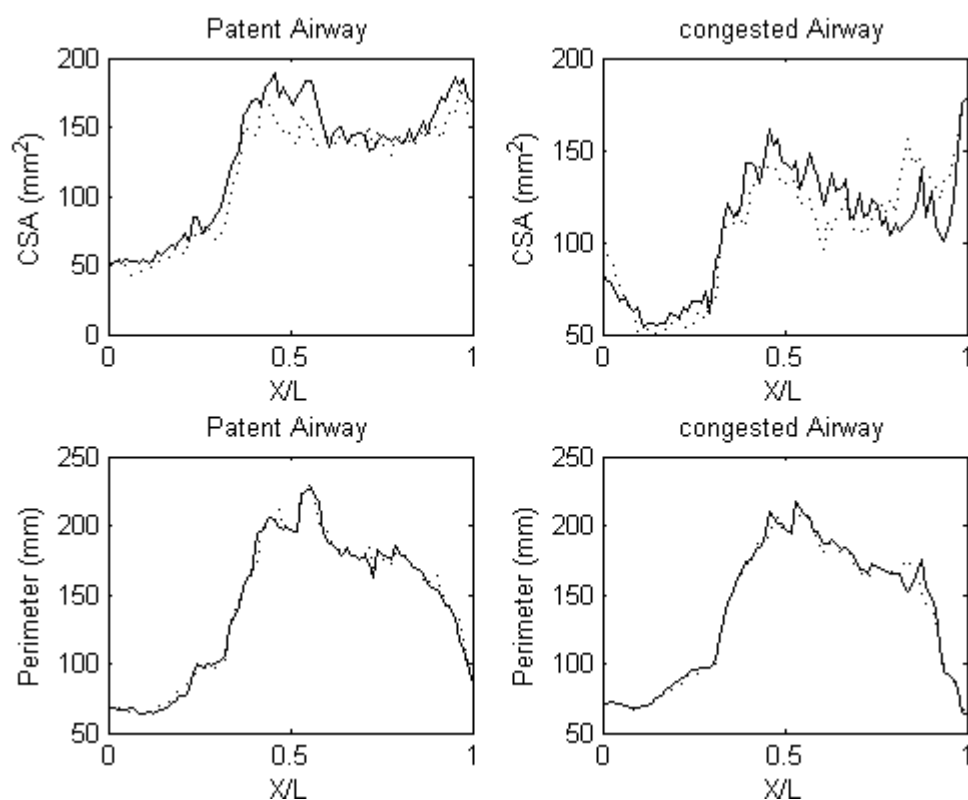


**Figure B3.4: Airway geometric data. — Ambient, - - - pressurized.**

Participant 107    Pressure Ambient/15 cm H<sub>2</sub>O    Congested left    Patent Right

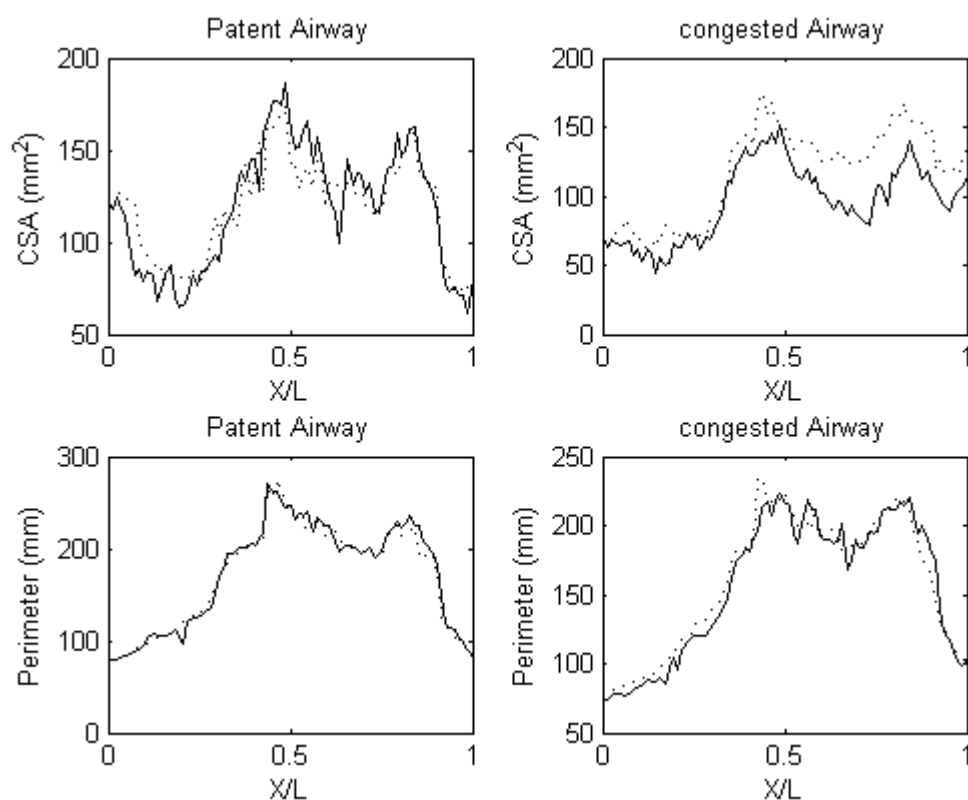


**Figure B3.5: Airway geometric data. — Ambient, - - - - pressurized.**

Participant 109    Pressure Ambient/15 cm H<sub>2</sub>O    Congested left    Patent Right

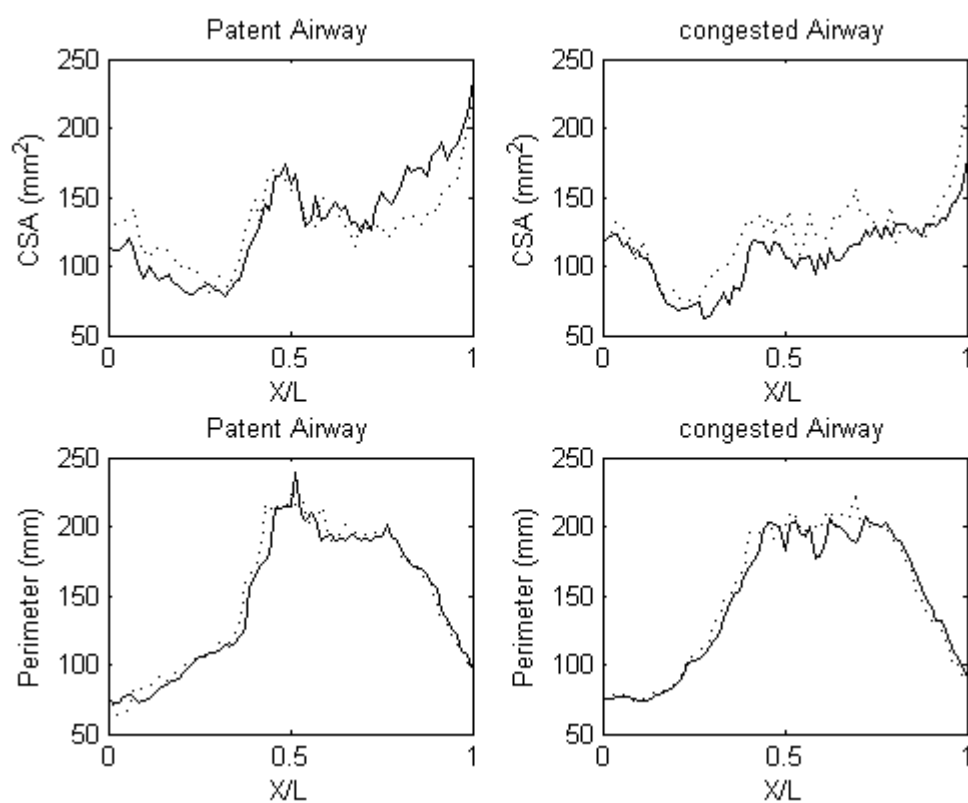


**Figure B3.6: Airway geometric data. — Ambient, - - - - pressurized.**

Participant 108    Pressure Ambient/20 cm H<sub>2</sub>O    Congested left    Patent Right

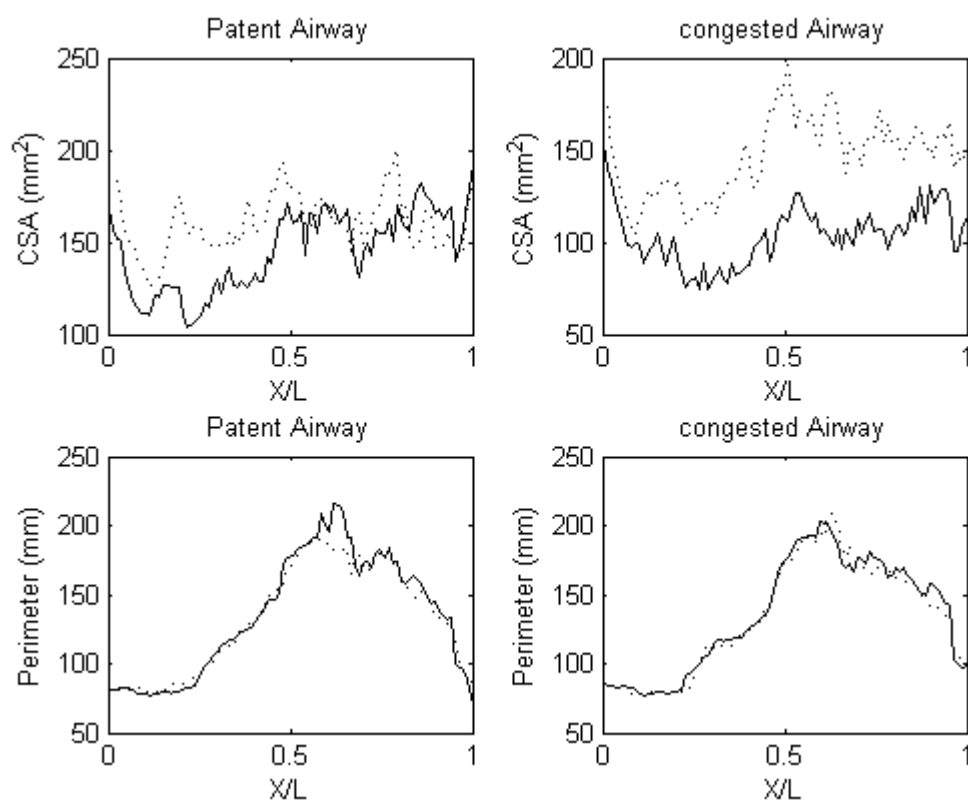


**Figure B3.7: Airway geometric data. — Ambient, - - - - pressurized.**

Participant 115    Pressure Ambient/20 cm H<sub>2</sub>O    Congested left    Patent Right

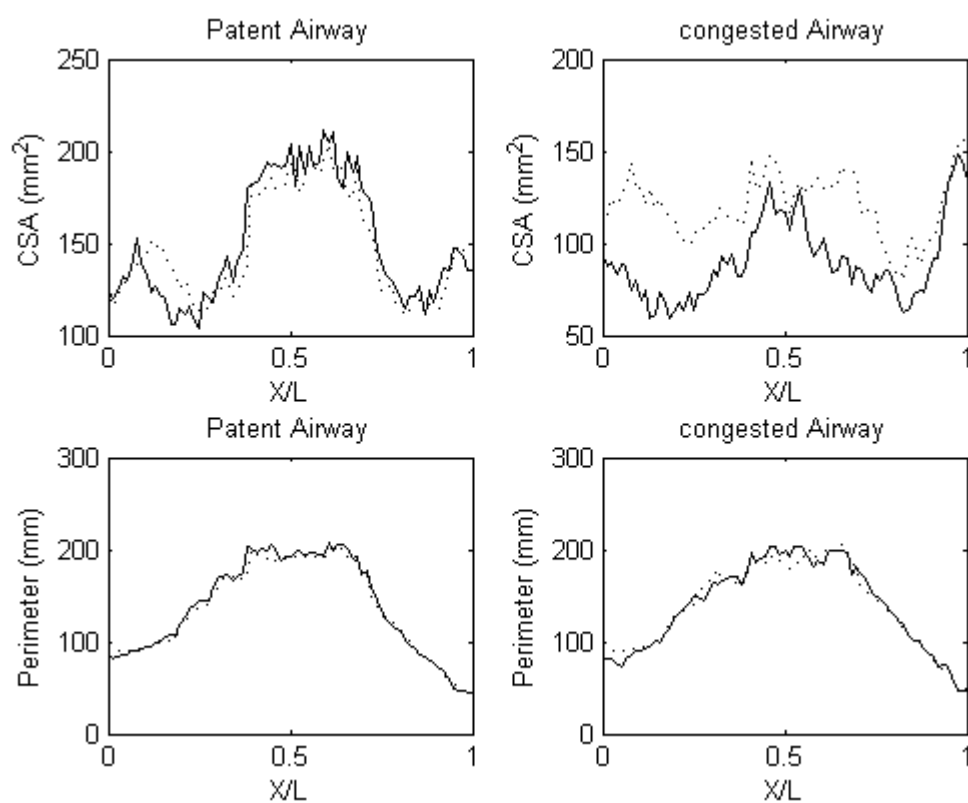


**Figure B3.8: Airway geometric data. — Ambient, - - - - pressurized.**

## APPENDIX C: MUCOSAL ASL SUPPLY RESPONSE AIR-PRESSURE EXPERIMENT

### C1 Experimental Protocol and Equipment

Supplementary information pertaining to the tracheal tissue experiment into air-pressure elicited change in ASL water supply during n-PAP breathing is contained within this appendix.

#### C1.1 Overview of Experiment

Measurement of total water efflux was achieved by exposing a whole bovine trachea *in-vivo* to airflow stresses generated during normal tidal breathing. Removal of water vapour from the air contained within a closed breathing circuit will create a water demand on the epithelial cells. The rate of water efflux can be determined by considering mass conservation within a closed volume of air as shown by Figure C.1.

Here, at any instant in time, the rate of change of water mass contained within the fixed air volume  $\left(\frac{dm}{dt}_{ASL,air}\right)$  is determined by the difference between the rate of epithelial cell water supply into the ASL layer  $\left(\frac{dm}{dt}_{ASL,cell}\right)$  and the rate of removal of water vapour leaving the control volume  $\left(\frac{dm}{dt}_{ASL,des}\right)$  through the action of a desiccant

By applying conservation of mass we find within the fixed air volume we find:

$$\frac{dm}{dt}_{ASL,air} = \frac{dm}{dt}_{ASL,cell} - \frac{dm}{dt}_{ASL,des} \quad (C1.1)$$

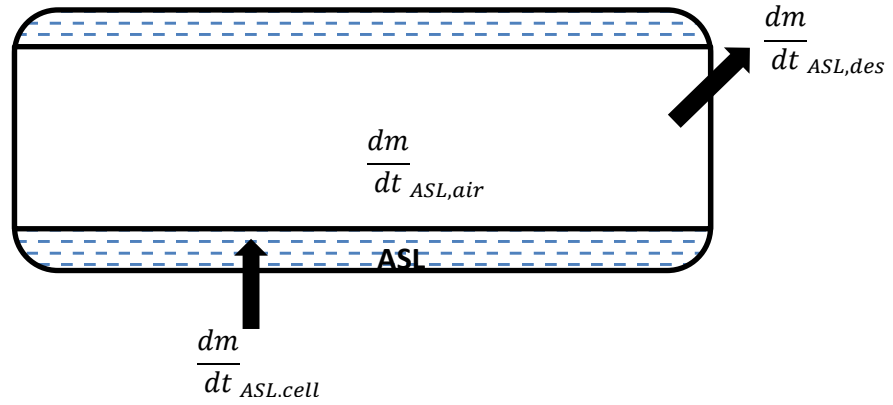


**Figure C 1.1: Schematic representation of principle of test apparatus operation.**

Where Rearranging (C1.1) enables the rate of epithelial cell water efflux to be determined:

$$\frac{dm}{dt}_{ASL,cell} = \frac{dm}{dt}_{ASL,air} + \frac{dm}{dt}_{ASL,des} \quad (C1.2)$$

As mentioned in Chapter 2, the ASL layer normally acts as buffer volume between the epithelial cells and air. This layer is very small, being in the range of 7-10  $\mu\text{m}$  height, so an assumption is made that, provided the ASL volume remains present, any change in ASL water volume is insignificant since its total volume is so small. Confirmation of this is achieved by ensuring the presence of the ASL layer both prior to and immediately after testing. The maximal rate of specific cellular water supply ( $\dot{m}_{w,s}$ ) required for the nasal air-conditioning computational model is determined by dividing the maximum rate cellular water supply ( $\dot{m}_{w,cell}$ ) by the total trachea surface area exposed to the tidal airflow.

## C1.2 Dissection and Mounting

As discussed in Chapter 5, immediately upon arrival, any attached connective tissue was removed and an intact length of tracheal tissue was cut to approximately 300 mm long. The presence of an intact ASL layer was visually confirmed by observation of a wetted internal surface. One end of the tracheal sample was then securely attached to a glass tube of a suitable diameter, so as to be a neat fit within the trachea sample, by three PVC plastic cable ties to ensure a gas-tight seal.

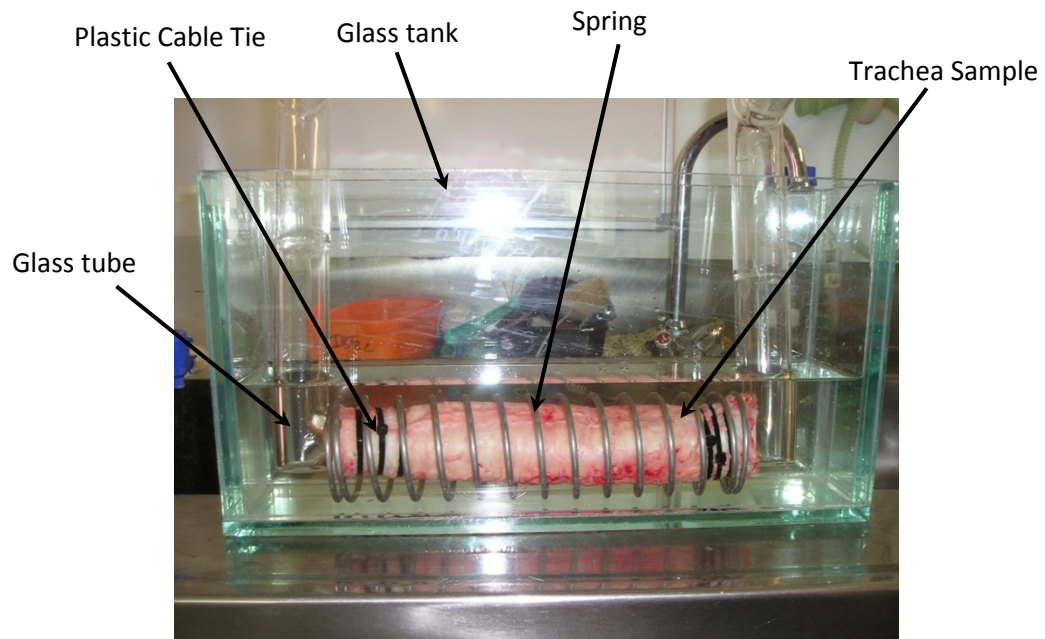


**Figure C 1.2: Trachea *in-toto* immersed in physiological salt solution within tissue bath.**

The tracheal sample is then passed through a stainless steel spring, grade 6061, to provide a distributed mass to resist buoyancy forces and ensure the trachea remains immersed in the PSS contained within a glass tissue bath. The second glass tube, again selected to be a neat fit inside the trachea, was inserted into the other end of the trachea and again securely attached by three PVC plastic cable ties. With the two glass pipes firmly sealed to the trachea, the inside of the tissue was rinsed with 100 ml of physiological salt solution (PSS) to remove a red colored foam contaminant lining the tracheal internal surface. Any surplus PSS was allowed to drain from the tracheal sample and glass tubing for a period of 3 minutes before the whole trachea and glass tube assembly was immersed in PSS contained within the glass tissue bath, Figure C1.2.

### **C1.3 Pre-Test Tissue Viability**

To ensure tracheal tissue viability, an unused portion of the tracheal tissue was mounted on a silicon filled petri dish using bent syringe needles before being bathed in PSS. A small drop of Indian ink was then released from a 1 ml Pasteur Pipette into the tracheal tissue surface and observed under a microscope (Askmnia Citoval SN 43271) at 100X magnification. Both still, shown in Figure C1.3, and moving images of the transport of the iron particles present within the Indian ink were recorded for each sample.

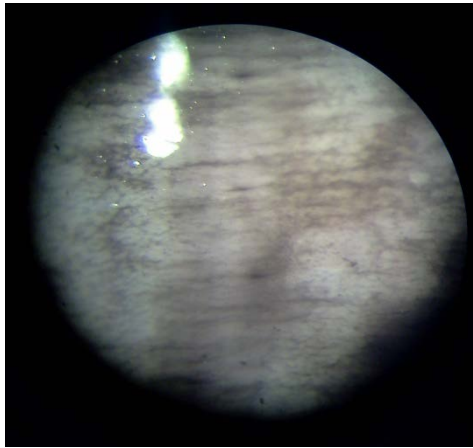


**Figure C 1.3: Still image of Indian ink on trachea surface.**

Images were recorded using a 30 Megapixel phone camera (LG Optimus P970) attached by a custom adaptor to the microscope eyepiece, Figure C1.4.

Confirmation of tissue viability was indicated by the presence of a coherent MTV occurring across the mucosal surface. This was visually confirmed by the transport of the small iron particles present within the Indian ink as a result of coordinated motile cilia beating.

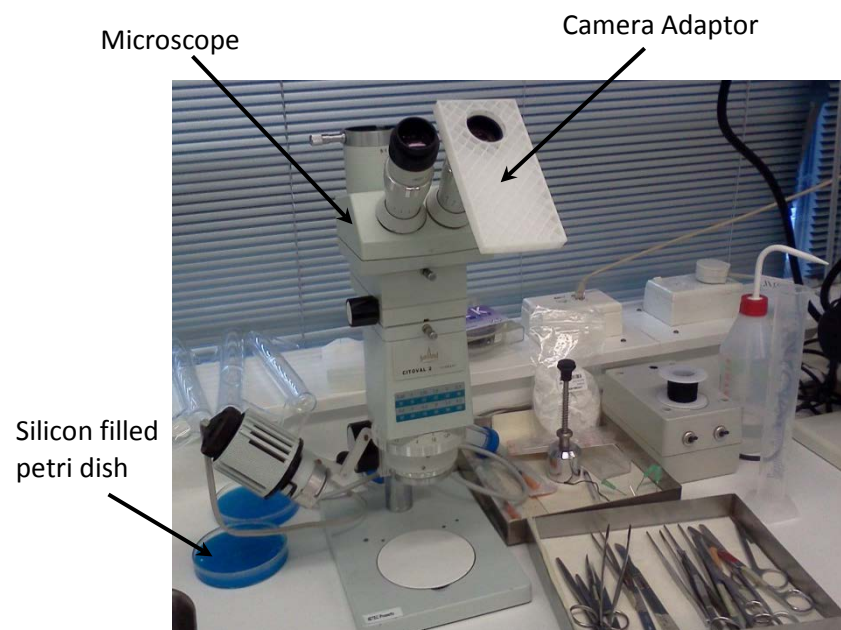


**Figure C 1.4: Custom camera adaptor mounted on microscope.**

#### **C1.4 Post-Test Tissue Viability Test and ASL Verification**

Confirmation of tissue viability was undertaken after operating the tissue test apparatus for a minimum time period of seven hours. Here the trachea was removed from the tissue bath and sectioned to enable visual confirmation of ASL presence by observation of a wetted surface. Additionally, a small portion was removed and mounted in a silicon filled petri dish in the same manner as described in Section C1.3 Pre-Test Tissue Viability.

Confirmation of tissue viability was again undertaken through visual confirmation of coherent MTV occurring across the mucosa surface.

#### **C1.5 Physiological Salt Solution**

Each trachea tissue test required two litres of physiological salt solution (PSS, composition in mM: 2.4  $\text{CaCl}_2$ , 25.7  $\text{NaHCO}_3$ , 5.6 Glucose Monohydrate, 0.82  $\text{MgSO}_4$ , 1.2  $\text{KH}_2\text{PO}_4$ , 3.39  $\text{KCl}$  and 110  $\text{NaCl}$ ) using distilled type 1 (ultrapure) Milli-Q® 18M $\Omega$  water. This water was sourced from a commercial Millipore system, Figure C1.6.



**Figure C 1.5: Post-test sectioned trachea.**



**Figure C 1.6: Commercial Type 1 ultrapure water Milli-Q® Millipore system.**

Type 1 ultrapure water has a resistance of  $18.2 \text{ M}\Omega \cdot \text{cm} @ 25^\circ\text{C}$  and total organic carbon (TOC)  $< 10 \text{ ppb}$ . This process entailed passing distilled water, Exelo ES51 water still, through four filters, Figure 4.8, into a 20 litre plastic storage container, Figure C1.7.



**Figure C 1.7: Type 1 ultrapure water, Milli-Q® in 20 litre plastic container.**



**Figure C 1.8: Precision scale and chemicals used to make physiological salt solution.**

At the commencement of the tissue test day, approximately 250 ml of distilled water, type 1 (ultrapure) Milli-Q®, was poured into a two litre glass bottle that had previously been rinsed with deionized water and dried. The mass of a variety of chemicals, listed ABOVE were measured using a precision electronic balance, AD Corporation SN 2905040, Figure D1.8, before being added to the distilled water.

Upon addition of all the chemicals the glass bottle was filled to contain a total volume of two litres and the chemicals mixed by mechanical agitation before a gas mixture of 5%CO<sub>2</sub>/95%O<sub>2</sub>, Alpha Gaz mix product code G19012, batch number QE6004, was bubbled through the solution, Figure C1.9.



**Figure C 1.9: Gassing physiological salt solution with 5% CO<sub>2</sub>/95% O<sub>2</sub>.**



**Figure C 1.10: Testing physiological salt solution PH.**

The pH was tested after a period gassing not less than 45 minutes, to achieve the desired PH of 7.4, Microcomputer PH-Vision 6071, Jenco Electronics Ltd., model 6071N, SN 611794, Figure C1.10. A small volume of PSS was removed from the 2 litre glass bottle to enable the pH to be tested before being discarded.

### **C1.6 Configuration of Test Apparatus**

As previously described in Chapter 5, the tissue mounting system containing PSS was placed in a water tank pre-heated by an immersion heater to 37°C located within an incubator (Steri-Cult 200, Froma Scientific Inc., Ohio, USA). The test apparatus was then assembled within the incubator space, shown schematically by Figure C1.11, trapping 2 litres of ambient air within the closed system. The transport ventilator was then configured to deliver a tidal volume of 1 litre and a frequency of 6 breaths per minute before the incubator door was closed. The temperature within the incubator space was then gradually raised from ambient to stable at 37°C over a 25 minute period.

Not only does this provide a means of preventing undesirable condensation from occurring within the apparatus holding the trapped air volume, but it also allows the surrounding air can be augmented above ambient pressure. A CPAP air delivery unit (Fisher & Paykel Healthcare HC234 AEA, SN 100731034279), connected by the standard CPAP air hose to the internal incubator air space heating system provided pressure augmentation. Air pressure within the incubator cabinet was measured with a simple U-tube manometer. Manual recording of incubator pressure was sufficient given this remained constant for the duration of each test.

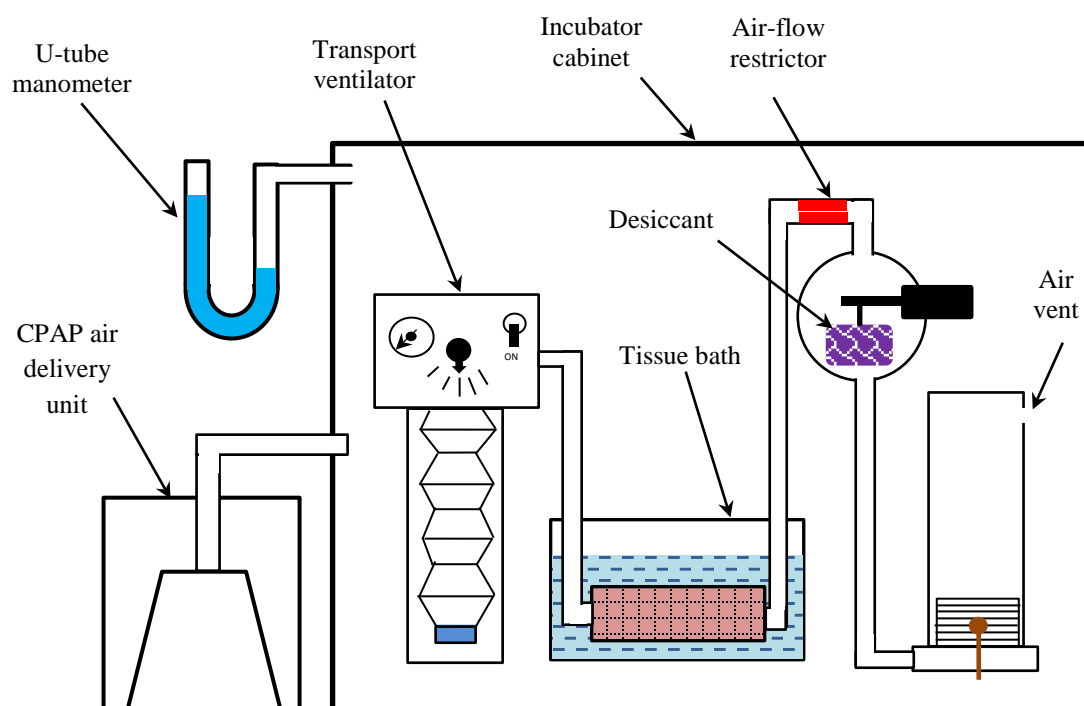


**Figure C 1.11: Schematic representation of apparatus set up within the incubator.**

The calibration of the cantilever strain gauge used to measure the mass of the silica gel desiccant (World Precision Instruments FORT 100, SN 02F 76536) was verified for each tissue test undertaken.

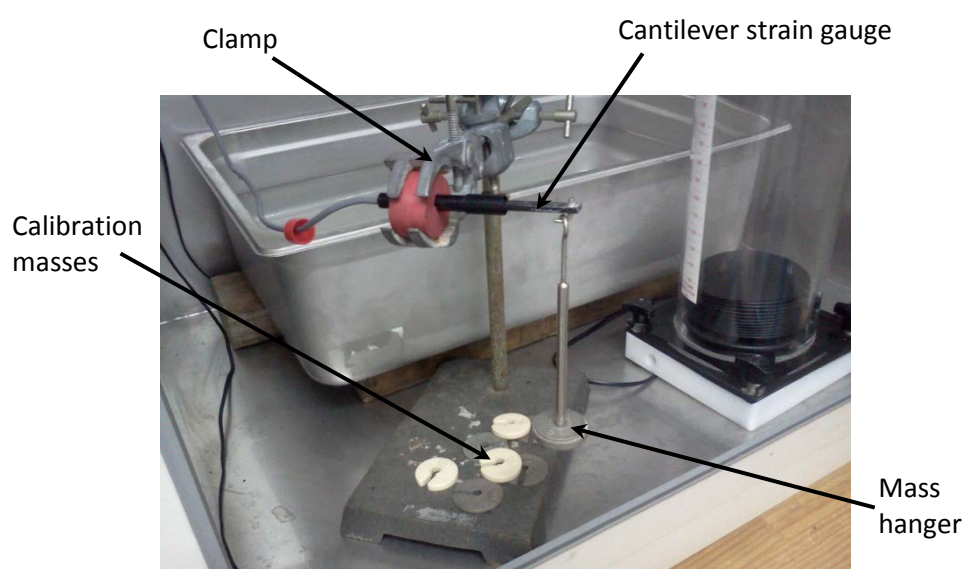


**Figure C 1.12: Calibration of cantilever strain gauge.**

### C1.7 Pre-Test Sensor Calibration

This involved the placement of known calibrated masses, ranging from 50 – 80 grams, in increments of 10 grams, on the desiccant bag supporting hook, Figure C1.12.

The cantilever stain gauge was supported in the same hard rubber bung, using a laboratory stand and clamps, as used to mount it within the glass sphere during the operation of the tissue testing apparatus. This was done to ensure the calibration process included any influence a soft support may have had on the instrument.

### C1.8 Assembly of Desiccant Chamber

The open weave fabric bag was inserted within the glass sphere and positioned to enable  $80 \pm 1$  grams of white non-indicating silica gel desiccant (UOP Ltd), of diameter 2-5mm, to be poured into opening. The bag was then closed by tying up the ribbon surrounding the bag opening before being pierced and suspended by the cantilever strain gauge hook. This enabled the bag mass to be measured by the cantilever strain gauge (Figure C1.13).

### C1.9 Silica Gel Absorption

The silica gel desiccant used in this experiment was characterized as having a rate of water vapor absorption that exponentially reduced over time, Figure C1.14, when exposed to moist air at a constant temperature and relative humidity [1].

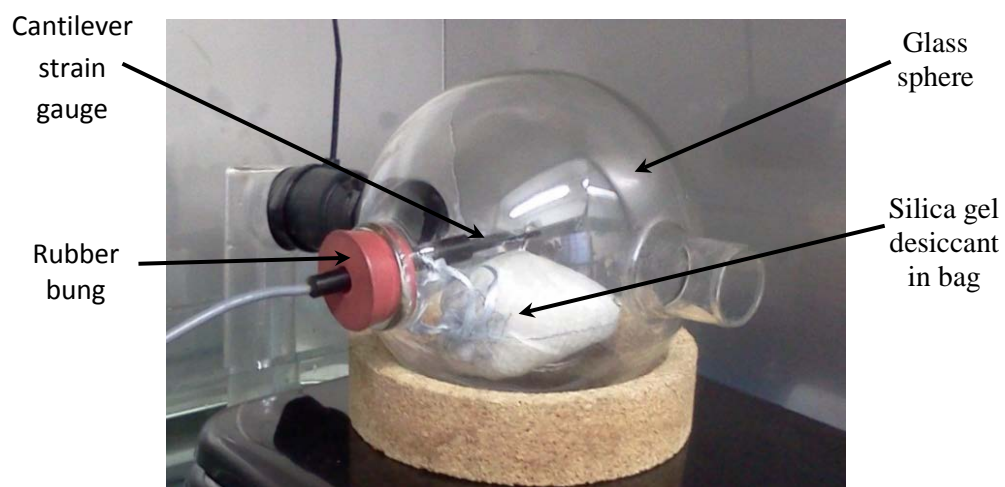


**Figure C 1.13: Silica gel bag supported by cantilever strain gauge within glass sphere.**

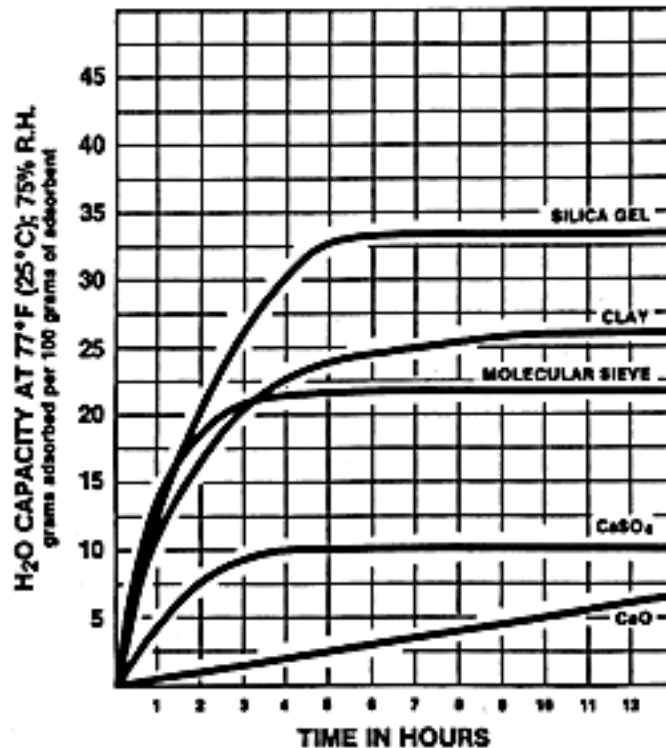


**Figure C 1.14: Equilibrium capacity of various water vapor desiccants at 25°C and 75% RH [1].**

As discussed in Chapter 5, the desiccant indirectly provides the water demand on the trachea tissue causing the tissue water supply response to be characterized by the behavior of the desiccant. Compounding this variable was the need to operate the experiment for around 35 minutes to achieve thermal stabilization prior to data being recorded. This time delay leads to a change in the rate in which the desiccant absorbs water vapour. To overcome this issue influencing the results, care was taken to ensure that each stage of the experiment was undertaken within identical time frames to ensure replication of these time dependent variables during all tests.

#### **C1.10 Assembly of Apparatus within Incubator Space**

A stainless steel bowl containing water and located within the incubator space was pre-heated by an immersion heater. Once the water temperature had stabilized at 37°C the glass tissue bath containing the tracheal tissue sample connected to glass tubes at either end and immersed in PSS was lowered in. The master bellows assembly containing the transport ventilator along with the assembled desiccant assembly chamber and slave bellows assembly were then mounted within the incubator and connected using thin wall elastomeric tubing sealed with electrical insulation tape secured by PVC cable ties (Figures C1.15 and C1.16).



**Figure C 1.15: Test apparatus assembled within incubator space. Note transport ventilator and master bellows assembly removed to aid clarity.**

The transport ventilator air supply hose along with data cables for both the cantilever strain gauge and air temperature/humidity sensor passed through a bulkhead gland fitting within the incubator wall.

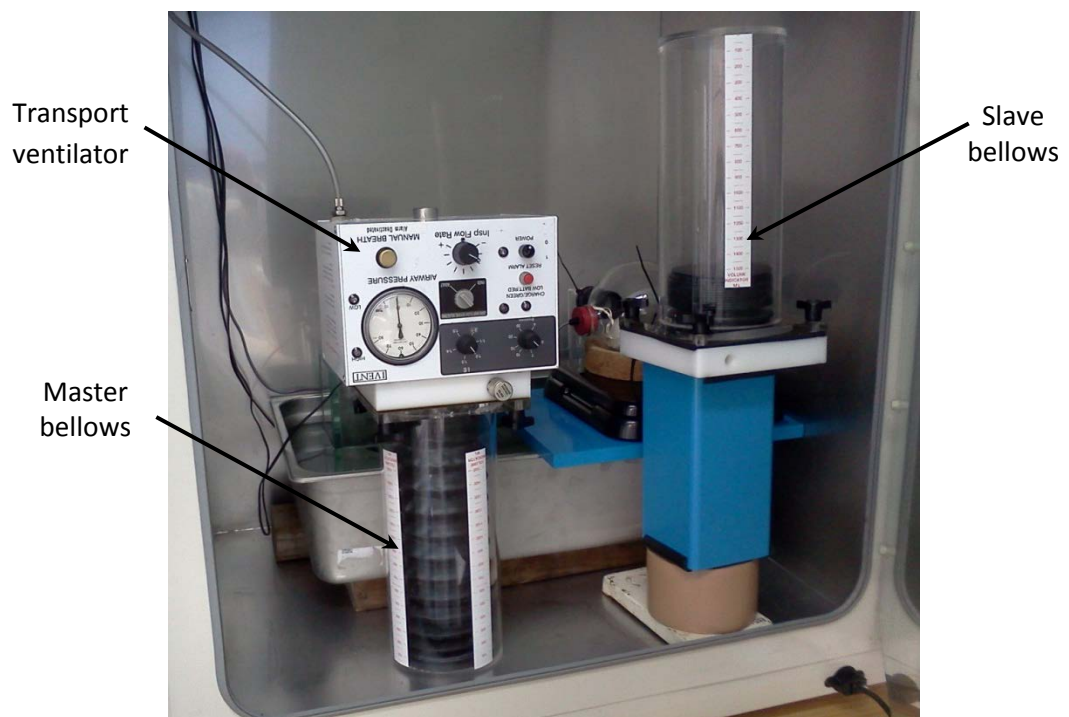


**Figure C 1.16: Complete test apparatus set up within incubator.**

During augmented air-pressure testing this opening was sealed by a soft rubber bung suitably modified to seal against air leaks but still allowing the pipe and cables to pass through the incubator wall.

Prior to switching on the transport ventilator and closing the incubator doors it was necessary to pre-set the ventilator settings to simulate tidal breathing. In order to achieve the desired pressure drop and air-flow shear stresses forces on the internal tracheal surface a simulated breathing rate of 6 breaths per minute and a tidal volume of 1 litre per breath were selected.

### **C1.11 Transport Ventilator Air Supply**

Quiet delivery of pressurized servo air to the transport ventilator driving the master bellows assembly was achieved by using a commercially available air-brush compressor (ROHS GS model AS18B 4 bar) capable of supplying air at 400 kPa pressure at a rate of 20 litres a minute.

The air-brush compressor was not rated for continuous operation or the high volume experienced in this application so it suffered from overheating. This problem was overcome by turning the room air-conditioning down to a temperature of 18°C and using an office fan to aid forced convective heat loss from the compressor driving motor (Figure C1.17).



**Figure C 1.17: Air-brush compressor supplying servo air to transport ventilator.**

### C1.12 Preparation for Augmented Pressure Testing

Additional preparation was required during tissue tests undertaken under augmented pressure. These included:

1. Incubator modification.
2. Incubator air-pressure supply.
3. Incubator pressure sensing.

Each of these additional attributes is described in detail in the following sections:

### C1.13 Incubator Modification

Apart from reducing the internal pressures generated within the incubator cabinet, air leakage also causes heat loss and the incoming cool air also provides additional thermal loading on the incubator heating system.

During preliminary testing it was found that the incubator glass door required additional bracing to overcome air leakage caused by distortion of the glass as a result of forces generated by the augmented air pressure. This was achieved by using a 6 mm thick galvanized steel strong-back to brace the glass door against the pressure forces (Figure C1.18).



**Figure C 1.18: Steel strong-back fitted to brace incubator glass door against air leakage.**



**Figure C 1.19: Glass side of steel strong-back showing felt webbing and disc magnets.**

The strong-back was secured to the incubator structure by 12 in number 15 mm diameter rare-earth disc magnets, Magnets New Zealand Neodymium ND2012 (Figure C1.19).

This was done because normal mechanical fasteners would not have been contained within the constrained space caused by the close fitting insulating outer door. Additionally, felt webbing (Bunnings Warehouse 35 x 3 mm) was attached on the inside face of the strong-back to both distribute the clamping force and protect the glass door from mechanical damage.

#### **C1.14 Air Pressure Supply**

A continuous source of air at a pre-determined pressure was supplied by the Fisher & Paykel Healthcare HC 234 AEA CPAP unit via the standard patient mask 20 mm flexible hose (Figure C1.20) to an air entry point within the incubator cabinet.

Air pressure delivered by the CPAP unit was adjusted to achieve the desired incubator cabinet pressure (Figure C1.21). Incubator pressure was varied from ambient pressure up to 15 cm H<sub>2</sub>O in increments of 5 cm H<sub>2</sub>O.



**Figure C 1.20: CPAP air supply unit pressurizing incubator internal space.**

### **C1.15 Incubator Pressure Sensing**

A simple U-tube manometer, filled with colored water, was connected to the incubator air space to read the static air pressure augmentation experienced by the tissue and the complete test apparatus (Figure C1.22).



**Figure C 1.21: CPAP air supply unit pressure display and control.**

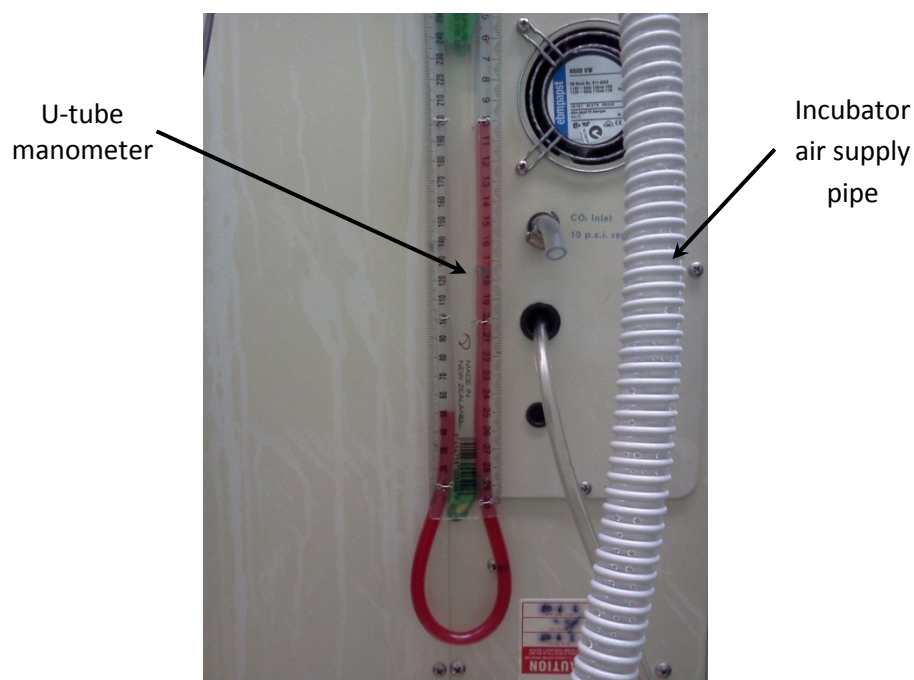


**Figure C 1.22: Simple U-tube manometer reading incubator air pressure augmentation.**

#### **C1.16 Thermal Stabilisation and Data Acquisition.**

Once the complete tissue test apparatus was assembled within the incubator the transport ventilator was started before the incubator door was closed and the incubator heating system started. Although the tissue water bath was able to be pre-heated to 37°C, the rest of the test apparatus was also required to be at the same temperature in order to avoid condensation occurring within the test apparatus. During this warming up phase the opportunity was taken to configure the setting of the LabVIEW™ data acquisition software and set the desiccant mass to zero so that only water mass absorbed from the air was recorded. Once the incubator temperature had stabilized at 37°C a further 10 minute period elapsed prior to commencement of data acquisition over a minimum period of seven hours.

#### **C1.2 Labview Program**

A customised Sensirion EK-H4 temperature and humidity sensor software interface was used to store simultaneously desiccant mass and air sensor data. Graphical representation of the LabView program is given in Figures C 2.1 and C 2.2.

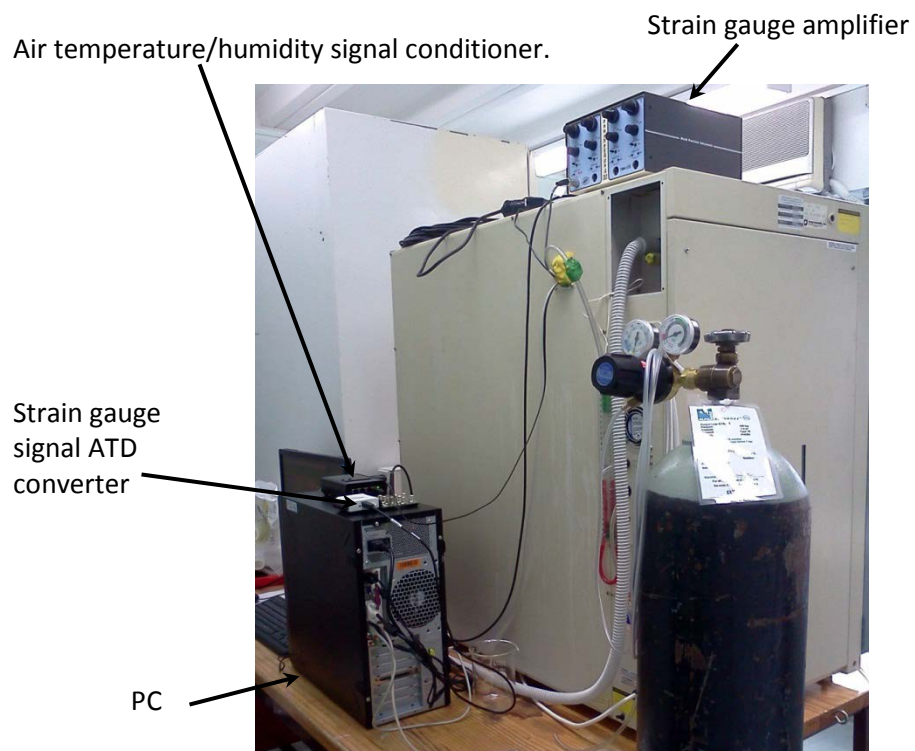


**Figure C 1.23: Rear view of incubator cabinet data acquisition apparatus set-up.**

#### **Appendix C1 References**

- [1] Sorbent-Systems. *Desiccant Chart Comparisons*. 2012; Available from: [http://www.sorbentsystems.com/desiccants\\_charts.html](http://www.sorbentsystems.com/desiccants_charts.html).

## Appendix C2 Labview Program

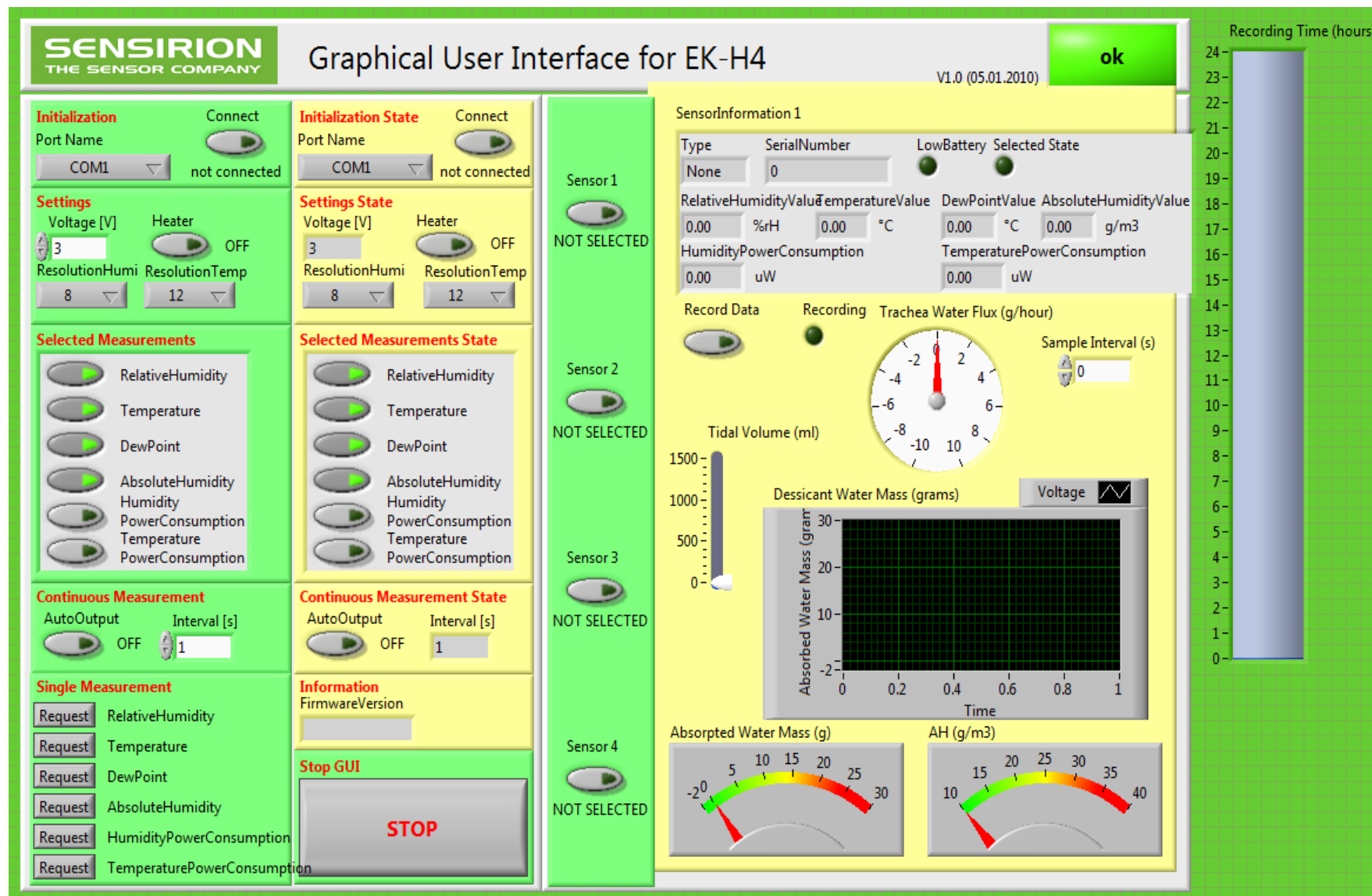


Figure C 2.1: Customized Sensirion® EKH5 LabVIEW™ software interface.

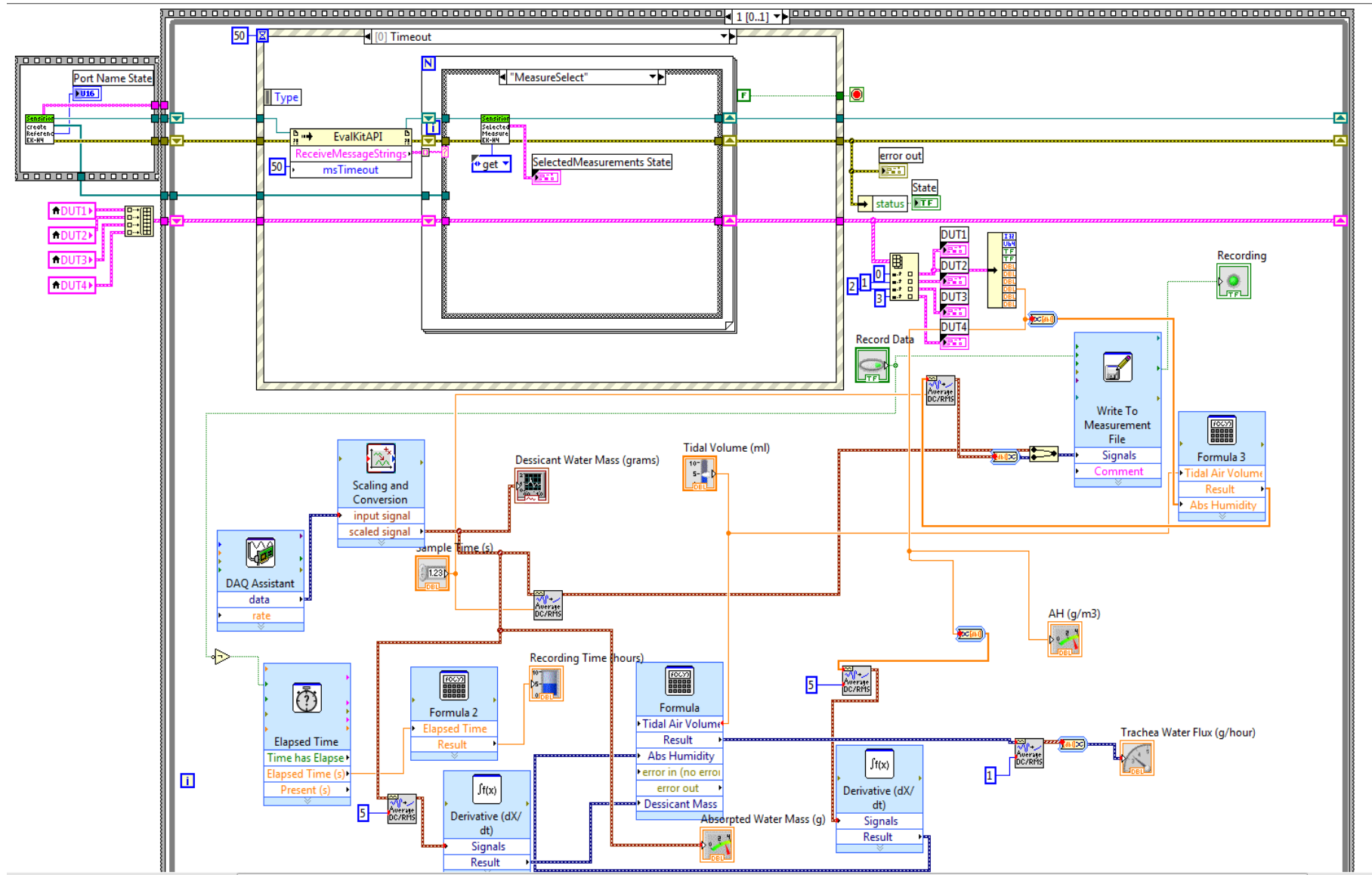


Figure C 2.2: Customized Sensirion® EKH5 LabVIEW™ software interface.

### Appendix C3 Pressure Drop Calculations

Based on pressure shock losses for a sharp contraction ( $k = 0.5$ ) and expansion ( $k = 1.0$ ) the head loss can be calculated using minor loss equation [1]:

$$h_f = k \frac{v^2}{2g} \quad (\text{D3.1})$$

Plotting the predicted pressure drop over the normal physiological range of tidal air mass-flow rates, shown by Figure C2.3, demonstrates good correlation to that found in previous clinical and simulated studies [2].

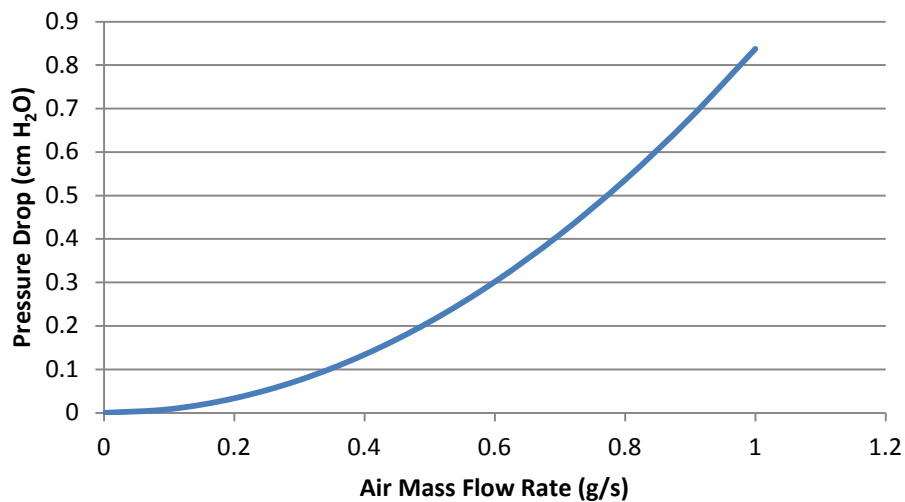


**Figure C2.3: Predicted pressure drop across 14mm diameter orifice.**

### Appendix C3 References

- [1] White, F.M., *Fluid Mechanics*. 3rd ed 1979, New York: McGraw-Hill. 736.
- [2] Wen, J., K. Inthavong, J. Tu, and S. Wang, *Numerical simulations for detailed airflow dynamics in a human nasal cavity*. *Respir. Physiol. Neurobiol.*, 2008. **161**(2): p. 125-135.

### Appendix C4 Experimental Data and Processing

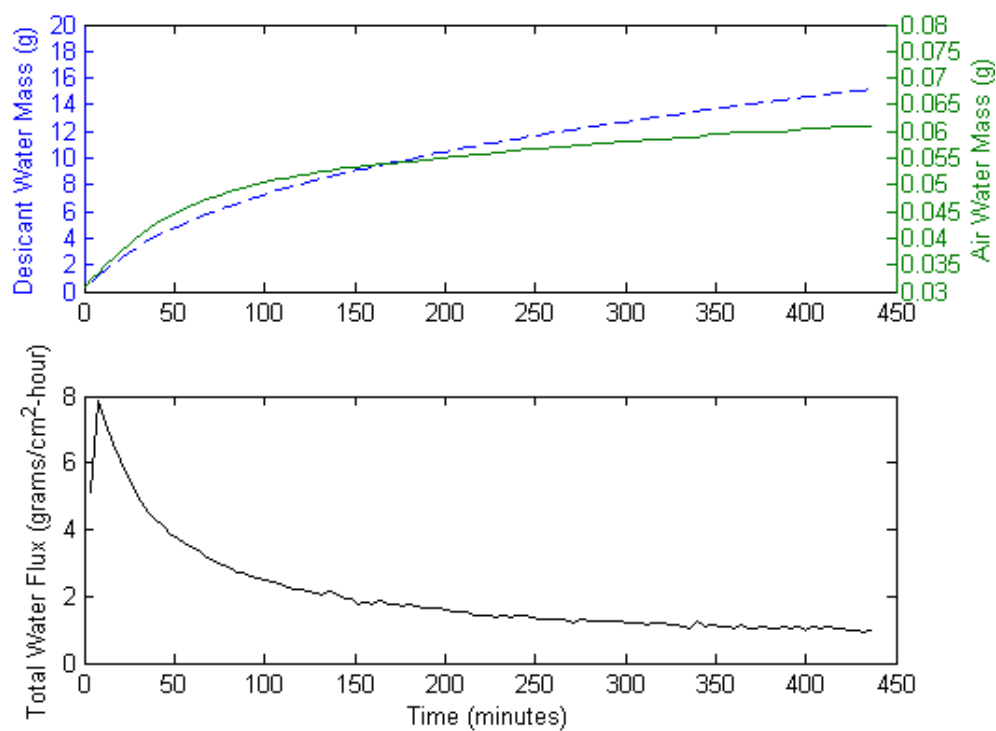
The raw data of desiccant water mass and air absolute humidity ( $\text{g H}_2\text{O}/\text{m}^3$  air) recorded for each is now presented. Due to the volume of data, this is presented in a graphical form. Included with each set of results is a presentation of the instantaneous net mucosal water flux ( $\text{g H}_2\text{O}/\text{cm}^2\text{-hour}$ ). This is found by differentiating the raw data of desiccant water mass and air water mass with respect to time.

#### C4.1 Ambient Pressure

Date: 08/08/12

Length: 220 mm

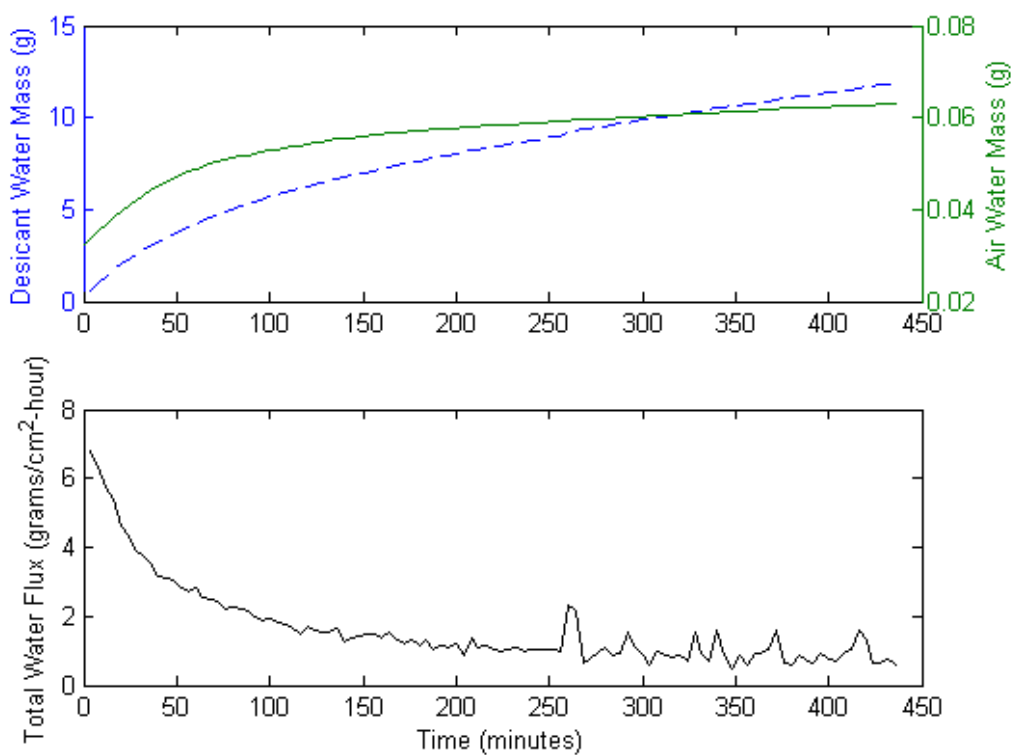
Diameter: 34 mm



Date: 15/08/12

Length: 220 mm

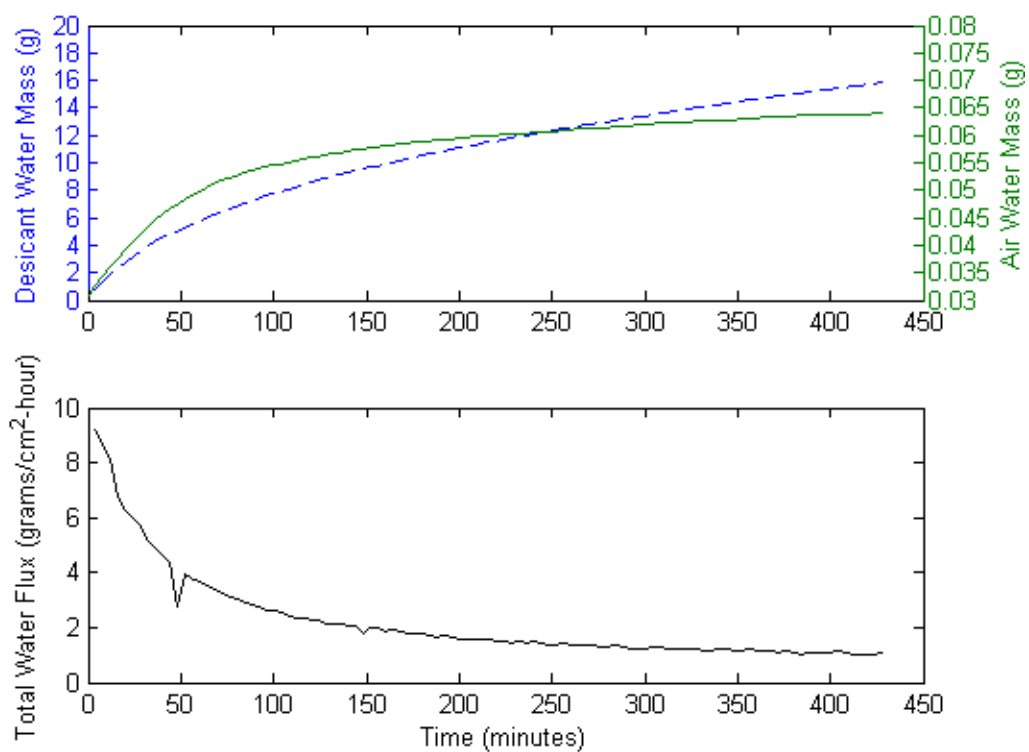
Diameter: 33 mm



Date: 17/08/12

Length: 250 mm

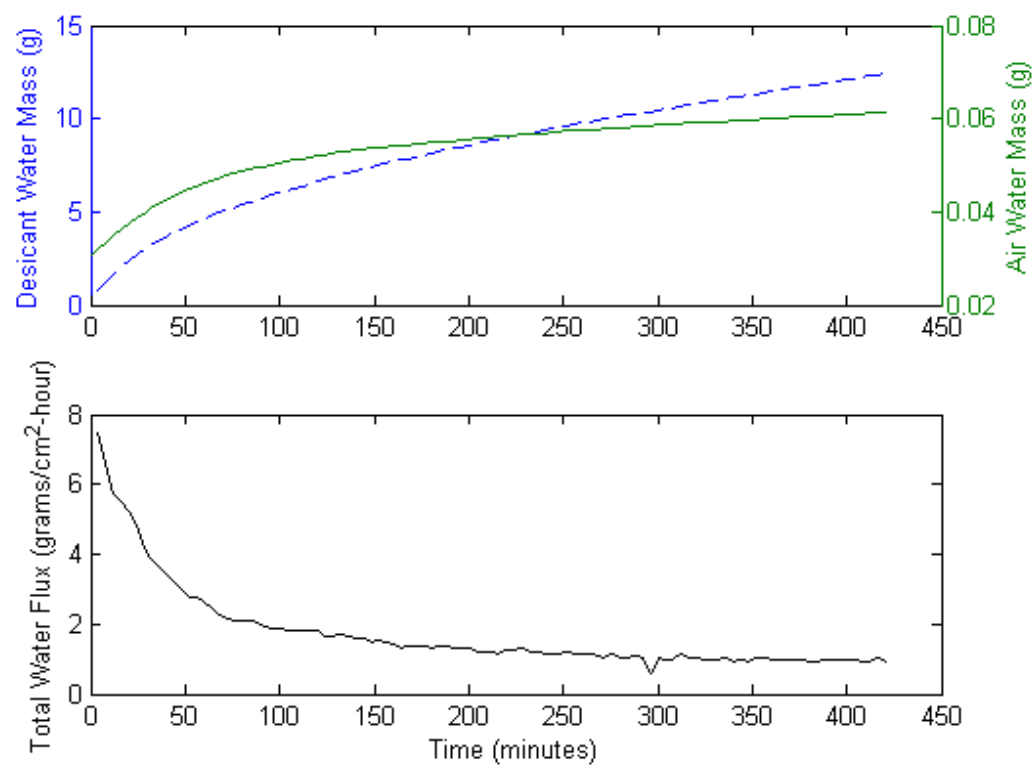
Diameter: 38 mm



Date: 06/08/12

Length: 240 mm

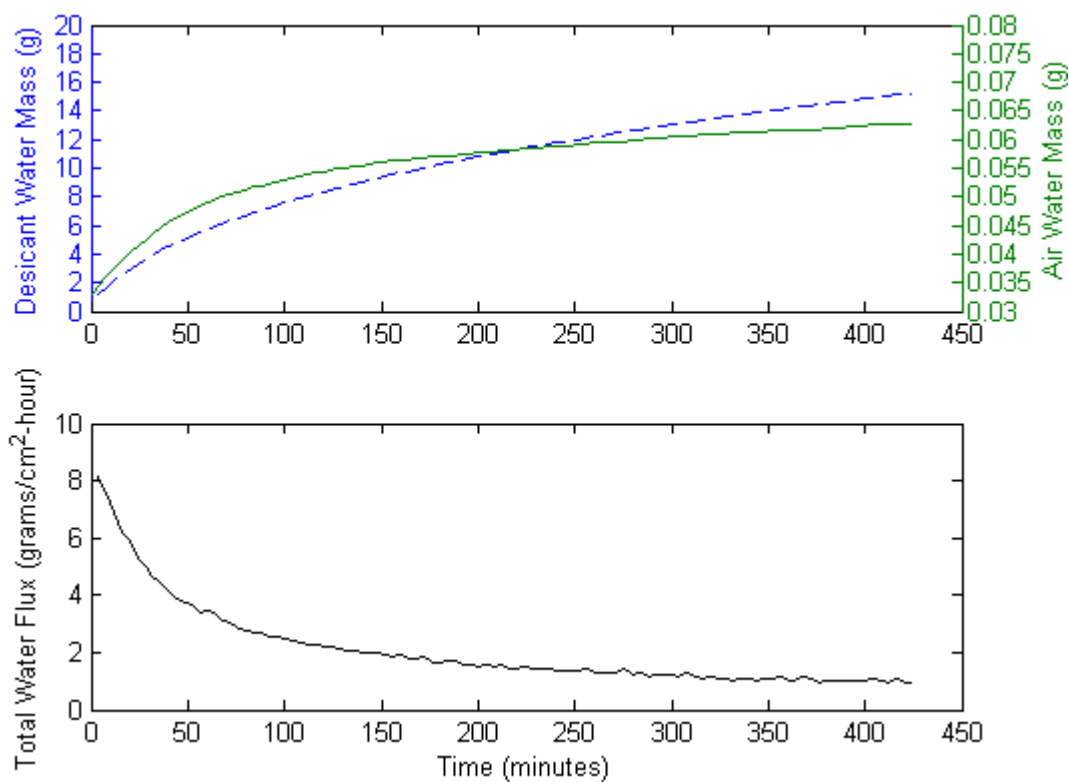
Diameter: 34 mm



Date: 20/08/12

Length: 240 mm

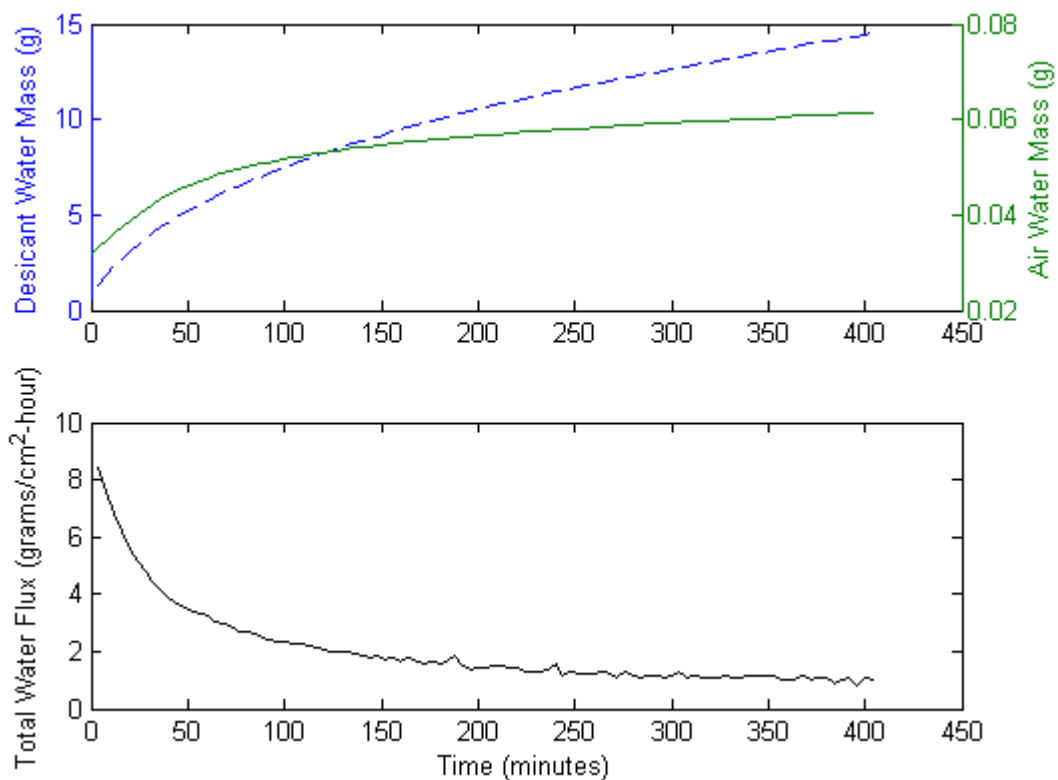
Diameter: 35 mm



Date: 22/08/12

Length: 230 mm

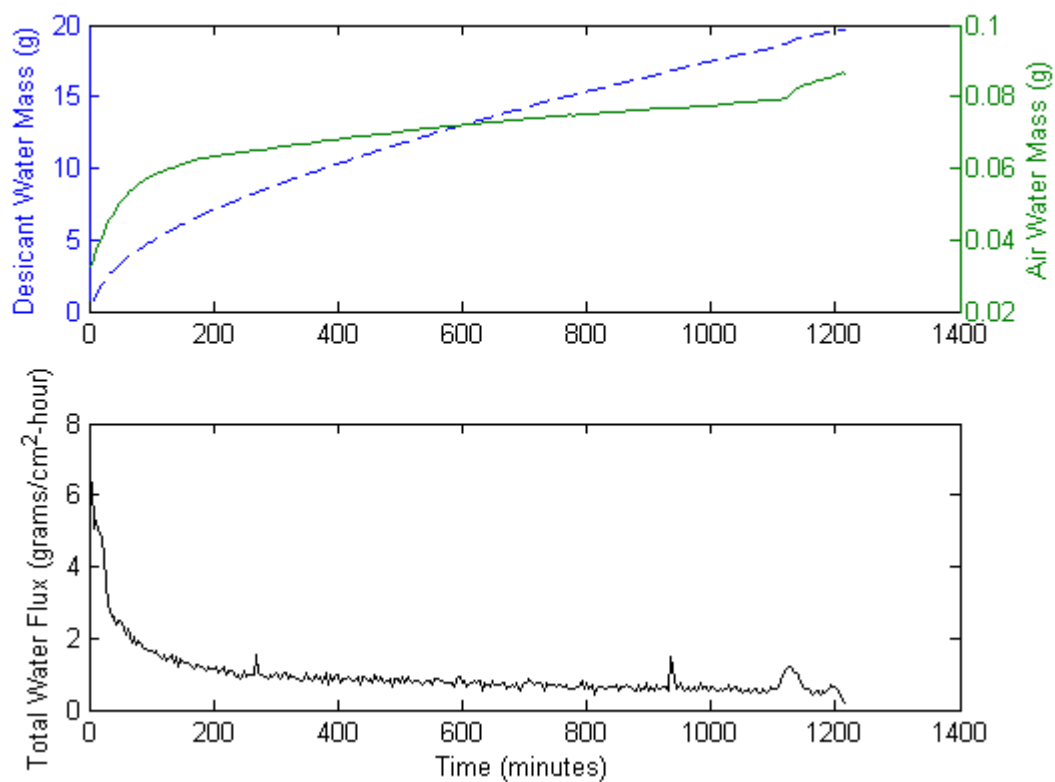
Diameter: 36 mm



Date: 21/08/12

Length: 220 mm

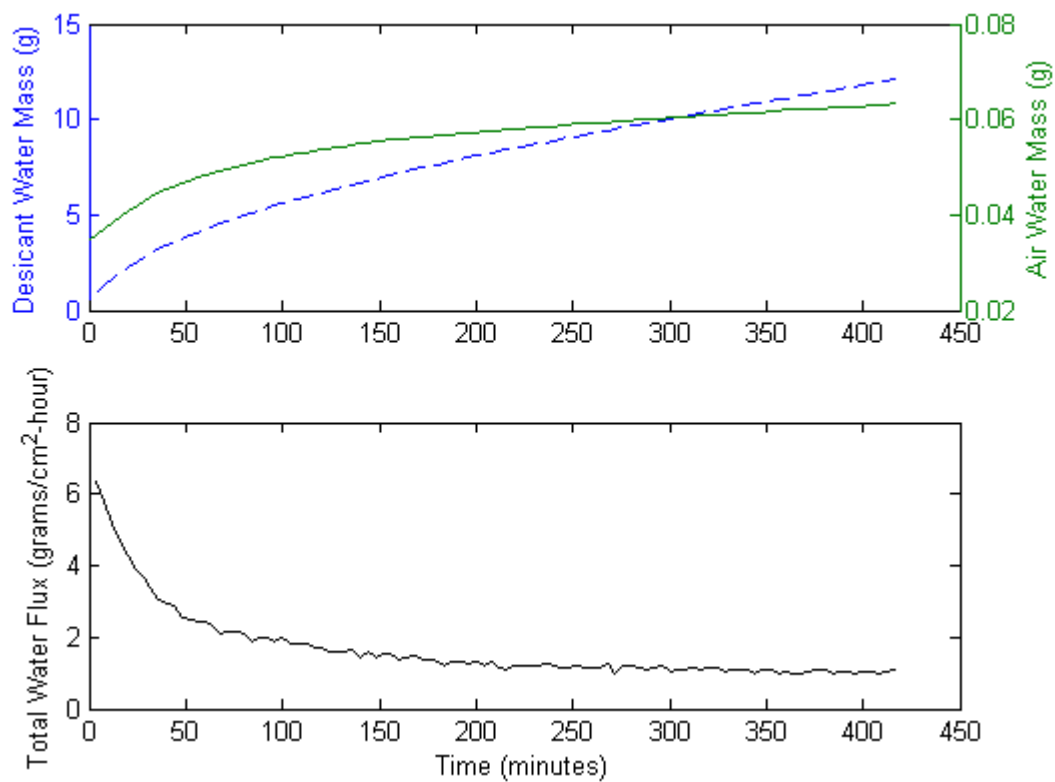
Diameter: 32 mm



Date: 31/05/12

Length: 220 mm

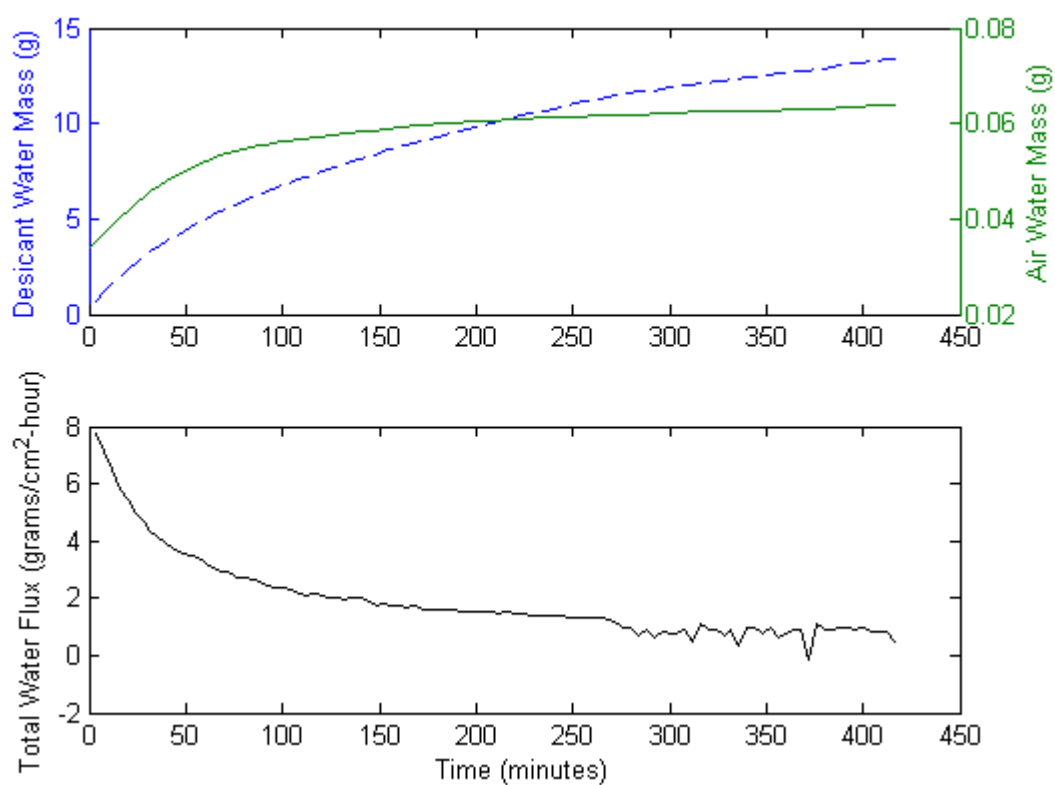
Diameter: 32 mm



Date: 11/09/12

Length: 240 mm

Diameter: 34 mm

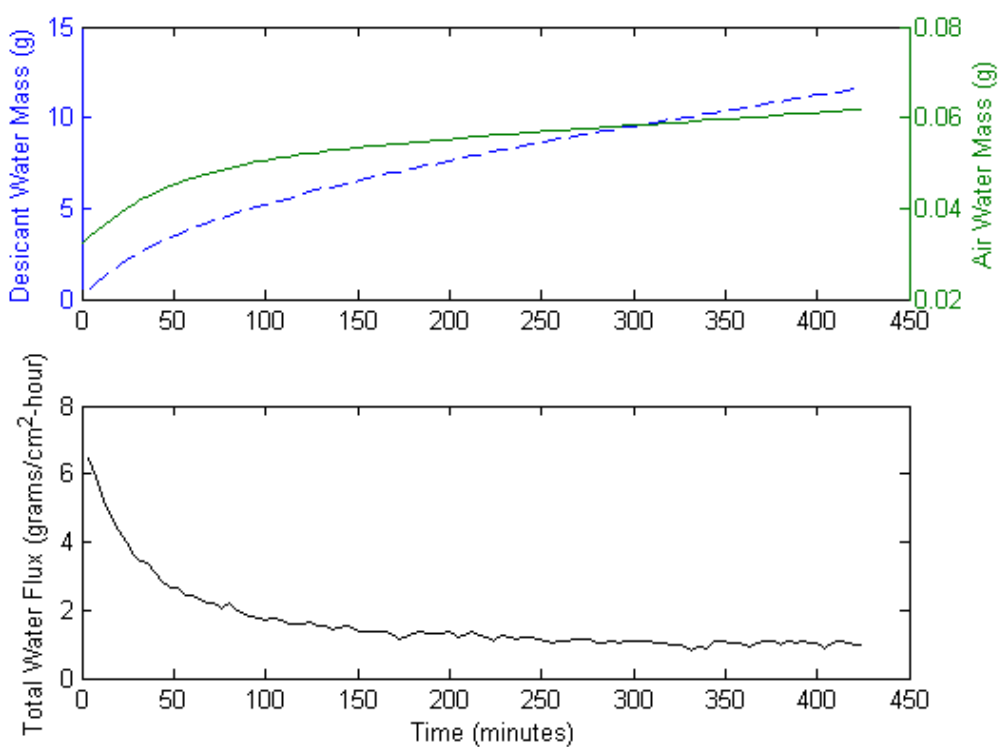


#### C4.2 5 cm H<sub>2</sub>O Pressure

Date: 05/06/12

Length: 240 mm

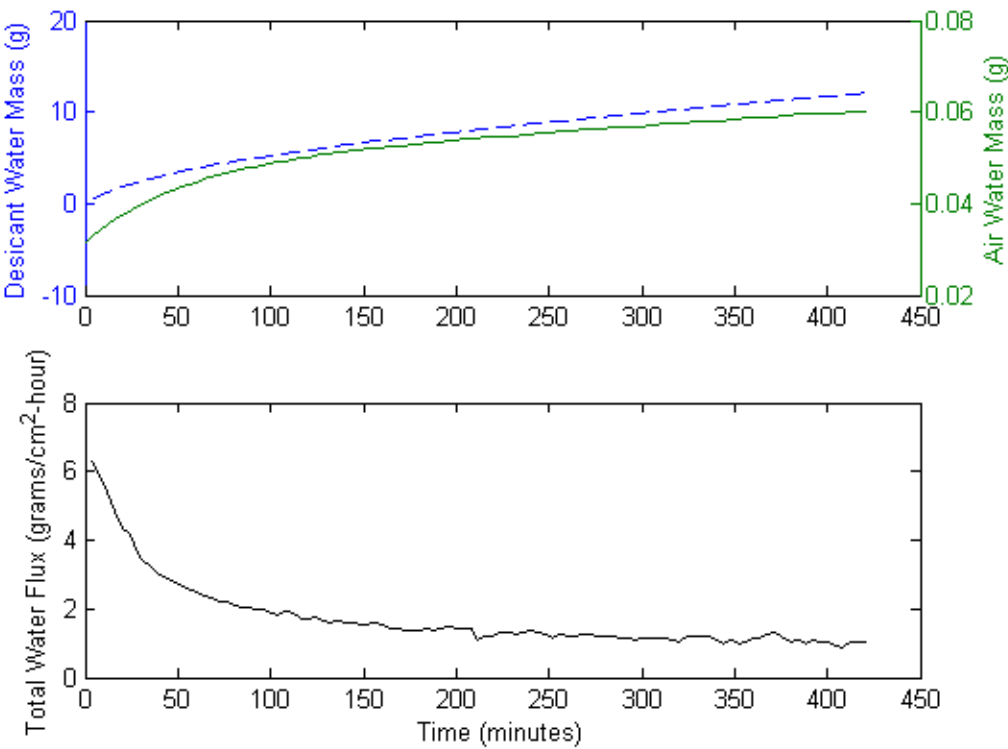
Diameter: 34 mm



Date: 06/06/12

Length: 240 mm

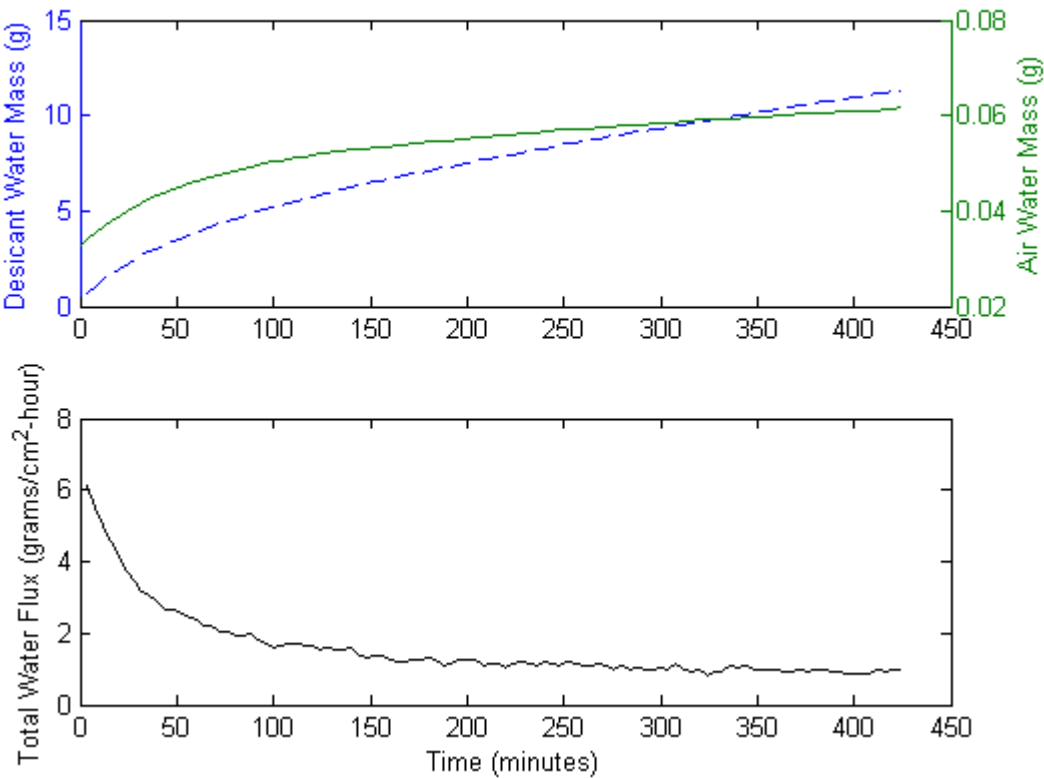
Diameter: 34 mm



Date: 07/06/12

Length: 240 mm

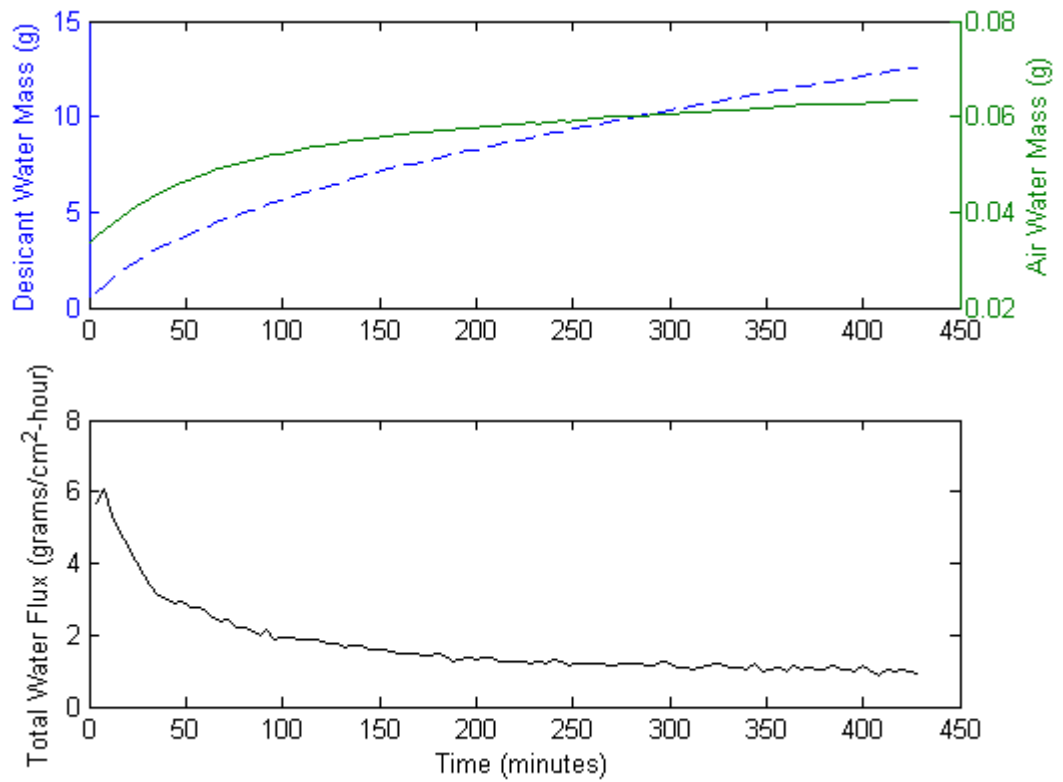
Diameter: 34 mm



Date: 11/06/12

Length: 240 mm

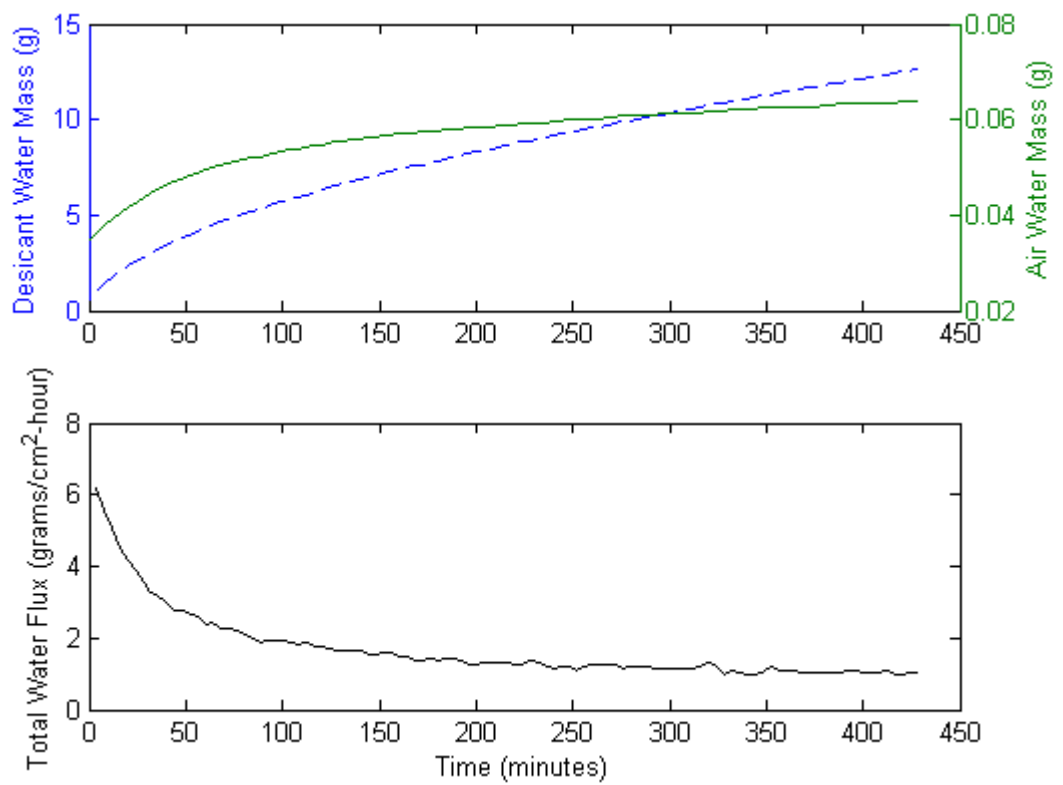
Diameter: 35 mm



Date: 12/06/12

Length: 250 mm

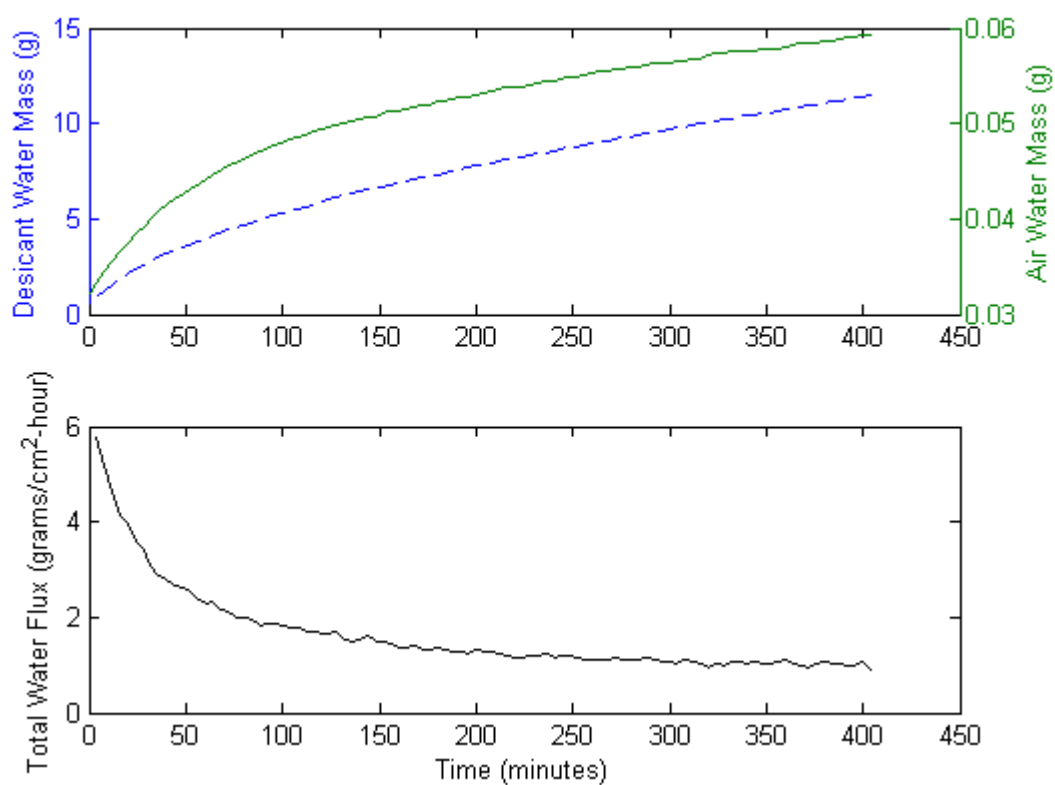
Diameter: 34 mm



Date: 13/06/12

Length: 240 mm

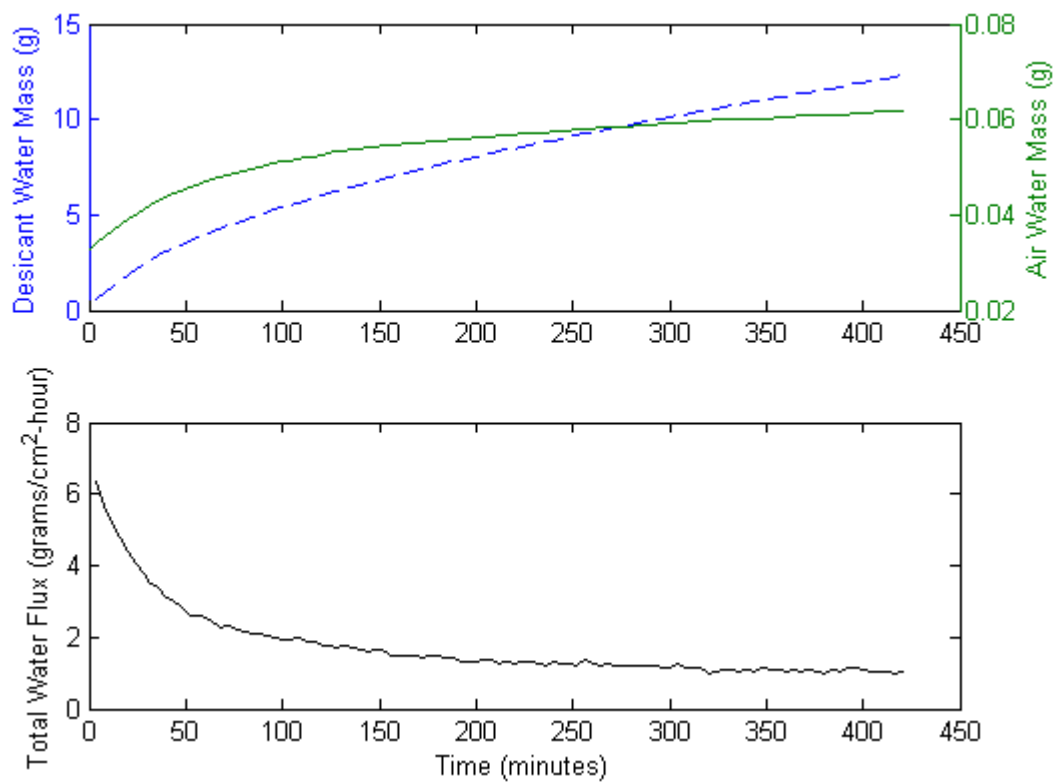
Diameter: 34 mm



Date: 14/06/12

Length: 230 mm

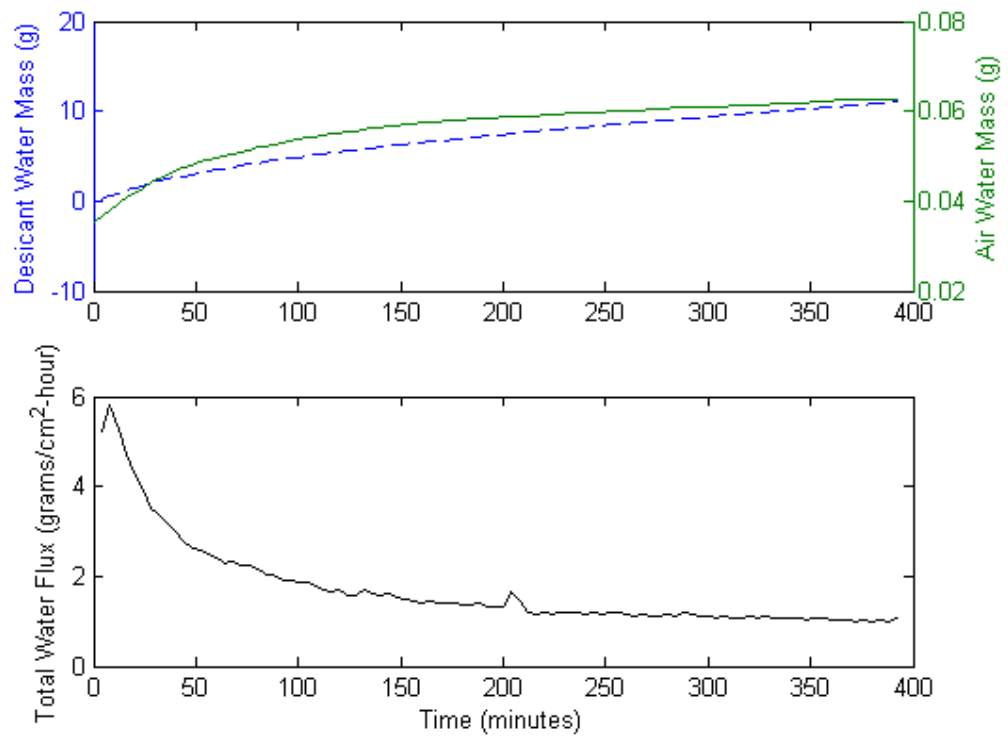
Diameter: 34 mm



Date: 20/06/12

Length: 240 mm

Diameter: 33 mm

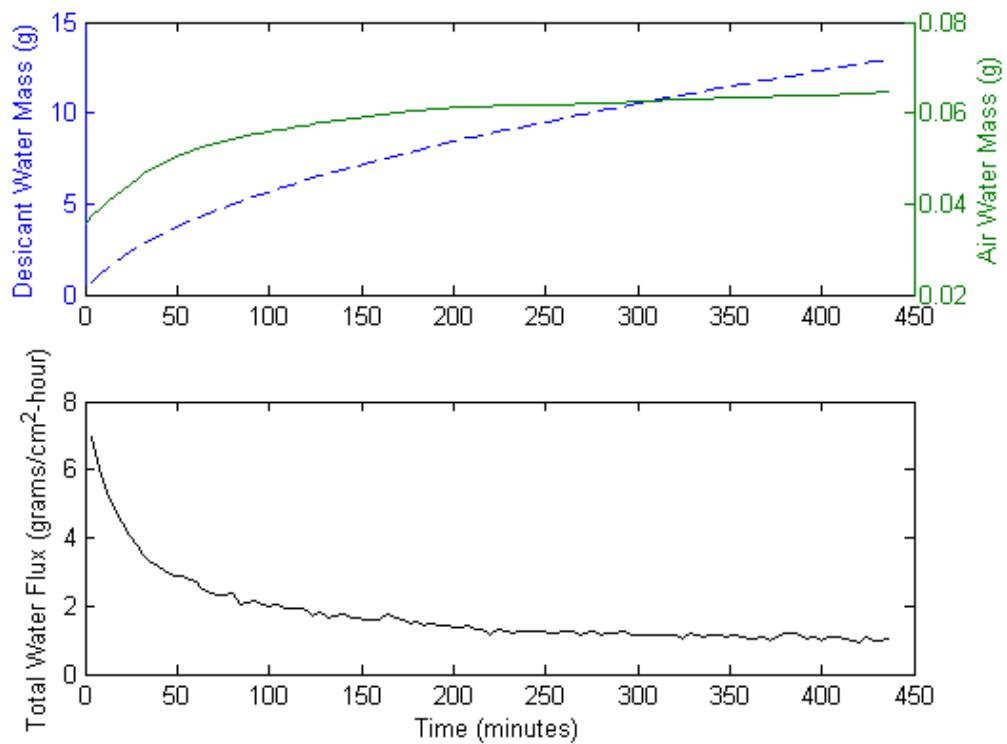


#### C4.2 10 cm H<sub>2</sub>O Pressure

Date: 26/06/12

Length: 250 mm

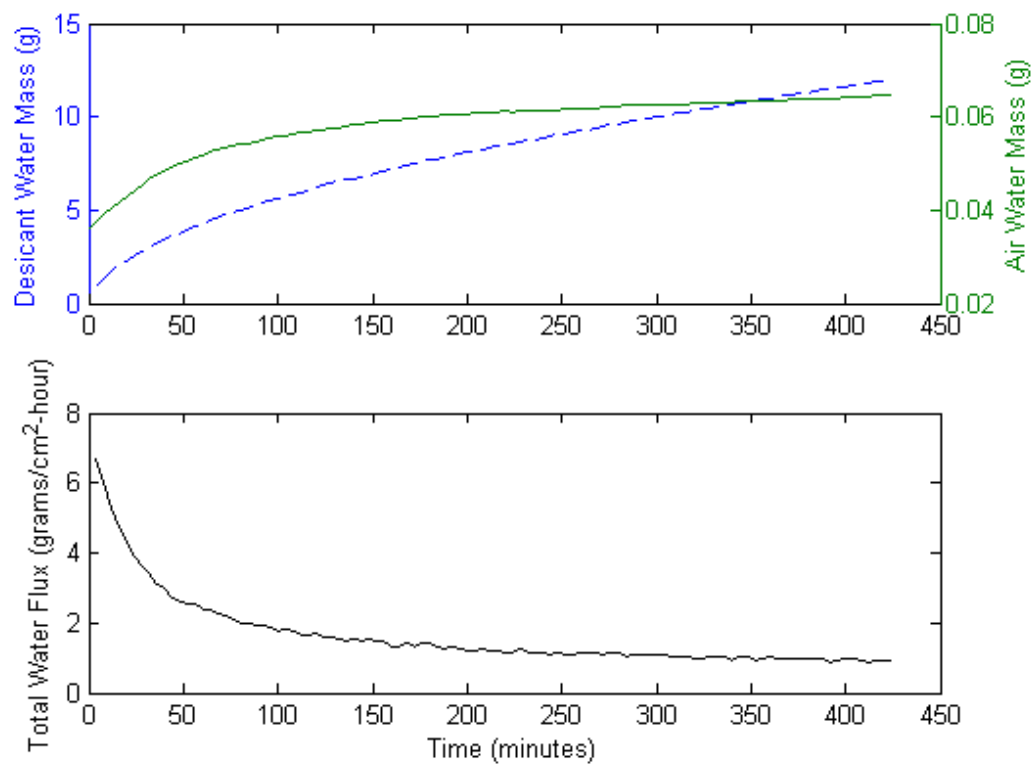
Diameter: 34 mm



Date: 21/06/12

Length: 250 mm

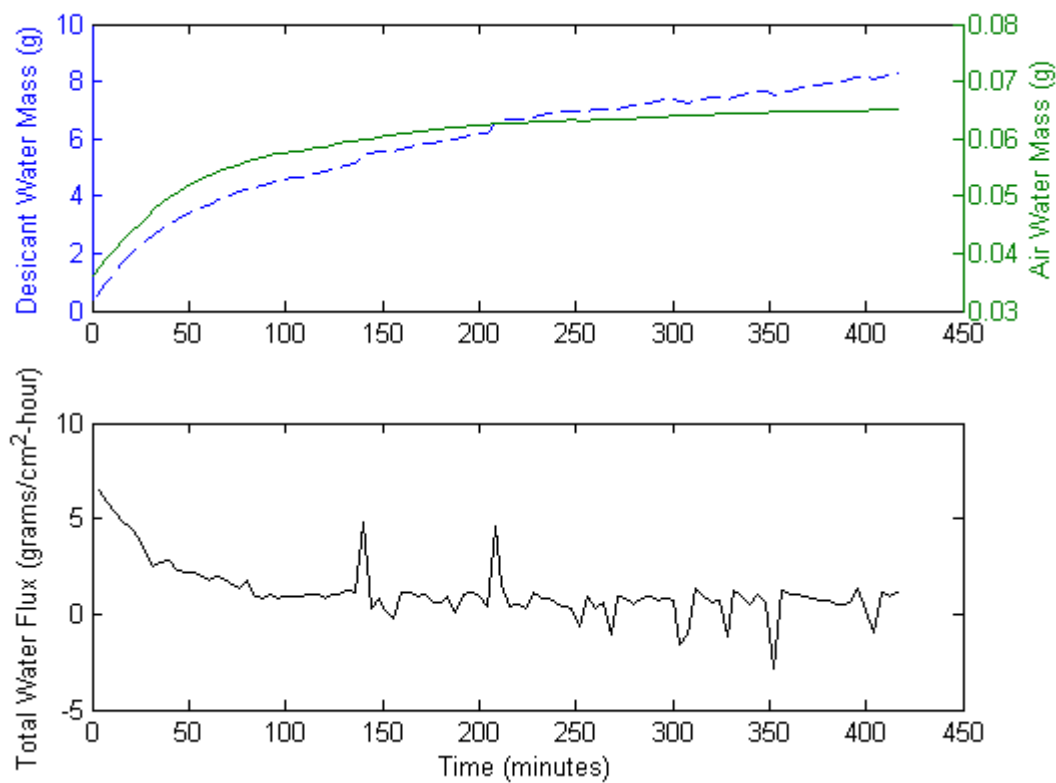
Diameter: 34 mm



Date: 25/06/12

Length: 250 mm

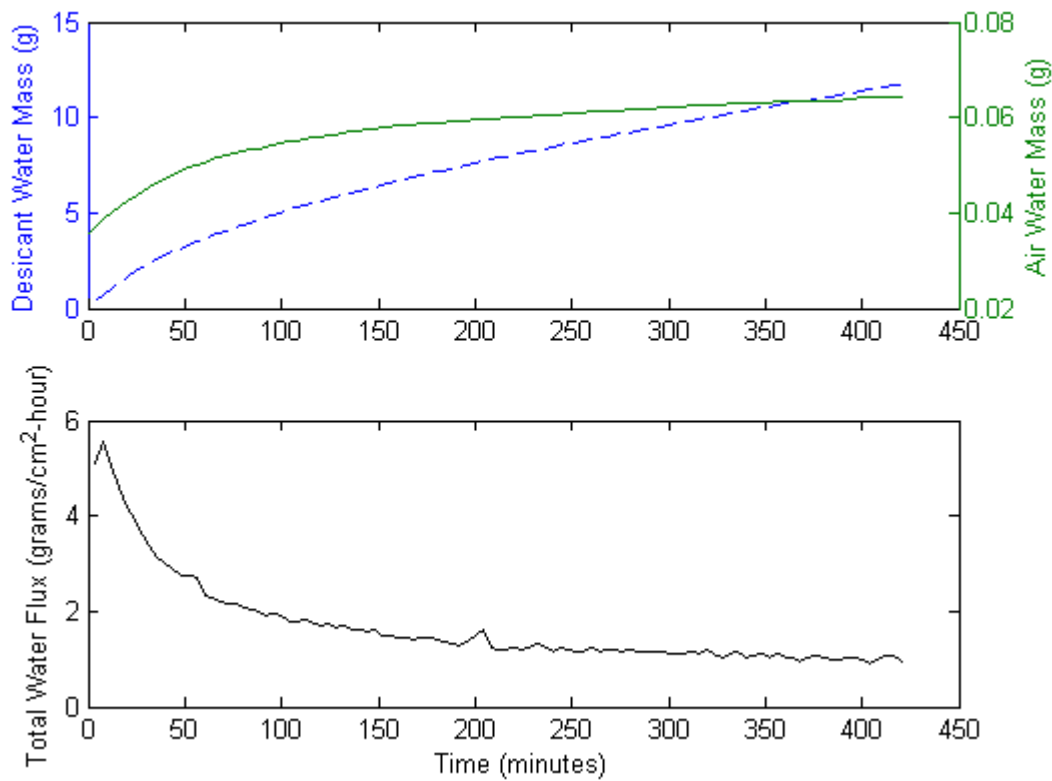
Diameter: 34 mm



Date: 18/06/12

Length: 240 mm

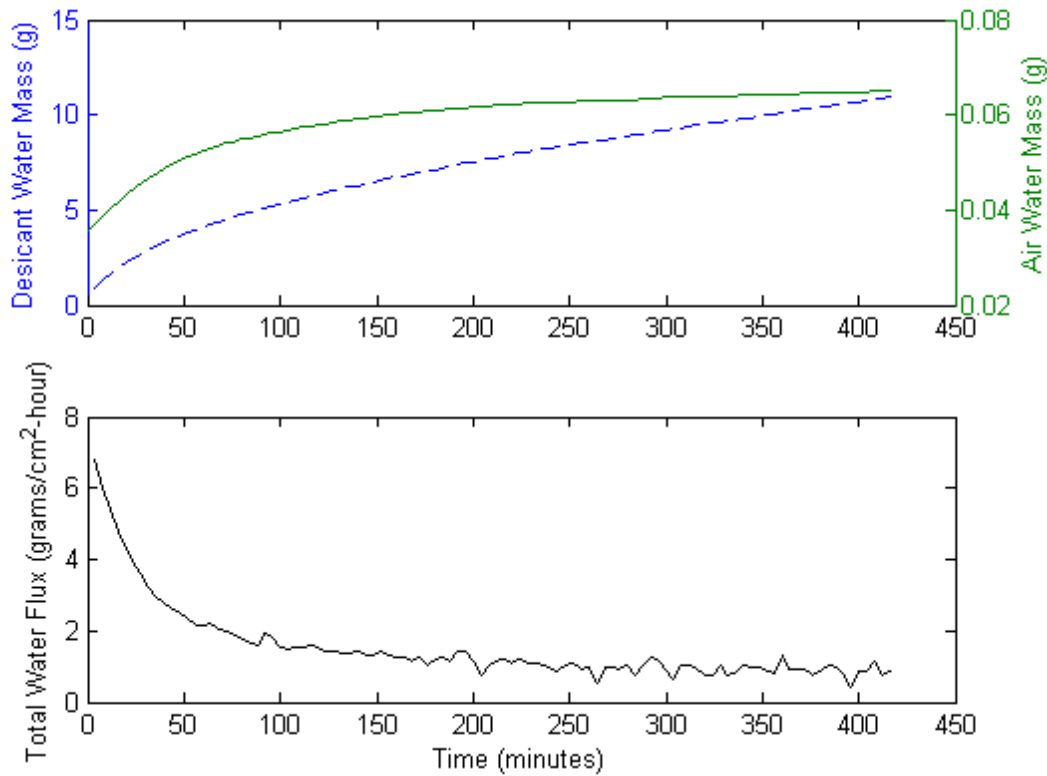
Diameter: 33 mm



Date: 19/06/12

Length: 250 mm

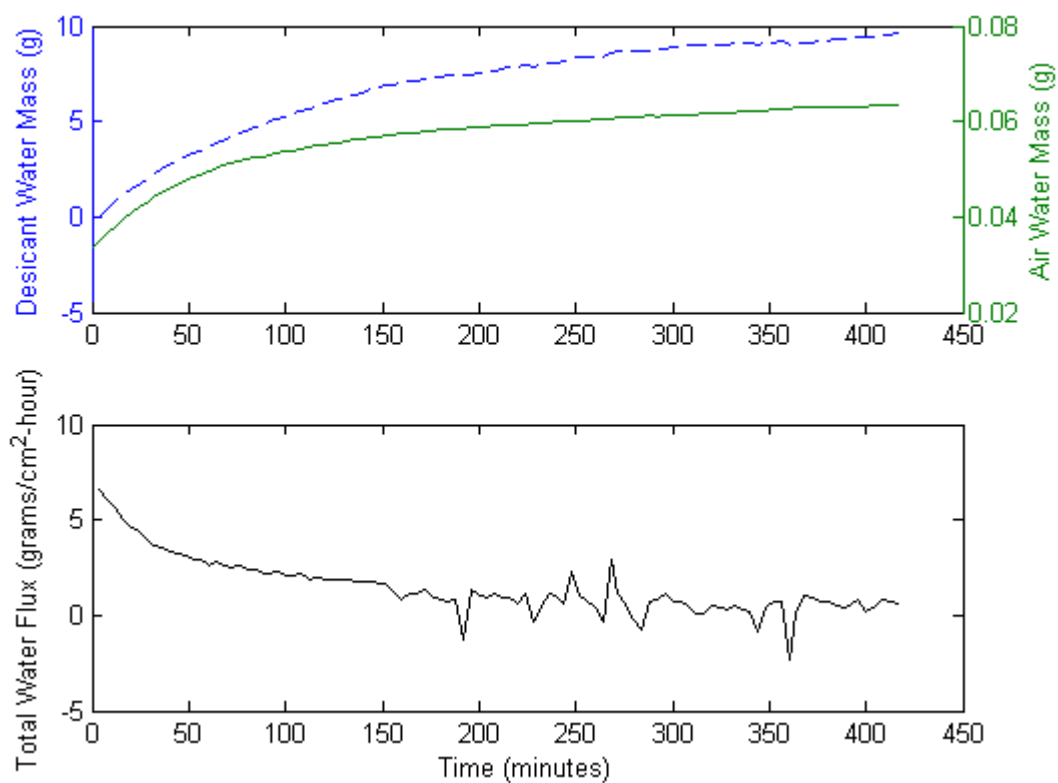
Diameter: 35 mm



Date: 05/09/12

Length: 250 mm

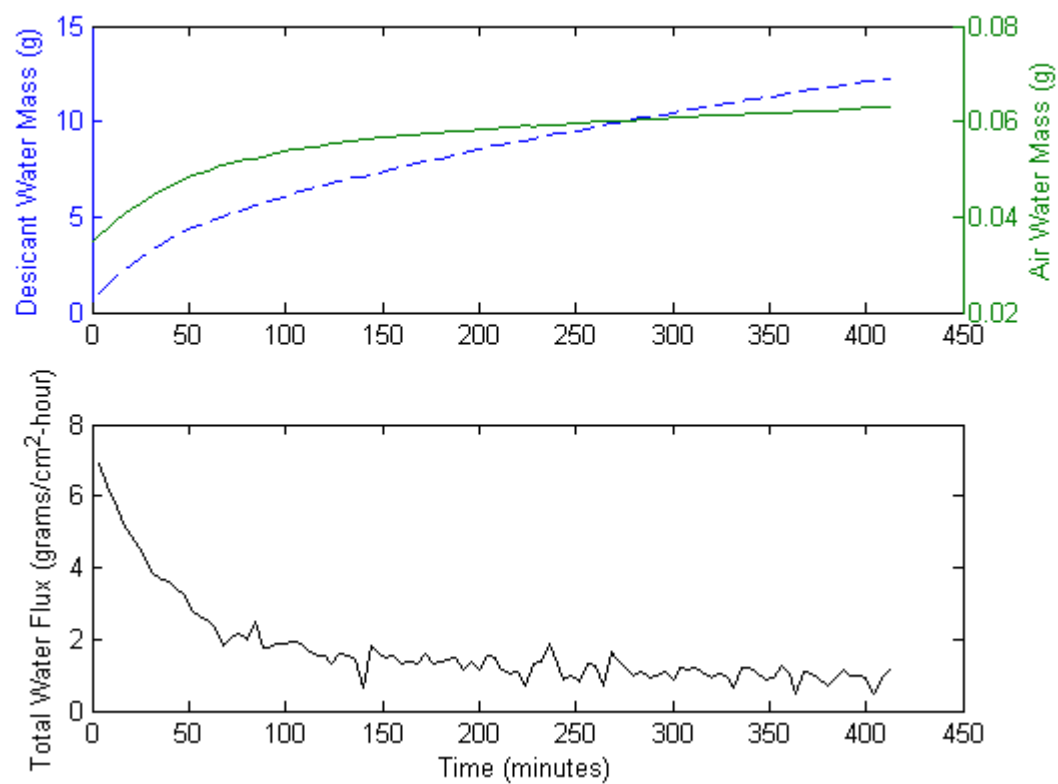
Diameter: 36 mm



Date: 06/09/12

Length: 240 mm

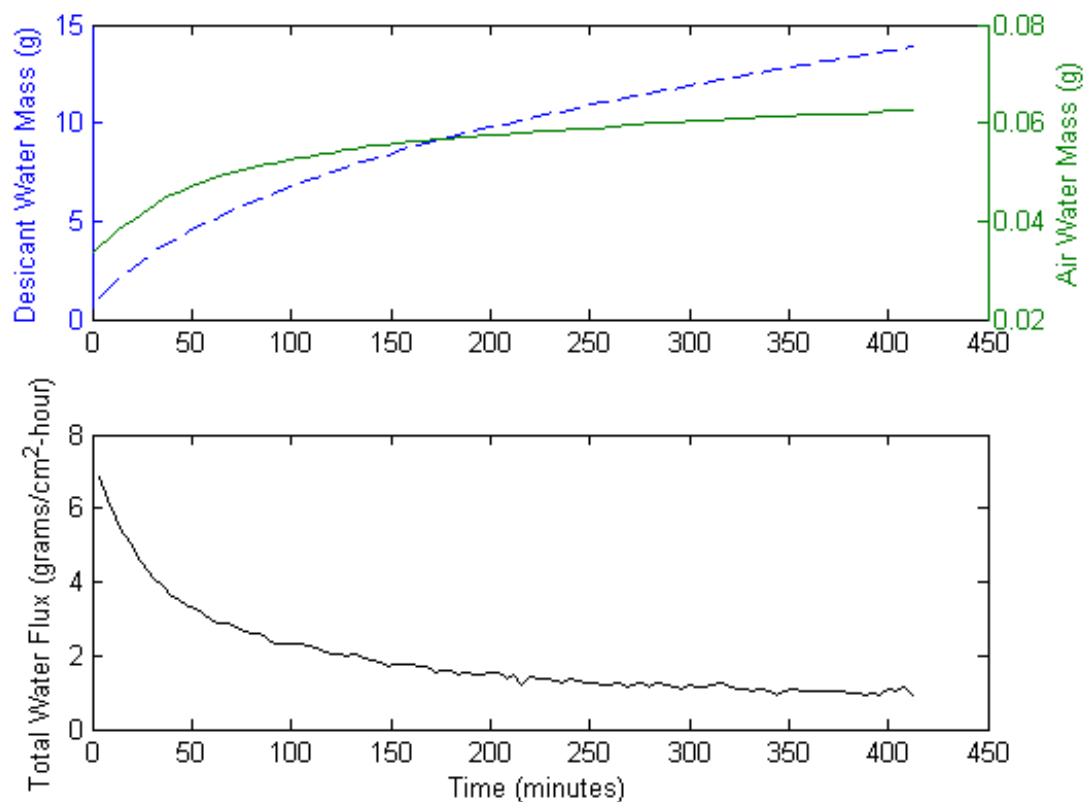
Diameter: 36 mm



Date: 10/09/12

Length: 250 mm

Diameter: 37 mm

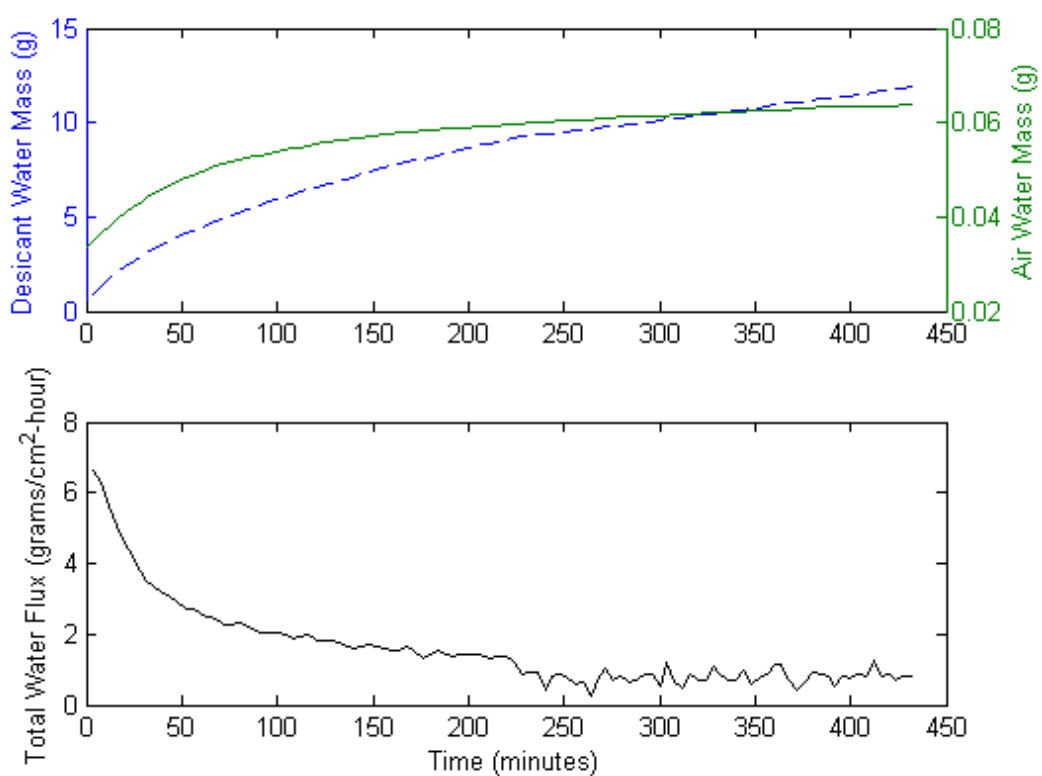


#### C4.4 15 cm H<sub>2</sub>O Pressure

Date: 27/06/12

Length: 240 mm

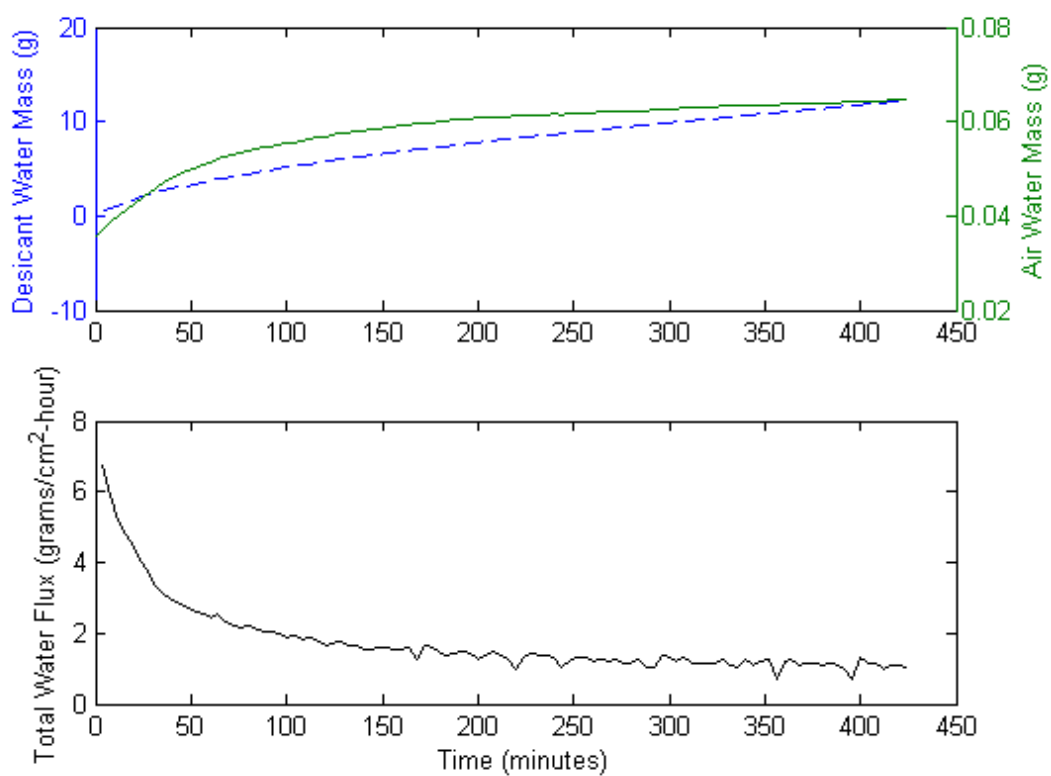
Diameter: 35 mm



Date: 28/06/12

Length: 240 mm

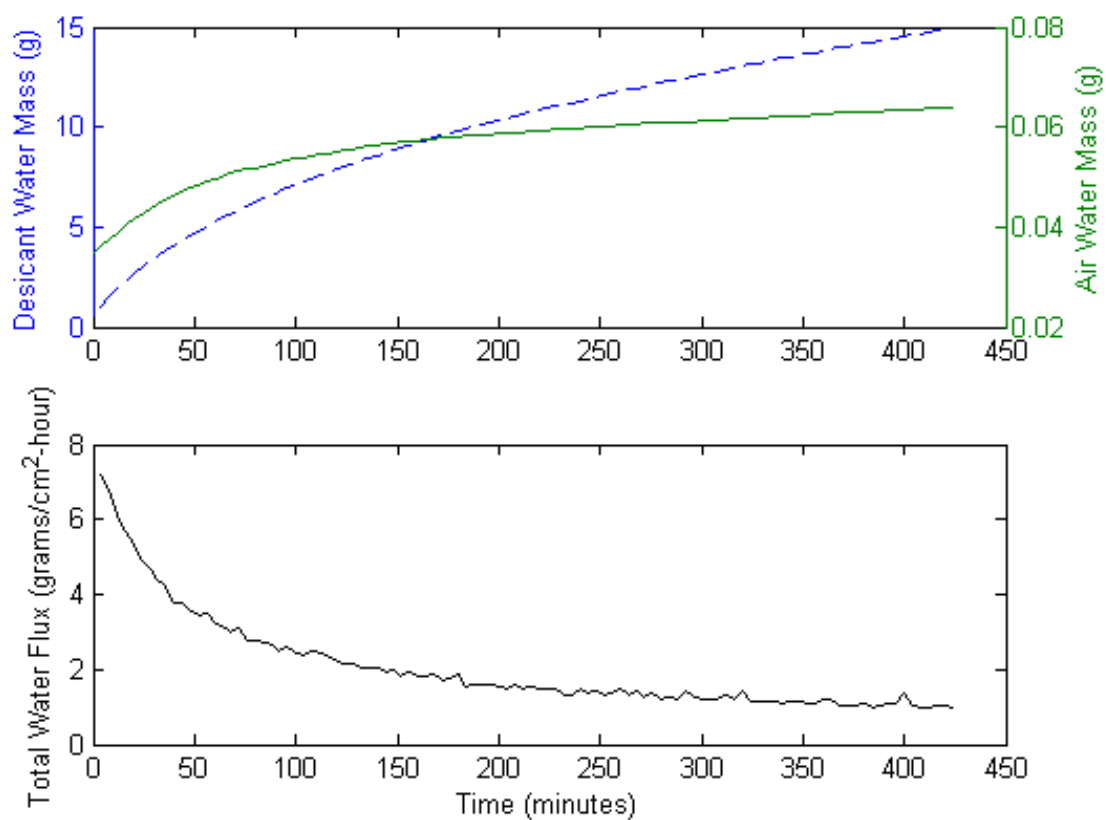
Diameter: 34 mm



Date: 24/08/12

Length: 250 mm

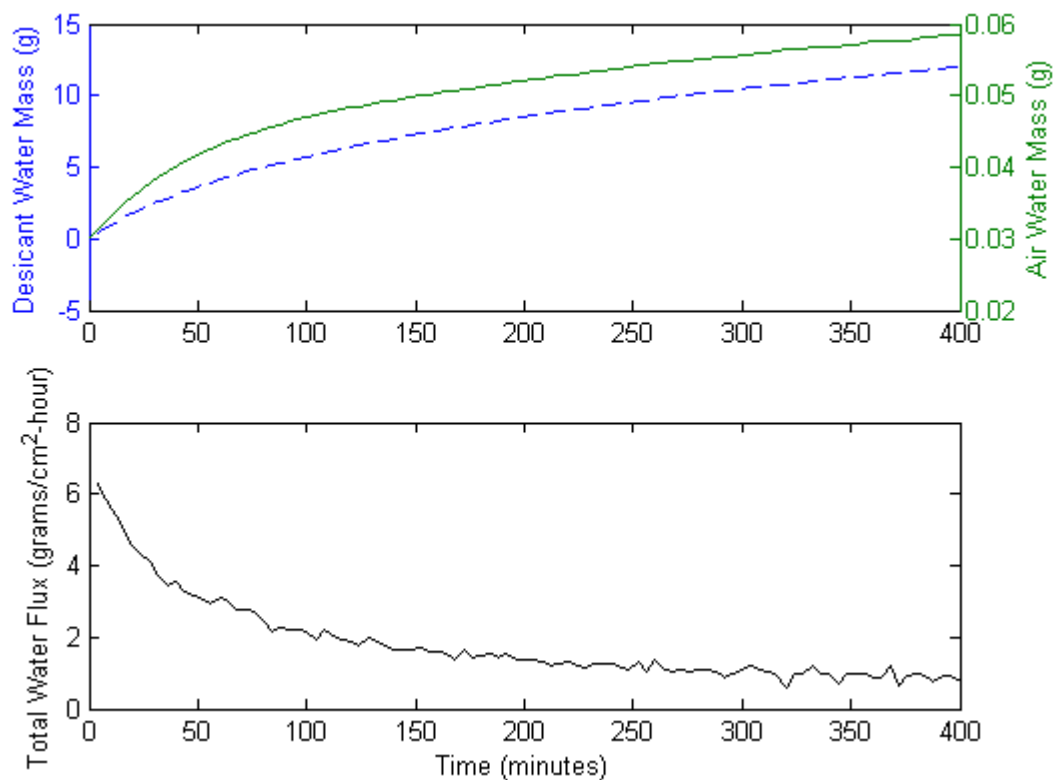
Diameter: 37 mm



Date: 27/08/12

Length: 250 mm

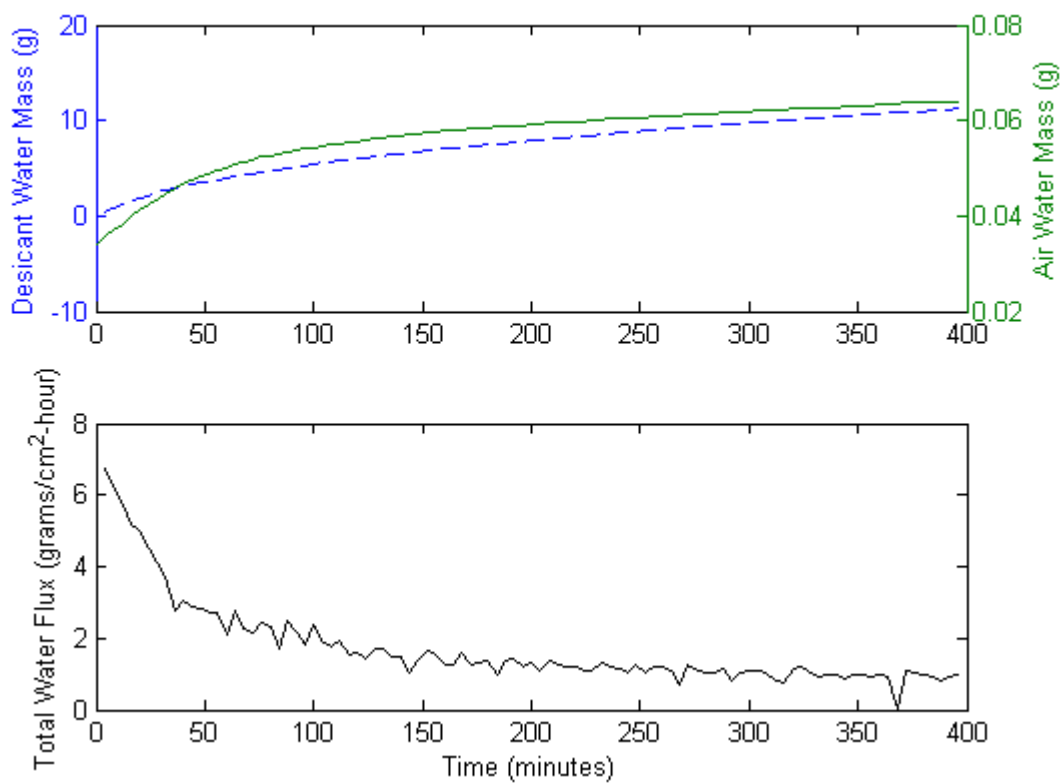
Diameter: 36 mm



Date: 29/08/12

Length: 240 mm

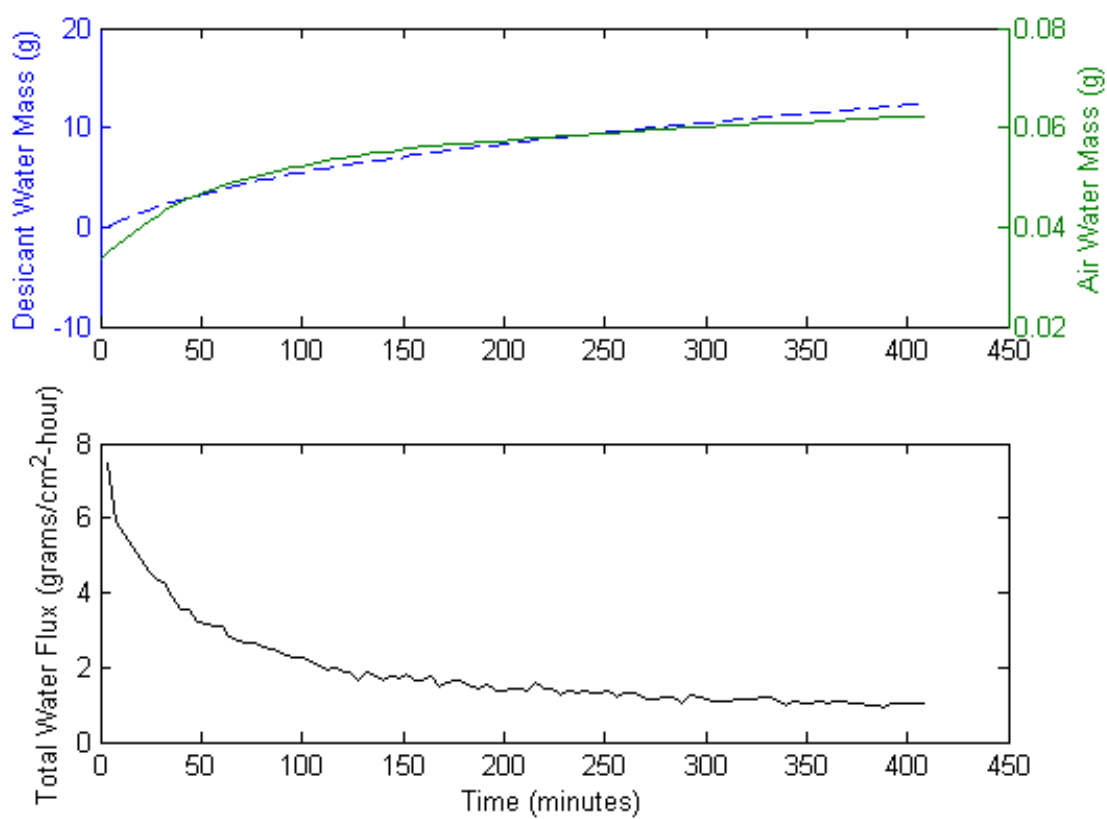
Diameter: 36 mm



Date: 30/08/12

Length: 250 mm

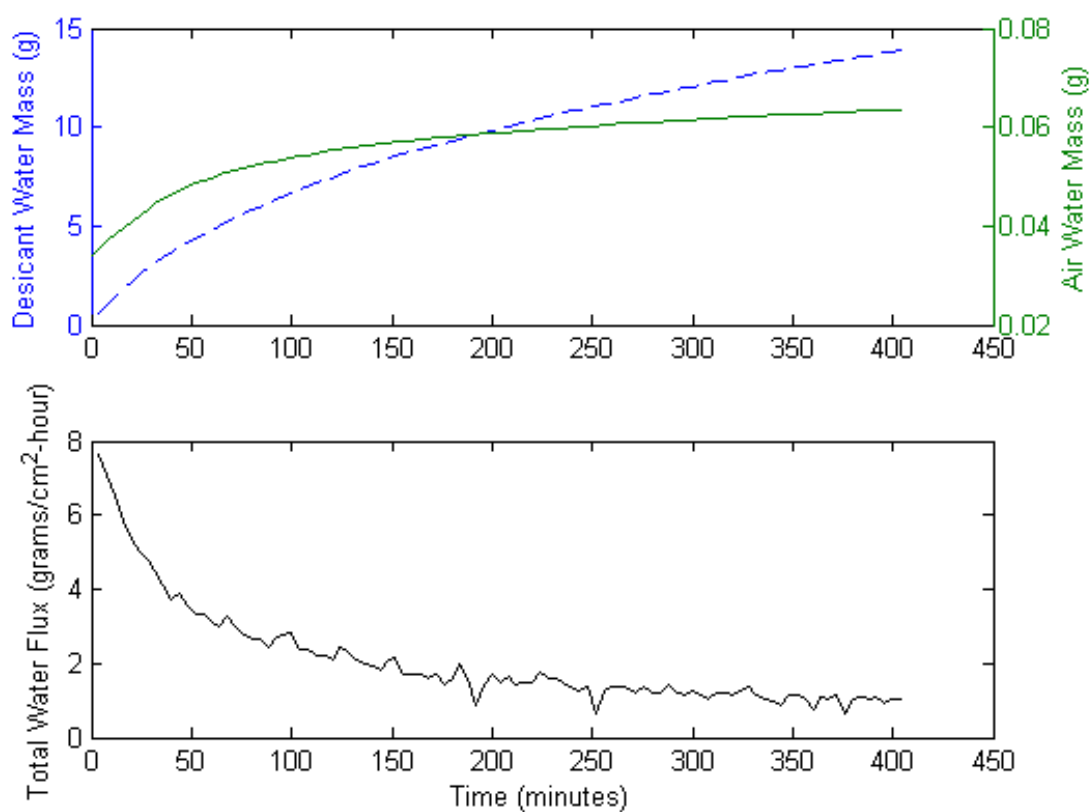
Diameter: 38 mm



Date: 03/09/12

Length: 250 mm

Diameter: 32 mm



Date: 04/09/12

Length: 250 mm

Diameter: 42 mm

